2009 SYNTHESIS AND PROCESSING CONTRACTORS' MEETING

Airlie Conference Center, Warrenton, Va., October 25-28, 2009

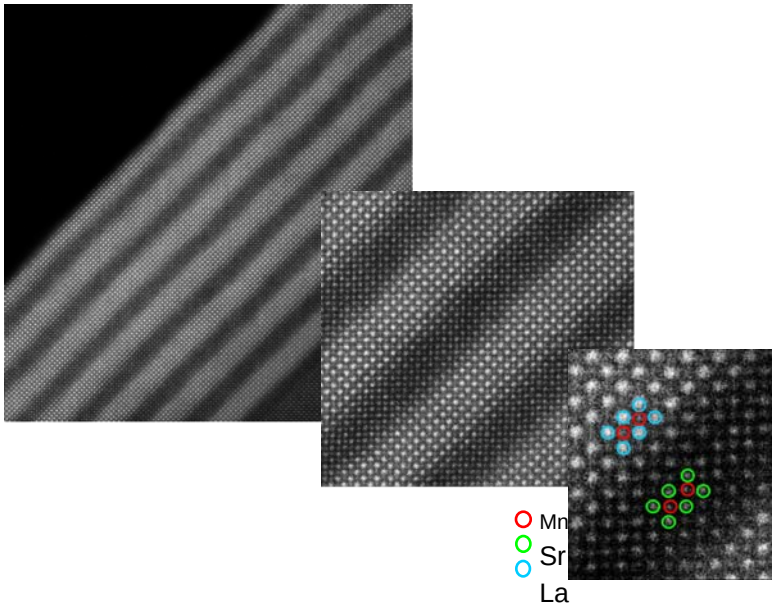

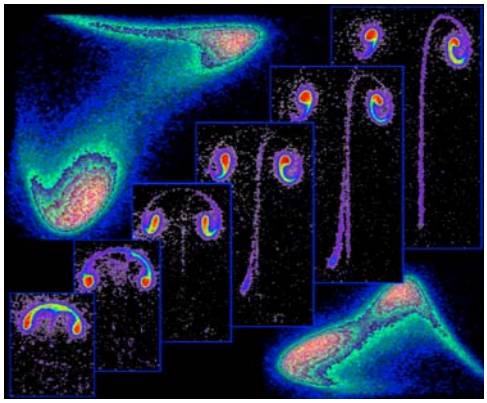

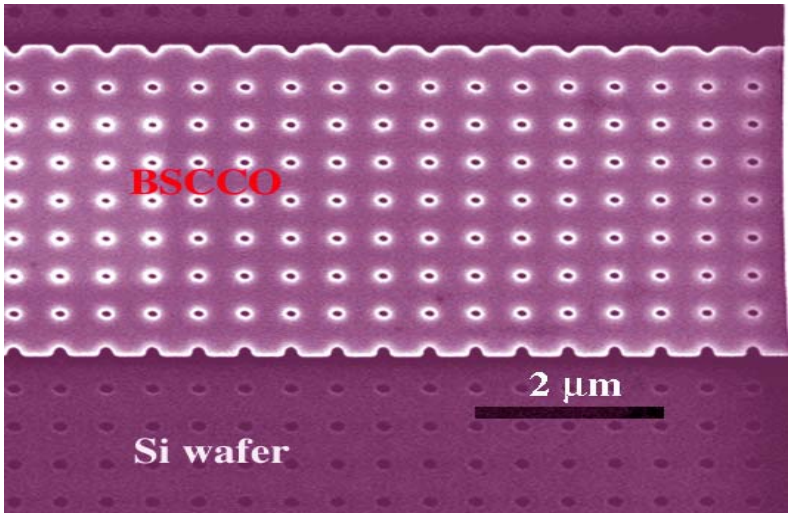

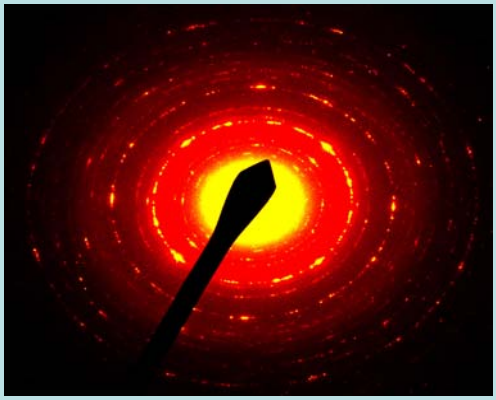

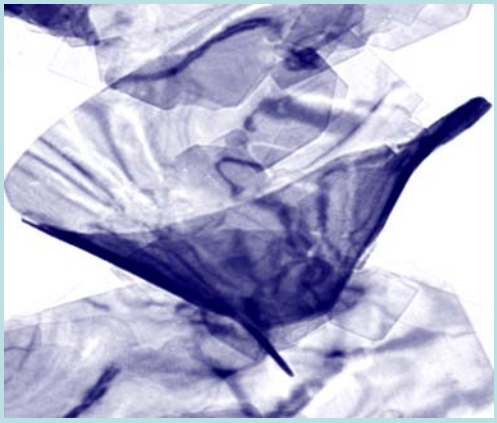

Office of Basic Energy Sciences
Division of Materials Science and Engineering

U.S. DEPARTMENT OF ENERGY Office of Science

On the Cover:
Top Left: Synthesis of manganites in $LaMnO_3/SrMnO_3$ superlattices. The La/Sr atoms are visible as bright/dim spots in this scanning transmission electron microscopy (STEM) image. The Sr/La cations are highly ordered, and the interfaces between $LaMnO_3$ and the $SrMnO_3$ are conducting, though both materials are gapped insulators.
Oxide MBE: S. May, T.S. Santos, A. Bhattacharya; STEM: Amish Shah, J.-M. Zuo.
Courtesy: Anand Bhattacharya (Argonne National Laboratory)

Bottom Left: Scanning electron microscopy (SEM) micrograph of a patterned $Bi_2Sr_2CaCu_2O_{8+x}$ nanoribbon. The holes with diameter of ~70 nm were achieved through focused-ion-beam (FIB) milling. $Bi_2Sr_2CaCu_2O_{8+x}$ is an extremely anisotropic high temperature superconductor with rich vortex physics including pancake and Josephson vortices. Single crystalline nanoribbons enable the pursuit of controlling vortex motions that can lead to novel properties such as terahertz radiation emission.
Courtesy: Zhilli Xiao (Northern Illinois University)

Top Right: The synthesis and confinement of nanoparticles by laser ablation of solid targets into background gases are studied with in situ gated-intensified CCD imaging and spectroscopy of the visible photoluminescence and Rayleigh scattering induced by a second, time-delayed sheet of laser light. (Si into 10 Torr He, false color representation of brightness)
Courtesy: David Geohegan (Oak Ridge National Laboratory)

Bottom Right: Transmission electron microscopy (TEM) images and electron diffraction (ED) pattern for PbO-type FeSe nanosheets (sheets are 50–200 nm diameter laterally by 2–3 nm thick)
Courtesy: Raymond Schaak (Pennsylvania State University)

This document was produced under contract number DE-AC05-06OR23100 between the U.S. Department of Energy and Oak Ridge Associated Universities.

Table of Contents

FOREWORD

This abstract book comprises the scientific content of the 2009 Synthesis and Processing Contractors' Meeting sponsored by the Division of Materials Sciences and Engineering (DMS&E) in the Office of Basic Energy Sciences (BES) of the U.S. Department of Energy (DOE). The meeting, held on October 25–28, 2009, at the Airlie Conference Center in Warrenton, Virginia, is the second contractors' meeting on this topic and is one among a series of research theme-based contractors' meetings being held by DMS&E.

The purpose of this contractors' meeting is to bring together all of the researchers funded by DMS&E within BES in the Synthesis and Processing core research activity and in related programs so that they can get a firsthand look at the broad range of materials science research that is being supported in this important research area. The meeting will serve as a forum for the discussion of new results and research highlights, thus fostering a greater awareness of significant new advances in the field and the research of others in the program. The confidential and collegial meeting environment is intended to provide unique opportunities to develop new collaborations among PIs, and new ideas. In addition, the meeting affords BES program managers an opportunity to assess the state of the entire program at one time on a periodic basis, in order to chart future directions and identify new programmatic needs.

This year's meeting focuses on four topics within the Synthesis and Processing portfolio, which include Nano-object Synthesis and Assembly, Thin Films, Bulk Materials and New Materials Discovery, and Soft and Hybrid Materials. In addition there are a few special topics that have been selected to be highlighted at this meeting, including Nanomaterials Synthesis and Characterization, Synthesis Methods in Plasmonics, as well as examples of new synthesis science at the DOE Nanoscale Science Research Centers and Energy Frontier Research Centers. While this is one way of organizing and presenting the research within this broad portfolio, there are many other synergies that could be highlighted and will be considered at future meetings.

Let me take this opportunity to express my thanks to all the meeting attendees, especially the invited presenters, for their active participation and sharing their ideas and new research results. A special thanks is given to the selected invited speakers from the DMS&E Condensed Matter Physics and Electron and Scanning Probe Microscopy core research activities, and the new Energy Frontier Research Centers, who graciously agreed to attend and share their perspectives. The dedicated efforts and invaluable advice of the Meeting Chairs, David Geohegan and Karen Winey, towards organizing this meeting are deeply appreciated. Finally, this meeting would not be possible without the logistical support from Christie Ashton at DMS&E and Joreé O'Neal at Oak Ridge Institute for Science and Education (ORISE).

Bonnie Gersten
Program Manager, Synthesis and Processing
Division of Materials Sciences and Engineering
Office of Basic Energy Sciences
U.S. Department of Energy

S&P 2009
Synthesis and Processing 2009
DOE-BES-DMSE Synthesis and Processing Science Contractors' Meeting

This meeting of DOE-BES-DMSE contractors will focus on current directions and challenges in Synthesis and Processing that are crucial for the discovery and exploration of novel materials and architectures. The Synthesis and Processing Science Core Research activities include:

(1) Studies to further the understanding between atomistic behavior and the predictive rational design of complex (spatially and dissimilar) materials with controlled defects and architectures including both atomistic to continuum approaches;
(2) The exploration of revolutionary and reliable new physical synthesis strategies (principally bottom-up approaches) and creative processing paradigm shifts; and
(3) The development of diagnostic tools to probe synthesis, in situ and in real time, with multi-technique probes that push the limits of both spatial and temporal resolutions.

This combination of novel synthesis approaches, diagnostic tools, and first-principle atomistic predictive design methods is focused on understanding the mechanisms of growth and the evolution of molecular and nanoscale structure. However a wide variety of processing approaches are used to controllably alter these structures, both in situ and ex situ, with a special emphasis on understanding interfacial interactions leading to the controllable self-assembly of architectures with tailored interfaces that often possess novel functionalities.

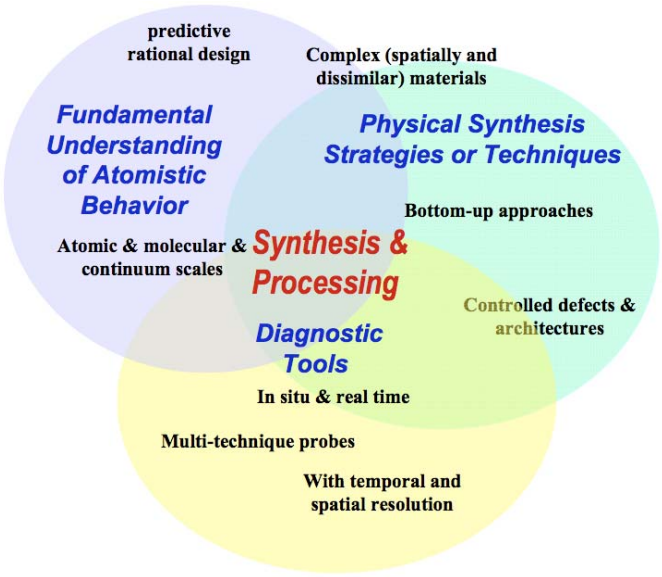

For this meeting, abstracts will be organized within six sessions:

I. **Bulk and Nano-materials: a. Synthesis and Characterization** and **b. New Materials Discovery** (poster session)
II. **The Nanoscale: a. Assembly; b. Object Synthesis and Assembly;** and **c. The Nanoscale** (poster session)
III. **Synthesis Methods in Plasmonics**: One and Two Dimensions
IV. **Thin Films**: **a.** and **b. Synthesis of Thin Film Interfaces; c. Thin Films** (poster session) and **d.** and **e. Fabricating Nanostructure from Films**: Synthesis and Processing
V. **Soft and Hybrid Materials**: Interfacial Interactions and Processing (poster

session)

VI. **Energy Frontier Centers and Nanocenters**

Each materials class presents its own challenges. However several synthesis and processing scientific themes crosscut the materials systems, including:

Crosscutting Questions

(1) **Synthesis Strategies for New Materials Discovery** – What new processing strategies and in situ techniques will enable the synthesis of new classes of materials?

(2) **Atomistic Deposition** – What synthesis and processing challenges must be overcome to enable the reliable and reproducible deposition of atoms for materials synthesis?

(3) **Designing Interfaces** – What are the basic principles for designing interfaces? How can interfaces be processed with atomic resolution? What are the new paradigms for soft/hard hybrid materials systems?

(4) **Theory-Driven Synthesis** – What are the first-principle–based theoretical approaches to describe experimentally accessible materials? Can material design and growth mechanism understanding be extended to predict the most thermodynamically plausible routes and techniques for synthesis?

(5) **Precision Processing and Defect Control***:* Can predictable and reliable, non-equilibrium processing be developed that is uniform over large scales? How can defects be controlled during processing?

(6) **Understanding Long- and Short-Range Forces**: Can the contributions of long- and short-range forces to the growth of nanoscale objects and the evolution of nanoscale morphology be understood? How do long-range interactions contribute to phase stability and interface motion?

Meeting Sessions will be organized to address the following questions:

I. Bulk and Nano-materials: a. Synthesis and Characterization and **b. New Materials Discovery** (poster session)

This session will focus on new directions in bulk material synthesis—an established discovery platform for new and well-characterized phases of materials (e.g., high-T_c superconductors, thermoelectrics, …) that are later synthesized as thin films and nanomaterials. Only a fraction of possible new materials combinations from the periodic table have been synthesized, and rational new approaches for the discovery of novel new bulk materials are needed. Progress in the field will be described and illustrated with ultrahard refractories, clathrates, and mesoporous materials. Along with new synthesis approaches, novel methods for characterization of phase composition, homogeneity, and structural anisotropy must be developed. Function-inspired synthesis strategies involve not only versatile methods to explore doping and phase characterization, but integrated materials properties measurements. Chemical synthesis techniques are also required for the design of mesoporous nano-architectures for tailored adsorption, separation, or optoelectronic properties.

II. The Nanoscale: a. Assembly; b. Object Synthesis and Assembly; and **c. The Nanoscale** (poster session)

This session will address synthesis and design of nanomaterials and fundamental understanding of growth processes through in situ diagnostics and real-time observations of growth. Nanoscale objects present special fundamental synthesis challenges because their nucleation and growth often occur rapidly in a competition between kinetics and thermodynamics. In situ and real-time diagnostics are inherently more difficult than those used to monitor the evolution of surfaces in thin film growth. Fundamental questions for quasi-one-dimensional nanomaterials (nanotubes, nanowires, nanoribbons, etc.) include competitive pathways for self-assembly and catalyst-driven (e.g., VLS) assembly. Unraveling the role of 'catalysts' is a key question, as high-temperature, gas-suspended catalyst nanoparticles are often likely molten, and prediction of their behavior requires knowledge of phase diagrams that still are unknown. Catalyst nanoparticles on a substrate at relatively low temperatures have been observed to be mostly crystalline by in situ TEM, yet serve multiple roles including chemical decomposition and localization points for self-assembly of intermediate species. Since nanomaterials are mostly surfaces, they are highly sensitive to the processing environment and the incorporation of defects. The controllable introduction of defects in synthesis and processing of nanomaterials is a key challenge. Materials properties that reflect the synthesis processes are often the most effective characterization features to assess the distribution of products. Measurements of both individual nanomaterial properties (e.g., scattering, photoluminescence) will be compared with those for ensembles (e.g., plasmonic, magneto optical, etc.).

III. Synthesis Methods in Plasmonics: One and Two Dimensions

This session will address some recent results and developments in the synthesis of materials that affect the plasmonic field. The synthesis of one-dimensional highly asymmetric core-capped nano-metals has allowed new assemblies of plasmonic structures in a variety of dielectric environments. New techniques for making ultrasmooth layers for the efficient propagation of surface waves at two dimensions and the modeling of such structures in a variety of dielectric environments have pushed the envelope of the state of the art. Some of the remaining synthesis and processing issues will be described in this session.

IV. Thin Films: **a.** and **b. Synthesis of Thin Film Interfaces; c. Thin Films** (poster session) and **d.** and **e. Fabricating Nanostructure from Films**: Synthesis and Processing

This session will address the synthesis and processing of quasi-two-dimensional materials—predominantly thin films, but including atomic sheets, flakes, and membranes. While molecular beam epitaxy has set the standard for controllable layer-by-layer synthesis of epitaxial thin films, the additional advantages of charged particles, pulsed fluxes, and higher kinetic energies in growth processes are illustrated by techniques such as plasma-assisted MBE, pulsed laser deposition, and pulsed CVD. New approaches for atomic layer deposition relying on surface charge-induced chemical deposition will be reviewed. Progress in the control of impurities and defects and

understanding the kinetic effects in surface diffusion and step migration through well-controlled deposition experiments will be presented. Atomic layer heteroepitaxy presents the opportunity to synthesize multiferroic thin films unit cell by unit cell, permitting the revelation of collective and emergent phenomena. Synthesis of multicomponent thin films designed to test these paradigms through their predicted properties will be described.

Modifications to surfaces through irradiation and sputtering using ion, laser, and other beams can be used to add functionality and order, but also reveal the mechanisms of defect creation, sputtering, diffusion, and restructuring.

V. Soft and Hybrid Materials: Interfacial Interactions and Processing (poster session)

This session will focus on defining the design rules for integrating soft with hard materials creating hybrid and dissimilar materials. Such materials hold the promise of tunable, multifunctional properties through the understanding of interfacial interactions and the development of associated processing strategies—for example, to create tailorable hard materials and robust soft materials, or for the self-assembly of bulk heterojunctions between inorganic nanowires/nanotubes and polymers for enhanced electron and hole-transport in organic photovoltaics and light-emitting devices. Therefore, understanding the self assembly of colloids, phase formation and segregation in block copolymers, and the energy-driven interactions in nanoparticle/polymer systems is crucial in the quest to develop soft/hard/hybrid materials that can hierarchically organize in 3D architectures by self-organization or through external stimuli. Controlling the topography of soft material surfaces is another processing challenge crucial to the development of nearly every functional thin film polymer hybrid structure.

VI. Energy Frontier Centers and Nanocenters

This session will overview some of the new initiatives and developments at the Department of Energy Basic Energy Sciences. What are the Energy Frontier Centers? How will they involve the community? How can you get involved in the Nanocenters?

Summary: Overall, this meeting will endeavor to establish working relationships and collaborations among the Contractors through the discovery and discussion of materials synthesis and processing challenges that crosscut materials classes.

This page is intentionally blank.

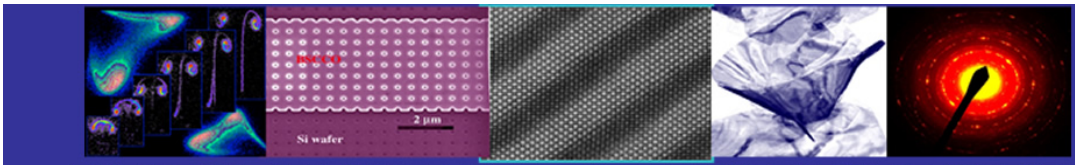

Synthesis and Processing Sciences Contractors Meeting

Sponsored by the U.S. Department of Energy, Office of Basic Energy Sciences
Airlie Conference Center, Warrenton, Virginia
October 25 - 28, 2009

Agenda

Sunday, October 25, 2009

3:00 – 6:00 pm	Arrival and Registration
5:00 – 6:00 pm	Reception (No Host)
6:00 – 7:00 pm	***** Dinner *****
7:00 – 7:40 pm	*Introductory Remarks* **Linda Horton** Director, Division of Materials Science and Engineering **Bonnie Gersten** Program Manager, Synthesis and Processing Science Meeting Chairs: **David Geohegan and Karen Winey** Oak Ridge National Laboratory/University of Pennsylvania
Session Ia	**Topic: Bulk and Nano-materials: Synthesis and Characterization** Chair: **Pavel Zinin**, University of Hawaii
7:40 – 8:10 pm	**Mildred Dresselhaus**, Massachusetts Institute of Technology *Thermoelectric Nanocomposites at Intermediate Temperature Range: Synthesis and Fundamental Studies*
8:10 – 8:40 pm	**Ralph Napolitano**, Ames Laboratory *Nanoscale Dynamics and Nonequilibrium Pathways to Crystallization in Deeply Undercooled Metallic Liquids*
8:40 – 9:10 pm	**Alexandra Navrotsky**, University of California at Davis *Thermochemistry of Anion Deficient and Charge Coupled Substitutions in Fluorite and Perovskite Based Materials*
9:10 – 9:40 pm	**Nigel Browning**, Lawrence Livermore National Laboratory *Observing Fundamental Mechanisms of Transient Dynamics in Materials by Ultrafast In Situ TEM*
9:40 – 10:30 pm	***Interaction and Discussion***

Monday, October 26, 2009

7:00 – 8:00 am	Breakfast
Session IIa	**Topic: The Nanoscale: Assembly** Chair: **Greg Exarhos**, Pacific Northwest National Laboratory
8:00 – 8:30 am	**Salvatore Torquato**, Princeton University *Inverse Optimization Techniques for Targeted Self-Assembly*

8:30 – 9:00 am	**Darrell Velegol**, The Pennsylvania State University *Nanoscale van der Waals Interactions*
9:00 – 9:30 am	**Chekesha Liddell**, Cornell University *Phase Behavior of Colloidal 'Mushroom Caps' under 2D and Quasi-2D Confinement*
9:30 – 10:00 am	**Jun Liu**, Pacific Northwest National Laboratory *Molecularly Organized Nanostructural Materials: From Two-Dimensional Crystallization to Three-Dimensional Self-Assembly*
10:00 – 10:30 am	***** Break *****
Session IIb	**Topic: The Nanoscale: Object Synthesis and Assembly** Chair: **Hanchen Huang**, University of Connecticut
10:30 – 11:00 am	**Stan Wong**, Brookhaven National Laboratory *Synthesis, Characterization, and Investigation of Charge Separation and Recombination in Carbon and Metal Oxide Nanostructures*
11:00 – 11:30 am	**David Geohegan**, Oak Ridge National Laboratory *Non-equilibrium Synthesis of Nanostructured Materials: Laser-Induced Processes*
11:30 am – 12:00 Noon	**Raymond E. Schaak**, The Pennsylvania State University *Low-Temperature Synthesis Routes to Intermetallic Superconductors*
12:00 Noon – 12:30 pm	**Zhili Xiao**, Northern Illinois University *Probing the Interaction between Magnetic Vortices and Periodic Pinning through Patterned Nanoribbons of High-Temperature Superconductors*
12:30 – 1:30 pm	***** Lunch *****
1:30 – 3:30 pm	***Interaction and Discussion***
3:30 - 4:00 pm	**Thomas Lograsso**, Ames Laboratory *Discussion on the National Academies Report on "Frontiers in Crystalline Matter: From Discovery to Technology"*
4:00 – 6:00 pm	***Posters: Session Ib: Bulk and Nano-Materials: New Materials Discovery and IIc: The Nanoscale***
6:00 – 7:00 pm	***** Dinner *****
Session III	**Topic: Synthesis Methods in Plasmonics** Chair: **Zhuomin Zhang**, Georgia Institute of Technology
7:00 – 7:30 pm	**George Chumanov**, Clemson University *Asymmetric Hybrid Nanoparticles*
7:30 – 8:00 pm	**David Norris**, University of Minnesota *Ultrasmooth Patterned Films for Plasmonics and Metamaterials*
8:00 – 8:30 pm	**Roberto Paiella**, Boston University *Plasmonic Dispersion Engineering for Light-Emission Efficiency Enhancement*
8:30 – 10:00 pm	***Interaction and Discussion*** (Cash Bar) Continuation of Poster Session

Tuesday, October 27, 2009

7:00 – 8:00 am	***** Breakfast *****
Session IVa	**Topic: Thin Films: Synthesis of Thin Film Interfaces** Chair: **Ian Fisher**, SLAC National Accelerator Laboratory
8:00 – 8:30 am	**Ivan Bozovic**, Brookhaven National Laboratory *Molecular Beam Epitaxy and Nanostructuring of Perovskite Oxide Materials toward an Understanding of Strongly Correlated Systems*
8:30 – 9:00 am	**Anand Bhattacharya**, Argonne National Laboratory *Digital Synthesis: A Pathway to New Materials at Interfaces of Complex Oxides*
9:00 – 9:30 am	**James Eckstein**, University of Illinois *How Perfect Should Each Digitally Synthesized Molecular Layer Be*?
9:30 – 10:00 am	**Jay Switzer**, Missouri University *Resistance Switching in Electrodeposited Superlattices in the Magnetite/Zinc Ferrite System*
10:00 – 10:30 am	***** Break *****
Session IVb	**Topic: Thin Films: Synthesis of Thin Film Interfaces (continued)** Chair: **Gyula Eres**, Oak Ridge National Laboratory
10:30 – 11:00 am	**Scott Chambers**, Pacific Northwest National Laboratory *Composition at the $LaAlO_3/SrTiO_3$ Interface—Some Surprises*
11:00 – 11:30 am	**Hans Christen**, Oak Ridge National Laboratory *Interfaces in Epitaxial Complex Oxides*
11:30 – 12:00 Noon	**Ramamoorthy Ramesh**, University of California at Berkeley *Science and Technology of Quantum Materials*
12:00 Noon – 12:30 pm	**Reji Thomas,** University of Puerto Rico *MOCVD Grown Ternary Rare-Earth Oxide as an Alternate Gate-Oxide and Buffer Layer for Logic and Memory Devices*
12:30 –1:30 pm	***** Lunch *****
1:30 – 4:00 pm	***Interaction and Discussion***
4:00 – 6:00 pm	***Poster Session: IVc: Thin Films and V: Soft and Hybrid Materials***
6:00 – 7:00 pm	***** Dinner *****
Session VI	**Topic: Energy Frontier Centers and Nanocenters** Chair: **Karen Winey**, University of Pennsylvania
7:00 – 8:00 pm	**Tof Carim,** DOE–Basic Energy Sciences, Program Manager *Discussion of DOE Energy Frontier Research Centers and Nanocenters*
8:00 – 8:30 pm	**Stacey Bent**, Stanford University *DOE Energy Frontier Research Center on Nanostructuring for Efficient Energy Conversion*
8:30 – 9:00 pm	**Peter Green**, University of Michigan *Center for Solar and Thermal Energy Conversion in Complex Materials*
9:00 –10:00 pm	***Interaction and Discussion*** (Cash Bar) Continuation of Poster Session

Wednesday, October 28, 2009

7:00 – 8:00 am	***** Breakfast *****
Session IVd	**Topic: Thin Films: Fabricating Nanostructure from Films: Synthesis and Processing** Chair: **Francisco Zaera**, University of California-Riverside
8:00 – 8:30 am	**Maria Tamargo**, The City College of New York *Synthesis of Submonolayer Type-II Quantum Dots to Enhance Materials Properties of Wide Bandgap Semiconductors*
8:30 – 9:00 am	**Max Lagally**, University of Wisconsin-Madison *Group IV Semiconductor Nanomembranes: New Properties through Novel Synthesis and Strain Engineering*
9:00 – 9:30 am	**Feng Liu**, University of Utah *Strain Superlattice: A Combination of Strain-Induced Self-Assembly and Strain-Engineered Band Structure*
9:30 – 10:00 am	***** Break *****
Session IVe	**Topic: Thin Films: Fabricating Nanostructure from Films: Synthesis and Processing (continued)** Chair: **David Geohegan**, Oak Ridge National Laboratory
10:00 – 10:30 am	**Michael L. Simpson**, Oak Ridge National Laboratory *Design and Synthesis of Nanomaterials*
10:30 – 11:00 am	**Michael J. Aziz**, Harvard University *Nanoscale Morphology Evolution Under Ion Irradiation*
11:00 – 11:30 am	**Eric Chason**, Brown University *Mechanisms of Sputter Ripple Formation: Coupling among Energetic Ions, Surface Kinetics, Stress and Composition*
11:30 – 12:00 Noon	*Closing Remarks* **Karen Winey** and **David Geohegan**, Meeting Chairs **Bonnie Gersten**, Program Manager, Synthesis and Processing
12:00 Noon	***** Lunch and Adjourn ***** (Optional box lunches available)

POSTER LIST

Poster Session Ib: Bulk and Nano-Materials: New Materials Discovery

University Grants:

1. Solution-Based Doping in Metal Oxides and Sulfides
   Meng Tao and Q. M. Zhang, University of Texas at Arlington

2. Synthesis of New Diamond-Like B-C Phases under High Pressure and Temperatures
   Pavel Zinin, L.-C. Ming, and S. Sharma, University of Hawaii

3. Molecular Hydrogen Storage in Novel Binary Clathrate Hydrates at Near-Ambient Temperatures and Pressures
   E. D. Sloan and **Carolyn A. Koh**, Colorado School of Mines

4. A Fundamental Study of Inorganic Clathrates and "Open-Framework" Materials
   George S. Nolas, University of South Florida

5. Computational Investigations of Solid-Liquid Interfaces
   Mark Asta, University of California at Davis

6. Atomistic Structure, Strength, and Kinetic Properties of Intergranular Films in Ceramics
   Stephen Garofalini, Rutgers University, presented by G. Lockwood

7. Three-Dimensional Evolution of Dendritic Mixtures
   C. Park*, L. Aegeson, A. Johnson, **Katsuyo Thornton***, and P. Voorhees,
   Northwestern University and *University of Michigan

Laboratory Grants:

8. The Dynamics of Structural Ordering in Metallic Liquids and Transitions to Amorphous and Crystallization Solids
   Kai-Ming Ho, S. H. Zhou, R. T. Ott, R. Trivedi, X. Song, E. Kalay, M. J. Kramer, M. I. Mendelev, S. G. Hao, C. Z. Wang, and R. E. Napolitano
   Ames Laboratory and Iowa State University

9. Fundamental Crystal-Melt Interface Behavior
   Mikhail. I. Mendelev, J. Monk, R. E. Napolitano, M. J. Kramer, and R. T. Ott,
   Ames Laboratory

10. The Atomic Structure of the Deeply Undercooled Metallic Liquid: Challenges to Experiments and Simulations
    Matthew J. Kramer, M. I. Mendelev, S. G. Hao, K. M. Ho, R. T. Ott, C. Z. Wang, and R. E. Napolitano, Ames Laboratory and Iowa State University

11. Novel Materials Preparation and Processing Methodologies II: In Situ High Energy X-ray Synchrotron Diffraction Study of the Synthesis and Stoichiometry of LaFeAsO and $LaFeAsO_{1-x}F_y$
    R. William McCallum, T. A. Lograsso, L. L. Jones, P. C. Canfield, and I. E. Anderson, Ames Laboratory

12. Microstructural Development and Synthesis of $ErRh_4B_4$ Single Crystals
    Thomas A. Lograsso, R. W. McCallum, L. L. Jones, P. C. Canfield, and I. E. Anderson, Ames Laboratory

13. Materials Preparation Center
    Larry L. Jones, T. A. Lograsso, R. W. McCallum, P. C. Canfield, and I. E. Anderson, Ames Laboratory

14. Correlated Materials – Synthesis and Physical Properties
    Ian Fisher, T. Geballe, A. Kapitulnik, S. Kivelson, and K. Moler, SLAC National Accelerator Laboratory

15. Exploratory Materials Synthesis and Characterization
    Cedomir Petrovic and R. Hu, Brookhaven National Laboratory

Poster Session IIc: The Nanoscale

University Grants:

16. Control of New Kinetic Barriers and Design of Nanorods
    L. G. Zhou, S. K. Xiang, C. G. Johansen, and **Hanchen Huang**, University of Connecticut

17. In Quest for Boron Nanostructures and Fullerenes: Key Issues of Stability and Synthetic Routes
    Boris Yakobson and Pulickel Ajayan, Rice University

18. Molecular Dynamics Simulation of Colloidal Nanoparticle Forces and Assembly
    Kristen A. Fichthorn, The Pennsylvania State University:

Laboratory Grants:

19. Hydrothermal Reaction Selectivity for Hierarchical Molecular Assembly
    Yoongsoon Shin, Jun Liu, and **Greg Exarhos**, Pacific Northwest National Laboratory

20. Non-equilibrium Synthesis of Nanostructured Materials: Real-Time Studies of Growth Kinetics
Gyula Eres, D. B. Geohegan, A. A. Puretzky, C. M. Rouleau, M. Yoon, and Z. Zhang, Oak Ridge National Laboratory

21. In Situ Studies of Solid Electrolyte Interphase on Nanostructured Materials
Chengdu Liang, N. Dudney, K. More, R. W. Shaw, J. Ankner, and K. An, Oak Ridge National Laboratory

Poster Session IVc: Thin Films

University Grants:

22. Demonstration of Coherent Thermal Emission in Multilayer Structures
Zhuomin Zhang, Georgia Institute of Technology

23. In Situ Visualization and Theoretical Modeling of Early-Stage Oxidation of Metal and Alloys
Guangwen Zhou and Xidong Chen*, State University of New York at Binghamton and Cedarville University*

24. Atomic Layer Deposition (ALD) of Metal and Metal Oxide Films: A Surface Science Study
Francisco Zaera, University of California at Riverside

25. Science of Heteroepitaxy for Energy-Efficient Lighting
Jung Han, Yale University

Laboratory Grants:

26. Growth and In Situ Characterization of Novel Thin Films Using Angle-Resolved Photoemission Spectroscopy
R. G. Moore and Z-X. Shen, SLAC National Accelerator Laboratory and Stanford

27. Creating a New Class of Materials: Multidimensional Multilayer Films
Paul B. Mirkarimi, Lawrence Livermore National Laboratory

28. Intrinsic and Laser-Irradiation–Induced Properties of Doped ZnO Films
S. A. Chambers[1], T. C. Droubay[1], T. C. Kaspar[1], J. McCloy[1], J. Ryan[1], C. M. Wang[1], V. Shutthanandan[1], L. Wang[2], G.E. Exarhos[1], D. R. Gamelin[3], C. R. Johnson[3], K. M. Whittaker[3], S. M. Heald[4], D. E. Keavney[4], A. Ney[5], T. Kammermeier[5], K. Ollefs[5], S. Ye[5], V. Ney[5], F. Wilhelm[6], and A. Rogalev[6];
[1]Pacific Northwest National Laboratory, [2]Carleton College, [3]University of Washington, [4]Argonne National Laboratory, [5]Universität Duisburg-Essen, [6]European Synchrotron Radiation Facility

29. The Atomic and Electronic Structure of Oxide Superlattices
Amish Shah, Anand Bhattacharya*, and **Jian -Min Zuo**, University of Illinois and Argonne National Laboratory*

30. The Oxide MBE Program at the Center for Nanoscale Materials at Argonne
Anand Bhattacharya, Argonne National Laboratory

31. Multifunctional Nanostructure for Magnetoelectric and Spintronics Applications
R. S. Katiyar, M. Gomez, G. Morell, L. Fonseca, W. Otano^, O. Perales+, M. S. Tomar+, Y. Ishikawa, R. Palai, **Reji Thomas**, A. Kumar, V. Makrov ,
University of Puerto Rico, Rio Piedras, Mayaguez+, Cayey^

Poster Session V: Soft and Hybrid Materials

University Grants:

32. Conduction Mechanisms and Structure of Ionomeric Single-Ion Conductors, Part 1: Structure
Ralph Colby, Janna K. Maranas, Karl T. Mueller, James Runt, and **Karen I. Winey***, The Pennsylvania State University and University of Pennsylvania*

33. Conduction Mechanisms and Structure of Ionomeric Single-Ion Conductors, Part 2: Dynamics
Ralph Colby, Janna K. Maranas, Karl T. Mueller, James Runt, and Karen I. Winey*, The Pennsylvania State University and University of Pennsylvania*

34. Nanoparticles Stabilize Thin Polymer Films: A Fundamental Study to Understand the Phenomenon
Michael Mackay, T-C. Tseng, V. Padmanabhan, and A. Frischknecht*
University of Delaware and Sandia National Laboratories

35. Diblock Copolymers under Nano-Confinement
Qiang (David) Wang and D. S. Dandy, Colorado State University

36. AC Electrohydrodynamic Instabilities in Thin Liquid Films: A Route to Hydrodynamic Self-Assembly of Topographical Patterns on Soft Materials
S. A. Roberts and **Satish Kumar**, University of Minnesota

37. Large Electrocaloric Effect near Room Temperature in P(VDF-TrFE) Based Ferroelectric Polymers
Qiming Zhang, The Pennsylvania State University

38. Thin Film Polymer Nanoparticle Composites: Morphology and Dynamics
Peter F. Green, University of Michigan

Session Ia

Bulk and Nano-materials – Synthesis and Characterization

Session Chair: Pavel Zinin, University of Hawaii

(This page intentionally left blank.)

Thermoelectric Nanocomposites at Intermediate Temperature Range: Synthesis and Fundamental Studies

M. S. Dresselhaus and G. Chen
millie@mgm.mit.edu and gchen2@mit.edu
Massachusetts Institute of Technology
Cambridge, MA 02139

Z. F. Ren
renzh@bc.edu
Department of Physics
Boston College, Chestnut Hill, MA 02467

Program Scope

With their ability to convert heat directly into electricity, thermoelectrics show great promise for a wide range of applications, from waste heat scavenging to topping cycles for more traditional heat engines. Unlike a heat engine, thermoelectric devices have no moving parts, and can easily be scaled down for small-scale applications. Thermoelectrics can also be used in cooling applications, and are especially effective when traditional working-fluid cooling cycles are not practical. Due to their present low efficiency, the demand for thermoelectrics has remained low for several decades, mainly limited to niche applications, such as deep-space power sources (radioisotope thermal generators) and miniature refrigerators. However, new scientific and technological advances are creating opportunities for a new generation of thermoelectric devices that seem promising for many potential applications. The goal of this project is to use modeling, measurement, and materials synthesis in an effort to better understand thermoelectric phenomena and to create bulk thermoelectric materials operating in the intermediate temperature range that are appropriate for low concentration solar thermal conversion of sun light into electricity.

Recent Progress

Our grant proposal focused on four topics: (1) nanocomposite synthesis and interface control; (2) transport property characterization and scattering mechanism studies; (3) phonon transport modeling; and (4) electron transport modeling. In addition, we perform structural characterization and thermoelectric property measurements on various samples to test the progress being made in the four topics listed above. Below we summarize our progress after one year of work on this grant, with an emphasis given to what has been accomplished in the last four months since our last progress report.

Nanocomposite Synthesis and Interface Control

During the past year we have had success in synthesizing advanced thermoelectric materials including $MnSi_{2-x}$, Si and Si containing a few percent Ge, and PbTe, but the focus was on PbTe.

A promising intermediate-temperature thermoelectric material is the silicide $MnSi_{2-x}$; besides good performance, the material is attractive because its constituent elements are nontoxic, plentiful, and relatively cheap. We have been successful in ball milling and hot pressing samples

of this bulk material to make a bulk nanocomposite material of multi-millimeter size with fairly good thermoelectric properties.

PbTe is the most studied thermoelectric material in the intermediate temperature range. Doping PbTe with 2% thallium has been shown[R1] to improve the power factor ($S^2\sigma$) and thermoelectric figure of merit (ZT) of PbTe. To build on these results, we are preparing PbTe doped with 2% thallium by a ball-milling and hot-pressing technique in order to reduce the thermal conductivity and further increase ZT. To date we have achieved a similar power factor improvement, but significant grain growth has prevented us from reducing the thermal conductivity.

Transport Property Characterization and Scattering Mechanism Studies

Impedance spectroscopy measurements are being undertaken to obtain the energy barrier height at the grain interfaces of our nanostructured samples. This barrier height is an important input parameter for modeling the charge carrier transport inside our nanocomposites. The AC impedance measurement challenge is that the self-inductance will overshadow the capacitance signal at high frequencies, which is indicated by the sign change in the imaginary part of the measured impedance. The transition frequency is typically 1 kHz without any shielding. However, theoretical modeling suggests that we normally need to reach 10 kHz to obtain a steady state capacitance because at lower frequencies the grain boundary band bending will result in a dramatically increased boundary capacitance. During the last year, we focused on using a copper holder to shield the electromagnetic field around the sample and in this way to eliminate its self-inductance. For one PbTe sample with a dopant level of $\sim 1\times10^{17}$ cm^{-3}, the transition frequency was 95 kHz and we obtained a reasonably good fit for the frequency-dependent grain boundary capacitance. The fitting suggested a reasonable 0.3 eV energy barrier height for the grain boundary. We continue to work on improving the reliability of these measurements.

To further overcome the measurement issue in bulk samples, we developed a technique to measure the AC impedance of micron-sized samples and we demonstrated this measurement technique on a PbTe sample with micron-sized grains. A simple analysis of these data agreed reasonably well with the frequency-dependent capacitance extracted from the measurement data for the middle segment of the sample (which was a 3D network of grains). We are currently improving our sample preparation techniques in order to measure the impedance across a single grain.

We have also developed an optical characterization technique for understanding the band structure of thermoelectric materials. It is difficult to measure optical properties of thermoelectric materials, such as the absorption coefficient, due to the strong optical absorption of thermoelectric materials. We have developed a technique that can be used to measure the absorption of small bandgap, heavily absorbing materials. We are currently developing analytical tools to understand the optical spectra, and from such spectral results to deduce information about the electronic structure of thermoelectric materials of interest.

Phonon and Electron Transport Modeling

We have constructed models of grain boundary scattering for both electrons and phonons in nanocomposite materials and we have used the resulting scattering rates to calculate the thermoelectric properties of our nanomaterials. We find that the models are able to explain the experimental data, thereby helping us to understand transport in these complex materials and to design new strategies to improve the figure of merit. Recently, we used the Boltzmann transport equation under the relaxation time approximation to calculate the thermoelectric properties of n-type and p-type SiGe nanocomposites[P7]. We account for the strong grain boundary scattering mechanism in nanocomposites using phonon and electron grain boundary scattering models. The results from this analysis are in excellent agreement with recently reported measurements for our n-type nanocomposite materials, but the experimental Seebeck coefficient for the p-type nanocomposite is approximately 25% higher than the model's prediction. The reason for this discrepancy is not clear at the present time and warrants further investigation. Using new mobility measurements and our model, we find that dopant precipitation is an important process in both n-type and p-type nanocomposites, in contrast to bulk SiGe, where dopant precipitation is found to be most significant only in n-type materials. The model also shows that the potential barrier at the grain boundary required to explain the data is several times larger than the value estimated using the Poisson equation, indicating the presence of crystal defects in the material. This suggests that an increase in mobility is possible by reducing the number of defects or reducing the number of trapping states at the grain boundaries. We have also applied the model to skutterudite systems. The key issue we encounter is the uncertainties in the calculated band structures, which prompted us to investigate the use of optical spectroscopy data, combined with first principles calculations, to make predictions about the band structures of thermoelectric materials with many grain boundaries.

We are also developing Kinetic Monte Carlo simulation approaches based on both experimental data and parameters obtained with density functional theory in the gradient-generalized approximation. The simulations involve realistic diffusion mechanisms by vacancy jumps, and point defect sources which drive the vacancy concentration towards its equilibrium value during isothermal heat treatments. The goal of the simulation is to provide understanding of electronic structures at the grain boundary, which is critical for modelling thermoelectric transport.

Future Plans

We intend to continue producing thermoelectric materials using our ball-mill, hot-press technique. We will develop better measurement techniques so that we can quantify our advances made in materials property performance. Through modeling and fundamental physics experiments, we will gain better insight into the physics behind these materials property gains.

Future work includes development of both the electron model, and a combination of the electron and phonon model to develop a consistent interpretation of the ingot and nanocomposite thermoelectric properties, and the characterization of a smaller grain size nanocomposite material with improved thermoelectric properties. For materials synthesis, we will focus on the addition of Tl in the PbTe system. The goal is to prevent the grain growth so that bulk materials with grain size smaller than 100 nm, having precipitates of about 1-20 nm size, embedded inside the grains and along the grain boundaries can be prepared. It is hoped that in this way thermal conductivity values below 1.5 $W \cdot m^{-1} \cdot K^{-1}$ at room temperature and 0.8 $W \cdot m^{-1} \cdot K^{-1}$ below 500 °C

can be achieved. If such a low thermal conductivity value can be achieved, then a ZT above 2 at 500 °C should be within reach. Kinetic Monte Carlo and Density Functional Theory modeling research will include studying the effect of the vacancy concentration on the electronic conductivity and on the Seebeck coefficient for materials systems of interest.

References

R1. Joseph P. Heremans, Vladimir Jovovic, Eric S. Toberer, Ali Saramat, Ken Kurosaki, Anek Charoenphakdee, Shinsuke Yamanaka, G. Jeffrey Snyder, "Enhancement of Thermoelectric Efficiency in PbTe by Distortion of the Electronic Density of States", *Science* **321**, 554 – 557 (2008).

DOE Sponsored Publications 2008-2009

P1. J. Yang, Q. Hao, H. Wang, Y. C. Lan, Q. Y. He, A. J. Minnich, D. Z. Wang, J. A. Harriman, V. M. Varki, M. S. Dresselhaus, G. Chen, and Z. F. Ren, "Solubility Study of Yb in n-type Skutterudites $Yb_xCo_4Sb_{12}$ and Their Enhanced Thermoelectric Properties", *Phys. Rev B* (in press).

P2. Y. C. Lan, A. J. Minnich, G. Chen, and Z. F. Ren, "Enhancement of Thermoelectric Figure-of-Merit by A Nanostructure Approach", *Advanced Functional Materials*, (submitted).

P3. A. Muto, D. Kraemer, Q. Hao, Z. F. Ren, and G. Chen, "Thermoelectric Properties and Efficiency Measurements under Large Temperature Differences", *Rev. Sci. Instrum.* **80**, 093901 (2009).

P4. G. H. Zhu, H. Lee, Y. C. Lan, X. W. Wang, G. Joshi, D. Z. Wang, J. Yang, D. Vashaee, H. Guilbert, A. Pillitteri, M. S. Dresselhaus, G. Chen, Z. F. Ren, "Increased Phonon Scattering by Nanograins and Point Defects in Nanostructured Silicon with a Low Concentration of Germanium", *Phys. Rev. Lett*. **102**, 196803 (2009).

P5. A. J. Minnich, M. S. Dresselhaus, Z. F. Ren, and G. Chen, "Bulk Nanostructured Thermoelectric Materials: Current Research and Future Prospects", *Energy & Enrironmental Science* **2**, 466 – 479 (2009), published online on Feb 27, 2009.

P6. Y. C. Lan, B. Poudel, Y. Ma, D. Z. Wang, M. S. Dresselhaus, G. Chen, and Z. F. Ren, "Structure Study of Bulk Nanograined Thermoelectric Bismuth Antimony Telluride" *NanoLetters* **9**, 1419 – 1422 (2009), published online on Feb 25, 2009.

P7. A. J. Minnich, H. Lee, X. W. Wang, G. Joshi, M. S. Dresselhaus, Z. F. Ren, G. Chen, and D. Vashaee. "Modeling study of nanocomposite SiGe alloys." Submitted to *Physical Review B*.

Nanoscale dynamics and nonequilibrium pathways to crystallization in deeply undercooled metallic liquids

K.M. Ho,[*] S. H. Zhou[*], R.T. Ott, R. Trivedi[*#], X. Song[*], E. Kalay, M. J. Kramer,[*#]
M.I. Mendelev,[*] S.G. Hao,[*] C.Z. Wang[*] and R. E. Napolitano[*#]
kmh@ameslab.gov
[*]Materials Science and Engineering Division, Ames Labs DOE
[#]Department of Materials Science and Engineering, Iowa State University

Program Scope

The challenge of achieving new materials with remarkable properties requires controlling structural dynamics at multiple length scales. This challenge is most profound at the nanoscale, where the fundamental link between atomistic interactions and short-/medium-range order must be understood. In this research effort, we investigate these critical connections and focus on the nonequilibrium pathways to nanostructured materials associated with deeply undercooled metallic liquids. Indeed, one of the five Grand Challenges recently put forth by the Basic Energy Sciences Advisory Committee[1] poses the question: "*How do we characterize and control matter away - especially far away - from equilibrium?* An emerging area of materials discovery that highlights the importance of this question is the utilization of amorphous phases as integral components in nonequilibrium pathways to new materials. Moreover, we note that glass-forming metallic systems give rise to distinctly nonequilibrium phases and structural dynamics that offer an immense opportunity for the realization and control of these materials[2,3]. Impeding such progress, however, is our limited ability to classify, characterize, and quantify the various elements of noncrystalline order which are central to structural dynamics and phase transition involving undercooled metallic liquids. As a means to facilitate the effective navigation of the energetic and dynamical landscapes that govern phase transformations and multiscale structural evolution under these far-from-equilibrium conditions, this project is focused specifically on understanding and quantifying the structural and chemical ordering dynamics in highly undercooled metallic liquids and their role in the competition between crystalline and amorphous solids. Critical challenges here include (i) the characterization of the key components of noncrystalline order in liquids and glasses, (ii) overcoming the challenges of disparate time scales in understanding and predicting the structural dynamics in amorphous phases, (iii) quantifying the energetics and kinetics associated with crystallization reactions and other phase transitions under far-from-equilibrium conditions involving glasses or undercooled liquids, and (iv) reconciling theoretical modeling and experimental measurements in terms of thermodynamic models for the relative stability of nonequilibrium phases. Here, we present recent computational and experimental results and discuss critical future directions with regard to these issues.

Recent Progress

We have developed a robust scheme based on cluster description of structures using Voronoi tessellation method for investigating the atomic packing and arrangement in metallic liquids and glasses. Along with the cluster population, the spatial and time correlations as well as the chemistry among various clusters have been investigated. From our analysis of RMC and EAM models for Zr-Cu glass systems, we find that the glass structure consists of a heterogeneous mixture of interpenetrating 13-atom icosahedral clusters connected in a string-like fashion forming a solid-like backbone network within a liquid-like matrix. It is interesting that a precursor of the development of the icosahedral network in the glass system can already be

observed in metallic liquid system at relatively small undercooling much above the glass transition temperature. Using *ab-initio* MD simulations, we observed that icosahedral clusters with an index of <0,0,12,0> have a strong tendency to aggregate in the supercooled metallic liquid although their population is not abundant enough to form a well-connected network. The material surrounding these icosahedral clusters exhibit slow dynamics compared with the rest of the system, and this "slowing down" becomes more pronounced in the presence of icosahedral aggregation. Based on these observations, we proposed a positive-feedback mechanism in which the aggregation of icosahedral clusters into a percolating network is responsible for slowing down the dynamics of the whole system, eventually locking the system into a heterogeneous glass structure with rapid cooling. We are examining the generality of this behavior for other alloy systems. Very recently, we have also developed a real space alignment method which can identify the orders in metallic liquid and glass that go beyond the first shell of the cluster and allow us to exam the medium range order in the system. As shown Fig.1, our analysis reveals that, as $Cu_{64.5}Zr_{35.5}$ is cooled from the liquid state, icosahedal order centered at Cu atoms is developed and extends to the third shell in the glass state.

To understand the dynamics of the structural transitions that occur on cooling the liquid, we employ MD simulations and rapid cooling (e.g. melt-spinning) experiments. However, the constraints of these methods do not permit direct comparison. In particular, MD methods can access cooling rates greater than ~10^9 K/s, while experimental methods of rapid cooling are limited to rates up to 10^6 K/s. Accordingly, the use of atomistic modelling to investigate the slow dynamics of deeply undercooled liquids and glasses has been a fundamental and longstanding problem. Addressing this problem, we have employed a theoretical two-state continuum approach to model the development of local order in a glass-forming alloy during cooling and to investigate the effect of cooling rates at time scales that span the range between experiments and atomistic simulations. In this analytical model, evolution of the icosahedral fraction in the system depends on the temperature-dependence of free energy of the icosahedral and non-icosahedral "states" and the activation barriers between them. The model also includes a packing efficiency term that accounts for the morphology of the icosahedral aggregation. To date, we have parameterized the model only in an empirical manner, but the results suggest that the approach is capturing the essential physics of the structural dynamics. Fig.2 shows the model results for the development of icosahedral fraction upon cooling at different rates. Also shown are the MD results for various cooling rates. The presence of the low-temperature plateau that increases in icosahedral fraction with decreasing cooling rate and then remains constant for cooling rates below ~10^8 K/s suggests that there may be an important intermediate time scale associated with the icosahedral aggregation dynamics. The relevance of this intermediate time (i.e. fast enough cooling to avoid crystallization but slow enough to permit medium-range ordering through aggregation mechanisms) may be that it serves to clearly distinguish between an unstable "liquid-like" quenched glass that might result from ultra-fast cooling and a true metastable glassy state that exhibits its own characteristic structural features.

In conjunction with the atomistic and analytical modelling of the liquid/glass dynamics, we have investigated crystallization dynamics in CuZr using in situ high energy X-ray diffraction (HEXRD), differential scanning calorimetry (DSC), and transmission electron microscopy (TEM). Using both continuous heating and isothermal treatments, we have quantified the crystallization kinetics and have identified several critical aspects of phase selection for the observed transformations. For example, Fig. 3 shows TEM micrographs of the structure at two stages of the crystallization transformation, where a transient metastable phase serves to stimulate growth of the metastable CuZr(B2) phase. This study has clearly revealed that the

thermal history is very important with regard to the phase sequence observed and the competition between various metastable phases and that quantifying the relative energetics of the competing metastable phases and the undercooled liquid is essential to predicting structural dynamics. Accordingly, we have undertaken a comprehensive effort to model the thermodynamics of the CuZr system, and have revealed several important features of the Cu-Zr phase diagram. Moreover, our modelling effort has enabled quantification of the energetics that drive the observed transitions. For example, Fig. 4 shows the Gibbs free energy (relative to the liquid phase) for the various competing stable and metastable phases, as a function of temperature. These models are required for analysis of experimental observation and for modelling transformation dynamics at the continuum level.

Future Plans

Based on our ongoing investigation of new methods to characterize and quantify short- and medium-range ordering in amorphous phases, we will continue to develop thermodynamic and kinetic models to describe the dynamics of structural evolution. These modeling efforts will include atomistic simulations, cluster-level simulations, and continuum-scale simulations. Experimentally, we will use a variety of methods (e.g. melt-spinning, magnetic-levitation-splat-cooling, electrostatic-levitation-free cooling, injection-wedge-casting) to control extreme thermal pathways and, in some cases, use alloying additions (e.g. Ni, Al), to enhance experimental access to deeply undercooled regime from both high and low temperatures. Model predictions will be compared with experimental measurements and observed structures toward the objective of new theoretical descriptions of liquid/glass dynamics and structural evolution.

References

1 Hemminger, J. & (Chair). Vol. http://www.sc.doe.gov/bes/reports/files/GC_rpt.pdf (ed D. o. Energy) (DOE, 2008).

2 Kelton, K. F. *Intermetallics* **14**, 966, (2006).

3 Inoue, A. *et al. Materials Science and Engineering a-Structural Materials Properties Microstructure and Processing* **441**, 18, (2006).

Publications supported by the DOE project over the last two years

1. Hao, S. G. *et al.* Experimental and ab initio structural studies of liquid Zr_2Ni. *Phys. Rev. B* **79**, 104206 (2009).
2. Mendelev, M. I., *et al.* Analysis of semi-empirical interatomic potentials appropriate for simulation of crystalline and liquid Al and Cu. *Phil. Mag.* **88**, 1723 (2008).
3. Mendelev, *et al.* Molecular dynamics simulation of diffusion in supercooled Cu-Zr alloys. *Phil. Mag.* **89**, 109 (2009).
4. Mendelev, M. I. *et al.* Development of suitable interatomic potentials for simulation of liquid and amorphous Cu-Zr alloys. *Phil. Mag.* **89**, 967 (2009).
5. Ott, R. T. *et al.* Anelastic strain and structural anisotropy in homogeneously deformed Cu64.5Zr35.5 metallic glass. *Acta Materialia* **56**, 5575 (2008).
6. Wang, S. Y. *et al.* Short- and medium-range order in a $Zr_{73}Pt_{27}$ glass: Experimental and simulation studies. *Phys. Rev. B* **78**, 184204 (2008).
7. Wang, S. Y. *et al.* Experimental and ab initio molecular dynamics simulation studies of liquid $Al_{60}Cu_{40}$ alloy. *Phys. Rev. B* **79,** 144205 (2009).

8. S. H. Zhou and R. E. Napolitano, Energetics of nonequilibrium solidification in Al-Sm, *Phys. Rev. B* 78 (2008) 184111.
9. S. H. Zhou and R. E. Napolitano, "Identification of the B33 martensite phase in Cu-Zr using first-principles and X-ray diffraction", *Scripta Materialia* **59** (2008) 1143-1146.
10. S.H. Zhou and R.E. Napolitano, "Modeling of thermodynamic properties and phase equilibria for the Al-Sm binary system", *Met .Mat. Trans. A* **39** (2008) 502-512.

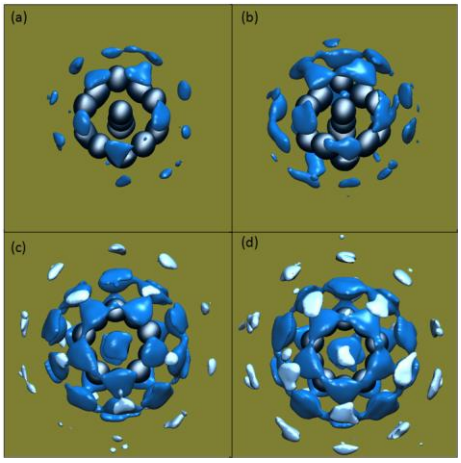

Fig.1. Our recently developed real-space alignment analysis showing the development of short- and medium- range (2nd and 3rd shell) order with decreasing temperature. (a) 1500 K, (b) 1100 K, (c) 700 K and (d) 300 K.

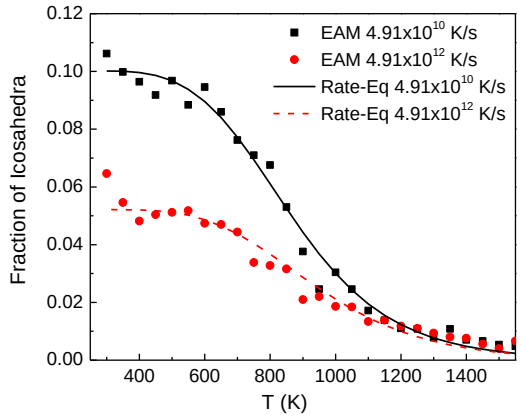

Fig.2. Analytical prediction of icosahedral fraction during cooling at two rates, compared with EAM-MD results.

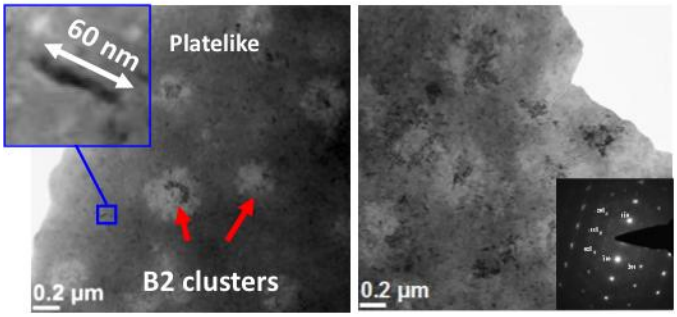

Fig.3 (above) Bright field TEM images showing a transient plate-like phase that stimulates the growth of the CuZr(B2) phase below its range of stability. (left) at peak transition rate, (right) near completion of crystallization.

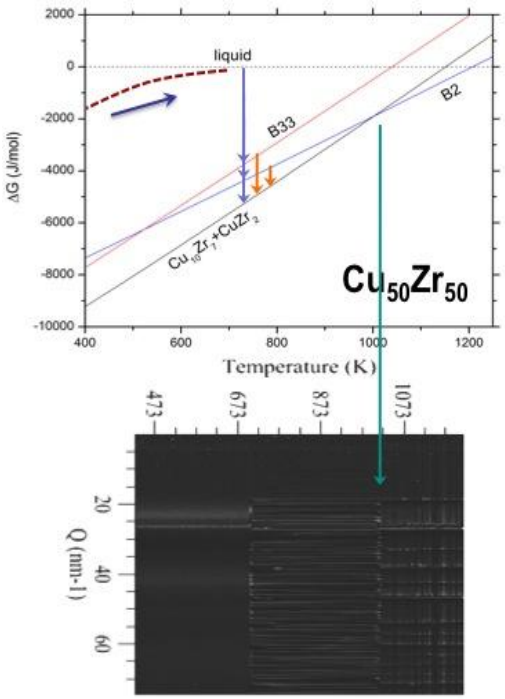

Fig.4 (right) Thermodynamic model predictions of the Gibbs free energy for the $Cu_{50}Zr_{50}$ composition, compared with the in situ HEXRD data indicating the phase transitions observed on heating from the glass. Note the large driving force for stable and metastable crystalline phases.

Thermochemistry of Anion Deficient and Charge Coupled Substitutions in Fluorite and Perovskite based Materials

Alexandra Navrotsky
University of California at Davis

Oxides having the fluorite structure offer a richness of defect chemistry, closely linked to their applications as solid electrolytes, gas separation membranes, and catalysts. Substituting the tetravalent ion, typically Zr, Hf, or Ce, by trivalent ions, typically yttrium and the rare earths, preserves the cubic fluorite structure to ambient conditions and produces materials with high oxygen mobility. Despite extensive studies of ionic conductivity, diffusion, and defect association by experiment and computation, there has been little work till recently on the direct experimental determination of enthalpies of formation. The extreme refractory nature of these oxides has been a stumbling block to calorimetry, but recent advances in oxide melt solution calorimetry using our custom built Calvet microcalorimeters at 700-800 ^{o}C makes it possible to make such measurements. Here I summarize our findings for ZrO_2-, HfO_2-, CeO_2- and UO_2-based systems doped with oxides of the lanthanides and yttrium, $REO_{1.5}$. I also discuss recent developments in measuring the surface and interfacial energies of YSZ and related materials, thus linking bulk, surface, interface, and nanoscale behavior.

The rare earth doped zirconia and hafnia systems all show similar behaviour, namely a strongly curved enthalpy of drop solution which implies strongly negative heats of mixing (Simoncic and Navrotsky 2007) (Fig. 1). By simultaneously fitting calorimetric data for a number of Zr and Hf systems, they obtained good constraints on the transformation enthalpies of ZrO_2 and HfO_2 from monoclinic to cubic fluorite structure and of each of the rare earth oxides from its parent structure (mostly C-type rare earth oxide, bixbyite) to disordered fluorite.

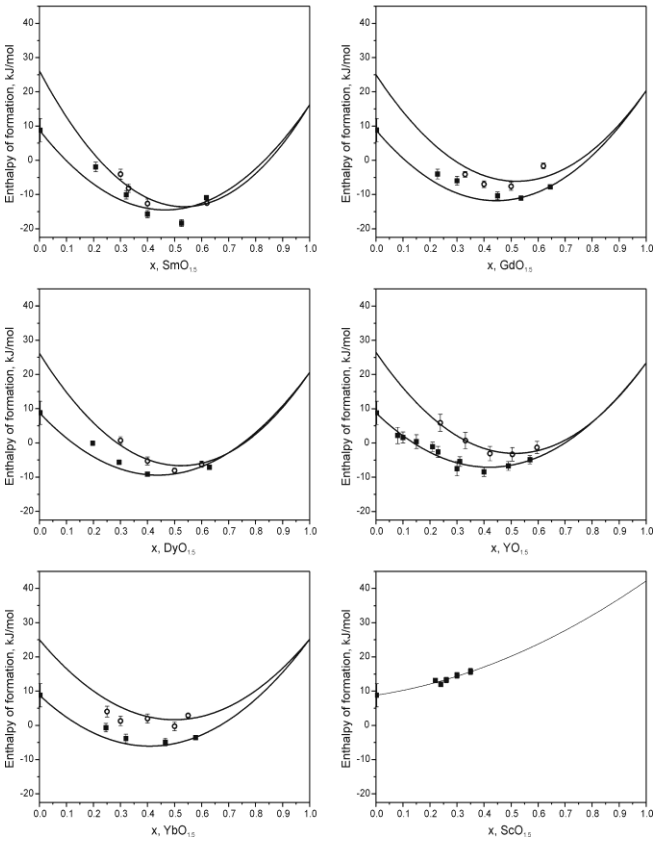

Fig. 1 *Enthalpies of formation of RE-doped zirconia and hafnia solid solutions (Simoncic and Navrotsky 2007)* The upper curves are for hafnia, lower for zirconia.

Formation enthalpies from binary oxides become less exothermic with decreasing dopant radius and enthalpies of phase transition from the C-type rare earth structure to fluorite also depend linearly on ionic

radius. The enthalpy of transformation of HfO_2 from monoclinic to fluorite structure is significantly larger than that of ZrO_2. In all these cases, the trivalent dopant is larger than the tetravalent host, Zr or Hf. Thus the size difference between RE and Hf diminishes as the dopant radius decreases, implying less strain from size mismatch of the cations, and a smaller endothermic contribution to the enthalpy of mixing. Yet the interaction parameter becomes more endothermic; thus the above effect does not appear to dominate the energetics. Rather, the dominant effect may be the competition of Hf and RE for vacancy location, that is, the difference in binding energy for a nearest neighbor versus a next nearest neighbour cluster. The trend in interaction parameters suggests that clusters with the vacancy located next nearest neighbor to the dopant (and nearest neighbor to Zr or Hf) are more stable with increasing dopant radius (decreasing ionic potential). In other words, the transfer of the vacancy from a REO_7 to a ZrO_7 or HfO_7 configuration becomes more energetically favorable as the RE radius increases. This is in accord with the calculations of Khan et al. (1998), who show that the difference in binding energies between nearest neighbor and next neatest neighbor dopant-vacancy clusters increases (favoring the latter) in the order Y(0.44 eV), Gd (0.50 eV), Nd (0.56 eV), La (0.60 eV) in stabilized zirconia.

In contrast, the ceria-based systems show slightly positive heats of mixing (Chen et al. 2006, Chen and Navrotsky 2007, Lee et al. 2008). This suggests that the ceria is acting as a diluent in all cases, and the vacancies remain predominantly nearest neighbor to the trivalent dopant, consistent with theoretical predictions. There is no tendency for Ce^{4+} to associate with a vacancy and become 7-coordinate. The most positive heats of formation occur near the Ce–rich end of the series.

The CeO_2 – ZrO_2 system (Lee et al. 2008) shows endothermic enthalpy of formation from oxides for composition in the range studied (up to 45 % Zr substitution),. Since no significant vacancy concentrations are created, one would expect no stabilization from ordering but a destabilization from size mismatch and a term arising from the enthalpy difference between cubic and monoclinic zirconia. Constraining the enthalpies at both ends (zero at x = 0 and 8.8 at x = 1), and fitting the heat of formation data gives a large positive interaction parameter, consistent with the large size difference between Zr and Ce.

These systematic trends enable us to predict that the system UO_2-$REO_{1.5}$, when it is constrained to have little oxidized uranium in oxidation state higher that 4^+ should behave similarly to doped ceria, with small positive heats of mixing, since the oxygen vacancies would be expected to remain near the trivalent dopant. This has indeed been borne out by a calorimetric study on yttria and calcia doped urania Mazeina et al 2007).

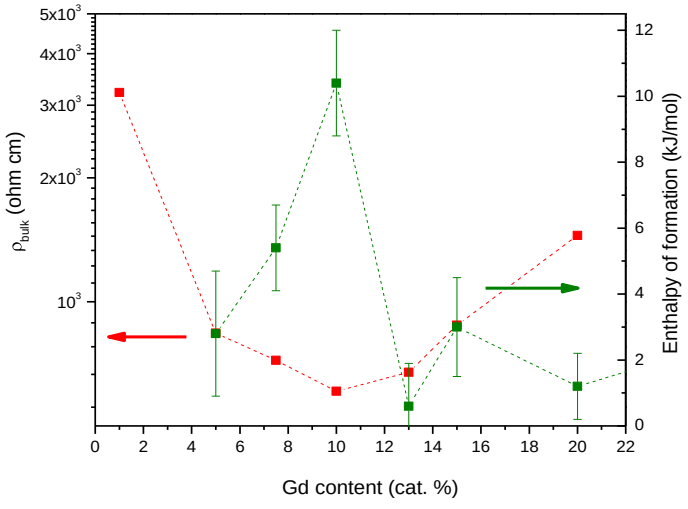

Fig. 2 *Ionic conductivity and enthalpy of mixing in gadolinia doped ceria (Avila Paredes et al. 2009)*

Further insight can be gained by comparing the energetics and the ionic

conductivity in doped ceria. For both Gd-doped ceria (Fig. 2) and La-doped ceria we have found that the compositions of maximum conductivity and of most endothermic heat of mixing coincide (Avila Paredes et al. 2009). We interpret this as further evidence that the conductivity maximum indeed arises from the formation of clusters or associates, which are lower in enthalpy but also lower in entropy than isolated defects (dopant cations and oxygen vacancies) and which decrease ionic conductivity by trapping the vacancies. We suggest that this composition of maximum conductivity may indeed be a point of change or anomaly in a number of physical properties. Work in progress on thoria-based systems suggests a similar correlation between ionic conductivity and mixing energetics.

Surfaces and interfaces are important in determining (and often degrading) ionic conductivity. Using calorimetric methodology developed in other DOE funded projects on minerals and nanomaterials, we have determined the enthalpies of drop-solution of a series of nanograined YSZ powders. We have also measured the enthalpy of water adsorption on these nanoparticle surfaces. The data are combined to obtain the surface energies of dry and wet YSZ nanoparticles (see Fig.3). We have also synthesized dense ceramics with nanosized grains of zirconia and YSZ. Oxide melt solution calorimetry of these materials provides their interfacial energies (Chen et al. 2009), which are smaller than the surface energies of isolated nanoparticles (see xx).

Fig. 3. *Surface enthalpy of hydrated (left) and anhydrous (right) nanocrystalline* $Zr_{1-x}Y_xO_{2-x/2}$ *as a function of yttria content, also data for zrconia and yttria end-members*

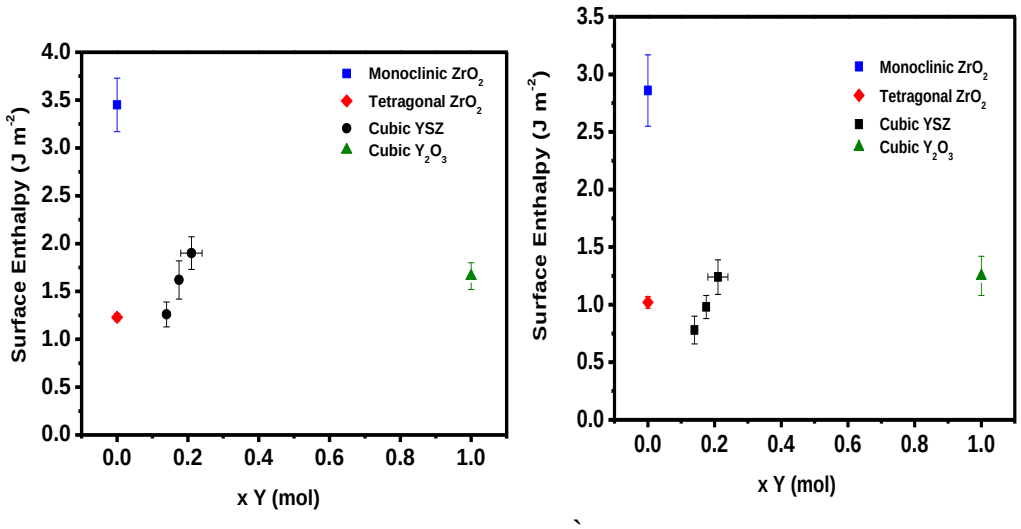

We are extending work to oxide ion conductors of apatite and mellilite structures, in which oxygen interstitials rather than vacancies appear to be the active conducting species. These maintain high conductivity to lower temperatures. We seek basic thermochemical properties, which at present are totally unknown, as well as possible correlations between defect energetics and conductivity.

From the point of view of basic science, this work addresses a number of DOE grand challenges as well as use-inspired fundamental questions. Understanding the relations of thermodynamics, structure and bonding addresses the grand challenge of *"how do we design and perfect atom- and energy-efficient synthesis of revolutionary new forms of matter with tailored properties?"* The materials we study address basic research needs for the *hydrogen economy* (solid oxide fuel cells, separation membranes, catalysts) and for *advanced nuclear energy systems* (reactor fuels and waste forms).

The present grant is complementary to a recently funded EFRC, Materials Science of Actinides, centered at Notre Dame, in which the Peter A. Rock Thermochemistry Laboratory at UC Davis is a major participant.

References

H.J. Avila Paredes, T. Shvareva, W Chen, A. Navrotsky and S. Kim (2009) "A Correlation between the Ionic Conductivities and the Formation Enthalpies of Trivalent-doped Ceria", Phys. Chem. Chem. Phys.(in press)

S. Chen, H.J. Avila-Paredes, S. Kim, J. Zhao, Z. Munir and A. Navrotsky, (2009) "Direct Calorimetric Measurement of Grain Boundary and Surface Enthalpies in Yttria Stabilized Zirconia" *Phys. Chem. Chem. Phys.* 11(17), 3039-3042

W. Chen, A. Navrotsky, Y. P. Xiong, and H. Yokokawa (2007) "Energetics of Cerium-Zirconium Substitution in the $xCe_{0.8}Y_{0.2}O_{1.9}$ - (1-x) $Zr_{0.8}Y_{0.2}O_{1.9}$ System", *J. Am. Ceram. Soc*., 90, 584-589.

W. Chen and A. Navrotsky, (2008) "Thermochemical Study of Trivalent-doped Ceria Systems: CeO_2-$MO_{1.5}$ (M = La, Gd, and Y)", *J. Mater. Res*., 21, 3242-3251

T. Lee, C. Stanek, K. McClellan, J. Mitchell, and A. Navrotsky (2008) "Enthalpy of Formation of the Cubic Fluorite Phase in the Ceria-Zirconia System", *J Mater Res*, 23(4), 1105-1112 (2008).

L. Mazeina, A. Navrotsky, and M. Greenblatt (2008). "Calorimetric Determination of Energetics of Solid Solutions of UO_{2+x} with CaO and Y_2O_3", *J. Nucl. Mater*. 373, 39-43

P. Simoncic and A. Navrotsky (2007) "Systematics of Phase Transition and Mixing Energetics in Rare Earth, Yttrium and Scandium Stabilized Zirconia and Hafnia", , *J. Am. Ceram. Soc*., 90(7), 2143-2150

Observing Fundamental Mechanisms of Transient Dynamics in Materials by Ultrafast In-Situ TEM

N. D. Browning (PI), G. H. Campbell (PI), T. B. LaGrange, and B. W. Reed
browning20@llnl.gov, ghcampbell@llnl.gov, lagrange2@llnl.gov, reed12@llnl.gov

Condensed Matter and Materials Division, Physical and Life Sciences Directorate, Lawrence Livermore National Laboratory, PO Box 808, Livermore, Ca 94550

Program Scope

The aim of this program is to develop a fundamental understanding of materials dynamics (from μs to ns) in systems where the required combination of spatial and temporal resolution can only be reached by the dynamic transmission electron microscope (DTEM). In this regime, the DTEM is capable of studying complex transient phenomena with several orders of magnitude time resolution advantage over any existing in-situ TEM. Using these unique nanosecond *in situ* capabilities, we seek to study complex transient phenomena associated with rapid processes in materials. This capability is being used to develop new insights into active sites on nanoscale catalysts and mechanisms in catalyzed growth of nanostructures. Additionally, we plan to explore the atomic level mechanisms and microstructural features for nucleation and growth mechanisms associated with phase transformations in materials, specifically in martensite formations and crystallization reactions from the amorphous phase. We also aim to study the transient phase evolution in rapid solid-state reactions, such as those occurring in reactive multilayer foils (RMLF). More recent work on the DTEM also aims to investigate biomolecular processes and in particular, the underlying thermodynamic and kinetic factors that lead to organization of macromolecules and drive assembly at macromolecular-inorganic interfaces.

Recent Progress

The first example of the use of the DTEM to study nanoscale catalysis has been the utilization of the DTEM to grow Si nanowires (NWs) by *in situ* pulsed laser ablation (Figure 1). One of the unique aspects of this work is that the Si NWs were fabricated without resistive heating or the flow of reactant gases. Although the result was obtained without time resolution (this experiment was a test of the specimen drive laser) this result establishes the ability to fabricate nanoscale systems in the DTEM under non-equilibrium conditions while simultaneously having the ability to image the growing nanostructures after each laser pulse. In future studies, dynamic observations will be incorporated into the experiment that may allow for a more complete understanding of the origin of texture, morphology, and extended defects in NWs during nucleation and growth. Such observations should allow for a more comprehensive model of the mechanisms involved in 1D nanostructure production, and hence have a great impact on the future of the use of NWs in electronic device fabrication. Thus, in future we will be able to determine the local microstructure and morphology before, during and after laser-assisted NW formation, giving us insight into the processing parameters that influence growth.

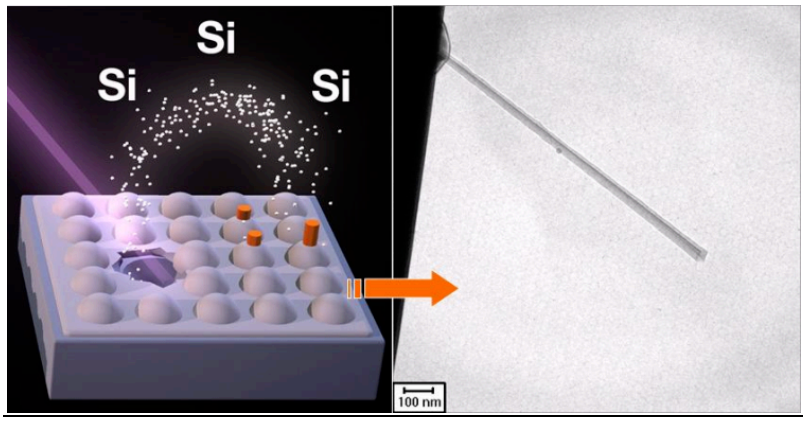

Figure 1: *In situ* pulsed laser ablation synthesis of Si nanowires within the DTEM.

The second example of *in situ* materials processing in the DTEM is on nickel titanium alloys of nearly equal atomic ratio, which were sputtered to create amorphous thin film structures for investigation. These films were heated inside the DTEM to temperatures of 1150 K with the specimen treatment laser, which completes the heating within its 12 ns pulse duration. Images were acquired after various delay times as the specimen is crystallizing and an example is shown in Figure 2. The nucleation events that initiate the crystallization occur rapidly. The advantage of a real space imaging technique such as DTEM is that it allows the counting of nucleation sites as a function of time after heating the thin foil to quantify average nucleation rates and crystallization kinetics. The image shown in Figure 2 is an example of this type of data that allows for quantitative evaluation of nucleation rates for comparison with models of the process. Reciprocal space (i.e. diffraction) measurements, also possible in the DTEM, give complementary information about phase fractions and crystallography but very little information about morphology.

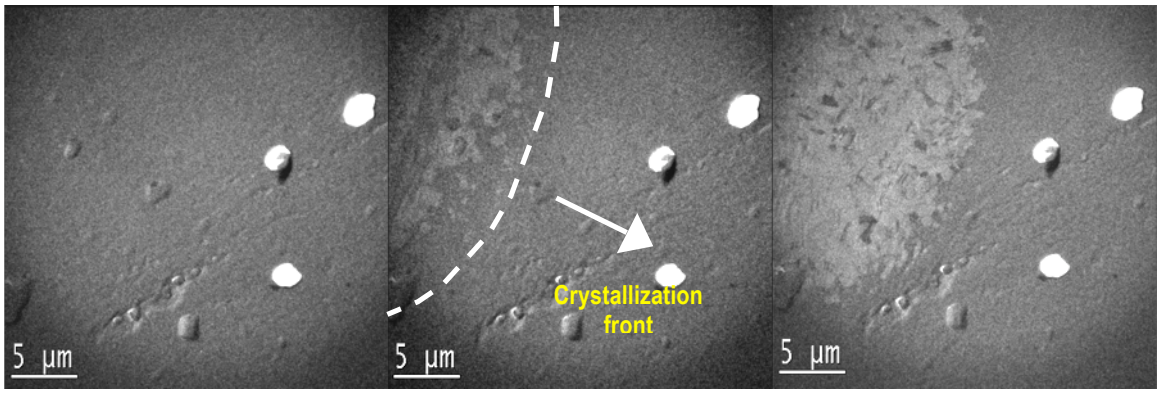

Figure 2: Time resolved images with 15 ns exposure times of laser irradiated NiTi alloy with initially amorphous structure. Prior to laser irradiation (a) the region of the thin film shows various defects, such as pinholes and surface contours. In (b) the specimen is at elevated temperature (1150K) 1.75 μs after laser irradiation at a spot centered outside the imaged area in the upper left-hand corner and the crystallized front is seen at the upper left growing into the region. Individual crystal nuclei can be seen forming. In (c) the specimen has crystallized as far as it will go and returned to room temperature.

Future Plans

The research performed during the first few years of this project has established the experimental and theoretical framework for analyzing the dynamic properties of nanoscale systems. The aim for the future of this project is to complete the following tasks

1. Complete the installation and calibration of the in-situ stage for both high spatial resolution STEM experiments (not in the DTEM) and high temporal resolution measurements. This calibration includes the effect of the windows and the gas pressure on the resolution achievable in the microscope. This work will also calibrate particle size measurements from annular dark field TEM with the Z-contrast STEM.
2. Install the capabilities for annular dark field TEM imaging with variable temporal resolution in the DTEM. The variable temporal resolution will be achieved by installing an arbitrary waveform generator that will allow the source laser (and hence the electron beam) to be varied between 10μs and 10ns in duration. The dark field TEM imaging will allow the DTEM characterization to be approximated to Z-contrast STEM and permit the quantified size, shape/orientation and composition analysis to be performed in the DTEM.
3. Correlate DTEM observations of Au nanocluster mobility/sintering under variable gas pressures and temperatures directly with MD simulations to elucidate the effects of metal-support interactions on catalytic properties.
4. Install in-situ liquid stage and observe the nucleation and growth of Fe3)4 within ferritin protein cages.
5. Install arbitrary waveform laser on the cathode drive to enable multiple exposures during a single experiment such that interface velocities can be measured directly. This capability will separate out the nucleation rate and the growth rate into separate measurements for more detailed parameter determination in phase transformation kinetics models.

This work performed under the auspices of the U.S. Department of Energy, Office of Science, Office of Basic Energy Sciences, Division of Materials Sciences and Engineering by Lawrence Livermore National Laboratory under Contract DE-AC52-07NA27344

DOE Sponsored Publications 2008-2009

"Validation and Generalization of a Method for Precise Size Measurements of Metal Nanoclusters", B. W. Reed, D. G. Morgan, N. L. Okamoto, A. Kulkarni, B. C. Gates and N. D. Browning, in press *Ultramicroscopy*

"The Evolution of Ultrafast Electron Microscope Instrumentation", B. W. Reed, M. R. Armstrong, N. D. Browning, G. H. Campbell, J. E. Evans, T. B. LaGrange, and D. J. Masiel, *Microscopy and Microanalysis* **15***,* 272-281 (2009)

"Strongly Driven Crystallization Processes in Metallic Glasses" Thomas LaGrange, David S. Grummon, Nigel D. Browning, Wayne E. King, and G. H. Campbell, *Applied Physics Letters* **94**, 184101 (2009)

"Laser Based *In Situ* Techniques: Novel Methods for Generating Extreme Conditions in TEM Samples", M. L. Taheri, T. B. Lagrange, B. W. Reed, M. R. Armstrong, G. H. Campbell, W. J. DeHope, J. S. Kim, W. E. King, D. J. Masiel, and N. D. Browning, *Microscopy Research and Techniques* **72**, 122-130 (2009)

"Nanosecond time resolved investigations using the *in situ* of Dynamic Transmission Electron Microscope (DTEM)", Thomas LaGrange, Geoffrey H. Campbell, B. W. Reed, Mitra Taheri, J. Bradley Pesavento, Judy S. Kim and Nigel D. Browning, *Ultramicroscopy***108**, 1441-1449 (2008)

"In-Situ Synthesis of Nanowires in the Dynamic TEM", M.L. Taheri, B.W. Reed, T. B. Lagrange & N. D. Browning, *Small* **4**, 2187-2190 (2008)

"Imaging of Transient Structures using Nanosecond in situ TEM", J. S. Kim, T. B. LaGrange, B. W. Reed, N. D. Browning, M. L. Taheri, M. R. Armstrong, W. E. King, and G. H. Campbell, *Science* **321**, 1472-1475 (2008)

"Determination of Nanocluster Sizes from Dark-Field Scanning Transmission Electron Microscopy Images", Norihiko L. Okamoto, Bryan W. Reed, Shareghe Mehraeen, Apoorva Kulkarni, David G. Morgan, Bruce C. Gates, and Nigel D. Browning, J*ournal of Physical Chemistry C* **112**, 1759-1763 (2008)

Session IIa

The Nanoscale: Assembly

Session Chair: Greg Exarhos, Pacific Northwest National Laboratory

(This page intentionally left blank.)

Inverse Optimization Techniques for Targeted Self-Assembly

Salvatore Torquato
Department of Chemistry, Princeton Institute for the Science and Technology of Materials,
and the Princeton Center for Theoretical Science
Princeton University, Princeton, N.J. 08544 USA
torquato@princeton.edu
http://cherrypit.princeton.edu

Abstract

Program Scope

The term "self-assembly" typically describes processes in which entities (atoms, molecules, aggregates of molecules, etc.) spontaneously arrange themselves into a larger ordered and functioning structure. Biology offers wonderful examples, including the spontaneous formation of the DNA double helix from two complementary oligonucleotide chains, the formation of lipid bilayers to produce membranes, and the folding of proteins into a biologically active state. On the synthetic side, molecular self-assembly is a potentially powerful method to fabricate nanostructures as an alternative to nanolithography. For example, it has been demonstrated that intricate two-dimensional structures can emerge by the placement of organic molecules onto inorganic surfaces [1]. Block copolymers can self-assemble into ordered arrays that have possible use as photonic band-gap materials [2]. Highly robust self-assembly of unique, small clusters of microspheres that can themselves be used for self-assembly of more complex architectures has been demonstrated [3]. DNA-mediated assembly of micrometer-size polystyrene particles in solution could enable one to build complex structures starting from a mesoscale template or seed followed by self-assembly [4]. These examples offer glimpses into the materials science of the future – devising building blocks with specific interactions that can self-organize on a larger set of length scales.

This is an emerging field with a wealth of experimental data that has been supported theoretically and computationally using the "forward" approach of statistical mechanics. Such an approach has generated a long and insightful tradition. The forward approach identifies a known material system that possesses scientific and/or technological interest, creates a manageable approximation to the interparticle interactions that operate in that material, and exploits simulation and analytical methods to predict non-obvious details concerning structural, thermodynamic and kinetic features of the system.

Several years ago, we proposed that *inverse* statistical-mechanical methods could be employed to find optimized interactions that most robustly and spontaneously lead to a targeted many-particle configuration of the system for a wide range of conditions [5, 6]. We will discuss these nascent developments in this connection as well as other closely related inverse realizability

problems that we have introduced, all of which are solved using various optimization techniques. Results produced by these inverse approaches have already led to a deeper fundamental understanding of the mathematical relationship between the collective structural behavior of many-body systems and the interactions: a basic problem in materials science and condensed matter theory. As will be shown, such methodologies hold great promise to control self-assembly in many-particle systems to a degree that surpasses the less-than-optimal path that nature has provided. Indeed, employing such inverse optimization methods, we envision being able to "tailor" potentials that produce varying degrees of disorder, thus extending the traditional idea of self-assembly to incorporate both amorphous and crystalline structures as well as quasicrystals.

The idea of *tailoring* potentials to generate targeted structures is motivated by the rich array of fundamental issues and questions offered by this fascinating inverse statistical-mechanical problem as well as our recent ability to identify the structures that have optimal bulk properties or desirable performance characteristics. The latter includes novel crystal and quasicrystal structures for photonic band-gap applications, materials with negative or vanishing thermal expansion coefficients, with negative Poisson ratios, materials with optimal or novel transport and mechanical properties, mesoporous solids for applications in catalysis, separations, sensors and electronics, and systems characterized by entropically driven inverse freezing, to mention a few examples.

Output from these optimization techniques could then be applied to create *de novo* colloidal particles or polymer systems with interactions that yield these structures at the nanoscopic and microscopic length scales. Colloidal particles suspended in solution provide an ideal experimental testbed to realize the optimized potentials, since both repulsive and attractive interactions can be tuned (*e.g.*, via particle surface modification or the addition of electrolytes) [7] and therefore offer a panoply of *possible* potentials that far extends the range offered by molecular systems.

Recent Progress

The research program has been aimed at first devising completely new inverse statistical-mechanical methods and then applying them for novel material design. The following is a list of the highlights of our accomplishments during last two years:

- Optimized isotropic pair interactions for unusual crystal ground states, including low-coordinated crystals, such as the diamond structure [8, 9];
- Novel low-temperature behavior obtained from designed interactions [10, 11];
- Designing isotropic pair interactions for anomalous thermal expansion behavior [12];
- Designing isotropic pair interactions for negative Poisson's ratio behavior [13];
- Inverse methods for the creation of disordered ground states [9, 14]; and
- Duality relations for classical ground states [9, 15, 16].

Figure 1 illustrates some of the novel target many-particle configurations that we have devised using our inverse statistical-mechanical techniques. Both structure and bulk properties can be optimized.

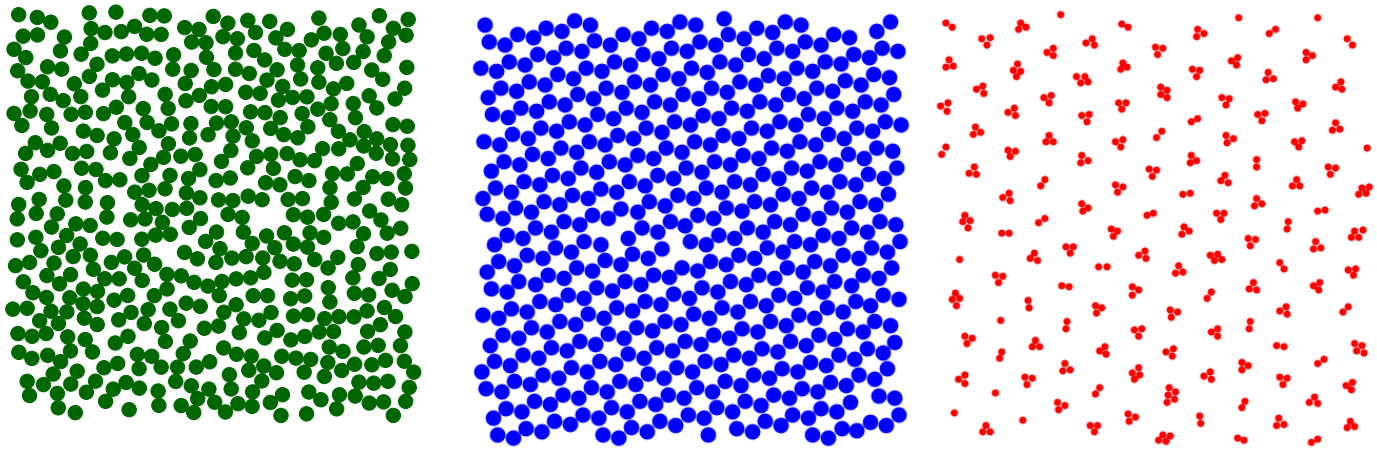

Figure 1: We have devised inverse statistical-mechanical optimization techniques so that many-particle interactions can be optimized to self-assemble into novel targeted configurations. Here we illustrate two-dimensional examples of targeted configurations: Left panel: an amorphous structure; Middle panel: low-coordinated honeycomb crystal structure (blue); and Right panel: crystals of compact clusters (red). We have also extended these results to three dimensions where, among other examples, we have formulated isotropic pair interactions leading to the low-coordinated diamond crystal as well as single-component systems having negative thermal expansion behavior and negative Poisson's ratio.

Future Plans

Our interest in future work will be in finding the interaction potential, not necessarily pairwise additive or spherically symmetric, that optimally stabilizes a targeted many-body system, which may be a crystal, disordered or quasicrystal structure, by incorporating structural information that is not limited to the pair correlation function and generally accounts for complete configurational information. Our primary interest is in the possible many-body structures that may be generated, some of which may include interesting but known structures, while others may represent entirely new structural motifs. We plan on extending our inverse methods to multicomponent systems. Moreover, the inverse methods described here can be employed to find targeted structures for metastable states as well as nonequilibrium configurations. Finally, an important component of future research will be the development of robust potentials (even if not optimal) for targeted structures and bulk properties that can be synthesized experimentally with colloids or other soft matter systems.

References

1. G. M. Whitesides and P. E. Laibinis. Wet chemical approaches to the characterization of organic-surfaces - self-assembled monolayers, wetting, and the physical organic-chemistry of the solid liquid interface. *Langmuir*, 6:87–96, 1990.

2. S. A. Jenekhe and X. L. Chen. Self-assembly of ordered microporous materials from

rod-coil block copolymers. *Science*, 283:372–375, 1999.

3. V. N. Manoharan, M. T. Elsesser, and D. J. Pine. Dense packing and symmetry in small clusters of microspheres. *Science*, 301:483–487, 2003.

4. M. P. Valignat, O. Theodoly, J. C. Crocker, W. B. Russel, and P. M. Chaikin. Reversible self-assembly and directed assembly of DNA-linked micrometer-sized colloids. *Proc. Nat. Acad. Sci.*, 102:4225–4229, 2005.

5. M. C. Rechtsman, F. H. Stillinger, and S. Torquato. Optimized interactions for targeted self-assembly: Application to honeycomb lattice. *Phys. Rev. Lett.*, 95:228301:1–4, 2005.

6. M. C. Rechtsman, F. H. Stillinger, and S. Torquato. Designed isotropic potentials via inverse methods for self-assembly. *Phys. Rev. E*, 73:011406:1–12, 2006.

7. W. B. Russel, D. A. Saville, and W. R. Schowalter. *Colloidal Dispersions*. Cambridge University Press, Cambridge, England, 1989.

Publications Over the Past 2 years Acknowledging DOE-BES Support on This Grant

8. M. Rechtsman, F. H. Stillinger, and S. Torquato. Synthetic diamond and wurtzite structures self-assemble with isotropic pair interactions. *Phys. Rev. E*, 75:031403, 2007.

9. S. Torquato. Inverse optimization techniques for targeted self-assembly. *Soft Matter*, 5:1157–1173, 2009.

10. R. D. Batten, F. H. Stillinger, and S. Torquato. Novel low-temperature behavior in classical many-particle systems. *Phys. Rev. Lett.*, 103:050602, 2009.

11. R. D. Batten, F. H. Stillinger, and S. Torquato. Interactions leading to disordered ground states and unusual low-temperature behavior. *Phys. Rev. E*, 80:031105, 2009.

12. M. C. Rechtsman, F. H. Stillinger, and S. Torquato. Negative thermal expansion in single-component systems with isotropic interaction. *J. Phys. Chem. A*, 111:12816–12821, 2007.

13. M. C. Rechtsman, F. H. Stillinger, and S. Torquato. Negative poisson's ratio materials via isotropic interactions. *Phys. Rev. Lett.*, 101:085501, 2008.

14. R. D. Batten, F. H. Stillinger, and S. Torquato. Classical disordered ground states: Super-ideal gases, and stealth and equi-luminous materials. *J. Appl. Phys.*, 104:033504:1–12, 2008.

15. S. Torquato and F. H. Stillinger. New duality relations for classical ground states,. *Phys. Rev. Lett.*, 100:020602:1–4, 2008.

16. C. E. Zachary, F. H. Stillinger, and S. Torquato. Gaussian-core model phase diagram and pair correlations in high euclidean dimensions. *J. Chem. Phys.*, 128:224505:1–16, 2008.

Nanoscale van der Waals Interactions

Milton W. Cole[a,c], Darrell Velegol[b,c,f], Hye-Young Kim[e], Amand A. Lucas[d]

[a]Department of Physics, [b]Department of Chemical Engineering and the [c]Materials Research Institute, The Pennsylvania State University, University Park, PA 16802

[d]Laboratoire de physique du solide, Facultes Universitaires Notre-Dame de la Paix, 61 rue de Bruxelles, B5000 Namur, Belgium

[e]Department of Chemistry & Physics, Southeastern Louisiana University, Hammond LA 70402

[f]corresponding authors: velegol@psu.edu, miltoncole@aol.com

10 September 2009[1]

i) Program Scope

Van der Waals (VDW) interactions are often considered to be "weak" or "physical" or "nonbonding" interactions between atoms, molecules, or even particles. All atoms experience VDW attractions in their electronic ground state. They are due purely to quantum mechanics, given by zero-point fluctuating densities of electronic charge within the atoms. Although VDW forces are small compared with covalent or electrostatic bonds, since they are often the only attractive interaction present, the VDW forces are central in many physical systems. As examples, liquids such as heptane condense due to VDW energetics; and surface tension for wax droplets is largely due to VDW energetics.

In our current research, we are interested in attractive forces between nanoparticles. VDW interactions were first hypothesized in the late 19th century by J. D. van der Waals in his Ph.D. thesis to explain vapor-liquid equations of state. But not until the advent of quantum mechanics were the origins of VDW interactions explained qualitatively, and even quantitatively, by Fritz London.[2] Many others have since studied these interactions, improving the accuracy of VDW force calculations between atomic or small molecule systems.[3,4] Extending the calculations to large systems has proved challenging, unless one makes the explicit assumption that interactions are pairwise additive; unfortunately, this is a bad approximation except for materials with low polarizability.

For colloidal particles in general, one often uses DLP (Dzyaloshinskii, Lifhsitz and Pitaevskii) theory.[5] They evaluated VDW interactions exactly, for the case of uniform, continuum media and several simple geometries.[6] In principle, continuum Lifshitz theory (as we call the DLP method) gives the full many-body, retarded interaction for all sizes and all separations between ideal geometries such as spheres.[7] In practice, surface roughness renders the continuum model inadequate at close separations, precisely where the VDW attraction exceeds the thermal energy (kT) for nanoscale systems. Nevertheless, since about 1960,[2,3,4,8] many researchers have considered the prediction of VDW forces, to be straightforward in principle, for *all* situations, especially by Lifshitz theory.

However, at the *nanoscale* VDW forces are not so readily predicted, or even estimated. The nanoscale problem includes these complicating issues: 1) Atoms are located at specific locations, not well characterized by continuum models or simple geometries; their placement includes corners, sharp edges, and roughness that can be comparable to the particle size. 2) Nanoscale systems have a permittivity – a macroscopic concept from electrodynamics – that varies near the boundaries of an object, because of local field effects and/or structural effects, so that the bulk approximation is not adequate. 3) Nanoscale systems sometimes have part of their interacting material sufficiently close for a "nonretarded" VDW model to be applicable, while other pieces are farther apart, requiring a "retarded" theory due to the finite speed of light.

ii) Recent progress for the "coupled dipole method" (CDM) and results

In most of our calculations of nanoscale VDW interactions, we have used a very different approach. In the limit of small separations, where retardation can be ignored, and in the limit of zero temperature, we combine quantum physics, classical electrostatics, and classical mechanics to find the VDW energies precisely. This "coupled dipole method" (CDM) is uniquely positioned to evaluate VDW energies between atoms, molecules, clusters, and particles at the nanoscale. Regimes involving particles nearly touching, or with surface roughness, are where the CDM works well, and unlike Lifshitz theory, the CDM is not limited to ideal shapes like spheres, cylinders, or half spaces. The method has no difficulty handling *arbitrary* shapes.

The CDM evaluates the VDW energy from the spectrum of collective motions of the ensemble of electric dipoles, one at each atomic position, which fluctuate in the presence of their mutual interactions. Thus, the method captures the complete "dipole conversation" in the system, which is the essence of the many-body effects. In the model we approximate that each electron obeys the classical motion embodied in the Drude model described earlier, although this is not a strict requirement of the technique. In the Drude model, two parameters, a static polarizability (α_0) and a resonant frequency (ω_0), characterize the electron's dynamics within an atom. The atom's dipole interacts with all other instantaneous dipoles by classical electrostatic dipole interactions. The eigenfrequencies $\{\omega_i\}$ of the resulting collective electron motions provide the zero-point energies, $\{\hbar\omega_i/2\}$. The total VDW energy is the sum, over the 3N normal modes, of these energies. Then the VDW interaction energy, V_{int} , is given by the difference between this sum and the energy of this collection of the N atoms when they are infinitely far apart.

The research has produced a number of findings. One finding, shown below in Figure 1, is that for an infinite line of atoms, while the 3-body contribution is only 2% of the 2-body contribution, the total contribution of higher order terms (i.e., beyond 3-body) exceeds the 3-body term, and indeed becomes comparable to 2-body terms. Thus, *a small magnitude of the three-body term implies neither that higher order terms are individually small or that they mutually cancel*. We note in passing that Figure 1 reveals a limitation in the CDM which is inherent. Above a critical value (ν~0.208 for the one-dimensional chain), no solution exists. For such large ν values, the system is unstable, because the force provided by the local field (due to the surrounding dipoles) exceeds the spring restoring force.

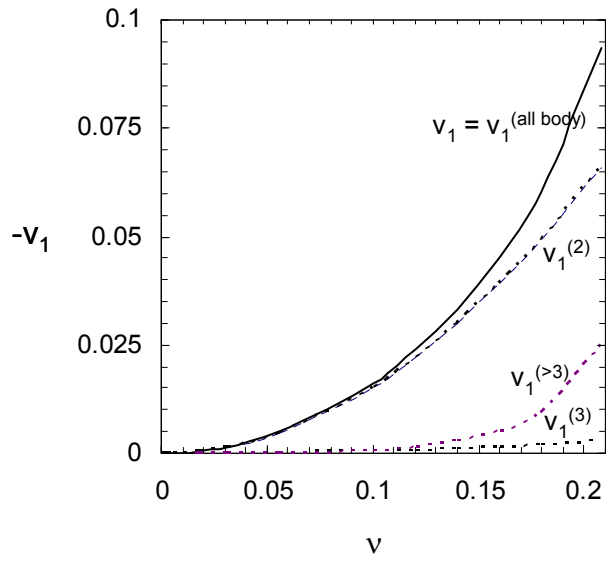

Figure 1. The dimensionless energy per atom (v_1) of an infinite line of atoms. The full (all body) calculation for v_1 was done with the CDM. For all values of ν, up to a "critical value" of 0.208, the 3-body contribution per atom ($v_1^{(3)}$) is small, while higher order interactions ($v_1^{(>3)}$) cannot be neglected, especially beyond ν > 0.15.

It is comforting to note, however, that for symmetric shapes, the CDM reduces to known Lifshitz results for spheres, as shown in Figure 2. We see that at large interparticle separations, the CDM gives the same results as Lifshitz theory for spheres, as given by Langbein,[9] as expected. However, as the separation between particles diminishes, continuum theories – whether the Langbein solution or the Hamaker approach – diverge, giving unphysically large results. In contrast, the discrete 2-body sums give results within 10 or 20% of the CDM.

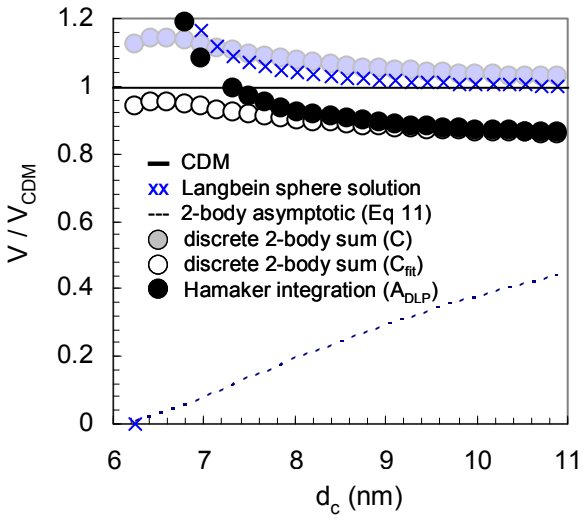

Figure 2. Ratio of various methods for computing VDW forces to the exact CDM method, for two identical spheres with N = 2340 atoms in each. The center-to-center distance between the spheres (d) is the same for both the continuum and discrete methods. The cluster diameters are both 5.88 nm. Due to the discrete placement of the atoms within the cluster, analytical methods (e.g., Langbein, Hamaker) far over-estimate the result for small gaps, although the Langbein result is within 2% when the gap is 3 nm. The 2-body sum with C approaches the exact CDM value at far distances, since multi-body effects essentially disappear.

iii) Future plans, challenges, and opportunities ahead

There are several critical avenues for future study, and many researchers will be needed to answer the large variety of problems. 1) One focus of future development must be the extension of the CDM method to metallic systems or systems such as fullerenes and carbon nanotubes for which CDM fails by producing instabilities. One avenue we are pursuing is to generalize the CDM to "chunks" of

matter, thus embodying the nonlocal response of the medium. 2) Another avenue of research is in examining retardation in the CDM. We are examining methods similar to those that have been used for continua. 3) Larger systems are a computational challenge. Methods are required for connecting continua results for the bulk of a material system with CDM results for the interface regions, where precise atomic placement could be assessed properly. In addition, it is possible that the chunking method mentioned above for metals could be used for regions of material, rather than using the CDM for individual atoms. 4) Finite temperature results require that we include effects due to the thermal energy (kT). These effects can be significant, for example in aqueous systems, since water has a permanent dipole and that permanent dipole contributes to the polarization of the medium. 5) Applications like surface tension, solvophobicity/philicity, contact angles, and others can be examined at the nanoscale, even at the molecular level, using the CDM. At present, few results exist for these parameters. It is clear that for nanoscale systems, the VDW forces play a critical and often dominant role.[10,11,12,13]

iv) References

[1] Parts of the text of this abstract have been taken from our publication: Cole, Milton W.; Velegol, Darrell; Kim, Hye-Young; Lucas, Amand A. "Nanoscale van der Waals Interactions," *Molecular Simulation*, **35**, 849-866 (2009). Invited review article..

[2] J. S. Rowlinson, *Cohesion: A Scientific History of Intermolecular Forces*, Cambridge, 2002.

[3] H. Margenau and N. R. Kestner, *Theory of Intermolecular Forces*, Pergamon, Oxford, 1971.

[4] V. Adrian Parsegian, *Van der Waals Forces*. (Cambridge U. P.: New York, 2005).

[5] Dzyaloshinskii, I.E.; Lifshitz, E.M.; Pitaevskii, L.P. *Adv. Phys*. **1961**, 10, 165.

[6] Lucas, A.A. Prog. Surf. Sci., **14**, 1-52 (1983).

[7] Mahanty, J.; Ninham, B.W. *Dispersion Forces*. New York: Academic Press (1976).

[8] Jacob N. Israelachvili, *Intermolecular and Surface forces*. 2nd ed. (Academic, New York, 1992).

[9] Dieter W. Langbein, *Theory of Van Der Waals Attraction*, Springer Tracts in Modern Physics 72, Springer (New York) 1974.

[10] We acknowledge support from DOE grant DE-FG02-07ER46414, and important discussions with Silvina Gatica, Jerry Mahan, Jorge Sofo, Kristen Fichthorn, Leonidas Gergidis, Slava Rotkin and Adrian Parsegian.

v) Publications resulting from this DOE grant

[11] Cole, Milton W.; Velegol, Darrell. "Van der Waals Energy of a 1-Dimensional Lattice." *Molecular Physics*, **106**, 1587-1596 (2008).

[12] Cole, Milton W.; Velegol, Darrell; Kim, Hye-Young; Lucas, Amand A. "Nanoscale van der Waals Interactions," *Molecular Simulation*, **35**, 849-866 (2009).

[13] Cole, Milton W.; Velegol, Darrell; Kim, Hye-Young. "Importance of Multi-body Effects in Lines of Particles." *J. Nanophotonics* (in preparation).

Phase Behavior of Colloidal 'Mushroom Caps' Under 2D and Quasi-2D Confinement

Chekesha M. Liddell
cliddell@ccmr.cornell.edu
Department of Materials Science and Engineering
Cornell University, Ithaca, NY 14853

Program Scope

A variety of monodisperse 'designer' particles with selectively engineered features— janus or patchy surfaces, faceted polyholyderal shape, 2- 3- or 4- lobed clusters, lock-and-key concave/convex shape complementarity, zig-zag chain ('w' particles)— are being prepared in scalable quantity.[1] The developments in colloidal synthesis and fine particle technology herald that the era of well-defined self-organized mesoscale structures sought for applications in photonics, biomaterials, and micromechanics is fast approaching. Building blocks capable of promoting the structural diversity and regularity of molecular solids, block copolymers and/or amphiphiles are in particular envisioned as a route to stronger light-matter interactions and novel optical properties of materials.[2] Though nonspherical colloidal dimers and tetrahedra have been suggested as prime building blocks for the self-assembly of diamond-analog structures with the most stable and largest photonic band gaps,[3] control of the structures that actually form spontaneously or with programmed anisotropic interactions from these building blocks using common assembly techniques still requires investigation.

Additionally, methods that provide self-assembly of ***any arbitrary shape*** into ordered structures are integral to the realization of low cost complex structures, in contrast to approaches such as uniaxial thermal stretching[4] or thermopolymerization-induced pressing[5] that have relied on simple sphere deformation. A few reports demonstrate convective assembly (evaporation-mediated assembly or controlled drying) with or without a magnetic field for nonspherical particles in the submicron size range. Spherocylinders, 'mushroom caps', and ellipsoids were reported to form a body-centered tetragonal crystal,[6] layer-by-layer close-packed hexagonal sheets,[7] and a triclinic dry particulate 3D film,[8] respectively. Monte Carlo simulations excluding an applied orienting field reveal that disorder-order and order-order structural transitions to crystals and other solids with unconventional order can occur as a function of building block shape and density (i.e., volume fraction of particles) alone.[9-12] Figure 1 highlights for example, the 2D aperiodic (or degenerate) crystal, oblique crystal, and rotator (or plastic) crystal predicted in phase diagrams for dimers with varying degree of fusion between the two lobes.

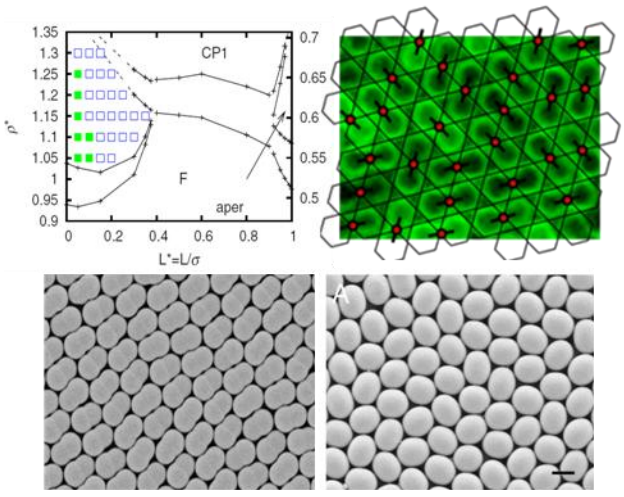

Fig. 1. Phase behavior of colloidal dimers.[9, 13-15] Predicted transitions with system density from (i) fluid [F] to plastic crystal [squares] to orientationally ordered solid [CP1] for high-fused lobe morphology, (ii) F to CP1 for mid-range lobe-fusion, and (iii) fluid to aperiodic or degenerate crystal for nearly tangent-lobed dimers.

Recent Progress

Here we report a sub-project of the DOE award, 'Self-Assembly of Non-Spherical Colloids: New Reduced Symmetry Crystals and Mesophases for Templating Functional Materials at Fine Scales'. Phase transitions of mushroom cap-shaped colloids (i.e., hemisphere capped with a half-torus) are systematically investigated as a function of density and confinement height in a custom wedge cell.[13-15] Surface modification of the polystyrene colloids with fluorescent silica enables their visualization in real time using confocal microscopy during the self-organization process. Phases are characterized by fast Fourier transform, voronoi constructions, radial and orientational distribution functions, and autocorrelation functions as quantitative and qualitative measures of order and symmetry.

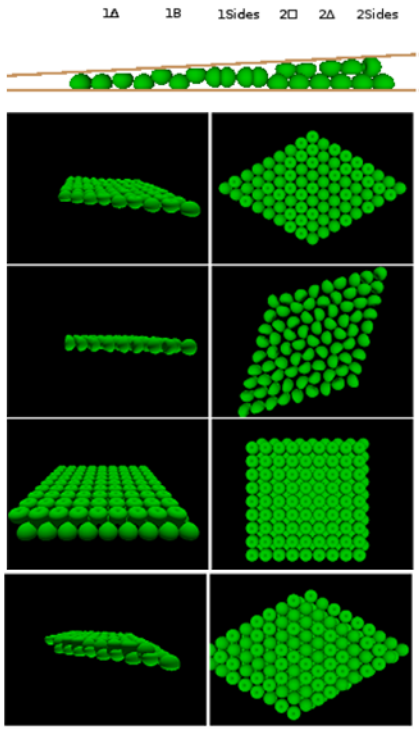

Fig. 2. Effect of confinement height on phase behavior of mushroom caps. Buckled phase only shown in side view.

In prior work, we commented that the convective assembly process allows reversible attachments as local configurations are sampled along with controlled densification of anisotropic particles when they are driven to the air-liquid-solid interface (while the suspension medium evaporates) so that high density structures of the phase diagram can be realized.[14] Under confinement in a wedge cell of glass coverslips, however, the system of 1.2 micron diameter mushroom caps in water was densified by gravitational settling over a period of 3 to 14 days. Polyvinylpyrolidone (PVP) was adsorbed onto the colloids and the glass surfaces to stabilize the particles against aggregation and to prevent their uncontrolled adhesion to the walls of the cell. Cells were laid flat and the particles were allowed to equilibrate prior to imaging.

We find the mushroom caps to adopt a series of high density packings commensurate with the confinement height in the sequence— [1] hexagonal monolayer (triangular lattice, 1Δ); [2] buckled (1B) monolayer, in which adjacent particles are promoted or demoted along the z-height distorting the hexagonal packing to a rectangular one; [3] rotator crystal on an oblique lattice, where the axis of spherical symmetry reorients parallel rather than perpendicular to the plane of the substrate (1sides, Fig. 3); [4] bilayer square (2□) with the lower layer particles centered in the interstitials of the top layer; [5] bilayer hexagonal (2Δ); [6] bilayer rotator crystal (2sides). The ideal density of each phase at the minimum geometrically allowed height was calculated and used to rationalize the stability range of each structure observed. In comparison, spheres are known to exhibit layering transitions through buckling and 'square' symmetry structures, for example, the sequence 1Δ-1B-2□-2Δ is known.[18] Additionally, anisotropic shapes have been shown to undergo realignment of the major axis to efficiently fill space in a transition height region rather than buckling.[13] The mushroom cap particle geometry has associated projection profiles of anisotropic and isotropic systems simultaneously. Thus, features of both systems

are apparent in the phase behavior of the mushroom caps and they provide an expanded range of phases over spheres or the rod-like dimer cases. As shown in the schematic of Figure 2, the structures exhibit diverse characteristic ordering, including positional order with bifurcated orientational order (cap up or cap down), positional order only and random orientational order, or both positional and orientational order (traditional crystal). We plan to perform Monte Carlo simulations of hemisphere model particles corresponding to the experimental mushroom cap system to further understand the dynamics of the phase formation.

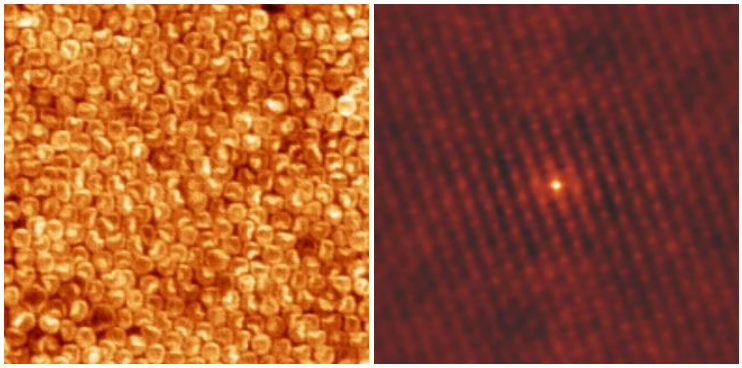

Fig. 3. Confocal microscopy image of the rotator phase ('2sides') of colloidal mushroom caps in a wedge cell at one of the heights intermediate between one and two layers of close-packed hexagonal structures (left). Autocorrelation function indicating oblique lattice symmetry by the defined spot pattern (right).

Future Plans

Our approach to explore the relationships between the shape of the colloidal building blocks and the micro/nanostructures that can be formed from them involves mapping out a comprehensive series of experimental and theoretical phase diagrams under a variety of conditions controlling the thermodynamics and kinetics of the condensed matter system during assembly. For selected cases, we have characterized structures and their defect dynamics and also assessed how these properties differ for spherical versus nonspherical particles.

We have observed that the defects produced in degenerate crystals of peanut-shaped dimers are longer-lived than those created in crystals of spheres.[15, 19] We plan to examine this difference rigorously by measuring the decay rate of defects after an impurity particle is no longer moving. Initial results suggest that in crystals of spheres, the defects produced by the motion of the impurity particle quickly leave the crystal grain within 3 minutes after the perturbation, either by annihilation with other defects, or by gliding to a grain boundary. In degenerate crystals, however, some of the defects induced by the deformation do not immediately disappear. These remaining defects tend to persist for very long times, ranging from 20 minutes to several days. For the dimer systems, after the first stage in which defects annihilate, the remaining defects have more difficulty migrating to the grain boundaries. In essence, they may be thought of as caged in much the same way that colloidal particles in a glassy suspension have been described as caged by their nearest neighbors.[20] To reach the grain boundary, defects in the dimer system often create new defects that facilitate their motions. This leads to a correlation in the defect positions and motions. Therefore, we have a dynamically heterogeneous system where certain particles are moving in correlated 'conga lines' while others are hindered, reminiscent of particle (not defect) behavior observed in glassy colloidal suspensions where there are multiple relaxation mechanisms and timescales associated with each mechanism.

In comparison with simulations, we plan to measure the defect-defect correlation function in dimers and spheres once grains have been deformed in the respective crystals. We expect that in dimers the defects will be correlated with one another in space and velocity, but in the sphere system they will be uncorrelated. An implication of the work may be toward tuning mechanical properties via entangled particle orientations rather than by defect pinning sites in crystals, promoting for example unconventional strengthening mechanisms.

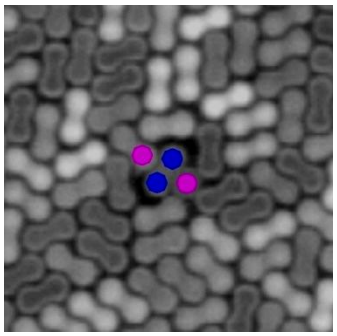

Fig. 4. Stable defect configuration in a degenerate crystal. These defects would not be stable in disconnected spherical lobes. If the two 7-fold lobes (blued) were not bonded and were allowed to separate, the defects would immediately annihilate. Initial investigations of the annealing mechanisms of these longer-lived defects revealed that in addition to the restrictions on defect glide, further limitations to defect motion are caused by geometric constraints from particle orientations. We find that certain defect configurations which would quickly annihilate in crystals of spheres are extremely stable in degenerate crystals of dimers.

References

1. Glotzer, S. C.; Solomon M. J. *Nat. Mater.* **2007**, *6*, 557-562.
2. Yang, S. M.; Kim, S. H.; Lim, J. M.; Yi, G. R. *J. Mater. Chem.* **2008**, 18, 2177-2190.
3. Lu, Y.; Yin, Y.; Xia Y. *Adv. Mater.* **2001**, 13, 415-420.
4. Lu, Y.; Yin, Y.; Li, Z.-Y.; Xia Y. *Langmuir* **2002**, 18, 7722-7727.
5. Sun, Z. Q.; Chen, X.; Zhang, J. H.; Chen, Z. M.; Zhang, K.; Yan, X.; Wang, Y. F.; Yu, W. Z.; Yang, B. *Langmuir* **2005**, 21, 8987-8991.
6. Mock, E. B.; Zukoski, C. F. *Langmuir* **2007**, 23, 8760-8771.
7. Hosein, I. D.; Liddell, C. M. *Langmuir* **2007**, 23, 8810-8814.
8. Ding,T.; Song, K.; Clays, K.; Tung, C.-H. *Adv. Mater.* **2009**, 21, 1936–1940.
9. Marechal M.; Dijkstra, M. *Phys. Rev. E*, **2008** 77, 061405-1 – 061405-10.
10. Branka A. C.; Wojciechowski, K. W. *Phys. Rev. Lett.* **1983** 50, 846-849.
11. Bolhuis P.; Frenkel, D. *J. Chem. Phys.* **1997** 106, 666-687.
12. Wojciechowski, K. W. *Phys. Lett. A* **1987** 122, 377-380.
13. Lee, S. H.; Fung, E. Y.; Riley E.; Liddell C. M. *Langmuir*, **2009** 25, 7193-7195.
14. Hosein, I. D.; John, B. S.; Lee, S. H.; Escobedo, F. A.; Liddell C. M. *J. Mater. Chem.*, **2009** 19, 344-349.
15. Lee, S. H.; Gerbode, S. J.; John, B. S.; Escobedo, F. A.; Cohen, I.; Liddell. C. M. *J. Mater. Chem.* **2008** 18, 4912-4916.
16. Pieranski, P.; Strzelecki, L.; Pansu, B. *Phys. Rev. Lett.* **1983**, 50, 900.
17. Schmidt, M.; Lowen, H. *Phys. Rev. Lett.* **1996**, 76, 4552.
18. Fortini, A.; Dijkstra, M. J. *Phys.: Condens. Matter* **2006**, 18, L371.
19. Gerbode, S. J.; Lee, S. H.; Liddell, C. M.; Cohen. I. *Phys. Rev. Lett.*, **2008** 101, 058302-1 – 058302-4.
20. Weeks, E. R.; Crocker, J. C.; Weitz, D. A. *J. Phys.: Cond. Mat.* **2007** 19, 205131.

DOE sponsored publications since Sept. 2008

1. S. H. Lee, E. Y. Fung, E. Riley and C. M. Liddell. “Asymmetric Colloidal Dimers Under Quasi-2D Confinement.” *Langmuir*, 25 (2009): 7193-7195.
2. U. Agarwal and F. A. Escobedo. “Phase Behavior of Space-Filling Hard Multi-Faceted Particles.” *submitted to J. Chem. Phys., Sept. 2009*.

Molecularly Organized Nanostructural Materials: From Two-Dimensional Crystallization to Three-Dimensional Self-Assembly

Jun Liu, Gregory J. Exarhos, Li-Qiong Wang, Yongsoon Shin,
Maria Sushko, Praveen Thallapally, Donghai Wang
Jun.liu@pnl.gov
Division of Chemical and Materials Sciences
Pacific Northwest National Laboratory
Richland, WA 99352

Program Scope

The overall goal of this project is to investigate a combination of self-assembly and controlled nucleation and growth approaches for synthesizing nanostructured materials with controlled three-dimensional architectures and desired stable crystalline phases of conductive or semiconducting metal oxides suitable for energy applications. Of importance is the understanding of crystallization in self-assembled materials in order to control both resident porosity and pore interconnectivity in these materials because these traits impart certain properties to the material that are underpinning for energy technologies including conversion and storage. The project contains the following components:

- Manipulation of the kinetics of competing self-assembly and precipitation reactions
- Use of molecular ligands to control nucleation and growth
- Multiscale modeling of the self-assembly process in solution
- *In situ* spectroscopic probes of structure-forming reactions and evolving porosity

Recent Progress

Nanocomposite materials have attracted wide attention because of the potential to optimize mechanical, electrical and chemical properties. Traditional approaches for making such materials mostly rely on mechanical or chemical mixing which usually produces a random distribution of the constitutive phases. Many groups have explored more complicated methods such as layer-by-layer deposition, but these methods are time consuming and difficult to scale up to bulk three-dimensional materials. In the past, we and many other groups have performed extensive study of controlled nucleation and growth on functionalized surfaces based on the principles used in biomineralization. A wide range of metal oxides and polymers films have been prepared with controlled orientation, crystalline structures and systematic variations of the morphologies. However, this approach has been limited to thin films and supported two-dimensional structures, as well as single phase materials.

An important new direction for this project is to explore a novel strategy to extend the two-dimensionally controlled nucleation and growth method to three-dimensional functional nanocomposite materials. This strategy involves the integration of controlled nucleation and growth and three-dimensional self-assembly process. Rather than using a hard substrate or functionalized surface to make supported thin films and coating (Pathway 1 in Figure 1), we use other novel nanostructured materials as the molecular

template as well as one of the critical component for forming the self-assembled materials. For example, we use molecularly dispersed graphene sheets as the template. The graphene sheets are dispersed in the hydrophobic domains of surfactant molecules or polymers. The functional groups on the absorbed surfactant surfaces controls the crystallization of metal oxide on the graphene surfaces, forming a well-dispersed metal oxide and graphene nanocomposite that shows significantly better conductivity that conventional nanocomposites and carbon nanotube composite materials for energy storage.

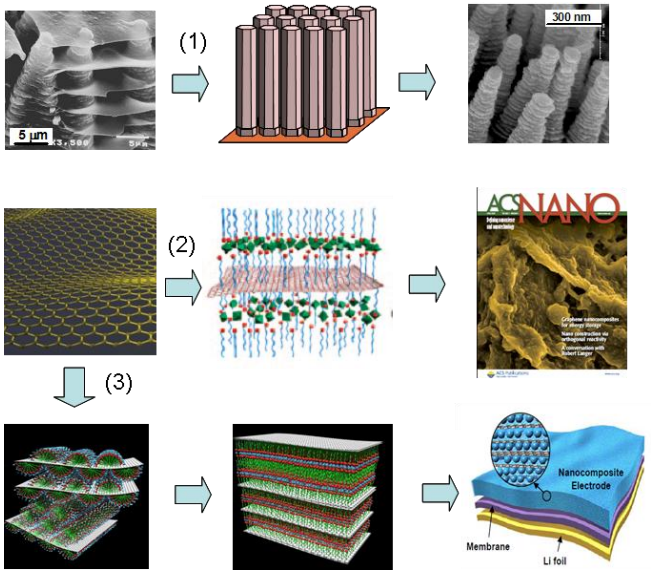

Figure 1. New pathways for three-dimensional self-assembly of metal oxide carbon nanostructures using extended graphene molecular sheets as the template and the fundamental building block. Pathway 1: Conventional nucleation and growth of two-dimensional nanostructures supported on substrates based on lessons from biology. Pathway 2: Controlled nucleation and deposition of metal oxides on graphene sheets for novel metal oxide-graphene nanocomposite. Parthway 3: Self-assembly of ordered graphene-metal oxide nanocomposites.

Furthermore, we demonstrate that we can use the extended graphene sheets solubilized in the hydrophobic domains as the fundamental building blocks for the self-assembly of three-dimensionally ordered architectures (Pathway 3). The graphene sheets and metal oxide precursors self-assemble into ordered three-dimensional composites structures. The metal oxides are then crystallized between the graphene sheets as controlled by the functional head groups of the surfactants. This self-assembly method process produces a new class of nanocomposite materials with well-controlled architectures on the nano- and microscales. Such materials show much improved conductivity and mechanical stability. The self-assembly process can be further used to directly fabricate energy storage devices in one step.

In order to understand the origin of the improved properties, we used ^{129}Xe NMR to probe the interconnectivity of micro- and nano-porosity, which plays an important role in the performance of porous materials. The pore geometry in most porous materials is complex with interconnected cages, channels and micropores. It is challenging to directly characterize the interconnectivity of the pores in nano or meso-porous materials. Techniques such as small angle x-ray or neutron scattering and gas absorption do not provide direct information on how channels and cages are connected.

Hyperpolarized (HP) ^{129}Xe NMR is used to probe the porosity and interconnectivity of pores in highly crystalline mesoporous metal oxide (TiO_2) and TiO_2-graphene nanocomposites. We have demonstrated that HP ^{129}Xe NMR can be used to unambiguous differentiation between similar sized pores within different crystalline phases. Both anatase and rutile pores of 4 nm size were identified in mesoporous TiO_2. In contrast to other pore characterization methods, we are also able to probe

interconnectivity between pores constrained to different phases. The cross peaks in 2D chemical shift exchange (EXSY) NMR spectra show exchange takes place between both types of pores with a short mixing time of 5 ms, indicating that these two types of pores are well interconnected.

A small percentage of graphene in TiO_2 was found to greatly enhance ion transport rate in our recent study. HP ^{129}Xe NMR studies on TiO_2 with and without graphene help us to understand how the nanostructures of TiO_2-graphen influence the ion transport. Comparative HP ^{129}Xe NMR studies of pure TiO_2 and TiO_2-graphene show that TiO_2 and graphene are mixed uniformly on the nanoscale and the resulting hybrid nanostructure has better connected channels among different domains upon adding 1% graphene in TiO_2. The better connected channels may be one of the factors that enhance the transport property of TiO_2-graphene.

The recent progress on this project has the potential to bridge the gap of two-dimensional crystallization and three-dimensional self-assembly. In addition, in the past, self-assembled oxide materials are mostly limited to single phase materials and nanoparticle based systems. Our study points to a new direction for self-assembly using multiple phases and multilength building blocks. Currently many nanoscale building blocks are available besides graphene sheets, such as carbon nanotubes, nanowires and nanorods, and ceramic nanoplates. Similar principles should apply for such nanoscale building blocks and will lead to truly multifunctional composite materials with controlled architectures. The materials developed under this project already demonstrated superior kinetics and stability as compared with conventional composite materials.

Future Plan

We will focus on the fundamental understanding of the nature of the interactions between graphene sheets, the surfactant, and the metal oxides. High resolution electron microscopy, NMR and other spectroscopic techniques, as well as atomic force microscopy will be used to probe the nature of the chemical binding, and the kinetics of surface absorption and nucleation processes. We will also perform systematic studies of similar self-assembly and nucleation processes involving different nanoscale building blocks in order to develop the general guiding principles for a wide range of materials. Finally, we will develop multiscale modeling capabilities that can not only address the ternary self-assembly problems we encountered here, but also the transport properties in such materials.

References

1. (a) G. Decher, "Fuzzy nanoassemblies: Toward layered polymeric multicomposites," *Science* 277, 1232 (1997); (b) A. C. Balazs, T. Emrick, T. P. Russell, "Nanoparticle polymer composites: Where two small worlds meet," *Science* 314, 1107 (2006). (c) P. Podsiadlo *et al.*, "Ultrastrong and stiff layered polymer nanocomposites," *Science* 318, 80 (2007). (d) L. J. Bonderer, A. R. Studart, L. J. Gauckler, "Bioinspired design and assembly of platelet reinforced polymer films," *Science* 319, 1069 (2008).
2. I. A. Aksay *et al.*, "Biomimetic pathways for assembling inorganic thin films," *Science* 273, 892 (1996).
3. (a) D. Wang, J. Liu, Q. Huo, Z. Nie, W. Lu, R. E. Williford, Y. Jiang, "Surface-Mediated

Growth of Transparent, Oriented and Well-Defined Nanocrystalline Anatase Titania Films," *J. of the Am. Chem. Soc.*, 128, 13670-13671, 2006; (b) Z. R. Tian, J. A. Voigt, J. Liu, B. McKenzie, H. F. Xu, "Large Oriented Arrays and Continuous Films of TiO2 Based Nanotubes," *J. Am. Chem. Soc*., 125, 12384-12385, 2003.

4. (a) J. W. P Hsu, Z. R. Tian, N. C. Simmons, C. M. Matzke, J. A. Voigt, J. Liu, "Spatial Organization of Zinc Oxide Nanorods," Nano Letters, 5, 83-86, 2005; (b) T. L. Sounart, J. Liu, J. A. Voigt,J. W. P Hsu, E. D. Spoerke, Z. Tian,Y. Jian, "Sequential Nucleation and Growth of Complex Nanostructured Films," *Advanced Functional Materials*, 16, 335-344, 2006; (c) Tian ZRR, JA Voigt, J Liu, B McKenzie, MJ McDermott, MA Rodriguez, H Konishi, and HF Xu. 2003"Complex and Oriented ZnO Nanostructures," *Nature Materials* 2(12):821-826; (d) Z. Tian, J. A. Voigt, J. Liu, B. Mckenzie, M. J. Mcdermott, "Biomimetic Arrays of Oriented Helical ZnO Nanorods and Columns," *J. Am. Chem. Soc*., 124, 12954-12955, 2002.
5. (a) Z. R. Tian, J. Liu, H. Xu, J. A. Voigt, B. Mckenzie, C. M. Matzke, "Shape-Selective Growth, Patterning, and Alignment of Cubic Nanostructured Crystals via Self-Assembly," *Nano Letters*, 83-86, 2003; (b) Z. R.Tian, J. Liu, J. A. Voigt, H. Xu, M. J. Mcdermott, "Dendritic Growth of Cubically Ordered Nanoporous Materials through Self-Assembly," *Nano Letters*, 3, 89-92, 2003; (c)Z. R. Tian, J. Liu, J. A. Voigt, B. Mckenzie, H. Xu, "Hierarchical and Self-Similar Growth of Self-Assembled Crystals," *Angew. Chem. Int. Ed*., 42, 413-417, 2003.
6. J. Liu, Y. Lin, L. Liang, J. A. Voigt, D. L. Huber, Z. R. Tian., E. Coker, B. Mckenzie, M. J. Mcdermott, "Templateless Assembly of Molecularly Aligned Conductive Polymer Nanowires: A New Approach for Oriented Nanostructures," *Chem.: A European J*. 9, 604-611, 2003.
7. L. Liang, J. Liu, C. F. Jr. Windisch, G. J. Exarhos, Y. Lin, "Direct Assembly of Large Arrays of Oriented Conducting Polymer Nanowires," *Angew. Chemie. Int. Ed*., 41, 3665-3668, 2002.

Selected Publications from the Project

1. D. Wang, D. Choi, J. Li, Z. Yang, Z. Nie, R. Kou, D. Hu, C. Wang, L. V. Saraf, J. Zhang, I. A. Aksay, J. Liu "Self-Assembled TiO_2-Graphene Hybrid Nanostructures for Enhanced Li-Ion Insertion," *ACS Nano*, ***cover article***, 3, 907-914, 2009.

2. L. -Q. Wang, D. Wang, J. Liu, G. J. Exarhos, S. Pawsey, I. Moudrakovski: "Probing Porosity and Pore Interconnectivity in Crystalline Mesoporous TiO_2 Using Hyperpolarized ^{129}Xe NMR," *J. Phys. Chem. C, 2009, 113 (16), pp 6485–6490.*

3. Wang D, D Choi, Z Yang, VV Viswanathan, Z Nie, CM Wang, Y Song, J Zhang, and J Liu. "Synthesis and Li-ion Insertion Properties of Highly Crystalline Mesoporous Rutile TiO_2." *Chemistry of Materials* 20(10):3435-3442, 2008.

4. Jun Liu, Guozhong Cao, Zhenguo Yang, Donghai Wang, Dan Dubois, Xiaodong Zhou, Gordon L. Graff, Larry R. Pederson, and Ji-Guang Zhang, "Oriented Nanostructures for Energy Conversion and Storage," *ChemSusChem*, 1, 676-697. ***Invited review***, ***cover article***, 2008.

5. L.-Q. Wang, X. –D. Zhou, C. Yao, G. J. Exarhos, C. F. Windisch Jr, L. R. Pederson, "Probing Proton Dynamics in ZnO Nanorods Quantified by *in situ* Solid-State ^{1}H Nuclear Magnetic Resonance Spectroscopy" *Applied Physics Letters*, 91, 173107 (2007).

6. L. –Q. Wang, S. Pawsey, I. Moudrakovski, G. J. Exarhos, J. Ripmeester, J. L. C. Rowsell and O. M. Yaghi "Hyperpolarized ^{129}Xe Nuclear Magnetic Resonance Studies of Isoreticular Metal-Organic Frameworks,"*J. of Phys. Chem. C. 111, 6060, 2007.*

Session IIb

The Nanoscale: Object Synthesis and Assembly

Session Chair: Hanchen Huang, University of Connecticut

(This page intentionally left blank.)

SYNTHESIS, CHARACTERIZATION, AND INVESTIGATION OF CHARGE SEPARATION AND RECOMBINATION IN CARBON AND METAL OXIDE NANOSTRUCTURES

Stanislaus S. Wong and James A. Misewich
Email: sswong@notes.cc.sunysb.edu
Condensed Matter Physics and Materials Sciences Department
Brookhaven National Laboratory
Upton, NY 11973

1. Program Scope

Since their discovery in 1991, carbon nanotubes (CNT) have been the focus of intense interest and potential for significant technological impact that has already been demonstrated, including a demonstration of the world's smallest complementary transistors and a demonstration, from one of the Principal Investigators (PIs), of the world's smallest electrically controllable light source. However, many challenges remain in the synthesis and characterization of the carbon nanotube materials family. Outstanding fundamental chemistry challenges include an enhancement of BNL's synthetic chemistry knowledge that would lead to better-defined control over the nature of carbon nanotubes. Ideally we would like higher purity materials, functionalized nanotubes, control of chirality and electronic structure of nanotubes, and an ability to assemble these materials into functional assemblies. In addition, fundamental physical problems include the development of a better understanding of the connection between structure and electronic states. This includes the development of an understanding of excitonic effects, which are expected to be large in quasi 1-d materials. Other challenges include a complete understanding of the emerging optoelectric properties of carbon nanotubes. Since the recently discovered electroluminescence in carbon nanotubes is a physically distinct method of producing light when compared with conventional semiconductor diode sources (e.g., the nanotube has no impurity doping profile and therefore no depletion field), progress in our fundamental understanding of this process has potential for application in diverse technological areas such as efficient lighting or for photovoltaic applications. Of particular interest are the properties of novel nanotube-quantum dot (CNT-QD) heterostructures, which have been synthesized by one of the PIs. This CNT-QD system combines a 1d system (CNT) with a 0d system (QD) in a new heterostructure in an attempt to combine the attractive charge transport and optical properties of each subsystem to produce a mixed dimensional hybrid with potential for efficient conversion of photons to separated electron and hole pairs for application in solar energy cells. The science of low-dimensional systems has advanced greatly in recent years; however, understanding and controlling the coupling of two low d systems with different dimensionality presents a new challenge that this research will address.

2. Recent Progress

We have demonstrated a covalent route towards site-selective synthesis of multiwalled carbon nanotube (MWNT)-nanoparticle conjugates containing two different types of nanoscale species, i.e. Au nanoparticles and CdSe quantum dots (QDs). We have quantitatively probed the effects of varying oxidation treatments, precursor concentrations, and incubation times in order to rationally affect the spatial coverage and distribution of either Au NPs or semiconducting QDs on the MWNT sidewalls and tips.

The degree of nanoparticulate coverage was found to primarily vary with the intensity of the oxidation treatment, though the hydrophobicity of the nanotube as well as the chemical and steric characteristics of the nanocrystals also played a role in determining the ultimate architecture. In general, the stronger the oxidation treatment, the denser the coating of nanoparticles and/or quantum dots on the nanotube surface. For instance, a combined H_2SO_4 / HNO_3 treatment with prolonged oxidation followed by sonication nondiscriminately and aggressively attacked the entire nanotube surface, creating a large number of defect sites not only at the ends but also along the sidewalls. In fact, this harsh protocol not only led to the highest percentage of gold nanoparticles that we were able to experimentally achieve along the sidewalls of the MWNTs (94.6 %) but also the highest overall density observed (20 particles / μm). In addition, the use of larger concentrations of precursor nanocrystals along with longer incubation times was also conducive to the observation of higher nanoparticle densities on our nanotube templates. For example, successively higher particle concentrations (50 to 200 mM) incubated with MWNTs yielded a correspondingly higher achievable density of Au nanoparticles. Finally, to determine the effect of incubation time on overall nanocrystal coverage on nanotube surfaces, we tested both CdSe and Au nanocrystals in the presence of oxidized MWNTs. H_2SO_4 /HNO_3-treated MWNTs were incubated with AET-CdSe nanocrystals for different incubation/reaction times of 0.5, 2, and 48 h with a constant CdSe concentration of 100 nM. The density of QDs increased significantly from a low of approximately zero particles per micron on the CNT surface to 71.3 particles / μm upon increasing incubation times from 0.5 to 48 h.

While none of these trends were perfect, our findings suggest a reasonable way of fabricating a series of novel CNT-nanocrystal/nanoparticle heterostructure composites with potentially tailorable electronic or optical properties. By controlling the additional oxidation time of MWNT-Au/CdSe starting materials, MWNT-Au-CdSe and MWNT-CdSe-Au conjugates with different percentages of NPs and QDs could be obtained (Figures 1 and 2). Interesting charge-transfer as well as energy transfer behavior between CNTs and the corresponding nanoparticles/quantum dots have been observed,[1, 2] and will likely render such conjugates as key components in a range of nanoscale devices important for photocatalytic and solar applications.

Recent Progress on Other Projects

Ambient Large-Scale Template-Mediated Synthesis of High-Aspect Ratio Single-Crystalline, Chemically Doped Rare-Earth Phosphate Nanowires

A simple, effective, and versatile template-directed method has been developed for the successful large-scale preparation of Tb-doped $CePO_4$ nanowires possessing very high aspect ratio, under ambient room temperature conditions. Sheaf-like bundles of ultrathin 1D nanostructures may initially form through a crystal splitting growth mechanism, followed by continuous growth out of template membrane pore channels, until they finally fracture in solution. This new synthetic approach is important not only because it involves a number of intriguing fundamental steps, but also because this environmentally benign route can be readily extended to the synthesis of other kinds of rare-earth phosphate nanomaterials either with or without dopants.

3. Future Plans

Covalently modifying the CNT surface using functional groups containing desirable, pendant moieties has been an important and popular method for creating CNT-based hybrid nanostructures because it is involves a relatively robust, straightforward, and facile protocol. There are several advantages to this particular approach. First, the shape and size of individual nanoparticles or nanocrystals can be easily tailored by sophisticated synthesis methods prior to combination with CNTs, thereby mitigating the influence of the CNTs themselves on the nucleation and growth processes of either nanoparticles or quantum dots. Secondly, covalent bonds can rigidly connect the linker molecules and CNTs in a reliable and robust manner, such that the nanoparticles will not become easily dislodged even after either sonication or extensive washing. Third, the physical integrity and hence, corresponding optoelectronic properties of a double-walled carbon nanotube (DWNT) structure need not be necessarily compromised. Therefore, we have recently been working on the covalent, linker-mediated synthesis of a DWNT-NC heterostructure, prepared by anchoring derivatized CdSe quantum dots (QDs) onto the surface of complementarily functionalized DWNTs. The resulting heterostructure should possess interesting optical characteristics including photoluminescent behavior.

In our recent results, we have demonstrated that a conventional covalent approach can be applied to the reliable and reproducible synthesis of DWNT-CdSe heterostructures. In addition, the optical properties of our DWNT-CdSe heterostructures suggest that the likelihood of intertwining interactions between QDs and DWNTs that govern their overall photophysical behavior. Importantly, we should note that the interpretation of our results may have been complicated by the presence of MWNTs in our DWNT samples. Our data highlight the caveat that ostensibly good-quality commercial samples are often contaminated by a relatively large quantity of non-DWNT-containing structures. Thus, while additional experimental and theoretical studies on the effect of chemical functionalization on the properties of DWNTs are still needed, the experimental evidence thus far suggests that DWNT-QD heterostructures exhibit potential for incorporation into devices such as photovoltaic cells.

4. References

1. Lee, J.; Javed, T.; Skeini, T.; Govorov, A. O.; Bryant, G. W.; Kotov, N. A., Bioconjugated Ag nanoparticles and CdTe nanowires: Metamaterials with field-enhanced light absorption. *Angewandte Chemie-International Edition* **2006,** *45*, (29), 4819-4823.
2. Govorov, A. O.; Bryant, G. W.; Zhang, W.; Skeini, T.; Lee, J.; Kotov, N. A.; Slocik, J. M.; Naik, R. R., Exciton-plasmon interaction and hybrid excitons in semiconductor-metal nanoparticle assemblies. *Nano Letters* **2006,** *6*, (5), 984-994.

5. Relevant Publications over the last two years.

Xiaohui Peng, Jingyi Chen, James A. Misewich, and Stanislaus S. Wong, "Carbon Nanotube-Nanocrystal Heterostructures", invited Critical Review, *Chem. Soc. Rev.* (inside cover), **38(4),** 1076-1098 (2009).

Xiaohui Peng and Stanislaus S. Wong, "Controlling Nanocrystal Density and Location on Carbon Nanotube Templates", *Chem. Mater.,* **21(4),** 682-694 (2009).

Xiaohui Peng and Stanislaus S. Wong, "Functional Covalent Chemistry of Carbon Nanotube Surfaces", invited Progress Report, *Adv. Mater.*, **21(6),** 625-642 (2009).

Mandakini Kanungo, Hugh S. Isaacs, and Stanislaus S. Wong, "Quantitative Control over Electrodeposition of Silica films onto Single-Walled Carbon Nanotube Surfaces", invited contribution (Richard E. Smalley Memorial issue), *J. Phys. Chem. C*, **111(48),** 17730-17742 (2007).

An additional 12 sponsored publications in 2007-2009 from current/preceding grants.

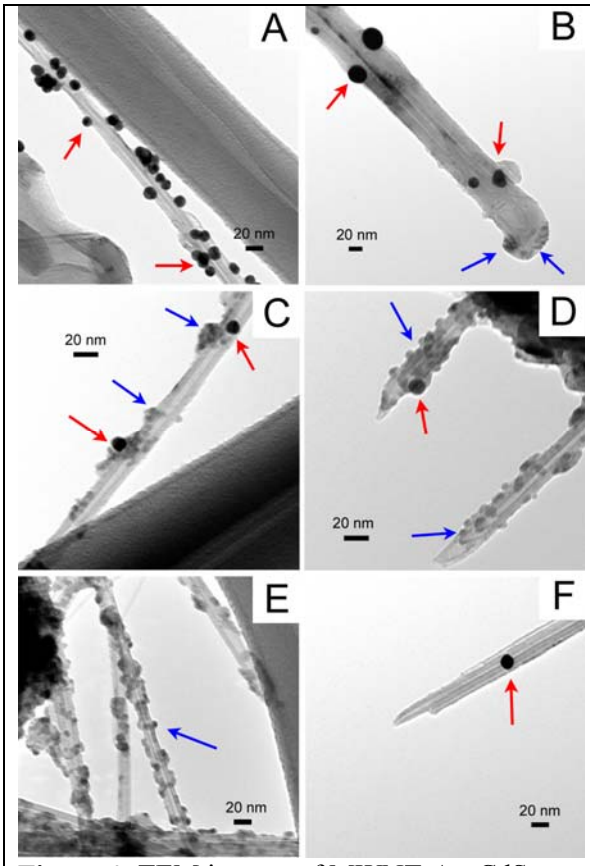

Figure 1. TEM images of MWNT-Au-CdSe conjugates. MWNT-Au (red arrows) were reacted with AET-CdSe nanocrystals (blue arrows) in the presence of EDC for 2 days, followed by additional oxidation in 1 M HNO_3 for (A) 0.5 h, (B) 1 h, (C) 6 h, (D) 12 h, and (E) 24 h; (F) MWNT-Au conjugate after 1 M HNO_3 oxidation for 24 h without incubation with AET-CdSe nanocrystals. MWNTs were initially oxidized using a H_2SO_4 /HNO_3 treatment.

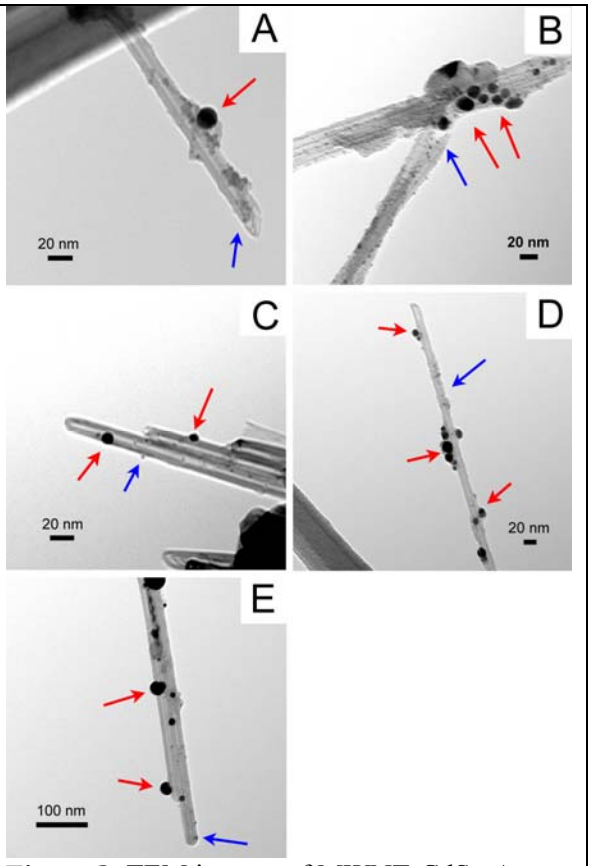

Figure 2. TEM images of MWNT-CdSe-Au conjugates. MWNT-CdSe conjugates (blue arrows) were thiolated and subsequently incubated with Au NPs (red arrows) for 2 h, following an additional oxidation in 1 M HNO_3 for (A) 0.5 h, (B) 1 h, (C) 6 h, (D) 12 h, and (E) 24 h. MWNTs were oxidized by a H_2SO_4 /HNO_3 treatment.

Non-Equilibrium Synthesis of Nanostructured Materials: Laser-Induced Processes

David Geohegan[1,2], Alex Puretzky[1,2], Christopher Rouleau[1,2], Mina Yoon[2], Gyula Eres[2], Jeremy Jackson[1,2], Karren More[2], and Gerd Duscher[3]
geohegandb@ornl.gov
[1]Center for Nanophase Materials Sciences and [2]Materials Science and Technology Divison
Oak Ridge National Laboratory, Oak Ridge, TN 37831
and the [3]Dept. of Materials Science and Engineering, Univ. of Tennessee, Knoxville, 37996

Program Scope

The spatial confinement and unique atomic configurations which determine the electronic energy levels, chemical reactivity, and physical properties of nanomaterials are often determined during their synthesis. However, theoretical calculations show that energy barriers can severely limit the number of interesting structural and compositional configurations formed under equilibrium synthesis conditions. This program explores the influence of thermodynamic and kinetic pathways on the formation of nanomaterials in metastable configurations with an approach which couples in situ, real-time diagnostics of growth conditions and growth kinetics with ex situ atomic scale characterization, and forefront computer modeling and simulation. Both high- and low-temperature non-equilibrium synthesis routes are explored, and the competition between catalyst-free self assembly of nanostructures and catalyst-activated growth mechanisms are investigated.

Non-equilibrium growth processes utilizing pulsed laser interactions and pulsed gas jets are investigated. Laser vaporization provides high kinetic energies to overcome energy barriers, and interactions with background gases or liquids provide the spatial confinement, transient thermal gradients, and chemical reactivity required to stabilize unique nanostructures with novel properties. In situ imaging, spectroscopy, and plasma diagnostics are used to understand the principal ejecta from laser-irradiated targets, and their subsequent self-assembly or catalyst-assisted assembly into novel nanostructures in these environments. Of special interest are synthesis processes resulting in 1) oxide, carbon, and alloy nanomaterials produced in metastable states by catalyst-free or catalyst-mediated processes, 2) doped, decorated, and filled nanomaterial hybrids designed to induce permanent electric fields or distribute charge within nanostructures.

Recent Progress

Non-equilibrium methods are used to produce single-wall carbon nanohorns (SWNHs) that are produced *without catalyst* by laser- or arc-vaporizing pure carbon into a background gas.[1] Despite the application of time-resolved, in situ diagnostics,[2,3] the understanding of how carbon self-assembles so efficiently into single-wall carbon tubules under these non-equilibrium conditions remains a major question which relates more generally to the formation of graphene, endohedral fullerenes,[4] and related materials such as boron nitride nanohorns.[5] Recently, we investigated the factors influencing the growth rates, size, and morphology of SWNHs and their ball-shaped aggregates by varying the growth times, temperatures, and spatial confinement of ablation plumes using a high-power pulsed laser with tunable pulse width, repetition rate, and energy per pulse. In situ pyrometery of the target temperature was used to develop a 3D model of heat transfer and an efficient laser ablation approach for the synthesis of SWNHs with uniform sizes and morphologies. Figure 1 shows the two regimes of laser ablation that we explored: *continuous* ablation that provides sustained temperatures sufficient for self-organization of the ablated species into "long" SWNH units and *cumulative* ablation which is optimal for growth of "short" SWNHs. Comparing *ex situ* high resolution transmission electron microscopy (HRTEM) analysis and pore size distributions of the products with the growth times measured by *in situ* videography and pyrometry we revealed that the length of the nanohorns varied, and correlated well with the time spent within the high temperature growth zone, with the length increasing at a rate of ~1 nm/ms of available growth time. This growth rate indicates that C *self-assembles* into nanostructures at rates comparable to some of the highest measured previously for *catalyst-assisted* nanotube growth.

Controlling the non-equilibrium growth conditions allowed variation of not only the individual nanohorn structure but also the aggregate size. At present the two are linked. Understanding the dynamics of the aggregation process is important to control the size and porosity of aggregates formed by this "bottom-up" self-assembly process. The size, shape, and porosity of the aggregated nanomaterials are very important for possible applications of these materials (e.g., in supercapacitors, hydrogen storage, and drug delivery).[6-8] Since the nanohorn aggregates are found to be strongly welded together, we must consider not only the formation of the nanohorn subunit but also their aggregation and annealing, as these determine important characteristics such as porosity, internal structure, and bonding.

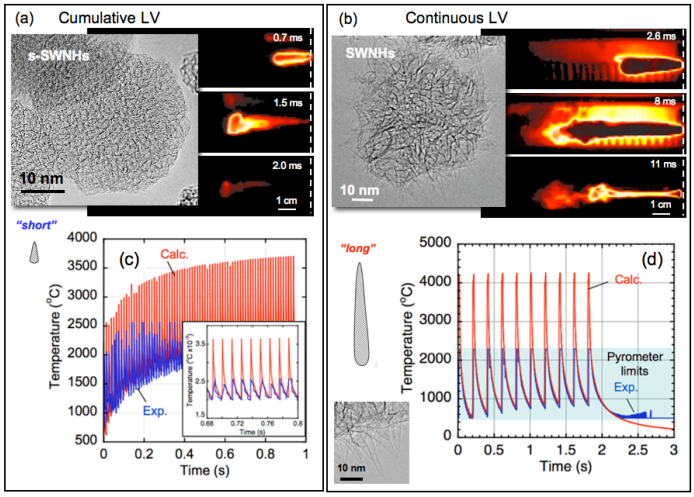

Figure 1. (**top**) Micrographs of SWNHs synthesized using short, multiple laser shots and long, less frequent laser shots - (**a**) and (**b**), respectively. Also shown are side on images of the laser plume at 3 different times after the laser fires, indicating that the plume is 'on' for far longer in the continuous LV case. This promotes longer annealing times at high temperature, thereby producing longer SWNH subunits. (**bottom**) Time-resolved pyrometric data acquired during cumulative- and continuous-LV - (**a**) and (**b**), respectively. Note that it takes almost 400ms for the target to reach 3500C in the cumulative case, where as it takes orders of magnitude less in the continuous case. (Ref. 5)

To explore the competition between catalyst-assisted and catalyst-free carbon nanostructure growth, metal catalysts such as Ni or Co were co-vaporized with carbon under the optimal conditions for SWNH growth. Under these conditions, the self-assembly of C into SWNHs was found to compete comparably with SWNT formation. To optimize SWNT formation over SWNH formation, the plume temperature must be rapidly reduced to near the carbon-metal eutectic temperature and sufficient growth time must be provided for the SWNT nuclei to consume the nearby carbon sheets and clusters to assemble long SWNTs by condensed phase conversion.[9] Under these conditions, the carbon clusters condense first, followed ~1 ms later by condensation of the metal vapor after the plume had cooled to ~1500°C. Ideally, one could prepare the metal catalysts prior to the formation of the C nanoparticles to understand how metal nanoparticles interact with the carbon precursors.

The self-assembly of carbon nanohorns is correlated with times spent at high temperatures. Calculations of minimum energy configurations for stable nanostructures, including the effects of defect inclusion and entropy, were performed to understand the driving forces for the synthesis of different carbon nanostructures formed at high temperatures. Nanohorns were predicted to form preferentially, as compared to graphene or nanotubes, at temperatures $1500 < T < 2900$K due to the entropy gain from defect formation vs. strain energy. However, if hydrogen gas was included to terminate dangling bonds, the stability favored hydrogen-terminated graphene.

Recent experiments have confirmed these predictions. Experiments performed under typical nanohorn growth conditions, however using hydrogen as an additional background gas to argon, reveal an evolution of morphologies with increasing hydrogen pressure and the production of open graphene flakes, as shown in Figure 2(a),(b). Z-Contrast STEM image intensity analysis reveal that single-layer open carbon sheets are formed, as well as 2, 3, and more layers. The hydrogen apparently interrupts the nanohorn closure process, lending support to the theory that SWNHs are formed from the closure of partially-formed graphene sheets.

Metal atoms introduced into the growth environment often change the product distribution in non-equilibrium synthesis, and their effect is typically referred to as catalytically-induced growth. While metal atoms can be incorporated in the nanostructure (as in endohedral fullerenes)[4] most often they co-condense into nanoparticles to serve as nucleation centers for the growth of nanotubes and nanowires, providing alternative pathways when self-assembly processes are absent. For example, Figure 2(e) shows

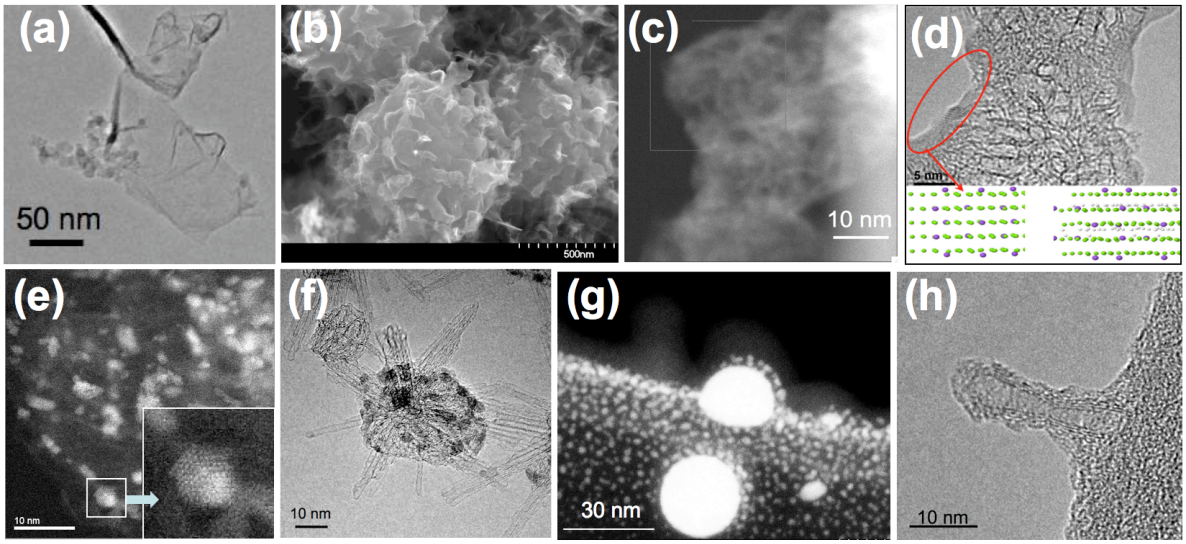

Figure 2. Variety of nanostructures synthesized by laser-induced processes. Laser-vaporization (LV)-produced (a) graphene sheets and their (b) micron-sized aggregates. SWNHs produced by LV, then oxidized and smoothly-coated by Ca (c) Z-contrast HAAC-STEM and (d) HRTEM bright field micrographs. (e) Z-contrast images of Gd layers on SWNHs as-synthesized by LV. (f) HRTEM of SWNT "urchins" radiating from Gd nanoparticles formed by co-ablation. (g) AuAl alloy nanoparticles from fs-laser ablation in vacuum. (h) Polymer-encapsulated single SWNHs.

high resolution TEM images of Gd flakes which have condensed on SWNHs during their aggregation, while (within the same sample) Figure 2(f) shows larger Gd nanoparticle aggregates which catalytically-induce the growth of SWNT "urchin" structures.

Modeling efforts to understand the interactions of metals with C nanostructures have been undertaken to determine the pathways and energy barriers for the formation of 3D structures, and to predict which metals may form smooth coatings on nanostructured carbons (e.g. Figure 3 for Ti). Alkaline earth metals, including Sr and Ca, are predicted to form smooth coatings on C due to charge transfer interactions. [4] These coatings have recently been verified by Z-STEM and EELS, as shown in Fig. 2(c),(d).

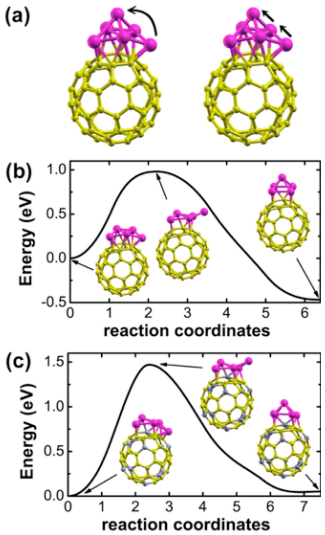

Figure 3. (a) Two possible mechanisms of 2D layer to 3D cluster transformation for Ti_5C_{60} complex, i.e., direct hopping (left) and position exchange (right). Energy barriers of direct hopping for Ti_5C_{60} (b) and for $Ti_5C_{48}B_{12}$ (c). (Ref. 9)

Future Plans

Hybrid nanostructures which distribute charge to produce new properties will be investigated theoretically and experimentally. For example we predict that the creation of a high electric field at the surface of atomic-layer Ca-coated C-nanostructures will significantly alter the adsorption binding energies of molecules such as hydrogen. Similarly, controlling the composition and interfaces in plasmonic or donor/acceptor hybrid nanomaterials is fundamental to control their optoelectronic properties. We will utilize pulsed laser vaporization to prepare new doped, decorated, and filled, 'charged nanostructures' through controllable synthesis and coating of nanomaterials in special, windowed reactors utilizing pulsed laser and gas delivery. Separate lasers will be used for synthesis of nanoparticles, coating or modification, and *in situ* spectroscopy and imaging diagnostics. Direct synthesis of nanoparticles by laser-induced phase explosion will be explored. Through differential control between synthesis and coating in the gas phase, we hope to understand and control the synthesis of core-shell nanostructures, metastable alloy nanoparticles, and ultra-thin films

of metals (such as Ca, Mg, and Al) on nanoparticle and carbon supports for comparison with theoretical predictions. We plan to characterize such structures using Z-STEM and EELS or vibrational spectroscopy and high-resolution electron microscopy. The optical properties of the nanoparticles will be probed *in situ* as they grow, while their performance as catalysts for synthesis will be assessed by introducing the nanoparticles directly into CVD growth reactors.

References

1. S. Iijima, M. Yudasaka, R. Yamada, S. Bandow, K. Suenaga, F. Kokai, and K. Takahashi, *Chem. Phys. Lett.* **309** (3-4), 165-170 (1999).
2. F. Kokai, K. Takahashi, D. Kasuya, M. Yudasaka, and S. Iijima, *Appl. Surf. Sci.* **197**, 650-655 (2002); D. Kasuya, M. Yudasaka, K. Takahashi, F. Kokai, and S. Iijima, *J. Phys. Chem. B* **106** (19), 4947-4951 (2002).
3. M. D. Cheng, D. W. Lee, B. Zhao, H. Hu, D. J. Styers-Barnett, A. A. Puretzky, D. W. DePaoli, D. B. Geohegan, E. A. Ford, and P. Angelini, *Nanotechnol.* **18** (18), 185604 (2007).; A. A. Puretzky, D. J. Styers-Barnett, C. M. Rouleau, H. Hu, B. Zhao, I. N. Ivanov, and D. B. Geohegan, *Appl. Phys. A* **93** (4), 849-855 (2008).
4. T. Akasaka and N. Nagase, *Endofullerenes: A New Family of Carbon Clusters*. (Kluwer Academic, Dordrecht, 2002).
5. C. Zhi, Y. Bando, C. Tang, D. Golberg, R. Xie, and T. Sekiguchi, *Appl. Phys. Lett.*, **87**, 063107 (2005).
6. C. M. Yang, Y. J. Kim, M. Endo, H. Kanoh, M. Yudasaka, S. Iijima, and K. Kaneko, *J. Am. Chem. Soc.* **129** (1), 20-21 (2007).
7. H. Tanaka, H. Kanoh, M. El-Merraoui, W. A. Steele, M. Yudasaka, S. Iijima, and K. Kaneko, *J. Phys. Chem. B* **108** (45), 17457-17465 (2004).
8. T. Murakami, H. Sawada, G. Tamura, M. Yudasaka, S. Iijima, and K. Tsucbida, *Nanomed.* **3** (4), 453-463 (2008).
9. D. B. Geohegan, H. Schittenhelm, X. Fan, S. J. Pennycook, A. A. Puretzky, M. A. Guillorn, D. A. Blom, and D. C. Joy, *Appl. Phys. Lett.* **78** (21), 3307-3309 (2001).

DOE Sponsored Publications 2008-2009 from Current Grant (selected of 24)

1. D. B. Geohegan, A. A. Puretzky, C. M. Rouleau, J. J. Jackson, G. Eres, Z. Liu, D. Styers-Barnett, H. Hu, B. Zhao, K. Xiao, I. Ivanov, and K. More, "*Laser Interactions in Nanomaterials Synthesis"*, Book Chapter in *Springer Series in Materials Science* (2009).
2. G. Eres, C.M. Rouleau, M. Yoon, A.A. Puretzky, D.B. Geohegan, "*Model for Self Assembly of Carbon Nanotubes from Acetylene Based on Real-Time Studies of Vertically Aligned Growth Kinetics"*, J. Phys. Chem. C 113, 15484 (2009).
3. M. Yoon, S. Yang, and Z. Zhang, *"Interaction between hydrogen molecules and metallofullerenes*", J. Chem. Phys. 131, 064707 (2009).
4. M. Yoon, S. Yang, C. Hicke, E. Wang, D. Geohegan, and Z. Zhang *"Calcium as the superior coating metal in functionalization of carbon fullerenes for high-capacity hydrogen storage." Phys. Rev. Lett.* **100**(20), 206806 (2008).
5. A. A. Puretzky, G. Eres, C.M. Rouleau, I. N. Ivanov, and D. B. Geohegan *"Real-time imaging of vertically aligned carbon nanotube array growth kinetics." Nanotechnol.* **19**(5) 055605 (2008).
6. A. A. Puretzky, D. Styers-Barnett, C. M. Rouleau, B. Zhao, H. Hu, I. N. Ivanov D. B. Geohegan, *"Cumulative and Continuous Synthesis of Single Wall Carbon Nanotubes and Nanohorns" Appl. Phys. A* **93**(4), 849-855 (2008).
7. Z. Liu, D. J. Styers-Barnett, A. A. Puretzky, C. M. Rouleau, D. Yuan, I. N. Ivanov, K. Xiao, J. Liu, and D. B. Geohegan, *"Pulsed Laser CVD Investigations for Single-Wall Carbon Nanotube Growth Dynamics", Appl. Phys. A* **93**(4), 987-993 (2008).
8. S. Yang, M. Yoon, C. Hicke, E. Wang, and Z. Zhang, "*Electron transfer and localization in endohedral metallofullerenes: Ab initio density functional theory calculations"*, *Phys. Rev. B* **78**, 115435 (2008).
9. S. Yang, M. Yoon, E. Wang, and Z. Zhang, "*Energetics and kinetics of Ti clustering on neutral and charged C_{60} surfaces"*, *J. Chem. Phys.* **129**, 13407 (2008).
10. C.M. Rouleau, G. Eres, H. Cui, H.M. Christen, A.A. Puretzky, D.B. Geohegan, "*Altering the catalytic activity of thin metal catalyst films for controlled growth of chemical vapor deposited vertically aligned carbon nanotube arrays*" , *Appl. Phys. A* **93**(4), 1005-1009 (2008).

Low-Temperature Synthesis Routes to Intermetallic Superconductors

Raymond E. Schaak
res20@psu.edu
Department of Chemistry and Materials Research Institute
The Pennsylvania State University, University Park, PA 16802

Program Scope

Superconducting materials pass current without resistance and have high current-carrying capabilities, making them central to applications that underpin our energy infrastructure. Among the many classes of materials that exhibit superconductivity, intermetallic superconductors play a prominent role in both modern research and applications. Therefore, improving their properties and performance, as well as discovering new superconducting intermetallic compounds, is an important research thrust. Intermetallic superconductors are traditionally synthesized using high-temperature, high-pressure, thin film, or gas-phase vacuum deposition methods. Our group has been developing alternative low-temperature solution chemistry techniques for synthesizing intermetallic compounds, using conditions that facilitate the formation of a large number of known and new transition metal intermetallics as bulk-scale crystals and powders, as well as size- and shape- controlled nanoparticles. The proposed project goals involved developing and applying solution chemistry methods for accessing elusive and metastable intermetallic compounds, controlling particle size and crystallite morphology for superconducting nanocrystals, scaling up reactions to facilitate the synthesis of bulk powders and crystals, and discovering new compounds and materials using previously unexplored synthetic conditions. Toward these goals, we set out to approach the synthesis of Nb_3M (*M* = Ga, Ge, Sn), Bi-*M* (*M* = In, Cu), and analogues of $MgCNi_3$ as model systems for studying the formation, stability, and properties of intermetallic superconductors made using this previously unexplored chemical synthesis regime. Tackling these goals required us to address several fundamental scientific challenges involving the chemical synthesis of bulk-scale and nanostructured metals and intermetallics – (a) incorporating early transition metals and post transition metals into nanoscale and bulk crystals using low-temperature solution chemistry methods, (b) targeting a particular phase in a binary system that contains multiple stable phases, (c) accessing non-equilibrium, metastable, or low-temperature intermetallic phases, (d) synthesizing crystalline metal borides and carbides using direct solution chemistry methods, and (e) scaling up syntheses for processing into monoliths, bulk-scale powders, and crystals.

Recent Progress

As a result of this research, we learned how to access nanoparticles and bulk powders of compounds containing elements that are typically very challenging to incorporate using standard solution-based syntheses: Nb, Mo, W, Mn, Zn, Ga, Ge, and In. We established guidelines for accessing multiple stable compounds in a given binary system for phase-selective synthesis. We discovered several new non-equilibrium intermetallics and found straightforward methods for synthesizing low-temperature phases that are challenging to prepare using traditional high-temperature methods. We generated several nanocrystalline metal carbides, borides, and hydrides directly in solution. Finally, we developed a novel benchtop "beaker chemistry" method to form bulk powders and mm-scale single crystals of superconducting intermetallics.

Our most recent progress is highlighted below. The fundamental scientific advances that have resulted from this research have also impacted other aspects of energy-related research, including catalysis, thermoelectrics, hydrogen storage, and batteries.

Our most recent non-equilibrium targets were the $L1_2$-type Au_3M (M = Fe, Co, Ni) intermetallics, which have not previously been isolated as bulk solids yet are of interest for their coupled magneto-optical properties.[1] We can synthesize bulk quantities of these $L1_2$-type intermetallics as nanocrystals using air-free solution chemistry methods. The Au_3Fe nanocrystals are superparamagnetic with T_B = 12 K, which differs from the magnetic behavior exhibited by nanocrystalline Fe, FeO_x, and Fe-Au alloys.[2] We have also developed straightforward chemical methods for accessing high-quality nanocrystals in elemental systems that have either been elusive, not of acceptable quality, or have required prohibitively harsh chemistry.[3,4] The first air-stable spherical nanocrystals of α-Mn were synthesized using air-free solution chemistry methods, and they are paramagnetic with no evidence of the antiferromagnetism exhibited by bulk α-Mn. Room-temperature benchtop chemistry methods, using water and isopropanol as solvents, were used to synthesize size- and shape-controlled nanocrystals of Ge and In. The In nanocrystals are superconducting with significantly higher critical fields than bulk In.

We also developed a benchtop "beaker chemistry" method for combining and reacting bulk elemental powders in high-boiling glycol or fatty acid solvents (T_B > 300 °C) to form bulk powders and single crystals of intermetallic compounds such as SbSn, $FeSn_2$, Cu_6Sn_5, $CoSn_3$, Ni_3Sn_4, $FeGa_3$, $NiGa_4$, Cu_9Ga_4, $CoGa_3$, Ni_2In_3, InSb, and BiIn, as well as the superconducting intermetallics Bi_3In_5, $BiIn_2$, and Bi_3Ni and the low-temperature phase $CoSn_3$. Modifications to these techniques can also generate bulk powders of $Bi_{0.5}Sb_{1.5}Te_3$ and $AgSbTe_2$, which are recently-reported thermoelectric materials.[5] Preliminary measurements on gram-scale sintered pellets of nanostructured $Bi_{0.5}Sb_{1.5}Te_3$ indicate that they are p-type with a room-temperature Seebeck coefficient of ~ 200 μV/K, which compares favorably with prior reports.[5] Finally, we have applied our solution chemistry tools to the new superconducting FeSe system, generating single-crystal nanosheets (2-3 nm thick × 200-1000 nm laterally) of PbO-type FeSe, as well as FeTe, $FeTe_2$, and members of the Fe(Se,Te) and Fe(Te,S) solid solutions. Magnetic measurements showed no evidence of the Meissner effect that would indicate superconductivity, which is interesting and could be due to the finite thickness of the sheets and/or non-optimal composition. These results all feed cohesively into the project goals: developing solution chemistry methods for synthesizing nanocrystalline and bulk intermetallic superconductors at low temperatures, with particular emphasis on discovering new non-equilibrium phases and exploring the physical properties in comparison with analogous materials made by more traditional methods.

Future Plans

We are focusing on applying our low-temperature solution chemistry techniques to the targeted and exploratory synthesis of new and non-equilibrium intermetallics of relevance to superconductivity and other energy-related applications. We are also expanding our crystal growth efforts in order to establish the maximum size and purity achievable, as well as the properties of these crystals. We hypothesize that single crystals of low-temperature and non-equilibrium phases should be achievable, and (in analogy to flux-based syntheses[6]) new phases should be able to be discovered. Finally, we are applying a suite of chemical tools to the FeSe

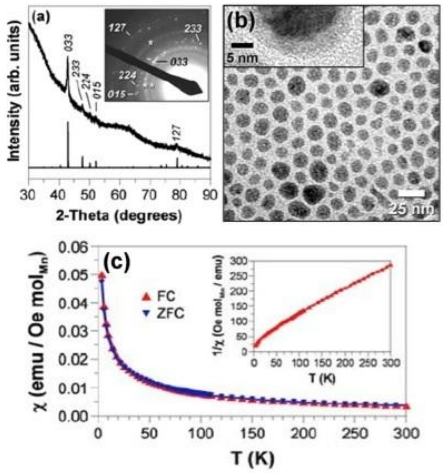

XRD, TEM, and χ vs. T data for Mn nanoparticles

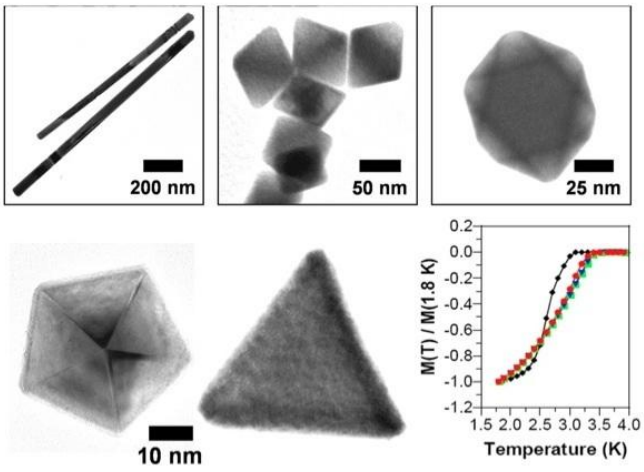

TEM images and M vs. T data (100 Oe) for In nanoparticles.

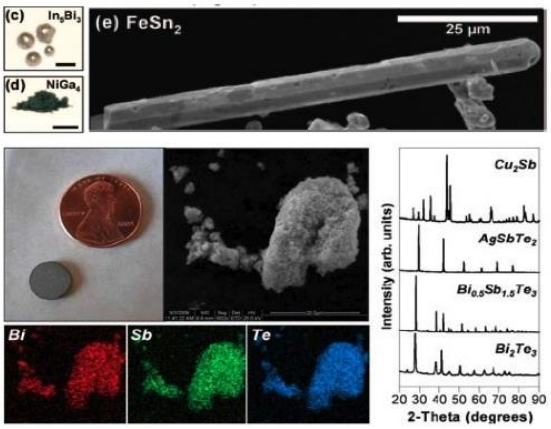

Top: Bulk products of intermetallics synthesized using "beaker chemistry." Bottom: Bulk sintered pellet and SEM data for nanostructured $Bi_{0.5}Sb_{1.5}Te_3$ powder.

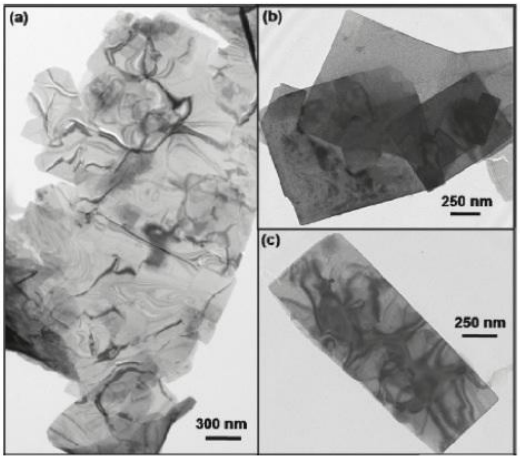

TEM images of single crystal PbO-type FeSe nanosheets.

superconductor system[7] in order to simultaneously fine-tune several key parameters and study unique aspects of the superconducting behavior in this and related systems.

References

1. (a) Sargolzaei, M.; Opahle, I.; Richter, M. *Phys. Status Solidi B* **2006**, *243*, 286–289. (b) Reichert, H.; Schops, A.; Ramsteiner, I. B.; Bugaev, V. N.; Shchyglo, O.; Udiansky, A.; Dosch, H.; Asta, M.; Drautz, R.; Honkimaki, V. *Phys. Rev. Lett.* **2005**, *95*, 235703. (c) Wolverton, C.; Zunger, A. *Comput. Mater. Sci.* **1997**, *8*, 107–121.
2. (a) Taniguchi, T.; Yamanaka, K.; Sumioka, H.; Yamazaki, T.; Tabata, Y.; Kawarazaki, S. *Phys. Rev. Lett.* **2004**, *93*, 246605–4. (b) Chiang, I-C.; Chen, D.-H. *Adv. Funct. Mater.* **2007**, *17*, 1311–1316.
3. (a) Ward, M. B.; Brydson, R.; Cochrane, R. F. *J. Phys.: Conf. Ser.* **2006**, *26*, 296. (b) Si, P. Z.; Brueck, E.; Zhang, Z. D.; Tegus, O.; Zhang, W. S.; Buschow, K. H. J.; Klaasse, J. C. P. *Mater. Res. Bull.* **2005**, *40*, 29.
4. (a) Wu, F.-Y.; Yang, C. C.; Wu, C.-M.; Wang, C.-W.; Li, W.-H. *J. Appl. Phys.* **2007**, *101*, 09G111. (b) Khanna, P. K.; Jun, K.-W.; Hong, K. B.; Baeg, J.-O.; Chikate, R. C.; Das, B. K. *Mater. Lett.* **2005**, *59*, 1032. (c) Tsai, K.-L.; Dye, J. L. *J. Am. Chem. Soc.* **1991**, *113*, 1650. (d) Soulantica, K.; Maisonnat, A.; Fromen, M.-C.; Casanove, M.-J.; Lecante, P.; Chaudret, B. *Angew. Chem., Int. Ed.* **2001**, *40*, 448. (e) Taylor, B. R.; Kauzlarich, S. M.; Delgado, G. R.; Lee, H. W. H. *Chem. Mater.*

1999, *11*, 2493. (f) Gerung, H.; Bunge, S. D.; Boyle, T. J.; Brinker, C. J.; Han, S. M. *Chem. Commun.* **2005**, 1914. (g) Lu, X.; Ziegler, K. J.; Ghezelbash, A.; Johnston, K. P.; Korgel, B. A. *Nano Lett.* **2004**, *4*, 969. (h) Lee, D. C.; Pietryga, J. M.; Robel, I.; Werder, D. J.; Schaller, R. D.; Klimov, V. I. *J. Am. Chem. Soc.* **2009**, *131*, 3436.

5. (a) Poudel, B.; Hao, Q.; Ma, Y.; Lan, Y.C.; Minnich, A.; Yu, B.; Yan, X.; Wang, D.Z.; Muto, A.; Vashaee, D.; Chen, X.Y.; Liu, J.M.; Dresselhaus, M.S.; Chen, G.; Ren, Z. *Science* **2008**, *320*, 634. (b) Wang, H.; Li, J.F.; Zou, M.M.; Sui, T. *Appl. Phys. Lett.* **2008**, *93*, 202106.
6. Kanatzidis, M.G.; Pottgen, R.; Jeitschko, W. *Angew. Chem. Int. Ed.* **2005**, *44*, 6996.
7. Wen, H.-H. *Adv. Mater.* **2008**, *20*, 3764-3769.

Publications (2007 – 2009, from this DOE grant)

1. Cable, R.E.; Schaak, R.E. "Solution Synthesis of Nanocrystalline *M*-Zn (*M* = Pd, Au, Cu) Intermetallic Compounds via Chemical Conversion of Metal Nanoparticle Precursors," *Chem. Mater.* **2007**, *19*, 4098-4104.
2. Henderson, N.L.; Baek, J.; Halasyamani, P.S.; Schaak, R.E. "Ambient Pressure Synthesis of SHG-Active $Eu_2Ti_2O_7$ with a [110] Layered Perovskite Structure: Suppressing Pyrochlore Formation by Oxidation of Perovskite-Type $EuTiO_3$," *Chem. Mater.* **2007**, *19*, 1883-1885.
3. Henderson, N.L.; Schaak, R.E. "Low Temperature Solution-Mediated Synthesis of Polycrystalline Intermetallic Compounds from Bulk Metal Powders," *Chem. Mater.* **2008**, *20*, 3212-3217.
4. Vasquez, Y.; Henkes, A.E.; Bauer, J.C.; Schaak, R.E. "Nanocrystal Conversion Chemistry: A Unified and Materials-General Strategy for the Template Based Synthesis of Nanocrystalline Solids," *J. Solid State Chem.* **2008**, *181*, 1509-1523.
5. Chou, N.H.; Schaak, R.E. "Room-Temperature Chemical Synthesis of Shape-Controlled Indium Nanoparticles," *J. Am. Chem. Soc.* **2008**, *130*, 8140-8141.
6. Vasquez, Y.; Luo, Z.; Schaak, R.E. "Low-Temperature Solution Synthesis of the Non-Equilibrium Ordered Intermetallic Compounds Au_3Fe, Au_3Co, and Au_3Ni as Nanocrystals," *J. Am. Chem. Soc.* **2008**, *130*, 11866-11867.
7. Schaefer, Z.L.; Ke, X.; Schiffer, P.E.; Schaak, R.E. "Direct Solution Synthesis, Reaction Pathway Studies, and Structural Characterization of Crystalline Ni_3B Nanoparticles," *J. Phys. Chem. C* **2008**, *112*, 19846-19851.
8. Henderson, N.L.; Straesser, M.D.; Sabato, P.D.; Schaak, R.E. "Toward Green Metallurgy: Low-Temperature Solution Synthesis of Bulk-Scale Intermetallic Compounds in Edible Plant and Seed Oils," *Green Chem.* **2009**, *11*, 974-978.
9. Liu, Q.; Yan, H.; Bauer, J.C.; Henderson, N.L.; Goodman, D.W.; Batteas, J.D.; Schaak, R.E. "Synthesis of CuPt Nanorod Catalysts with Tunable Lengths," *J. Am. Chem. Soc.* **2009**, *131*, 5720-5721.
10. Phan, T.H.; Schaak, R.E. "Polyol Synthesis of Palladium Hydride: Bulk Powders vs. Nanocrystals," *Chem. Commun.* **2009**, 3026-3028.
11. Avery, K.N.; Schaak, J.E.; Schaak, R.E. "M13 Bacteriophage as a Biological Scaffold for Magnetically-Recoverable Metal Nanowire Catalysts: Combining Specific and Non-Specific Interactions to Design Multi-Functional Nanocomposites," *Chem. Mater.* **2009**, *21*, 2176-2178. [Featured in ***Chemical & Engineering News***]
12. Bondi, J.F.; Oyler, K.D.; Chou, N.H.; Ke, X.; Schiffer, P.E.; Schaak, R.E. "Chemical Synthesis of Manganese Nanoparticles," *J. Am. Chem. Soc.* **2009**, *131*, 9144-9145.
13. Oyler, K.D.; Ke, X.; Sines, I.T.; Schiffer, P.E.; Schaak, R.E. "Chemical Synthesis of Lamellar FeSe, FeTe, and Fe(Se,Te) Nanocrystals," *Chem. Mater.* **2009**, *21*, 3655-3661.
14. Chou, N.H.; Oyler, K.D.; Motl, N.M.; Schaak, R.E. "Colloidal Synthesis of Germanium Nanocrystals Using Room-Temperature Benchtop Chemistry," *Chem. Mater.* **2009**, *21*, ASAP Article [DOI: 10.1021/cm902088y].

Probing the Interaction Between Magnetic Vortices and Periodic Pinning Through Patterned Nanoribbons of High-temperature Superconductors

Zhili Xiao
zxiao@niu.edu
Department of Physics, Northern Illinois University, DeKalb, Illinois 60115

Program Scope

Superconducting nanowires have been a subject of intensive research in recent years due to their intriguing properties and novel potential applications [1-5]. On one hand, they are highly desirable in future electronic nanodevices. For example, nanowires of zero-resistance are ideal interconnects since they can circumvent the damaging heat produced by energy dissipation in a normal nano-conductor whose high resistance is inversely proportional to its cross-section area. Furthermore, in the resistive state they can also act as superconducting quantum interference devices [1,2]. On the other hand, superconducting nanowires provide unique platforms to investigate and discover novel superconducting phenomena in confined geometries: for example, Tian et al. reported an anti-proximity effect in Zn nanowires with bulk superconducting electrodes [3]. Quasi one-dimensional (1D) superconducting nanowires with diameters comparable to the zero-temperature superconducting coherence length ξ_0 have been the research subject of thermal and quantum [4,5] phase slip phenomena which induce dissipation at temperatures near and away from the superconducting critical temperature, T_c, respectively. Pursuing research on superconducting nanowires will provide fundamental experimental results which will benefit nanoscale superconductivity and nanodevices.

One of the grand challenges in current research on superconducting nanowires is to explore the physical properties of individual superconducting nanowires. The main obstacles are the surface contamination and oxidation (in the metal nanowires) which hinder the conventional four-probe resistive measurements, in addition to electrostatic charge problems which destroys nanowires in four-probe resistive measurements.

In this DOE funded project we have been developing methods to synthesize a new class of superconducting nanowires which are stable in atmosphere, enabling the exploration of superconducting properties and potential applications of individual nanostructures. We also aim to fabricate other superconducting nanostructures with high-aspect ratios, for example, superconducting nanoribbons.

Recent Progress

Vortex matter with periodic pinnings can serve as a model system for studying periodic elastic media such as charge density waves and electron crystals driven on substrates with arrays of obstacles (or defects) [6]. It also offers the possibility to increase the critical current of a superconductor due to the enhanced pinning strength at matching fields where the density of the flux quanta is equal or multiple times of that of the pins [7]. Due to the limitation of sample preparation and patterning techniques, current research on vortex matter with periodic pinnings has been mainly conducted in superconducting thin films by introducing arrays of holes [7]. However, random pinning resulting in high critical currents can dominate in thin films at low temperatures and cause Joule heating problems since high currents are needed to depin vortices. Thus, transport measurements [7] are usually conducted at temperatures near the zero-field critical temperature T_{c0}. As pointed out by Misko et al. [8], both high pinning disorder and

thermal fluctuation can hinder the observation of the various dynamic phases, their transitions and the resulting features in the macroscopically measurable quantities, e.g. the N shaped *V-I* curves. Furthermore, pinning strength plays a crucial role in the vortex dynamics [6] and the easiest way to change it is to vary temperature. Thus, exploration on the rich vortex dynamic phases requires a clean system with extremely weak random pinning, allowing resistive measurements at low temperatures.

$Bi_2Sr_2CaCu_2O_8$ (BSCCO-2212) crystals with $T_{c0} \approx 80$K are well-known for their weak random pinning. However, existing technologies are unable to introduce through-holes into thick crystals. By modifying a whisker growth method [9] we successfully fabricated BSCCO-2212 crystalline nanoribbons with thickness of tens to few hundreds nanometers and width of a few micrometers: the oxides of the associated elements were mixed and melted at 1200^{o}C in an alumina boat for 30 minutes and then quenched in between two copper plates to form a glassy pellet. Ribbons of various sizes grew out of the pellet after it is annealed in a steady flow of O_2 gas at 860^{o}C for 40 hours. After dispersed into an ethanol solution, the ribbons were spin-coated on a silicon substrate. Electric contacts to a selected nanoribbon were made by optical lithography technique followed by sputtering 250 nm thick gold and lift-off. Square arrays of holes with desired diameters and lattice spacings were patterned with focused-ion-beam (FIB) milling (FEI Nova 600). The right panel of Fig. 1 shows a BSCCO-2212 nanoribbon with a square array of holes with diameter of ~30 nm and hole-hole spacing of 500 nm. Such nanoribbons enable us to pursue superconducting phenomena in an extended temperature range of ~40K (down to $0.5T_{c0}$) through resistive measurements.

We carried out systematic resistive measurements on the patterned BSCCO-2212 nanoribbons at various temperatures, magnetic fields and field orientations. We observed the 'matching effect' which represents itself as peaks (dips) in the field dependences of the critical current (magnetoresisance). Furthermore, the appearance of the matching effect is found to be temperature, magnetic field and driving force dependent: the amplitudes of the critical current peaks and magnetoresistance dips increase at fields around the melting line in the magnetic field versus temperature (*H-T*) phase diagram; at low temperatures magnetoresistance dips can be observed at high driving forces while no peaks appear in the critical current at the same fields. We also observed N-shaped *V-I* characteristics similar to those observed in semiconductor and plasma devices for the first time.

Our results demonstrate that patterned crystalline nanoribbons of high-temperature superconductors can be a unique platform and an effective tool in revealing various vortex phases and their transitions, resulting in discoveries of new superconducting phenomena.

Future Plans

As part of the proposed project on synthesis and properties of superconducting nanowires and nanoribbons, we plan to carry out the following experiments in the near future:

(i). *High quality $Bi_2Sr_2CaCu_2O_{8+x}$ (BSCCO-2212) crystalline nanoribbons and their growth mechanisms*: most of the synthesized BSCCO-2212 nanoribbons contain second phases (typically $Bi_2Sr_2Ca_2Cu_3O_{10+x}$). We will conduct systematic exploration of the growth conditions, with emphasis on the effect of the composition ratio of the starting glassy plate.

(ii). *Hole arrays of various symmetries*: the magnetic vortices in a superconductor form an Abrokosov triangular lattice. The symmetry of the hole-array will definitely affect its interaction with the vortex lattice and results in different physical properties or phenomena.

We will introduce hole arrays with triangular, honeycomb and rectangular symmetries into BSCCO-2212 nanoribbons and explore their transport properties.

(iii). *Nanoribbons of high-T_c superconductors with lower anisotropy*: it is known that BSCCO is extremely anisotropic. That is, the vortices in BSCCO-2212 nanoribbons can be two-dimensional (2D) (pancake vortices). They can behave completely different from 3D vortices. Thus, we will fabricate nanoribbons of $YBa_2Cu_3O_{7-x}$ and pattern them with FIB technique.

(iv). *Nanoribbons of the newly discovered pnictides*: we proposed to grow nanostructures of the Fe-based superconductors to explore possible confinement effects. It will be extremely interesting to study the interaction of the iron atoms in the crystalline lattice and the magnetic vortices which can be arranged in lattices of various symmetries by the artificially fabricated hole-arrays.

References

[1]. A. Johansson *et al*., *Phys. Rev. Lett*. **95**, article # 116805 (2005).

[2]. D. S. Hopkins et al., *Science* **308**, 1763 (2005).

[3]. M. L. Tian *et al*., *Phys. Rev. Lett*. **95**, article # 076802 (2005).

[4]. A. Bezryadin, C. N. Lau, and M. Tinkham, *Nature* **404**, 971 (2000).

[5]. F. Altomare *et al*., *Phys. Rev. Lett.* **97**, article # 017001 (2006).

[6]. C. Reichhardt, C. J. Olson, and Franco Nori, *Phys. Rev. Lett*. **78**, 2648 (1997); C. Reichhardt and G. T. Zimanyi, *Phys. Rev. B* **61**, 14354 (2000).

[7]. M. Kemmler *et al*., *Phys. Rev. Lett.* **97**, 147003 (2006); U. Patel *et al*., *Phys. Rev. B*. **76**, 020508 (2007); A. D. Thakur *et al*., *Appl. Phys. Lett*. **94**, 262501 (2009).

[8]. V. R. Misko *et al*., *Phys. Rev. Lett.* **96**, 127004 (2006).

[9]. I. Matsubara *et al*., *J. Crystal Growth* **128**, 719 (1993).

Publications in the Past Two Years

"Magnetoresistance oscillations in granular superconducting niobium nitride nanowires", U. Patel, Z. L. Xiao, A. Gurevich, S. Avci, J. Hua, R. Divan, U. Welp, and W. K. Kwok, *Phys. Rev. B* **80**, 147003 (2009).

"Growth and superconductivity of $FeSe_x$ crystals", U. Patel, J. Hua, S. H. Yu, S. Avci, Z. L. Xiao, H. Claus, J. Schlueter, V. V. Vlasko-Vlasov, U. Welp, and W. K. Kwok, *Appl. Phys. Lett.* **94**, 082508 (2009).

"Multi-gap nodeless superconductivity in iron selenide $FeSe_x$: evident from quasiparticle heat transport", J. K. Dong, T. Y. Guan, S. Y. Zhou, X. Qiu, L. Ding, C. Zhang, U. Patel, Z. L. Xiao, S. Y. Li, *Phys. Rev. B* **80**, 024518 (2009).

"Effect of sample geometry on the phase boundary of a mesoscopic superconducting loop", G. R. Berdiyorov, S. H. Yu, Z. L. Xiao, F. M. Peeters, J. Hua, A. Imre, and W. K. Kwok, *Phys. Rev. B* **80**, 064511 (2009).

"Magnetoresistance anisotropy of a one-dimensional superconducting niobium strip", J. Hua, Z. L. Xiao, A. Imre, S. H. Yu, U. Patel, L. E. Ocola, R. Divan, A. Koshelev, J. Pearson, U. Welp, and W. K. Kwok, *Phys. Rev. Lett.* **101**, 077003 (2008).

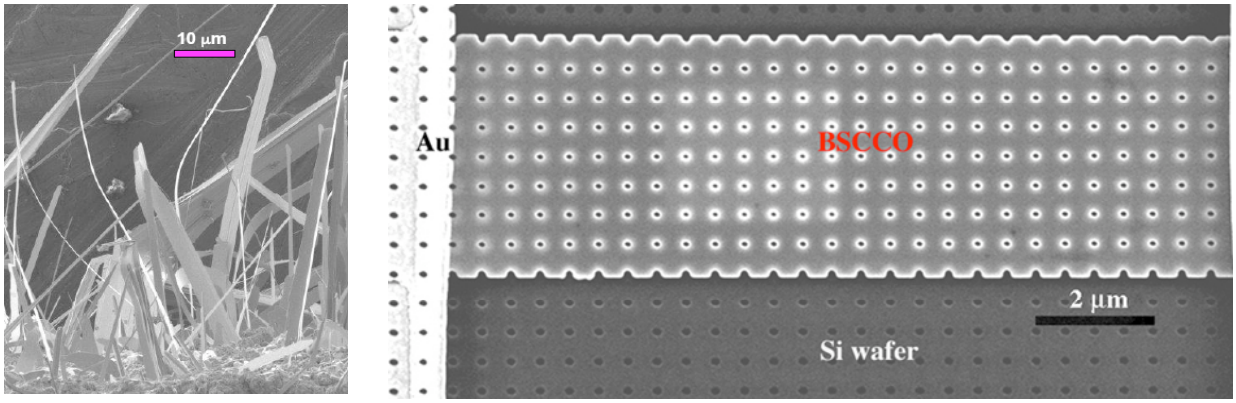

FIG.1. Left panel: $Bi_2Sr_2CaCu_2O_{8+x}$ (BSCCO-2212) wires and ribbons grown out of a glassy BSCCO-2212 plate; Right panel: a patterned BSCCO-2212 ribbon with Au electrical leads on Si substrate.

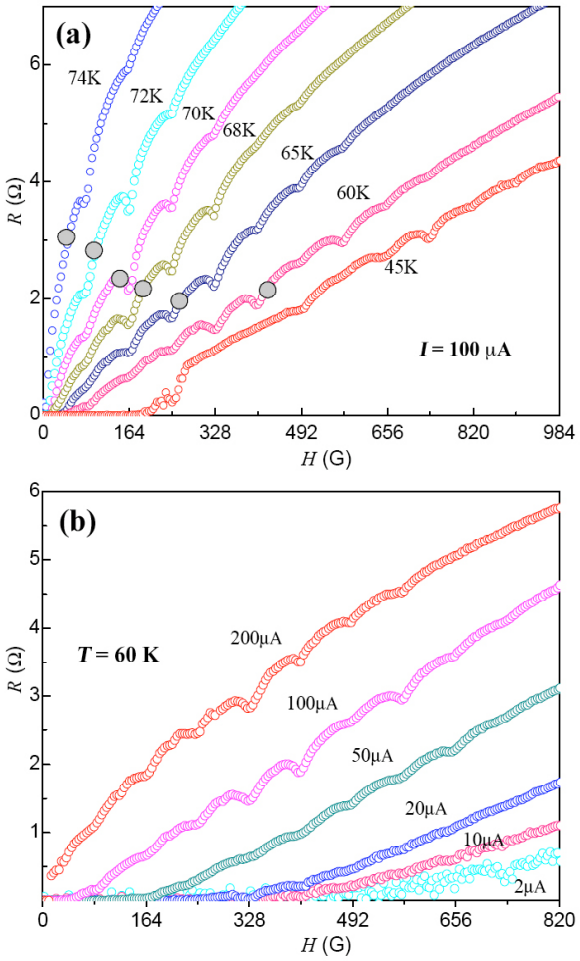

FIG.2. Magnetoresistance of the patterned BSCCO-2212 ribbon shown in the right panel of Fig.1: (a) at 100 μA and various temperatures; (b) at 60 K and various currents.

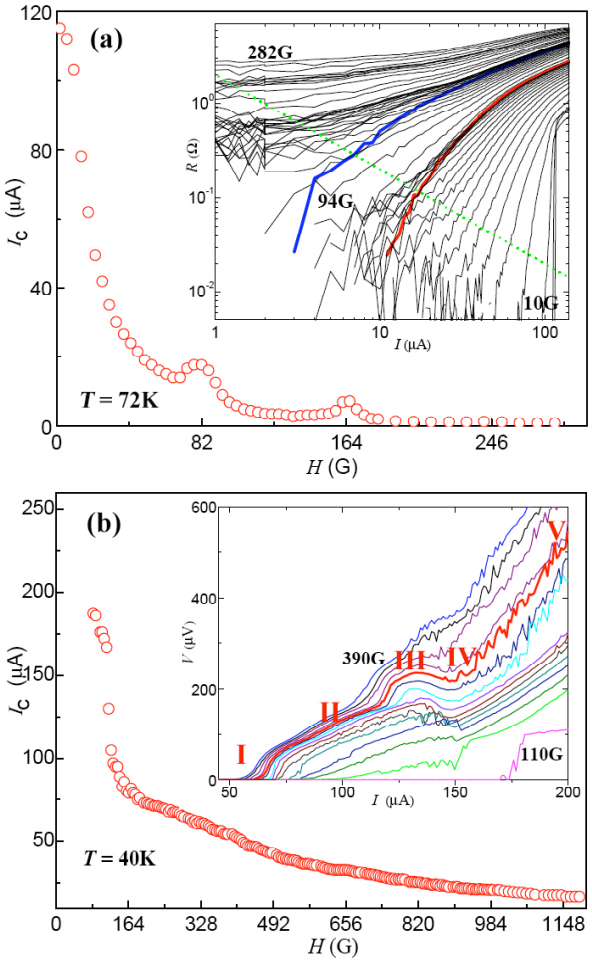

FIG.3. Magnetic field dependence of the critical current I_c at 72K (a) and 40K (b), respectively. The insets present the associated voltage-current (V-I) characteristics at these two temperatures but in various magnetic fields.

Poster Session

Ib. Bulk and Nano-Materials: New Materials Discovery

IIc. The Nanoscale

(This page intentionally left blank.)

Solution-Based Doping in Metal Oxides and Sulfides

M. Tao and Q. M. Zhang
(mtao@uta.edu)
Departments of Electrical Engineering and Physics, University of Texas at Arlington, Arlington, Texas 76019, USA

Program Scope

With the current rate of global energy consumption at ~15 TW [1], solar cells need to be deployed at the TW scale or they will not make a noticeable impact on our future energy mix. Most of the current solar cell technologies are limited by natural resources for TW-scale deployment. To bypass these limitations, a new solar cell material needs to be identified, which should be abundant, low cost and non-toxic. Table I lists some of the desirable properties for the new solar cell material suitable for TW-scale deployment. A recent study [2] suggests that candidate materials for TW-scale solar cells are largely metal oxides and sulfides including Cu, Fe, Zn and Ni, which meet the requirements for low cost and material abundance. The Principal Investigator has been pursuing transition-metal chalcogenides (TMC, including oxides) for solar cells for the last 9 years. This project will initially focus on Cu_2O and later expand to other transition-metal sulfides such as FeS_2 and NiS. Electrochemical synthesis of Cu_2O and later transition-metal sulfides will be investigated. A fundamental understanding of the structural, chemical, electrical and optical properties of these metal oxide and sulfides as related to solar cell applications will be pursued.

Table 1. Material requirements for TW-scale solar cells.

Material requirements	*Materials meeting requirement*
1. Availability	Si, organic, Gratzel, *TMC*
2. Cost	Organic, Gratzel, *TMC*
3. Low-cost synthesis	CdTe, $CuInSe_2$, organic, Gratzel, *TMC*
4. Toxicity	Si, organic, *TMC*
5. Stability	Si, III-V, CdTe, $CuInSe_2$, *TMC*
6. Carrier mobility	Si, III-V, CdTe, $CuInSe_2$, *TMC*
7. Carrier lifetime	Si, III-V, CdTe, $CuInSe_2$, *TMC*
8. Broad-spectrum absorption	Si, III-V, CdTe, $CuInSe_2$, *TMC*
9. Band gap 1.4 eV	III-V, CdTe, $CuInSe_2$, *TMC?*
10. Conduction type	Si, III-V, CdTe, $CuInSe_2$, *TMC*
11. Conductivity	Si, III-V, *TMC?*

All the commercial solar cells today utilize p-n junctions for charge separation. This requires the ability to achieve both n-type and p-type in the solar cell material. In addition, the resistivity of the n-type and p-type solar cell material has to be controlled within a specific range for optimum efficiency. For example, the optimum resistivity of p-type base in wafer-silicon solar cells is ~1 Ω-cm. In the semiconductor industry, the conduction type (n-type or p-type) is controlled by the type of dopant (Group III or Group V) and the resistivity is controlled by the amount of dopant introduced into silicon. However, the semiconductor industry utilizes vacuum-based techniques, such as diffusion and ion implantation, for doping, which are inherently high cost due to the large complex vacuum systems. To achieve low-cost solar cells, this project will focus on *solution-based doping techniques* to control the conduction type and resistivity of Cu_2O and selected transition-metal sulfides such as FeS_2 and NiS.

Table 2. Potential n-type and p-type dopants for Cu_2O.

n-Type		p-Type	
Cu^+ Site	O^{2-} Site	Cu^+ Site	O^{2-} Site
Mg, Ca	F, Cl	Li? Na?	N, P, As

N-type and p-type dopants in Cu_2O and transition-metal sulfides need to be identified. In Cu_2O, dopant atoms can substitute either Cu atoms or O atoms. If the dopant atom occupies a Cu site in Cu_2O, Group II elements, such as Mg and Ca, become possibilities for n-type doping. However, if the dopant atom occupies an O site in Cu_2O, Group

Table 3. Band gap values for metal oxides and their conduction type.

TiO_2	NiO	CdO	Co_3O_4	Fe_2O_3	PbO_2	CuO	Cu_2O
3.5	3.8	2.5	2.2	2.2	2.8	1.1	2.1
N	P	N	N	N	N	P	P

VII elements, such as F and Cl, are candidates for n-type doping and Group V elements, such as P and N, are possible p-type dopants. Table 2 lists dopant candidates for Cu_2O. For transition-metal sulfides, n-type and p-type dopant candidates can be identified based a similar valence argument.

Recent Progress

Justifications for Cu_2O

The semiconductor for terrestrial solar cells needs to have, ideally, a direct band gap of 1.4 eV for maximum efficiency [3]. Table 3 compiles the band gap values for several metal oxides. The band gap values of Cu oxides are the closest to the optimum band gap of 1.4 eV than all other metal oxides we have found. Their band gap values were one of the main reasons for us to begin investigation of Cu oxides for solar cell applications 7 years ago.

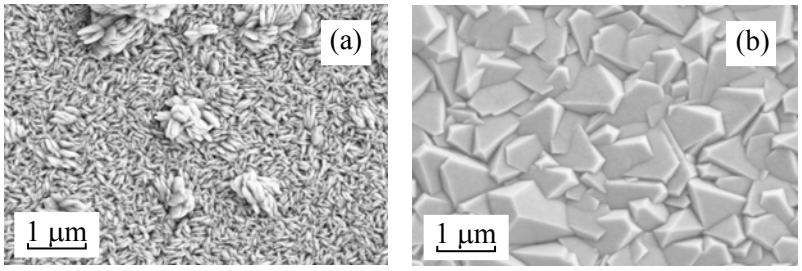

Fig. 1. Morphology by SEM of (a) CuO and (b) Cu_2O electrodeposited at 60°C and pH of (a) 13 and (b) 10.2.

Out of the two Cu oxides, Cu_2O and CuO, we have determined that Cu_2O has a better chance to achieve low-cost high-efficiency solar cells over CuO [4-6]. One reason is the indirect band gap of CuO, which results in a low absorption coefficient and would require a thick film (~50 μm) to completely absorb sunlight. With the direct band gap of Cu_2O, a film of ~2 μm is enough for complete absorption. Another reason is the 10× smaller hole mobility in CuO than in Cu_2O [7], since high mobility typically translates into high efficiency. The third reason is the poor crystallinity of electrodeposited CuO as compared to electrodeposited Cu_2O, which suggests low carrier mobility and low minority carrier lifetime for CuO. Fig. 1 shows the morphology of electrodeposited CuO and Cu_2O by SEM with a deposition temperature of 60°C. The CuO film has tiny grains (<100 nm) and is porous, while the Cu_2O film shows large grains of ~1 μm. The amorphous-like morphology of CuO is likely due to the low symmetry of its monoclinic crystal structure.

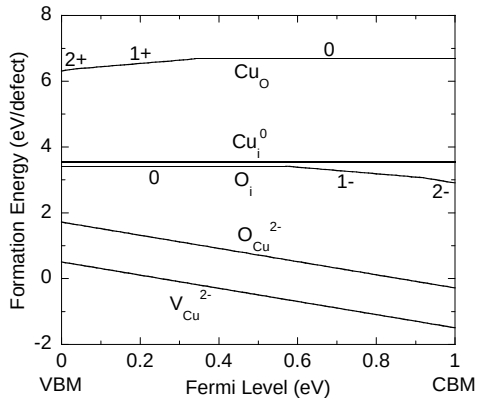

Fig. 2. Formation energy of native point defects in CuO as a function of Fermi level in an O-rich environment [4].

Understanding of p-Type Conductivity in Cu Oxides

Both Cu_2O and CuO are naturally p-type. The conduction type of a metal oxide is largely determined by its native point defects and chemical stoichiometry. For Cu oxides, Cu vacancies have been suggested to be the source of holes [4]. As an example, Fig. 2 shows our simulation on formation energy of various native point defects in CuO as a function of Fermi level in an O-rich environment. Doubly-charged Cu vacancies, V_{Cu}^{2-}, have the lowest formation energy (<1 eV), so they appear in high concentration leading to p-type conductivity. This conclusion is likely true for Cu_2O as well. Without n-type Cu_2O, early studies on Cu_2O solar cells had to rely on Schottky junctions, such as

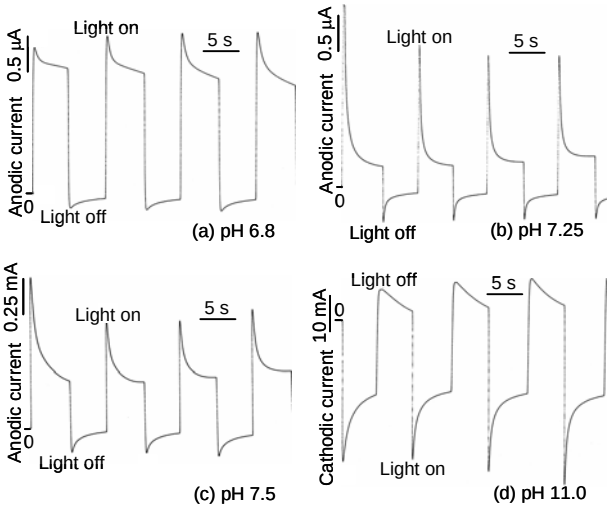

Fig. 3. Photocurrent responses from Cu_2O electrodeposited at pH of: (a) 6.8, (b) 7.25, (c) 7.5 and (d) 11.

Cu/Cu_2O, and p-n heterojunctions, such as n-type ZnO/p-type Cu_2O, which did not provide high efficiency. The long-held consensus in the solar cell community is that the best approach to improve the efficiency of Cu_2O solar cells is to achieve both p-type and n-type Cu_2O and thus p-n homojunctions of Cu_2O [8].

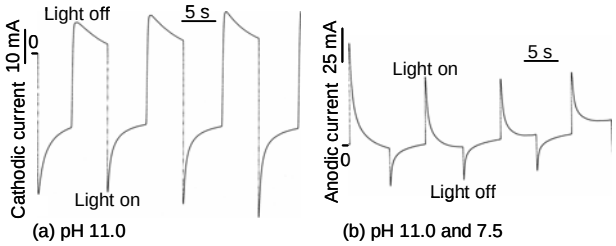

Fig. 4. Photocurrent responses from Cu_2O electrodeposited at pH of: (a) 11 and (b) first at 11 and then at 7.5.

Control of Conduction Type by Solution pH in Cu_2O

We have conducted a fundamental study on the effect of solution pH on the conduction type of electrodeposited Cu_2O and found that the naturally p-type Cu_2O is converted to n-type at low solution pH [9]. Fig. 3 shows photocurrent responses from Cu_2O samples electrodeposited at solution pH 6.8, 7.25, 7.5 and 11. Photocurrent generated upon illumination has opposite directions for n-type and p-type semiconductors. Samples deposited at pH below 7.5 show anodic photocurrents, indicating n-type conductivity. The sample deposited at pH of 11 shows a cathodic photocurrent, indicating a p-type semiconductor. These results demonstrate that solution pH can control the conduction type of electrodeposited Cu_2O.

Electrodeposited p-n Junctions in Cu_2O

With both p-type and n-type Cu_2O, a 2-step process was adopted to deposit n-type and p-type Cu_2O in sequence for the formation of a p-n junction of Cu_2O. First, p-type Cu_2O was deposited at pH 11 on a Cu substrate, and then n-type Cu_2O was deposited directly onto the p-type Cu_2O at pH 7.5. Photocurrent responses were recorded after deposition at pH 11 and after subsequent deposition at pH 7.5. As shown in Fig. 4, Cu_2O deposited at pH 11 shows a typical p-type response. However, after deposition of another Cu_2O film at pH 7.5, the photocurrent response shows n-type semiconductor behavior. This demonstrates that n-type Cu_2O has been successfully deposited on p-type Cu_2O and a p-n junction of Cu_2O has been formed.

Fig. 5 shows the I-V curves of a Cu_2O p-n junction before and after breakdown. In Fig. 5(a), the I-V curve displays a rectification effect of a p-n junction. The inset in Fig. 5(a) is a logarithmic plot of the I-V curve. The nonlinear forward current suggests a large series resistance in the junction. As the reverse bias passes -6 V, the p-n junction breaks down. The I-V curve after breakdown no longer displays any rectification but linear, as shown in Fig. 5(b). This I-V characterization demonstrates the first p-n homojunction by solution deposition in any semiconductor, and thus the feasibility of solution fabrication of high-efficiency Cu_2O solar cells.

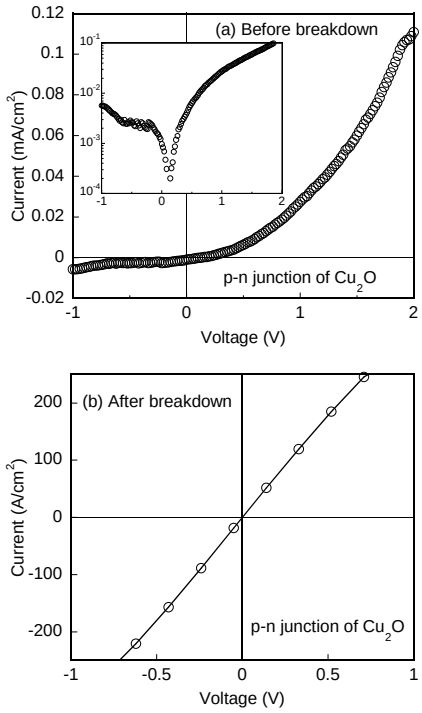

Fig. 5. I-V curves of an n-type Cu_2O/p-type Cu_2O junction: (a) before breakdown and (b) after breakdown. The inset in (a) is a logarithmic plot of the I-V data in (a).

N-Type Cu_2O by Electrochemical Doping

We have recently demonstrated n-type Cu_2O by doping it with Cl during electrodeposition [10], which reduces the resistivity of Cu_2O from MΩ-cm to below 10 Ω-cm. The method is based on co-precipitation of Cu_2O with CuCl. Out of all the halogens as n-type dopant candidates for O sites, F is best size-matched to O, but CuF is soluble in water. We choose Cl as the n-type dopant for O sites in Cu_2O. The solubility product constant of CuCl is 1.72×10^{-7} at 25°C. This means that even small amounts of Cu^+

and Cl^- in the solution will react with each other and form solid CuCl. $CuCl_2$ was used as the Cl precursor during electrodeposition of Cu_2O. Fig. 6 shows photocurrent response from a Cl-doped Cu_2O sample. The anodic current indicates an n-type semiconductor. XRD confirms that the sample is pure Cu_2O (data not shown).

The resistivity of Cl-doped Cu_2O as a function of $CuCl_2$ concentration in the deposition solution is shown in Fig. 7. Without doping, the resistivity of electrodeposited Cu_2O is 40 MΩ-cm, which is too high to produce an efficient solar cell. However, with 0.1 M $CuCl_2$ in the solution, the resistivity of the Cu_2O is significantly reduced to 75 Ω-cm, an over $10^5\times$ reduction. With higher $CuCl_2$ concentrations in the solution (from 0.01 to 0.15 M), the resistivity of Cl-doped Cu_2O is reduced from 157 Ω-cm to 48 Ω-cm (insert in Fig. 7). The lowest resistivity we have achieved so far with Cl-doped Cu_2O is 7 Ω-cm, which is close to the optimum resistivity for an efficient solar cell, ~1 Ω-cm.

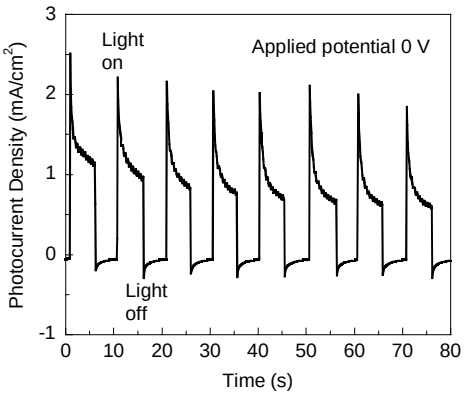

Fig. 6. Photocurrent response from Cl-doped Cu_2O. The anodic current indicates an n-type semiconductor.

Future Plans

Over the next 3 years, this project will involve the following research activities:

1) Electrochemical synthesis of Cu_2O and FeS_2;
2) Investigation of the structural, chemical, electrical and optical properties of these chalcogenides;
2) Identification of n-type and p-type dopants for Cu_2O and FeS_2;
3) Introduction of dopants into Cu_2O and FeS_2 by solution-based methods;
4) Molecular dynamic simulations of the atomic structures of dopants in Cu_2O and FeS_2;
5) Investigation of the electrical properties of doped Cu_2O and FeS_2; and
6) Demonstration of well-behaved p-n junctions in Cu_2O or FeS_2.

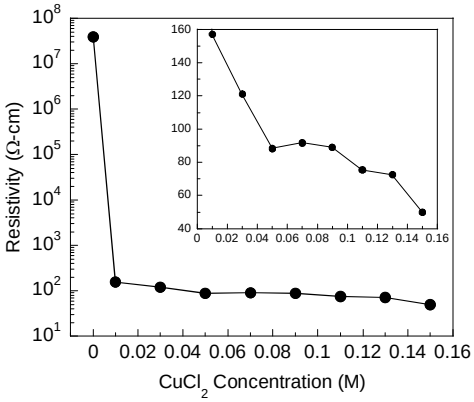

Fig. 7. Resistivity of Cl-doped Cu_2O as a function of $CuCl_2$ concentration in deposition solution.

References

[1] U.S. Department of Energy, Basic Research Needs for Solar Energy Utilization (April 2005).
[2] C. Wadia, A. P. Alivisatos and D. M. Kammen, Environ. Sci. Technol. 43, 2072 (2009).
[3] C. H. Henry, J. Appl. Phys. 51, 4494 (1980).
[4] D. Wu, Q. Zhang, and M. Tao, Phys. Rev. B 73, 235206 (2006).
[5] L. Wang, K. Han, and M. Tao, J. Electrochem. Soc. 154, D91 (2007).
[6] L. Wang, K. Han. G. Song, X. Yang, and M. Tao, Conference Record of 4th World Conference on Photovoltaic Energy Conversion (Hawaii, 2006).
[7] T. Ito, H. Yamaguchi, and K. Okabe, J. Mater. Sci. 33, 3555 (1998).
[8] L. C. Olsen, F. W. Addis, and W. Miller, Solar Cells 7, 247 (1982).
[9] L. Wang and M. Tao, Electrochem. Solid-State Lett. 10, H248 (2007).
[10] X. Han, K. Han, and M. Tao, Electrochem. Solid State Lett. 12, H89 (2009).

Synthesis of new Diamond-like B-C Phases Under High Pressure and Temperatures

Pavel Zinin, Li Chung Ming and Shiv Sharma
zinin@soest.hawaii.edu
Hawaii Institute of Geophysics and Planetology,
University of Hawaii, Honolulu, HI 96822

Program Scope

The finding of the new diamond-like B-C phases is of fundamental importance. These phases are potential high-temperature superconductors and their development is important for understanding the nature of high-temperature superconductivity. They will shed light on the nature of the bonding of the boron atoms in a diamond-like structure. Recently, theoretical simulations of pressure- and temperature-induced phase transition in the B-C system conducted by Lowther [1] demonstrated that the incorporation of B atoms into a diamond structure should not lead to a drastic distortion of the cubic cell of a diamond. The unit cells obtained in the phases predicted theoretically (i.e., 3.745 Å for cubic BC and 3.642 Å for nearly cubic BC_3) are slightly larger than that of a diamond (3.5667 Å) [1]. The aim of the this research is to synthesize a new class of *diamond-like* materials containing only boron and carbon in the B-C system, and to study the regularities of formation of novel dense phases over a wide P-T-range using a laser heated diamond anvil cell (up to 100 GPa and 2500^{o}C). Within the DOE project, we synthesized a novel cubic BC_4 (*c*-BC_4) phase under high pressure and high temperature (HPHT) conditions [2]. Identification of the phase was done using x-ray diffraction scattering, electron microprobe (EMP) technique, and Raman scattering.

Recent Progress

The pressure- and temperature-induced phase transformation of *g*-BC_4 was studied at a pressure up to 44 GPa using laser-heated diamond anvil cells and angle-dispersive powder X-ray diffraction (ADXD) at Advanced Photon Source (APS), Argonne National Laboratory. X-ray diffraction measurements were performed using a monochromatic synchrotron radiation source (λ = 0.368138 Å) at the 16-ID-B beamline of the HPCAT facility at the APS. The Raman spectra excited by a Nd-YAG laser (532-nm, Coherent Compass, Dieburg, Germany) were taken with a confocal Raman system (WiTec alpha300). A symmetrical DAC was used in this study. The laser moved stepwise vertically and horizontally to heat the whole sample area and the duration of the laser heating at each point was about 10 seconds. After quenching, each sample was decompressed gradually stepwise to atmospheric pressure.

Electron microprobe analysis of the recovered BCx sample was performed using JEOL *Hyperprobe* JXA-8500F at the School of Ocean and Earth Science and Technology, University of Hawaii. In order to ensure a reliable result, a pure B_4C powder was used as the standard for calibration of boron and carbon in the sample, and the rinsed BCx sample in the gasket was first fixed with an epoxy resin and then polished until an optically flat surface from the sample was fully exposed. The result obtained from EMP measurements gives a C/B ratio of around 4 (C/B = 3.91 ± 0.26).

Two samples were loaded to 24 and 44 GPa, and laser-heated to 1984 and 2020 K, respectively. After laser-heating, the sample pressure was measured again. It was found that the sample pressure remained the same for the first sample at 24 GPa, while the pressure dropped from 44 GPa to 37 GPa in the second sample. The large pressure drop in the second sample is most likely related to volume change as a result of the transition to a denser phase in the sample. The x-ray spectra of the starting material BC_4 (*g*-BC_4(I)) is shown in figure 1. A weak peak at 2.384 Å is believed to be from the B_4C left in the starting material during the process of synthesis [3]. The positions of the other eight peaks on the x-ray spectrum can be indexed using a hexagonal unit cell with *a*=2.4537±0.0031

Å and c= 13.45±0.37 Å. Parameters of the unit cell of g-BC_4(I) are close to those of graphite (a=2.463 Å and c= 6.714 Å) (JCPDS # 23-64) if the c-axis is doubled.

The diffraction pattern from the recovered sample at 24 GPa is similar to that in the starting material except the major diffraction peaks are more symmetric in shape and less in number (i.e., a change from 8 to 5 peaks), indicating a subtle change has taken place in the BC_4 specimen at this pressure. Tthe 4 diffraction peaks thus obtained can be best fitted using a new hexagonal unit cell with lattice parameters a=2.4654±0.013 Å and c=6.468±0.028 Å, that compare well with those in the graphite.

The x-ray spectrum of the post-lasered BC_4 (c-BC_4) specimen recovered from 37 GPa shows a completely different diffraction pattern (figure 2), indicating a phase transition has indeed taken place. All the graphite-like x-ray diffraction peaks were replaced by a completely new set of peaks. The fact that all the new diffraction lines are sharp and well defined implies the high-pressure phase is well crystallized. The new phase can be indexed by a cubic unit cell with lattice parameter, a_0 = 3.5866±0.0003 Å. The 4 peaks are indexed as the (111), (220), (311) and (400), respectively, and together with their respective intensity are in good agreement with those in the diamond structure with both boron and carbon atoms randomly distributed in the 8 positions in the diamond-like structure. Two weak peaks at 3.73 and 2.347 Å are probably from the B_4C phase in the starting material, indicating that B_4C remains intact, untransformed, and uncrystallized at a pressure of up to 44 GPa.The zero-pressure lattice parameter of the cubic phase obtained in this study is larger than that of diamond (i.e., a_0=3.5667 Å, JCPDS No. 6-0675), which is consistent with theoretical prediction [1].

The Raman spectrum of the g-BC_4(II) phase recovered from 24 GPa shows two broad modes at 1342 and 1583 cm-1, which are the D and G modes, respectively, typical for graphitic materials. The Raman spectrum of the cubic c-BC_4 and map of the Raman peak intensity at 1193 cm^{-1} over the sample surface are shown in figures 3 and 4. The Raman spectrum of the c-BC_4 phase is different from those of g-BC_4(II) recovered from 24 GPa and of graphitic BC_x phases studied by Zinin *et al* [3], which supports the observation that a new phase has occurred. It displays a broad peak at 450 cm^{-1}, a second peak at 1193 cm^{-1}, another broad peak at 684 cm^{-1}, a much narrower peak around 1287 cm^{-1}. The Raman spectrum of the c-BC_4 phase is similar to that of the dl-BC_3 phase with a strong peak at 1193 cm^{-1}[4].

In conclusion, a new cubic phase, c-BC_4 was synthesized by direct transformation from a graphitic phase at pressure 44 GPa and temperature 2020 K in a laser-heated DAC. Identification of the cubic phase was obtained from x-ray diffraction and Raman spectroscopy measurements. The zero-pressure lattice parameter of the c-BC_4 calculated from diffraction peaks is 3.587 Å. The composition of the new phase was determined from EMP measurements and gave a value of C/B ratio around 4 (C/B = 3.91 ± 0.26). The x-ray diffraction measurements of the recovered sample synthesized at a pressure of 24 GPa and a temperature of 1984 K showed a very subtle transition from the hexagonal phase g-BC_4(I) phase at ambient conditions to a new hexagonal phase g-BC_4(II) phase with a volume change of 0.3%.

Future Plans

Synthesis of the cubic BC_4 phases confirms the theoretical prediction on the cubic BCx phases with high B/C ratio. We plan to continue our research in three directions: (a) to conduct synthesis of BCx phases with B/C ratio higher that ¼; and (b) to conduct comprehensive study of the elastic, electrical, and vibrational properties of the novel c-BC_4 phases as well as graphitic BC_x phases; (c) to conduct feasibility studies on synthesis of dense C_3N_4 phases. To measure the isothermal compressibility of the recently synthesized diamond-like BCx phases (including a diamond-like cubic BC_4 phase from a post-lasered graphitic phase at 37 GPa) we plan to use synchrotron-based

x-ray diffraction at the APS. Important part of the characterization is study of the nanostructure of the cubic BCx phases. Such a characterization can be achieved by using transmission electron microscopy-electron energy loss spectroscopy (TEM-EELS). A more accurate determination of the chemical composition of the recovered high-pressure BCx samples using the FIB-TEM available to users at National Microscopy Lab, ANL.

In collaboration with the Universite du Maine, France, we plan to measure both the longitudinal and shear waves of cubic and graphitic-BCx phases under high pressure using our newly developed laser-ultrasonic technique in a diamond-anvil cell (LU-DAC) so that we can measure their elastic properties as a function of pressure and possibly determine the pressure requires to bridge atoms between BC_x layers.

References

1. Lowther, J.E., Potential super-hard phases and the stability of diamond-like boron-carbon structures. *J. Phys. Condes. Matter.* **17** (2005) 3221-3229.
2. Ming, L.C., P.V. Zinin, X.R. Liu, Y. Nakamoto, and R. Jia, Synthesis of Dense BC_x Phases under High-Pressure and High-Temperature". *J. Phys. Conf. Ser.* (2009) in press.
3. Zinin, P.V., L.C. Ming, S.K. Sharma, Y. Liu, and S.M. Hong, Ultraviolet Raman spectroscopy of the graphitic BCx phases. *Diam. Relat. Mater.* **18** (2009) 1123-1128.

DOE Sponsored Publications in 2007-2009 from Current Grant

- P. V. Zinin, L. C. Ming, S. K. Sharma, S. M. Hong, Y. Xie, T. Irifune, T. Shinmei. "Synthesis of new cubic C_3N_4 and BC_x phases under high pressure and high temperature". *J. Phys. Conf. Ser.* **121** (2008) 062002.
- N. Chigarev, P. Zinin, L. C. Ming, G. Amulele, A. Bulou, V. Gusev. "Laser generation and detection of longitudinal and shear acoustic waves in a diamond anvil cell". *App. Phys. Lett.*, **93** (2008) 181905.
- P. V. Zinin, L. C. Ming, S. K. Sharma, Y. Liu, S. M. Hong. "Ultraviolet Raman spectroscopy of the graphitic BCx phases". *Diam. Related Mater.* **18** (2009) 1123–1128.
- P. Zinin, L. Ming, S. Sharma, V. Khabashesku, X. Liu, S. Hong, S. Endo. "Ultraviolet and near-infrared Raman spectroscopy of graphitic C_3N_4 phase". *Chem. Phys. Lett.*, **472** (2009) 69–73.
- J. E. Lowther, P. V. Zinin, L. C. Ming. "Vibrational energies of graphene and hexagonal structured planar B-C complexes". *Phys. Rev. B,* **79** (2009) 033401.
- L. C. Ming, P. V. Zinin, X. R. Liu, Y. Nakamoto, R. Jia, "Synthesis of Dense BC_x Phases under High-Pressure and High-Temperature", *J. Phys. Conf. Ser.*, in press (2009).

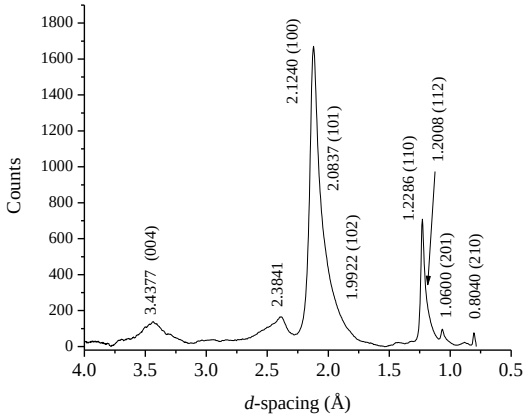

Figure 1. X-ray diffraction of the graphitic BC_4 (*g*-BC_4(I)) as the starting material, where the broad peak around 2.384 Å is from the B_4C.

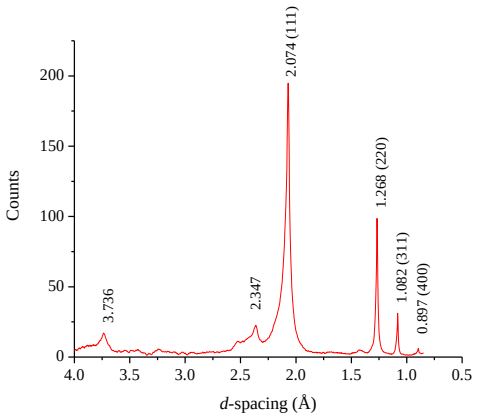

Figure 2. The ambient x-ray diffraction pattern of a post-lasered BC_4 (*c*-BC_4(II)) phase recovered from 37 GPa. Two weak and broad peaks at 3.736 and 2.347 are from the B_4C in the starting material.

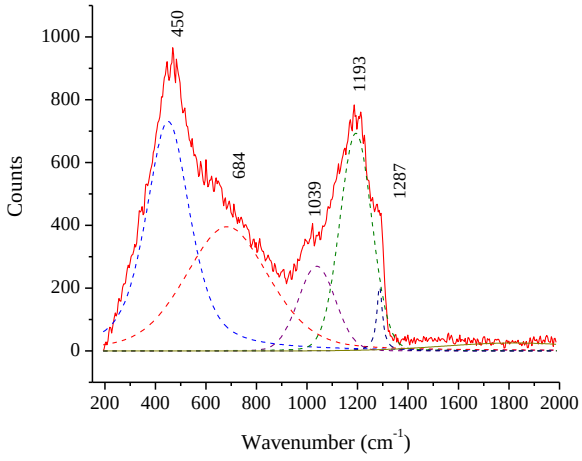

Figure 3. Raman spectrum (532 nm) of *c*-BC_4 phase: integration time was 4 min, laser power was 2 mW.

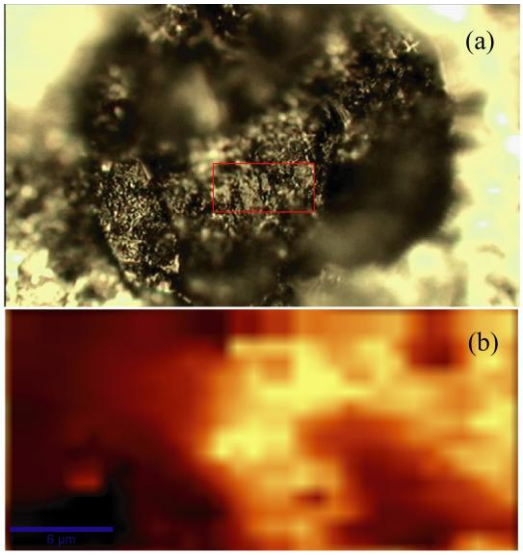

Figure 4. (a) Optical image of the *c*-BC_4 phase and (b) a map of the Raman peak intensity at 1193 cm^{-1} shown in a yellow colour scale, showing the distribution of the cubic BC_4 phase in the recovered sample.

Molecular Hydrogen Storage in Novel Binary Clathrate Hydrates at Near-Ambient Temperatures and Pressures

PIs: E. Dendy Sloan and Carolyn A. Koh
Center for Hydrate Research, Chemical Engineering Department
Colorado School of Mines, Golden, CO 80401
esloan@mines.edu, ckoh@mines.edu

(i) Program Scope

The program has two objectives that are vital for realizing the potential of a new class of hydrogen storage materials: (1) to design, synthesize, and develop novel chemical-clathrate hybrid materials and molecular hydrogen clathrates that will efficiently store and release H_2 from clathrate host frameworks and from clathrate guest molecules at near-ambient temperatures and pressures, (2) obtain a fundamental understanding of the molecular level structure and the kinetics and mechanisms of formation and H_2 release in these novel crystalline compounds. The H_2 storage capacity of the new clathrate materials and proof-of-principle hybrid technology will be developed and optimized by scanning a broad range of synthesis pressure, temperature and composition conditions. A wide range of new clathrate host and promoter molecules will be investigated, including amines and organic hydrogen-bonded host crystals.

(ii) Recent Progress

Extending the chemical-clathrate hybrid concept to a clathrate hydrate hybrid system of hydrogen

We have demonstrated for the first time the proof-of-concept of chemical-clathrate hybrid storage of H_2 using an organic compound hydroquinone (HQ) (Figure 1) [1]. This is the first storage scheme in which both molecular storage of H_2 within hydrate cavities and chemical storage in the host molecule are utilized. Using Raman spectroscopy and X-ray diffraction analysis, we have confirmed that H_2 molecules can be enclathrated into HQ under sufficient hydrogen pressure. The host molecule of this clathrate-chemical hybrid system, HQ, has been also used to directly power a fuel cell. At the anode side of the fuel cell, HQ loses its chemically bound hydrogen in the hydroxyl group while producing electricity. This approach in taking advantage of additional chemically stored hydrogen in the host molecule promises an improvement in weight storage capacity of clathrate materials and is the first time that these two systems have been combined in a hybrid technology for H_2 storage [1].

While the presence of large guests such as tetrahydrofuran (THF) and tetra-*n*-butylammonium bromide (TBAB) drastically reduces the formation pressure of H_2 hydrate at a given temperature, weight storage capacity of H_2 in the material also decreases because the large guests occupy the large cavities of the hydrate structure instead of H_2. To help overcome this trade-off between stability and weight storage capacity, the chemical-clathrate hybrid concept was applied to clathrate hydrates of H_2.

We have recently shown for the first time that tetra-*n*-butylammonium borohydride (TBABh) can store hydrogen both in molecular form in the hydrate cavities and chemically bound to the borohydride anion [2] (Figure 2). Raman spectroscopy was used to confirm the presence of encaged H_2 in the small cages of the hydrate. X-ray diffraction revealed that the structure of TBABh + H_2 hydrate is analogous to that of TBAB + H_2 hydrate. An acid catalyzed hydrolysis reaction was used to produce additional hydrogen from the borohydride anion, and the reaction showed nearly 100% conversion. Using gas evolution and differential scanning calorimetry measurements, we showed that TBABh + H_2 hydrate is more stable and stores more hydrogen (27%) than the THF + H_2 hydrate system [2].

Raman spectroscopic studies of hydrogen hydrates

Detailed Raman spectroscopic studies have been performed in order to better understand the quantum behavior of hydrogen molecules stored within the hydrate cavities. Vibrational bands show that the molecules vibrate at lower frequencies than in the gas phase and a pair of peaks (ortho- and para-H_2) is present for each environment in the hydrogen hydrate. For a simple hydrate of hydrogen, four pairs of peaks are present for single occupancy in the small cavities and double, triple, and quadruple occupancies in the large cavities. Integrating these peaks results in an under-estimation of the large cavity H_2 content, implying that a H_2 molecule in a small cavity is more polarizable than H_2 molecules in a large cavity [3].

Rotational bands show that enclathrated H_2 molecules have orientationally dependent rotation, suggesting that the small and large cavities are orientationally anisotropic. The Raman spectrum of D_2 hydrate was also analyzed, and this indicated that D_2 was a suitable substitute for H_2 in hydrate formation [3].

Thermodynamic prediction of hydrates containing THF and H_2

A thermodynamic model based on the CSMGem framework (an in-house program based on the van der Waals and Platteeuw theory) was developed for hydrate systems containing THF and H_2. With the newly developed model, thermodynamic predictions of many simple or binary hydrates containing THF or H_2 can be made for the first time. The model predictions are in excellent agreement with experimentally determined *p-T* phase diagrams. Such a model is very useful since THF binary hydrates of hydrogen are currently being investigated as a potential storage material. The model also indicates that the degree to which the cavities are filled with hydrogen is largely a function of formation pressure, which has an implication in hydrogen storage, where high occupancy is desired [4].

(iii) Future Plans

We have used hydroquinone as a proof-of-concept for chemical-clathrate hybrid storage of hydrogen. In this system, hydroquinone forms a host framework and is able to enclathrate hydrogen molecules. There are a large number of compounds that can form a similar framework by hydrogen bonding. The possibility of storing hydrogen in some of these compounds will be

further explored.

Many researchers have reported the hydrogen storage in binary clathrate and semi-clathrate hydrates. The storage capacities of H_2 in the hydrates were approximately 1 wt% H_2 or less, except for the result of the tuning effect reported by the KAIST group [5]. In spite of efforts by many other fine researchers, however, no one has been able to repeat the tuning effect with the same method as KAIST group. Recently, we found a new approach for increasing the H_2 storage capacity the THF+H_2 binary hydrates. We will further investigate the mechanism of the tuning effect to provide efficient H_2 storage near ambient temperature and pressure.

(iv) References

[1] Strobel, T.A.; Kim, Y.; Andrews, G.S.; Ferrell, J.R.; Koh, C.A.; Herring, A.M.; Sloan, E.D., *J. Am. Chem. Soc.* (2008), **130**, 14975-14977.

[2] Shin, K.; Kim, Y.; Strobel, T.A.; Prasad, P.S.R.; Sugahara, T.; Lee, H.; Sloan, E.D.; Sum, A.K.; Koh, C.A., *J. Phys. Chem. B* (2009), **113**, 6415–6418.

[3] Strobel, T.A.; Sloan, E.D.; Koh, C.A., *J. Chem. Phys.* (2009), **130**, 014506.

[4] Strobel, T.A.; Sloan, E.D.; Koh, C.A., *Fluid Phase Equilibria* (2009), **280**, 61–67.

[5] Lee, H.; Lee, J.-W.; Kim, D.Y.; Park, J.; Yu-Taek Seo, Y.-T.; Zeng, H.; Moudrakovski, I.L.; Ratcliffe, C.I.; Ripmeester, J.A.. *Nature* (2005), **434**, 743-746.

(v) Publications resulting from work supported by the DOE project over the last two years

A New Approach for Increasing Hydrogen Storage Capacity Using Tetrahydrofuran, Sugahara, T.; Haag, J.C.; Prasad, P.S.R.; Warntjes, A.A.; Sloan, E.D.; Sum, A.K.; Koh, C.A., *Journal of the American Chemical Society* (2009), submitted.

Properties of the Clathrates of Hydrogen and Developments in Their Applicability for Hydrogen Storage, Strobel, T.A.; Hester, K.C.; Koh, C.A.; Sum, A.K.; Sloan, E.D. Jr., *Chemical Physics Letters* (2009), **478**, 97-109.

Hydrogen Storage in Double Clathrates with tert-Butylamine, Prasad, P.S.R.; Sugahara, T.; Sum, A.K.; Sloan, E.D.; Koh, C.A., *Journal of Physical Chemistry A* (2009), **113**, 6540–6543.

Tetra-n-butylammonium Borohydride Semi-clathrate: A Hybrid Clathrate Hydrate for Hydrogen Storage, Shin, K.; Kim, Y.; Strobel, T.A.; Prasad, P.S.R.; Sugahara, T.; Lee, H.; Sloan, E.D.; Sum, A.K.; Koh, C.A., *Journal of Physical Chemistry B* (2009), **113**, 6415–6418.

Thermodynamic Predictions of Various Tetrahydrofuran and Hydrogen Clathrate Hydrates, Strobel, T.A.; Sloan, E.D.; Koh, C.A., *Fluid Phase Equilibria* (2009), **280**, 61–67.

Raman Spectroscopic Studies of Hydrogen Clathrate Hydrates, Strobel, T.A.; Sloan, E.D.; Koh, C.A., *Journal of Chemical Physics* (2009), **130**, 014506.

Chemical-Clathrate Hybrid Hydrogen Storage: Storage in Both Guest and Host, Strobel, T.A.; Kim, Y.; Andrews, G.S.; Ferrell, J.R.; Koh, C.A.; Herring, A.M.; Sloan, E.D., *Journal of the American Chemical Society* (2008), **130**, 14975-14977.

Water Cavities of Structure H Clathrate Hydrate Stabilized by Molecular Hydrogen, Strobel, T.A.; Koh, C.A.; Sloan, E.D., *Journal of Physical Chemistry B* (2008), **112**, 1885-1887.

Natural Gas Hydrates: Recent Advances and Challenges in Energy and Environmental Applications, Koh, C.A.; Sloan, E.D, *AIChE Journal* (Invited Perspective Cover Article) (2007), **53**, 1636-1643.

Clathrate Hydrates Under Pressure, Mao, W.; Koh, C.A.; Sloan, E.D., *Physics* Today (Invited Article) (2007), **60**, 42-47.

A Hydrogen Clathrate Hydrate with Cyclohexanone: Structure and Stability, Strobel, T.A.; Hester, K.C.; Sloan, E.D.; Koh, C.A., *Journal of the American Chemical Society* (2007), **129**, 9544-9545.

Hydrogen Storage Properties of Clathrate Hydrate Materials, Strobel, T.A.; Koh, C.A.; Sloan, E.D., *Fluid Phase Equilibria* (2007), **261**, 382-389.

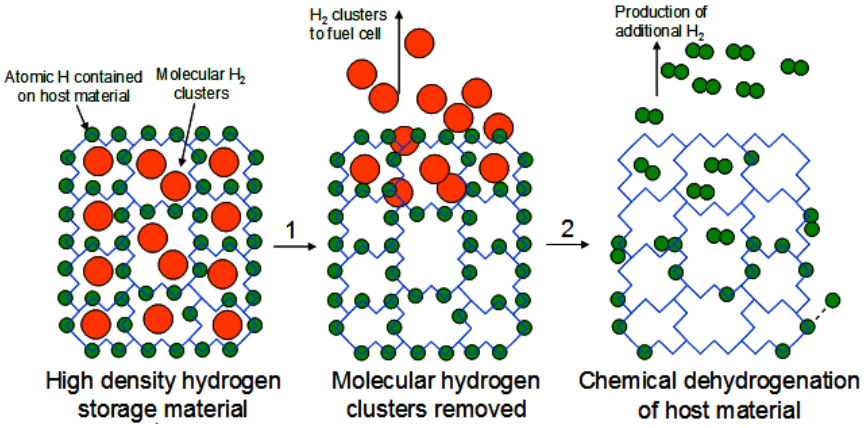

Figure 1. A conceptual picture of chemical-clathrate hybrid storage of hydrogen [1]

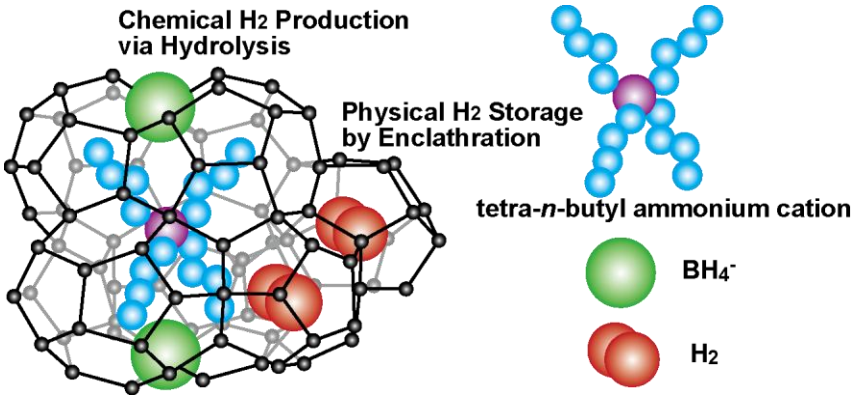

Figure 2. Water cavities with enclathrated TBABh and H_2 molecules. TBA^+ is situated within the large cavities, and BH_4^- replaces a water molecule. H_2 is located in the small cavities. [2]

A Fundamental Study of Inorganic Clathrates and "Open-Framework" Materials

George S. Nolas
gnolas@cas.usf.edu
Department of Physics, University of South Florida, Tampa, FL USA

Program Scope

Due to formidable synthetic challenges, many materials of scientific and technological interest are first obtained as microcrystalline powders. High purity, high yield processing techniques are often lacking and thus care must be taken in interpretation of the observed structural, chemical, and physical properties of these powder or polycrystalline materials, which can be strongly influenced by grain boundary effects, surface composition, and, most notably, impurity phases. New processing techniques are of interest in order to investigate the intrinsic properties of these materials and elucidate their fundamental physical properties. In addition, techniques in synthesizing metastable materials continue to be of scientific and technological interest. A canonical example of such materials is the intermetallic clathrates.[1, 2]. Characterized by a covalently bonded cage-like framework crystal structure isotypic to the clathrate hydrates, this material system has stimulated a broad interest from both fundamental and applied vantage points.[1, 2, 3] Na_xSi_{136} represent a prototypical example. Figure 1 shows the clathrate-II structure together with low and high Na containing Si compositions. Yet in the four decades since the discovery [4] of this material system, the preparation of compositions of high purity and yield, in addition to single crystals, was not achieved. We have developed processing techniques not only to synthesize phase-pure high yield specimens reproducibly but also single crystals for the first time. We also employed this technique to synthesize new "open-framework" compounds and investigate their physical properties.

Recent Progress

The series of high purity Na_xSi_{136} specimens shown in Figure 1 were prepared in high yield by an *optimized* form of the thermal decomposition technique of the precursor Na_4Si_4.[1] The Na1 and Na2 fractional occupancies are plotted in Figure 2 as normalized occupancies of the Si_{20} and Si_{28} cages, respectively, along with the lattice parameters *a*, as a function of the total Na content *x*. The first important observation is that the larger Si_{28} cages are almost exclusively filled first as Na is incorporated into the structure. Not until the Si_{28} cages are nearly completely filled (near $x \sim 8$) do the smaller Si_{20} cages begin to be occupied. Figure 2 also shows that the lattice parameter exhibits a clear minimum with Na content, decreasing slightly upon filling the Si_{28} cages, but then increasing as the Si_{20} cages are then occupied. Thus occupation of the two distinct cages has distinct and opposite effects on the structure. **This effect is observed unequivocally for the first time experimentally** and corroborated by theoretical density functional theory computations.[5]

In collaboration with the Max Planck Institute for the Chemical Physics of Solids in Dresden, Germany, a collaboration that was included in our proposal for renewal, **we have synthesized** [6] **and measured the intrinsic transport properties of single crystals of type II silicon clathrates for the first time** employing a Spark Plasma

Sintering (SPS) approach. The defining characteristic of the SPS process is the pulsed DC electrical current, typically on the order of several hundred Amperes, that is sourced through the specimen and die assembly while they are simultaneously held under applied uniaxial pressure. Thus, the specimen is heated internally, as opposed to externally as in conventional hot-pressing. Although a complete understanding of the role of the electric field and the beneficial mechanisms involved in this process is developing, and the existence or nature of the inter-grain plasma is still under investigation, the SPS method has allowed us to grow silicon clathrate-II single crystals for the first time.

Single crystal X-ray diffraction showed low residuals of the structure refinement, indicative of the quality of the crystallinity of the crystals. Our structural analyses indicate that all silicon framework sites are completely occupied, and both sodium sites show full occupation. A very large atomic displacement parameter (ADP) was observed for Na2 centred at the 8*b* site in the Si_{28} cage. A difference Fourier map calculated with Na2 removed from the model shows only a broadly smeared, essentially spherical residual density with a clear maximum at the 8*b* site. Powder X-ray diffraction (PXRD) pattern for a specimen ground from $Na_{24}Si_{136}$ crystals corroborate the phase purity of the specimen. All reflections are indexed with the clathrate-II crystal structure (space group $Fd\bar{3}m$, blue tick marks in Figure 2).

Specific heat (C_p) measurements on the single crystals clearly indicate an Einstein mode of 55 K for Na inside the Si_{28} polyhedra and corroborate a large dynamic contribution to the disordered Na@Si_{28} (Figure 2). The frequency of this "rattle" mode falls well inside the frequency range of the host Si_{136} acoustic phonon branches predicted from density functional theory calculations [7] indicating the potential for a resonant phonon interaction, analogous to clathrate-I materials.[8**]** The data also indicates a considerable electronic contribution to the specific heat and a substantial electronic density of states at the Fermi level, results that are corroborated by transport measurements (Figure 2). This agrees with DFT calculations [5, 9] for $Na_{24}Si_{136}$ which predict the Fermi level to coincide with a prominent peak in the electronic density of states, and also corroborates the metallic transport properties further revealed below. Fitting the experimental data with two Einstein modes (Θ_{E1} and Θ_{E2}), Debye temperature (Θ_D) and electronic contribution to C_p (Θ_e) provides the best fit to the data, as shown in the Figure 2.[10]

Future Plans

Most recently we have begun to grow single crystals of both clathrate-I and II materials by a newer technique, not using the SPS approach outlined above. This new processing technique will allow us to further study these crystals, via temperature dependent single crystal X-ray diffraction, electrical and thermal transport and NMR, for example, and begin a complete investigation into the dynamics and guest-host bonding in these materials. We will also employ the new processing techniques thus far develop to synthesize and investigate compounds of other structure types. Furthermore, we continue an investigation into developing different processing techniques in synthesizing new compositions and crystal structures.

References

1. M. Beekman and G.S. Nolas, J. Mater. Chem. **18**, 842 (2008), and refs therein.
2. G.S. Nolas, G.A. Slack and S.B. Schujman, in *Semiconductors and Semimetals*, Vol. 69, ed. T.M. Tritt, Academic Press, 2001, p 255, and references therein.
3. G.S. Nolas, J.W. Sharp and H.J. Goldsmid, *Thermoelectrics: Basics Principles and New Materials Developments* (Springer-Verlag, Heidelberg, 2001), and refs therein.
4. J.S. Kasper, P. Hagenmuller, M. Pouchard, C. Cros, *Science* **150**, 1713 *(1965).*
5. M. Beekman, E.N. Nenghabi, C.W. Myles, and G.S. Nolas, unpublished (manuscript in preparation).
6. M. Beekman, M. Baitinger, H. Borrmann, W. Schnelle, K. Meier, G.S. Nolas, Y. Grin, J. Amer. Chem. Soc. **131**, 9642 (2009).
7. X. Tang, J. Dong, P. Hitchins, O. Shebanova, J. Gryko, P. Barnes, J.K. Cockcroft, M. Vickers, and P.F. McMillan, Phys. Rev. B **74**, 14109 (2006).
8. G.S. Nolas, T.J.R. Weakley, J.L. Cohn and R. Sharma, Phys. Rev. B **61**, 3845 (2000).
9. J.C. Conesa, C. Tablero, and P. Wahnon, J. Chem. Phys. **120**, 6142 (2004).
10. M. Beekman, M. Baitinger, W. Schnelle, Y. Grin, and G.S. Nolas, unpublished (manuscript in preparation).

DOE Sponsored Publications and Presentations, 2007 – 2009:

Seven (7) published journal article (listed below)
Seven (7) published conference proceedings
Ten (10) Plenary and Invited Conference Presentations, Seminars and Colloquia
Six (6) contributing conference presentations from students and collaborators

DOE Sponsored Journal Article Publications, 2007 – 2009:

1. M. Beekman, M. Baitinger, H. Borrmann, W. Schnelle, K. Meier, G.S. Nolas, Y. Grin, 'Preparation and crystal growth of $Na_{24}Si_{136}$: An electrochemical solid state route', J. Amer. Chem. Soc. **131**, 9642 (2009).
2. M. Beekman, J.A. Kaduk, J. Gryko, W. Wong-Ng, A. Shapiro and G.S. Nolas, 'Synthesis and characterization of framework-substituted $Cs_8Na_{16}Cu_5Ge_{131}$', J. Alloy Comp. **470**, 365 (2009).
3. A.N. Mansour, M. Beekman, W. Wong-Ng, and G.S. Nolas, 'Local structure of Cu in $Cs_8Na_{16}Cu_5Ge_{131}$ type II clathrate', J. Solid State Chem, Journal of Solid State Chemistry **182**, 107 (2009).
4. K. Biswas, C.W. Myles, M. Sanati and G. S. Nolas, 'Thermal properties of guest-free Si136 and Ge136 clathrates: A first-principles study', J. Appl. Phys. **104**, 033535 (2008).
5. M. Beekman and G.S. Nolas, 'Inorganic clathrate-II materials of group 14: synthesis routes and physical properties', J. Mater. Chem. **18**, 842 (2008).
6. C.L. Condron, S.M. Kauzlarich and G. S. Nolas, 'Structure and Thermoelectric Characterization of $A_xBa_{8-x}Al_{14}Si_{31}$ (A = Sr, Eu) Single Crystals', Inorganic Chem **46**, 2556 (2007).
7. M. Beekman, W. Wong-Ng, J.A. Kaduk, A. Shipario, and G.S. Nolas, 'Synthesis and single-crystal X-ray diffraction studies of new framework substituted type II clathrates, $Cs_8Na_{16}Ag_xGe_{136-x}$ ($x < 7$)', J. Solid State Chem **180**, 1076 (2007).

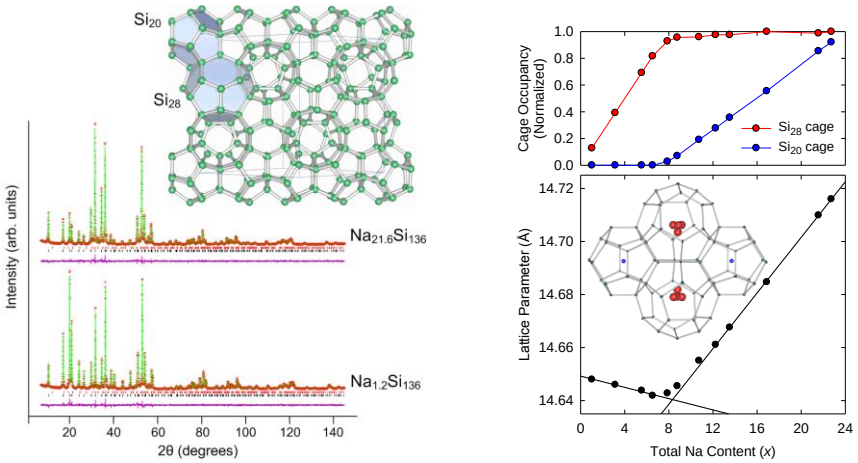

Figure 1 LEFT: Rietveld refinement powder X-ray diffraction plots for $Na_{21.6}Si_{136}$ and $Na_{1.2}Si_{136}$ polycrystalline specimens. Lower tickmarks indicate reflection positions for Na_xSi_{136}, while upper tickmarks indicate reflections for a trace impurity phase, clathrate-I Na_8Si_{46}. Also shown is a depiction of the Si_{136} host framework, with the two distinct polyhedra emphasized. Na atoms occupy the interiors of these polyhedra. RIGHT: Refined relative cage occupancies (top) and lattice parameters (bottom) as a function of the total Na content, *x*. Black lines are linear fits to the data for highest and lowest four Na contents, respectively. Inset: Structure fragment for $Na_{5.5}Si_{136}$ with ADP ellipsoids shown for 60% probability.

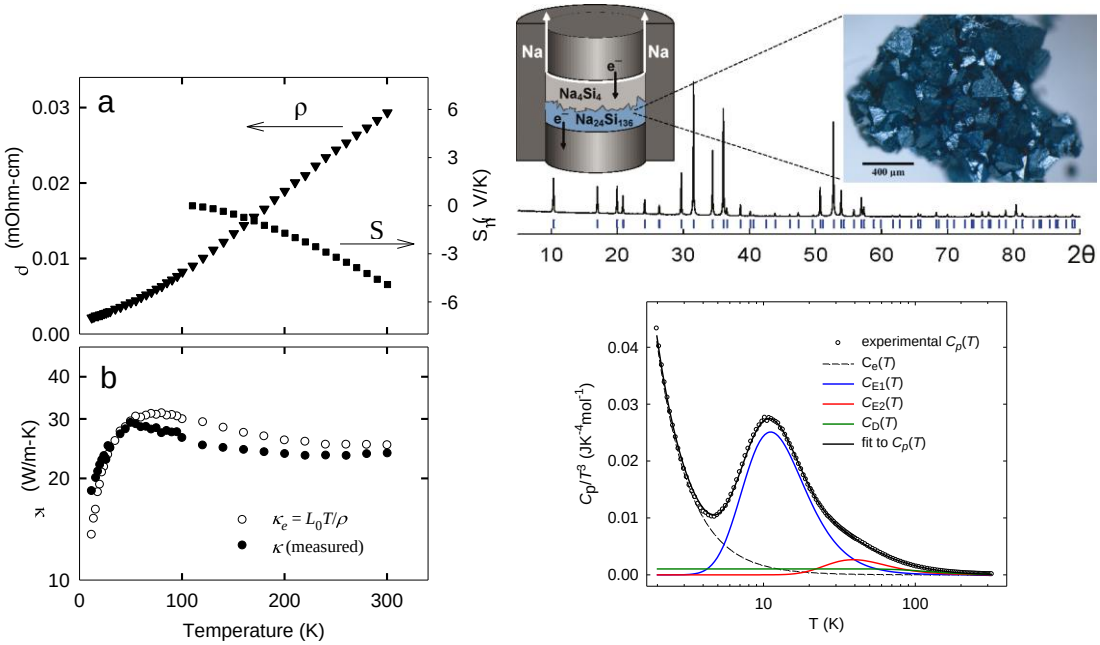

Figure 2 The synthesis and single crystal growth of clathrate-II $Na_{24}Si_{136}$ is performed in one step applying SPS to the precursor Na_4Si_4 demonstrating a new route to the synthesis of intermetallic compounds facilitated by the electric field and current. Heat capacity, as well as electrical and thermal transport, reveals the intrinsic transport properties of these materials for the first time. These crystals demonstrate highly metallic transport properties, as expected from theoretical and crystal chemistry considerations.

Computational Investigations of Solid-Liquid Interfaces

Mark Asta
Chemical Engineering & Materials Science Department, University of California, Davis
One Shields Ave., Davis, CA 95616
Email: mdasta@ucdavis.edu

I. Program Scope – In a wide variety of materials synthesis and processing contexts, atomistic processes at solid-liquid interfaces (SLIs) play a critical role governing defect formation, growth morphologies, and microstructural evolution. Accurate knowledge of SLI free energies, mobilities and non-equilibrium segregation coefficients are critical for predictive modeling of such growth phenomena, yet direct experimental measurement of these properties remains elusive in many cases. In this program atomistic simulation methodologies are being developed and applied to derive detailed insights into the structural and dynamical properties of SLIs, and their relationship with the thermodynamic and kinetic parameters that impact structural evolution on larger scales.

II. Recent Progress – Our recent research has involved three main thrusts. The first concerns the structural and dynamic properties of *faceted solid-liquid interfaces*. While crystal-melt interfaces in elemental materials are typically molecularly rough, featuring highly isotropic interfacial free energies, SLIs between chemically dissimilar materials are generally much more anisotropic, and often feature one or more faceted orientations. Faceted SLIs are found in a wide variety of synthesis and processing contexts, ranging from heterogeneous nucleation assisted by grain refiners in alloy casting, to semiconductor nanowire growth from liquid catalysts. While atomistic simulations have been extensively employed in studies of molecularly rough crystal-melt interfaces [V.5], far less effort has been devoted to faceted systems. Outstanding questions remain concerning the nature of the interfacial atomic structure, and how it relates to the energetic and kinetic properties underlying growth dynamics.

Our work has led to the development of molecular dynamics (MD) simulation approaches and analysis tools to characterize structural order at faceted crystal-melt interfaces, and to compute the thermodynamic and dynamic properties of SLI steps, related to terrace-nucleation kinetics [V.3]. Most recently this work has been extended to faceted, chemically heterogeneous interfaces. This class of SLIs has been shown to be amenable to high-resolution structural characterization by electron microscopy and X-Ray scattering techniques [IV.1-IV.5], and they thus offer unique possibilities for direct comparisons between measurements and simulation results. An example of our work is shown in Fig. 1, from a MD simulation of interfaces between liquid Pb and solid Cu. The layering of the first few Pb interfacial layers is clearly apparent in this figure, and within the interfacial layers pronounced

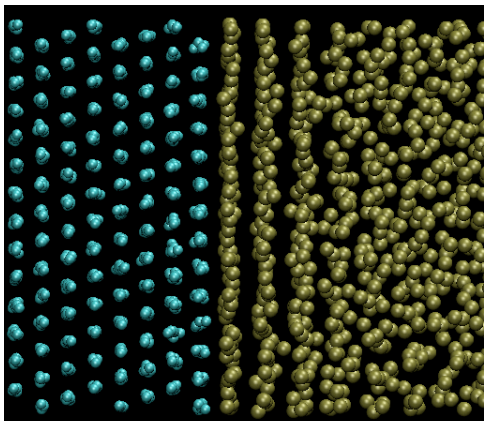

Figure 1: Snapshot of a faceted interface between liquid Pb (gold) and Cu (blue). From collaborative research by Palofox, Laird and Asta.

lateral structural ordering is observed in the simulations (not shown). Such structural ordering at SLIs is expected to have important consequences for wetting and freezing phenomena, particularly at the nanoscale [IV.1]. The simulations being undertaken in this work provide a framework for deriving expanded insights into such interface structural features, and their relation to SLI properties.

The second thrust concerns *solute effects on crystal-melt interface properties* in alloys, for both near-equilibrium and far-from equilibrium growth conditions. This work is primarily motivated within the context of the development of a predictive multiscale framework for modeling dendrite growth. Modeling of dendritic solidification is key to understanding how changes in processing conditions affect microstructures and associated mechanical properties of many solidification-processed materials [V.5].

Phase-field modeling, motivated by experimental investigations in Al and Mg alloys, demonstrate that solute-induced changes in the anisotropy of the crystal-melt interfacial energy (γ) can give rise to dramatic morphological transitions resulting from changes in the growth orientations of dendrite tips [IV.5,V.5]. These studies highlight a critical need to quantify composition dependencies of γ, in order to accurately model alloy solidification microstructures. Recent MD calculations of anisotropic crystal-melt interfacial free energies demonstrate unequivocally that composition-induced variations in γ anisotropies are large on the scale of the magnitudes required to induce observed changes in growth morphologies; when coupled with calculations of interface excess quantities [V.7,V.10], these results are beginning to provide insights into the nature of solute interactions with SLIs, and their associated effects on equilibrium properties.

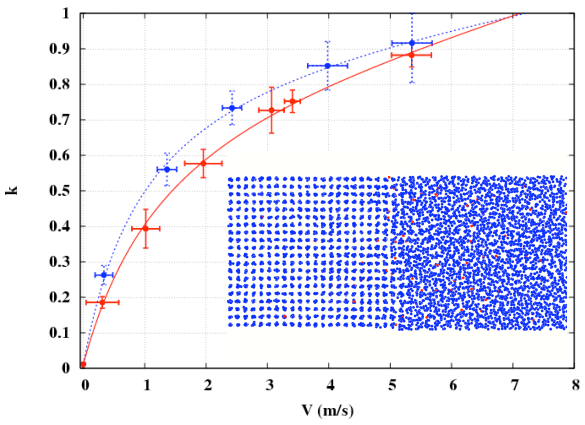

Figure 2: MD calculated partition coefficients (k) as a function of interface velocity (V). The inset is an interfacial region from an MD snapshot.

Under the non-equilibrium conditions characteristic of rapid solidification, solute effects on solidification microstructures arise also due to their influence on interface mobilities, and the related phenomenon of solute trapping. We have recently developed a non-equilibrium MD methodology for the study of such properties. As shown in Fig. 2, the non-equilibrium partitioning of solute between solid and liquid phases (k) as a function of interface velocity (V) has been calculated in a model fcc alloy system, considering two different interface orientations. The MD work is the first of its type to demonstrate anisotropic behavior in the $k(V)$ relationship. It is also providing new results related to the effects of solute atoms on the interfacial mobility, and the associated magnitude of solute drag.

The third research direction involves the calculation of the *thermodynamic forces underlying grain coalescence and grain-boundary premelting* phenomena in metals. This work has involved the development of an equilibrium MD method [V.6] for calculating structural contributions to grain-boundary disjoining potentials. The

disjoining potential parametrizes the dependence of the excess interfacial free energy of a grain-boundary on the width of the premelted layer, and it is thus a key quantity underlying the attractive or repulsive forces that govern grain coalescence during solidification. The MD method for calculating this quantity is based on analyses of equilibrium fluctuations in the boundary width, as illustrated in Fig. 3. This work is part of a larger CMSN (Computational Materials Science Network) sponsored collaborative effort aimed at the development of multiscale methods for modeling phenomena such as hot-tearing, associated with the late stages of solidification.

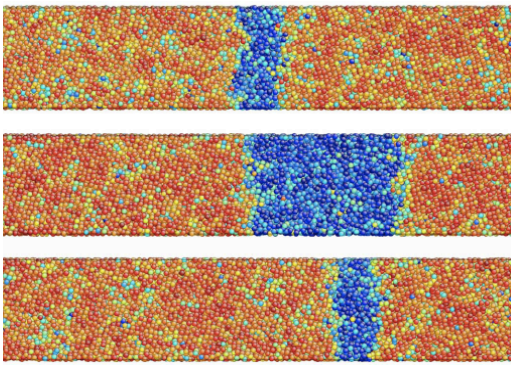

Figure 3: Equilibrium width fluctuations in an MD simulation of a premelted twist grain boundary in Ni. The atoms are colored red (solid) or blue (liquid) based on the value of a local structural order parameter.

III. Future Work – Future work on faceted SLIs will involve an expanded collaboration with the group of U. Dahmen at the National Center for Electron Microscopy (NCEM). Through this collaboration we will aim to exploit opportunities for making direct comparisons between in-situ microscopy measurements and modeling results for the atomic structure of liquid nanoparticles confined in chemically dissimilar solids. Of particular interest is the nature of the ordering in the liquid induced by the faceted SLIs in these systems. We will also investigate the melting/freezing dynamics and equilibrium fluctuations of these particles as a framework for probing fundamental SLI thermodynamic and kinetic properties, and their dependencies on system size.

Future investigations into the nature of the coupling between solute composition, interfacial free energy anisotropies, and growth morphologies in alloy solidification will focus on the Al-Mg system, for which experimental investigations are underway at Ames Laboratory to study changes in dendrite growth shapes induced by Mg additions to Al. Our work to date has involved the development of a classical interatomic potential for Al-Mg, in collaboration with M. Mendelev at Ames, and J.J. Hoyt at McMaster University, which accurately models the Al-rich solidus and liquidus phase boundaries [V.9]. The potential is currently being used in calculations of concentration dependent values of γ and associated crystalline anisotropies. Future work on non-equilibrium properties of solid-liquid interfaces will involve further development of the methodologies described above, to compute interface mobilities as well as *k(V)* in alloys, and to probe the variations in these properties induced by changes in solute concentration.

Finally, this research project has continued to maintain a focus on heterophase solid-solid as well as solid-liquid interfaces in cases where opportunities for direct comparisons with experimental measurements are possible. Our previous work on interfaces between precipitate and matrix phases in Al-Sc alloys is being extended in the study of highly monodisperse core-shell precipitates in Al-Sc-Li alloys, which are the subject of detailed experimental investigations led by V. Radmilovic and U. Dahmen at NCEM. Our efforts will involve the application of first-principles calculations to elucidate

the energetic driving forces [V.1] and kinetic mechanisms underlying the formation of the observed nanoscale precipitate microstructures, and their highly monodisperse size distributions. Such first-principles calculations also proved useful in determining the magnitude of the threshold displacement energy for Li atoms in Al-Sc-Li alloys, which helped to explain an observed non-monotonic dependence of radiation damage on imaging voltage [V.8] for these light atoms.

IV. References:

1. W. D. Kaplan and Y. Kauffmann, "Structural Order in Liquids Induced by Interfaces in Crystals," *Annu. Rev. Mater. Res.* **36**, 1-48 (2006).
2. S. H. Oh, Y. Kauffmann, C. Scheu, W. D. Kaplan, and M. Ruhle, "Ordered Liquid Aluminum at the Interface with Sapphire," *Science* **310**, 661-663 (2005).
3. S. E. Donnelly, R. C. Birtcher, C. W. Allen, I. Morrison, K. Furuya, M. Song, K. Mitsuishi, and U. Dahmen "Ordering in a Fluid Intert Gas Confined by Flat Surfaces," *Science* **296**, 507-510 (2002).
4. J. M. Howe and H. Saka, "In Situ Transmission Electron Microscopy Studies of the Solid-Liquid Interface," *MRS Bulletin* **29**, 951-957 (2004).
5. H. Reichert, O. Klein, H. Dosch, M. Denk, V. Honkimaki and T. Lippman, "Observation of Five-Fold Local Symmetry in Liquid Lead," *Nature* **408**, 839-841 (2000).
6. T. Haxhimali, A. Karma, F. Gonzales and M. Rappaz, "Orientation Selection in Dendritic Evolution," *Nature Mat.* **5**, 660-664 (2006).

V. Publications *(2008-2009):*

1. G. Ghosh, A. van de Walle, and M. Asta, "First-Principles Calculations of Structural and Energetic Properties of BCC, FCC and HCP Solid Solutions in the Al-TM (TM=Ti,Zr,Hf) Systems: A Comparison of Cluster Expansion and Supercell Methods," *Acta Mater.* **56**, 3203-3221 (2008).
2. M. I. Mendelev, M. J. Kramer, C. A. Becker and M. Asta, "Analysis of Semi-Empirical Interatomic Potentials Appropriate for Simulation of Crystalline and Liquid Al and Cu," *Phil. Mag.* **88**, 1723-1750 (2008).
3. D. Buta, M. Asta and J. J. Hoyt, "Structure and Dynamics of a Faceted Crystal-Melt Interface," *Phys. Rev. E* **78**, 031605 (2008).
4. S. Angioletti-Uberti, M. Asta, M. W. Finnis and P. D. Lee, "Solid-Liquid Phase Equilibria from Free Energy Perturbation Calculations," *Phys. Rev. B* **78**, 134203 (2008).
5. M. Asta, C. Beckermann, A. Karma, W. Kurz, R. Napolitano, M. Plapp, G. Purdy, M. Rappaz, and R. Trivedi, "Solidification Microstructures and Solid State Parallels: Recent Developments, Future Directions," *Acta Mater.* **57**, 941-971 (2009).
6. J. J. Hoyt, D. Olmsted, S. Jindal, M. Asta, and A. Karma, "Method for Computing Short-Range Forces Driving Grain Boundary Premelting," *Phys. Rev. E* 79, 020601(R) (2009).
7. C. A. Becker, D. L. Olmsted, M. Asta, J. J. Hoyt and S. M. Foiles, "Atomistic Simulations of Crystal-Melt Interfaces in a Model Binary Alloy: Interfacial Free Energies, Adsorption Coefficients and Excess Entropy," *Phys. Rev. B* **79**, 054109 (2009).
8. M. D. Rossell, R. Erni, M. Asta, V. Radmilovic and U. Dahmen, "Atomic-Resolution Imaging of Lithium in Al_3Li Precipitates," *Phys. Rev. B* **80**, 024110 (2009).
9. M. I. Mendelev, M. Asta, M. J. Rahman and J. J. Hoyt, "Development of Interatomic Potentials Appropriate for Simulation of Solid-Liquid Interface Properties in Al-Mg Alloys," *Phil. Mag.* (in press).
10. B. B. Laird, R. L. Davidchack, Y. Yang and M. Asta, "Determination of the Solid-Liquid Interfacial Free Energy Along a Coexistence Line by Gibbs-Cahn Integration," *J. Chem. Phys.* (in press).

Atomistic Structure, Strength, and Kinetic Properties of Intergranular Films in Ceramics

Stephen H. Garofalini
Department of Materials Science and Engineering
Rutgers University
Piscataway, NJ, 08855

Program Scope

Polycrystalline ceramics often contain a glassy intergranular film (IGF) between the crystals that occupies only a small volume percentage of the bulk ceramic, but can significantly influence various mechanical, thermal, chemical, and optical properties. There has been significant effort to address the fundamentally important scientific and engineering issues associated with the atomistic details of these films in order to design material properties [1-3]. Although significant progress has been made experimentally in recent years[4-6], the glassy nature of the IGF and its very thin width between crystals has made the understanding the atomistic structure and fundamental behavior of IGFs experimentally formidable, allowing for application of computational techniques to address these issues.

Our research is designed to provide information of the atomistic structure of the glassy IGF and the IGF/crystal interface and their effect on the fracture behavior of the IGFs related to both kinetically and thermodynamically controlled design of the intergranular films. We apply molecular dynamics (MD) computer simulations and have developed and applied Atomic Density Functional (ADF) (also called Phase Field Crystal (PFC)) calculations to this problem. Both MD and ADF offer important complementary approaches to understanding these intergranular films, with the ADF offering an opportunity to generate equilibrium compositions and configurations that are equivalent to long time behavior that are otherwise computationally too difficult to obtain in MD.

Recent Progress

In our MD simulations, we have shown the kinetically complex competition of anisotropic dissolution and anisotropic grain growth occurring during liquid phase sintering that could be controlled with processing variations. We have evaluated fracture in the IGFs in silicon nitride crystals as a function of IGF thickness as well as IGF composition. We have introduced Rare Earth ions (currently, La) into the IGF, observing the adsorption of the La to sites on the prism surface similar to HADDF-STEM results.

In our ADF work, direct application of known or published interatomic potentials in the ADF calculations is of interest. Previous ADF(PFC) studies generally use a phenomenological free energy functional form based on known crystal structure, potentially biasing the density evolution. Our approach is designed to allow us to incorporate well-known and previously published interatomic potentials into the ADF format. This will uniquely allow formation of an equilibrium structure based on an interatomic potential, enabling a direct connection between an equilibrium structure and further MD calculations of dynamics as well as enabling a new method of evaluating the validity of an interatomic potential. In the initial development of the method, we employed a simple Lennard-Jones (12-6) interatomic potential to describe the evolution of a two-dimensional system from the liquid to the polycrystalline state.

Fracture Behavior

Thickness of the IGF between Si_3N_4 crystals has been shown in our simulations to affect fracture strength. As shown in figure 1, the SiO_2 IGF with a film thickness ≥ 2nm shows fracture similar to bulk amorphous silica (given by the dashed line) and thinner films showing increased fracture strength. We were able to attribute this difference to a significant increase in the concentration of 6-membered rings in the thinner IGF than the thicker IGF, giving the thinner IGF a characteristic more akin to crystalline silica (which contains predominantly 6-membered rings), which has a higher fracture strength than glassy silica. Interestingly, Doblinger et al. [7] mentions experimental observation of increasing strength with decreasing IGF thickness, but do not discuss details. Our most recent results show the effect of composition on maximum stress, in which there is a change in the 'effective' composition of the glassy IGF caused by segregation of specific species to the IGF/crystal interface that causes a change in maximum stress.

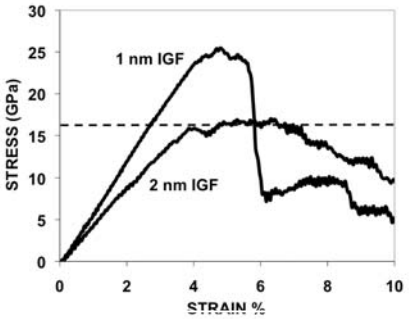

Figure 1. Stress-strain of 1nm and 2nm thick SiO_2 IGFs in nitride crystals, compared to bulk SiO_2 stress maximum (dashed line).

Location of Rare Earth Ions at Interface

We have developed an interatomic potential for La additions in the silicate IGF. Figure 2 shows the locations of the La ions at the prism orientation of the Si_3N_4 crystal surface from (A) HAADF-STEM results by Winkelman et al.[8]and (B) our MD simulation results. The drawing at the left shows the predominant locations of the La ions at sites 1 and 2, which are shown in the HAADF-STEM at the black arrows, and which are consistent with the locations we observe in our simulations (red arrows in B).

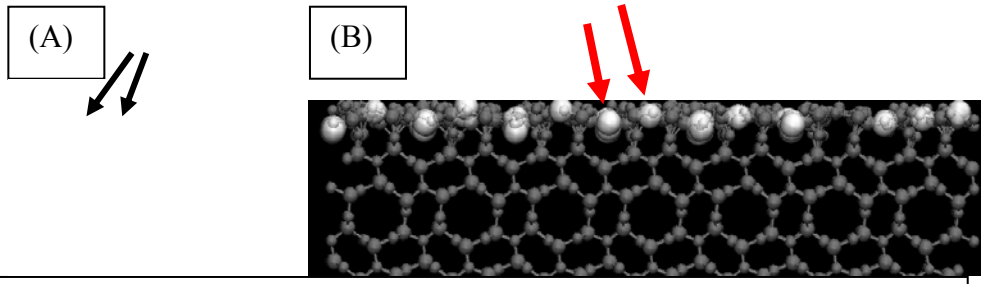

Figure 2. Experimental HAADF-STEM micrograph of La at nitride surface (A) from Winkelman et al[4] and (B) our MD simulation results, with arrows showing location of La ions at sites 1 and 2 from drawing at left in both experiment and simulations.

These results and our recent results showing the effect of interface segregation on IGF composition and resultant fracture will merge in our subsequent studies in which the La ions saturate interface sites that otherwise adsorbed Ca (modifier ions) in the IGF that altered strength. This competition of La and Ca for these interface sites will play an important role in strength, especially with different rare earths, which we plan to evaluate. Currently, we observe changes in fracture stress as a function of La concentration, enabling analysis of the structural changes that cause the property change, which has eluded experimental determination.

Equilibrium Structures and Compositions

We have used a known interatomic potential with a softened core in the ADF equations rather than using a phenomenological free energy functional form. *Our approach is designed to*

allow us to incorporate existing interatomic potentials into the ADF format, thus connecting directly to previous and future MD simulations. The free energy of a system with density modulation of atom $\rho(\vec{r})$ around the average density $\overline{\rho}$ is given as:

$$F = \frac{1}{2}\iint \delta\rho(\vec{r}) W(\vec{r}-\vec{r}')\delta\rho(\vec{r}')d\vec{r}d\vec{r}' + k_B T\int(\rho(\vec{r})\ln\frac{\rho(\vec{r})}{\rho_l} - \delta\rho(\vec{r}))d\vec{r},$$

where $\delta\rho(\vec{r}) = \rho(\vec{r}) - \overline{\rho}$ and ρ_l is the liquid density. In our model, $W(\vec{r}-\vec{r}')$ is an interatomic potential from the literature and causes the first term on the rhs to bias the system to large values of ρ (equivalent to atom positions), while the second term on the rhs is the entropy term that opposes this order. We began using a simple LJ12-6 pair potential to develop code and methodology, with plans to move to our more realistic multibody potentials that describe our systems. Long time runs enabled us to observe the evolution of a liquid to a polycrystalline configuration, followed by grain growth. An example is shown in figure 3.

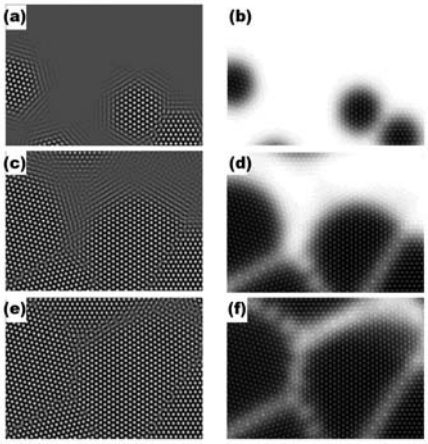

Figure 3. Evolution of a polycrystalline system from the liquid, with densities shown on the left (a,c,e) and free energies on the right (b,d,f). Bright spots in density plots indicate high density (atomic positions), showing mostly liquid in (a), with eventual nucleation and grain growth; bright spots on free energy plots indicate high energy. Our methodology works, enabling introduction of more complex and realistic interatomic potentials in the future.

This approach was computationally intensive, given the simplicity of the interatomic potential. However, a more complex interatomic potential would provide the same computational time evolution, indicating a potentially significant time savings in comparison to GCMD of complex oxides such as those in the IGFs studied in our project.

Future Plans

Previous studies indicated that the location of rare earth ions at the crystal surface might play a role in the mechanical properties of nitride ceramics. However, recent experiments showed that the location of rare earth atoms (Yb) at the nitride crystal surface was not changed by processing, but mechanical properties were changed [9]. They inferred from their data is that 'something else' must be occurring to affect strength. This 'something else' is related to the structure of the rare earth within the glassy film and it's effect on the structure of the other ions in the IGF, each of which are still experimentally elusive. We intend to evaluate these properties using both ADF and MD computations. The former needs additional work to implement the complex potentials currently used in MC and MD simulations of oxides and nitrides as opposed to the simpler LJ potential that we previously used.

References

(1) Tanaka, I.; Kleebe, H. J.; Cinibulk, M. K.; Bruley, J.; Clarke, D. R.; Rühle, M. *J. Am. Ceram. Soc.* **1994**, *77*, 911.

(2) Kleebe, H.-J. *J. Ceram. Soc. Japan* **1997**, *105*, 453.
(3) Becher, P. "The Role of Intergranular Phases and Films in Ceramic Systems"; Workshop on Interfaces in Silicon-Based Ceramics, 1998, Berkeley, CA.
(4) Ziegler, A.; Kisielowski, C.; Hoffmann, M. J.; Ritchie, R. O. *J. Am. Ceram. Soc.* **2003**, *86*, 1777.
(5) Shibata, N.; Pennycook, S. J.; Gosnell, T. R.; Painter, G. S.; Shelton, W. A.; Becher, P. F. *Nature* **2004**, *428*, 730.
(6) Winkelman, G. B.; Dwyer, C.; Hudson, T. S.; Nguyen-Mahn, D.; Doblinger, M.; Satet, R. L.; Hoffmann, M. J.; Cockayne, D. J. H. *Appl. Phys. Lett.* **2005**, *87*, 061911.
(7) Doblinger, M.; Winkelman, G. B.; Dwyer, C.; Marsh, C.; Kirkland, A. I.; Cockayne, D. J. H.; Hoffmann, M. J. *Acta Mater.* **2006**, *54*, 1949.
(8) Winkelman, G. B.; Dwyer, C.; Marsh, C.; Hudson, T. S.; Nguyen-Mahn, D.; Doblinger, M.; Cockayne, D. J. H. *Mater. Sci. and Eng. A* **2006**, *422*, 77.
(9) Ziegler, A.; Cinibulk, M. K.; Kisielowski, C.; Ritchie, R. O. *Appl. Phys. Lett.* **2007**, *91*, 141906.

Publications from 2007-2009

1. "Molecular dynamics simulations of the effect of the composition of the intergranular film on fracture in Si_3N_4", S. H. Garofalini and S. Zhang, J. Am. Ceram. Soc. (in press).
2. "Effect of thickness of the intergranular film on fracture in Si_3N_4", S. Zhang, and S. H. Garofalini, J. Am. Ceram. Soc.92 (2009)147-151.
3. "Modeling of microstructural evolution using atomic density function and effective pair potentials", J. Kim and S. H. Garofalini, Phys. Rev. B 78 (2008) 144109.
4. "Anisotropic dissolution of α-alumina (0001) and $(11\bar{2}0)$ surfaces into adjoining silicates", G. K. Lockwood, S. Zhang, and S. H. Garofalini, J. Am. Ceram. Soc., 91 (2008) 3536-3541.
5. "Molecular dynamics simulations of beta-SiC using both fixed charge and variable charge models", Y. Ma and S. H. Garofalini, J. Chem. Phys. 128 (2008) 084505.
6. "Molecular dynamics simulations of the location of La ions in lanthanum silicon oxy-nitride intergranular films is silicon nitride", Y. Jiang and S. H. Garofalini (in preparation).

Three-Dimensional Evolution of Dendritic Mixtures

C. Park*, L. Aageson, A. Johnson, K. Thornton* and P. Voorhees
Department of Materials Science and Engineering
Northwestern University, Evanston IL
*University of Michigan
Ann Arbor, MI

Program Scope

Dendrites frequently form during solidification into an undercooled melt. These dendrites possess secondary and sometimes even tertiary arms. While the tip radius and velocity of the dendrite are set by the growth conditions, the sidebranches behind the tip undergo a coarsening process under nearly isothermal conditions. The resulting two-phase mixtures are topologically and morphology complex with spatially varying mean and Gaussian curvatures. These dendritic two-phase mixtures are one example from a large class of morphologically and topologically complex structures found in nature that undergo coarsening. Included in this class are two-phase mixtures produced following phase separation in polymer blends, ordered crystalline materials, and fluids. Understanding the coarsening process in these systems requires theory, simulation, and experiments that capture their three-dimensional topology and morphology

Recent Progress

We have made progress along two major directions. 4D X-ray tomography has been used to examine interfacial evolution in the vicinity of a topological singularity. Secondly, we have examined the dynamics of coarsening by focusing on the evolution of interfacial curvature and interfacial velocities.

The topology and connectivity of a multiphase material can have an important effect on its properties. Such multiphase materials include solid-liquid mixtures, fuel cells, steels, and composites with intermetallic phases. It is well known that these multiphase systems can be morphologically unstable if there is sufficient atomic mobility. For example, interfacial energy will induce the interface between a rod and matrix to develop undulations by the well-known Rayleigh instability. These undulations increase in amplitude and lead to a pinching of the rods, a topological singularity, and spheriodization of the structure. Here we examine the interfacial morphology of a solid-liquid mixture in an Al-15 wt. % Cu alloy. Thus the interfaces evolve by bulk diffusion of solute through the high diffusivity liquid. The interfacial morphologies of tubes of liquid were observed in-situ using X-ray tomography at the every 150 s over a 12-hour period. Hundreds of pinching events were observed during this time. Fig. 1 shows one pinching event as it approaches the time of pinch off, and just after. We show theoretically and experimentally that sufficiently close to the pinching event the interfacial morphology for systems evolving by interfacial-energy-driven bulk diffusion

becomes universal; the interfacial shape is independent of the initial morphology of the rod-like phase and material system.

The theoretical shape is determined by scaling all dimensions by $(t_s\text{-}t)^{-1/3}$, where t_s is the time at which the singularity occurs. Using these new coordinates it is possible to find a solution to the diffusion equation along with Gibbs-Thompson boundary conditions that gives the time independent shape for the interface morphology, see Fig. 2. Far from the singularity, that occurs $\xi = 0$, the interface shape is a cone with a unique cone angle of 76^o.

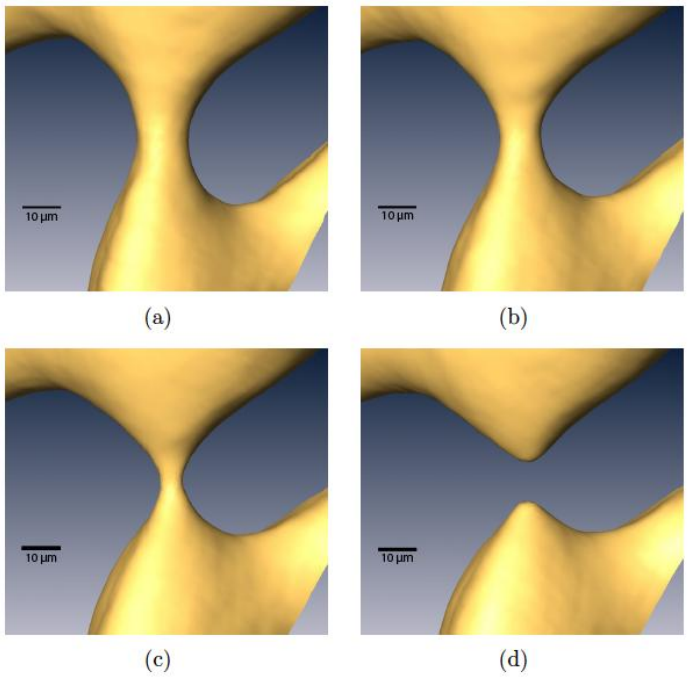

Figure 1. A liquid tube approaching (a-c) and just after (d) the topological singularity due to interfacial-energy driven bulk diffusion. Elapsed time after (a): (b) 750 s, (c) 1,350 s, (d) 1,650 s.

We test this prediction using 4D X-ray tomography. Using an affine transformation, we align the experimental data to the theoretically predicted shape, and linearly scale the predicted shape such that the diameter at the center of the pinching tube was the same as that measured experimentally. This process was repeated for a series of times leading to the singularity. We calculate the distance from the theoretically predicted shape to the closest point on the experimentally measured shape. We find an excellent agreement between theory and experiment in both the interfacial morphology and the kinetics of the pinching process. This work is done in collaboration with S. Poulsen and E. Lauridsen from RISO laboratory, M. Stampanoni of the Paul Scherrer Institute and M. Miksis from Northwestern University.

To understand the evolution of interfaces, the properties of interfaces such as curvatures at each interfacial patch must be calculated accurately. Since these quantities depend on the local change of the interfacial shape, noise and grid effects can overwhelm the data. A straightforward calculation of the mean curvature is shown in Fig. 3, using the phase-field order parameter obtained from a simulation of coarsening using Allen-Cahn dynamics. Since this is a simulated data, the order parameter is sufficiently smooth locally; the ripples that appear are due to the coarse grid. The simplest method to remove the ripples is by volume smoothing, but this will lead to loss of small but possibly important interfacial features.

In order to compute interfacial properties accurately while retaining small features in the dataset, we have developed a method combining the level-set and diffusion smoothing methods. The level-set method uses the order-parameter of the phase-field model as an initial condition and ensures the magnitude of the gradient of the level-set function to be a specified constant. The level-set function is given by the distance (to the constant factor) from the nearest interface, and therefore provides information such as the interfacial normal accurately over a larger region near the interfaces, and ensures that the change in the function stems only from the shape of the interfaces. The diffusion equation is used to remove the noise in the second derivatives with minimal change in the interfacial positions. Fig. 4 shows the mean curvature calculated using this method for the same structure shown in Fig. 3.

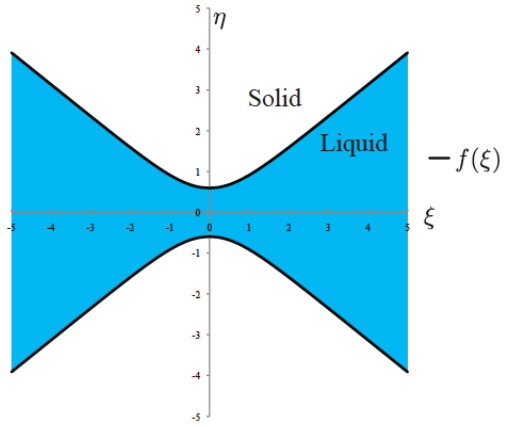

Figure 2. Theoretically predicted interfacial morphology, $f(\xi)$, as a function of the axial coordinate ξ. The shape is symmetric about ξ and asymptotes to a cone for large ξ.

As evident from the comparison between Figs. 3 and 4 the new method enhances the quantitative analysis of the evolving interfaces. As an alternative to more traditional smoothing methods such as the volume smoothing, our method improves accuracy of the calculated properties by reducing the movement of the interfaces during the smoothing of dataset.

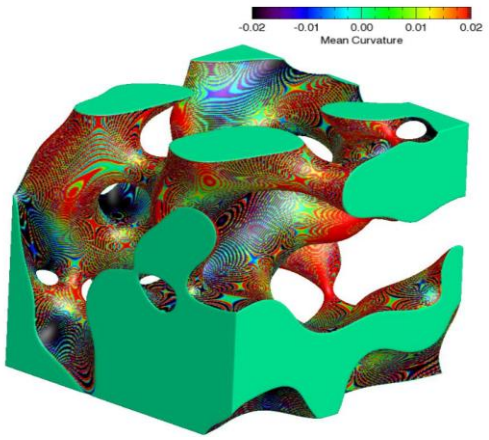

Figure 3. The interfacial morphology of the Allen-Cahn structure, colored with the mean curvature that is calculated directly from the order parameter.

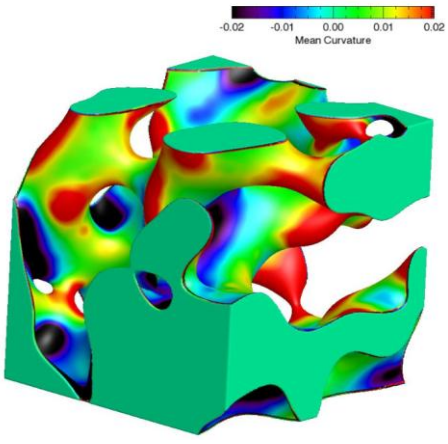

Figure 4. The interfacial morphology of the Allen-Cahn structure, colored with the mean curvature that is calculated from the combination of the level-set method with the diffusion smoothing.

Future Plans

Using the smoothing approach discussed above we will analyze both experimental and theoretical data. We will employ the 4D X-ray tomography data of coarsening in dendritic solid-liquid mixtures in the Al-Cu system and simulation data of coarsening under Allen-Cahn and Cahn-Hilliard dynamics. We will be seeking connections between interfacial velocities and interfacial curvature. These studies will be used to form the basis for the theory of coarsening in complex microstructures.

Publications

- Y. Kwon, K. Thornton and P.W. Voorhees, *The Topology and Morphology of Bicontinuous Interfaces During Coarsening,* Euro Physics Letters, **86** 46005 (2009).

- Y. Kwon, K. Thornton and P.W. Voorhees, *Morphology and Topology of Domains Coarsening via Nonconserved and Conserved Dynamics,* Phi. Mag., in press.

- L. Aageson, A. Johnson, J. Fife, S. Poulson, E. Lauridsen, M. Miksis, M. Stampanoni, and P. Voorhees, *Universality and Topological Singularities in Materials: Self-Similar Pinch-Off of Rod,* submitted.

- L. Aageson, T. Pusztai and P.W. Voorhees, *The Morphology and Topology of Equiaxed Dendritic Solid-Liquid Mixtures: A Comparison Between Simulation and Experiment,* submitted.

- J.L. Fife, J.C. Li, D.C. Dunand and P.W. Voorhees, *Morphological Analysis of Pores in Directionally Freeze-Cast Titanium Foams*, J. Mater. Res., **24**, 117-124 (2009).

- J.L. Fife and P.W. Voorhees, *Self-Similar Microstructural Evolution Of Dendritic Solid-Liquid Mixtures During Coarsening, Scripta Mater.* **60**, 839-842 (2009).

- J.L. Fife and P.W. Voorhees, *The Morphological Evolution of Equiaxed Dendritic Microstructures During Coarsening, Acta Mater.* **57**, 2418-2428 (2009).

Fundamental crystal-melt interface behavior

M.I. Mendelev, J. Monk, R.E. Napolitano, M.J. Kramer and R.T. Ott
mendelev@ameslab.gov
Materials Science and Engineering Program
Ames Laboratory US DOE, Ames, IA, 50011

Program Scope

The fundamental nature of structural selection during phase transitions in an undercooled liquid involves the simultaneous action of numerous physical forces, collectively governing the natural evolution of multiscale morphological hierarchy. This dynamical process includes energetic contributions that operate at (i) the *atomistic*- or *nano*scale, where the chemical and structural ordering in both crystalline and noncrystalline phases are important factors, (ii) the *capillary* scale, where interfacial properties may drive or influence structural evolution, (iii) the *microstructural* scale, where competition between various growth mechanisms and morphologies gives rise to complex structure, and (iv) various longer range thermal and chemical *transport* scales. Considered in concert, the prediction and control of phase selection and morphological dynamics, particularly far from equilibrium, is indeed a formidable task, but recent advances have let to quantitatively accurate predictive modeling methods that can be used to simulate many of the relevant structural and chemical features that evolve upon solidification. These methods, however, rely on accurate parameterization of fundamental thermodynamic and kinetic properties. The present subtask addresses these issues, integrating fundamental thermodynamic measurements[1], new approaches in bulk thermodynamic modeling[2], *ab initio* calculations[3], investigation of bulk and solid-liquid interface (SLI) behavior with molecular dynamics simulations (MD)[4], experimental measurement of SLI properties[5], and investigation of microstructural dynamics through experiments and continuum-level simulation. In this work we combine MD simulations of SLIs with *in situ* X-ray scattering experiments to quantify the SLI kinetics and identify the governing mechanisms. Such progress represents significant fundamental advancement in the area of structural dynamics in solid-liquid phase transitions.

Recent Progress

Molecular dynamics simulation of SLI properties requires using simulation cells containing tens of thousands of atoms and simulation times on the order of 1 ns. With these spatial and temporal scales precluding the use of first-principles methods, semi-empirical interatomic potentials are needed. A critical requirement for these potentials is that they accurately describe both the structures and properties of the solid and liquid phases. While there are several successful techniques to develop semi-empirical potentials suitable for simulation of solid phase properties in the literature (e.g., see Refs [6-10]), most of these potentials are not appropriate for the simulation of liquid or amorphous alloys. Therefore, we have developed a method for the construction of semi-empirical potentials where the data from diffraction experiments are used as input information along with the other literature and *ab initio* data on solid phases[11]. Using this method we have developed a semi-empirical potential for Cu-Zr alloys. Figure 1 shows that the new interatomic potential does predict a glass structure that is in very good agreement with experimental measurements.

Along with other solid phase properties, we tested the mechanical stability of bcc Zr and B2 $Cu_{50}Zr_{50}$ phases using this new interatomic potential. The ratio of elastic constants C_{11}/C_{12} as

function of temperature (Fig. 2) shows that both the bcc Zr and B2 phases are mechanically unstable at T=0 but stable above the room temperature, which is consistent with predictions from *ab initio* calculations. (It should be noted that this does not necessarily mean that these phases are thermodynamically stable.) Another critical feature of the newly developed potential is its ability to accurately describe the melting temperatures of pure Cu and Zr as well as the parameters of the hcp→bcc transformation in pure Zr. The accurate description of the solid and liquid properties makes the new potentials ideal for simulations of the SLI properties.

The kinetics of the SLI were investigated using the MD simulation scheme shown in Figure 3, where the simulation cell (~30,000 atoms) includes a crystalline layer sandwiched between two liquid layers with the interfaces macroscopically normal to the z axis, which is aligned with the <100> direction in the crystal. The simulation cell has periodic boundaries in the x and y directions and free surfaces in ±z directions. This scheme permits investigation of SLI migration in either direction, since the system can be driven to melt or freeze through well controlled adjustments in temperature. The new interatomic potential exhibits appropriate phase selection, where "freezing-mode" simulations yield fcc, bcc, and B2 structures for pure Cu, pure Zr, and $Cu_{50}Zr_{50}$, respectively, in agreement with experiment. Driven in either direction, the SLI velocity is determined from the time dependence of the total internal energy of the simulation cell. Figure 4 shows the SLI velocity, V as function of undercooling, $\Delta T=T-T_m$ for Cu, Zr and B2, where $V(\Delta T)$ is linear for the pure metals but nonlinear for the $Cu_{50}Zr_{50}$ alloy.

The kinetic coefficients determined from these simulations are 60 cm/(s·K) and 75 cm/(s·K) for pure Cu and Zr, respectively. Simulation results suggest that the $Cu_{50}Zr_{50}$ SLI is inherently different from that of the pure components, exhibiting a kinetic coefficient that is at least two orders of magnitude smaller. This result indicates the critical role of short-range chemical ordering during solidification. While the solid phase growing from the $Cu_{50}Zr_{50}$ liquid alloy always has a bcc structure, the occupancy of the lattice sites does not always completely correspond to the B2 symmetry. Figure 5 shows that near the melting temperature, the number of defects in growing B2 phase is rather small. However, at large supercooling the number of defects is much larger. This effect cannot be explained by the fact that the growth rate is larger at larger supercooling because it is actually smaller (see the insert in Fig. 4).

Since there is no partitioning requirement for growth of the $Cu_{50}Zr_{50}$ solid phase from the liquid alloy, this system provides an excellent opportunity to study interface kinetics using both computational and experimental means, without the superposition of diffusion kinetics. The obtained kinetic coefficients will be used as input in our phase field simulation.

Recent Progress on Other Projects

Unfortunately, there are no literature data to date to confirm our MD simulation results. Therefore, we are building a unique DS experimental setup to directly image the SLI in real time using high energy X-rays (Fig. 6). Proof-of-concept DS/tomography experiments have been performed at sector 13 at the Advanced Photon Sources at Argonne National Laboratory. We have confirmed our ability to directly image the solid/liquid interface. Over the next year, these experiments will be used to directly measure the SLI kinetic coefficient over a range of imposed temperature gradients.

Future Plans

We will continue to use MD simulations to quantify SLI kinetics, focusing specifically on the role of (i) chemical and structural ordering, (ii) crystalline anisotropy, and (iii) alloy

composition. Given that there are no reported literature data to date to confirm our MD simulation results, we have developed a unique DS experimental setup to directly image the SLI in real time using high energy (synchrotron) X-rays (Fig. 6). Proof-of-concept DS/tomography experiments have been performed at sector 13 at the Advanced Photon Sources at Argonne National Laboratory. We have confirmed our ability to directly image the solid/liquid interface. Over the next year, these experiments will be further developed to improve image resolution and temperature control capabilities to enable accurate direct measurement of the SLI kinetic coefficient in a systematic manner.

References:

[1] S. H. Zhou and R. E. Napolitano, Metall. Mater. Trans. A-Phys. Metall. Mater. Sci. **38A**, 1145 (2007).

[2] S. H. Zhou and R. E. Napolitano, Metall. Mater. Trans. A-Phys. Metall. Mater. Sci. **39A**, 502 (2008).

[3] S. Y. Wang, C. Z. Wang, M. Z. Li, L. Huang, R. T. Ott, M. J. Kramer, D. J. Sordelet, and K. M. Ho, Physical Review B **78** (2008).

[4] M. I. Mendelev, J. Schmalian, C. Z. Wang, J. R. Morris, and K. M. Ho, Physical Review B **74**, 104206 (2006).

[5] R. E. Napolitano and S. Liu, Physical Review B **70**, 11 (2004).

[6] M. S. Daw and M. I. Baskes, Physical Review B **29**, 6443 (1984).

[7] F. Ercolessi and J. B. Adams, Europhysics Letters **26**, 583 (1994).

[8] M. W. Finnis and J. E. Sinclair, Philosophical Magazine a-Physics of Condensed Matter Structure Defects and Mechanical Properties **50**, 45 (1984).

[9] M. I. Mendelev, S. Han, D. J. Srolovitz, G. J. Ackland, D. Y. Sun, and M. Asta, Philosophical Magazine **83**, 3977 (2003).

[10] Y. Mishin, M. J. Mehl, D. A. Papaconstantopoulos, A. F. Voter, and J. D. Kress, Physical Review B **6322** (2001).

[11] M. I. Mendelev, M. J. Kramer, R. T. Ott, D. J. Sordelet, D. Yagodin, and P. Popel, Philosophical Magazine **89**, 967 (2009).

DOE Sponsored Publications in 2008-2009 from Current Project

1. M.I. Mendelev, M.J. Kramer, C.A. Becker and M. Asta, Analysis of Semi-Empirical Interatomic Potentials Appropriate for Simulation of Crystalline and Liquid Al and Cu, Phil. Mag. **88**, 1723 - 1750 (2008).

2. M. Li, C.Z. Wang, M.I. Mendelev and K.M. Ho, Molecular dynamics investigation of dynamical heterogeneity and local structure in the supercooled liquid and glass states of Al, Phys. Rev. B **77**, 184202 (2008).

3. M.I. Mendelev, M.J. Kramer, R.T. Ott and D.J. Sordelet, Molecular dynamics simulation of diffusion in supercooled Cu-Zr alloys, Phil. Mag. **89**, 109-126 (2009).

4. M.I. Mendelev, M.J. Kramer, R.T. Ott, D.J. Sordelet, D. Yagodin and P. Popel, Development of suitable interatomic potentials for simulation of liquid and amorphous Cu-Zr alloys, Phil. Mag. **89**, 967-987 (2009).

5. M.I. Mendelev, M. Asta, M.J. Rahman and J.J. Hoyt, Development of Interatomic Potentials Appropriate for Simulation of, Solid-Liquid Interface Properties in Al-Mg Alloys, Phil. Mag., in press.

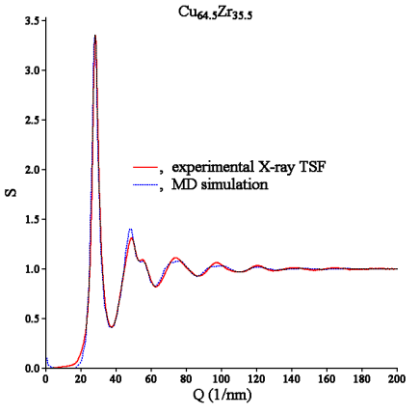

Figure 1. X-ray TSF of amorphous $Cu_{64.5}Zr_{35.5}$ at T=300 K.

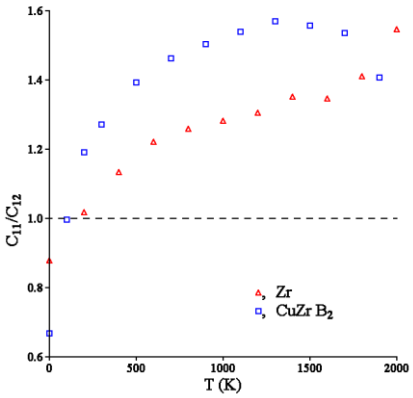

Figure 2. Mechanical stability of the bcc Zr and B2 phases.

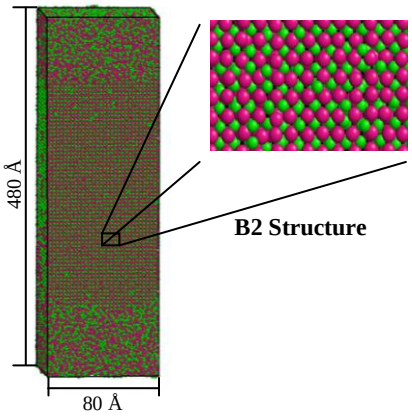

Figure 3. Simulation scheme.

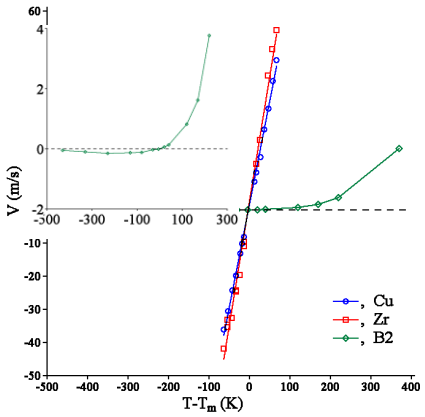

Figure 4. SLI velocity in pure metals and B2.

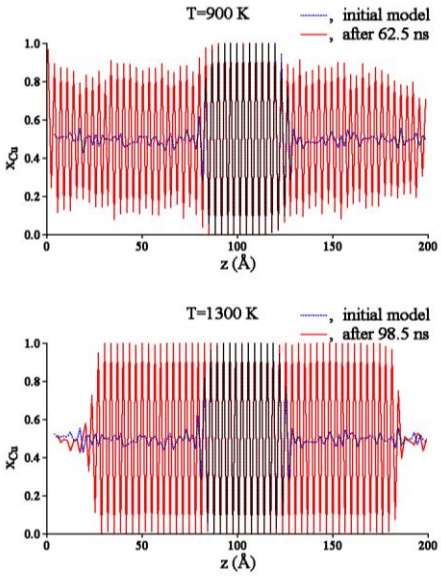

Figure 5. Cu concentration in the <100> direction.

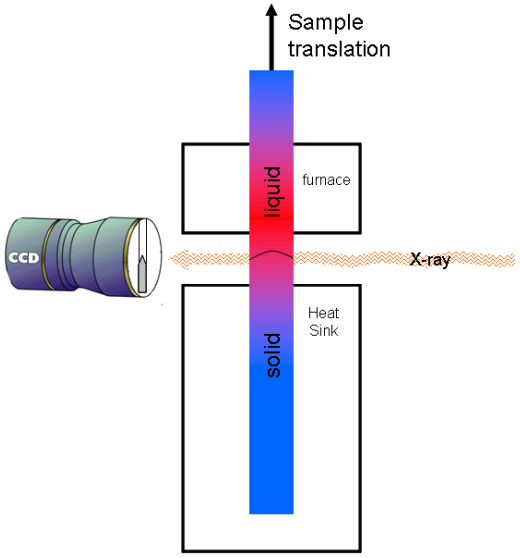

Figure 6. Experimental setup to study the SLI migration.

The Atomic Structure of the Deeply Undercooled Metallic Liquid: Challenges to Experiments and Simulations

M. J. Kramer,[*#] M.I. Mendelev,[*] S.G. Hao,[*] K.M. Ho,[*] R. T. Ott,[*]
C.Z. Wang[*] and R. E. Napolitano[*#]
mjkramer@ameslab.gov
[*]Materials Science and Engineering Division, Ames Labs DOE
[#]Department of Materials Science and Engineering, Iowa State University

Program Scope

There is increased recognition that local atomistic structures of liquid phases are critical in dictating the transformation pathways in metallic alloy systems.[1-2] Solid phases that have short-range order (SRO) and medium-range order (MRO) similar to that of the corresponding liquid structures generally have smaller interfacial free energies between the amorphous and ordered phases.[3-4] These competing energetics are an influential factor when cooling a liquid metallic alloys in not only the selective nucleation of certain structures among many competing ones, but also for avoiding crystallization to form a glass. This broader fundamental challenge can be addressed by answering the following questions:

- *How does the observed collective structure of an amorphous solid or its liquid correlate to the pair-wise and many-body interactions that give rise to topological and chemical order,*
- *How is the structure affected by composition and temperature?*

By performing state-of-the-art scattering experiments that are closely coupled to atomistic simulations for select model binary and ternary alloys, we can ascertain the chemical and kinetic factors that control structural ordering in deeply undercooled liquids. The overall goal of this project is to develop a set of order parameters that accurately describe the salient structural changes that occur in liquid systems during cooling. The order parameters will be incorporated into continuum and solution-based descriptions of the thermodynamics of the system. The establishment of such a theoretical framework will provide a model where structural and dynamics properties can be unified to simulate the structural evolution in undercooled liquid systems.

Recent Progress

Reliable structural determination of liquid metallic alloys is not a trivial undertaking.[5] On the experimental side, well controlled undercoolings can only be achieved with high-purity samples free of external stimuli for nucleation. The liquid scattering experiments were conducted at the Advanced Photon Source (APS) at sector 6ID-D. Samples of Cu_xZr_{1-x}, $PdZr_2$, and $Cu_{1-x}Ni_xZr_2$ were electro-statically levitated and laser heated to ~300 K above the melting temperature (T_m) followed by free-cooling while collecting the forward scattered high-energy X-rays on an area detector. Data sufficient for pair-distribution function (PDF) analysis could be obtained with exposures times of ~0.1 s. Concurrent temperature and density measurements were also obtained. Zr-based alloys were chosen since they represent compounds ranging in glass-formability,[6] a wide variety of stable and meta-stable phase relationships,[7] and differences in their electronic configuration[8] and ionic radii.[9]

There are a number of simulation techniques that can provide 3D descriptions of the liquid structure, each having its strengths and weaknesses. *Ab initio* methods were used to calculate liquid structures, but this approach is limited to small models (a few hundred atoms) and very high cooling rates (~10^{12} K/s) due to high computational overhead. Simulations were performed on most of the deeply undercooled alloys mentioned above. Larger systems and

longer simulation times can be performed using classical molecular dynamics (MD) simulations, which utilize empirical inter-atomic potentials (e.g. embedded atom method (EAM)). However, this method requires a considerable amount of time and effort to develop accurate inter-atomic potentials. Work was recently completed on the development of a Cu-Zr potential, which provides structures that are in very good agreement with X-ray scattering measurements (Fig. 1) [10-11] and appears to correctly predict several aspects of the mechanical behavior.[12]

Major challenges in describing the structure of undercooled liquids and amorphous solids is that experiments reduce the higher-order atomic correlations to a 1D pair correlation while the simulations occur on spatial and temporal scales that are orders of magnitude different than the experiments. Therefore, the experimentally measured total scattering function (S(q)) or its Fourier Transformation, the PDF, is typically compared to the simulations. If these data agree and the simulations also accurately predict other measured thermophysical properties, it increases the confidence in the simulated structures and properties. The accuracy of the simulations is critical since they provide information that cannot be easily obtained experimentally.

Another challenge in characterizing the structure of liquids involves effectively describing the developing order that occurs during undercooling. The development of MRO can be seen qualitatively in the sharpening of the peaks in the partial-pair correlation function (PPCF) of the real-space data for the EAM-MD simulation of the $Cu_{64.5}Zr_{35.5}$ alloy as it is cooled from the liquid to the amorphous state (Fig. 2) and observed in the reciprocal space data from the experiments (Fig. 1). Common methods for describing the SRO, such as the Bond Orientation Order,[13] Honeycutt-Anderson analysis[14] and Voronoi Tessellation[15] do not capture the higher order correlations that are developing in the undercooled liquid nor do they provide a framework for

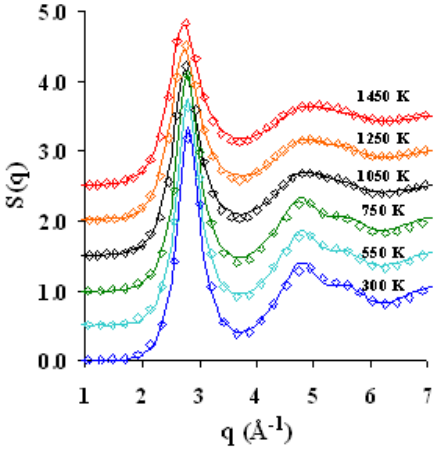

Fig. 1. EAM-MD (solid lines) and experimental data for $Cu_{64.5}Zr_{35.5}$ alloy heated to the glass transition (300 to 750 K) and its liquid cooled from 1450 down to 1050 K (open symbols).

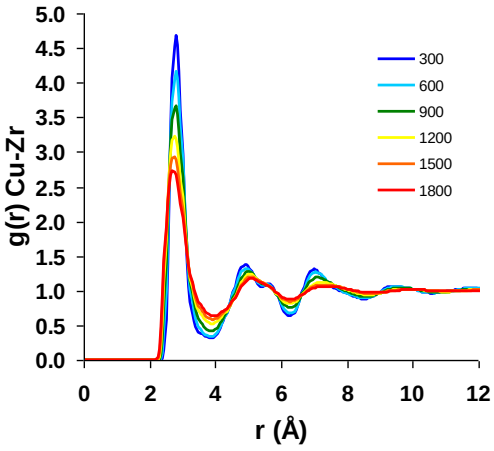

Fig. 2. EAM-MD of the Cu-Zr PPCF for the simulated $Cu_{64.5}Zr_{35.5}$ alloy cooled from 1800 K. Note the significant changes in the shape of the distributions above T_g ~ 750 K.

rigorously correlating these structures to their stable or meta-stable phases. What is needed is a new approach that more accurately describes the developing structural order in a disordered system.

One approach we have developed to analyze the MRO is to determine the connectivity of the neighboring Voronoi Polyhedra (VP). In this method, we look at the difference in distribution of the neighboring type of VPs to the most common VPs within that structure. The

connectivity map in Fig. 3 shows which VP types are spatially correlated or anti-correlated compared to a random distribution. From this analysis technique the highest correlated VP in the $Cu_{64.5}Zr_{35.5}$ are the icosahedral <0,0,12,0> with a strong affinity for identical neighbors. Furthermore, we find that (i) the <0,0,12,0> has the longest average life-time of all VPs, (ii) they tend to form connected 'solid-like' backbone structures, (iii) the number and size of these 'backbones' increase with undercooling and (iv) the glass is characterized by a dense network of <0,0,12,0> VPs which are separated by more 'liquid-like' VPs. The icosahedral and distorted icosahedral VPs also have a lower energy compared to the average liquid or glass. Interestingly, the region in the binary Cu-Zr phase diagram associated with the best glass forming regions has the highest density of the <0,0,12,0> and also the lowest diffusivity in the undercooled liquid.[16]

Future Plans

Our current and future work is to address the limitations of experiments and simulations cited above. Experimental efforts will be expanded to develop methods that will allow for capturing higher-order correlations not accessible by scattering methods. In particular, fluctuation electron microscopy has promise in this area. We will also develop hybrid methods to extend the 'effective cooling rate' of the simulations to longer length scales. One method will be combining EAM-MD and *ab inito* techniques to allow for EAM-MD simulations that cool the models and then equilibrate them at that temperature with *ab initio*. We are also working on more robust algorithms to describe both the SRO and MRO in amorphous systems. For instance, traditional Voronoi Tessellation cannot distinguish between face-centered cubic-like and icosahedral-like VPs. We are currently extending the suite of alloys to a wider range of compositions to test the universality of the current observations in the Cu-Zr system. Substitutions to the binary system and new alloys will be selected to focus on the competing contributions of atomic size and electronic states on the local order which develops in the metallic liquid. For example, Ni substitutions are particularly interesting since the atomic radii are nearly the same but different *s* electron allowing for more *d*-band stabilized compounds.[8] Moreover, additions of Al to Zr-based alloys allows for bond shortening, stabilizing the ternary glass over the binary, but it is unclear if this also true in the liquid? Lastly, additions of non-metals, B, Si and P, are key additions in several good glass forming systems, but the glasses that form do not appear to have any significant icosahedral order, which raises the question as to the generality of the role of icosahedral ordering in glass-forming metals.

Fig. 3. On top is a histogram of the distribution, in percent, for the most common VPs. On the bottom is a correlation map showing the 14 most common VP for the simulated $Cu_{64.5}Zr_{35.5}$ liquid (1300 K). Warm colors indicate higher than random probability that the VP are neighbors.

References

1 Holland-Moritz, D. *et al. Materials Science & Engineering, A: Structural Materials: Properties, Microstructure and Processing* **A375-A377**, 98, (2004).
2 Kelton, K. F. *Intermetallics* **14**, 966, (2006).
3 Holzer, J. C. & Kelton, K. F. *Acta Metallurgica Et Materialia* **39**, 1833, (1991).
4 Lee, G. W. *et al. Physical Review B: Condensed Matter and Materials Physics* **72**, 174107, (2005).
5 Hennet, L. *et al. International Journal of Thermophysics* **26**, 1127, (2005).
6 Altounian, Z. *et al. Journal of Applied Physics* **54**, 3111, (1983).
7 Arias, D. & Abriata, J. P. *Bulletin of Alloy Phase Diagrams* **11**, 452, (1990).
8 Kramer, M. J. *et al. Metallurgical and Materials Transactions a-Physical Metallurgy and Materials Science* **39A**, 1847, (2008).
9 Egami, T. *Materials Research Society Symposium Proceedings* **754**, 47, (2003).
10 Mendelev, M. I. *et al. Journal of Applied Physics* **102**, 093518 (2007).
11 Mendelev, M. I. *et al. Philosophical Magazine* **89**, 967, (2009).
12 Mendelev, M. I. *et al. Journal of Applied Physics* **104**, 123532 (2008).
13 Steinhardt, P. J. *et al. Physical Review Letters* **47**, 1297, (1981).
14 Honeycutt, J. D. & Andersen, H. C. *Journal of Physical Chemistry* **91**, 4950, (1987).
15 Finney, J. L. *Nature* **266**, 309, (1977).
16 Mendelev, M. I. *et al. Philosophical Magazine* **89**, 109, (2009).

Publications supported by the DOE project over the last two years

Hao, S. G. *et al.* Experimental and ab initio structural studies of liquid Zr_2Ni. *Phys. Rev. B* **79**, 104206 (2009).

Kramer, M. J., *et al.*. Phase stability and transformations in the Zr_2NiCu_{1-x} amorphous system. *Metal. and Mat. Trans. A-Phys. Metal. and Mat. Sci*. **39A**, 1847 (2008).

Mendelev, M. I., *et al.* Analysis of semi-empirical interatomic potentials appropriate for simulation of crystalline and liquid Al and Cu. *Phil. Mag.* **88**, 1723 (2008).

Mendelev, *et al.* Molecular dynamics simulation of diffusion in supercooled Cu-Zr alloys. *Phil. Mag.* **89**, 109 (2009).

Mendelev, M. I. *et al.* Development of suitable interatomic potentials for simulation of liquid and amorphous Cu-Zr alloys. *Phil. Mag.* **89**, 967 (2009).

Mendelev, M. I. *et al.* Deformation behavior of an amorphous Cu64.5Zr35.5 alloy: A combined computer simulation and experimental study. *Journal of Applied Physics* **104**, 123532 (2008).

Mendelev, *et al.* Determining strain in amorphous alloys: Uncertainties with analyzing structural changes during deformation. *Journal of Applied Physics* **105**, - (2009).

Ott, R. T. *et al.* Anelastic strain and structural anisotropy in homogeneously deformed Cu64.5Zr35.5 metallic glass. *Acta Materialia* **56**, 5575 (2008).

Ott, R. T. *et al*, Strain dependence of peak widths of reciprocal- and real-space distribution functions of metallic glasses from in situ x-ray scattering and molecular dynamics simulations. *Phys. Rev. B* **80**, 064101 (2009).

Sordelet, D. J. *et al.* Structure of Zr_xPt_{100-x} ($73 <= x <= 77$) metallic Glasses. *Metal. and Mat. Trans. A-Phys. Metal. and Mat. Sci.* **39A**, 1908 (2008).

Wang, S. Y. *et al.* Short- and medium-range order in a $Zr_{73}Pt_{27}$ glass: Experimental and simulation studies. *Phys. Rev. B* **78**, 184204 (2008).

Wang, S. Y. *et al.* Experimental and ab initio molecular dynamics simulation studies of liquid $Al_{60}Cu_{40}$ alloy. *Phys. Rev. B* **79,** 144205 (2009)

In situ High Energy X-ray Synchrotron Diffraction Study of the Synthesis and Stoichiometry of $LaFeAsO$ and $LaFeAsO_{1-x}F_y$

R. W. McCallum, T. A. Lograsso, L. L. Jones, P.C. Canfield and I. E. Anderson
Ames Laboratory, Ames IA 50014

Program Scope

The growth, control and modification of novel materials in single crystal and polycrystalline form, represent a national core competency that is essential for scientific advancement within and across traditional disciplinary boundaries, and are critical components of the USDOE Basic Energy Sciences' mission. The objectives of this program are to advance the ability to synthesize and characterize high purity, high quality novel materials; develop unique capabilities and processing knowledge in the preparation, purification, and fabrication of metallic elements, alloys, and compounds; and to understand and quantify the role of synthesis in controlling chemical inhomogeneities and structural defects that influence the properties of highly responsive materials (superconductors, magnetostrictive (Fe-X alloys) and ferromagnetic shape memory alloys (Ni-Mn-X alloys). Our efforts are grouped into three areas; 1) growth-based activities that are currently focused on identifying operating limits for solution growth methods by defining stable morphological growth regimes; 2) use-inspired materials investigations of highly magneto-responsive materials and superconductors aimed at developing synthesis capabilities and protocols for high-quality single phase samples with well controlled microstructures in both single and polycrystalline form; and 3) utilizing our synthesis and characterization capabilities to understand synthesis-structure relationships that will lead to the control manipulation and optimization of specific energy-relevant material systems.

This research effort is integrated with the Materials Preparation Center (MPC) at the Ames Laboratory. The Materials Preparation Center is a specialized research center, managed through the BES Synthesis & Processing core research area, whose mission is to provide high-purity, high-quality materials in support of scientific research programs at the Ames Laboratory and to the general scientific community. (see related Abstract)

Within each of these task areas referenced above, a variety of research projects are active and ongoing. For this meeting we review 1) the use of in situ high energy x-ray synchrotron diffraction in identifying the reaction pathways and stoichiometry of $LaFeAsO$ and $LaFeAsO_{1-x}F_x$ and 2) the results of defining growth regimes and protocols for bulk single crystals of the ferromagnetic superconductor $ErRh_4B_4$ (see related Abstract).

Recent Progress

In situ High Energy X-ray Synchrotron Diffraction Study of the Synthesis and Stoichiometry of $LaFeAsO$ and $LaFeAsO_{1-x}F_y$ [1]

The discovery of high transition temperature (T_c) superconductivity with structural units of (FeAs) layers has attracted extensive attention in the scientific community. Like the cuprates,

---

[1] McCallum, R. W.; Yan, J.-Q.; Rustan, G. E.; Mun, E. D.; Singh, Yogesh; Das, S.; Nath, R.; Bud'ko, S. L.; Dennis, K. W.; Johnston, D. C.; Canfield, P. C.; Kramer, M. J.; Kreyssig, A.; Lograsso, T. A.; Goldman, A. I. **In situ high energy x-ray synchrotron diffraction study of the synthesis and stoichiometry of LaFeAsO and LaFeAsO1-xFy.** Journal of Applied Physics (2009), 105(12), 123912/1-123912/11.

this series of materials share a common structural feature, in this case the (FeAs) layers. However, in these materials, the planes may be separated by either oxide layers, such as $RO_{1-x}F_x$ in $RFeAsO_{1-x}F_x$ (R = light rare earth element), or metallic layers, such as AE metal in $AE_{1-x}K_xFe_2As_2$ (AE = Ca, Sr, or Ba) and Li in LiFeAs, offering the opportunity to study superconductivity in both oxides and intermetallics in closely related compounds. The preparation of polycrystalline $RFeAsO_{1-x}F_x$ has been plagued by high levels of irreproducibility characterized by large run to run variations in phase purity and superconducting fraction. The root cause of these problems is the fact that 3 to 5 reactants must be combined into a homogenous sample. In addition, the low melting temperature of Fe-As binary compounds was viewed as a possible source of phase segregation during preparation when liquid is formed and migrates through the under the influence of capillary forces, temperature gradients and gravity . Given the fact that La_2O_3, LaF_3, LaOF, LaAs, and Fe_2O_3 all melt above 1500 °C, the diffusion of the refractory components is expected to be limited below the melting of the Fe-As phase mixtures between 840°C and 1040°C.

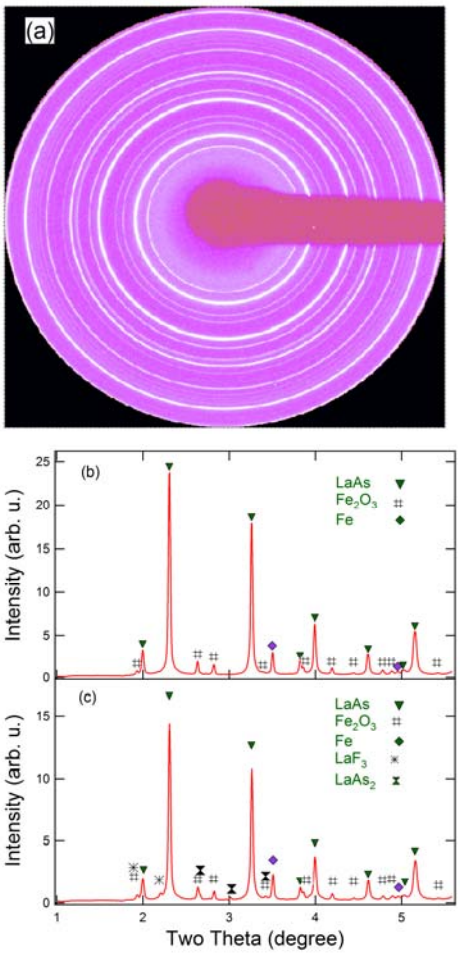

Figure 1. (a) Typical X-ray diffraction image recorded on the CCD detector for composition A at 200 °C. (b) 1-D plot of angle-integrated intensity vs 2θ for composition A at 200 °C. (c) 1-D plot of angle-integrated intensity vs 2θ for composition B at 100 °C

In order to gain a more complete understanding of the sample preparation of $RFeAsO_{1-x}F_y$ materials, we have undertaken a detailed study of the reaction route in both undoped and fluorine doped LaFeAsO. This study utilized both Differential Thermal Analysis (DTA) and *in situ* high temperature x-ray diffraction. The High-Energy X-Ray Diffraction (HEXRD) studies were performed at station 6ID-D in the MUCAT sector at the Advanced Photon Source (APS), Argonne National Laboratory. High energy x-rays from a synchrotron allow for data to be taken in transmission geometry so that the bulk of the sample is measured. The use of a charge coupled device (CCD) area detector allows the acquisition of high quality diffraction patterns in time slices as short as 20 seconds. This rapid acquisition rate, coupled with continuous heating, allows for a real time determination of phases and phase distributions as a function of temperature that can be correlated with thermal analysis measurements. In this way, the reaction pathway for a given set of starting materials is determined including the formation and elimination of intermediate phases leading in turn to the formation of the $RFeAsO_{1-x}F_y$ phase. Residual impurity phases are also identified.

From the analysis of the high temperature diffraction data we have determined the phase evolution as a function of temperature in the formation of the FeAs based superconductors $LaFeAsO_{1-x}$ and $LaFeAsO_{1-x}F_y$ under ambient pressure conditions. Based on the analysis of the

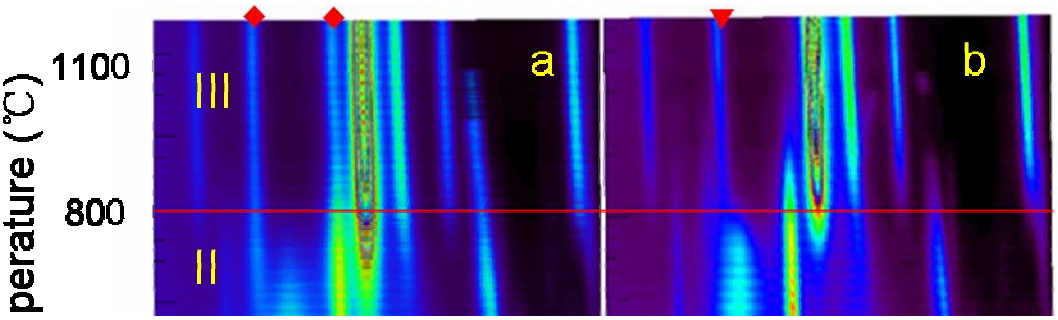

phase evolution for $LaFeAsO_{1-x}$, we have proposed a reaction path which has significant implications with respect to the formation of single phase materials. Consistent with thermal analysis results, the control of the reaction in the proximity of the Fe-Fe_2As eutectic at 840 ºC is important for controlling the reaction rates and sample homogeneity. From an analysis of the observed phase composition at high temperature, we conclude that the materials may form with a large oxygen deficiency at the reaction temperature. The determination of this oxygen deficiency is highly dependent on the second phases which are present in the fully reacted material. This oxygen deficiency plays a significant role in the phase formation and may control the amount of F which is actually doped into the sample. While this oxygen deficiency controls the ability to make single phase samples, it also raises significant questions as to the doping of the (FeAs) layers in nominal $RFeAsO_{1-x}F_x$.

Future Plans

While La is the prototype for the RFeAsO, superconductors, Sm has the highest superconducting transition temperature. Although the reaction path of the Sm compounds is similar to that of the La compounds, there are differences which are currently being evaluated and will be presented in a second paper focusing on the high temperature x-ray diffraction determination of the reaction path. The question as to the range of oxygen stoichiometry over which the $LaFeAsO_{1-x}$ forms is also under further investigation. Having determined the reaction path we have directed a significant portion of our effort toward obtaining millimeter sized single crystals of the $LaFeAsO_{1-x}$ and $LaFeAsO_{1-x}F_y$ superconductors. Previously, small single crystals have only been obtained from growths performed in a high pressure cell. These crystals have been sub millimeter in size. We are currently refining an ambient pressure flux growth method which has produced plate-like single crystals of $LaFeAsO_{1-x}$ several millimeters in the lateral dimensions and of order 0.5 millimeter thick. The process is being refined to produce larger single crystals and to allow controlled doping. A variant of the process will be developed in an attempt to produce large single crystals using a floating solvent approach.

In a more general outlook, we will continue to develop safe effective processing protocols for the producing of single and polycrystalline materials containing volatile and or toxic materials. This will include safe methods of preparing materials at higher temperatures and the use of such processes as physical vapor transport and traveling solvent crystal growth. The procedures which we have developed for the production of binary arsenide's for precursor materials will be transferred to the Materials Preparation Center (MPC see related abstract) so that these materials can be made available to the broader scientific community.

Publications attributable to research performed under this research program (2008-2009)

J. M. Hill, R. J. McQueeney, R. Wu, K. Dennis, R. W. McCallum, M. Huang and T. A. Lograsso, "The Low Temperature Heat Capacity of $Fe_{1-x}Ga_x$, $0.0 < x < 0.194$", Phys. Rev. B, **77**, 014430 (2008).

J.-Q. Yan, A. Kreyssig, S. Nandi, N. Ni, S. L. Bud'ko, A. Kracher, R. J. McQueeney, R. W. McCallum, T. A. Lograsso, A. I. Goldman and P. C. Canfield, "Structural Transition and Anisotropic Properties of Single Crystalline $SrFe_2As_2$", Phys. Rev. B, **78**, 024516 (2008).

S. Nandi, A. Kreyssig, J. Q. Yan, M. D. Vannette, J. C. Lang, L. Tan, J. W. Kim, R. Prozorov, T. A. Lograsso, R. J. McQueeney and A. I. Goldman, "Magnetic Structure of Dy^{3+} in Hexagonal Multiferroic $DyMnO_3$", Phys. Rev. B, **78**, 075118 (2008).

S. Nandi, A. Kreyssig, L. Tan, J. W. Kim, J. Q. Yan, J. C. Lang, D. Haskel, R. J. McQueeney and A. I. Goldman, "Nature of Ho Magnetism in Multiferroic $HoMnO_3$", Phys. Rev. Lett. **100**, 217201 (2008).

Y. Janssen, K. W. Dennis, R. Prozorov, P. C. Canfield and R. W. McCallum. "Exotic (Anti)Ferromagnetism in Single Crystals of $Pr_6Ni_2Si_3$", Phys. Rev. B, **77**, 214407 (2008).

E. M. Levin, X. W. Fang, S. L. Bud'ko, W. E. Straszheim, R. W. McCallum and K. Schmidt-Rohr, "Magnetization and ^{13}C NMR Spin-lattice Relaxation of Nano-diamond Powder", Phys. Rev. B, **77**, 054418(2008).

J.-S. Zhou, Y. Ren, J.-Q. Yan, J. F. Mitchell, and J. B. Goodenough, "Frustrated Superexchange Interaction Versus Orbital Order in a $LaVO_3$ Crystal", Phys. Rev. Lett., **100**, 046401 (2008).

G. Petculescu, J. B. LeBlanc, M. Wun-Fogle, J. B. Restorff, D. Wu, T. A. Lograsso and A. E. Clark, "Magnetoelastic Coupling in $Fe_{100-x}Ge_x$ Single Crystals with $5 < x < 18$", J. Appl. Phys., **105**, 07A932 (2009).

A. Niazi, S. L. Bud'ko, D. L. Schlagel, J.-Q. Yan, T. A. Lograsso, A. Kreyssig, S. Das, S. Nandi, A. I. Goldman, A. Honecker, R. W. McCallum, M. Reehuis, O. Pieper, B. Lake and D. C. Johnston, "Single-Crystal Growth, Crystallography, Magnetic Susceptibility, Heat Capacity, and Thermal Expansion of the Antiferromagnetic S=1 Chain Compound CaV_2O_4", Phys. Rev. B, **79**, 104432 (2009).

R. W. McCallum, J.-Q. Yan, G. E. Rustan, E. D. Mun, Y. Singh, S. Das, R. C. Nath, S. L. Bud'ko, K. W. Dennis, D. C. Johnston, P. C. Canfield, M. J. Kramer, A. Kreyssig, T. A. Lograsso and A. I. Goldman, "*In situ* High Energy X-ray Synchrotron Diffraction Study of the Synthesis and Stoichiometry of LaFeAsO and $LaFeAsO_{1-x}F_x$", J. Appl. Physics, **15**, 123912 (2009).

C. Ma, J.-Q. Yan, K. W. Dennis, R. W. McCallum and X. Tan, "Size-dependent Magnetic Properties of High Oxygen Content $YMn_2O_{5\pm\delta}$ Multiferroic Nanoparticles", J. Appl. Phys., **105**, 033908 . (2009).

A. Kreyssig, R. Prozorov, C. D. Dewhurst, P. C. Canfield, R. W. McCallum and A. I. Goldman, "Probing Fractal Magnetic Domains on Multiple Length Scales in $Nd_2Fe_{14}B$", Phys. Rev. Lett., **102**, 047204 (2009).

Microstructural Development and Synthesis of $ErRh_4B_4$ Single Crystals

Novel Materials Preparation and Processing Methodologies
T.A. Lograsso, R. W. McCallum, L. L. Jones, P.C. Canfield and I. E. Anderson
Ames Laboratory, Ames IA 50014

Program Scope

The growth, control and modification of novel materials in single crystal and polycrystalline form, represent a national core competency that is essential for scientific advancement within and across traditional disciplinary boundaries, and are critical components of the USDOE Basic Energy Sciences' mission. The objectives of this program are to advance the ability to synthesize and characterize high purity, high quality novel materials; develop unique capabilities and processing knowledge in the preparation, purification, and fabrication of metallic elements and alloys; and to understand and quantify the role of synthesis in controlling chemical inhomogeneities and structural defects that influence the properties of highly responsive materials (Fe-As based superconductors, magnetostrictive (Fe-X alloys) and ferromagnetic shape memory alloys (Ni-Mn-X alloys). Our efforts are grouped into three areas; 1) growth-based activities that are currently focused on identifying operating limits for solution growth methods by defining stable morphological growth regimes; 2) use-inspired materials investigations of highly magneto-responsive materials and superconductors aimed at developing synthesis capabilities and protocols for high-quality single phase samples with well controlled microstructures in both single and polycrystalline form; and 3) utilizing our synthesis and characterization capabilities to understand synthesis-structure relationships that will lead to the control manipulation and optimization of specific energy-relevant material systems.

This research effort is integrated with the Materials Preparation Center (MPC) at the Ames Laboratory. The Materials Preparation Center is a specialized research center, managed through the BES Synthesis & Processing core research area, whose mission is to provide high-purity, high-quality materials in support of scientific research programs at the Ames Laboratory and to the general scientific community. The MPC is a national resource for bulk materials synthesis and processing of a wide variety of use-inspired, energy-relevant materials in both single and polycrystalline forms, spanning a range of sizes with well-controlled microstructures. These materials and processing capabilities are accessible by the scientific community through a Work for Others program (see related Abstract). In accomplishing this mission, MPC develops and maintains a broad spectrum of expertise and capabilities for synthesis and processing including purification, single crystal growth techniques, casting operations, mechanical fabrication, powder processing and rapid solidification processing. This breadth of capabilities allows us to address synthesis challenges at every stage of a materials development, from initial discovery and fundamental scientific investigations to assessing a materials' technological potential, thereby hastening the implementation of new materials in addressing the Nation's technological needs.

Within each of these task areas reference above, a variety of research projects are active and ongoing. For this meeting we review results of defining growth regimes and protocols for bulk single crystals of the ferromagnetic superconductor $ErRh_4B_4$ and the use of in situ high energy x-ray synchrotron diffraction in identifying the reaction pathways and stoichiometry of LaFeAsO and $LaFeAsO_{1-x}F_x$. (see related Abstract).

Recent Progress

Microstructural Development and Synthesis of $ErRh_4B_4$ Single Crystals

$ErRh_4B_4$ represents one of a handful of compounds that display superconductivity (T_C = 8.7 K) and ferromagnetic ordering (T_{FM} = 0.7 K). [1, 2] Up until the discovery of systems $ErRh_4B_4$, magnetism and superconductivity were thought to be mutually exclusive phenomena. In order to fully characterize the unique properties of this system, large single crystals (>1cm^3) are required. Unfortunately these crystals have proven difficult to grow due to the reactivity of the constituent elements, the lack of phase diagram information and relatively high melting points. Except for one instance where the solidification of a non-stoichiometric Er-Rh-B melt yielded a 0.3 g single crystal, there have only been reports of long needles (0.2×0.2×5mm) obtained from a solution growth technique using copper as an inert flux.[3] The difficulties encountered in the growth of $ErRh_4B_4$ single crystals are not uncommon when dealing with ternary systems. These growth issues make $ErRh_4B_4$ a test system for the development of efficient single crystal growth protocols that can be applied to a variety of ternary systems that lack the required phase information. To develop the proper growth protocols, microstructural and thermal analyses were performed on $ErRh_4B_4$ (1-4-4) as well as several surrounding compositions to further define the liquidus surface and solidification behavior of this compound. Microstructural analysis indicates that the primary surface is exposed between 1-4-4 and the eutectic constituent comprised of $RhB_{1.1}$ and 1-4-4 compounds (Figure 1a). The microstructure of compositions between 1-4-4 and the eutectic suggest that 1-4-4 solidifies dendritically with non-faceted morphologies and that compositional segregation of the liquid occurs directly toward the eutectic composition. It was found that for compositions close to 1-4-4, where 1-4-4 is nucleated directly from liquid (primary solidification), approximately 75% by volume will solidify as 1-4-4. DTA analysis indicates that stoichiometric 1-4-4 decomposes via a peritectic reaction at 1439°C (Figure 1b). On cooling the eutectic temperature of 1240°C suggests a maximum growth temperature range of 200°C. Based on the observed growth morphologies and DTA results it was concluded that a Bridgman approach would be most applicable. Optimization of the Bridgman growth temperature and pulling rate led to a planar growth front and the solidification of single phase 1-

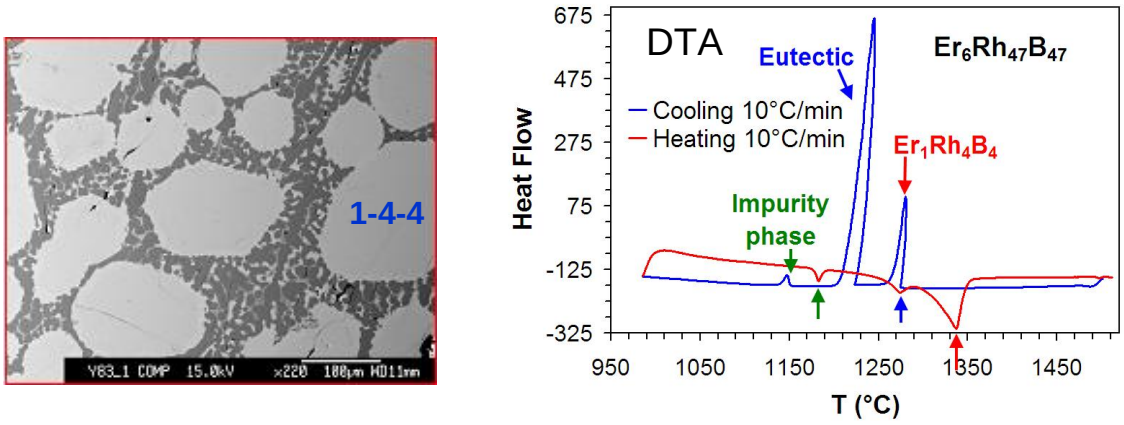

(a) (b)

Figure 1 Microstructural and thermal analyses of the solidification path of an $Er_6Rh_{47}B_{47}$ alloy. Primary solidification of the $ErRh_4B_4$ dendrites with limited faceting suggests Bridgman growth under planar growth conditions could be utilized for bulk single crystal growth

4-4 over a large fraction of the ingot (see Figure 2). AC susceptibility measurements of crystals cut from the single phase region feature a superconducting transition T_C = 8.54 K with a width of 0.15 K consistent with previous work.

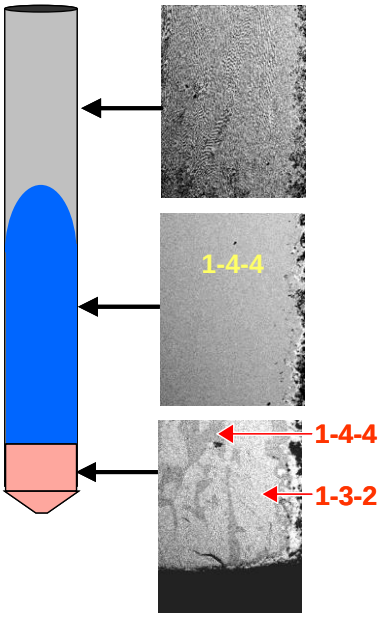

Figure 2 Directional solidification (Bridgman configuration) leads to phase separation via sequential solidification across the ternary liquidus surface (shown schematically on left). Bulk single crystal has been harvested from the central region where single phase planar solidification of $ErRh_4B_4$ occurred.

Future Plans

The trial and error approach to finding optimal composition and growth conditions for solution growth can be minimized by the use of relevant phase diagrams and a basic understanding of the faceted growth of crystals. Unfortunately, solution growth does not lend itself very well to modeling efforts as it is practiced, due to a lack of control of heat transfer and a coupling of growth temperatures and kinetics that do not allow for independent control over faceted/non-faceted growth regimes. Currently there is overall agreement that the slope of the liquidus as a function of composition is key to determining the proper growth parameters (composition and cooling rate) for a given solution growth run [5-7, 10, 11, 16]. This consensus is based on detailed models of faceted growth that are tied to supersaturation gradients across the face of the growing facet. A faster cooling rate leads to a larger supersaturation gradient and dendritic growth while a slower cooling rate minimizes undercooling leading to a lower supersaturation gradient and faceted growth. Although the importance of the liquidus is agreed upon, the proper region of the liquidus to grow over is not. In contrast, thermodynamic considerations by Saroch *et al.* [4] claim that the stable region for faceted crystal habits coincide with relatively flat regions of the liquidus curve (surface). To properly resolve this issue and understand the dynamics between stable faceted crystal habits regimes and those faceted growth regimes stabilized by kinetic considerations, these two effects need to be decoupled. We will employ directional solidification studies to establish independent control over growth temperatures and growth rate in the Pb-Pr alloy system by altering the nominal compositions and controlling the temperature gradient at the solidifying interface. We will model the solidification behavior using phase field methods to correlate the microstructural development with the materials parameters and growth conditions. Further we will utilize thin tube methods to isolate convection effects.

References

1. W. A. Fertig, D. C. Johnston, L. E. Delong, R. W. McCallum, M. B. Maple, and B. T. Matthias, Phys. Rev. Lett. **38**, 987 (1971).
2. S. K. Sinha, G. W. Crabtree, D. G. Hinks, and H. Mook, Phys. Rev. Lett. **48**, 950 (1982).
3. T. Takei, T. Shishido, H. Iwasaki, and Y. Muto, Jpn. J. Appl. Phys. **22**, 1463 (1983).
4. M. Saroch, K. S. Dubey, P. Ramachandrarao, J. Crystal Growth **126**, 701 (1993).

Publications attributable to research performed under this research program (2008-2009)

A.E. Clark, J.B. Restorff, M. Wun-Fogle, D. Wu, and T.A. Lograsso, "Temperature Dependence of the Magnetostriction and Magnetoelastic Coupling in Fe-Al and Fe-Co Alloys", J. Appl. Phys., **103,** 07B310 (2008).

D. Wu, Q. Xing and T.A. Lograsso, "Magnetostriction of Iron-Germanium Single Crystals", J. Appl. Phys., **103**, 07B307 (2008).

J. M. Hill, R. J. McQueeney, R. Wu, K. Dennis, R. W. McCallum, M. Huang and T. A. Lograsso, "The Low Temperature Heat Capacity of $Fe_{1-x}Ga_x$, $0.0 < x < 0.194$", Phys. Rev. B, 77**,** 014430 (2008).

A. E. Clark, J. B. Restorff, M. Wun-Fogle, D. Wu and T. A. Lograsso, "Temperature Dependence of the Magnetostriction and Magnetoelastic Coupling in Fe-Al and Fe-Co Alloys", J. Appl. Phys., **103**, 07B310 (2008).

D. L. Schlagel, R. W. McCallum and T. A. Lograsso, "Influence of Solidification Microstructure on the Magnetic Properties of Ni-Mn-Sn Heusler Alloys", J. Alloys Compd., **463,** 38 (2008).

Q. Xing, Y. Du, R. McQueeney and T. A. Lograsso, "Structural Investigations of Fe-Ga Alloys: Phase Relations and Magnetostrictive Behavior", Acta Mat., **56**, 4536 (2008).

D. L. Schlagel, W. M. Yuhasz, K. W. Dennis, R. W. McCallum and T. A. Lograsso, "Temperature Dependence of the Field Induced Phase Transformation in $Ni_{50}Mn_{37}Sn_{13}$", Scripta Mat, **59**, 1083 (2008).

Q. Xing and T. A. Lograsso, "Phase Identification of Quenched Fe-25 at% Ga", Scripta Mat, **60**, 373 (2009).

W. M. Yuhasz, D. L. Schlagel, Q. Xing, K. W. Dennis, R. W. McCallum and T. A. Lograsso, "Influence of Annealing and Phase Decomposition on the Magnetostructural Transitions in $Ni_{50}Mn_{39}Sn_{11}$", J. Appl. Phys., **105**, 07A921 (2009).

G. Petculescu and J. B. LeBlanc, M. Wun-Fogle and J. B. Restorff, D. Wu and T. A. Lograsso, A. E. Clark, "Magnetoelastic Coupling in $Fe_{100-x}Ge_x$ Single Crystals with $5 < x < 18$", J. Appl. Phys., **105**, 07A932 (2009).

R. S. Dhaka, S. W. D'Souza, M. Maniraj, A. Chakrabarti, D. L. Schlagel, T. A. Lograsso, and S. R. Barman, "Photoemission Study of the (100) Surface of Ni_2MnGa and Mn_2NiGa Ferromagnetic Shape Memory Alloys", Surface Science, **603**, 1999 (2009).

X. Moya, D. Gonzalez-Alonso, Ll. Manosa, A. Planes, V. O. Garlea, T. A. Lograsso, D. L. Schlagel, J. L. Zarestky, S. Aksoy and M. Acet, " Lattice Dynamics in Magnetic Superelastic Ni-Mn-In Alloys. Neutron Scattering and Ultrasonic Experiments", Phys Rev B, **79**, 214118 (2009).

Materials Preparation Center
L. L. Jones, T.A. Lograsso, R. W. McCallum, P.C. Canfield and I. E. Anderson
Ames Laboratory, Ames IA 50014

Program Scope

The Materials Preparation Center (MPC) is a BES-DMSE specialized research center with unique capabilities in preparation, purification, processing, and fabrication of well characterized materials for research and development. The MPC is focused on establishing and maintaining materials synthesis and processing capabilities crucial for the discovery and development of a wide variety of use-inspired, energy-relevant materials in both single and polycrystalline forms, spanning a range of sizes with well-controlled microstructures. The primary mission of the MPC is to develop innovative and superior processes for materials preparation, and to provide research-grade, controlled-purity materials and crystals that are otherwise not available to the academic, governmental, and industrial research communities. The MPC is widely recognized for its leadership in the area of materials synthesis. This leadership has been built from a combination of understanding the synthesis of and the underlying physics of a material, a willingness to collaborate widely through sample sharing, openness to divulging proprietary techniques, a desire for advancing synthesis through education, and open accessibility to the materials and processing capabilities of the Ames Laboratory through the MPC. Most notably, the MPC is regarded as the premier worldwide source of high purity rare earth metals, alloys and compounds.

The MPC currently conducts a variety of activities from fundamental research, to use-inspired R&D, to preparation of custom materials upon request. The integration of MPC within the BES funded research activity, *Novel Materials Preparation and Processing Methodologies*, coupled with close interactions with other research groups in Ames Laboratory, helps to strengthen and enhance the scientific and technical expertise of the MPC over broad classes of materials as well as develop processing capabilities and novel materials. This relationship results in a synergy that strengthens both the development of processing and material synthesis capabilities and the scientific understanding that is achieved in the research efforts at Ames Laboratory. While the research arm of the MPC is incorporated within *Novel Material*, the MPC interacts with the general scientific community through its “Work for Others” (WFO) activities. The processing capabilities and novel materials developed through the integration of fundamental research activities with the MPC is quickly made available to researchers worldwide. One measure of the impact of the MPC capabilities on the materials science research is that over 75 publications annually cite the MPC as the source of their materials. .Selected articles are listed in the Publication section.

MPC maintains and operates a wide range of equipment for the preparation and processing of a variety of metallic materials. Facilities included are: melting and casting systems; vacuum and inert gas atmosphere furnaces; mechanical processing equipment; rapid solidification systems for atomization and melt spinning; and crystal growth systems for preparation of single crystal elemental and intermetallic compounds. This breadth of process allows the MPC to select appropriate methods and develop protocols for synthesis of a wide range of novel materials. Processing equipment operated by the MPC includes both general-use commercial equipment and unique research equipment that has enabled new processes to be designed and developed by researchers in the Ames Laboratory. There are four functional sections within the MPC: (1) high

purity rare earth metals and alloys; (2) general alloy preparation; (3) single crystal synthesis; and (4) metallic powder atomization. Each area is provided scientific and technical guidance by a Principal Investigator (PI) whose individual expertise is aligned with the function of each section.

Recent Progress

Purification processes play an important critical role in the preparation of high purity metals, compounds and precursors. MPC's capability in uranium purification processing has enabled the understanding of the underlying mechanism in highly correlated electron systems. In these systems, the low temperature behavior of specific heat and resistivity are strongly affected by a small amount of impurity due to the formation of an impurity band in the hybridization gap. Electrotransport purified uranium prepared by MPC overcomes this barrier. MPC has resumed the purification of uranium in support of these research activities.

Successful synthesis of high purity thin film nanomaterials requires the use of high purity multi-component sputter targets of novel materials. Sputter targets are often prepared from powder precursors that contain significant amounts of oxygen. Melt processing, while helping to maintain high purity, is not always an applicable route to target preparation due to brittle compound formation. However, melt processing to maintain high purity, followed by careful comminution under low oxygen conditions results in high purity pressed and sintered sputter targets with significantly lower impurity levels. MPC's equipment and capabilities are well suited to provide this type of processing to ensure the highest purity materials for thin film research.

Developing methods to take novel materials from the research scale to the bulk scale has been a strategy employed by MPC to enable use-inspired materials. A bulk scale method has been developed at Ames to convert plasma synthesized boron and carbon doped boron powders into MgB_2 superconductors. Utilizing the protocols developed in research scale processing the MPC has worked with researchers to produce larger quantities of MgB_2. Such larger quantities are required for the fabrication of sputter targets for thin film deposition studies.

During FY2008 (most recent year of complete data) the MPC provided materials and services to academic, governmental, and industrial scientists providing MPC with $660K in external revenue. The MPC's WFO efforts supported 179 external materials request, which include 128 different scientists at 93 academic, national and industrial laboratories worldwide.

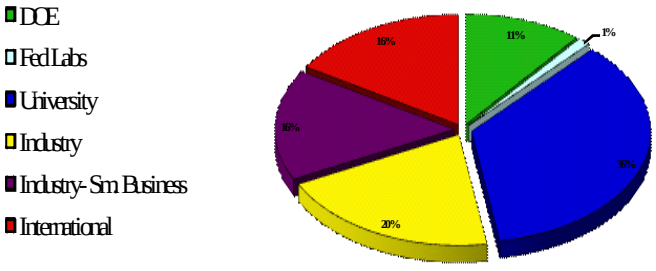

Future Plans

The availability of MPC rare earth metals and compounds is a key underpinning element to many of the experimental research efforts at the Ames Laboratory as well as throughout the DOE materials science and condensed matter physics community. As a Specialized Research Center the MPC is working to provide higher purity rare earth metals and compounds with lower oxygen content through better fluoride processing known as "hot topping". Improved purity of

LaF_3 and rare earth metals is critical to studies such as $RFeAsO_{1-x}F_y$ materials (see related Abstract).
MPC's unique experience in the preparation of reactive rare earth and alkaline earth elements provides a core competency in the preparation and handling of reactive materials. Expansion of inert processing to incorporate preparation capabilities (arc and resistance melting), structure characterization (XRD, microscopy), and thermal property measurement (DTA, DSC) are future goals These capabilities will support current and proposed efforts to synthesize light metal (Li and Ca) aluminides, efforts to evaluate hydrogen storage capacity, and investigate the kinetics of the absorption/desorption of hydrogen from surface of single crystals. These Ca-based compounds, first discovered at the Ames Laboratory in 1998, have been identified as potential candidates for hydrogen storage materials. Additionally, this type of facility will be central to a new effort to evaluate low melting reactive metals for extension of solution growth methods to broader classes of compounds.

The recent discovery of superconductivity in FeAs based materials has highlighted the need to be able to produce high quality samples from materials containing volatile and toxic components. $RFeAsO_{1-x}F_x$ (R = light rare earth element), $AE_{1-x}K_xFe_2As_2$ (AE = Ca, Sr, or Ba) and in LiFeAs. Have superconducting transition temperatures reaching into the 40K region. Studies of $REFeAsO_{1-x}F_x$ within *Novel Materials Preparation and Processing Methodologies* have identified the reaction path by which these materials form (see related abstract). A critical step in the preparation of the FeAs superconductors is the preparation of binary arsenic precursors. It is the preparation of these precursors which requires elemental arsenic that presents the most significant safety hazards in preparing the superconducting materials. The Novel Materials PI's, working in conjunction with Ames Laboratory Environmental Health and Safety personnel developed safe methods of producing the As based precursors. The standard method of producing these materials is to seal the reactants in a quartz ampoule prior to reaction. However, this technique is susceptible to catastrophic failure if deviations from the expected behavior occur. It is therefore necessary to insure that there a secondary safeguards in place which will contain the reactants in the event of a failure of the quartz ampoule. In the Ames approach, the ampoule can be quartz, tantalum, molybdenum, Inconel, or other suitable metals. The metal ampoules are seal using the laser welder so that they can contain any compatible gas or turbopumped vacuum. The ampoules may contain additional crucibles if required to prevent reaction with one or more of the constituents. In order to provide secondary containment within a standard tube furnace, a specially designed superalloy (Haynes 230) retort is used. The retort is capable of withstanding the shock wave expected to accompany the catastrophic failure of an ampoule. Haynes 230 has both the strength and corrosion resistance to be used in air to 1200 C. In the event of an ampoule failure, any reaction products are contained within the retort or vented up the chemical hood. The equipment and procedures developed are designed to allow the production of novel compounds containing volatile and/or toxic constituents. These include but are not limited to As, Cd, S, Se, Te, P, Zn, K, Rb, and Mg. The procedures which were developed for the production of binary arsenides for precursor materials will be transferred to the Materials Preparation Center so that these materials can be made available to the broader scientific community.

A new effort is being initiated with the intended to design and fabricate novel nanometric structural materials based on immiscible metallic alloys as the method for developing a suite of highly controlled nanoparticulate synthesis. The synthesis method intended for this study is highly localized, ultra-short duration spark erosion. One important scientific question to be

answered is whether an extreme mutual insolubility can significantly enhance the stability of multiphase nanostructures against coarsening. If proven, this could enable extensive studies of the scaling laws for many physical properties and may establish an effective route for designing practical nano-materials based on particulate precursors with a technological range of use temperatures. The highly controlled nanoparticulate synthesis capabilities developed during these studies will be transferred to MPC. The availability of MPC produced high purity, compositionally controlled nanometric materials will build on the internationally recognized core competency of the MPC for generation of powder processed materials.

Examples of worldwide research made possible by materials prepared by the MPC

S. H. Zhou, and R. E. Napolitano, "Identification of the B33 Martensite Phase in Cu-Zr Using First-principles and X-ray Diffraction", Scripta Mater., **59**, 1143(2008).

T.-S. You, M.-K. Han and G. J. Miller, "On the 'Coloring Problem' in YMgZn and Related Phases", Inorg. Chim. Acta, **361**, 3053 (2008).

D. A. Sokolov, M. C. Aronson, G. L. Strycker, M. D. Lumsden, S. E. Nagler and R. Erwin, "Elastic Neutron Scattering in Quantum Critical Antiferromagnet $Cr_{0.963}V_{0.037}$", Physica B, **403**, 1276 (2008).

A. Mehta and J. D. Corbett, "$Er_{17}Ru_6Te_3$: A Highly Condensed Metal-rich Ternary Telluride", J. Solid State Chem., **181**, 871 (2008).

T. C. Kaspar, T. Droubay, S. M. Heald, M. H. Engelhard, P. Nachimuthu and S. A. Chambers, "Hidden Ferromagnetic Secondary Phases in Cobalt-doped ZnO Epitaxial Thin Films", Phys. Rev. B, **77**, 201303 (2008).

D. Kaczorowski, and T. Komatsubara "Complex Magnetic Behavior in Single-crystalline $CeRh_3Si_2$", Physica B, **403**, 1362 (2008).

K. Y. Shin, J. Laverock, Y. Q. Wu, C. L. Condron, M. F. Toney, S. B. Dugdale, M. J. Kramer and I. R. Fisher, "Charge Density Wave Formation in R_2Te_5 (R=Nd, Sm, and Gd)", Phys. Rev. B, **77**, 165101 (2008).

M. Debessai, J. J. Hamlin and J. S. Schilling, "Comparison of the Pressure Dependences of T_c in the Trivalent d-electron Superconductors Sc, Y, La, and Lu up to Megabar Pressures", Phys. Rev. B, **78**, 064519 (2008).

S. Bhattacharyya, J. R. Jinschek, A. Khachaturyan, H. Cao, J. F. Li and D. Viehland, "Nanodispersed DO_3-phase Nanostructures Observed in Magnetostrictive Fe-19% Ga Galfenol Alloys", Phys. Rev. B, **77**, 104107 (2008).

J. Atulasimha, A. B. Flatau and J. R. Cullen, "Analysis of the Effect of Gallium Content on the Magnetomechanical Behavior of Single-crystal FeGa Alloys Using an Energy-based Model", Smart Mater. Struct., **17**, 025027 (2008).

J. A. Wollmershauser, S. Kabra and S. R. Agnew, "In situ Neutron Diffraction Study of the Plastic Deformation Mechanisms of B2 Ordered Intermetallic Alloys: NiAl, CuZn, and CeAg", Acta Mater., **57**, 213 (2009).

R. Teghil, L. D'Alessio, A. De Bonis, D. Ferro, A. Galasso, G. Lanza, A. Santagata, P. Villani and D. J. Sordelet, "Ultra-short Pulse Laser Ablation of $Al_{70}Cu_{20}Fe_{10}$ Alloy: Nanoparticles Generation and Thin Films Deposition", Thin Solid Films, **517**, 1880 (2009).

X. Moya, D. Gonzalez-Alonso, L. Manosa and A. Planes, "Lattice Dynamics in Magnetic Superelastic Ni-Mn-In Alloys: Neutron Scattering and Ultrasonic Experiments", Phys. Rev. B, **79**, 214118 (2009).

M. Debessai, T. Matsuoka, J. J. Hamlin, S. Schilling and K. Shimizu, "Pressure-induced Superconducting State of Europium Metal at Low Temperatures", Phys. Rev. Lett., **102**, 197002 (2009).

Correlated Materials - Synthesis and Physical Properties

Ian Fisher, Ted Geballe, Aharon Kapitulnik, Steve Kivelson and Kathryn Moler

Stanford Institute for Materials and Energy Sciences (SIMES),
SLAC National Accelerator Laboratory
2575 Sand Hill Road, Menlo Park, California 94025, USA
irfisher@stanford.edu

1. Program Scope

This FWP is part of the newly formed Stanford Institute for Materials and Energy Sciences (SIMES), a joint venture between the SLAC National Accelerator Laboratory and Stanford University. Within our specific FWP, our efforts aim to address the grand challenge of "emergence" as well as a number of "Basic Research Needs" areas for energy applications in the realm of quantum materials. Understanding and ultimately controlling this class of materials has the potential to profoundly impact the next generation of electronic materials relevant to addressing our nation's energy needs. From new quantum states that enable computing with vastly lower power consumption, to new superconductors that better suit power transmission requirements, quantum materials hold the promise of advanced applications as well as providing some of the deepest and most challenging intellectual questions. Our research encompasses the fields of superconductivity, charge and spin order, non-Fermi liquid behavior, and most recently topological insulators. Our focus is on understanding fundamental factors determining the often complex electronic properties of these materials. We combine crystal growth and characterization of novel materials (Fisher & Geballe), local electronic (Kapitulnik) and magnetic (Moler) measurements, and theory (Kivelson). We collaborate extensively, both within SIMES and externally, and materials synthesized as part of this program enable research at diverse other universities and laboratories.

2. Recent Progress

For this meeting we will particularly focus on the synthesis aspects of our program. Specific areas of interest impacted by our synthesis efforts over the last two years can be loosely grouped in the realms of superconductivity, charge density wave formation, and topological insulators.

(a) Superconductivity in Fe-pnictides

The Fe-pnictides appear to provide a new paradigm for high temperature superconductivity. Born out of a multiband itinerant antiferromagnetic state (Fig. 1(a)), evidence points to spin fluctuations associated with a partially nested Fermi surface playing a decisive role. Our experiments have focused on probes of the electronic structure (principally quantum oscillations), of the magnetic structure, and of the superconducting gap symmetry. All of these measurements rely on the availability of high quality single crystals: for example, quantum oscillations are exponentially damped by impurity scattering, and evidence for nodes in the superconducting gap can be smeared by scattering. We have used both a self flux and also a Sn flux to grow high quality single crystals of several families of Fe-pnictides. Our experiments have revealed, among other results, the key role played by Fermi surface nesting (see for example refs [3,5,6]), and the presence of line nodes in the superconducting gap of LaFePO [7].

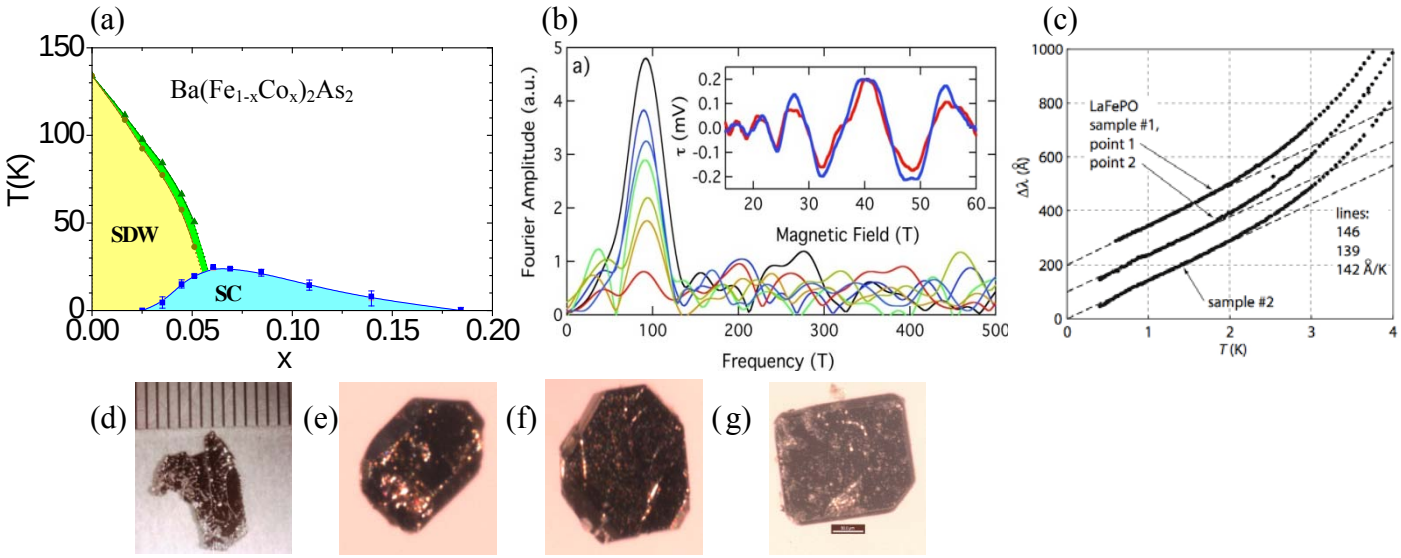

Fig. 1 (a) Phase diagram of Co-doped $BaFe_2As_2$ [4]. A universal feature of the Fe-pnictide superconductors is the proximity of superconductivity (SC) to antiferromagnetism (SDW). (b) Quantum oscillations in $BaFe_2As_2$. Analysis of data like these enables us to determine the topology of the reconstructed Fermi surface [6], relevant to understanding the electronic behavior. (c) Linear penetration depth in LaFePO revealed by scanning SQUID susceptometry, indicating the presence of line nodes in the superconducting gap [7]. Photographs show representative crystals of some of the Fe pnictides that we have looked at recently; (d) $Ba(Fe_{1-x}Co_x)_2As_2$ (over a mm scale) , (e) $SrFe_2P_2$, (f) $CaFe_2P_2$, and (g) LaFePO. Crystals (e) – (g) are each 200 – 300 microns on a side.

(b) Charge density wave formation in rare earth tellurides

Charge density wave compounds provide weak-coupling analogs of more strongly correlated charge ordered materials, for instance stripe and checkerboard phases in complex oxides. Their investigation reveals factors affecting the symmetry of the ordered states, as well as addressing issues associated with Fermi surface reconstruction. Recently we have identified the rare earth (R) tellurides RTe_n (n=2, 2.5, 3) as being an ideal model system for this type of study. The materials possess a wonderful admixture of simplicity (of band structure and also lattice modulation), "tunablilty" (including band filling, chemical pressure and disorder) and gap size, to permit a range of illuminating experiments. We are able to grow high quality single crystals of all three members of the homologous series directly from a binary melt.

The tritelluride family (n = 3) provides one example. Via a combination of electrical resistivity and high resolution x-ray diffraction measurements we discovered the CDW transition in this family of compounds, paving the way for a series of further experiments. The CDW transition temperature varies monotonically across the series (Fig. 2(a)), which can be principally attributed to the effect of chemical pressure on the electronic structure. More surprisingly, our experiments revealed a second CDW transition for the heaviest members of the series, with a wave vector almost identical to the first but oriented at 90 degrees in the Te plane (a "rectangular" CDW state if we borrow the language of "stripes" and "checkerboards" from charge ordered states), and with a transition temperature that *increases* with increasing chemical pressure [2]. It turns out that this effect is directly related to the amount of FS remaining after formation of the first CDW. The symmetry of the CDW can be readily appreciated from STM measurements (Fig 2(b) and ref [1]). The CDW states are not innocent bystanders, but actively compete with both magnetic and superconducting groundstates at low T.

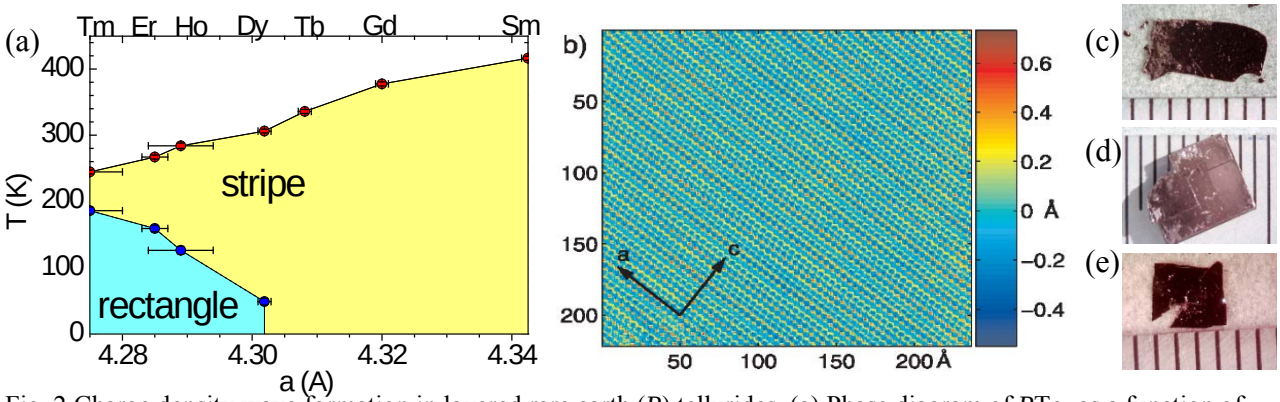

Fig. 2 Charge density wave formation in layered rare earth (R) tellurides. (a) Phase diagram of $R\mathrm{Te}_3$ as a function of the in-plane lattice parameter a, revealing two competing CDW phases [2]. These CDW states also compete with magnetic and superconducting groundstates at low temperature. (b) STM image showing the real space lattice modulation of TbTe_3 in the CDW state [1]. Photographs show examples of single crystals of (c) $R\mathrm{Te}_2$, (d) $R\mathrm{Te}_3$ and (e) $R_2\mathrm{Te}_5$, which comprise the single, double, and alternating single-double layer compounds respectively. Crystals are shown over a mm scale.

(c) Topological insulators

The quantum spin Hall (QSH) effect is a new quantum state of matter comprising an insulating gap in the bulk and gapless states at the edge where opposite spin states counter-propagate. The two opposite spin states form a single massless Dirac fermion at the edge, and the crossing of their dispersion branches at a time reversal invariant point is protected by the Kramers theorem. This robust protection is a consequence of the Z_2 topological quantum number of the bulk quantum states. The dissipationless edge state transport of the QSH state may enable low power spintronics devices. Recently, the stoichiometric materials $\mathrm{Bi}_2\mathrm{Te}_3$ and $\mathrm{Bi}_2\mathrm{Se}_3$ have been theoretically predicted to be 3D topological insulators whose surface states consist of a single Dirac cone at the Γ point. We have been able to grow large, high quality, single crystals of these materials, and to systematically tune the Fermi level with respect to the bulk bands. Probing the electronic structure via ARPES [8] (in collaboration with Y. Chen and ZX Shen), quantum oscillations, and STM (Fig 3) reveal the presence and properties of the bulk bands and the surface states, enabling detailed exploration of their properties.

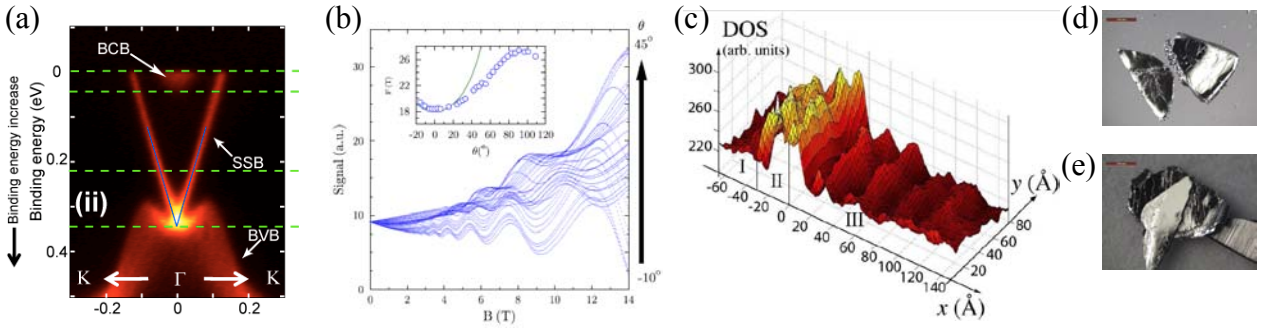

Fig. 3 Probes of the electronic structure of the topological insulators $\mathrm{Bi}_2\mathrm{Te}_3$ and $\mathrm{Bi}_2\mathrm{Se}_3$. (a) ARPES measurements for a n-type sample of $\mathrm{Bi}_2\mathrm{Te}_3$, showing the bulk conduction band (BCB), bulk valence band (BVB) and surface state band (SSB) [8]. Tuning the Fermi level by careful compositional control and/or via additional dopants so that E_F lies between the BCB and BVB in principle leads to a bulk insulator with a conducting surface. (b) Quantum oscillations in $\mathrm{Bi}_2\mathrm{Se}_3$ arising from the bulk bands. Understanding how the bulk bands behave on approaching the surface of the material is a key aspect to finding successful applications for these materials. (c) STM imaging of electronic waves on the surface of $\mathrm{Bi}_2\mathrm{Te}_3$, revealing the presence and properties of the surface states. Photographs of single crystals of (d) $\mathrm{Bi}_2\mathrm{Se}_3$ and (e) $\mathrm{Bi}_2\mathrm{Te}_3$ shown with a mm scale.

3. Future Plans

The synthesis aspect of our FWP will continue to focus on the classes of materials described above. Building on our initial work, over the next two years our crystal growth program will move in the following directions.

(a) Superconductivity in Fe-pnictides:

- Determine the phase diagram and Fermi surface evolution for various combinations of dopants, including a detailed exploration of physical properties related to gap symmetry
- Explore related materials, extending the search for superconductivity

(b) Charge density wave formation:

- Substitutional studies probe interplay of various ground states and the role of disorder
- Related ternary and quaternary phases

(c) Topological insulators:

- Reconcile bulk and surface probes of the electronic structure in Bi_2Se_3 and Bi_2Te_3
- Synthesis and properties of topological Mott insulators

4. Selected list of publications resulting from work supported by the DOE project over the last two years*

1) *STM Studies of $TbTe_3$: Evidence for a Fully Incommensurate Charge Density Wave*
A. Fang, N. Ru, I. R. Fisher and A. Kapitulnik, Phys. Rev. Lett. **99**, 046401 (2007). (4 pages)

2) *Effect of chemical pressure on the charge density wave transition in rare earth tritellurides RTe_3*
N. Ru, C. L. Condron, G. Y. Margulis, K. Y. Shin, J. Laverock, S. B. Dugdale, M. F. Toney and I. R. Fisher, Phys. Rev. B. **77**, 035114 (2008). (9 pages)

3) *Fermi surface of superconducting LaFePO determined by quantum oscillations*
A.I. Coldea, J.D. Fletcher, A. Carrington, J.G. Analytis, A.F. Bangura, J.-H. Chu, A.S. Erickson, I.R. Fisher, N.E. Hussey, R.D. McDonald, Phys. Rev. Lett. **101**, 216402 (2008). (4 pages)

4) *Determination of the phase diagram of the electron doped superconductor $Ba(Fe_{1-x}Co_x)_2As_2$,*
J.-H. Chu, J. G. Analytis, C. Kucharczyk & I. R.Fisher, Phys. Rev. B **79**, 014506 (2009). (6 pages).

5) *Fermi surface of $SrFe_2P_2$ determined by de Haas-van Alphen effect*
J. G. Analytis, C.M.J. Andrew, A. I. Coldea, A. McCollam, J.-H. Chu, R. D. McDonald, I. R. Fisher, and A. Carrington, Phys. Rev. Lett. **103**, 076401 (2009). (4 pages)

6) *Quantum oscillations in the parent pnictide $BaFe_2As_2$: itinerant electrons in the reconstructed state,*
J. G. Analytis, R. D. McDonald, J.-H. Chu, S. C. Riggs, A. F. Bangura, Chris Kucharczyk, M. Johannes, & I. R.Fisher, Phys. Rev. B **80**, 064507 (2009). (5 pages)

7) *Evidence for Nodal Superconductivity in LaFePO from Scanning SQUID Susceptometry*
Clifford W. Hicks, Thomas M. Lippman, Martin E. Huber, James G. Analytis, Jiun-Haw Chu, Ann S. Erickson, Ian R. Fisher, Kathryn A. Moler, Phys. Rev. Lett. **103**, 127003 (2009).

8) *Large Gap Topological Insulator Bi_2Te_3 with a Single Dirac Cone on the Surface*
Y. L. Chen, J. G. Analytis, J. H. Chu, Z. K. Liu, S. K. Mo, X. L. Qi, H. J. Zhang, D. H. Lu, X. Dai, Z. Fang, S. C. Zhang, I. R. Fisher, Z. Hussain, Z. X. Shen
Science **325**, 178-181 (2009).

* out of 44 total publications for this period

Exploratory Materials Synthesis and Characterization

Cedomir Petrovic and 1 graduate student (Rongwei Hu, up to August 2009)

Condensed Matter Physics and Materials, Science, Brookhaven National Laboratory, Upton NY 11973

i) Program Scope

The focus of our program is design, discovery and characterization of new materials in condensed matter physics. Single crystals are at the forefront of exploratory synthesis since they carry information on anisotropy. Materials synthesis techniques include crystal growth from solvents at high and low temperatures, crystal growth and deposition from vapors, solid state and gas reactions, and intermetallic alloy arc melting. Innovative synthetic techniques are developed in order to boost exploratory efforts. Bulk physical and structural characterization measurements serve as a feedback in synthesis and are the essential component of the program. They include measurement of electrical and thermal transport, heat capacity, magnetization and X-ray diffraction. The same methods are used to probe electronic systems at low temperatures, high magnetic fields and pressures. We use high magnetic fields at NHFML and high resolution X ray beamlines at NSLS. Extensive collaborations exist at BNL and with universities at the Northeast and throughout the US. This program includes training of next generation of scientists. Students from neighboring universities (Brown, Columbia, Johns Hopkins) are being educated in materials physics, arts and crafts of crystal growth, materials synthesis and characterization.

ii) Recent progress

1. New synthesis/crystal growth methods: In – Situ Decanting High Temperature Flux (ISDHTF) method

Figure 1: AlB_{12} crystals

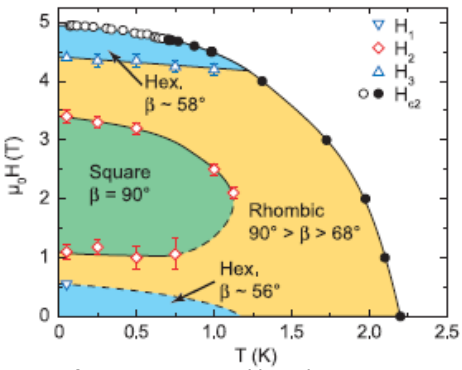

Figure 2: VL transitions in $CeCoIn_5$ (Science 319, 180 (2008))

High temperature metallic solutions are method of choice for synthesis of many important correlated electron systems such as heavy fermions or iron based superconductors. The method is well suited for synthesis of both congruently and incongruently melting crystals. The crystals, however, have to be etched or mechanically removed from the solidified flux after being cooled to room temperature. Fisk and Remeika introduced decanting outside the furnace using the quartz wool for filtration, centrifuge at room temperature and encapsulating crucibles in quartz tubes to prevent oxidation [1]. Using this method crystal cannot be decanted at temperatures above ~ 1100°C. At high temperatures there is a substantial difference between actual and desired temperature of decanting. ISDHTF method developed in Petrovic lab at BNL enables inside the furnace decanting below 1700°C. In FY 07-09 we introduced new crucibles and inside rotation assembly that places growth crucible closer to perimeter of rotation. This enables higher centrifugal acceleration of ~ 10g at 500 rpm. This is important due to viscosity of the molten metal. In situ decanting has been tested up to 1450°C (Fig. 1, showing AlB_{12} crystals decanted at 1290°C).

2. Exploratory synthesis and characterization of novel materials

a) Large high quality crystals of $CeCoIn_5$ paved way for several important experiments. Full breadth of vortex lattice symmetries up to H_{c2} for the first time has been observed in a d-wave heavy fermion superconductor (Fig. 2) [2]. In addition, a violation of Wiedemann – Franz (WF) law has been observed [3]. WF law is one of the oldest laws of condensed matter physics and a corner stone of the standard theory of metals. Electrical resistivity for interplane charge and heat transport no longer tracks thermal resistivity at magnetic field induced quantum critical point (QCP), causing a violation of WF law and Lorentz number $L < L_0$. In contrast, WF law is valid for arbitrary scattering strength, disorder and interactions since it does not depend on quasiparticle mass. It is therefore surprising to observe its violation in a good metal without proximity to Mott insulating state. Finally, a spin resonance in the $CeCoIn_5$, chemically homogeneous d-wave superconductor has been observed [4]. The presence of a resonance peak is indicative of strong coupling between *f* electron magnetism and superconductivity. It is consistent with a d-wave gap order parameter satisfying $\Delta(q + Q_0) = -\Delta(q)$. A large reduction in the magnetic RKKY spin exchange energy for $T < T_C$ was seen. Its relation to d-wave superconductivity and a spin resonance, otherwise reminiscent to the one observed in $Bi_2Sr_2CaCu_2O_{8+\delta}$ and $YBa_2Cu_3O_7$, remains to be understood. The resonance peak is well-defined in the absence of long-ranged spatial correlations. This is further evidence that $CeCoIn_5$ is similar to cuprates where resonance was seen in the absence of long ranged spin correlations, but different from isotropic heavy fermion superconductor UPd_2Al_3 which has long range spin order.

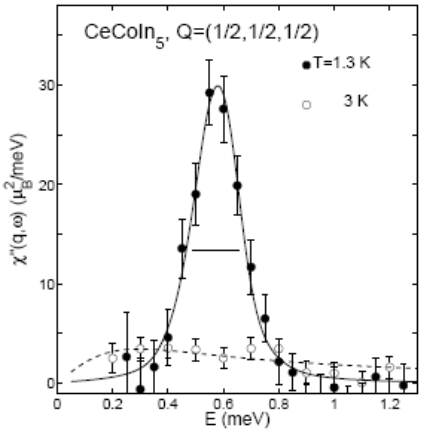

Figure 3: Spin Resonance in $CeCoIn_5$ (PRL 100, 087001 (2008))

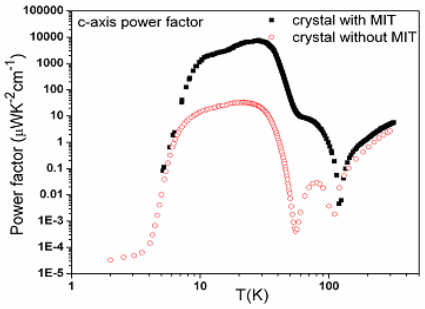

Figure 4: Power factor in $FeSb_2$

b) Giant thermoelectric power factor was discovered in single crystals of $FeSb_2$ with metal insulator transition (collaboration Qiang Li BNL, Fig. 4). Due to its simple crystal structure, $FeSb_2$ can serve as a test ground for ab initio and DMFT theoretical models of large thermoelectric response. Colossal magnetoresistance, multiband transport and giant mobility in one carrier band were also discovered.

c) Isolated single crystal phase α-$YbAlB_4$, a structure closely related to first Yb based heavy fermion superconductor β-$YbAlB_4$ (work performed at ISSP University of Tokyo).

d) High spin polarization (P=0.6), highest among any Si and Ge based material and ferromagnetic T_C=319K discovered in new half metallic ferromagnet Mn_4FeGe_3. This material has spin polarization second only to CrO_2 (P=0.98) and $La_{1-x}Sr_xMnO_3$ (P=0.78).

e) We synthesized many oxide pyrochlores, many transition metal chalcogenide and halide crystals using innovative solvents. Many crystals were made to support efforts in materials science and chemistry at BNL (thermoelectrics, catalysis).

f) Extensive collaboration in progress with many research groups at BNL and elsewhere (Columbia, Brown, Johns Hopkins, UIUC, Ameslab, Toronto, Sherbrooke, UBC…).

III) Future Plan

1. Development of new tools and synthesis/crystal growth methods

a) We will improve the decanting performance of the ISDHTF for use with various fluxes by using new crucible sets in order to make Mn, Ge and Si rich crystal phases with narrow range of liquid coexistence.
b) The large gradient (1000°C) multi-zone vapor transport furnace was designed to explore physical and chemical vapor transport (PVT and CVT) of crystals. In closed tubes the PVT growth rate R is proportional to supersaturation σ and quilibrium vapor pressure $P_{eq}(T_C)$ at the growth site. R is heavily influenced by the temperature of the growth site (T_C), increasing with the increase of T_C, whereas there is little dependence on the temperature of vaporization site (T_V). $P(T_C)$ is much more sensitive to changes in T_C than σ [5]. Long reaction tubes promote interaction with the vapor and the wall chamber, inhibiting σ at long distances. Tunable temperature gradients $\Delta T = T_V - T_C$ will be used to tune reaction rates. For example, in Fe-Si CVT many different phases and/or crystal morphologies crystallize at different temperature gradients from the source.

2. Exploratory synthesis and characterization of novel materials

a) Iron based superconductors within EFRC on superconductivity. We have synthesized large single crystals of $Fe_{1+y}(Te_{1-x}S_x)_z$ and performed comprehensive investigation of bulk physical properties and stoichiometry. We discovered smallest H_{c2} anisotropy in the whole family of iron based superconductors and high critical current density. Collaborations with PI's from EFRC are ongoing. We will explore poorly metallic ternary phases with FeSe and FeTe units with first order like magnetic transitions.
b) The increased power of computational methods stimulated predictions for new superconductors [6-7]. We will explore 2D B networks, icosahedral B_{12} and cage – like C clusters (C_{20}, C_{28}, C_{36}) with large electron – phonon coupling σ-character bands. Bonding in borides depends on metal/boron ratio. Above 12, B forms icosahedral clusters. Using ISDHTF it will be possible to dissolve compounds with high B.
c) We will continue our collaboration on the k-space inhomogeneity in quasi 2D 115 heavy fermion superconductors with Louis Taillefer (Shérbrooke), complemented with neutron scattering experiments by Broholm (Johns Hopkins). Breakup of quasiparticle transport and WF law violation around QCP at H_{c2} in $CeCoIn_5$ raises an issue if the quasiparticle breakup is generic feature, present in other materials at the QCP or is it connected with the proximity to superconducting phase [3]? And what is the analogy to underdoped cuprates where Fermi surface aggregates into isolated regions that support conventional charge and transport?
d) Quantum criticality in heavy fermions is connected with the nature of magnetic interactions. Poorly explored, yet important perturbation parameter is disorder. Weak free energy singularities in Griffiths phase of disordered magnetic systems are greatly amplified at QCP. Quantum Griffiths phases are likely to play a key role in disorder driven non-Fermi liquid behavior in heavy fermions [8]. Our goal is to search in 115 heavy fermion superconductors for cluster glass phase proposed to exist between uniformly ordered phase and paramagnetic Fermi liquid. This will enable us to address several questions. What is the influence of the glassy phase on non-Fermi liquid behavior in d-wave quasi 2D heavy fermion superconductors and how does it relate to high T_C cuprates? How does it relate to more isotropic heavy fermions and other magnetic materials (eg. MnSi or $YbRh_2Si_2$) in the pressure, field or composition tuned non-Fermi liquid state where we can also vary disorder in crystals using innovative synthesis methods? Strong correlations and disorder govern physics of Kondo insulator – like material with giant thermoelectric power factor $FeSb_2$. MuSR measurements on $Fe_{1-x}Co_xSb_2$ show that the volume of weak magnetic order ($M \sim 10^{-2}\mu_B$) increases below ferromagnetic T_C, for every investigated sample, reaching only 25-50%. This result excludes impurity related magnetism. Partial electronic order is reminiscent to MnSi when $T_N \rightarrow 0$, but in $Fe_{1-x}Co_xSb_2$ the underlying magnetic fluctuations can be ferromagnetic or antiferromagnetic depending on the dopant. Thermodynamic measurements on $Fe(Sb_{1-x}Te_x)_2$ are consistent with ferromagnetic Griffiths clusters on the metallic side of the MIT which is induced at 0.1 atomic % of Te. The novel partially ordered metallic phase observed in $FeSb_2$ may be

relevant to physics of electronic segregation in high T_C and heavy fermion superconductors. EMSC will pursue this further by investigations of thermal, magnetic and transport properties at low temperatures as well as by muSR with our collaborators (Uemura, Luke).

e) We will search for new ferromagnetic materials for spin injection among transition metal Si,Ge phases. Increasing number of ab initio predictions for half metallicity in novel materials are awaiting experimental verification, for example various ternary phases with cobalt and silicon including Heuslers, half Heuslers and 53 phases isostructural to Mn_5Ge_3. Electrical and magnetic properties of such systems are sensitive to atomic defects and disorder, with some types of atomic interchange having larger influence on half metallicity. Materials synthesized at different temperatures had different types and degrees of disorder. Development of new crucible sets to use with Si wil enable us to use the full power of ISDHTF. It will be possible to simultaneously vary soaking and decanting temperature very close to solidification point at the phase diagram and consequently to correlate structural and spin – injection characteristics of materials.

f) We plan on exploratory synthesis of thermoelectrics in collaboration with Clemson University including, B,C based clathrates. At BNL we collaborate on $FeSb_2$ with Advanced Energy Materials and X ray scattering groups.

iv) References

[1] Z. Fisk, J. P. Remeika in K.A. Gschneider, Jr. L. Eyring (Eds), Handbook on the Physical Chemistry of rare earths, Vol. 12, 1989, Elsevier Amsterdam

[2] A. D. Bianchi et al., Science 319, 177 (2008)

[3] M. A. Tanatar et al., Science 316, 1320 (2007)

[4] C. Stock et al., Phys. Rev. Lett. 087001 (2008)

[5] H. Yumoto et al., Jpn. J. Appl. Phys. 32, 887 (1993)

[6] E. Spanò et al., Phys. Rev. B 72, 014530 (2005)

[7] F. Zipoli et al., Phys. Rev. B 74, 205408 (2006)

[8] Jose´ A. Hoyos et al., Phys. Rev. Lett. 99, 230601 (2007)

v) Selected publications FY 07-09 (Full list at http://www.bnl.gov/cmpmsd/emsc/pubs.asp)

1. "Violation of a universal law at a quantum critical point", M.A. Tanatar, J. Paglione, C. Petrovic and L. Taillefer, **Science 316, 1320 (2007)**
2. "Hybrid gap structure in the heavy-fermion superconductor $CeIrIn_5$", H. Shakeripour, M. A. Tanatar, S. Y. Li, L. Taillefer and C. Petrovic, **Phys. Rev. Lett 99, 187004 (2007)**
3. "Enhanced Curie temperature and spin polarization in Mn_4FeGe_3", T. Y. Chen, C. L. Chien and C. Petrovic, **Applied Phys. Lett. 91, 142505 (2007)**
4. "Superconducting vortices in $CeCoIn_5$: beyond Ginzburg-Landau paradigm", A. D. Bianchi, M. Kenzelmann, L. DeBeer – Schmitt, J. S. White, E. M. Forgan, J. Mesot, M. Zolliker, J. Kohlbrecher, R. Movshovich, E. D. Bauer, J. L. Sarrao, Z. Fisk, C. Petrovic and M. R. Eskildsen, **Science 319, 177 (2008)**
5. "Giant carrier mobility in single crystals of $FeSb_2$", Rongwei Hu, V. F. Mitrovic and C. Petrovic. **Applied Phys. Lett. 92, 182108 (2008)**
6. "Spin resonance in the d wave superconductor $CeCoIn_5$", C. Stock, C. L. Broholm, J. Hudis, H. J. Kang and C. Petrovic, **Phys. Rev. Lett. 100, 087001 (2008)**

Control of New Kinetic Barriers & Design of Nanorods

L. G. Zhou, S. K. Xiang, C. G. Johansen, and Hanchen Huang
hanchen@uconn.edu
Department of Mechanical Engineering
University of Connecticut, Storrs, CT 06029

Program Scope:

Diffusion kinetics dictates the shape and structure of many nanostructures. In fact, the very stability of a nanostructure depends on diffusion and reaction kinetics. This is particularly true for nanorods. During the synthesis, say by physical vapor depositions, newly deposited atoms diffuse on surfaces and their diffusion determines the dimension and morphology of nanorods. Our previous studies have revealed the existence and variation of the three-dimensional Ehrlich-Schwoebel (3D ES) barrier. In the current project, we focus on (1) control of the 3D ES barrier using surfactants and (2) design of nanorods based on the knowledge of the 3D ES barrier and on the integration of this knowledge and those from previous studies of peers.

Recent Progress:

Among the recent progresses, the most encouraging is the discovery of the origin of nanorods diameter; others include the understanding of how 3D ES barrier varies as surfactant decorates steps and top layers of surfaces, how the 3D ES barrier dictates the facet orientations of nanorods, and how twin boundaries form and how they affect facet orientation of nanorods/nanowires. The following presentation focuses on this particular discovery of the origin of nanorods diameter [1].

The diameter of nanorods is on the order of 200 nm, while the axial dimension is usually beyond microns. The synthesis of nanorods has been a common practice, and the glancing angle deposition (GLAD) technique has been patented by a Canadian group [2]. Using the technique, or its variation such as [3] simultaneous opposite direction GLAD (SO-GLAD), numerous research groups synthesize nanorods and networks of nanorods. Interesting, no one has ever questioned why the diameter of the nanorods is on the order of 200 nm. A back-of-envelope calculation shows that the diffusion

distance of surface adatoms is on the order of 100,000 nm. Although the diffusion distance is a very rough approximation of nanorods diameter, the three orders of magnitude difference indicates missing links - elements of fundament physics.

Based on the knowledge of 3D ES barrier, we study the morphology evolution of nanorods during synthesis. The kinetic process involving the 3D ES barrier competes with other processes such as atomic deposition on surface, adatom diffusion on surface, and adatom diffusion down monolayer steps. Taking copper as the prototype of nanorods material and using kinetic Monte Carlo simulations, we have shown that a new characteristic length scale L_{3D} exists. This length scale is the dimension of surface islands bounded by steps of multiple atomic layers. In comparison, the dimension of monolayer atomic islands is L_{2D}, which is no larger than L_{3D}. Further, through analytical formulation, we have shown that the criterion defining this L3D is the balance of mass transport between top and sides of a nanorod; in contrast, the conventional wedding cake model [4, 5] relies on the criterion of nucleation on top of a nanorod. As shown in the Figure 1, at room temperature and under typical deposition rate of 1 micron/minute, the L_{3D} is on the order of 100 nm. If the 3D ES barrier were removed to the conventional ES barrier, this length scale would become at least 1000 nm (and is expected to be much larger).

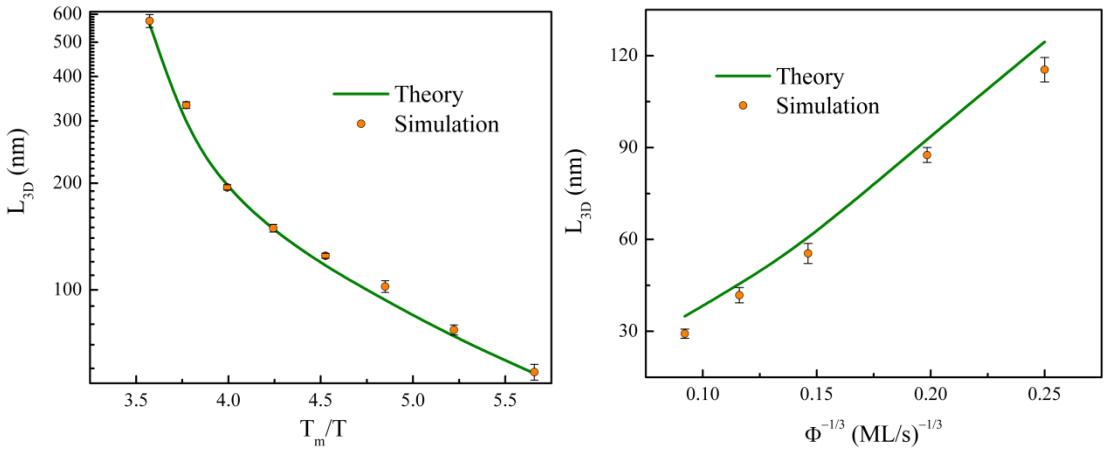

Figure 1: L_{3D} as a function of (left) substrate temperature and (right) deposition rate.

As a direct impact of this discovery, we now know that nanorods diameter is on the order of 200 nm because the diameter is dictated by the length scale L_{3D}, which in turn results from the 3D ES barrier and the balance of mass transport across it. As the second impact, we can now design to control porosity - the separation between nanorods. Using ab initio calculations, we show that addition of surfactants can reduce

the 3D ES barrier and therefore reduce the porosity; this is confirmed experimentally using magnetron sputtering deposition of copper with a monolayer indium. As a more generic impact, we expect this new length scale to affect other aspects of surface processing. For example, the wedding cake model/theory has taken into account other length scales, and incorporation of the new L_{3D} in such theories should lead to further discoveries in and/or better understanding of surface processing.

Future Plan:

There are two aspects in the future plan. The first aspect is to carry analytical formulations of incorporating the new length scale L_{3D} in surface processing theories such as the wedding cake model; and to continue the studies of surfactant effects on diffusion and L_{3D}. This aspect is on a solid ground, and we can have a clear prospect of what will be accomplished. The other aspect is to explore new modeling capabilities in nanorods processing. Specifically, the limitation now is the representation of nanostructures rigorously and efficiently. Existing approaches allow the representation in some cases and fail in others. This situation challenges us to explore new approaches, and we are such a path of exploration.

References:

1. L. G. Zhou and H. C. Huang, **Phys. Rev. Lett.** *101*, 266102 (2008).
2. K. Robbie and M. J. Brett, **U. S. Patent** No. 5, 866, 204 (1999).
3. J. Wang, H. C. Huang, S. V. Kesapragada, and D. Gall, **Nano Lett.** *5*, 2505 (2005); and references therein.
4. J. Krug, **J. Stat. Phys.** *87*, 505 (1997).
5. J. Krug, P. Politi, and T. Michely, **Phys. Rev. B** *61*, 14037 (2000).

Publications:

1. Hanchen Huang and Helena van Swygenhoven, "Atomistic Simulations of Mechanics of Nanostructures", **MRS Bulletin** *34*, 160-163 (2009).

2. Harold S. Park, Wei Cai, Horacio D. Espinosa, and Hanchen Huang, "Mechanics of Crystalline Nanowires", **MRS Bulletin** *34*, 178-183 (2009).

3. C. G. Johansen, Hanchen Huang, and T. M. Lu, "Diffusion and Formation Energies of Adatoms and Vacancies on Magnesium Surfaces", **Computational Materials Science** (2009) in press doi:10.1016/j.commatsci.2009.06.022.

4. Dilpuneet Aidhy, Paul C. Millett, Simon R. Phillpot, Dieter Wolf, and Hanchen Huang, "Kinetically-driven Point-defect Clustering in Irradiated MgO by Molecular-dynamics Simulation", **Scripta Materialia** *60*, 691-694 (2009).

5. H. W. Shim, Jaron D. Kuppers, and Hanchen Huang, "Strong Friction of Silicon Carbide Nanowire Films", **Nanotechnology** *20*, 25704-1-4 (2009); highlighted in news report **http://nanotechweb.org/cws/article/lab/37263**.

6. L. G. Zhou and Hanchen Huang, "A Characteristic Length Scale of Nanorods Diameter during Growth", **Physical Review Letters** *101*, 266102-1-4 (2008).

7. H. W. Shim, Y. F. Zhang, and Hanchen Huang, "Twin Formation During SiC Nanowire Synthesis", **Journal of Applied Physics** *104*, 63511-1-5 (2008).

8. H. W. Shim, J. G. Kuppers, and Hanchen Huang, "High-temperature Stability of Silicon Carbide Nanowires", **Journal of Nanoscience and Nanotechnology** *8*, 3999-4002 (2008).

9. S. K. Xiang and Hanchen Huang, "Ab initio Determination of Three-dimensional Ehrlich-Schwoebel Barriers on Cu{111}", **Applied Physics Letters** *92*, 101923-1-3 (2008).

10. Hanchen Huang, "Predictive Modelling of Nanorods Synthesis", **Journal of Physics: Conference Series** *107*, 12006-1-4 (2008).

In Quest for Boron Nanostructures and Fullerenes: Key Issues of Stability and Synthetic Routes

Boris I. Yakobson and Pulickel Ajayan
biy@rice.edu
Department of Mechanical Engineering & Materials Science, Department of Chemistry, and the Smalley Institute for Nanoscale Science and Technology, Rice University, Houston, TX 77005

Among the allotropes of carbon, all sp^2-types are closely related and have been extensively studied: spherical *fullerenes*, cylindrical *nanotubes* (often also considered as members of fullerene family), and graphene (flat mono-atomic sheet of *graphite*). For boron, carbon's left neighbor in the periodic table, the landscape of fullerene-like possibilities is just beginning to emerge.

Our project, beginning in August 2009, aims to advance the understanding of the boron assembly into nanoscale structures, while also to initiate a series of experimental synthetic trials. The effort is two-pronged, including theoretical models and assessment of possible structures and properties, and experiments on synthesis and characterization. Embarking into possibly extensive field, we include in our scope all basic possibilities: (1) hollow fullerene-type clusters and their "stuffed" variety, (2) boron nanotubes, (3) mono-atomic boron sheets—analog of graphene monolayers, and (4) boron-based or boron-enriched combinations with C, N, and H. Theory will allow us to gain better understanding of these nanostructures stability, chemical inertness (with respect to mutual fusion into bulk, oxidation, etc.) Quantum-chemistry methods including the first-principles based approaches, molecular dynamics, density functional energy calculations, nudged-elastic-band evaluation of kinetic barriers, and saddle point computations will be adapted for this purpose. We have so far explored the stability of boron buckyball B_{80} and closely related hollow structures [1-3]. This was followed by the proposal in the literature of so called α-sheet. Furthermore, analysis shows interesting properties of not only the α-sheets but their logical folded version—boron nanotubes [4-5].

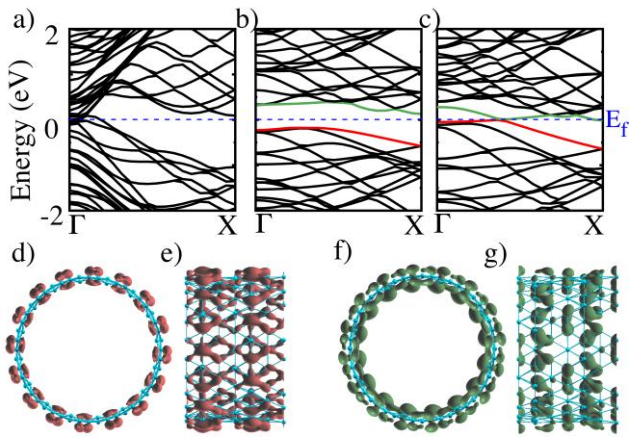

Band structure of (a) (18,0), and *relaxed* (b) and *unrelaxed* (c) (8,8) tubes. Views of band-decomposed charge density for HO [(d) and (e)] and LU bands [(f) and (g)], for relaxed (8,8) tube [4].

At the same time, recent theoretical investigation shows that the pure boron clusters may lack the chemical inertness of carbon analogs. For example, a pair of two B_{80} undergoes fusion with the barrier lower [6] than in the process of C_{60} polymerization. This emphasizes the challenges on the way of experimental production and retention of pure B-structures due to their higher reactivity.

Actual experimental evidence so far remains rather sparse, due to either lack of

systematic exploration or fundamental difficulties yet to be determined. The focus of the experimental part will be to develop new synthetic protocols for the creation of pure crystalline boron nanotubes, nanosheets and buckyballs, using methods such as laser evaporation, chemical vapor deposition, and chemical substitution reactions using boron containing targets and precursors. Template based approaches will also be followed to deposit pure boron nanostructures on porous scaffolds. The synthesized structures will be characterized using a variety of microscopy, scanning probe and spectroscopy techniques such as SEM, TEM, AFM/STM, TGA, XPS, FTIR and Raman. We will also perform electrical transport measurements of sheets and nanotubes, to explore the electronic structure of these materials and compare with theoretical predictions. Initial attempts of sytnthesis of boron nanoparticles are under way by chemical methods. One approach is the reduction of boron trichloride BCl_3 by Li metal in liquid ammonia, in anticipation that the reaction $BCl_3 + 3Li \rightarrow LiCl_3 + B$ (particles) may yield interesting structures [7].

Boron nanostructures, if systematically produced, would open variety of opportunities. B-fullerenes must lead to a branch of chemistry in a way similar to C_{60}, but with its own and unexpected novelties. Nanotubes should possess electronic properties beneficially more uniform than in the case of carbon, where inherent intermixing of metallic and semi-conducting species remains a serious obstacle for obtaining well characterized material.

References

1. "The boron buckyball", N. Gonzalez Szwacki, A. Sadrzadeh, and B.I. Yakobson, *Phys. Rev. Lett*., **98**, 166804 (2007).
2. "B_{80} fullerene: An *ab initio* prediction of geometry, stability, and electronic structure", N. Gonzalez Szwacki, A. Sadrzadeh, and B.I. Yakobson, Phys. Rev. Lett., **100**, 159901 (2008).
3. "The boron buckyball and its precursors: An electronic structure study", A. Sadrzadeh, O.V. Pupysheva, A.K. Singh, and B.I. Yakobson, J. Phys. Chem. A**,** **112**, 13679-13683 (2008).
4. "Probing properties of boron α-tubes by *ab initio* calculations", A.K. Singh, A. Sadrzadeh, and B.I. Yakobson, Nano Letters, **8**, 1314 (2008).
5. "New boron barrelenes and tubulenes", L.A. Chernozatonskii, P.B. Sorokin, and B.I. Yakobson, JETP Letters, **8**, 489-493 (2008).
6. Arta Sadrzadeh and B.I. Yakobson, in preparation.
7. Ashavani Kumar and P.M. Ajayan, in preparation.

Molecular Dynamics Simulation of Colloidal Nanoparticle Forces and Assembly

Kristen A. Fichthorn
fichthorn@psu.edu
Departments of Chemical Engineering and Physics
The Pennsylvania State University
University Park, PA 16802

Program Scope

Nanoparticles hold great promise for a diverse array of materials applications, ranging from nanoelectronic circuits and sensors to bulk materials with novel mechanical properties to biological materials. Two critical challenges with using nanocolloids in these and other technologies are stability and bottom-up assembly of the particles, both of which are governed by nanoparticle forces. From a theoretical point of view, it is unclear if traditional, macroscopic colloidal theories for interparticle forces (*e.g.*, DLVO theory) can describe colloidal nanoparticles. With molecular dynamics (MD) simulations, we can simulate colloidal nanoparticles to understand their forces. These studies can yield atomic-scale detail that is not currently accessible with experimental methods.

The forces between colloidal nanoparticles are also important in crystallization, where the formation of nanoparticle aggregates can occur. Here an interesting phenomenon is oriented attachment, in which nanocrystals approach one another and merge along specific crystallographic directions to form twinned or single-crystal structures [1-3]. The ability to direct crystallization through oriented attachment is an exciting prospect that could allow for the creation of new nanostructures with well-defined sizes and shapes. MD simulations can model nanoparticle aggregation and furnish many details of this process that are not accessible experimentally.

Recent Progress

A. MD Simulation of the Aggregation of Titanium Dioxide Nanocrystals: Preferential Alignment [4]

We used classical MD simulations to study the aggregation of various titanium dioxide (anatase) nanocrystals in vacuum. We consider charge-neutral nanocrystals with variations of the truncated tetragonal bipyramidal Wulff shape. Nanocrystalline anatase has been experimentally observed to possess approximate Wulff shapes [3]. The model nanocrystals are shown in Fig. 1, where we see that in addition to Wulff shapes, we consider asymmetric nanocrystals, which mimic possible off-Wulff shapes that could occur during crystal growth. The asymmetric nanoparticles possess permanent dipole moments, while the symmetric nanocrystals do not. Thus, we studied the effect of dipole-dipole interactions, which have been proposed to play a role in oriented attachment [1,2].

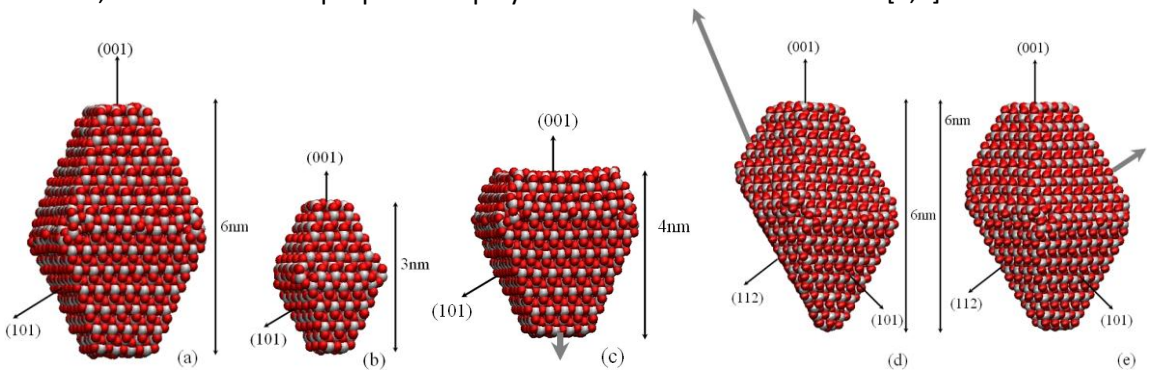

Figure 1: We studied (a) large crystals with Wulff shapes; (b) small crystals with Wulff shapes; (c), (d), (e) truncations of the Wulff shape, in which the relative magnitudes and directions of the dipole moments are indicated by gray arrows. Oxygen atoms are red (dark) and titanium atoms are white (light).

All the particles studied exhibit a strong tendency to aggregate with certain preferred orientations in a ``hinge'' mechanism. Our simulations indicate that electrostatic forces between under-coordinated atoms on the edges between nanocrystal facets drive this phenomenon. We find that aggregation rarely occurs along the direction of the dipoles - even when the permanent dipole moment is as large as 250 Debye. Although the dipole-dipole interaction is the leading term in the multipole expansion of the electrostatic potential for neutral particles, higher order multipole moments (*e.g*., quadrupole, octupole, *etc.*) can also contribute to the electrostatic potential. Here, these high-order multipoles dominate the electrostatic potential at short separations and they are created by regions of positive and negative charge associated with under-coordinated surface atoms, as shown in Fig. 2. The observed mechanism for preferential alignment may be a driving force for oriented attachment and the growth of anisotropic structures during crystallization.

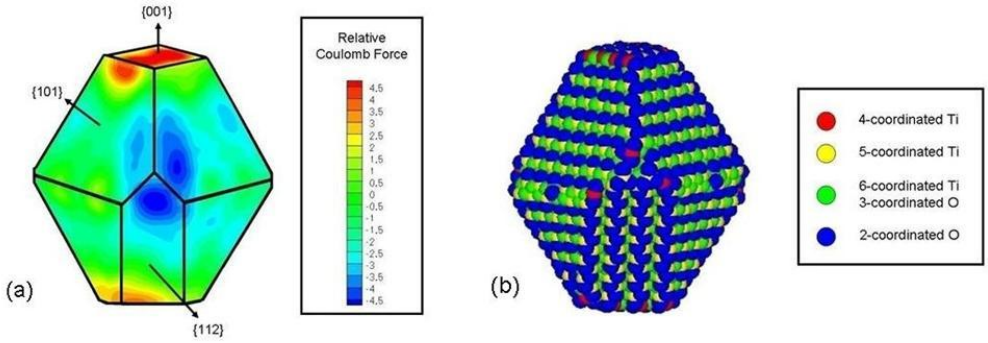

Figure 2: (a) Projected map of the electrostatic potential in planes parallel to the nanocrystal facets on the particle shown in Fig. 1(e). The coordination numbers of the surface atoms are indicated in (b). Nanoparticle aggregation occurs between the red (positively charged) and blue (negatively charged) regions shown in (a).

B. MD Simulation of the Directed Alignment of Au Nanocrystals in Alkane Solvent: Solvation and van der Waals Forces [5]

We used MD simulations to study the approach of icosahedral gold nanoparticles in hexane solvent, where we find an interesting interplay between solvent-mediated forces and van der Waals attraction. In the absence of solvent, the nanoparticles approach one another in a facet-to-facet orientation, due to van der Waals forces, as shown in Fig. 3(a). Hexane solvent tends to decorate the nanoparticle facets, leaving the vertices and edges bare, so that in solvent, the nanoparticles approach each other in a vertex-to-vertex fashion [Fig. 3(b)]. This study shows the critical role of solvent in achieving nanoparticle alignment.

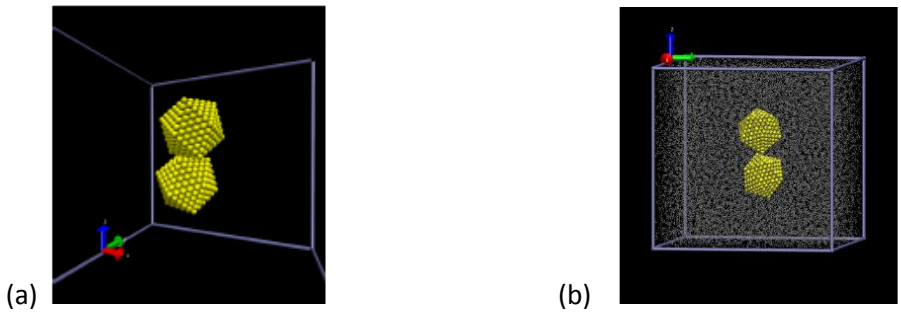

Figure 3: Snapshots from MD simulations of nanoparticle aggregation (a) in vacuum and (b) in solvent. For clarity, hexane solvent molecules are not shown to scale.

C. Entropic forces and directed alignment of hard squares in suspensions of rods and disks [6]

We used Monte Carlo simulations to study the depletion forces and directed alignment of two-dimensional hard squares by hard rods and disks. We determined the effects of size and concentration of rods and disks on the potential of mean force between the squares. Rods and disks produce a depletion attraction between the squares, which increases with increasing concentration and size. Under certain disk concentrations and sizes, the depletion interaction becomes oscillatory exhibiting both attraction and repulsion. We also probed the relative orientation that two squares adopt as they approach each other in a sea of depletant. We observe rich behavior, in which the relative orientation varies with inter-particle separation and depends on the size and concentration of the rods and disks.

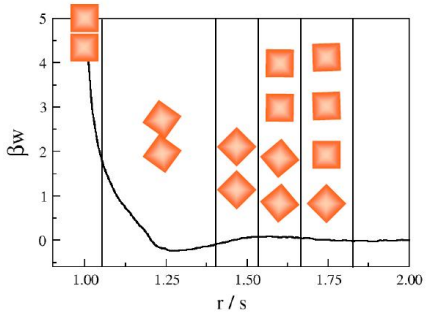

Figure 4: Potential of mean force (βw) as a function of square spacing, along with preferred orientations of the squares at various separations.

D. Assembly of gold nanowires by sedimentation from solution: Experiments and simulation [7]

We investigated the ordering of gold nanowires that settle from aqueous suspension onto a glass substrate due to gravity. The wires, 320 nm in cross-sectional diameter and 2, 4, or 7 microns in length, were coated with 2-mercaptoethanesulfonic acid to provide electrostatic repulsion and prevent aggregation. The layer of wires in direct contact with the substrate was examined from below and found to exhibit smectic-like ordering, the extent of which depends on wire length with the shortest (2 μm) wires exhibiting the best ordering. To understand the assembly in this system, we used canonical Monte Carlo simulations to model the two-dimensional ordering of the wires on a substrate. We account for van der Waals and electrostatic interactions between the wires. The simulations reproduce the experimental trends and show that roughness at the ends of the wires, which locally increase electrostatic repulsion, is critical to correctly predicting the experimentally observed smectic ordering.

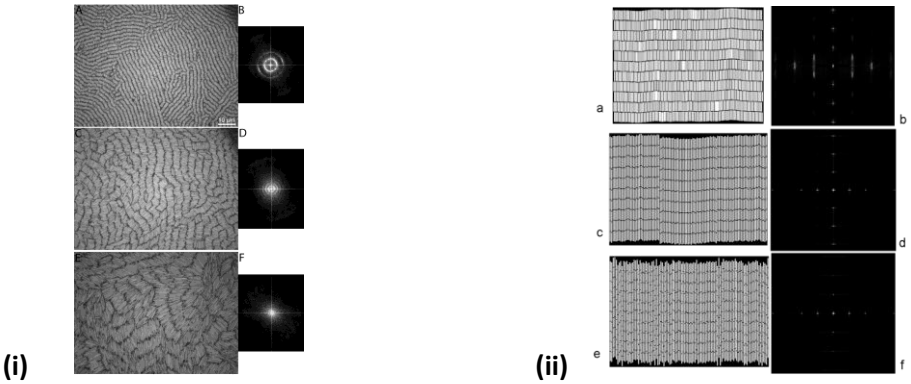

Figure 5: Snapshot of experimental (i) and simulated (ii) nanowire assemblies and their Fourier transforms for 2 μm (a,b), 4 μm (c,d), and 7 μm (e,f) wires.

Future Plans

Work is continuing on projects (A) and (B) described above. We are currently simulating TiO_2 nanoparticles in an aqueous environment to understand the role of hydroxyl groups and hydration on

nanoparticle alignment and aggregation. These simulations will be directly relevant to the experimental studies of the crystallization of colloidal anatase [3], where oriented attachment was first discovered. Additionally, we are probing the long-time restructuring of the anatase nanoparticles after they aggregate using accelerated MD simulations. We note that accelerated MD is an area of strength in our group [8,9]. In our MD studies to date [4], the aggregates are polycrystalline and, hence, are not the monocrystals observed in experiment [3]. By using accelerated MD simulations, we will see if monocrystals form over times that are short on the experimental scale, but long over the (ns) time scale of regular MD. These studies will provide the first insight into long-time aspects of the sintering process.

For the gold/hexane system, we are looking at two different angles. First, we are simulating the aggregation of the nanoparticles in solvent. Our simulations show that these particles should have vertex-to-vertex alignment when their closest atoms are just 1 Å apart and we would like to know if the particles actually aggregate vertex-to-vertex. Strong bonding and van der Waals interactions both favor aggregation in the facet-to-facet configuration and vertex-to-vertex aggregation would be favored by kinetics and solvation forces. We are also simulating the interactions between a "long" (anisotropic) nanoparticle and a compact icosahedron. The hypothesis is that solvation forces are the most repulsive for large, smooth surfaces, which allow solvent molecules to achieve good ordering. Anisotropic nanoparticles will have long, smooth sides, where solvent can order well, and small ends, where solvent cannot order. Thus, we expect a small, uniform nanoparticle to be attracted to the end more than to the sides. These simulations will provide insight into the formation of anisotropic structures during crystallization.

References

1. Niederberger, M.; Colfen, H. *Phys. Chem. Chem. Phys.* **2006**, *8*, 3271.
2. Zhang, Q.; Liu, S.-J.; Yu, S.-H. *J. Mater. Chem.* **2009**, *19*, 191.
3. Penn, R. L.; Banfield, J. F. *Geochim. Cosmochim. Acta* **1999**, *63*, 1549.
4. Alimohammadi, M.; Fichthorn, K.A. *Nano Letters* [Publication Date (Web): August 31, 2009; **DOI:** 10.1021/nl9024215]
5. Gergidis, L.; Fichthorn, K.A. (In preparation).
6. Triplett, D.; Fichthorn, K.A. (In preparation).
7. Triplett, D.; Dillenback, L.M.; Smith, B.D.; Rodriguez, D. H.; St. Angelo, S.; Gonzalez, P.; Keating, C.D.; Fichthorn, K.A. *J. Phys. Chem. C* (submitted).
8. Miron, R.A.; Fichthorn, K.A. *J. Chem. Phys.* **2003**, *119*, 6210.
9. Miron, R.A.; Fichthorn, K.A. *Phys. Rev. Lett.* **2004**, *93*, 128301.

Publications

1. M. Alimohammadi and K. A. Fichthorn, "Molecular Dynamics Simulation of the Aggregation of Titanium Dioxide Nanocrystals: Preferential Alignment", *Nano Letters* [Publication Date (Web): August 31, 2009; **DOI:** 10.1021/nl9024215]
2. L. Gergidis and K. A. Fichthorn, "Molecular Dynamics Simulation of the Directed Alignment of Au Nanocrystals in Alkane Solvent: Solvation and van der Waals Forces" (In preparation).
3. D. A. Triplett and K. A. Fichthorn, "Entropic forces and directed alignment of hard squares in suspensions of rods and disks" (In preparation).
4. D. A. Triplett, L. M. Dillenback, B. D. Smith, D. H. Rodriguez, S. St. Angelo, P. Gonzalez, C. D. Keating, and K. A. Fichthorn, *J. Phys. Chem. C* (submitted).

Hydrothermal Reaction Selectivity for Hierarchical Molecular Assembly

Yongsoon Shin, Jun Liu, and Gregory J. Exarhos
greg.exarhos@pnl.gov
Division of Chemical and Materials Sciences
Pacific Northwest National Laboratory, Richland, WA 99352

Program Scope

Uniform nano-architectures are generated using hydrothermal solution-templated growth approaches and post growth modification techniques that invoke chemical control of molecular self-assembly at interfaces. Synthesis strategies are based upon a fundamental understanding of coupled formation reactions in these nearly energy-neutral processes that drive molecular organization and that can be manipulated kinetically. Materials derived from this approach are characterized with respect to phase composition and homogeneity, structural anisotropy, porosity, and attendant molecular structure by means of diffraction measurements, optical spectroscopies, and traditional electron microscopy approaches that are complemented by non-conventional magnetic resonance measurements. Research progress pursuant to hydrothermally driven condensation reactions involving formation of carbon spheres and core-shell titania-carbon hybrid materials is reported here. Of interest is controlling the sp^2 to sp^3 carbon bond ratio that in turn affects electrical conductivity thereby enabling their use in composite electrode materials for energy storage applications.

Recent Progress

Acid catalyzed conversion of biomolecules that are comprised principally of C6 and C5 sugar molecular units proceeds through condensation reactions that sequentially remove water molecules from the sugars to form oxygenated hydrocarbons like 5-hydroxymethyl furfural and eventually carbon agglomerates as the reaction proceeds to completion. A summary of the cogent condensation and hydrolysis reactions that lead to these species is shown in Figure 1. Aqueous sugar solutions undergo intra-molecular rather than inter-molecular condensation in a closed system at moderate temperatures and pressures to several atmospheres. Under such conditions, HMF readily forms and it can further convert molecularly to either levulinic acid (LA) and formic acid (FA) or by self-assembly to form carbon spheres. The research challenge is to discover the conditions by which complete conversion to carbon spheres becomes the dominant pathway and also to determine how the ratio of sp^2 to sp^3 bonding among the carbon atoms can be controlled.

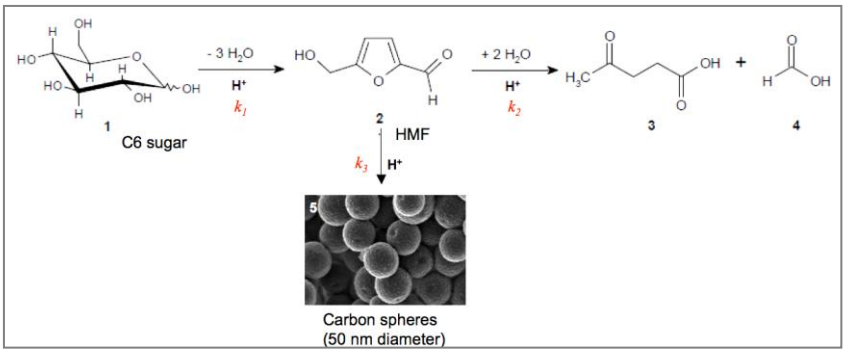

Figure 1. Key condensation pathways for dehydration of sugar in a closed system.

Formation of

HMF is promoted when aqueous sugar solutions are heated in a closed system. Previous work has shown that low pH frustrates the forward hydrolysis reaction that converts HMF to LA and FA while promoting subsequent condensation to form carbon spheres [1]. This architecture is achieved by a partitioning of the slowly evolving hydrophobic phase from the aqueous solution with sugar playing the role of a surfactant. Sphere size correlates with the initial sugar concentration and the structure of the sugar molecule used. In general, fructose, which is a strained 5-member ring, reacts an order of magnitude faster than glucose and produces significantly larger carbon spheres. While increased processing temperature increases the rate of conversion to carbon spheres, little change in sphere size occurs and size distribution remains monodisperse. Processing at pressures considerably higher than ambient by backfilling the reaction vessel with nitrogen results in little change in reaction rate or sphere size.

Other carbohydrates including the cyclodextrines also convert to carbon spheres when aqueous solutions are subjected to mild heating in a closed system [2]. The basket shaped α- and β- cyclodextrines comprised of six and seven member glucose units respectively form spheres with a significantly higher sp^3 content than the much more soluble 8-member basket (γ-cyclodextrine). This conversion also involves formation of HMF. The ubiquity of this molecule has been demonstrated in the literature in studies involving cellulose conversion to fuels in heated ionic liquids [3]. It is not unexpected, then, that aqueous solutions of HMF also will convert to carbon spheres when heated in a closed system. Very recent work here has confirmed this prediction although the highly dispersed carbon formed in solution has not as yet been isolated or analyzed.

The research thus far indicates that concentrated sugar solutions at low pH tend to rapidly convert to carbon spheres and suggests that the presence of other species in solution that would act to enhance formation of HMF would also enhance the conversion rate and influence the nature of the bonding in the resulting carbon. To test this idea, a nickel (II) acetate catalyst was introduced into the reaction vessel at concentrations on the order of one hundredth that of the sugar. This approach was predicated upon recent work that demonstrated accelerated formation of HMF from cellulose exposed to trivalent chromium in an ionic liquid. Under these homogeneous reaction conditions, carbon spheres self-assemble albeit at an accelerated rate. Sphere size again correlates with the initial concentration of sugar in the starting solution. A mild acid wash is used to remove nickel from the carbonaceous material.

The work to this point demonstrates the efficacy of sugar to convert to carbon spheres under hydrothermal conditions in a closed system and that the presence of a catalyst (nickel acetate) can promote the transformation. Since low pH is known to enhance the reaction kinetics from previous *in situ* Raman measurements, introduction of an acid catalyst was suspected to behave analogously and to provide a route for preparing core-shell architectures. Recent activity has been focused on the heterogeneous conversion of sugar to carbon mediated by titania nano-particles dispersed throughout the reaction mixture. Initial studies investigated Degussa P25 titania dispersed in fructose solution at a concentration of several milligrams of titania per gram of sugar. TEM images of the centrifuged reaction mixture following heating at 150º C for several hours in a closed system are shown in Figure 2. The inhomogeneity of the titania both in terms size and shape irregularity and crystalline phase (both anatase and rutile are present) are evident in the figure. However, all particles indeed become coated with a carbon shell.

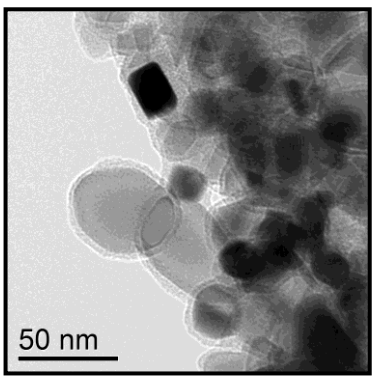

Figure 2a. Degussa P25 titania coated with carbon following hydrothermal dehydration of fructose. Size, shape, and phase inhomogeneity are evident.

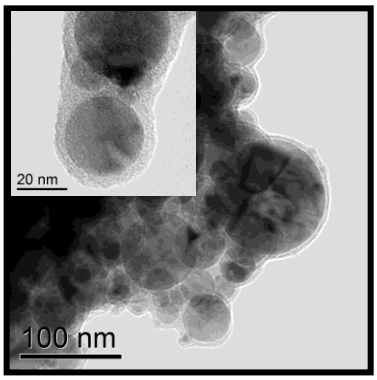

Figure 2b. Carbon shell formation from hydrothermal dehydration of aqueous fructose solution promoted by anatase phase (TiO_2).

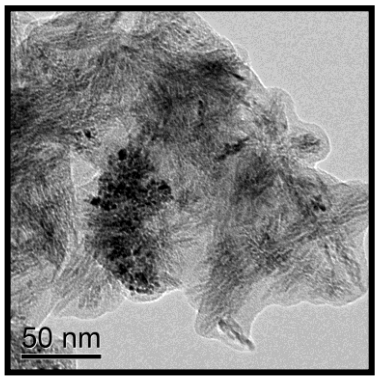

Figure 2c. Carbon shell formation from hydrothermal dehydration of aqueous fructose solution promoted by rutile phase (TiO_2).

The reaction was repeated on phase pure anatase and rutile particles of distributed size and shape. Figure 3 shows that both phases nucleate and grow carbon shell films that encapsulate the dispersed particles. Anatase shows a higher reactivity that rutile. At this point, recent studies have demonstrated that hybrid core-shell structures can be derived from dehydration of aqueous sugar solutions in a closed system and that the carbonaceous phase completely encapsulates the transition metal oxide phase.

Future Plans

Proposed follow-on work will pursue routes for preparing monodisperse particles of titania (anatase), coating the core particles with carbon shells, and modifying the chemical bonding intrinsic to the carbon shells to produce conducting phases. The first activity will investigate biomolecular templating approaches invoking viral cages as reaction vessels. Figure 3 renders a schematic viral cage having a fixed internal volume. Such structures are readily dispersed in solution where ambient pH can be manipulated to open or close ports in the surrounding wall for ingress or egress of reactants. The idea is to admit titania precursors and hydrolyze them in acidic solution to internally form an anatase phase. Denaturing the protein cage will release monodisperse titania particles into solution for subsequent purification.

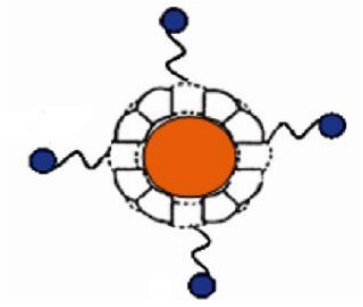

Figure 3. Schematic of a viral cage to be used as a reaction vessel for the formation of monodisperse titania. Variable internal pore volumes on the order of tens of nanometers are available.

The titania nanoparticles will then be coated with carbon shells by means of the sugar dehydration reaction discussed previously. For such materials to be useful in hybrid battery electrode applications, the carbon shell must be rendered electrically conducting. To achieve this, control over the sp^2/sp^3 carbon bond ratio is required accompanied by minimization of oxygen functionality within the carbonaceous shell. Initial experiments suggest that processing these materials in solvents having dielectric constants different from that of water and choosing appropriate sugar precursors are promising approaches.

The long term strategy is to further develop this approach as a means to prepare organized carbon/ceramic and carbon/carbon nano-composite materials.

References

[1] Yao C, Y Shin, LQ Wang, CF Windisch, JR, WD Samuels, BW Arey, CM Wang, WM Risen Jr., and GJ Exarhos. 2007. "Hydrothermal Dehydration of Aqueous Fructose Solutions in a Closed System." Journal of Physical Chemistry C 111(42):15141-15145.

[2] Y. Shin, L-Q Wang, I-T Bae, B.W. Arey, and G.J. Exarhos. Hydrothermal Syntheses of Colloidal Carbon Spheres from Cyclodextrins, 2008. J. Phys. Chem. C112, 14236.

[3] H. Zhao, J. E. Holladay, H. Brown, Z. C. Zhang, Metal Chlorides in Ionic Liquid Solvents Convert Sugars to 5-Hydroxymethylfurfural, 2007. Science 316(5831) 1597.

Selected Project Publications

1. C. Yao, Y. Shin, L-Q Wang, C.F. Windisch, Jr., W.D. Samuels, B.W. Arey, C.M. Wang, W.M. Risen Jr., and G.J. Exarhos. 2007. "Hydrothermal Dehydration of Aqueous Fructose Solutions in a Closed System." Journal of Physical Chemistry C 111(42):15141-15145.

2. J.H. Chang, M.E. Park, Y. Shin, G.J. Exarhos, K.J. Kim, S.C. Lee, and K.S. Oh. 2007. "Functional Scaffolds of Bicontinuous, Thermoresponsive L3-phase Silica-Hydroxyapatite Nanocomposites." Journal of Materials Chemistry 17(3):238-242.

3. Y. Shin, G.A. Baker, L.Q. Wang, and G.J. Exarhos. 2008. "Investigation of the hygroscopic growth of self-assembled layers of N-alkyl-N-methylpyrrolidinium bromides at the interface between air and organic salt ." Colloids and Surfaces. A, Physicochemical and Engineering Aspects 318(1-3):254-258.

4. Y. Shin, I.T. Bae, B.W. Arey, and G.J. Exarhos. 2008. "Facile stabilization of gold-silver alloy nanoparticles on cellulose nanocrystal." Journal of Physical Chemistry C 112(13):4844-4848.

5. Y. Shin, L-Q Wang, I-T Bae, B.W. Arey, and G.J. Exarhos. Hydrothermal Syntheses of Colloidal Carbon Spheres from Cyclodextrins, 2008. J. Phys. Chem. C112, 14236-14240.

6. Y. Shin, I.-T. Bae, G. J. Exarhos, "Green" approach for self-assembly of platinum nanoparticles into nanowires in aqueous glucose solutions. *Colloids and Surfaces A* 2009 In press.

7. Y. Shin, G. J. Exarhos, "Template synthesis of nanostructured metals using cellulose nanocrystal" Chapter contribution in Biomass Nanotechnology (eds: L. Lucia and O. Rojas), Wiley-Blackwell. 2009 In press.

Non-Equilibrium Synthesis of Nanostructured Materials: Real-Time Studies of Growth Kinetics

Gyula Eres, D.B. Geohegan, A.A. Puretzky, C.M. Rouleau, M. Yoon, Z. Zhang
eresg@ornl.gov
Materials Science and Technology Division
Oak Ridge National Laboratory, Oak Ridge, TN 37831

Program Scope

The special properties of nanomaterials result from spatial confinement and unique atomic configurations which determine their electronic energy levels, chemical reactivity, and physical properties. Theoretical calculations show that energy barriers can severely restrict the number of useful configurations that occur under equilibrium conditions. However, numerous metastable configurations evolve during synthesis as a result of competition between thermodynamic and kinetic pathways. Non-equilibrium growth methods transcend the energy barriers for nanostructure formation, and are important tools for materials discovery. The kinetic and chemical energy supplied by lasers, plasmas, and supersonic beams are used to access a parameter space that is out of reach for thermal growth methods. Measurements of the time scales, temperatures, and kinetics of nanomaterial formation in the nonequilibrium regime are enabled by time-resolved, in situ diagnostic techniques. Identifying and isolating the chemical reaction pathways for nanomaterial synthesis represents a key challenge in current synthesis science. For example, despite vivid imagery of nanotube and nanowire growth in environmental electron microscopes, major questions remain about the chemistry of catalyst-assisted growth. Another important question in non-equilibrium synthesis concerns the understanding of the factors that govern and control the product distribution. These mechanisms are often complex and specific steps can be difficult to isolate. However, knowing the type of kinetics is often sufficient to attain a reasonable description of the product distribution. The goal of this research program is to explore the link between growth mechanisms and the resulting structure of nanoscale materials in order to discover and controllably synthesize novel nanomaterials with enhanced properties. The focus is on synthesis processes that can be used to control the structure and composition of a variety of materials including carbon structure formation and wide bandgap semiconductor doping by applying the principles of nonequilibrium synthesis.

Recent Progress

The elimination of secondary gas phase reactions by using a molecular beam environment has greatly simplified the study of the kinetics of carbon structure formation.[1] We have shown that acetylene is a primary precursor and plays a special role in these processes, and have studied vertically aligned nanotube array (VANTA) growth by CVD using molecular beams (MB) of acetylene.[1] Our real-time measurements of MB-CVD VANTA growth kinetics revealed two intriguing results. In addition to the widely-reported deceleration stage of growth, two other stages were found: an onset of growth preceded by an incubation period, and a rapid acceleration of growth. Together, the three stages form an S-shaped growth curve (Fig. 1), which is a characteristic signature of a specific kinetics known as *autocatalysis*.[2] Autocatalytic behavior is often observed in carbon network formation including polymerization and soot growth in connection with acetylene pyrolysis.[2] Using MB-CVD we were able to study specifically the surface catalyzed processes, including the threshold acetylene flux for vertical alignment and the induction period that precedes the onset of vertically aligned growth.[3] These kinetic features strongly imply a heterogeneous chain reaction, leading to a new picture for the growth of CNTs in VANTA. To model the observed autocatalytic kinetics, a five-step self-assembly of acetylene molecules during CNT growth was formulated. Each step illustrates a type or a class of intermediate products and their kinetic tendencies in the growth of CNTs that can be validated by specific experiments. Step one corresponds to dynamic blocking of active sites by adsorbed acetylene

molecules. The transfer of catalytic activity from the metal catalyst film to surface carbon species is necessary to enable propagation of the chain reaction. The next step in self-assembly of carbon is formation of high temperature intermediates such as polyyne chains. Cross-linking of polyyne chains creates nascent graphene fragments that coalesce into tubular graphitic structures. The stabilization of the tubular structures completes the self-assembly process that is governed by free energy minimization of the resulting structure. The nanotube growth stops when no more carbon bonds (active sites) are open to add more acetylene. This kinetic picture is consistent with the formation of a distribution of fullerene type side products confirmed by post growth analysis and a complex distribution of nanotube diameters, chiralities, lengths and alignment. This work identifies general features of carbon nanostructure formation in which carbon species catalyze incorporation of new carbon. These results suggest that molecular pathways play a more important role in the formation of graphene sheets and carbon nanotubes than in it is recognized by the particle centric models of carbon dissolution and precipitation.[4]

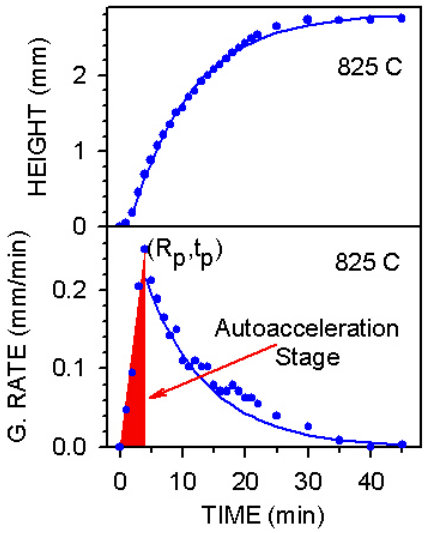

Figure 1. Thickness profile in VANTA growth obtained by CCD imaging of VANTA growth in real-time at 825°C. The growth rate curve shows the autoacceleration stage at the onset of growth.

A pulsed growth method was developed with the goal of exploring the kinetics of the autoacceleration stage on a faster time scale. Of the top outstanding questions regarding nanotube growth, the fundamental understanding of nucleation kinetics are perhaps the most crucial and least studied. In these measurements pulsed feedstock gas introduction was combined with *in situ* reflectivity monitoring and *ex situ* SEM and TEM analysis of VANTAs. Operating at low pressures and fast gas flows, C_2H_2

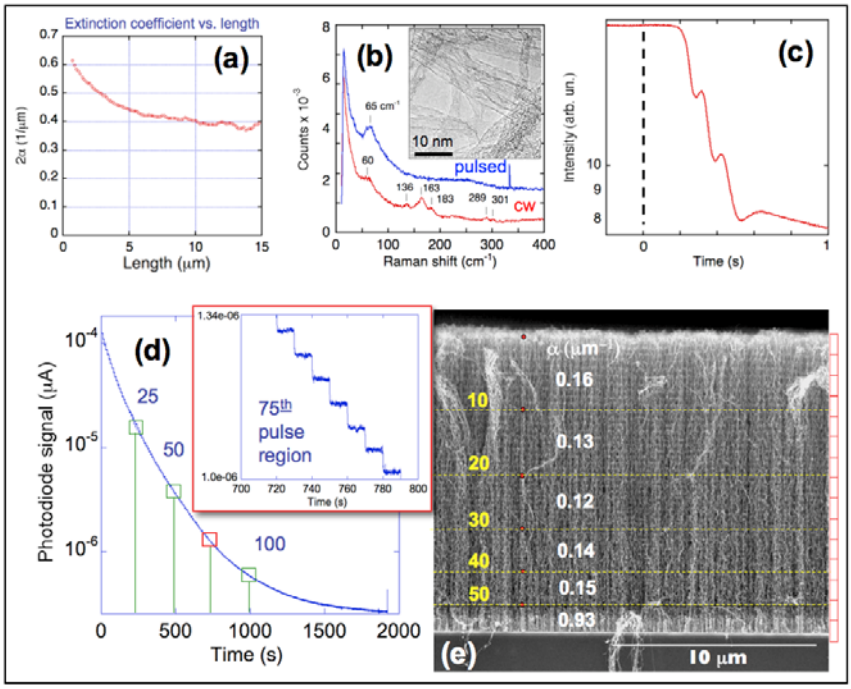

Figure 2. (a) Optical extinction coefficient vs. length measured *in situ* during VANTA growth in 6 Torr of $Ar/H_2/C_2H_2$. (b) Raman spectra RBM region showing narrowing of diameters in pulsed vs. cw-grown VANTAs (c) Optical reflectivity signal of nucleation and rapid growth of ~ 1 μm-long VANTAs after a single gas pulse at t=0. (d) Reflectivity signal for the incremental growth of nanotubes over 150 gas pulses (e) The corresponding VANTA shows 52 bands of growth during the first 52 pulses, followed by a high-density unaligned region at the bottom of the array.

gas pulses from a pulsed valve were injected into fast propagating jets of Ar/H_2 inside a high temperature CVD reactor. The growth kinetics of VANTAs were investigated using a single gas pulse (Fig. 2(c)) and sequences of multiple gas pulses (Fig. 2(d)) of acetylene. The instantaneous growth rate per pulse was varied from 0.02 mm/s up to extremely high rates of 7 mm/s depending on the feedstock supply. It was discovered that the high flux pulsed growth conditions narrow and shift the SWNT diameter distribution toward large (~3.8 nm) diameters as indicated by both the appearance of the broad radial breathing mode (RBM) around 65 cm^{-1} in the Raman spectrum and our TEM measurements (Fig.2(b)). Repeatedly stopping and starting the growth using gas pulses results in the synthesis of vertically stacked SWNT arrays separated by "horizontal" bands - corresponding to incomplete tubular structures grown at the beginning of each gas pulse (Fig. 2(d),(e)). The appearance of the dense disordered layer at the top of each segment was explained by highly active smaller catalyst particles that generate tube-like structures and maintain their activity for a relatively short time due to rapid overcoating with carbon. At low feedstock fluxes these particles generate very long SWNTs. This implies that different catalyst nanoparticles respond differently to the changing feedstock flux within each pulse, some shuting down, and then renucleating on successive pulses. Using this technique the growth rate and induction delay on successive pulses were measured for some of the first observations of renucleation kinetics. Nanotubes were found to renucleate effectively after hundreds of growth interruptions, with small-diameter SWNTs showing little evidence of wall defects under HRTEM.

Recent Progress on Other Projects

We are using theoretical modeling and simulations to develop oxide materials with enhanced nanoscale interface properties. By modeling the energetics and kinetics of dopant incorporation in TiO_2 and ZnO using DFT calculations this effort resulted in a conceptually new approach for doping of wide bandgap materials. The calculations show that the dopant incorporation barriers are substantially lowered if instead of a single element[5] two elements with different valence states are simultaneously incorporated.[6] The net doping referred to as non-compensated *n*-*p* codoping can be either *n*- or *p*-type depending on the valence states of the chosen pair. For example in Fig. 3 a Cr-N pair is a net *n*-type, and V-C pair is a net *p*-type dopant. This work establishes non-compensated co-doping as a promising approach not just for bandgap narrowing but also for solving long standing doping challenges such as *p*-type doping of ZnO. Bandgap narrowing of anatase TiO_2 to around 2 eV was demonstrated in preliminary studies using Cr-N doping of particles synthesized by wet chemistry.[6] A line of complementary characterization techniques was used to confirm various essential predictions of the concept, including band gap narrowing and dramatically enhanced photoabsorption in the visible region. However, these studies also reveal a disproportionately high loss of N during the anatase crystallization step and a correspondingly low concentration of N in substitutional sites.

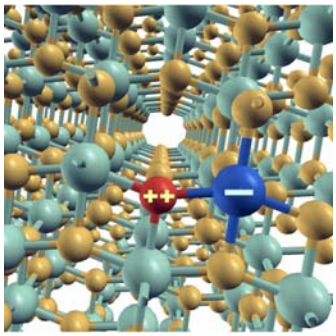

Figure 3. Non-compensated doping where an n-type dopant (V,Cr) replaces a host Ti atom and a p-type dopant (C, N) replaces an adjacent O atom.

Future Plans

We propose to use the non-equilibrium features of PLD to exert direct control over dopant incorporation by non-compensated n-p codoping in the synthesis of TiO_2 nanoparticles. A wide range of dopant element pairs can be explored during growth under different synthesis conditions to overcome undesirable dopant loss. The experimental configuration is based on crossing two PLD plumes, one of the host material target, for example TiO_2 or ZnO and the other of the dopant target containing for example a single dopant or a dopant pair.[7] Certain dopants such as N will be supplemented from a reactive gas phase background. A novel feature of this approach is that the dopant incorporation will be controlled by adjusting the delay between the two plumes while keeping the target composition fixed. Optical diagnostics combined with laser induced fluorescence will be used to monitor a wide range of parameters including the dopant composition, the particles size and the bandgap of nascent particles. Real-time monitoring of the bandgap of nascent particles is being attempted for the first time with the

objectives to understand the synthesis process and to develop a general technique for controlling the optical properties of wide bandgap materials with doping.

References

1. G. Eres, A. A. Kinkhabwala, H. T. Cui, D. B. Geohegan, A. A. Puretzky, and D. H. Lowndes, "Molecular beam-controlled nucleation and growth of vertically aligned single-wall carbon nanotube arrays," *Journal of Physical Chemistry B* **109** (35), 16684-16694 (2005).
2. M. Frenklach and D. Clary, "Aspects of Autocatalytic Reaction-Kinetics," *Industrial & Engineering Chemistry Fundamentals* **22** (4), 433-436 (1983).
3. G. Eres, C.M. Rouleau, M. Yoon, A.A. Puretzky, D.B. Geohegan, Model for Self Assembly of Carbon Nanotubes from Acetylene Based on Real-Time Studies of Vertically Aligned Growth Kinetics, *J. Phys. Chem. C* **113**, 15484 (2009).
4. A. A. Puretzky, D. B. Geohegan, S. Jesse, I. N. Ivanov, and G. Eres, "In situ measurements and modeling of carbon nanotube array growth kinetics during chemical vapor deposition," *Applied Physics a-Materials Science & Processing* **81** (2), 223-240 (2005).
5. S. H. Cheung, P. Nachimuthu, A. G. Joly, M. H. Engelhard, M. K. Bowman, and S. A. Chambers, "N incorporation and electronic structure in N-doped TiO2(110) rutile," *Surface Science* **601** (7), 1754-1762 (2007).
6. W. Zhu, X. Qiu, V. Iancu, X. Chen, H. Pan, W. Wang, N. Dimitrijevic, T. Rajh, H. M. Meyer III, M. P. Paranthaman, M. Stocks, H. Weitering, B. Gu, Gyula Eres, and Z. Zhang, Bandgap narrowing of titanium oxide semiconductors by non-compensated anion-cation codoping for enhanced visible-light photoactivity, (submitted to *Phys. Rev. Lett.*)
7. P. R. Willmott, "Deposition of complex multielemental thin films," *Progress in Surface Science* **76** (6-8), 163-217 (2004).

DOE Sponsored Publications in 2008-2009 from Current Grant (selected of 24)

1. Gyula Eres, C.M. Rouleau, M. Yoon, A.A. Puretzky, D.B. Geohegan, Model for Self Assembly of Carbon Nanotubes from Acetylene Based on Real-Time Studies of Vertically Aligned Growth Kinetics, *J. Phys. Chem. C* **113**, 15484 (2009).
2. H. Pan, X. Qiu, I. N. Ivanov, H. M. Meyer, W. Wang, W. Zhu, M. P. Paranthaman, Z. Zhang, Gyula Eres, and B. Gu, Fabrication and characterization of brookite-rich, visible light-active TiO_2 films for water splitting, accepted *Applied Catalysis B*
3. Y. Yue, G. Eres, X. Wang, L. Guo, Characterization of thermal transport in micro/nanoscale wires by steady-state electro-Raman-thermal technique, *Appl. Phys. A* **97**, 19 (2009).
4. Z. Zhou, G. Eres, R. Jin, A. Subedi, D. Mandrus, E.H. Kim, The performance of in situ grown Schottky-barrier single wall carbon nanotube field-effect transistors, *Nanotechnology* **20**, 085709 (2009).
5. M. H. Upton, R. F. Klie, J. P. Hill, T. Gog, D. Casa, W. Ku, Y. Zhu, M.Y. Sfeir, J. Misewich, G. Eres, D. Lowndes, Effect of number of walls on plasmon behavior in carbon nanotubes, *Carbon*, 47, 162 (2009).
6. C.M. Rouleau, G. Eres, H. Cui, H.M. Christen, A.A. Puretzky, D.B. Geohegan, "Altering the catalytic activity of thin metal catalyst films for controlled growth of chemical vapor deposited vertically aligned carbon nanotube arrays" , *Appl. Phys. A* **93**(4), 1005-1009 (2008).
7. A. A. Puretzky, G. Eres, C.M. Rouleau, I. N. Ivanov, and D. B. Geohegan "Real-time imaging of vertically aligned carbon nanotube array growth kinetics." *Nanotechnology* **19**(5) 055605 (2008).
8. D. B. Geohegan, A. A. Puretzky, C. M. Rouleau, J. J. Jackson, G. Eres, Z. Liu, D. Styers-Barnett, H. Hu, B. Zhao, K. Xiao, I. Ivanov, and K. More, "Laser Interactions in Nanomaterials Synthesis", Book Chapter in *Springer Series in Materials Science* (2009).

In situ Studies of Solid Electrolyte Interphase on Nanostructured Materials

Chengdu Liang, Nancy Dudney, Karren More, Robert W. Shaw, John Ankner, and Ke An
liangcn@ornl.gov
Oak Ridge National Laboratory
Oak Ridge, TN 37831-6493

Program scope

Nanostructured materials hold great promise for advanced electrical energy storage systems because of their advantageous properties of high surface area and short diffusion path of ions. However, these advantages have been offset by side reactions that lead to the formation of the solid electrolyte interphase (SEI), which plays two major roles in electrical energy storage (EES) systems: (1) transport of the Li^+ and (2) impedance of the side reactions between the electroactive materials and the liquid electrolyte. The dynamically changing nature of the SEI makes the conventional *ex situ* studies inadequate to provide precise descriptions of the growth mechanisms, structure, and dynamic properties of the SEI. **The overall goal of this project is to develop a molecular level understanding of the growth mechanisms, structure, and dynamic properties of the SEI that results from the oxidative decomposition of liquid electrolytes at the nanostructured cathodes.** To reach this goal, we propose herein to use three synergistically linked *in situ* characterization techniques, including transmission electron microscopy (TEM), sum frequency generation (SFG) spectroscopy, and neutron scattering (NS), with the added component of materials synthesis to probe the chemistry and physics of the SEI under real electrochemical conditions. The three *in situ* techniques will provide insight to the SEI from different scientific angles and render new fundamental answers to these questions: (1) How does the SEI physically and chemically evolve at reduced (nm-scale) dimensions? (2) How does the mass transport of Li^+ occur in the SEI under electrochemical conditions at real time? (3) How do the dynamic structural and compositional changes of the SEI relate to the electrochemical properties of the electrode materials at the nm-scale in terms of electric energy storage capacity, charge/discharge rate, and temporal physiochemical stability? With a thorough fundamental understanding of Li^+ transport and SEI formation, we could rationally design novel chemistries and advanced materials for EES systems with high energy and power densities. Probing the novel phenomena emerging at the nanometer scale at real time and harnessing the emergent properties of nanomaterials are key to the development of advanced energy materials, which will have far-reaching implications for the missions of the Department of Energy. To deploy the advanced EES systems is an essential step toward substantial future energy strategy and of vital importance for the nation's energy independence and security.

Future Plans

Our approach will to be use controlled chemical syntheses to precisely tailor nanostructured materials and interfaces for *in situ* characterization studies of the SEI. Nanostructured oxides and phosphates of transitional metals, such as Co, Ni, Fe, and Mn, will be synthesized so that individual crystal facets can be studied; these materials will be assembled into specially designed electrochemical cells that will enable *in situ*

measurements, thus providing real-time information under a variety of conditions. The *in situ* characterization techniques are essential to providing fundamental information not currently available about: 1) the evolving physical structure and phase formation within the growing SEI via S/TEM imaging; 2) the chemical structure of the SEI from surface vibrational spectroscopy data; and 3) depth profiles and transport mechanism of Li^+ in the SEI from neutron scattering by using isotope substitution techniques. Bench-top electrochemical experiments will be carried out to validate the *in situ* characterization data. Based on the *in situ* experimental results the formation, growth, structure, and transport properties of the SEI will be thoroughly understood. By establishing a fundamental understanding of the mechanisms of Li^+ transport and SEI formation, we will design and synthesize advanced materials for EES with high energy- and power-densities at high charge/discharge rates.

Session III

Synthesis Methods in Plasmonics

Session Chair: Zhoumin Zhang, Georgia Institute of Technology

(This page intentionally left blank.)

Asymmetric Hybrid Nanoparticles

George Chumanov
gchumak@clemson.ecu
Department of Chemistry
Clemson University, Clemson, SC 29634

Program Scope

Nanoscale materials attract considerable interest because of their unusual properties and potential for practical applications. Most of the activity in this field is focused on the synthesis of homogeneous nanoparticles from metals, metal oxides, semiconductors, and polymers. It is well recognized that properties of nanoparticles can be further enhanced if they are made as hybrid structures. This research is concerned with the synthesis, characterization, and application of plasmonic Ag nanoparticles (NPs) and structures. One of the main emphases is on asymmetric hybrid nanoparticles (AHN) that are composed of a core with several caps. Combined properties of the core and the caps as well as new properties that arise from core-cap and cap-cap interactions render the development of AHNs fundamentally and practically important. In addition, specific chemical reactivity of the caps enables directional self-assembly of AHNs into complex architectures that are not possible with only spherical nanoparticles. Plasmonic NPs exhibit unique optical properties arising from the excitation of the collective oscillations of the conduction electrons. Plasmon resonances can be tuned across the visible spectral range by varying the particle size, shape, and dielectric environment. Their excitation in Ag NPs represents the most efficient mechanism by which light interacts with matter. Because of this efficiency, tunability, and photochemical robustness, plasmonic AHNs are ideal for applications involving interaction with light. We design novel structures for optical applications.

Recent progress

AHNs were fabricated by vacuum evaporation of thin layers of SiO, LiF, Ti, Al, Cr, Ni, and Fe onto Ag nanoparticles immobilized on glass substrates modified with poly-(4-vinylpyridine). After the deposition, the particles were stripped into solution and characterized by UV-Vis spectroscopy as well as transmission and scanning electron microscopy. The presence of the caps shifted the plasmon resonance into the red spectral region according to the refractive index of the cap material. In the case of metals, specifically Fe, the cap damped the plasmon resonance and to minimize this effect, a thin layer of SiO was deposited between the Ag core and Fe cap. A thin layer of SiO also was deposited on top of the Fe cap to protect the latter from oxidation in the aqueous environment (Fig. 1). The Fe cap rendered magnetic properties to plasmonic AHNs. It was demonstrated that the AHNs technology enables manipulation of resonance properties of plasmonic nanoparticles. At the same time, new properties can be added as was exemplified by the deposition of the magnetic caps onto the surface of Ag NPs. Placing a dielectric spacer layer between the magnetic cap and the surface of the plasmonic particle represents a general strategy for minimizing the interference of the caps with plasmon resonances of the core.

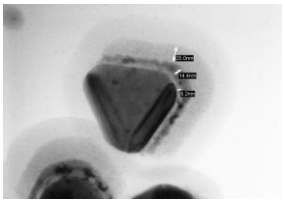

Fig. 1 Triple layered magnetic plasmonic AHNs composed of 90 nm Ag core, 8.2 nm SiO spacer, 14.4 nm Fe cap, and 25 nm SiO overlayer to protect oxidation of Fe.

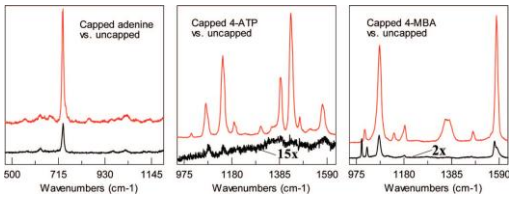

Fig. 2. SERS of capped (red) and uncapped (black) AHNs.

A different type of AHNs was synthesized comprising the *silver core – molecule – silver cap* structure. These AHNs were demonstrated to produce strong surface-enhanced Raman scattering. The SERS signal was impressively strong so signals with ca. 10^2 signal-to-noise ration were measured from a single particle in only one second with ca. 10 microwatt exciatation power (Fig. 2). From the analysis of the data, *plasmon-induced electronic coupling* was concluded to be the major Raman enhancement mechanism. The hybrid nanoparticles also exhibited polarization dependant elastic light scattering that was attributed to the particle anisotropy which resulted from the addition of the silver cap. The disparities in the scattering along different particle axes were attributed to the plasmon modes that have similar frequencies but, upon deposition of the cap, have changed their character from radiative to absorbing. There are three degenerate modes corresponding to the electron oscillations along three equal axes in a spherical plasmonic particle. Upon the deposition of the cap, one mode corresponding to the electron oscillations along the core-cap axis becomes different. These AHNs can potentially be used as optical labels for spectral multiplexing and hyperspectral imaging. AHNs composed of metal core – molecular layer – metal cap structure present a new type of composite nanoparticles that exhibit new properties enabling novel applications and devices.

Plasmon coupling in arrays of plasmonic particles was investigated as a function of dielectric environment, particle size and interparticle distance. This fundamental ongoing study aims the development of general principles that guide light/matter interaction in strongly coupled systems with ultimate goal to discover systems with novel optical properties of practical importance. We have completed experimental and theoretical studies of the role of the dielectric environment on plasmon coupling. The studies were performed on 2D arrays of immobilized Ag NPs. The immobilization was accomplished with a thin PMMA layer. This newly developed technique provides a convenient method for stabilizing particles against surface aggregation and preserving their original arrangement. In the frame of the applied method we simulated a change in the SNPs' surrounding medium, which was caused by forming the PMMA layer between the individual SNPs in the arrays, by introducing the effective refractive index with the value intermediate between those of air and the PMMA and dependent on the PMMA thickness. On the basis of experimental data and theoretical modeling, it was concluded that the plasmon coupling is more efficient in the media with higher dielectric function, contrary to previous believes. The quasi-crystalline approximation of the statistical theory of multiple scattering of waves was used to model the extinction spectra of the arrays (Fig. 3). The lateral electrodynamic interactions between individual particles in the array were considered as the interference of multiply scattered waves in both the near and the far field regions. The resulting field at any point of space was a sum of multiply scattered waves from individual NPs, including their relative phases and the field produced by all waves multiply scattered by other particles. The spatial distribution of particles in the arrays determines the correlation effects for the electrodynamic interactions and was described statistically by the radial distribution function g(r) calculated in the Percus-Yevick approximation for hard spheres.

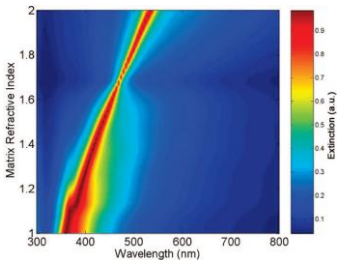

Fig. 3 Result of the modeling of plasmon coupling in 2D arras of AHNs

Future plans

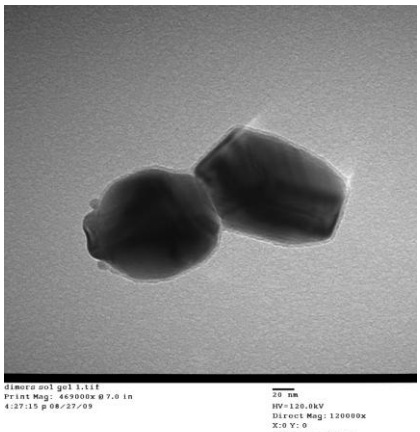

Fig. 4 A dimer of plasmonic AHNs synthesized by template assisted self-assembly. Notice a 10 nm thick silica shell around the dimer as well as a thin organic layer between the two particles that promoted the assembly of this structure.

Near-future work will proceed along several venues. First, we will continue the ongoing fundamental studies of plasmon coupling, as described above. Second, we will continue studies of ring structures of plasmonic NPs fabricated by template assisted self-assembly. We have recently accomplished the controlled synthesis of nanoparticle dimers using the template assisted self-assembly technique of AHNs (Fig. 4) Third, preliminary results suggest that it is possible to synthesize the following AHN structures: Ag core/organic layer/Ag cap/SiO cap/Fe cap/SiO cap. Such structures have potential to function as advanced optical labels because they exhibit strong SERS (as per our results in the previous report) as well as have magnetic response, permitting the SERS signal to be modulated via a rotating magnetic field. As we previously demonstrated, the scattering intensity from such AHNs is several orders of magnitude stronger when excited along the major axis as compared to the excitation along the minor axis. Fourth, we have initiated studies of a novel heterogeneous AHN structure for potential photovoltaic applications. This structure consists of Ag core/AgSe cap/Se cap. Whereas Se is known p-type semiconductor, our resent Hall measurements strongly suggest that AgSe is an n-type semiconductor. If this is confirmed, the structure is a pn-heterojunction that could produce photocurrent when excited in the plasmon resonance of the Ag core. These studies currently constitute one of our main efforts.

DOE Sponsored Publications in 2007-2009 from Current Grant

1. Malynych, S., Chumanov, G., Extinction spectra of quasi-spherical silver sub-micron particles", *J. Quantitative Spectroscopy & Radiative Transfer*, **106**, 297-303 (2007).

2. Stephen D. Hudson, George Chumanov, "Synthesis and Characterization of Plasmonic Asymmetric Hybrid Nanoparticles" *Chemistry of Materials*, **19**, 4222-4227 (2007).

3. Mark Kinnan, George Chumanov, "Surface Enhanced Raman Scattering from Silver Nanoparticle Arrays on Silver Mirror Films: Plasmon-Induced Electronic Coupling as the Enhancement Mechanism" *J. Phys. Chem. C*, **111**, 18010-18017 (2007).

4. S. Malynych, and G. Chumanov, "Narrow Plasmon Mode in 2D Arrays of Silver Nanoparticles Self-Assembled on Thin Silver Films" *J. Microscopy*, **229**, 567–574 (2008).

5. Bogdan Zdyrko, Mark K. Kinnan, George Chumanov, Igor Luzinov, "Fabrication of optically active flexible polymer films with embedded chain-like arrays of silver nanoparticles" *Chem. Com.*, **11**, 1284 - 1286 (2008).

6. Mark K. Kinnan, Amar Kumbhar, George Chumanov, "Surface Enhanced Raman Scattering from Plasma Reduced Silver Salts", *Applied Spectroscopy*, **62**, 721-726, (2008). The article featured on the cover page of the journal.

7. Bogdan Zdyrko, Olha Hoy, Mark K. Kinnan, George Chumanov, and Igor Luzinov, "Nano-patterning with Polymer Brushes via Solvent-Assisted Polymer Grafting", *Soft Matter*, **4**, 2213-2219, (2008).

8. John C. Heckel, Fatimah F. Farhan, George Chumanov, "Synthesis of Carbon Shells Around Silver Nanoparticles", *Coll. Polym. Sci*., **286**, 1545-1552 (2008).

9. Stephen D. Hudson, George Chumanov, "SERS and Resonance Elastic Scattering from Capped Single Ag Nanoparticles", *J. Phys. Chem. C*, **112**, 19866–19871 (2008).

10. Ramaratnam, K., Iyer, S. K., Kinnan, M. K., Chumanov, G., Brown, Ph., Luzinov, I. "Ultrahydrophobic Textiles Using Nanoparticles: Lotus Approach", *J. Engineered Fibers and Fabrics*, **3**, 1-14 (2008).

11. Stephen D. Hudson, George Chumanov, "Bioanalytical Applications of SERS" (Invited Review), *Analytical and Bioanalytical Chemistry*, **394**, 679–686 (2009).

12. Mark K Kinnan, Svetlana Kachan, Courtenay K Simmons, George Chumanov, "Plasmon Coupling in Two-Dimensional Arrays of Silver Nanoparticles: I. Effect of the Dielectric Medium", *J. Phys. Chem. C*, **113**, 7079-7084 (2009).

13. Amar S. Kumbhar and George Chumanov, "Encapsulation of Silver Nanoparticles into Polystyrene Microspheres", *Chem. Mater*., **21**, 2835–2839 (2009).

14. John C. Heckel, Lydia M. Kisley, Joe Mannion, George Chumanov "Synthesis and Self-Assembly of Polymer Coated Silver Nanoparticles", *Langmuir*, **25**, 9671–9676 (2009).

15. John Henson, John C. Heckel, Emmanouil Dimakis, Josh Abell, Anirban Bhattacharyya, George Chumanov, Theodore D. Moustakas, and Roberto Paiella, "Plasmon Enhanced Light Emission from InGaN Quantum Wells via Coupling to Chemically Synthesized Silver Nanoparticles" *App. Phys. Lett*., **submitted** (2009).

16. Serhiy Z. Malynych, Alexander Tokarev, Stephen Hudson, George Chumanov, John Ballato, and Konstantin G.Kornev, "Magneto-Controlled Illumination with Opto- Fluidics, *Applied Optics*, **submitted** (2009).

Ultrasmooth Patterned Films for Plasmonics and Metamaterials

David J. Norris (PI)
dnorris@umn.edu
Department of Chemical Engineering & Materials Science
University of Minnesota, Minneapolis, MN 55455

Program Scope

Photonic crystals are materials that are periodically structured on an optical length scale. It was previously demonstrated that the glow, or thermal emission, of tungsten photonic crystals that have a specific structure – known as the "woodpile structure" – could be modified to reduce the amount of infrared radiation from the material.[1] This effect can improve the efficiency of thermal emission sources and for thermophotovoltaic devices, which convert heat into electricity.[2] The study of this effect had been limited because the fabrication of metallic woodpile structures had previously required a complex fabrication process. In this project we have been pursuing several approaches to simplify the fabrication of metallic photonic materials that are useful for modification of thermal emission. First, we have used the self-assembly of micrometer-scale spheres into colloidal crystals known as synthetic opals.[3-5] These opals can then be infiltrated with a metal and the spheres removed to obtain a structure, known as an inverse opal, in which a three-dimensional array of bubbles is embedded in a film. Second, we have used direct laser writing, in which the focus of an infrared laser is moved through a thin film of photoresist to form lines by multiphoton polymerization.[6] Proper layering of such lines can lead to a scaffold with the woodpile structure.

Recent Progress

Our prior work on three-dimensional metallic photonic crystals led us to consider whether simple metallic films could also provide useful thermal emission. In particular, we were interested if they could control the direction of the emission. If possible, this would have serious implications for thermophotovoltaics (TPV). For example, in solar TPV, a material must absorb all of the energy from sunlight as heat and then thermally re-emit IR light. If this IR emission has a narrow spectrum that is well-matched to a photocell, it can, in principle, be efficiently converted into electricity. Indeed, we previously demonstrated how the thermal emission spectrum from tungsten woodpiles could be useful for solar TPV.[6] However, because this emission is not directional, it would be difficult to collect by a photocell in a real TPV device. Thus, it would be highly desirable to discover a structure that controlled not only the spectrum but also the direction of the thermal emission. The emission could then be "beamed" efficiently to the photocell and converted to electricity.

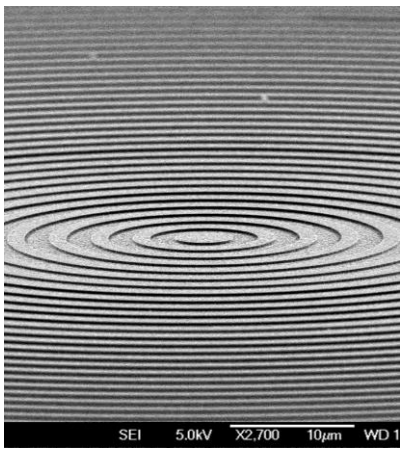

Fig. 1 SEM image of a bull's eye patterned on a tungsten film. The periodicity and depth of the grooves are 3.5 μm and 160 nm, respectively. The scale bar is 10 μm.

We recently discovered that a very simple pattern can produce a highly directional beam of thermal emission. Namely, a bull's eye structure (Fig. 1), in which the surface of a metal film is patterned with a series of circular concentric grooves,

can produce a beam that is narrow both in its spectrum and angular divergence.[7] By tailoring both the spacing between the grooves and the metal, the emission wavelength can be tuned. While we initially fabricated tungsten bull's eyes with optical lithography and reactive ion etching, a different fabrication technique was required to reduce surface roughness and improve optical performance.

Surprisingly, no techniques existed previously to obtain such structures. Metal films deposited by evaporation are inherently rough due to polycrystallinity. Moreover, when such films are patterned, for example by focused ion beam or reactive ion etching, this roughness is increased as the grains are exposed. When this roughness is present, effects, such as our thermal beaming, can be diminished.

More generally, surface roughness in patterned metal films has been a serious problem for the field of plasmonics, where devices have been developed to utilize and manipulate surface plasmons.[10-12] Surface plasmons are special electromagnetic waves that exist at a metal interface.[13] They are restricted to propagate at the surface and have an intensity that decays both into the bulk metal and the surrounding medium. Because surface plasmons are a mixture of both optical waves and electronic surface oscillations, they have a unique hybrid character. The photonic component allows surface plasmons to interact with light, while the electronic component allows this light to be concentrated in nanometer-scale volumes. This has fundamental implications as well as applications ranging from sensors to solar cells.

In a typical device, surface plasmons are excited when light irradiates an exposed metal surface. If the interface is perfectly flat, this is not allowed by momentum conservation. However, if the surface is patterned, light can couple to surface plasmons via diffraction. Moreover, once the plasmons are created, patterning provides a means to channel, concentrate, and manipulate them as they move along the interface. However, due to unwanted roughness, surface plasmons have suffered from increased scattering and limited propagation. This has restricted the study of many phenomena, including intense localized light. Consequently, the fabrication of smooth patterned films was recognized as a major challenge for the field of plasmonics.

To fabricate our bull's eye structures while simultaneously satisfying the broader requirements for plasmonics, we developed an extremely simple, general

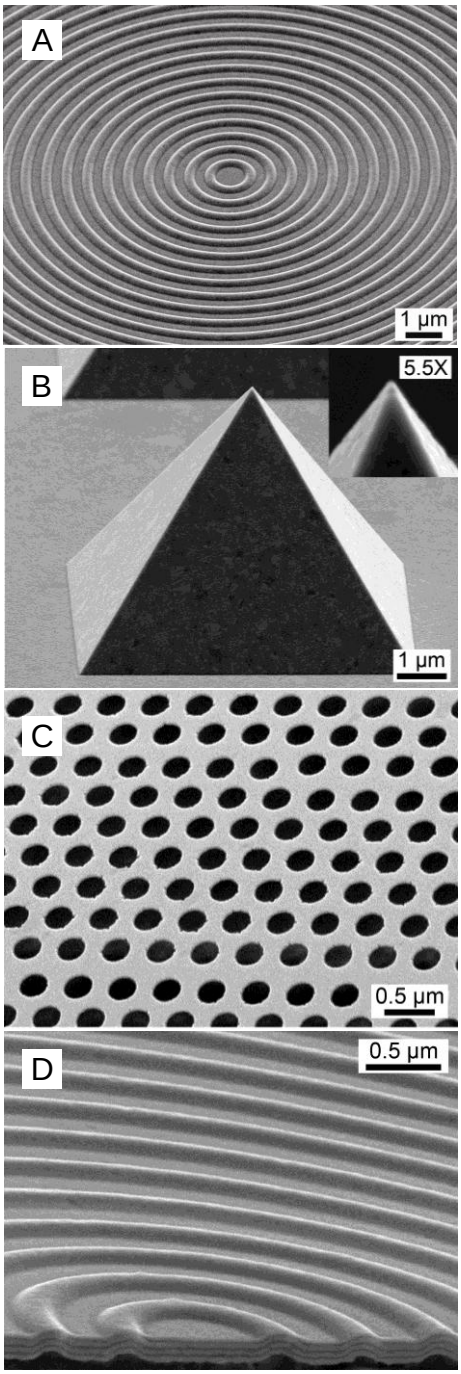

Fig. 2 SEMs of several ultrasmooth patterned metal films obtained by a new simple, high-throughput method. (A) a silver bull's eye, (B) an ultrasharp silver pyramid with a radius of curvature at the tip of 10 nm, (C) a silver hole array, and (D) a cross-section of a multilayer silver/alumina film that can be used as an optical metamaterial.

technique for producing ultrasmooth patterned metal surfaces (see Fig. 2).[8] It also provides a high-throughput fabrication procedure that can produce wafer-scale films. Our approach starts by patterning a silicon wafer and depositing a metal film on it. The metal can then be peeled off to expose an ultrasmooth metal replica of the patterned wafer. This process works due to the poor adhesion but good wettability of many metals on silicon.[9] It is not only simple but offers several critical advantages: (i) Although the metal film still has a rough surface on its "top" interface after deposition, the opposite side is used, which was templated by the silicon wafer. Indeed, roughnesses as low as 0.4 nm have been observed. (ii) Because the wafer, and not the metal, is patterned, no ion impurities are implanted in the metal, which has been a problem in previous approaches. (iii) Since a wafer acts as the template, all of the tools developed for microelectronics can be utilized for patterning. (iv) After the metal film is removed, this template is ready to produce additional metal structures of the same pattern. Thus, an inexpensive, high-throughput, large-area, and reproducible approach to plasmonic structures is obtained.

Because of these benefits, we expect our technique to impact not only our research on bull's eyes for the modification of thermal emission, but also more broadly. A variety of ultrasmooth plasmonic structures will be available for the first time. For example, a sharp tip with smooth side walls, such as that shown in Fig. 2B, can lead to extreme localization of surface plasmons in nanometer-scale volumes. This has immediate implications for not only sensing, but many nonlinear optical spectroscopies and microscopies. In addition, the fabrication method can produce structures known as metamaterials. Such solids can exhibit properties not found in natural materials (*e.g.*, a negative index of refraction). They have been studied as a route to new optical devices such as superlenses and invisibility cloaks. Figure 2D shows a smooth patterned film made via template-stripping that consists of alternating layers of silver and alumina. Similar films have been fabricated via low-throughput conventional methods to obtain negative index materials. With our approach, many more structures can be quickly fabricated and studied. Moreover, these films have built-in metal contacts and can be formed on flexible substrates, useful for device applications.

Future Plans

To date, we have demonstrated ultrasmooth patterned films from noble metals such as silver, gold, and copper. For thermal emission, refractory metals that have much higher melting temperatures must be used. Therefore, we are currently working to extend our approach to metals such as tungsten. Thus, smooth tungsten bull's eyes will be available for thermal emission measurements. Also, the behavior of heated tungsten pyramids will be examined. More generally, we believe that our simple approach, will be applicable to a broad class of materials, such that patterned multilayer films that include layers of metal, dielectric, and semiconductor can be produced. This should be useful for many applications, including solar cells and solid-state lighting.

Another related aspect of our work is to probe whether metal films can be produced that have useful grain structures on their exposed surfaces. We will examine the texturing in our films and test whether our approach can be used to create thin patterned films that are single crystalline. For plasmonic applications, this can further reduce optical losses and improve the performance of devices.

References

1. J. G. Fleming, S. Y. Lin, I. El-Kady, R. Biswas, and K. M. Ho, Nature **417**, 52 (2002).
2. S. Y. Lin, J. Moreno, and J. G. Fleming, Appl. Phys. Lett. **83**, 380 (2003).
3. N. R. Denny, S. E. Han, D. J. Norris, and A. Stein, Chem. Mater. **19**, 4563 (2007).
4. S. E. Han, A. Stein, and D. J. Norris, Phys. Rev. Lett. **99**, 053906 (4 pages) (2007).
5. Y. Jun, P. Nagpal, and D. J. Norris, Adv. Mater. **20**, 606 (2008).
6. P. Nagpal, S. E. Han, A. Stein, and D. J. Norris, Nano Lett. **8**, 3238 (2008).
7. S. E. Han, P. Nagpal, and D. J. Norris, Phys. Rev. Lett. (submitted).
8. P. Nagpal, N. C. Lindquist, S. H. Oh, and D. J. Norris, Science **325**, 594 (2009).
9. M. Hegner, P. Wagner, and G. Semenza, Surf Sci **291**, 39 (1993).
10. H. A. Atwater, Sci. Am. **296**, 56 (2007).
11. C. Genet and T. W. Ebbesen, Nature **445**, 39 (2007).
12. A. Polman, Science **322**, 868 (2008).
13. H. Raether, *Surface Plasmons*. (Springer-Verlag, Berlin, 1988).

Publications Resulting from Work Supported by the DOE Project over the Last Two Years

1. Denny, N. R., Han, S. E., Norris, D. J. & Stein, A.; "Effects of thermal processes on the structure of monolithic tungsten and tungsten alloy photonic crystals," *Chem. Mater.* **19**, 4563-4569 (2007).
2. Han, S. E., Stein, A. & Norris, D. J.; "Tailoring self-assembled metallic photonic crystals for modified thermal emission," *Phys. Rev. Lett.* **99**, 053906, 4 pages (2007).
3. Jun, Y., Nagpal, P. & Norris, D. J.; "Thermally stable organic-inorganic hybrid photoresists for fabrication of photonic band gap structures with direct laser writing," *Adv. Mater.* **20**, 606-610 (2008).
4. Nagpal, P., Han, S. E., Stein, A. & Norris, D. J.; "Efficient low-temperature thermo-photovoltaic emitters from metallic photonic crystals," *Nano Lett.* **8**, 3238-3243 (2008).
5. Nagpal, P., Lindquist, N.C., Oh, S.-H. & Norris, D. J.; "Ultra-smooth patterned metals for plasmonics and metamaterials," *Science* **325**, 594-597 (2009).

Plasmonic Dispersion Engineering for Light-Emission Efficiency Enhancement

R. Paiella
Department of Electrical Engineering and Photonics Center, Boston University, Boston, MA 02215
Phone: 617-353-8883, Fax: 617-353-1283, Email: rpaiella@bu.edu

1. Program Scope

This project is focused on the development and characterization of plasmonic nanostructures integrated with semiconductor photonic materials and designed to enhance their light-emission efficiency. In particular we employ epitaxial films based on the family of nitride semiconductors InGaN and AlGaN, whose energy bandgap can be tuned throughout the visible and UV spectrum by varying the alloy composition. Consequently, these materials are technologically important for a wide range of optoelectronic applications such as lasers, light emitting diodes (LEDs), photodetectors, and solar cells.

In general, surface plasmon polaritons (SPPs) at metal surfaces and localized plasmonic resonances of metallic nanostructures can be used to increase the spontaneous emission rate of nearby radiative media, by virtue of their highly confined electromagnetic fields and large densities of optical modes [1]. The overall light output intensity of these media can therefore be enhanced, provided that a suitable nanostructure is present that can efficiently scatter the emitted SPPs into radiation [2]. The goal of this project is to theoretically and experimentally investigate several configurations of metallic nanostructures designed for this application. Particular emphasis is focused on the geometrical tuning of the plasmonic resonance to match the emission wavelength of the supporting semiconductor material, which is a key requirement for strong exciton/SPP coupling.

2. Recent Progress

Tunable plasmonic resonances in strongly coupled metallo-dielectric stacks

In this context, we have theoretically proposed and experimentally demonstrated a fundamentally new class of tunable SPP resonances based on nanoscale metallo-dielectric stacks [3,4]. These heterostructures allow tailoring the SPP dispersion curves $\omega(k)$ so as to introduce tunable singularities in the SPP density of modes (which is inversely proportional to the slope $d\omega/dk$), and hence in the spontaneous emission rate of nearby emissive layers (which is proportional to the SPP density of modes). The photon energies of these resonances depend on the stack layer thicknesses and compositions, and thus can be controlled by design through the choice of these parameters.

This idea is illustrated in Fig. 1 for the case of a (4-nm)Al/(10-nm)HfO_2/(10-nm)Ag/HfO_2 structure, designed to produce a resonance in the SPP density of modes near 350 nm (far removed from the natural resonance of all common noble-metal films). As indicated by the dotted circle in Fig. 1(a), the SPP dispersion curves of this structure exhibit a region of negligibly small slope $d\omega/dk$ – and hence highly enhanced SPP density of modes – near this target wavelength ($\hbar\omega$ = 3.5 eV), resulting from the mixing and anticrossing of SPP modes localized at neighboring interfaces in the stack. The calculated spontaneous-emission-rate enhancement factor F of an emissive layer at a small distance t_{sp} from this stack is plotted versus wavelength in Fig. 1(c), for different values of t_{sp}. As expected, a pronounced peak in the enhancement factor at the target wavelength of 350 nm is clearly observed. The wavevector-resolved enhancement factor is plotted versus in-plane wavevector k and photon energy $\hbar\omega$ in the log10-scale color map of Fig. 1(b), to illustrate its direct correlation with the dispersion curves of Fig. 1(a).

For the experimental demonstration of this novel SPP tuning mechanism, we have measured the photoluminescence (PL) spectra of several samples derived from the same GaN/AlGaN quantum-well

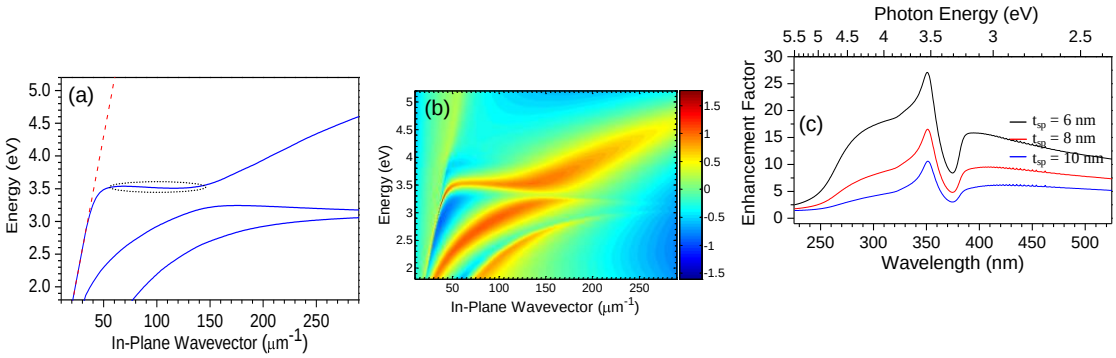

Fig. 1: (a) SPP dispersion curves of a (4-nm)Al/(10-nm)HfO_2/(10-nm)Ag/HfO_2 stack on an AlGaN substrate. (b) Spontaneous-emission-rate enhancement factor of a nearby (8-nm) active layer, plotted as a log10-scale color map on the k-$\hbar\omega$ plane. (c) Spontaneous-emission-rate enhancement factor from (b), integrated over k and plotted versus wavelength, for different values of the spacer thickness between the active layer and the stack.

(QW) structure emitting near 350 nm. These included samples coated with a single Al film, with the Al/HfO_2/Ag/HfO_2 multiple-layer structure of Fig. 1 (denoted ML(A) in Fig. 2 below), and with a similar stack except for a ~30% thinner Al film (ML(B)).

Shown in Fig. 2(a) are the ratios between the PL spectrum of a reference uncoated piece and those of the three metal-coated samples just described. All three ratios are greater than one, indicating insufficient roughness in the deposited films to effectively scatter the emitted SPPs into radiation. Thus, the increased recombination rate due to emission of SPPs here manifests itself as a proportional decrease in the amount of collected light [5]. In Fig. 2(b) we show the calculated PL intensity ratios between the reference uncoated sample and each coated structure of Fig. 2(a), computed from the spontaneous-emission-rate enhancement factor F as described in detail in ref. [4]. The overall agreement between these theoretical and experimental traces is remarkable. In particular, the expected resonance peak in the PL intensity ratio brought about by the Al/HfO_2/Ag/HfO_2 stacks is clearly observed in both theoretical and experimental plots. Furthermore, in both figures this peak undergoes an obvious red shift as the thickness of the Al film is decreased. These results therefore demonstrate the ability of metallo-dielectric stacks to tune the resonance of SPPs and more in general to engineer their dispersion characteristics.

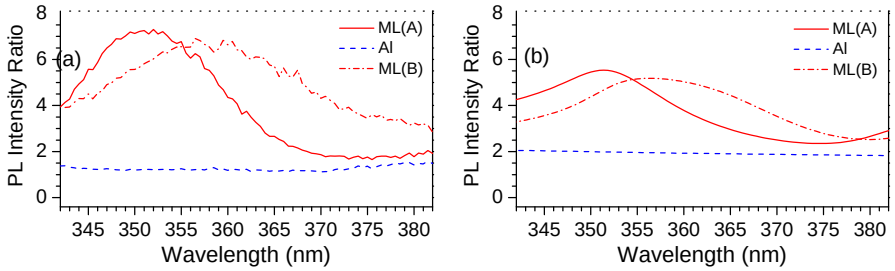

Fig. 2: (a) Ratios between the measured PL spectrum of a reference uncoated sample and those of the three metal-coated samples described in the text. (b) Theoretical PL-intensity ratios for the same three structures.

<u>Plasmon-enhanced light emission using chemically synthesized silver nanoparticles</u>

Recently we have also demonstrated plasmon-enhanced light emission using chemically synthesized single-crystal Ag nanoparticles (NPs) [6], which were fabricated and supplied by Dr. Chumanov's group at Clemson University [7]. These NPs feature strong localized plasmonic resonances at blue/green wavelengths with large scattering cross-sections and minimal absorption losses. To illustrate, a measured extinction spectrum of the NPs used in this work is shown in Fig. 3(a). For ease of assembly with planar epitaxial samples, the NPs are embedded on the surface of flexible and optically transparent films of poly(dimethylsiloxane) (PDMS) [7], which are then simply adhered on top of the light emitting material. A scanning electron microscopy (SEM) image of an array of embedded NPs is shown in Fig. 3(b).

In this work, several QW samples were characterized via PL measurements with a backside pumping and collection geometry. The PL spectra plotted in Fig. 4(a) were measured with an InGaN/GaN QW sample emitting near 480 nm, with no coating (black curve) and with a control PDMS film containing no NPs (blue curve). As shown by these data, application of the control film leads to a decrease in the measured PL intensity, due to the smaller amount of pump light reflected in the QWs by the nitride/PDMS interface versus nitride/air. On the other hand, application of the NP film leads to a strong increase in PL intensity as illustrated in Fig. 4(b). Normalizing to the data of Fig. 4(a) to account for the reduced pump reflection, the emission efficiency is found to be enhanced by a factor of about 4.2.

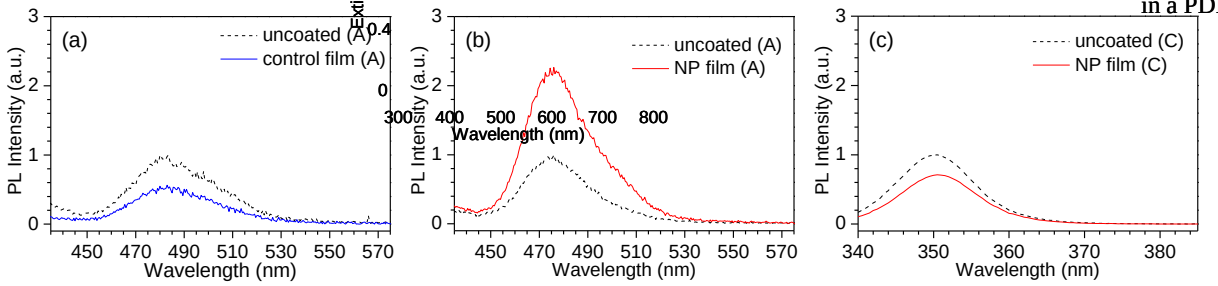

Fig. 4: Exemplary PL spectra from various combinations of coated and uncoated samples.

The same experiment was also carried out with GaN/AlGaN QW samples emitting near 350 nm, i.e., well outside of the NP plasmonic resonance of Fig. 3(a). As shown in Fig. 4(c), in this case the NP film produces a decrease in PL intensity by roughly the same amount observed with the control film, which confirms the plasmonic origin of the enhancement of Fig. 4(b).

Tunable plasmonic resonances in two-dimensional silver nanoparticle arrays

Metallic NPs can also be directly fabricated on light emitting substrates using "top-down" techniques such as electron-beam lithography (EBL). Compared to the chemically synthesized NPs of the previous section, lithographically defined nanostructures can offer a higher degree of control and flexibility for device integration. Recently we have fabricated by EBL and characterized a wide range of periodic arrays of Ag NPs [8]. An SEM image of one of these arrays is shown in Fig. 5(a).

In particular, we have investigated the geometrical tunability of the plasmonic resonance of NP arrays of varying NP height. To illustrate, in Fig. 5(b) we plot the measured transmission spectra of six arrays with 130-nm NP diameter, 240-nm pitch, and NP height ranging from 20 to 160 nm. A pronounced dipolar resonance is seen in each spectrum, whose wavelength strongly decreases with increasing height until it saturates at heights comparable to the diameter. Figure 5(c) is a compilation of measured resonance wavelengths versus array pitch for different NP heights and fixed diameter of 130 nm: altogether these arrays cover a broad spectral range, extending to well below 500nm. Furthermore, FDTD simulations indicate that control of the NP height also allows maximizing the NP scattering

efficiency and electromagnetic field enhancement, both of which are key parameters for the envisioned applications.

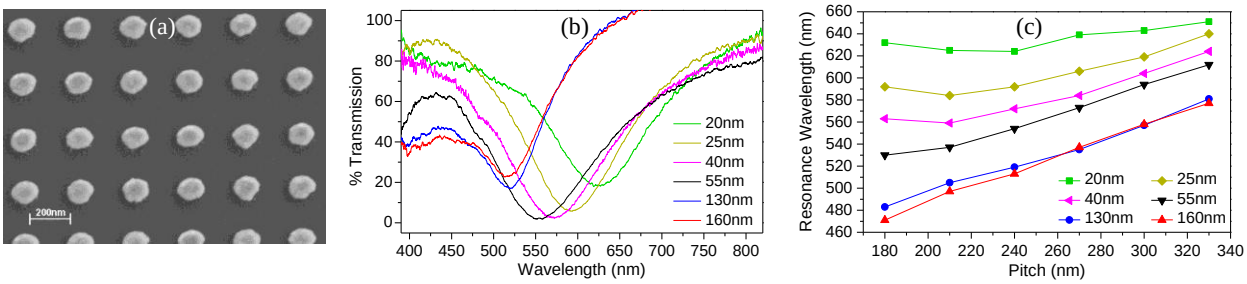

Fig. 5 (a) SEM image of a fabricated array. (b) Transmission spectra of Ag NP arrays of fixed pitch and diameter and varying heights (indicated in the legend). (c) Plasmonic resonance wavelengths of arrays of varying NP height and pitch.

3. Future Plans

In the immediate future we plan to demonstrate plasmon-enhanced light emission from green/blue emitting InGaN QW samples using the NP arrays just described. More complex geometries will then be developed and investigated, including nanohole arrays and coupled thin-film/NP-array systems, designed to optimize the tradeoff between efficient SPP scattering, tunability of the plasmonic resonance, and uniform area coverage. The same nanostructures will also be designed to simultaneously control the properties of the radiated optical beams, such as their degree of collimation, direction of propagation, and polarization state. In addition, we will demonstrate a higher level of integration where metallic nanostructures are introduced inside (as opposed to on top of) the epitaxial material, which will facilitate the use of the proposed plasmonic effects in more realistic device geometries.

4. References

[1] W. L. Barnes, J. Mod. Opt. **45**, 661 (1998).

[2] K. Okamoto, I. Niki, A. Shvartser, Y. Narukawa, T. Mukai, and A. Scherer, Nature Materials **3**, 601 (2004).

[3] R. Paiella, Appl. Phys. Lett. **87**, 111104 (2005).

[4] J. Henson, A. Bhattacharyya, T. D. Moustakas, and R. Paiella, J. Opt. Soc. Am. B **25**, 1328 (2008).

[5] I. Gontijo, M. Boroditsky, E. Yablonovitch, S. Keller, U. K. Mishra, and S. P. DenBaars, Phys. Rev. B **60**, 11564 (1999).

[6] J. Henson, J. C. Heckel, E. Dimakis, J. Abell, A. Bhattacharyya, G. Chumanov, T. D. Moustakas, and R. Paiella, Appl. Phys. Lett., accepted with minor revisions (2009).

[7] D. D. Evanoff Jr. and G. Chumanov, Chem. Phys. Chem. **6**, 1221 (2005).

[8] J. Henson, J. DiMaria, and R. Paiella, J. Appl. Phys., accepted with minor revisions (2009).

5. Publications related to this project over the last two years

J. Henson, A. Bhattacharyya, T. D. Moustakas, and R. Paiella, "Controlling the recombination rate of semiconductor active layers via coupling to dispersion-engineered surface plasmons," J. Opt. Soc. Am. B **25**, 1328 (2008).

J. Henson, J. DiMaria, and R. Paiella, "Influence of nanoparticle height on plasmonic resonance wavelength and electromagnetic field enhancement in two-dimensional arrays," J. Appl. Phys., accepted with minor revisions (2009).

J. Henson, J. C. Heckel, E. Dimakis, J. Abell, A. Bhattacharyya, G. Chumanov, T. D. Moustakas, and R. Paiella, "Plasmon-enhanced light emission from InGaN quantum wells via coupling to chemically synthesized silver nanoparticles," Appl. Phys. Lett., accepted with minor revisions (2009).

Session IVa

Thin Films: Synthesis of Thin Film Interfaces

Session Chair: Ian Fisher, SLAC National Accelerator Laboratory

(This page intentionally left blank.)

Molecular beam epitaxy and nano-structuring of perovskite oxide materials toward an understanding of strongly correlated systems

I. Bozovic, G. Logvenov, V. Butko, A. Gozar, A. Bollinger, O. Pelleg
bozovic@bnl.gov

Department of Condensed Matter Physics and Materials Science, Brookhaven National Laboratory, Upton NY 11973

Program Scope

The mechanism of high-temperature superconductivity (HTS) is one of the most important open problems in Condensed Matter Physics. Some of the most basic questions - what is the role of dimensionality in the HTS phenomenon, what are the spin and the charge of free carriers, what is the nature of superconducting transition, and what is the 'glue' (boson excitations) responsible for electron pairing - are still unresolved.

We use a unique molecular beam epitaxy (MBE) system (Figs. 1 and 2) for atomic-layer ('digital') synthesis of complex oxidex to fabricate single-crystal films of cuprates, nickelates, bismuthates, etc., as well as multilayers and superlattices with atomically perfect interfaces. We manufacture SIN, SIS, and SNS junctions, HTS nanowires, nanorings and nanodots, and perform on them experiments that were not previously possible and provide conclusive answers to at least some of the above questions. We have demonstrated that HTS and antiferromagnetic states phase-separate on an atomic scale, proven the Giant Proximity Effect, and discovered colossal photo-induced expansion[18] and high-T_c interface superconductivity[9]. Now we are addressing the role of dimensionality in the HTS phenomenon, the spin and the charge of free carriers, the nature of superconducting transition, and the source of the pairing 'glue'. We are also trying to synthesize new superconductors by leveraging on atomic-layer engineering, epitaxial strain and stabilization, and proximity effects including interface superconductivity.

Recent Progress

Electron-lattice coupling in cuprates. Ultrafast electron diffraction experiments (Fig. 3a) on MBE-grown $La_2CuO_{4+\delta}$ films revealed colossal photo-induced lattice expansion[18]. At the highest fluence used, the intermittent increase in *c*-axis lattice constant reaches 2.5% (Fig. 3b) - more than the thermal expansion upon heating from 4.2 K to the melting point. This implies very strong coupling of charge-transfer excitations to the lattice, and specifically to c-axis longitudinal acoustic phonons. According to numerical simulations, the coupling is also strong to out-of-plane optic vibrations[12]. Tunneling spectroscopy of SIS-type LSCO bicrystal junctions indeed showed that most of the phonon DOS features are strongly coupled to the superconducting gap[10].

Interface superconductivity. In bilayer films built from insulating (I = La_2CuO_4) and metallic (M = $La_{1.55}Sr_{0.45}CuO_4$) blocks, neither of which is superconducting per se, we have discovered[9] interface superconductivity, see Fig. 4. After annealing such *M-I* bilayers in ozone, we see $T_c > 50$ K - a large (25%) enhancement compared to single-phase films gown under the same conditions[9].

We have characterized these interfaces in detail using a suite of state-of-the art techniques. The chemical composition profile was determined using ion scattering spectroscopy (TOF-ISARS) and electron energy loss spectroscopy in scanning transmission electron microscopy, EELS-STEM[9]. The crystallographic structure was profiled by using synchrotron x-ray diffraction and coherent Bragg rod analysis (COBRA), a phase-retrieval technique that provides accurate positions of atoms within the unit cell in ultrathin films (H. Zhou *et al.,* arxiv. 0903.2097). The hole density profile in LSCO : LCO superlattices has been determined from soft resonant x-ray scattering (SRXRS)[2].

The greatest challenge was to profile the superconducting properties with atomic resolution; the standard techniques are limited by much larger length scales such as the penetration depth or the coherence length. We have

accomplished this by using a new method that we call "δ-doping tomography" (Fig. 5). In cuprates, replacing a small amount of Cu by Zn suppresses superconductivity very efficiently: e.g., 3% Zn doping in $La_{1.85}Sr_{0.15}CuO_4$ reduces T_c by about a factor of 2. We have synthesized and studied a series of samples in which we varied systematically - in increments of 0.5 unit cells - the position of CuO_2 layer δ-doped by 3% Zn. By studying the transport properties in such a set of samples, we were able to prove that interface HTS with $T_c = 32 \pm 4$ K occurs within a single CuO_2 plane[1], and to pinpoint its location (the second CuO_2 layer after the nominal interface, see Fig. 6). The mutual inductance measurements show the same N-dependence - both T_c and the magnitude of superconducting screening of the magnetic field are dramatically reduced only in the N = 2 samples[1].

Future Plans

Interface superconductivity. We will attempt to understand the origins of interface superconductivity and of T_c enhancement, and search for signatures of enhanced fluctuations and Kosterlitz-Thouless physics (formation of vortex-antivortex plasma) in ultrathin interfacial HTS layers.

Quantum critical points (QCPs) in overdoped cuprates. The MBE system at BNL was designed to enable synthesis of large libraries of compounds with systematic and position-addressable variation in composition. We will fabricate combinatorial libraries of HTS films and utilize them to study the doping dependence of both the normal state and the superconducting state properties (the carrier density, T_c, the penetration depth, etc.) with an unprecedented density and resolution in the doping level (down to $\Delta x < 0.0005$), looking for signs of QCPs.

Planar SIS junctions. Traditionally, the study of SIS tunneling characteristics had enabled, through the so-called McMillan-Rowell inversion procedure, extraction of the Eliashberg $\alpha^2F(\omega)$ function that contains information about the density of states of boson excitations responsible for electron pairing. We will experiment with a number of insulating materials ($LaAlO_3$, $LaSrAlO_4$, HfO_x, etc.) and fabricate SIN and/or SIS junctions with HTS electrodes, measure the I(V) characteristics, perform the tunneling spectroscopy of the SC gap, and try to extract the $\alpha^2F(\omega)$ function. In parallel, in collaboration with R. Ashoori at MIT, we will pursue Time-Domain Capacitance Spectroscopy (TDCS) of both the superconducting gap and pseudogap; this unique technique essentially eliminates junction heating and has a very high energy resolution.

Giant Proximity Effect (GPE). We have proven that GPE, arguably the first really unconventional property of the superconducting state in the cuprates, is real and intrinsic to HTS. In collaboration with E. Morenzoni and A. Suter (PSI Zurich, Switzerland) we will use low-energy μSR to verify that GPE indeed induces *bulk* superconductivity in the barrier layer, and study the doping dependence of GPE to determine in which part of the phase diagram it occurs.

HTS nano-structures. We will investigate systematically the effects of reduced dimensionality and confined geometries on HTS by synthesizing atomically smooth films of LSCO, BSCCO, or DBCO, lithographically fabricating nano-wires, nano-rings, nano-dots, etc., and studying their transport properties. By measuring $R(T)$, $\chi(T)$, $R_H(T)$, $j_c(T)$, etc., in trilayers and superlattices that contain just a single HTS CuO_2 plane, we can check what is the role (if any) of interlayer interactions in the mechanism of HTS. Using few unit cells thick HTS films, we can fabricate HTS nanowires with the cross-section down to ~10 nm^2 and test the role of hypothetical dynamic charge stripes. By studying magneto-transport, the Bohm-Aharonov effect, and Little-Parks oscillations in HTS nanorings, we will try to determine whether pairing indeed occurs at T_c or well above it as postulated in some theories of HTS. An independent check will be provided by studying the Coulomb-blockade steps, as a function of temperature and doping, in HTS nanodots and in single-Cooper-pair transistor devices.

Engineering new artificial superconductors. Trying to leverage on our discovery of interface HTS, we will synthesize a series of superlattices based on *M-I* and *M-S'* blocks. For *M* layers, we will primarily utilize $La_{1.55}Sr_{0.45}CuO_4$, but will also experiment with non-cuprate metals such as $La_{2-x}Sr_xNiO_4$, $La_{2-x}Sr_xCoO_4$, and $La_{2-x}Sr_xMnO_4$. For *I* blocks we will use La_2CuO_4, but will also experiment with $La_2CaCu_2O_6$, $La_2Ca_2Cu_3O_8$, and infinite layers compounds such as $CaCuO_2$, $SrCuO_2$, and $Ca_xSr_{1-x}CuO_2$. The idea is to provide free carriers into *I* layer by charge transfer and without chemical disorder, thus achieving a higher T_c.

DOE Sponsored Publications in 2007-2009 from Current Grant

1. G. Logvenov, A. Gozar and I. Bozovic, "High-temperature superconductivity in a single copper-oxygen plane", ***Science*** (2009) in press.
2. S. Smadici, J. C. T. Lee, S. Wang, P. Abbamonte, A. Gozar, G. Logvenov, C. Deville Cavellin and I. Bozovic, "Superconducting Transition at 38 K in Insulating-Overdoped La_2CuO_4-$La_{1.64}Sr_{0.36}CuO_4$ Superlattices: Evidence for Interface Electronic Redistribution from Resonant Soft X-Ray Scattering", ***Phys. Rev. Letters*** 102, 107004 (2009).
3. V. Butko, G. Logvenov, N. Bozovic, Z. Radovic and I. Bozovic, "Madelung Strain in Cuprate Superconductors – A Route to Enhancement of the Critical Temperature", ***Advanced Materials*** 21, 1-5 (2009).
4. S. V. Dordevic, L. W. Kohlman, L. C. Tung, Y.-J. Wang, A. Gozar, G. Logvenov and I. Bozovic, "Absence of magnetic field induced effects in the mid-infrared transmission of $La_{2-x}Sr_xCuO_4$ thin films", ***Phys. Rev. B*** 79, 134503 (2009).
5. I. Bozovic, A. Gozar, G. Logvenov, A. Bollinger, N. Bozovic and Zoran Radovic, "Insights in high-temperature superconductivity from the study of films and heterostructures synthesized by molecular beam epitaxy", *Journal of Superconductivity* 22, 223-7 (2009).
6. G. Logvenov, A. Gozar, V. Y. Butko, A. T. Bollinger, N. Bozovic, Z. Radovic and I. Bozovic, "Comprehensive study of high-T_c interface superconductivity", *J. Chem. Phys. Solids* (2009) in press.
7. J. A. Clayhold, O. Pelleg, A. T. Bollinger, G. Logvenov, B. M. Kerns, M. D. Schroer, D. W. Rench and I. Bozovic, "Statistical Characterization and Process Control for Improved Growth of $La_{2-x}Sr_xCuO_4$ Films", *Journal of Superconductivity (2009)* in press.
8. I. Božović, G. Logvenov, A. Gozar, A. Bollinger and O. Pelleg, Z. Radović and N. Božović, "Nano-structured films of cuprate superconductors and other complex oxides: MBE synthesis, characterization, and engineered properties", (Invited Keynote paper) *Proc. ICCE-17*, ed. by D. Hui, 2009.
9. A. Gozar, G. Logvenov, L. Fitting Kourkoutis, A. T. Bollinger, L. A. Giannuzzi, D. A. Muller, and I. Bozovic, "Interface superconductivity between a metal and a Mott insulator", ***Nature*** 455, 782-5 (2008). [Highlighted in The APS News in Physics, Physics World, Scientific American, MRS Bulletin, Superconductor Week, Washington Post, Reuters, and several hundred web sites in US, United Kingdom, Germany, Italy, Serbia, Russia, Turkey, Hungary, India, China, Vietnam, Malaysia, Saudi Arabia, etc.; listed as the Most Emailed Science News by Yahoo News and as the #3 on the 2008 top list of the American Ceramic Society.]
10. H. Shim, P. Chaudhari, G. Logvenov and I Bozovic, "Quasiparticle tunneling across a $La_{1.84}Sr_{0.16}CuO_4$ superconductor grain boundary junction", ***Phys. Rev. Letters*** 101, 247004 (2008).
11. N. Bozovic, I. Bozovic, and J. Misewich, "X-ray Nanocrystallography of Individual Carbon Nanotubes", ***Nano Letters*** 8, 4477–4482 (2008). [Highlighted by A. Sandhu, Nature Nanotechnology, doi:10.1038/nnano.2008.347, published online 7 November 2008.]
12. Z. Radovic, N. Bozovic and I. Bozovic, "Photoinduced expansion in cuprate superconductors: Evidence of strong electron-lattice coupling", ***Phys. Rev. B*** 77, 092508 (2008).
13. I. Božović, G. Logvenov, V. Butko, A. Gozar, A. Bollinger, O. Pelleg, N. Božović and Z. Radović, "Insights in high-T_c superconductivity from the study of MBE-grown films and heterostructures", *Proc. 3rd International conference "On problems of High Temperature Superconductivity"* ed. by V. Pudalov and I. Mitsin, Zvenigorod, Russia (2008).
14. G. Logvenov and I. Bozovic, "Artificial superlattices grown by MBE: can we design novel superconductors?", *Physica C* 468, 100–104 (2008).
15. J. A. Clayhold, B. M. Kerns, M. D. Schroer, D. W. Rench, I. Bozovic, A. T. Bollinger and G. Logvenov, "Combinatorial measurements of Hall effect and resistivity in oxide films", *Rev. Scient. Instr.* 79, 033908 (2008).
16. I. Bozovic, "Experiments with atomically smooth thin films of cuprate superconductors: strong electron-phonon coupling and other surprises", *Russian Physics Uspekhi* 178, 179-190 (2008).
17. G. Logvenov, V. Butko, C. Deville-Cavellin, J. Seo, A. Gozar, and I. Bozovic, "Engineering Interfaces in Cuprate Superconductors", *Physica B* 403, 1149–1150 (2008).
18. N. Gedik, D.-S. Yang, G. Logvenov, I. Bozovic and A. Zewail, "Non-equilibrium Phase Transitions in Cuprates Observed by Ultrafast Electron Crystallography." ***Science*** 316, 425 (2007).
19. A. Gozar, G. Logvenov, V. Butko and I. Bozovic, "Surface structure analysis of atomically smooth BaBiO", ***Phys. Rev. B*** 75, 201402 (2007).
20. J. Demsar, A. Gozar, V. K. Thorsmølle, A. J. Taylor and I. Bozovic, "Long-lived near-infrared photoinduced absorption in LaSrAlO$_4$ excited with visible light", ***Phys. Rev. B*** 76, 054304 (2007).
21. J. He, R. F. Klie, G. Logvenov, I. Bozovic and Y. Zhu, "Microstructure and possible strain relaxation mechanisms of $La_2CuO_{4+\delta}$ thin films grown on $LaSrAlO_4$ and $SrTiO_3$ substrates", Journal of Applied Physics 101, 073906 (2007).
22. G. Logvenov, I. Sveklo, and I. Bozovic, "Combinatorial Molecular Beam Epitaxy of $La_{2-x}Sr_xCuO_{4+d}$", Physica C 460, 416 -419 (2007)
23. I. Božović, G. Logvenov, A. Gozar, A. Bollinger, V. Butko, N. Božović and Z. Radović, "MBE synthesis of nano-structured films of cuprate superconductors and related oxides", *Proc. ICCE-15* ed. by D. Hui, 2007.
24. I. Bozovic, "Possible Jahn-Teller effect and strong electron-phonon coupling in beryllium hydride", in In High T_c Superconductors and Related Transition Metal Oxides, A. Bussmann-Holder, H. Keller, Eds., (Springer Verlag, 2007).

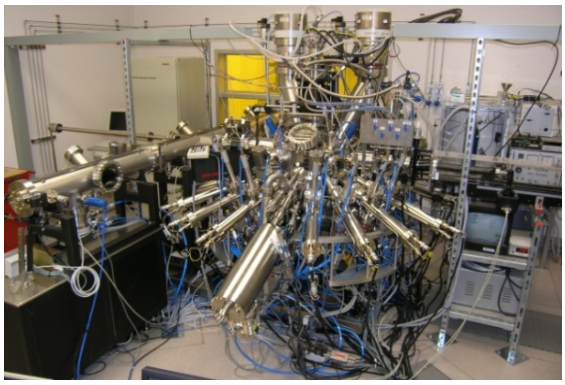

Fig. 1: The oxide molecular beam epitaxy system at BNL: the growth chamber

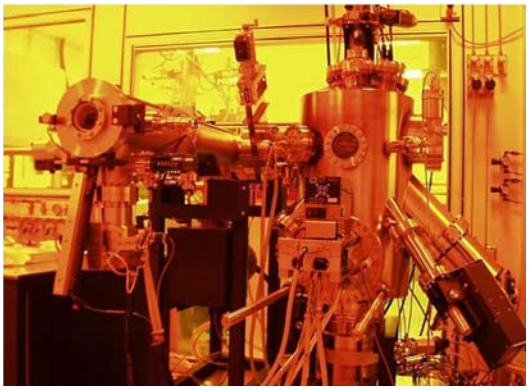

Fig. 2: The oxide molecular beam epitaxy system at BNL: the processing chamber

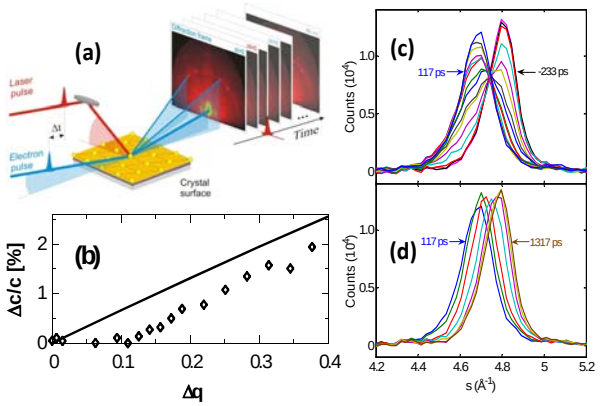

Fig. 3: (a) A movie of RHEED patterns taken at different delay times after photo-excitation. (b) The relative expansion of *c*-axis lattice constant as a function of the laser fluence, experiment (open squares) vs numerical simulations (solid line). (c) The time evolution of initial lattice expansion. (d) Subsequent lattice relaxation. [After Ref. 18.]

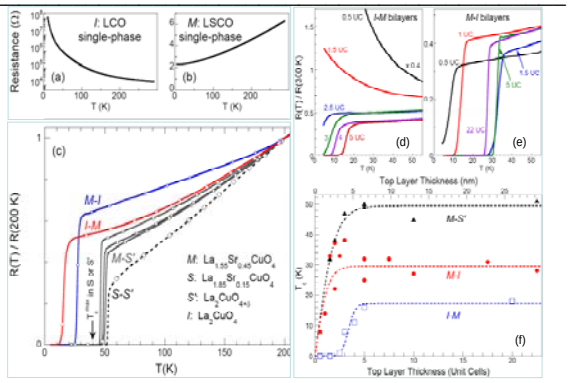

Fig. 4: (a) and (b): R(T) for single-phase *I* and *M* films, respectively. (c): R(T) normalized to T = 200 K for various bilayers. (d) Normalized resistance for several *I*-*M* bilayers where the thickness of the bottom *I* layer is fixed at 40 unit cells (UC) while the thickness of *M* layer is varied as indicated. (e) The same for *M*-*I* bilayers where the thickness of the top *I* layer is varied. (f) T_c as a function of the top layer thickness in *M*-*I*, *I*-*M* and *M*-*S*′ bilayers. [After Ref. 9.]

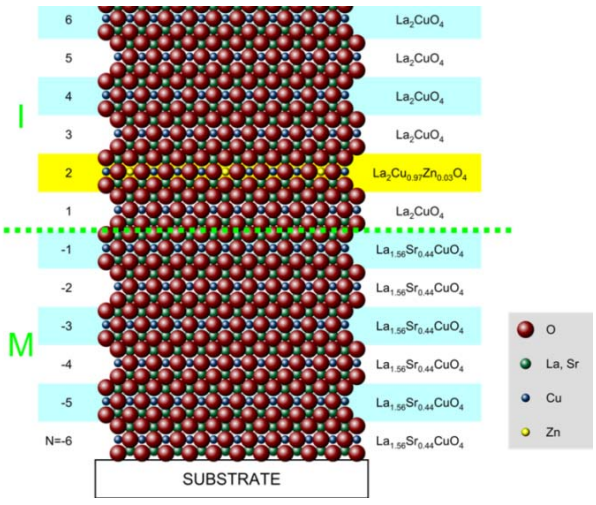

Fig. 5: Delta-doping tomography: a series of M-I bilayer samples that are identical except for replacing 3% of Cu by Zn in one CuO_2 layer, the position of which is changed systematically from N = -6 to N = 6.

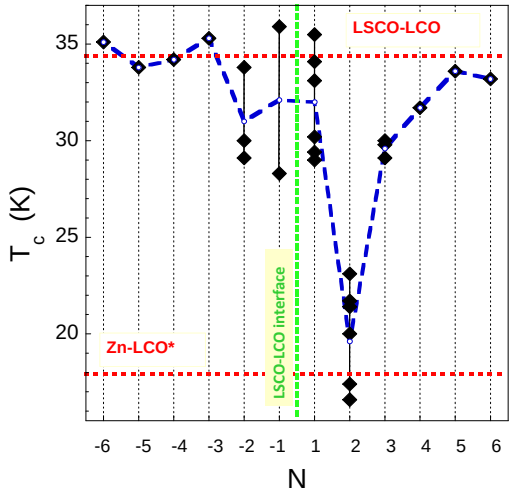

Fig. 6: Delta-doping tomography shows that HTS with $T_c = 32 \pm 4$ K is located in a single CuO_2 plane, the second after the LSCO-LCO interface – the only one that is affected by Zn doping. [After Ref. 1.]

Digital Synthesis: A Pathway to New Materials at Interfaces of Complex Oxides

Anand Bhattacharya
anand@anl.gov
Materials Science Division & Center for Nanoscale Materials
Argonne National Laboratory, Argonne, IL 60439

(i) Program Scope

The complex oxides host many fascinating and diverse collective states of condensed matter, with spin, charge and lattice degrees of freedom all playing their part. In our program, we seek to create, characterize, understand and manipulate novel states of condensed matter at interfaces of complex oxides using digital synthesis. Digital synthesis is a technique where ordered, undoped layers are stacked in integer sequences, and all charge transfer or doping takes place at atomically sharp interfaces, without the disorder that is associated with the usual chemical doping strategies. The richness of observed phenomena in the complex oxides, which have also presented some of the greatest challenges to our understanding, are due to the strongly interacting degrees of freedom in the materials. Surfaces and interfaces between complex oxides provide a unique environment for these degrees of freedom to 'reconstruct' and create new systems with properties that are qualitatively different from their bulk constituents. In this sense, they provide a pathway for discovering new materials.

Creating and understanding these interfacial states defines our program. More specifically, we seek to discover and explore novel states of condensed matter with attributes such as tunability of collective states with an external electric field, multiferroic superlattices, superconductivity at interfaces between materials that may not be superconducting themselves, long-range proximity effects, half-metallic, spin-polarized electron gases, and interfacial ferromagnetism between non-ferromagnetic constituents. We seek to explore properties of materials that are known to have interesting phases, such as the manganites and cuprates, where the effects of disorder have been engineered away by digital synthesis. We create these materials systems using state-of-the-art, ozone-assisted oxide Molecular Beam Epitaxy (MBE) at the Center for Nanoscale Materials (CNM) at Argonne, and at the University of Illinois at Urbana Champaign, and characterize them using the major DOE facilities for neutron and photon scattering, and at the new DOE Nanoscale Science Research Centers.

(ii) Recent Progress

(a) Enhanced Néel Temperatures in $(LaMnO_3)_m/(SrMnO_3)_{2m}$: We find striking evidence for enhanced ordering temperatures in ordered analogs of $La_{1/3}Sr_{2/3}MnO_3$. This material is known to be an AF insulator with A-type i.e. FM in plane, AF out of plane phase in composition in bulk single crystals, with a Néel temperature T_N near 240 K. In the superlattices, we found a sharp downturn in the resistivity at 320 K for m =1, at a temperature that progressively lowered with increasing m. Via neutron diffraction measurements (carried out with J.L. Zerestky and J. L. Robertson at HFIR, Oak Ridge), we found evidence for A-type AF order in superlattices of $(LaMnO_3)_m/(SrMnO_3)_{2m}$ for m = 1 and 2 (Fig. 1) whose Néel temperature T_N correlates with that for the downturn. Randomly alloyed films of the same composition show a T_N that is close to that for bulk samples. This implies that orbital occupancy and the resultant A-type AF order is

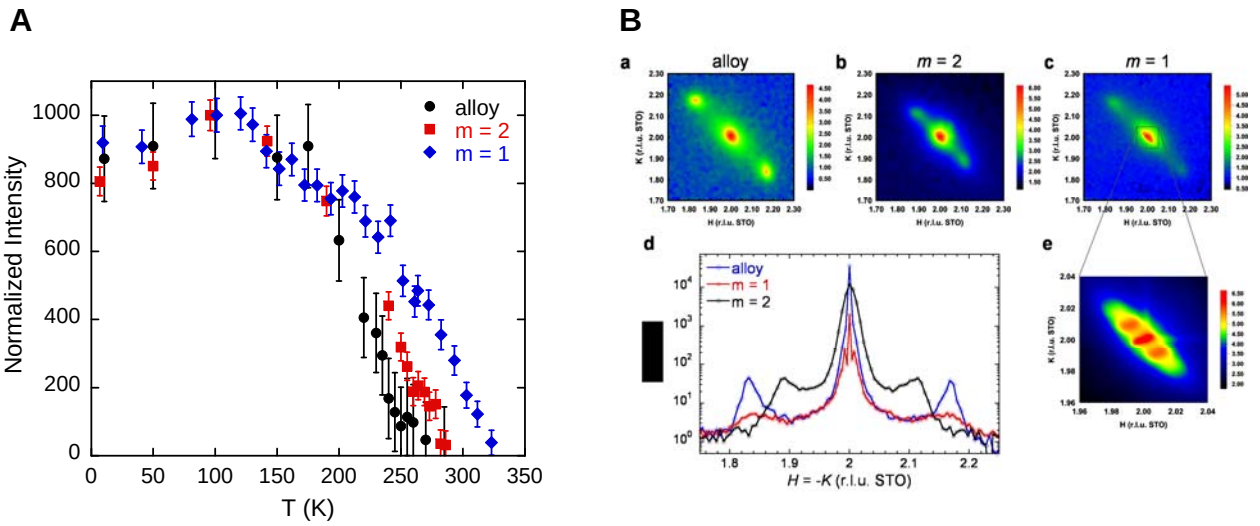

Fig. 1. A. The A-type AF order parameter as a function of temperature for $(LaMnO_3)_m/(SrMnO_3)_{2m}$ superlattices with m=1,2 and an equivalent random alloy with composition $La_{1/3}Sr_{2/3}MnO_3$, as determined by neutron scattering **B**. The corresponding evolution of the in-plane distortion as measured by grazing incidence x-ray scattering.

promoted by having superlattices where the (La/Sr) cations are ordered in digital layers, and the T_N is enhanced by more than 70 K. The exact mechanism for this enhancement is unknown at the time, though a very strong clue is provided by studies of in-plane x-ray diffraction from the ordered and disordered films. These measurements were carried out with our collaborators (Drs. P. J. Ryan, J.-W. Kim and E. Karapetrova) at the Advanced Photon Source, Argonne. For scattering along the $[110]$ direction, we find an in-plane periodic structure with a wavevector along $[1\bar{1}0]$, transverse to the scattering vector. In the random alloy, the period of this displacement (1.63 nm) is ~ 3 u.c. diagonals along $[1\bar{1}0]$. This period is increased to ~ 4.5 u.c. (2.5 nm) in the m = 2 superlattice, and is strongly suppressed in the m = 1 superlattice. Along with the suppression of the short-range periodicity, a longer period ordering (~58 u.c.) emerges along the same directions in the m = 1 superlattice. The m = 2 superlattice, which exhibits an intermediate T_N, has coexisting short-period (~ 4.5 u.c.) and long-period modulations. All periodicities measured in the alloy and superlattices are temperature independent within the range of our measurements (at 150, 300 and 350 K), are purely structural in nature, and not affected by magnetic ordering. A possible explanation for the observed in-plane structural modulation and its correlation with T_N involve cooperative tilts of the MnO_6 octahedra. If the 'wavelength' of the tilts are long, the angle of tilt between neighboring octahedra are relatively smaller, this would give rise to higher in-plane itinerancy and consequently a higher in-plane magnetic ordering temperature via double-exchange. In this scenario, the out-of-plane antiferromagnetic coupling strength is assumed to be higher than the observed T_N, which is limited by the in-plane ferromagnetic ordering (Pub. 1).

(b) The metal-insulator transition and magnetic structure of $(LaMnO_3)_{2n}/(SrMnO_3)_n$ superlattices: A metal-insulator transition is observed in $(LaMnO_3)_{2n}/(SrMnO_3)_n$ superlattices for $n\geq3$. Using measurements of the average magnetization and polarized neutron reflectometry, we established that a strongly modulated ferromagnetic order occurred in the insulating state, while a uniform magnetization is obtained in the metallic state. This provides direct evidence for a Mott metal-insulator transition driven by the distance between LMO/SMO interfaces. We

showed that the interfacial regions had states in the vicinity of the Fermi energy, but that they were localized by disorder. Intrinsic magnetic disorder arising out of frustration at interfaces between ferromagnetic and AF regions was shown to play a role in localizing the charge carriers. A key finding in the course of these studies (Fig. 2) was that a chemically smooth LMO/SMO

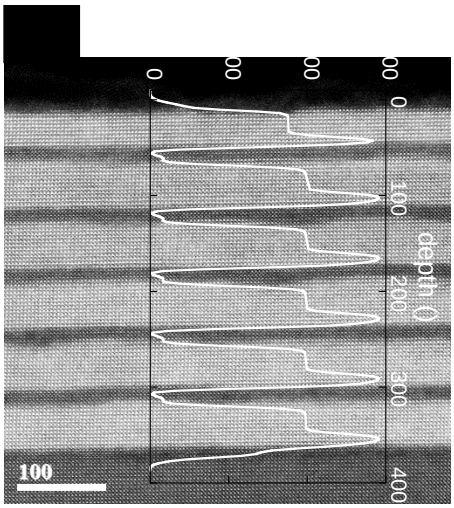

Fig. 2. Magnetization depth profile extracted from polarized neutron reflectometry. The magnetization is strongly suppressed in $SrMnO_3$, and large in $LaMnO_3$ (brighter in the Z-contrast image taken with a Scanning Transmission Electron Microscope, J.-M. Zuo's group at UIUC). The asymmetry in the magnetization profile may be correlated with interfacial roughness. The interface going from SMO to LMO is smooth, while that from LMO to SMO is rough. This may be due to differences in surface energy and wetting.

interface promoted magnetic order near the interface, whereas an interface with roughness on the scale of two unit cells was sufficient to disrupt the interfacial magnetic order (Pub. 4,5).

(c) The observation of a metal-insulator transition in $(LaNiO_3)_n/(SrMnO_3)_2$ superlattices: A metal insulator transition was discovered in $(LaNiO_3)_n/(SrMnO_3)_2$ superlattices, where a metallic state was obtained for $n \geq 4$. The transition showed an evolution from a metal to a variable-range hopping conductor to a gapped insulator as *n* was decreased (Pub. 3). These materials are interesting because of predictions of superconductivity in similar strained superlattices that incorporate thin nickelate layers between insulators (Ref. 1). We are currently investigating these systems to understand the role of interfacial charge transfer between $SrMnO_3$ and $LaNiO_3$.

(iii) Future Plans

Our research program will continue to address a number of broad goals that were outlined in section about the scope of our program, allowing the realization and exploration of novel properties at interfaces of complex oxides. At Argonne, our work is evolving naturally at this time to include materials such as cobaltates and titanates, and manganites with A-site cations such as Ca and Bi. We also plan to explore cuprates and vanadates. We are planning to compete for equipment funds at the Materials Science Division (MSD) to build an MBE system that will enable us to synthesize a range of complex oxides that incorporate relatively volatile constituents such as Pb and K and will be complementary to our existing oxide-MBE capabilities at the Center for Nanoscale Materials. This system will be designed specifically for rapid turnaround between different materials and will be used to carry out exploratory synthesis on a number of systems of interest. At Urbana, the synthesis program is exploring short period superlattices of t_{2g} transition metal perovskites. In an ongoing project with the Eckstein group, we are developing a state-of-the-art atomic absorption spectroscopy system (AAS) that will allow us to improve the degree of real-time flux control for a range of elements, and we anticipate that this will significantly improve the quality of our samples. We have developed a number of strong connections with researchers at various major DOE facilities for neutron and photon scattering

that will enable us to carry out very sophisticated probes of the collective states that are realized at interfaces (see Pub. 1,2,4,5,7).

(iv) References

1. "Orbital Order and Possible Superconductivity in LaNiO3/LaMO3 Superlattices", Jiří Chaloupka and Giniyat Khaliullin, *Phys. Rev. Lett.* **100**, 016404 (2008).

(v) Publications resulting from work supported by DOE BES from 2007-2009:

1. "Enhanced ordering temperatures in antiferromagnetic manganite superlattices", S. J. May, P. J. Ryan, J. L. Robertson, J.-W. Kim, T. S. Santos, S. G. E. te Velthuis, E. Karapetrova, J. L. Zarestky, J. N. Eckstein, S. D. Bader, and A. Bhattacharya, *manuscript accepted* for publication in *Nature Materials* (2009).

2. "Tuning between the metallic antiferromagnetic and ferromagnetic phases of $La_{1-x}Sr_xMnO_3$ near x=0.5 by digital synthesis", T. S. Santos, S. J. May, J. L. Robertson and A. Bhattacharya, *manuscript accepted* for publication in *Phys. Rev*. B (2009).

3. "Onset of metallic behavior in strained $(LaNiO_3)_n/(SrMnO_3)_2$ superlattices", S. J. May, T. S. Santos and A. Bhattacharya, *Phys. Rev.* B **79**, 115127 (2009).

4. "The metal-insulator transition and its relation to magnetic structure in $(LaMnO_3)_{2n}/(SrMnO_3)_n$ superlattices". A. Bhattacharya, S. J. May, S. G. E. te Velthuis, M. Warusawithana, X. Zhai, A. B. Shah, J.-M. Zuo, M. R. Fitzsimmons, S. D. Bader, J. N. Eckstein, *Phys. Rev. Lett.* **100**, 257203 (2008).

5. "Magnetically asymmetric interfaces in a $LaMnO_3/SrMnO_3$ superlattice due to structural asymmetries," S. J. May, A. B. Shah, S. G. E. te Velthuis, M. R. Fitzsimmons, J.-M. Zuo, X. Zhai, J. N. Eckstein, S. D. Bader and A. Bhattacharya, *Phys. Rev.* B **77**, 174409 (2008).

6. "Viscous spin exchange torque on precessional magnetization in $(LaMnO3)_{2n}/(SrMnO3)_n$ superlattices" H. B. Zhao, K. J. Smith, Y. Fan, G. Lüpke, A. Bhattacharya, S. D. Bader, M. Warusawithana, X. Zhai, J. N. Eckstein, *Phys. Rev. Lett.* **100,** 117208 (2008).

7. "Electronic Reconstruction at $SrMnO_3$-$LaMnO_3$ Superlattice Interfaces" Serban Smadici, Peter Abbamonte, Anand Bhattacharya, Xiaofang Zhai,Bin Jiang, Andrivo Rusydi James N. Eckstein, Samuel D. Bader, and Jian-Min Zuo, *Phys. Rev. Lett.* **99**, 196404 (2007).

8. "Signatures of enhanced ordering temperatures in digital superlattices of $(LaMnO_3)_m/(SrMnO_3)_{2m}$", A. Bhattacharya, X. Zhai, M. Warusawithana, J.N. Eckstein, S.D. Bader, *Appl. Phys. Lett.* **90,** 222503 (2007).

How Perfect Should Each Digitally Synthesized Molecular Layer Be?

Xiaofang Zhai, Mao Zheng, Maitri Warusawithana, Brian Mulcahy, and James Eckstein
eckstein@illinois.edu
Department of Physics and Fredrick Seitz Materials Research Laboratory
University of Illinois, Urbana, IL 61801

Program Scope

Constructing new materials by artificially assembling sequences of molecular layers of stable phases in a thin film sample by atomic layer-by-layer molecular beam epitaxy provides a way to obtain new electronic structure that can give rise to new emergent phenomena. This is the core of our program which we are carrying out in close collaboration with Bhattacharya's MBE group at Argonne. To date, the new artificial materials we've studied include superlattices with built-in poling arising from broken inversion symmetry leading to permanently polarized dielectrics [1], materials exhibiting new optical transitions between atomically interlaced adjacent layers [2], and ferromagnetism emerging at the interface between two antiferromagnetic phases [3].

One question which has not received a lot of attention is just how good each molecular layer has to be to make these materials show properties that arise from the layering architecture and not from defects. This point is more difficult for oxide phases such as ABO_3 perovskites, than in semiconductors like GaAs. In GaAs growth, the Ga to As ratio of almost exactly one is naturally achieved by desorption of excess arsenic. This does not happen in the case of the metal atom part of oxide perovskites. Here the metal atom composition, namely the A:B ratio, must be actively controlled with flux monitoring tools and active feedback to achieve a level of precision that provides intrinsic properties in each molecular layer. So the question arises what is the impact of being off composition on properties of layers as well as on their growth dynamics. We have studied this question using manganite phases which have incidentally been part of several of the experiments listed above. In manganites, the A site is an alloy of La and Sr, including as end members phases those containing pure La and pure Sr. The B-site is Mn, and the low energy electronic structure that governs transport and collective electronic phenomena occurs in MnO_3 states. We find that compositional deviations of one part in a thousand are important, even though single phase growth occurs over a very broad range of compositions. This importance comes about for two different reasons. First, the overall growth mode is strongly dependent on A:B. Surprisingly, when A is in excess the growth mode is 2D while when B is in excess

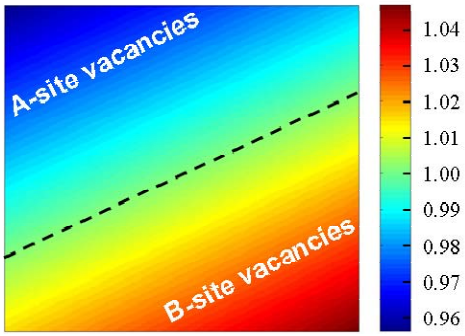

Figure 1. A/B composition ratio appearing over surface of a 14 mm × 14 mm sized wafer.

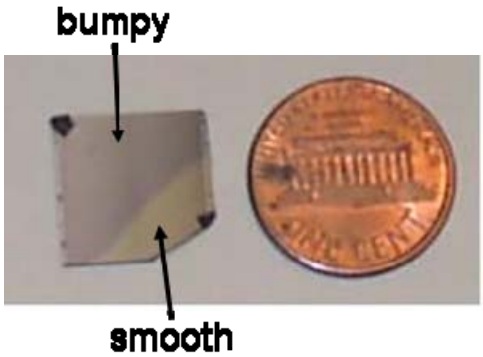

Figure 2. Two different regions are obviously seen visually. The sharp boundary is at [A]/[B] = 1.00. As described below in the text, the morphology of one region is bumpy, while that of the other is atomically smooth.

there is a proliferation of step edges that results after a few layers in the development of rolling hill topography. The size of these hills and their spacing depends on composition in a manner reminiscent of critical scaling in the vicinity of a continuous phase transition, where in this case the compositional deviation is the independent parameter playing the role of temperature. Secondly, an A-site excess results in B-site vacancies. Since the transport occurs through BO bonds, B-site vacancies lead to strong carrier scattering and disrupt transport and the emergence of any collective order dependent on transport.

Recent Progress

Samples grown in our MBE system without rotation have a small systematic composition spread that is mapped directly onto position. This is due to the fact that all of the sources are pointed at the substrate with an angle of 30° relative to the substrate normal. In the case of $LaMnO_3$, the Mn source is incident from the "north north west" while the La source is incident from the "east south east". This causes a flux gradient which in turn results in the composition spread as shown in figure 1 which shows the composition, y=[A]/[B], of the film versus position. Measurements by RBS confirm this quantitatively. This provides a very sensitive way of studying dependence of growth and transport on composition to the level of 1 part in 10^4. One part in 10^4 corresponds to 20 μm displacement perpendicular to the dashed line. Both morphology and transport can be probed at that scale. The impact of this spread is immediately obvious visually as shown in figure 2. The two regions have different color to the naked eye.

What is surprising about this is that the two regions are essentially the same crystal. The lattice spacing in both regions is strictly strained to the $SrTiO_3$ substrate value of 3.905 Å. There is no evidence in either region for lattice relaxation. On the other hand, the reflection high energy diffraction patterns from the two regions are noticeably different. In the SE region the RHEED is very nearly the same as from an annealed $SrTiO_3$ substrate. The specular reflection is sharp indicating a surface with flat areas uninterrupted by steps around 2000 Å in lateral size. RHEED from the NW region is shown in figure 3 and is quite different. It shows several interesting features. The specular reflection is stretched out in the propagation direction substantially. This indicates a much smaller size of flat domains coherently diffracting, about 20 Å in lateral size. In addition there is a periodicity observed in both the <100> and <110> substrate directions that indicates the emergence of a $\sqrt{2}$ x $\sqrt{2}$ surface reconstruction. The transition between these two regimes is sudden in composition and located at the same place that the change in appearance is seen. Furthermore, it can be shifted up or down on the substrate during growth by changing the composition of the layers being grown on top of a given wafer's surface. To move the boundary up, add [La] and to move it down add [Mn], or do just the opposite with the flux of the other metal atom beam. The change in reconstruction is rapidly visible. For example, if the RHEED beam position is located such that it

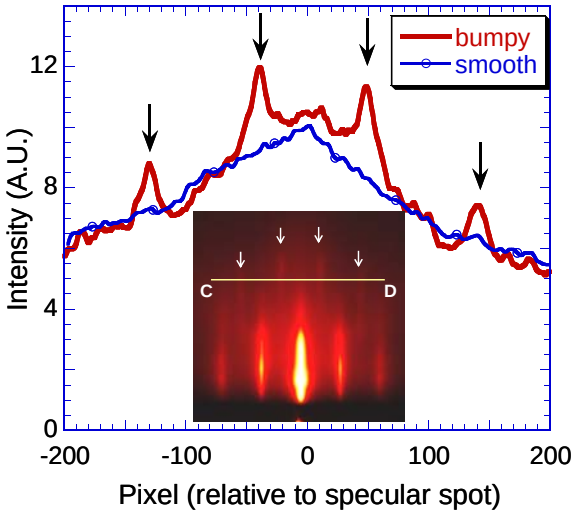

Figure 3. RHEED pattern observed in the bumpy NW region of the films. Notable are the elevated half-order spots seen looking in the STO <100> azimuth. The arrows match in the two figures. In the smooth SE region a sharp specular reflection is seen with no surface reconstruction.

is viewing a flat surface from the smooth region and the composition is adjusted by less than 1% to move to the other side of the compositional transition, the RHEED reconstruction is visible after the first monolayer with this composition is grown.

The reason for the qualitatively different specular reflections in these two regions is readily seen by examining the surface in detail using AFM. A sample of some images taken in the vicinity of the transition region is shown in figure 4. In the SE region the surface is terraced and the terrace density is essentially that of the substrate. This is the minimum terrace density a film can exhibit and it is caused by the miscut of the substrate which is a topological feature of the surface. In the case of these substrates, moving perpendicular to the terrace edge every ~400 unit cells or so a terrace emerges. The best a film can do is to follow this pattern. Beyond the boundary towards the NW direction the surface topography is much more interesting. At the boundary large, separated bumps appear. Moving from the boundary to the NW the bumps become more numerous and smaller in size until they completely fill the surface. The bumps far from the boundary are about 300 Å in lateral size and about 20 to 40 Å high. The bump size scales simply with deviation of composition from 1:1. The graph in figure 4 shows the inverse

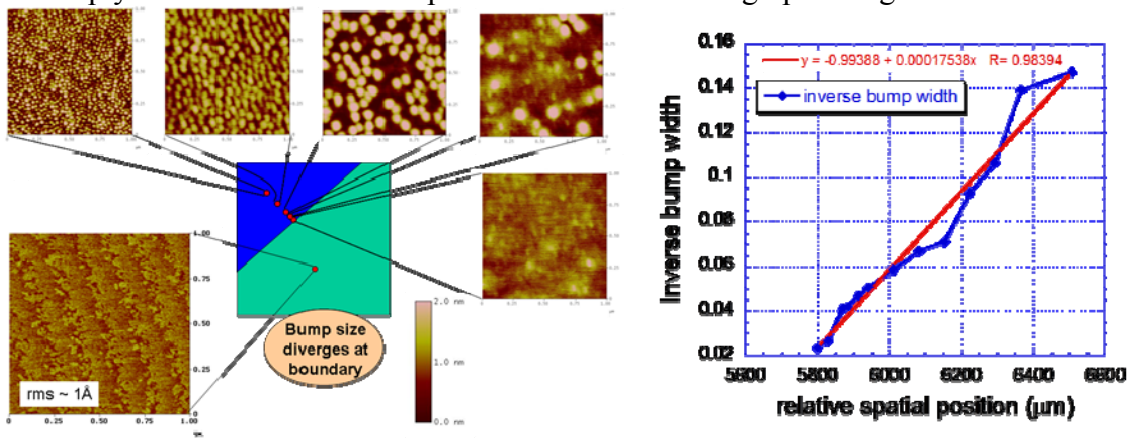

Figure 4. Surface morphology observed across the bumpy to smooth transition. Everywhere on the smooth side the surface is terraced with only the topologically required terrace density. Across the boundary large bumps appear with increasing density and smaller size the deeper into the bumpy side the sample is imaged. The bump size is inversely proportional to the composition difference, [B]- [A] which is similar to mean-field scaling of a susceptibility near a continuous phase transition. This suggests that there is a "phase transition" between two growth modes with critical scaling of the dynamics leading to the formation of the bumps.

bump size versus position on the surface of a sample. Each point represents the analysis of bump size from a 1 µm square region. Evidently, the bump size scales as $1/y-1$. This is similar to how linear susceptibilities near an ordering transition vary with temperature in 3D mean field theories and in fact in many magnetic and ferroelectric systems. In our data, compositional deviation plays the role of temperature. Apparently there is a continuous transition between two different growth modes occurring at the boundary. The sensitivity to composition suggests that only a small fraction of the surface is important. Since growth mainly occurs via step edge attachment, the most likely origin of this sensitivity is step edge composition. The data suggests that step edges terminated with the A-site cation are effective in trapping molecules diffusing on terraces, while B-site terminated steps are not. In the case of B-site terminated steps, terraces would then be populated with more diffusing molecules and there would be more opportunity for

new layers to form in the middle of an existing terrace. This leads to step edge proliferation and eventually mound formation. This is a new growth mode instability.

The composition is also important for transport. To study this, a mask was devised with closely spaced transport links, arranged to span the composition spread. This is shown in the inset to figure 5. Testing these links revealed that the residual resistivity significantly increased with B-site vacancy density but not with A-site vacancy density. This is reasonable since the transport bands are made up from B-site orbitals hybridized with oxygen orbitals. The onset of magnetism as seen in transport was also suppressed.

These two effects place a rather tight bound on acceptable composition control, about 0.1%. Exceeding this in either direction leads to either unstable growth with good transport or flat growth with poor transport. This may also happen for other perovskites, although differences in surface mobility may make the growth mode instability more or less important. Moreover, differences in bonding, π-bonded t_{2g} orbitals vs σ-bonded e_g orbitals may make determine the importance of B-site cations. Manganites may be quite sensitive to both, since surface mobility is high and transport is already fairly good for an oxide. In any case, if it is possible to achieve 0.1% composition control, then it is likely that atomic layered superlattices made up of components with near intrinsic properties will be obtained, thereby making possible a fundamental advance in complex materials engineering.

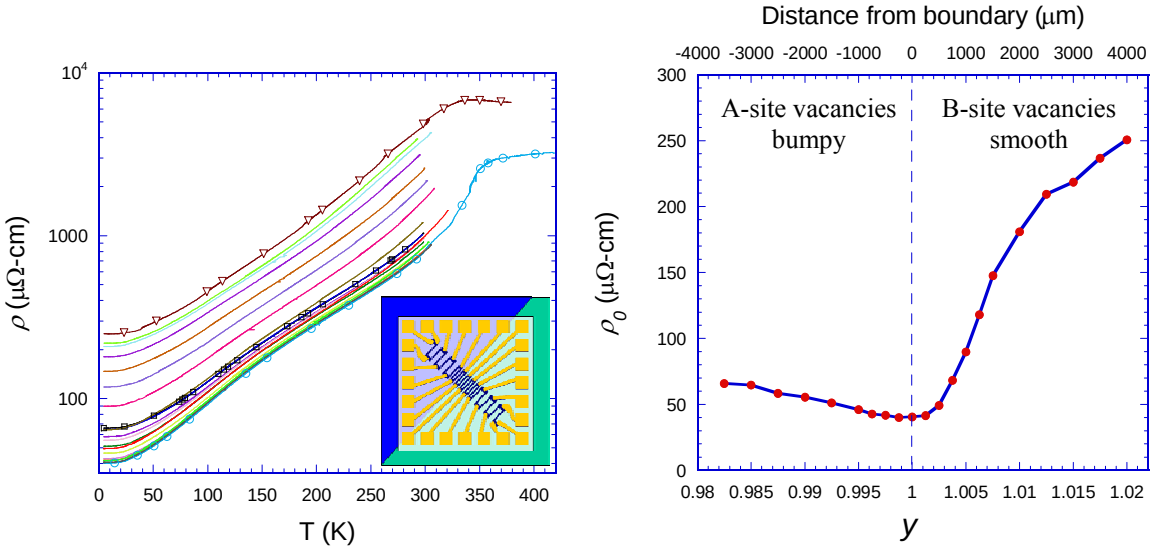

Figure 5. Many transport bars measured across the boundary showing a systematic dependence of resistance and residual resistivity on composition. For parts of the sample with Mn vacancies (smooth) the residual resistivity rises rapidly with increasing vacancy density. The vacancies lead to scattering which increases residual resistance. For the other side (bumpy) the scattering is only weakly dependent on composition. To obtain the best transport, the composition apparently should be controlled to within on part in a thousand.

References:

[1] M.P. Warusawithana, E.V. Colla, J.N. Eckstein, M.B. Weissman, Phys. Rev. Lett. **90**, 036802 (2003)
[2] Xiaofang Zhai and James N. Eckstein, to be published in Advanced Materials
[3] A. Bhattacharya, et. al., Phys Rev Lett **100**, 257203 (2008)

Resistance Switching in Electrodeposited Superlattices in the Magnetite/Zinc Ferrite System

Jay A. Switzer
Department of Chemistry & Materials Research Center
Missouri University of Science and Technology
Rolla, MO 65409-1170
jswitzer@mst.edu

Program Scope

The emphasis of our research is the epitaxial growth of metal oxide semiconductors (such as ZnO) and spintronic materials (such as magnetite and zinc ferrite) at the solid/solution interface using electrodeposition and chemical bath deposition. This year we showed that tilted nanospears of ZnO can be directly deposited onto Si(001) by chemical bath deposition, and that superlattices in the $Fe_3O_4/ZnFe_2O_4$ can be electrodeposited onto Au(111). In addition to the low cost of these deposition methods, we are also interested in the control of composition, orientation, and shape that they provide. For instance, in electrodeposition the composition of metal oxides can be controlled through the applied potential. We exploit this fact to produce superlattices in the magnetite/zinc ferrite system. Superlattices (i.e., periodic layered nanostructures with coherent stacking of atomic planes) are a unique type of nanomaterial, because they combine the nanometer-scale dimensions of the individual layer thicknesses with the utility of large-scale films that can be conveniently connected to the real world. The magnetite-based superlattices exhibit an unusual multistate resistance switching in perpendicular transport measurements that may be applicable to the fabrication of resistive random access memory (RRAM).

Recent Progress

Magnetite, Fe_3O_4, is a half metallic metal oxide with the inverse spinel structure. It exhibits ferrimagnetism below the Curie temperature of 860 K. It is also known to exhibit ferroelectric properties below the Verwey metal-to-insulator phase transition at 120 K. Zinc ferrite, $ZnFe_2O_4$, produced by substituting Fe(II) by diamagnetic Zn(II) ions, has the normal spinel structure, and is antiferromagnetic below the Néel temperature of 10 K. Recently, Lee et al. have shown that nanophase Fe_3O_4 exhibits resistance switching, an effect that may be applicable to resistive random access memory (RRAM).[1] They attribute the resistance switching to an electric field driven insulator-to-metal phase transition below the Verwey temperature due to strong electron-phonon coupling. We previously showed that it was possible to deposit both defect chemistry[2] and compositional[3-5] superlattices in the Tl_2O_3/PbO_2 system. Here, we show that defect chemistry superlattices based on Fe_3O_4 and compositional superlattices in the $Fe_3O_4/ZnFe_2O_4$ system can be electrodeposited as epitaxial films on Au(111) from a single plating bath by simply pulsing the applied potential. Due to the nanometer-scale thickness of the layers in these superlattices, they exhibit a unique and potentially important multistate resistance switching during perpendicular transport measurements that is not observed in bulk material.

In the deposition of superlattices we exploit the fact that Fe_3O_4 deposits by an electrochemical/chemical (EC) mechanism, and that the surface concentrations of Fe(II) and

Fe(III) can be precisely controlled through the applied potential. We prepare the films by electrochemical reduction of an 86 mM Fe(III)-TEA (triethanolamine) complex at 80 ^{o}C in alkaline solution.[6] The deposition is believed to occur by an electrochemical-chemical (EC) mechanism described by Eq. 1 and 2.

$$Fe(TEA)^{3+} + e^{-} \rightarrow Fe^{2+} + TEA \quad (1)$$

$$Fe^{2+} + 2Fe(TEA)^{3+} + 8OH^{-} \rightarrow Fe_3O_4 + 2TEA + 4H_2O \quad (2)$$

Because of the EC nature of the deposition reaction, it is possible to control the composition of the film through the applied potential. The deposition of Fe_3O_4 begins at a potential of -0.99 V, and the reaction becomes mass-transport-limited at potentials of about -1.1 V vs. Ag/AgCl. The mass transport limit is predominately controlled by convection. At low overpotentials at which i = 0, the surface concentration of $Fe(TEA)^{3+}$ should be equal to the bulk concentration, whereas at high overpotential at which the current reaches the mass-transport limit the surface concentration of $Fe(TEA)^{3+}$ should approach zero. Stoichiometric Fe_3O_4 should deposit at an applied potential of -1.065 V vs. Ag/AgCl. The material should have an excess of Fe(III) at potentials positive of -1.065 V, and an excess of Fe(II) at potentials more negative than -1.065 V vs. Ag/AgCl.

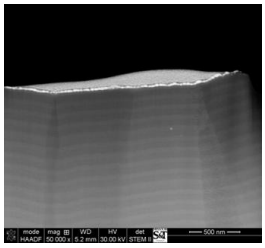

Fig. 1-HAADF (Z-contrast) image of compositional superlattice with 70 nm modulation wavelength

Defect chemistry superlattices based on Fe_3O_4 were deposited by pulsing the potential in the Fe(III)-TEA bath between -1.01 and -1.065 V vs. Ag/AgCl. Compositional superlattices in the $Fe_3O_4/ZnFe_2O_4$ system were deposited from the same bath with 30 mM Zn(II) added by pulsing between -0.99 and -1.05 V vs. Ag/AgCl. The modulation wavelength (i.e., bilayer thickness) was tuned by varying the dwell times, according to Faraday's law. The layered structure of a compositional superlattice is readily apparent in the high angle annular dark field (HAADF) image in Fig. 1 that we obtained in a focused ion beam microscope (FIB). The superlattice was designed to have a large modulation wavelength of 70 nm so that it could be easily imaged in the FIB. The light layers that are 25 nm thick correspond to the higher zinc content layer that was grown at -0.99 V vs. Ag/AgCl. The darker layers that are 45 nm thick correspond to the lower zinc content material that was grown at -1.05 V vs. Ag/AgCl. The superlattices were deposited as epitaxial films on single-crystal Au(111) substrates. X-ray diffraction provides direct evidence that these multilayered films are superlattices (i.e., crystallographically coherent). Fig 2 shows X-ray diffraction patterns of compositional superlattices in the $Fe_3O_4/ZnFe_2O_4$ system with modulation wavelengths of 12.5, 16.8, and 29.2 nm. The superperiodicity of the superlattices manifests itself as satellites around the (444) Bragg peak.

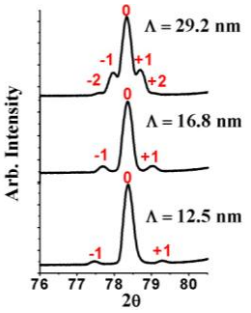

Fig. 2-X-ray patterns of compositional superlattices showing satellites due to superperiodicity

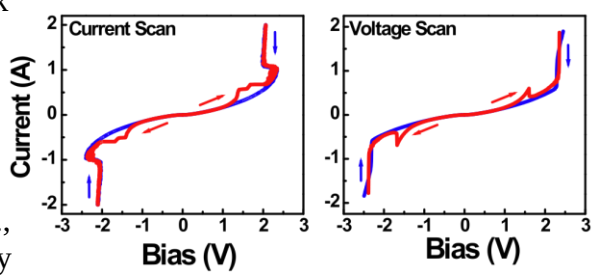

Fig. 3-Resistance switching in electrodeposited magnetite superlattice on Au(111) at 77 K. The modulation wavelength was 10.3 nm. The left scan was obtained by scanning the applied current at a 10 mA/s, and the right scan was obtained by scanning the applied voltage at 100 mV/s. Forward scans are red, and reverse scans are blue.

A unique feature of the electrodeposited

superlattices is the fact that they exhibit resistance switching during perpendicular transport measurements. Although this has been observed previously with magnetite samples, the resistance always decreased as the electric field was increased.[1,7,8] This jump in resistance was attributed to a field-assisted insulator-to-metal phase transition. As can be seen in Fig. 3, a magnetite superlattice on Au(111) with a modulation wavelength of 10.3 nm undergoes multistate resistance switching at 77 K, in which the resistance first increases at a bias of about 1.5 V and then abruptly decreases at a bias of about 2.3 V. In the current scan (left) of Fig. 3, negative differential resistance (NDR) and voltage oscillations are observed at the 2.3 V bias at which resistance switching is observed in the voltage sweep (right). It may be possible to exploit this resistance switching to design resistive random access memory (RRAM).[1,9]

Future Plans

Our main emphasis will be on the electrodeposition and characterization of superlattices based on magnetite. We plan to study the resistive switching of both defect chemistry and compositional superlattices in more detail. A major emphasis will be placed on determining the mechanism of resistance switching in the superlattices. Specifically, we will measure iV curves in perpendicular transport as a function of temperature and magnetic field. These measurements will be done in our Quantum Design PPMS system. Although researchers have previously observed resistive switching in single-crystal magnetite,[7,8] there are no studies in which a magnetic field effect has been observed. Also, by studying the temperature dependence of the resistance switching, we can determine the role that the Verwey metal-to-insulator transition plays in the resistance switching. We also plan to do these measurements for a series of superlattices with varying modulation wavelengths and strain. Our working hypothesis is that the phase transition is facilitated in the superlattices by residual strain due to the lattice mismatch between the layers. Some attempts will be made to incorporate other cations besides Zn(II) in the electrodeposited magnetite. We have done preliminary work on the Al(III) and Cr(III) ions (both amphoteric ions), but have had very limited success.

Another area of work will be the growth of epitaxial nanospears of ZnO on Si and on Cu_2O. We have shown this year that we can deposit tilted nanostructures of ZnO on Si(001). The Si was highly doped p^+-Si(001). We used this material because it does not etch appreciably in the highly alkaline solution. We also plan to try the deposition on lightly doped n- and p-Si. Our goal is to make heterojunctions that we can use to probe the ZnO/Si interfacial energetics. For this work we will do Mott-Schottky plots and iV curves to measure the barrier height and doping density. A challenge in this work will be to make contacts to the ZnO nanospears. One approach will be to test them in photoelectrochemical cells. Another approach will be to electrodeposit an insulating material between the ZnO nanospears, to avoid making contact to the Si substrate. A final area of work we would like to do with ZnO is produce epitaxial nanostructures on electrodeposited Cu_2O. This will be of interest for solar cells, because it will allow us to produce cells that absorb a larger percentage of the solar spectrum. We have previously shown that we can deposit epitaxial Cu_2O on both Si and InP, so our ultimate goal will be to produce ZnO/Cu_2O/Si and ZnO/Cu_2O/InP heterojunctions.

References

1. S. Lee, A. Fursina, J. T. Mayo, C. T. Yavuz, V. L. Colvin, R. G. Sumesh Sofin, I. V. Shvets, and D. Natelson, *Nature Materials* **7**, 130-133 (2008).
2. J. A. Switzer, C.-J. Hung, B. E. Breyfogle, M. G. Shumsky, R. Van Leeuwen, and T. D. Golden, *Science* **264**, 1573-1576 (1994).
3. J. A. Switzer, M. J. Shane, and R. J. Phillips, *Science* **247**, 444-446 (1990).
4. J. A. Switzer, R. P. Raffaelle, R. J. Phillips, C.-J. Hung, and T. D. Golden, *Science* **258**, 1918-1921 (1992).
5. H. M. Kothari, A. A. Vertegel, E. W. Bohannan, and J. A. Switzer, *Chem. Mater.* **14**, 2750-2756 (2002).
6. H. M. Kothari, E. A. Kulp, S. J. Limmer, P. Poizot, E. W. Bohannan, and J. A. Switzer, *J. Mater. Res.* **21**, 293-301 (2006).
7. T. Burch, P. P. Craig, C. Hedrick, T. A. Kitchens, J. I. Budnick, J. A. Cannon, M. Lipsicas, and D. Mattis, *Phys. Rev. Lett.* **23**, 1444-1447 (1969).
8. P. J. Freud and A. Z. Hed, *Phys. Rev. Lett.* **23**, 1440-1443 (1969).
9. R. Waser and M. Aono, *Nature Materials* **6**, 833-840 (2007).

DOE Sponsored Publications in 2009 from Current Grant

1. G. Mu, R. V. Gudavarthy, E. A. Kulp, and J. A. Switzer, "Tilted epitaxial ZnO nanospears on Si(001) by chemical bath deposition," *Chem. Mater.* **21**, 3960-3964 (2009).

2. E. A. Kulp, H. M. Kothari, S. J. Limmer, J. Yang, R. V. Gudavarthy, E. W. Bohannan, and J. A. Switzer, "Electrodeposition of epitaxial magnetite films and ferrihydrite nanoribbons on single-crystal gold," *Chem. Mater.*, manuscript #cm-2009-013514, accepted for publication (2009).

3. J. A. Switzer, E. A. Kulp, and R. V. Gudavarthy, "Resistance switching in electrodeposited superlattices in the magnetite/zinc ferrite system," *Science*, in preparation (2009).

Session IVb

Thin Films: Synthesis of Thin Film Interfaces (cont.)

Session Chair: Gyula Eres, Oak Ridge National Laboratory

(This page intentionally left blank.)

Composition at the $LaAlO_3/SrTiO_3$ interface – some surprises

S.A. Chambers (PI)[a], T.C. Droubay[a], L. Qiao[a], M.E. Engelhard[a], W. Jiang[a], V. Shutthanandan[a], P. Sushko,[b] T. Feng[c], H. D. Lee[c], T. Gustafsson[c], E. Garfunkel[c], H. Sato[d], Y. Hikita[d], H.Y. Hwang[d]
[a]Pacific Northwest National Laboratory, Richland, WA
[b]University College, London, United Kingdom
[c]Rutgers University, Piscataway, NJ, [d]University of Tokyo, Chiba, Japan

I. Program scope

This program focuses on the growth and properties of doped transition metal (TM) and complex oxides prepared as epitaxial films. Our methods include plasma assisted molecular beam epitaxy (MBE) and off-axis pulsed laser deposition (PLD). Our interests span the mechanistic growth details specific to the method being used, the dynamics of film morphological and structural evolution, and the resulting magnetic and electronic properties. Here we present our recent work on the properties of the LAO/STO interface – a system that has been of considerable interest because of observations of novel interface conductivity, despite being at the junction of two band insulators.

II. Recent Progress

Although both LAO and STO exhibit cubic perovskite structures in the bulk, is nonpolar along [001] whereas LAO is polar. This difference stems from the different formal charges on the cations. STO consists of alternating layers of $(Sr^{2+}O^{2-})^0$ and $(Ti^{4+}O^{2-}_2)^0$ along [001]. Both constituent layers are formally charge neutral, leading to nonpolarity. In contrast, LAO consists of alternating $(La^{3+}O^{2-})^+$ and $(Al^{3+}O^{2-}_2)^-$ layers, and thus exhibits polarity along [001]. Atomically abrupt LAO/STO interface formation thus gives rise to a polar discontinuity. Moreover, the LAO/STO interface exhibits novel electronic properties not seen in either of the bulk materials. Elementary electrostatic considerations suggest that perfect layer-by-layer growth of LAO on STO will lead to a diverging electric potential as a result of the accumulation of alternating dipoles within the LAO film – the so-called "polar catastrophe". This unstable situation can in principle be mitigated by transfer of half an electron per unit cell from $(La^{3+}O^{2-})^+$ to $(Ti^{4+}O^{2-}_2)^0$ at the interface for TiO_2-terminated STO, or half a hole per unit cell from $(Al^{3+}O^{2-}_2)^-$ to $(Sr^{2+}O^{2-})^0$ for SrO-terminated STO. Electronically, these two interfaces are formally *n*-type and *p*-type. In principle, both interfaces should exhibit some degree of conductivity. Moreover, if there is sharp band bending at the interface, the carriers should be confined to form a two-dimensional electron or hole gas (2DEG or 2DHG). In addition to charge transfer to avert the polar catastrophe, other more subtle physical causes for charge accumulation at the interface, such as aliovalent cation exchange, may be operative.

A number of laboratories report that epitaxial LAO grown on TiO_2-terminated STO(001) (the "*n*-type interface") exhibits conductivity when the LAO thickness is at least 4 unit cells (u.c.).[1-12] Moreover, many of the same laboratories also report that the *p*-type interface resulting from LAO growth on SrO-terminated STO(001) is insulating. The extremely high current level of research activity on this materials system stems from the fascinating physics and potential device applications. Among the various groups working on LAO/STO, PLD is by far the most commonly used growth method. It is

commonly assumed throughout this community that: (i) PLD results in the stoichiometric transfer of material from the LAO target to the epitaxial film, provided some ablation threshold has been exceeded, and, (ii) the resulting interface is essentially abrupt. That is, cation exchange is limited to the first few atomic layers away from the interface, with the extent of mixing falling off sharply with distance away from the interface.[4,13] However, recent results from our respective laboratories lead to different conclusions.

LAO/STO specimens prepared at the Universities of Augsburg and Tokyo, as well as PNNL, were characterized using high-resolution x-ray diffraction (XRD), Rutherford backscattering spectrometry (RBS), x-ray photoelectron spectroscopy (XPS) and medium energy ion scattering (MEIS). Although analysis of some of these data is in progress at the time of writing of this abstract, results to date reveal that contrary to popular opinion, epitaxial LAO on STO(001) prepared by PLD is decidedly nonstoichiometric, and that the interface is significantly intermixed.

Fig. 1 shows normal emission XPS and off-normal RBS for 25 unit cell (u.c.) LAO films (~95Å thick) on STO(001). In the case of XPS, the film composition was determined by direct comparison to La 4*d* and Al 2*p* peak areas for bulk LAO(001),

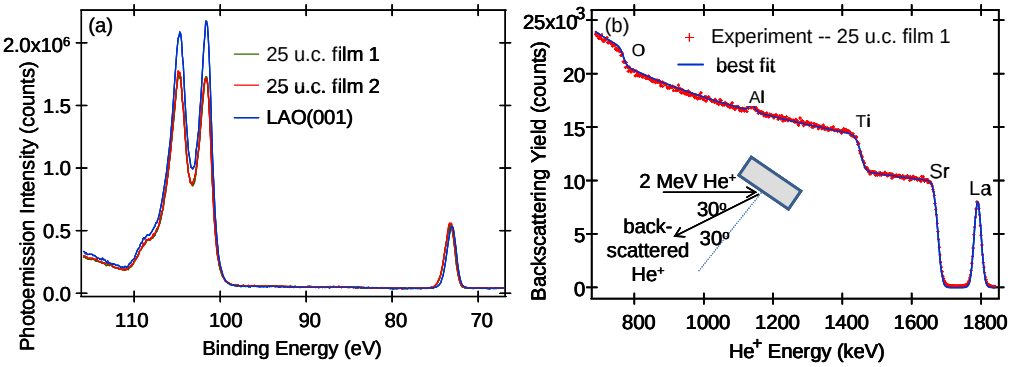

Fig. 1 La 4*d* (100-110 eV) and Al 2*p* (73 eV) core-level peaks at normal emission (a) and off-normal RBS (b) for 25 u.c. LAO/STO(001). The best fit to the RBS data corresponds to a volume-averaged composition of $La_{0.92(3)}Al_{1.1(1)}O_3$ where the number in parentheses is the uncertainty in the last digit.

and by modeling using the program SIMNRA for RBS. The two films analyzed by XPS yielded compositions of $La_{0.90(3)}Al_{1.14(2)}O_{2.9(1)}$ and $La_{0.91(3)}Al_{1.18(2)}O_{2.9(1)}$. The probe depth in these measurements was ~15 Å, about half the overall film thickness. These results are in good agreement with those from RBS (Fig. 1b), and reveal a substantial imbalance in the La and Al concentrations relative to those for a perfectly stoichiometric film.

Interface conductivity is reported for film thicknesses of 4 u.c. (~1.5 nm) or greater.[2] It is believed that a monotonically increasing electrostatic potential within the LAO film resulting from the dipoles causes the LAO valence band to cross the Fermi level of the STO, resulting in charge transfer from LAO and STO and the establishment of a 2DEG at the interface. We have investigated 4 u.c. LAO/STO(001) specimens which exhibit interface conductivity. Characteristic XPS spectra for one such specimen are shown in Fig. 2. The La 4*d* and Al 2*p* spectra are compared to those for bulk LAO(001) after scaling by a factor of $1 - \exp(-t/\lambda\sin\theta)$ to account for the thickness of the 4 u.c. film. Here, t is the film thickness and λ is the electron attenuation length (15 ± 2Å). Such scaling is required if the film thickness is less than $\sim 3\lambda\sin\theta$, the XPS probe depth.

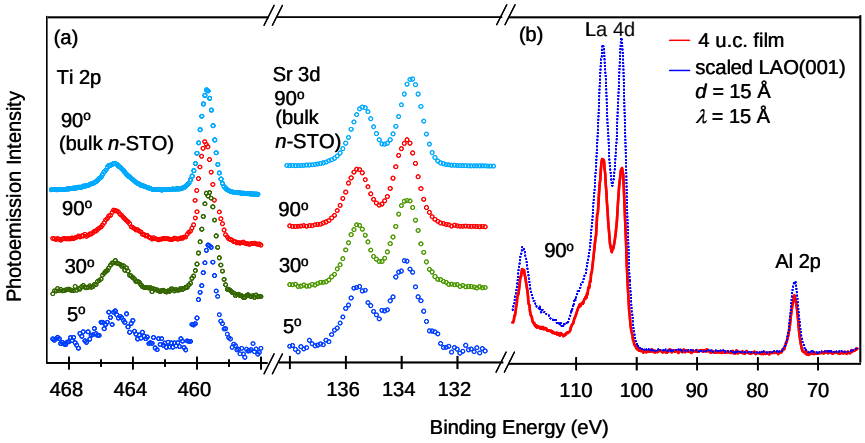

Fig. 2 Ti 2*p* and Sr 3*d* spectra at various electron emission angles (θ) relative to the surface plane (a) and La 4*d* and Al 2*p* at normal emission (b) for 4 u.c. LAO/STO(001). Also shown in (b) is a spectrum for bulk LAO(001) scaled by a factor of $1 - \exp(-t/\lambda\sin\theta)$ to generate a standard for a stoichiometric 4 u.c. film.

As with the 25 u.c. films, there is a marked imbalance in the La and Al within the film, with both elements exhibiting concentrations less than expected for a perfectly abrupt film. Interestingly, the La to Al atom ratio, which is given by $(\mathrm{La}4d/\mathrm{Al}2p)_{film}/(\mathrm{La}4d/\mathrm{Al}2p)_{bulk}$, is ~0.75, the same as that for the 25 u.c. films (0.76 ± 0.03). Moreover, there is substantial spectral intensity for Ti 2*p* and Sr 3*d* at $\theta = 5^{o}$. Due to the much longer photoelectron path length though the film at $\theta = 5^{o}$ compared to that at normal emission, this result cannot occur unless: (i) the film does not wet the substrate, resulting in patches of exposed substrate, or, (ii) Ti and Sr have outdiffused. RHEED during and after deposition reveals layer-by-layer growth and a flat surface, thereby ruling out film roughness and pointing to Ti and Sr outdiffusion. Indeed, if we assume that the interface is abrupt, *apparent* attenuation lengths for the Ti 2*p* and Sr 3*d* core electrons of the order of 90 - 100Å would be required to account for peak areas of the magnitudes observed. These numbers are physically unreasonable in light of the photoelectron kinetic energies.

In order to more quantitatively probe the atom profiles in the film and interface, we have used high-resolution RBS and MEIS. The MEIS data are currently being analyzed, and will be presented at the meeting. The HRRBS results are summarized in Fig. 3. The asymmetries on the low- (high-) energy sides of the La (Sr) backscattering peaks reveal interdiffusion of these two elements. The associated atom profiles (Fig. 3b) show that there is significant Ti and Sr in the film, and that La has diffused far into the substrate. The signal-to-background of the Al backscattering peak (not shown) is not sufficient to allow the motion of this atom to be tracked with the data at hand. However, the MEIS based on 100 keV ions backscattering is quite sensitive to Al and may yield quantitative atom profiles for all four elements. This analysis is currently underway.

Finally, density functional theory calculations reveal that the *coupled* (Al, Ti) and (La, Sr) exchange reactions are energetically favorable by up to 0.6 eV depending on the defect concentration and proximity to the interface. Moreover, exchange of La and Sr cations generate electron carriers in STO and hole carriers in LAO. These electrons and holes recombine if the La and Sr impurities are close to the nominal LAO/STO interface position, but recombination shuts down if the La and Sr impurities are separated by a few lattice constants. Finally, we find Al atoms do not fill up La vacancies in La-deficient LAO film. Instead, the vacancies promote out-diffusion of Sr atoms from the STO

substrate with the energy gain of more than 0.2 eV, which can be a major factor contributing to the Sr enrichment of the STO-supported LAO films.

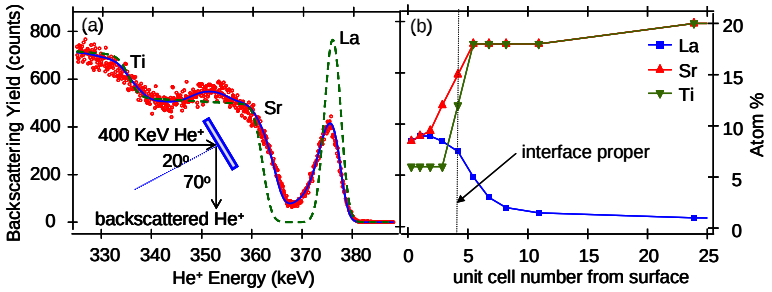

Fig. 3 (a) HRRBS (red) along with SIMNRA-generated model spectra for an abrupt (dashed) and heavily intermixed (blue) model of the interface. Atom profiles accompanying the intermixed model in (a)

III. Future Plans

We are currently measuring the angular distributions of elements given off during laser ablation of LAO to understand the complex PLD behavior of this particular perovskite. Our measurements reveal that within our PLD chamber, most target-substrate geometries result in LAO films that are La rich. However, there is a deposition geometry that results in stoichiometric LAO. We plan to optimize LAO on STO growth at this geometry and determine the associated heterojunction properties.

[1] A. Ohtomo, H. Y. Hwang, *Nature* **2004**, *427*, 423.
[2] S. Thiel, G. Hammerl, A. Schmehl, C. W. Schneider, J. Mannhart, *Science* **2006**, *313*, 1942.
[3] M. Takizawa, H. Wadati, K. Tanaka, M. Hashimoto, T. Yoshida, A. Fujimori, A. Chikamatsu, H. Kumigashira, M. Oshima, K. Shibuya, T. Mihara, T. Ohnishi, M. Lippmaa, M. Kawasaki, H. Koinuma, S. Okamoto, A. J. Millis, *Phys. Rev. Lett.* **2006**, *97*, 057601.
[4] N. Nakagawa, H. Y. Hwang, D. A. Muller, *Nat. Mat.* **2006**, *5*, 204.
[5] M. Huijben, G. Rijnders, D. H. A. Blank, S. Bals, S. Van Aert, J. Verbeeck, G. Van Tendeloo, A. Brinkman, H. Hilgenkamp, *Nat. Mat.* **2006**, *5*, 556.
[6] W. Siemons, G. Koster, H. Yamamoto, T. H. Geballe, D. H. A. Blank, M. R. Beasley, *Phys. Rev. B* **2007**, *76*, 155111.
[7] W. Siemons, G. Koster, H. Yamamoto, W. A. Harrison, G. Lucovsky, T. H. Geballe, D. H. A. Blank, M. R. Beasley, *Phys. Rev. Lett.* **2007**, *98*, 196802.
[8] G. Herranz, M. Basletic, M. Bibes, C. Carretero, E. Tafra, E. Jacquet, K. Bouzehouane, C. Deranlot, A. Hamzic, J.-M. Broto, A. Barthelemy, A. Fert, *Phys. Rev. Lett.* **2007**, *98*, 216803.
[9] A. D. Caviglia, S. Gariglio, N. Reyren, D. Jaccard, T. Schneider, M. Gabay, S. Thiel, G. Hammerl, J. Mannhart, J. M. Triscone, *Nature* **2008**, *456*, 624.
[10] K. Yoshimatsu, R. Yasuhara, H. Kumigashira, M. Oshima, *Phys. Rev. Lett.* **2008**, *101*, 026802.
[11] Z. S. Popovic, S. Satpathy, R. M. Martin, *Phys. Rev. Lett.* **2008**, *101*, 256801.
[12] M. Basletic, J. L. Maurice, C. Carretero, G. Herranz, O. Copie, M. Bibes, E. Jacquet, K. Bouzehouane, S. Fusil, A. Barthelemy, *Nat. Mat.* **2008**, *7*, 621.
[13] P. R. Willmott, S. A. Pauli, R. Herger, C. M. Schleputz, D. Martoccia, B. D. Patterson, B. Delley, R. Clarke, D. Kumah, C. Cionca, Y. Yacoby, *Phys. Rev. Lett.* **2007**, *99*, 155502.

IV. Sponsored Publications in 2008-2009

1. S.A. Chambers, Comment on "Origin of Metallic States at the Heterointerfaces between the Band Insulators $LaAlO_3$ and $SrTiO_3$", Phys. Rev. Lett. **2009**, *102*, 199703.
2. S.A. Chambers, "Epitaxial Growth and Properties of Doped Transition Metal and Complex Oxide Films", invited review article for Advanced Materials, **2009** in press.

Interfaces in Epitaxial Complex Oxides

H.M. Christen, H.N. Lee, G. Eres, C.M. Rouleau, B.C. Larson, J.Z. Tischler, and W. Zhu
christenhm@ornl.gov
Materials Science and Technology Division
Oak Ridge National Laboratory, Oak Ridge, TN 37831

I. Program Scope

Unexpected phenomena, including metallicity,[1] superconductivity,[2] and magnetism,[3] have recently been shown to emerge at interfaces between two insulating perovskite metal-oxides. While originally explained exclusively in terms of electronic reconstruction, recent work shows that the delicate interplay between electronic, magnetic, structural, and chemical effects at epitaxial interfaces must be considered in order to fully understand the observed phenomena. Therefore, the central goal of this effort is to understand how these effects emerge and interact to create new macroscopic behaviors, and how these interfacial properties are controlled by synthesis parameters and the selection of the constituent materials. The materials focus is on perovskite transition-metal oxides, a family exhibiting a rich variety of physical properties.[4] The work focuses on understanding and controlling epitaxial synthesis using pulsed-laser deposition (PLD)[5,6] including real-time in-situ synchrotron surface x-ray diffraction (SXRD).[7] Numerous specialized techniques are used to characterize the resulting properties of epitaxial heterostructures, including transport measurements, magnetometry, electron microscopy, optical spectroscopies, and neutron scattering. While a broad range of techniques is used to gain an in-depth description of interfacial properties, this talk will focus on magnetic properties at epitaxial interfaces, the interplay between chemical and electronic effects, and results from neutron reflectometry.

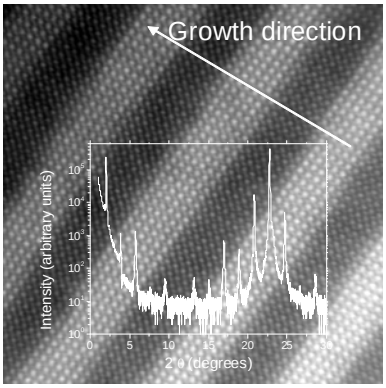

Fig. 1. Epitaxial $SrTiO_3$/$LaMnO_3$ superlattices. Foreground: x-ray diffraction θ-2θ scan showing superlattice reflections. Background: Z-contrast scanning transmission electron micrograph. (Microscopy by M. Varela, ORNL)

II. Recent Progress

Results from this program show broad range of effects at interfaces and in thin layers. For example, we show a surprising variability in materials' responses to epitaxial strain,[8,9] determine the intrinsic charge carrier density at specific interfaces between insulating perovskites,[10] and show that the traditional picture of layer-by-layer (LBL) growth needs to be completely revised in order to properly tune synthesis parameters for atomic scale control of interfacial systems.[6,7]

For the purpose of this presentation, the focus will be on results for epitaxial $SrTiO_3$/$LaMnO_3$ superlattices as well as more complex heterostructures (three-component superlattices containing $LaMnO_3$ layers). In $SrTiO_3$/$LaMnO_3$ superlattices (Fig. 1) we find a surprising enhancement of the total

magnetization when the thickness of each sublayer is reduced (Fig. 2),[11] but this magnetization disappears in $La_{0.5}Sr_{0.5}Mn_{0.5}Ti_{0.5}O_3$ (i.e. solid-solutions of $SrTiO_3$ and $LaMnO_3$).

Polarized neutron reflectometry was applied to the study of $SrTiO_3/LaMnO_3$ interfaces, as this method reveals the magnetization profile across a film with a spatial resolution better than 0.5 nm in the direction perpendicular to the interfaces. While bulk $LaMnO_3$ is an A-type antiferromagnet and films of $LaMnO_3$ exhibit weak ferromagnetism, a strong enhancement (approaching 4 μ_B/Mn) is observed in a region near the interface (Fig. 3).

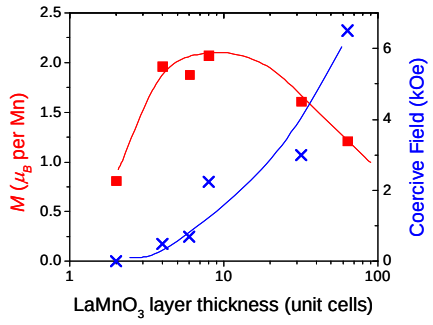

Fig. 2. Magnetic properties of $LaMnO_3/SrTiO_3$ superlattices as a function of the $LaMnO_3$ sublayer thickness.

III. Future Plans

In order to understand the interplay between synthesis parameters and physical properties of the resulting materials, we will focus on in-situ SXRD measurements of heteroepitaxial growth, on detailed microscopic and tomographic (laser-assisted local electrode atom probe, laser-LEAP) approaches to probe the chemical and structural reconstructions at epitaxial interfaces, and on optical spectroscopies as well as resonant x-ray scattering to probe interfacial electronic properties. This is motivated by the promising possibility to create new artificial materials (superlattices) with macroscopic properties that result from effects at atomic-scale controlled epitaxial interfaces. Future applications will include Mott transistors,[12] solar cells based on the bulk photovoltaic effect,[13] fuel cells,[14] battery applications,[15] and thermoelectrics.

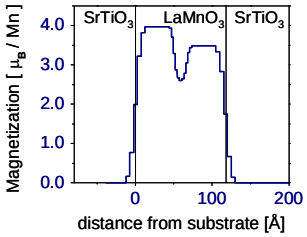

Fig. 3. Polarized neutron reflectometry results (magnetic scattering length density) showing a strong enhancement of the magnetization at the $LaMnO_3$/ $SrTiO_3$ interface. (Neutron reflectometry with V. Lauter, SNS, ORNL)

IV. References

1. A. Ohtomo and H. Y. Hwang, "A high-mobility electron gas at the $LaAlO_3/SrTiO_3$ heterointerface," *Nature* **427**, 423 (2004).
2. N. Reyren, S. Thiel, A. D. Caviglia, L. F. Kourkoutis, G. Hammerl, C. Richter, C. W. Schneider, T. Kopp, A.-S. Rüetschi, D. Jaccard, M. Gabay, D. A. Muller, J.-M. Triscone, J. Mannhart, "Superconducting Interfaces Between Insulating Oxides," *Science* **317**, 1196 (2007).
3. A. Brinkman, M. Huijben, M. Van Zalk, J. Huijben, U. Zeitler, J. C. Maan, W. G. Van der Wiel, G. Rijnders, D. H. A. Blank, and H. Hilgenkamp, "Magnetic effects at the interface between non-magnetic oxides," *Nat. Mater.* **6**, 493 (2007).
4. C.N.R. Rao, and B. Raveau, Transition Metal Oxide: Structure, Properties and Synthesis of Ceramic Oxides, 2nd ed., Wiley–VCH, New York, 1998.

5. H. N. Lee, H. M. Christen, M. F. Chisholm, C. M. Rouleau, and D. H. Lowndes, "Strong polarization enhancement in asymmetric three-component ferroelectric superlattices," *Nature* **433**, 395 (2005).
6. H. M. Christen and G. Eres, "Recent advances in pulsed-laser deposition of complex-oxides," *J. Phys.: Condens. Matter* **20**, 264005 (2008).
7. J. Z. Tischler, G. Eres, B.C. Larson, C.M. Rouleau, P. Zschack, and D.H. Lowndes, "Nonequilibrium interlayer transport in pulsed-laser deposition," *Phys. Rev. Lett.* **96**, 226104 (2006).
8. H.N. Lee, S. M. Nakhmanson, M. F. Chisholm, H. M Christen, K. M. Rabe, and D. Vanderbilt, "Suppressed Dependence of Polarization on Epitaxial Strain in Highly Polar Ferroelectrics," *Phys. Rev. Lett.* **98**, 217602 (2007).
9. D. H. Kim, H. N. Lee, M. D. Biegalski, and H. M. Christen, "Effect of Epitaxial Strain on Ferroelectric Polarization in Multiferroic $BiFeO_3$ Films," *Appl. Phys. Lett.* **92**, 12911 (2008).
10. S. S. A. Seo, W. S. Choi, H. N. Lee, L. Yu, K. W. Kim, C. Bernhard, and T. W. Noh, "Optical Study of the Free Carrier Response of $LaTiO_3/SrTiO_3$ Superlattices," *Phys. Rev. Lett.* **99**, 266801 (2007).
11. H. M. Christen, D. H. Kim, and C. M. Rouleau, "Interfaces in Perovskite Heterostructures," *Appl. Phys. A* **93**, 807 (2008).
12. C. H. Ahn, J. M. Triscone, and J. Mannhart, "Electric field effect in correlated oxide systems," *Nature* **424**, 1015 (2003).
13. V. M. Fridkin, "Bulk Photovoltaic Effect in Noncentrosymmetric Crystals," *Crystallogr. Rep.* **46**, 654 (2001).
14. J. Garcia-Barriocanal, A. Rivera-Calzada, M. Varela, Z. Sefrioui, M. R. Díaz-Guillen, K. J. Moreno, J. A. Díaz-Guillen, E. Iborra, A. F. Fuentes, S. J. Pennycook, C. Leon, and J. Santamaria, "Tailoring Disorder and Dimensionality: Strategies for Improved Solid Oxide Fuel Cell Electrolytes," *Chem. Phys. Chem.* **10**, 1003 (2009).
15. M. Thackeray, "An unexpected conductor," *Nat. Mater.* **1**, 81 (2002).

V. Publications resulting from work supported by the DOE project over the last two years (2008, 2009)

W. S. Choi, Z. Marton, S. Y. Jang, S. J. Moon, B. C. Jeon, J. H. Shin, S. S. A. Seo, T. W. Noh, K. Myung-Whun, H. N. Lee, and Y. S. Lee, "Effects of oxygen-reducing atmosphere annealing on $LaMnO_3$ epitaxial thin films," *J. Phys. D: Appl. Phys.* **42**, 165401 (2009).

H. M. Christen, G. J. MacDougall, H-S. Kim, D. H. Kim, L. A. Boatner, C. J. Callender Bennett, J. L. Zarestky, and S. E. Nagler, "Potassium tantalate substrates for neutron experiments on antiferromagnetic perovskite films," *Journal of Physics: Conference Series* (accepted for publication).

M. Z. Li, Y. G. Yao, B. A. Wu, Z. Y. Zhang, and E. G. Wang, "Strain effect on the instability of island formation in submonolayer heteroepitaxy," *Europhys. Lett*. **86**, 16001 (2009).

M. M. Özer, C.-Z. Wang, Z. Y. Zhang, and H. H. Weitering, "Quantum Size Effects in the Growth, Coarsening, and Properties of Ultra-thin Metal Films and Related

Nanostructures," *J. Low Temp. Phys.*, DOI 10.1007/s10909-009-9905-z, invited review (2009).
S. S. A. Seo and H. N. Lee, "Strain-coupled ferroelectric polarization in $BaTiO_3$-$CaTiO_3$ superlattices," *Appl. Phys. Lett.* **94**, 232904 (2009).
S. S. A. Seo, Z. Marton, W. S. Choi, G. W. J. Hassink, D. H. A. Blank, H. Y. Hwang, T. W. Noh, T. Egami, and H. N. Lee, "Multiple conducting carriers generated in $LaAlO_3$/$SrTiO_3$ heterostructures," *Appl. Phys. Lett.* **95**, 082107 (2009).
D. A. Tenne, H. N. Lee, R. S. Katiyar, and X. X. Xi, "Ferroelectric phase transitions in three-component short-period superlattices studied by ultraviolet Raman spectroscopy," *J. Appl. Phys.* **105**, 054106 (2009).
J. Cao, J. L. Musfeldt, D. J. Singh, B. Rahaman, T. Saha-Dasgupta, C. C. Torardi, B. C. Sales, H. M. Christen, and O. Swader, "Color Properties of Model Spin Chain Materials $VOHPO_4 \cdot 1/2H_2O$ and $(VO)_2P_2O_7$: Spectroscopy and Electronic Structure Calculations," *Phys. Rev. B* **77**, 165111 (2008).
H. M. Christen, M. Varela, and D. H. Kim, "The Effect of Strain and Strain Symmetry on the Charge-Order Transition in $Bi_{0.4}Ca_{0.6}MnO_3$ Films," *Phase Transitions* **81**, 717 (2008).
H. M. Christen and G. Eres, "Recent Advances in Pulsed-Laser Deposition of Complex-Oxides," *J. Phys. Cond. Matt.* **20**, 264005 (2008).
H. M. Christen, D. H. Kim, and C. M. Rouleau, "Interfaces in Perovskite Heterostructures," *Appl. Phys. A* **93**, 807 (2008).
W. Hong, Z. Suo, and Z. Y. Zhang, "Dynamics of Terraces on a Silicon Durface Due to the Combined Action of Strain and Electric Eurrent," *J. Mech. Phys. Solids* **56**, 267 (2008).
D. H. Kim, H. N. Lee, M. D. Biegalski, and H. M. Christen, "Effect of Epitaxial Strain on Ferroelectric Polarization in Multiferroic $BiFeO_3$ Films," *Appl. Phys. Lett.* **92**, 12911 (2008).
Lu, Z., M. J. Walock, P. R. LeClair, G. J. Mankey, P. Mani, D. Lott, F. Klose, H. Ambaye, V. Lauter, M. Wolff, A. Schreyer, H. M. Christen, and B. C. Sales, "Structural and magnetic properties of epitaxial Fe25Pt75," Presented at the 55th International Symposium of the American-Vacuum-Society, Boston, MA, 2008.
J. Ma, E. G. Wang, Z. Y. Zhang, and B. A. Wu, "Theory of the Excitation of the Vibrational Mode of an Adatom-Substrate System Under a Resonant Laser Field," *Phys. Rev. Lett.* **78**, 125303 (2008).
Y. N. Mo, W. G. Zhu, E. Kaxiras, and Z. Y. Zhang, "Electronic Nature of Step-Edge Barriers against Adatom Descent on Transition-Metal Surfaces," *Phys. Rev. Lett.* **101**, 216101 (2008).
C. M. Rouleau, H. M. Christen, H. Cui, G. Eres, A. A. Puretzky, and D. B. Geohegan, "Altering the Catalytic Activity of Thin Metal Catalyst Films for Controlled Growth of Chemical Vapor Deposited Vertically Aligned Carbon Nanotube Arrays," *Appl. Phys. A* **93**, 1005 (2008).

SCIENCE AND TECHNOLOGY OF QUANTUM MATERIALS

R. Ramesh, Department of Materials Science and Engineering and Department of Physics, Materials Science Division, Lawrence Berkeley Laboratory, University of California, Berkeley CA 94720.

Overview: Quantum physics provides the theoretical basis for our understanding of the electronic properties of *all* materials. However, there exists a fascinating sub-class of condensed matter systems, now widely known as "*quantum materials*," in which quantum mechanics plays an especially profound role in determining the nature of macroscopic order parameters and the phase-transitions between them. In some cases, such as supeconductors, this occurs because the order parameter is explicitly a quantum mechanical object. In many other such systems, quantum effects dominate the physics because of the interplay between competing order, frustration, strong interactions, and low-dimensionality. These systems display a marvelously rich and diverse range of physical phenomena. Transition metal oxides, *e.g.,* manganites, cuprates, ruthenates and cobaltates, are systems whose interacting charge, spin, orbital, and lattice degrees of freedom exemplify the diversity of quantum materials. The Quantum Materials Group was first organized in Fall 2006 as a unified FWP at LBNL. Our group includes experts in the theory of strongly correlated systems (**Lee**, **Vishwanath**), bulk crystal synthesis (**Birgeneau**, **Bourret**), thin-film synthesis (**Ramesh**), and characterization (**Birgeneau**, **Dynes**, **Lanzara**, and **Orenstein**). We bring to bear powerful experimental tools (transport, photoemission spectromicroscopy, optical spectroscopy, electron microscopy and spectroscopy, and neutron scattering) in conjunction with comprehensive theoretical approaches to understanding the complex phenomena that arise in quantum materials. With expertise in both single crystal and thin film growth, we are able to compare the properties of quantum phases in the bulk with those that occur in thin films and heterostructures. The work in this FWP is complemented by strategic collaborations with colleagues at other national labs, academic institutions as well as researchers around the world. In this talk, I will describe to you a specific portion of work in this FWP, namely that based on multiferroic oxide heterostructures.

Magnetoelectric Coupling in Multiferroics and Electric Field Control of Magnetism

In the last 5-10 years there has been a flurry of research focused on multiferroic and magnetoelectric materials.[1,2] From the investigation of bulk single crystals to novel characterization techniques that probe order parameters, this is truly a diverse field, rich with experimental and theoretical complexity. By definition, a multiferroic[3] is a material that simultaneously possesses two or more of the so-called "**ferroic**" order parameters – ferroelectricity, ferromagnetism, and ferroelasticity. Magnetoelectric coupling typically refers to the induction of magnetization by an electric field or polarization by a magnetic field and vice versa.[4] The promise of coupling between magnetic and electric order parameters and the potential to manipulate one through the other has captured the imagination of researchers worldwide. The ultimate goal for device functionality would be a single-phase multiferroic with strong coupling between ferroelectric and ferromagnetic order parameters, enabling control over the magnetic nature of the material with an applied electric field, at room temperature. Details of the fundamentals of multiferroics are described in several review articles[1,5,6].

The overlap required of ferroic materials to be classified as multiferroic is shown schematically in **Fig. 1a**. Only a small subgroup of all magnetically and electrically polarizable materials are either ferromagnetic or ferroelectric and fewer still simultaneously exhibit both order parameters (**Fig. 1b**). Magnetoelectricity is an independent phenomenon that can arise in any material with both magnetic and electronic polarizability, regardless of whether it is multiferroic or not. However, magnetoelectric coupling is expected to be enhanced in a material that is simultaneously ferromagnetic and ferroelectric.[7] The scarcity of ferromagnetic-ferroelectric multiferroics can be understood as a consequence of a number of limiting factors including symmetry, electronic structure, and chemistry.[8] In particular, there exists a contradiction between the conventional mechanism of off-centering in a ferroelectric and the formation of magnetic order. [8] Therefore, our focus has been in designing and indentifying new mechanisms that lead to magnetoelectric coupling and multiferroic behavior. It has been proposed that one can engineer multiferroic properties by chemically controlling the functionality on a site-by-site basis. Single phase multiferroism has been identified in only a few perovskite oxides and is typically achieved by making use of

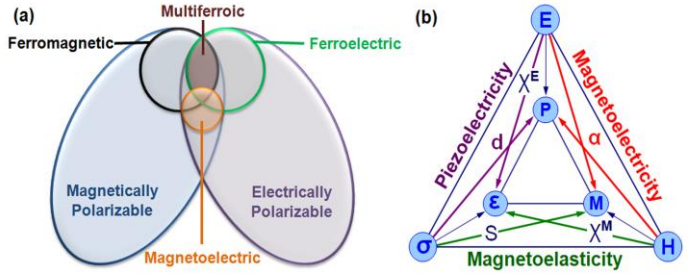

Fig. 1: (a) Relationship between multiferroic and magnetoelectric materials. Illustrates the requirements to achieve both in a material. (b) Schematic illustrating different types of coupling present in materials. Much attention has been given to materials where electric and magnetic order is coupled (magnetoelectrics).

the stereochemical activity of the lone pair on large (*A*-site) cations to provide ferroelectricity while retaining magnetism on the smaller (*B*-site) cations. This is the case in one of the most widely studied single-phase multiferroics – the antiferromagnetic, ferroelectric $BiFeO_3$ (BFO).[9]

Multiferroic $BiFeO_3$: This antiferromagnetic (T_N~350C) ferroelectric (T_C~820C) is by far the most studied multiferroic system worldwide, as a direct consequence of some of the pioneering work done within this program. Today, much progress has been made in understanding the structure, properties, and growth of thin films of BFO. High quality epitaxial BFO films have been grown via pulsed laser deposition(PLD),[9,10] radio-frequency (RF) sputtering,[11,12] metalorganic chemical vapor deposition (MOCVD),[13,14] and chemical solution deposition (CSD)[15] on a wide range of substrates including traditional oxide substrates as well as Si[10,16] and GaN.[17] This work has shown that high quality films, like those shown in **Fig. 2** can be produced. Typical XRD θ-2θ measurements (**Fig. 2a**) show the ability of researchers to produce high quality, fully epitaxial, single phase films of BFO (data here is for a BFO/$SrRuO_3$ (SRO)/$SrTiO_3$ (001) heterostructure). The quality of such heterostructures as produced by PLD can be probed further by transmission electron microscopy (TEM) (**Fig. 2b**), which reveals that the films are uniform over large areas with atomically abrupt, smooth, and coherent interfaces between BFO and a commonly used bottom electrode material SRO.

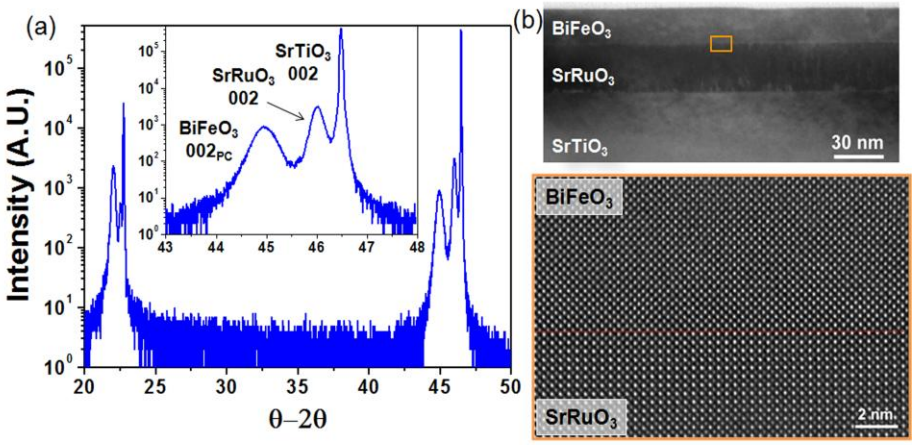

Fig. 2: (a) X-ray diffraction results from a fully epitaxial, single phase BFO/SRO/STO(001) heterostructure. (b) Low and high resolution transmission electron microscopy images of BFO/SRO/STO(001) heterostructure.

Electric field control of antiferromagnetism: **We have** observed the first visual evidence for electrical control of antiferromagnetic domain structures in a single-phase multiferroic at room temperature (**Fig. 3**). By combining piezoresponse force microscopy (PFM) imaging of ferroelectric domains and x-ray photoemission electron microscopy (PEEM, in collaboration with **Scholl**, ALS) imaging of antiferromagnetic domains we were able to observe direct changes in the nature of the antiferromagnetic domain structure in BFO with application of an applied electric field.[18] This research showed that the ferroelastic switching events (i.e., 71° and 109°) resulted in a corresponding rotation of the magnetization plane in BFO (**Fig. 3**) and has paved the way for further study of this material in attempts to gain room temperature control of ferromagnetism (which is discussed in detail later). This work has since been confirmed by neutron diffraction experiments in bulk BFO.[19] While significant progress has been made, much remains to be understood with respect to the two order parameters as well as the details of how they interact. This forms one focus of our proposed future research.

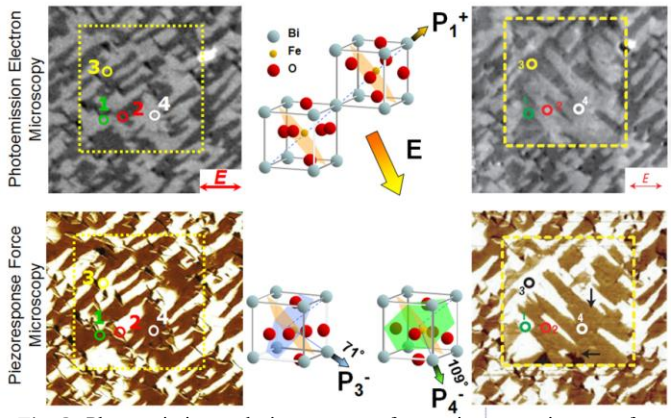

Fig. 3: Photoemission and piezoresponse force microscopy images of a (001)-oriented BFO film before and after the application of an electric field. This illustrates the coupling between antiferromagnetism (PEEM images, top) and ferroelectricity (PFM images, bottom).

Electrical Control of Ferromagnetism: The next question is this: can we control ferromagnetism with an electric field? In order to explore this, we use two types of heterostructures in conjunction with a variety of probes, including conventional magnetic measurements, photoemission based spectromicroscopy.

Exchange bias coupled ferromagnet-multiferroic heterostructures: To address the issue that emerged from our studies of the vertical nanostructures, we begain exploring heterostructures that involved exchange coupling between a ferromagnet and an antiferromagnet, i.e., the well-known Mikeljohn-Bean coupling,[20] with the key difference being the use of a ferroelectric antiferromagnet (i.e., a multiferroic) instead of an ordinary antiferromagnet. Within this framework, we are exploring two broad classes of heterostructures. One consists of a conventional ferromagnet (CoFe) in contact with BFO and the other is an epitaxial heterostructure consisting of an oxide ferromagnet ($SrRuO_3$, $La_{0.7}Sr_{0.3}MnO_3$) and BFO.

We use two types of electromagnetic coupling phenomena that are manifested in heterostructures consisting of a ferromagnet in intimate contact with the multiferroic $BiFeO_3$. The first is an internal, magnetoelectric coupling between antiferromagnetism and ferroelectricity in the $BiFeO_3$ film that leads to electric-field control of the antiferromagnetic order. The second is based on exchange interactions at the interface between a ferromagnet ($Co_{0.9}Fe_{0.1}$) and the antiferromagnet (**Fig. 4a** and **b**). We have discovered a one-to-one mapping of the ferroelectric and ferromagnetic domains, mediated by the collinear coupling between the magnetization in the ferromagnet and the projection of the antiferromagnetic order in the multiferroic (**Fig. 5**). Our preliminary experiments reveal the possibility to locally control ferromagnetism with an electric field[21].

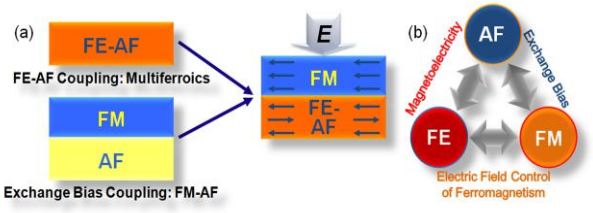

Fig 4: Schematics illustrating the design algorithm for gaining electrical control of ferromagnetism. (a) By combining multiferroics together with traditional ferromagnets, we can create heterostructures that might have new functionalities.

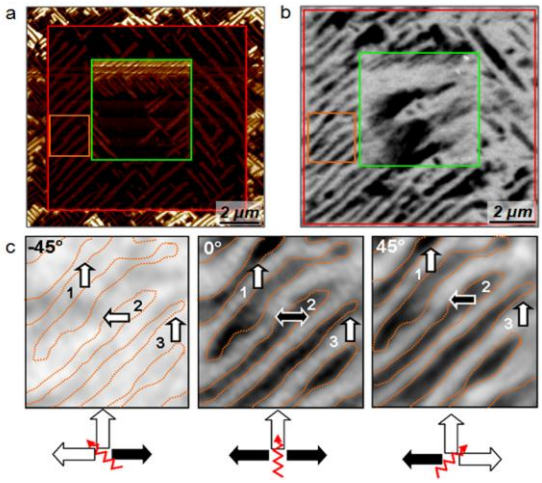

Fig. 5: **a**, In-plane PFM image showing the ferroelectric domain structure of a BFO film with a large (10 μm, red square) and small (5 μm, green square) electrically switched region. **b**, Corresponding XMCD–PEEM image taken at the Co L-edge for a CoFe film grown on the written pattern. Direct matching of domain structures is evident. Black contrast is interpreted as a spin pointing side-to-side in the image and grey as spin pointing up. **c**, Rotation of the sample in reference to the incoming right-circularly polarized light enables full determination of the nature of magnetism in the CoFe layer.

Magnetotransport at Ferroelectric domain walls in multiferroics: An exciting area of research that is emerging is that associated with the electronic structure and magnetism at domain walls. Our preliminary work has revealed two important and totally unexpected directions. First, we have discovered that specific types of ferroelectric domain walls can exhibit electronic conduction. These domain walls (mainly 180° and 109° type) can be created during growth or artificially using an atomic force microscope to write domain patterns. The origin of conduction is yet to be fully elucidated. Preliminary density functional theoretical work (in collaboration with Spaldin) suggests the origin to be a change in the band gap at the domain wall. In future work, we plan to explore this further with a combination of magnetotransport and optical measurements. In parallel studies, we have discovered that the magnetic interactions of a ferromagnet depend critically on the ferroelectric domain structure of the BFO. In our future work, we plan to carry out a comprehensive study of the magnetotransport properties of such domain walls, coupled with careful structural studies of the atomic structure of the domain wall as well as theoretical models of the electronic structure of the wall and how it influences transport and magnetism at the wall.

Coupling across multiferroic-ferromagnet interfaces: Our work so far has shown a lot of promise in using a ferromagnet (CoFe)-BFO heterostructure to study electric field control of ferromagnetism. However, research is still in the early stages. Our immediate goals are to explore the role of BFO orientation and domain structure on the coupling behavior. Our prior work has already demonstrated exquisite control over the BFO domain structure through proper choice of substrate orientation (for example, $SrTiO_3$ [100], [110] and [111]) and vicinality. A topic of considerable interest to us is the electronic structure as well as coupling across hetero-interfaces. As we outlined in the original version of this proposal, oxide interfaces are rapidly becoming an exciting and emerging field, with the potential to create new states of matter. Preliminary work has discovered the existence of strong magnetic interactions between an oxide ferromagnet (LSMO) and antiferromagnetic BFO. In our future work, we plan to pursue this with a combination of controlled epitaxial growth and photoemission spectromicroscopy. Preliminary theoretical modeling suggests the exciting possibility of orbital ordering in the LSMO layer at this interface

New multiferroics through epitaxial stabilization: An area of research that we have been pursuing in collaboration with Schlom is epitaxial stabilization as a route to create new multiferroics. We are working on two complementary systems: (i) epitaxially stabilized $FeTiO_3$; (ii) epitaxially stabilized $PbFeO_3$ (the lead analog of BFO); (iii) epitaxially stabilized tetragonal version of $BiFeO_3$. In the case of $FeTiO_3$, DFT calculations by Fennie[22] and co-workers has indicated the possibility of stabilizing a ferroelectric state through heteroepitaxial strain to complement the ferromagnetic state that already exists in this system. We have carried out preliminary experiments in this direction. However, clear indications for the onset of a piezoelectric order parameter is still lacking. We plan to use a combination of optical SHG coupled with XLD-PEEM to address this issue. Our approach will be to use epitaxial strain to stabilize the perovskite phase through a careful selection of the appropriate substrate material.

References:

[1] R. Ramesh and N. A. Spaldin, *Nature Mater.* **6,** 21 (2007).
[2] Y.-H. Chu, L. W. Martin L W, M. B. Holcomb, and R. Ramesh, *Mater. Today* **10**, 16 (2007).
[3] H. Schmid, *Ferroelectrics* **162,** 665 (1994).
[4] M.Fiebig, 2005 *J. Phys. D* **38** R123.
[5] G. A. Smolenski and I. E Chupis, *Sov. Phys. Usp.* **25**, 475 (1982).
[6] S.-W. Cheong and M. Mostovoy, *Nature Mater.* **6**, 13 (2008).
[7] W.Eerenstein, N.D.Mathur, and J.F.Scott 2006 *Nature* **442** 759.
[8] N.A.Hill 2000 *J. Phys. Chem.* **104** 6694.
[9] J.Wang, J.B.Neaton, H.Zheng, V.Nagarajan, S.B.Ogale, B.Liu, D.Viehland, V.Vaithyanathan, D.G.Schlom, U.V.Waghmare, N.A.Spaldin , K.M.Rabe, M.Wuttig, and R.Ramesh, *Science* **299** 1719 (2003).
[10] V.R.Palkar, J.John, and R.Pinto, *Appl. Phys. Lett.* **80** 1628 (2002).
[11] Y.H.Lee, C.C.Lee, Z.X.Liu, C.S.Liang, and J.M.Wu, *Electrochem. Solid-State Lett.* **8** F55 (2005).
[12] R.R.Das, D.M.Kim, S.H.Baek, F.Zavaliche, S.Y.Yang, X.Ke, S.K.Streiffer, M.S.Rzchowski, R.Ramesh, and C.B.Eom, *Appl. Phys. Lett.* **88** 242904 (2006).
[13] S.Y.Yang, F.Zavaliche, L.Mohaddes-Ardabili, V.Vaithyanathan, D.G.Schlom, Y.J.Lee, Y.H.Chu, M.P.Cruz, T.Zhao, and R.Ramesh, *Appl. Phys. Lett.* **87** 102903 (2005).
[14] R. Ueno, S.Okaura, H.Funakubo, and K.Saito, *Jpn. J. Appl. Phys.* **44** L1231 (2005).
[15] S.K.Singh, Y.K.Kim, H.Funakubo, and H.Ishiwara, *Appl. Phys. Lett.* **88** 062502 (2006).
[16] J.Wang, H.Zheng, Z.Ma, S.Prasertchoung, M.Wuttig, R.Droopad, J.Yu, K.Eisenbeiser, and R.Ramesh, *Appl. Phys. Lett.* **85** 2574 (2004).
[17] W. Tian, V.Vaithyanathan, D.G.Schlom, Q.Zhan, S.Y.Yang, Y.H.Chu, and R.Ramesh, *Appl. Phys. Lett.* **90** 172908(2007).
[18] T.Zhao, A.Scholl, F. Zavaliche, K. Lee, M.Barry, A.Doran, M.P.Cruz, Y.H.Chu, C.Ederer, N.A.Spaldin, R.R.Das, D.M.Kim, S.H.Baek, C.B.Eom, and R.Ramesh, *Nature Mater.* **5** 823 (2006).
[19] D.Lebeugle, D.Colson, A.Forget, M.Viret, A.M.Bataille, and A.Gukasov, condmat arXiv:0802.2915 (2008).
[20] J. Nogués and I. K. Schuller, *J. Magn. Magn. Mater.* **192**, 203 (1999).
[21] Y.H.Chu, L.W.Martin, M. Holcomb, M. Gajek, S.Han, Q.He, N.Balke, C.H.Yang, D.Lee, W.Liu, Q.Zhan, P.Yang, A.F. Rodriguez, A. Scholl, S. Wang and R. Ramesh, *Nature Materials*, **7**, 478(2008).
[22] C.Fennie, *Phys. Rev. Lett.* **100**, 167203 (2008).

MOCVD Grown Ternary Rare-Earth Oxide as an Alternate Gate-Oxide and Buffer Layer for Logic and Memory Devices

R. Thomas and R.S. Katiyar
etreji@yahoo.com; rkatiyar@uprrp.edu
Department of Physics and Institute for Functional Nanomaterials, University of Puerto Rico, San Juan, P.O. Box 23343, PR 00931, USA.

New dielectric materials with sufficiently high dielectric constant (high-k), large band gap, stability in contact with silicon and reasonable conduction/valance and offset with Si are urgently needed by the industry to replace SiO_2/SiON in the future CMOS technology with a sub-nanometer equivalent oxide thickness [1]. The oxides of Zr, Hf, and their silicates are widely considered as candidates for high-k materials [2,3]. While not disclosed; the most probable dielectric used, in the present day processors, is a form of nitrided hafnium silicates (HfSiON) [4]. However, its maximum dielectric value is merely ~14 and even it is susceptible to trap-related leakage currents which tend to increase with stress and that make it unsuitable as future high-k dielectric. A close look at the three different generations of gate-oxides, i) SiO_2, ii) SiON and iii) HfSiON reveals the success mainly due to the presence of Si in these dielectric materials, which maintained the overall MOSFET performances due to the perfect interface between Si and gate-oxide. So the real challenge is integrating a Si free gate-oxide on Si without compromising the transistor performance. In short, during the 40 years of CMOS technology, gate-oxides with dielectric constant in the range 3.9 to 14 (SiO_2, SiON to HfSiON) had been successfully used from technology node to another. But in order to set the target further another class of dielectrics with even higher dielectric constant (k~20-40) and lower leakage current and hysteresis are of great interest. With this purpose ternary oxides in the amorphous state are being considered as next generation dielectrics. We have therefore developed MOCVD routes to ternary dysprosium scandate ($DyScO_3$) deposition and its gate-oxide applications were studied.

For almost 40 years, the electronics industry has been searching for a universal memory that is fast, flexible, scalable, low-power, non-volatile and cheap to make. Ferroelectric Random Access Memory (FeRAM) is a non-volatile memory offering high-speed writing, low power consumption and long rewriting endurance, was one of the findings of that search [5,6]. It started off with a great promise, a couple of generations behind mainstream dynamic random access memory (DRAM) and flash memory. However, the manufacturing difficulties to scale up the densities still a problem to circumvent [7]. At present, DRAM and flash surged into the gigabit era, while ferroelectric memory makers still struggle to get above a megabit. The structure of FeRAMs is very similar to DRAMs except that a ferroelectric layer replaces the dielectric layer of the DRAMs and FeRAMS can be fabricated using similar processes as for DRAMs. The integration of 2-D ferroelectric capacitors with CMOS transistors, with the capacitor being located on the side of the transistor area is the main reason for the low-density FeRAM. The reason for this is the requirement for having a larger ferroelectric capacitor size to distinguish the off and on state signal by the sensor. Currently, the industry is looking ahead to the development of high density (≥ 1 MB) FeRAMs, which requires ferroelectric capacitor on top of the transistor via connection to the drain, to produce the nanoscale FeRAMs that will revolutionize the memory market. The high-density FeRAMs will require at least scaling the size of the ferroelectric capacitors to less than 100 nm in diameter. However, for such small dimensions, the polarization in a nanosized ferroelectric capacitor might not be enough to provide a suitable signal for a memory device. Therefore, the consensus in the community performing research on FeRAMs is that the high-density FeRAM architecture will need to feature 3-D capacitors in order to increase the area and the polarization needed to retain signal strength. However, it is challenging to develop 3-D ferroelectric films with conformality (i.e., uniform film thickness around the high-aspect ratio of the 3-D structure) and hence FeRAM 3-D capacitor technology for high-density are not considered rigorously. Another configuration which can be considered for the high density FeRAM is the one transistor. Since the 1T FeRAM consists of only one ferroelectric gate field-effect transistor (FET), the area required for one bit memory cell is extremely small, can be scaled down using the proportionality rule and thus hyper-advanced level of integration to obtain Gbit NVRAM can be achieved. In other words, it offers scope for capacity expansion compared to the conventional (1T-1C) FeRAM which has no

room for further capacity expansion without changing from 2D to 3D capacitors. The idea of 1 T-FeRAM is not new, but the interface between ferroelectric and silicon is a matter of concern [8]. The main reason behind problem is the high deposition temperature and oxidizing atmosphere required for the ferroelectric oxide thin film growth as it promote interdiffusion into silicon and vice versa. This accelerates fatigue and imprint which ultimately results in device failure. The insulating buffer layer that prevents interdiffusion between the components of the ferroelectric material and the Si substrate is then tried and the resulting structure is known as Metal-Ferroelectric-Insulator-Semiconductor (*MFIS*) structure [9]. However, insulating buffer layer has some disadvantage *viz.* generation of depolarization field in the ferroelectric film and increase of the operation voltage by weakening the electric field across the ferroelectric layer. To overcome these disadvantages, it is important to find a

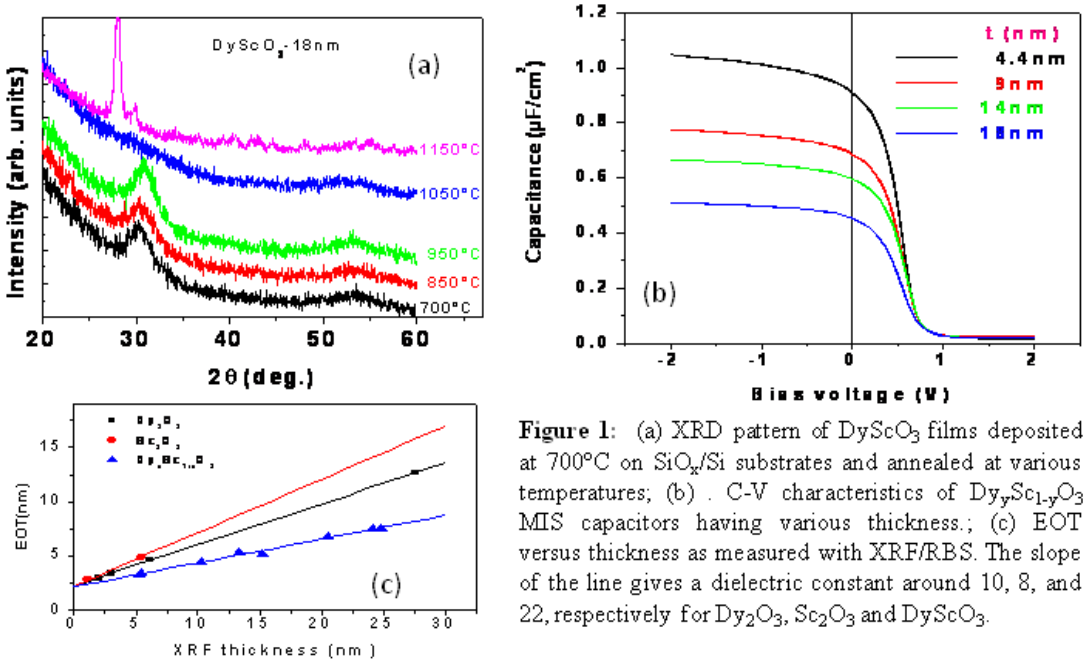

Figure 1: (a) XRD pattern of $DyScO_3$ films deposited at 700°C on SiO_x/Si substrates and annealed at various temperatures; (b) . C-V characteristics of $Dy_ySc_{1-y}O_3$ MIS capacitors having various thickness.; (c) EOT versus thickness as measured with XRF/RBS. The slope of the line gives a dielectric constant around 10, 8, and 22, respectively for Dy_2O_3, Sc_2O_3 and $DyScO_3$.

ferroelectric with low ε_r (compared to normal ferroelectrics) and an insulating buffer layer with high ε_r (compared to $\varepsilon_r = 3.9$ of SiO_2). Various materials *viz.* $LaAlO_3$, SiN, HfO_2, HfAlO etc. have been studied as buffer layers in the *MFIS* structures and coincidently, these materials are widely studied as an alternate high-k gate-oxide in metal-insulator-silicon (*MIS*) to replace conventional SiON dielectric in the sub-micron technology node. So the gate-oxide may be the ideal choice as a buffer layer due to the fact that, the interface between Si and the ferroelectric is the main concern in reliable device applications. Recently, a novel gate dielectric material, $DyScO_3$ (DSO) was considered and studies indicated that the films of this material on Si remained amorphous even at 1000°C annealing condition [10]. Considering the requirements of dielectric constant, electrical stability for high-*k* buffer layers, DSO seems to be promising as the buffer layer for *MFIS* structures for non-volatile memory applications, hence considered for the BNT and BFO integration with silicon.

Thin films were grown in an AIXTRON 2600G3 Planetary Reactor®, which has been described elsewhere [2]. The composition of the films was routinely determined by x-ray fluorescence (XRF) and additionally checked with Rutherford back scattering (RBS). Surface morphology and microstructure were investigated with atomic force microscopy (AFM) and x-ray diffraction (XRD) and high resolution transmission electron microscopy (HRTEM). Ferroelectric $Bi_{3.25}Nd_{0.75}Ti_3O_{12}$ and multiferroic $BiFeO_3$ thin films were prepared by chemical solution deposition on $DyScO_3$ (4nm)/Si substrates using spin coating at 2500 rpm for 30 s. After each coating the films were pyrolysed at 400°C. Multiple coatings were carried to get the desired thickness and finally the films were annealed at 700°C in air to ensure crystalline phase formation. Electrical tests of the MIS capacitors were done with sputter deposited Pt top electrodes after forming gas annealing of the completed gate stack at 450° C. For films deposited at 700°C, the grazing-incidence x-ray diffraction patterns show that the simple oxides Dy_2O_3, Sc_2O_3 crystallize into cubic structures, whereas the mixed oxide $DyScO_3$ films were amorphous, Fig.1. Nevertheless, we observe a broad peak around 30°, which indicates some short-range

order, which is consistent with the HRTEM studies. Under annealing in purified nitrogen this amorphous structure is stable for up to 1050°C. The post deposition annealing in oxygen also preserved the amorphous structure up to a temperature of about 950°C. Remarkably, the annealing at 1050°C resulted in nearly complete disappearance of the broad peak around 30°, however, crystalline peaks were observed only after annealing at higher temperatures, 1150°C in Fig.1a.

The surface morphology of the films was studied by AFM. A smooth, thickness independent (4-20 nm) surface morphology of the films with a rms roughness of ~0.1 nm was achieved when Dy/Sc~1. Post deposition annealing up to 950°C did not increase surface roughness in line with the XRD observation of the stability of the amorphous phase. Well behaved C-V curves without any hysteresis were observed over wide ranges in thickness and stoichiometry, Fig.1b. To extract the dielectric constant of the dysprosium scandate the capacity in accumulation was determined from C-V curves for films with different thickness. Fig.1c depicts the obtained EOT vs. physical thickness. This thickness was deduced from the atomic mass density of Dy and Sc directly obtained with XRF/RBS. The dielectric constant of the film is indicated as determined from the slope of the lines, which gave dielectric constant around 10, 8, and 22, respectively for Dy_2O_3, Sc_2O_3 and $DyScO_3$. I-V characteristics showed very promising leakage behaviour, e.g., leakage current at -1V was less 10^{-6} A/cm^2 for a 5 nm thick film and for thicker film it was even lower ($<10^{-8}$ A/cm^2). All these properties of $DySCO_3$ is promising for the gate-oxide application.

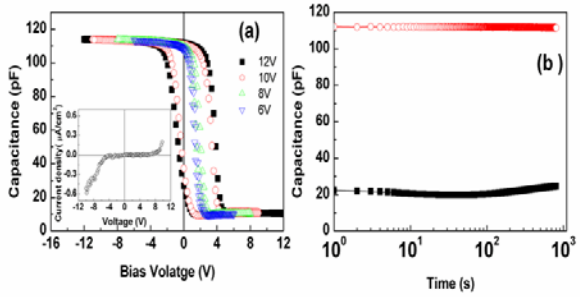

Figure 2 *(a) CV hysteresis at 1MHz of Pt/BNT/DSO/Si MFIS when cycled between various bias voltages (±12, ±10, ±8, and ±6 V); Inset shows current density vs. voltage characteristics of the same. (b) Results of the retention tests showing the capacitance at zero gate bias after poling the sample with a bias voltage pulse of ±12 V for 100s.*

Next we tried the $DyScO_3$ buffer layer to realize ferroelectric (BNT)/multiferroic (BFO) integration with Si for the non-volatile memory application. When the MFIS capacitor is cycled between ± V (with $V >> V_c$), the polarization switching introduces a clock-wise hysteresis in the CV curves for a p-type semiconductor and counterclock-wise hysteresis in the case of n-type semiconductor. Fig.2a shows the clock-wise CV hysteresis in the case of Pt/BNT/DSO/p-Si MFIS structures at different bias voltages. This suggests the ferroelectric nature of the BNT film on amorphous $DyScO_3$ buffer layer. The memory window is the difference between the flatband voltages, which was extracted by using Schroder method. In the present case, ΔV_{FB} reaches a maximum value of 4.0 V when the sweep voltage was 12V and saturated thereafter. The observed memory window was higher than the reported ΔV_{FB} ~ 0.9V of Pt/$(Bi,La)_4Ti_3O_{12}$/HfO_2/Si MFIS structures. As can be seen from the inset of Fig. 2a, the current density was of the order of 10^{-6} A/cm^2 at -12V. The retention measurements were performed by applying ±12V for 100s to set the on or off state. Figure 2b shows the results of the retention measurements on the present MFIS device. The capacitance change was very small upto 1000 s. The excellent data retention may be due to the low leakage current and improved interfacial quality between DSO and Si, which can effectively prevent the charge injection from the Si substrate to the BNT film.

Summarizing, dysprosium scandate was deposited as thin amorphous film by MOCVD for the first time. This film showed promising properties as a high-k gate oxide material. Structural stability with annealing, high dielectric constant, negligible hysteresis, very smooth surface morphology all seems good for this exotic material. But challenges remain as EOT scaling is required and we try to deposit at lower temperatures to avoid the SiO_2 formation between the high-k and Si. With new precursors and engineered Si substrates one can expect even better result with this material. Polycrystalline $BiFeO_3$, and $Bi_{3.25}Nd_{0.75}Ti_3O_{12}$ thin films were prepared by chemical solution. The buffer $DyScO_3$ layer does not have much influence on the crystalline structure of the deposited

FE or MF films. The surfaces of the films were smooth without any cracks and showed distribution of grains of varying sizes. $DyScO_3$ buffer layer between Si and FE/MF layers resulted in the leakage current reduction. A large memory window of about 4.0V was obtained and the structures showed excellent data retention due to low leakage current and improved interfacial quality between $DyScO_3$ film and Si.

Acknowledgement:

The Financial support from DOE-EPSCoR Grant #DE-FG02-08ER46526 is gratefully acknowledged.

References:

[1] Process Integration, Devices, and Structures, *International Technology Roadmap for Semiconductors: 2006 Update*. http://www.itrs.net

[2] R.Thomas, R.Bhakta, A.Milanov, U.Patil, A. Devi and P. Ehrhart, Chem. Vap. Dep. **13**, 98 (2007).

[3] R.Thomas, E.Rije, R.Bhakta, A.Milanov, U.Patil, A. Devi, Ehrhart and R.Waser, J. Elec. Chem. Soc, **154** G77 (2007).

[4] G. Moore "Biggest change in transistor technology in 40 years" http://www.intel.com.

[5] J. F. Scott and C. A. Paz de Araujo, Science **246,** 1400 (1989).

[6] J.F. Scott, Science, **315,** 954 (2007).

[7] O. Auciello and C. M. Foster, Annual Review of Materials Science, **28,** 501 (1998).

[8] D.R. Lampe, D.A. Adams, M. Austin. M. Polinsky. J. Dzimianski. S. Sinharoy, H. Buhay, P. Brabant and Y.M. Liu, Ferroelectrics **133**, 61 (1992).

[9] K. Siguchi, Y. Kurogi, and N. Endo, *J. Appl. Phys*. **46**, 2877 (1975).

[10] R . Thomas, P .Ehrhart, M.Luysberg, M .Boese, R .Waser, M .Roeckerath, E .Rije, J. S chubert, S.Van Elshocht and M.Caymax, J. Electrochemical Soc., **154**, G147 (2007).

*[11] N.M.Murari, R. Thomas, A.Winterman, R.E. Melgarejo, S.P. Pavunny and R. S. Katiyar, J. Appl. Phys, **106**, 014103 (2009)*

*[12] N.M. Murari, R. Thomas, A. Winterman, R.E. Melgarejo, S.P. Pavunny and R.S. Katiyar, J. Appl. Phys. **105**, 084110 (2009).*

*[13] R. Thomas, Ricardo E. Melgarejo, Dillip K. Pradhan, Naba K. Karan, Jose J. Saavedra-Arias, and Ram S. Katiyar, ECS Transactions **13,** 363 (2008).*

*[14] N. M. Murari, R. Thomas, S. P. Pavunny, J. R. Calzada, and R. S. Katiyar, Appl. Phys. Lett., **94**, 142907 (2009)*

[15] R. Thomas, R.E. Melgarejo, N.M. Murari, S.P. Pavunny, R.S. Katiyar, Solid State Communications (2009) doi:10.1016/j.ssc.2009.08.032

*[16] R. Thomas, J.J. Saavedra-Arias, N.K. Karan, N.M. Murari, R.S. Katiyar, P. Ehrhart, R. Waser, Solid State Communications **147**, 332 (2008)*

Poster Session

IVc. Thin Films

V. Soft and Hybrid Materials

(This page intentionally left blank.)

Demonstration of Coherent Thermal Emission in Multilayer Structures

Zhuomin Zhang zhuomin.zhang@me.gatech.edu
George W. Woodruff School of Mechanical Engineering
Georgia Institute of Technology, Atlanta, GA 30332

Program Scope

Controlling the directional and spectral properties of thermal radiation has important applications in aeronautics and astronautics, as well as in solar energy harvesting and infrared sensing. A large number of recent publications have dealt with enhanced transmission and emission properties in nanostructures by the excitation of surface plasmon and surface phonon polaritons, usually in grating structures. Likewise, there exist numerous publications on the fabrication of complicated photonic crystal (PC) structures. However, relatively few studies have been done on the effect of surface waves at the interface between a PC and another material. The aim of this project is to demonstration controlling thermal radiative properties, particularly with thin-film multilayer structures.

Recent Progress (references are according to the list of publications)

Recently, we have demonstrated coherent thermal emission using a multilayer structure consisting of a one-dimensional photonic crystal (1D PC) coated on a silver layer [2,7]. The left of Fig. 1 shows the fabricated PC-on-Ag structure. The sample fabrication started with sputtering a Ag film on a Si substrate with a Ti adhesive layer. Then, the truncated PC with six unit cells was formed on the Ag film using plasma-enhanced chemical vapor deposition of SiO_2 and Si_3N_4 layers. The Ag layer is much thicker than its radiation penetration depth, so that it can be assumed to be semi-infinite, i.e., opaque. Therefore, the adhesive Ti layer and the Si substrate do not affect the radiative properties of the PC-on-Ag structure. The thicknesses were obtained from fitting the reflectance dip wavelengths as follows: $d_1 = d_2 = 153$ nm and $d_t = 100$ nm (i.e., the surface termination layer). A Fourier-transform infrared (FTIR) spectrometer was used to measure the spectral reflectance at incidence angles of 10°, 30°, and 45°. In addition, a laser scatterometer was employed to measure the angle-resolved reflectance at the wavelength of 891 nm. The emissivity calculated from the measured reflectance exhibits temporal and spatial coherence. The key to enabling coherent emission is by exciting a surface wave at the PC-Ag interface in the stop band of the PC. As shown on the right of Fig. 1, the experimentally obtained resonance conditions matches closely with the dispersion relation calculated using a supercell method. Along with the dispersion curves also confirms the existence of surface waves where the field is highly localized near the PC-Ag interface. These findings demonstrate the feasibility of constructing coherent emission sources based on truncated 1D PC and may be used to improve the design of wavelength-selective coatings for future space flights and satellites.

We have also fabricated asymmetric Fabry-Perot resonance cavities and observed spatial and temporal coherence of thermal radiation using the FTIR and laser scatterometer. The structures are composed of a SiO_2 optical cavity with a thin Au film (< 30 nm) and a 200-nm Au film deposited on a Si substrate, as shown in Fig. 2a. The spectral measurement demonstrates

sharp reflectance dips (see Figs. 2b&c), while narrow angular lobes are observed in the angle-resolved measurement (see Fig. 2d). Experimental results suggest strong spectral and directional selectivity in thermal emission, which is related to the reflection by Kirchhoff's law since the samples are opaque. Theoretical calculations with the fitting geometric parameters agree well with the measurement results. This easy-to-fabricate structure has potential applications in solar cells, thermophotovoltaic devices, and radiation emitters. Details can be found from Ref. [8].

Recent Progress on Other Projects

It is well known that when the gap between two surfaces are less than the characteristic wavelength, thermal radiation can be greatly enhances due to photon tunneling and Planck's law of blackbody radiation does not apply. Tunneling has been thought as a quantum mechanical effect and the direction of energy propagation cannot be determined. Photon tunneling can also be understood as the coupling (interference) of a forward and backward evanescent waves. We have combined the fluctuational electrodynamics with the energy streamline method, based on the Poynting vectors, to explain the energy propagating in nanoscale thermal radiation. The key is that the evanescent waves with different magnitude of the parallel wavevector component are de-coupled in the case of thermal radiation, contrary to diffraction optics where all evanescent waves are coupled coherently. The de-coupling of evanescent waves discovered in this study allows the authors to demonstrate that, in the near-field regime, the energy pathways are curved and the photon energy propagates in infinite directions for thermal radiation due to the nature of random fluctuation [1,5]. Recently, we have studies the maximum near-field radiative transfer between two parallel plates separated by a vacuum gap from 0.1 to 100 nm [9]. By assuming a frequency-independent dielectric function and introducing a cutoff parallel wavevector component, we find the ideal dielectric function for the two media which will maximize the near-field radiative transfer is $-1+i\delta$, where δ is the imaginary part. For vacuum gaps greater than 1 nm, the near-field heat transfer peaks when $\delta << 1$, while at sub nanometer gaps, the peak in the energy transfer shifts towards larger values of δ. The determination of the maximum radiative flux at nanometer distances will benefit emerging applications of near-field radiation for energy harvesting and nanothermal manufacturing.

More recently, we investigated the use of metamaterial for tailoring the radiative properties. Coherent thermal emission can be achieved in the infrared region by exciting magnetic polaritons between metallic gratings and an opaque metallic film, separated by a dielectric spacer [4]. The coupling of the metallic strips and the film induces a magnetic response that is characterized by a negative permeability and positive permittivity. On the other hand, the metallic film intrinsically exhibits a negative permittivity and positive permeability in the near infrared. This artificial structure is equivalent to a pair of single-negative materials. By exciting surface magnetic polaritons, large emissivity peaks can be achieved at the resonance frequencies and are almost independent of the emission angle. The resonance frequency of the magnetic response can be predicted by an analogy to an inductor and capacitor circuit. We also found that magnetic polaritons can be used to quantitatively explain the resonance transmission or absorption in deep gratings. This subject has been extensively studied in the past decade and several explanations existed in the literature such as the interference or diffraction of evanescent waves, Fabry-Perot-like resonance, cavitylike resonances, coupled surface plasma polaritons. We have numerically shown that magnetic polaritons are responsible foe the cavitylike resonance.

Future Plan

We have finished the design and procurement of components for a high-temperature emissivity measurement facility (emissometer). We are in the process of testing the components and assembling the system, as well as preparing samples for the direct emissivity measurements. This has been a challenging experiment and we should be able to obtain direct measurements of the emissivity at elevated temperatures by the end of 2009.

Some samples have already been fabricated and we will study the temperature effect as well as thermal and mechanical stability of the samples. For example, we need to study the annealing effect and interface stability at high temperatures for the silicon dioxide and nitride film samples. We will also investigate different materials combinations and thickness effects.

We will continue to study the near-field radiative transfer mechanisms for energy conversion applications, as well as radiative properties in various nanostructures, including periodic gratings and including magnetic responses.

List of Publications Supported by the DoE Contract (additional five accepted not listed)

1. B.J. Lee, K. Park, and Z.M. Zhang, "Energy Pathways in Nanoscale Thermal Radiation," *Appl. Phys. Lett.* **91**, 153101 (2007).
2. B.J. Lee, Y.-B. Chen, and Z.M. Zhang, "Surface Waves Between Metallic Films and Truncated Photonic Crystals Observed with Reflectance Spectroscopy," *Opt. Lett.* **33**, 204 (2008).
3. K. Park, S. Basu, W.P. King, and Z.M. Zhang, "Performance Analysis of Near-Field Thermophotovoltaic Devices Considering Absorption Distribution," *J. Quant. Spectrosc. Radiat. Transfer*109, 305 (2008).
4. B.J. Lee, L.P. Wang, and Z.M. Zhang, "Coherent Thermal Emission by Excitation of Magnetic Polaritons between Periodic Strips and a Metallic Film," *Opt. Exp.* **16**, 11328.
5. B.J. Lee and Z.M. Zhang, "Lateral Shift in Near-Field Thermal Radiation with Surface Phonon Polaritons," *Nanos. Micros. Thermophys. Eng.* **12**, 238 (2008).
6. Q. Li, B.J. Lee, Z.M. Zhang, and D.W. Allen, "Light Scattering of Semitransparent Sintered Polytetrafluoroethylene Films," *J. Biomed. Opt.* **13**, 054064 (2008).
7. B.J. Lee and Z.M. Zhang, "Indirect Measurements of Coherent Thermal Emission from a Truncated Photonic Crystal Structure," *J. Thermophys. Heat Transfer* **23**, 9 (2009).
8. L.P. Wang, B.J. Lee, X.J. Wang, and Z.M. Zhang, "Spatial and Temporal Coherence of Thermal Radiation in Asymmetric Fabry-Perot Resonance Cavities," *Int. J. Heat Mass Transfer* **52**, 3024 (2009).
9. S. Basu and Z.M. Zhang, "Maximum Energy Transfer in Near-Field Thermal Radiation at Nanometer Distances," *J. Appl. Phys.* **105**, 093535 (2009).
10. X.J. Wang, J.D. Flicker, B.J. Lee, W.J. Ready, and Z.M. Zhang, 2009, "Visible and Near-Infrared Radiative Properties of Vertically Aligned Multi-Walled Carbon Nanotubes," *Nanotechnology* **20**, 215704 (2009).

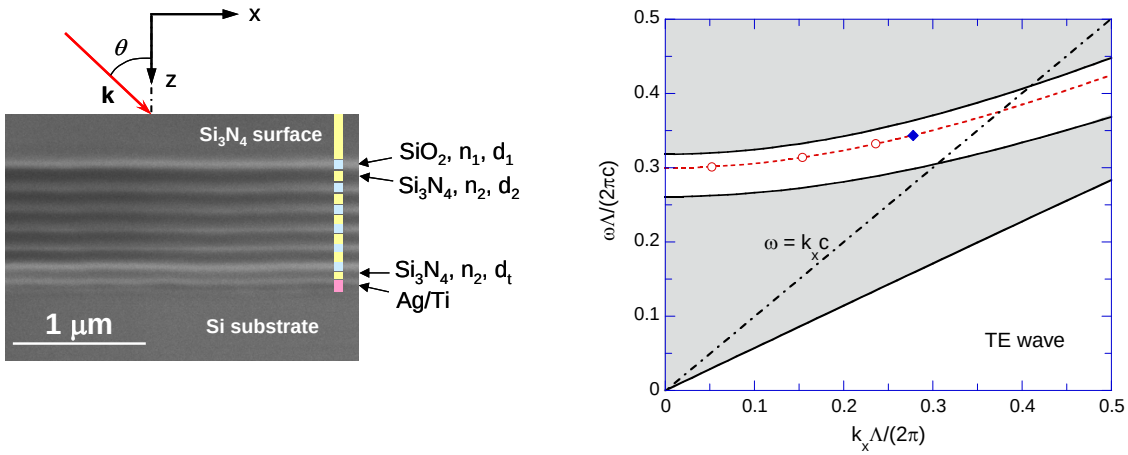

Fig. 1. (Left) Focused-ion-beam image of the fabricated PC-on-Ag structure. (Right) Band structure of the PC and the dispersion curve (dashed line) calculated from the supercell method for transverse-electromagnetic (TE) waves.

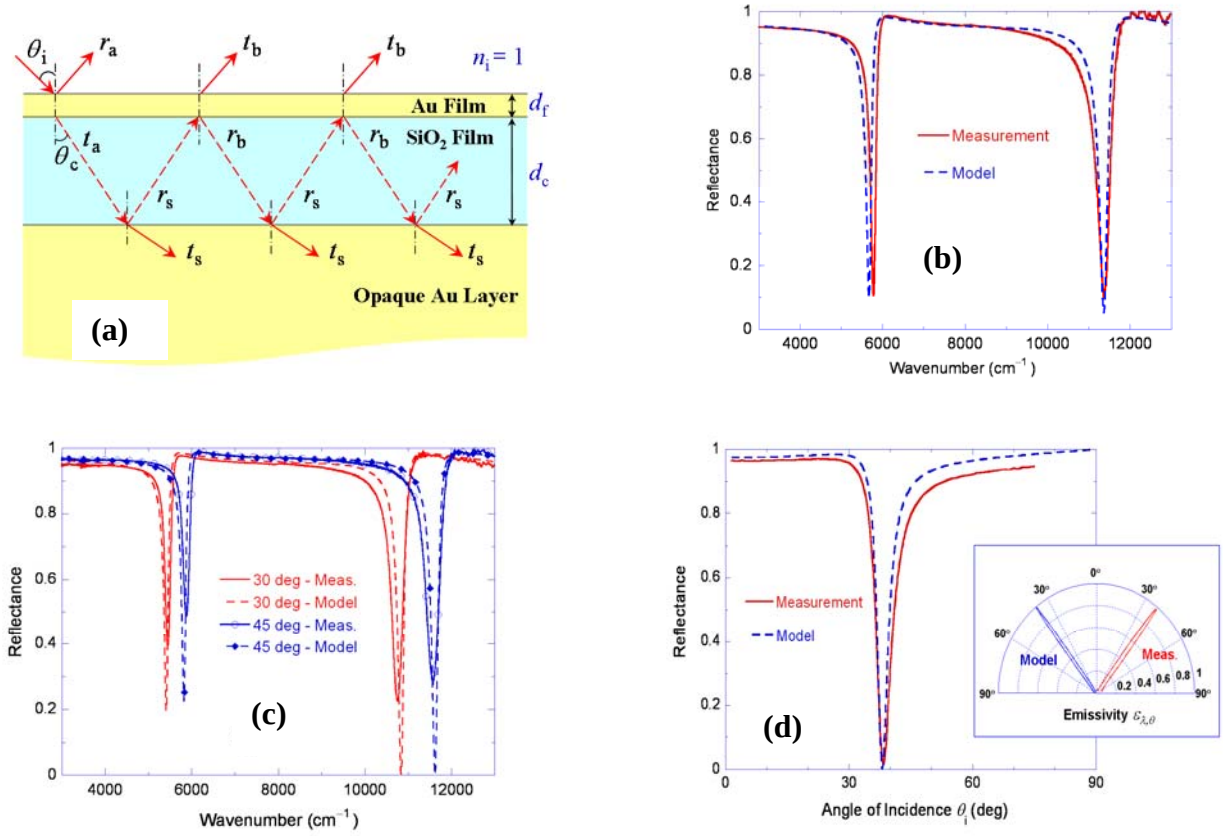

Fig. 2. Illustration of coherent emission from asymmetric Fabry-Perot structures: (a) schematic of the structure; (b) normal reflectance; (c) TE-wave reflectance at 30° and 45° incidence angles; (d) angle-resolved emissivity for TE-wave.

In Situ Visualization and Theoretical Modeling of Early-Stage Oxidation of Metal and Alloys

Guangwen Zhou[1], Xidong Chen[2]
gzhou@binghamton.edu
[1]Department of Mechanical Engineering, State University of New York, Binghamton, NY 13902
[2]Department of Science and Mathematics, Cedarville University, OH 45314

Program Scope

A fundamental understanding of metal and alloy oxidation is of significant importance to a wide range of applications including corrosion, catalysis, fuel reactions, electrochemistry, and thin film processing. However, quantitative description of oxide growth morphologies during early stages of oxidation of metal and alloys has received little attention. This dearth of research is, in large part, due to the complexity of the dynamics of oxide growth and the inability of traditional experimental techniques to measure the structure, chemistry, and kinetics at the nanoscale as the reaction progresses, as well as a lack of a universal theoretical approach to address this issue. Power laws based on statistical mechanics and scaling analysis have been recently employed to describe non-equilibrium growth phenomena, which greatly simplify the descriptive properties of surface morphologies [1, 2]. The objective of this program is to utilize unique *in situ* microscopy techniques (*in situ* scanned probe microscopy and *in situ* transmission electron microscopy) to visualize oxide formation at a nanometer scale and below. Experimental observations will then be correlated with the theory of dynamic scaling for a quantitative understanding of the atomic processes governing the early stages of oxidation of metals and alloys.

Recent Progress

We have employed *in situ* UHV-TEM to observe the early-stage oxidation of Cu(111) surfaces and have revealed the evolution of the oxide film morphology from initially ramified islands to irregularly connected oxide clusters. The growth morphology of such discontinuous, non-compact oxide films cannot be addressed by thermodynamics, i.e., the interplay between surface/interface energies and relaxation of the elastic energy due to the metal-oxide lattice mismatch, as adopted in the epitaxial growth of 3D compact oxide islands [3-5]. In contrast, our results of scaling analysis of the geometrical features of these oxide films and kinetic Monte Carlo (KMC) simulations of the oxide film growth demonstrate that the non-compact morphologies of these discontinuous oxide films are of kinetic origin [6].

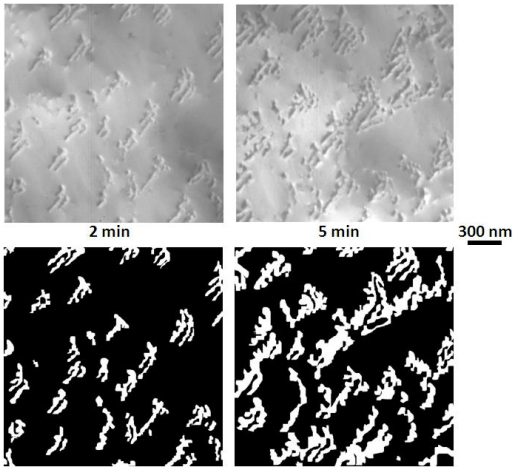

Figure 1: *In situ* TEM images of the oxide islands formed from the oxidation of a Cu(111) surface at 450°C and an oxygen pressure of pO_2=5 × 10^{-4} Tor (upper panel), and the corresponding white & black matrix (white = occupied, black = unoccupied). The images are 1024 × 1024 lattice units (lower panel).

Figure 1 shows representative images from *in situ* TEM observations of the morphological evolution of the oxide film during the oxidation of Cu(111) at 450°C under pO_2 = 5×10^{-4} Torr. When oxygen is introduced, Cu_2O islands nucleate rapidly and form a "discontinuous-branched" shape. Further oxidation results when these Cu_2O islands coalesce to create irregularly connected oxide clusters. Figure 1 reveals that these oxide islands have ramified morphologies, grow into each other, and form a percolating network as the oxidation progresses. These discontinuous, non-compact oxide films are irregularly shaped. They look like tree branches with stringy boundaries and certainly are not describable in terms of familiar Euclidean geometry. In order to quantitatively understand the features of the growth morphologies of the oxide films, the TEM images are digitized to a binary contrast with 1 and 0 for occupied (white) and vacant (black) sites respectively, as shown in the lower-panel images in Figure 1. The geometrical features of these non-compact oxide films are analyzed in terms of the scaling theory of percolation. Our kinetic Monte Carlo simulations reveal that the percolating oxide film growth is related to a mechanism of neighbor-dependent site percolation [6].

We have also used *in situ* TEM techniques to visualize the early-stage oxidation of Cu-Au alloys. Figure 2 is a bright-field TEM image showing how the morphology of a typical Cu_2O island evolves during oxidation of the (100) surface of Cu-15at.%Au at 600°C under 5×10^{-4} Torr oxygen partial pressure (pO_2). The selected area electron diffraction patterns reveal that regions far from the reaction front, such as *A*, have the Cu(100) face-centered cubic structure as observed prior to oxidation. The diffraction pattern from region *B* indicates that the oxide islands are single crystals that nucleate in an epitaxial orientation relationship with the substrate. The regions with dark contrast such as *C* are Au-rich and have the structure of the ordered $CuAu_3$ phase at room temperature. This phase is not observed prior to the onset of oxidation. Besides the structure characterization, this non-uniform partition of Au atoms around the dendritic oxide is also confirmed by energy dispersive spectroscopy (EDS) analysis of the alloy composition [7].

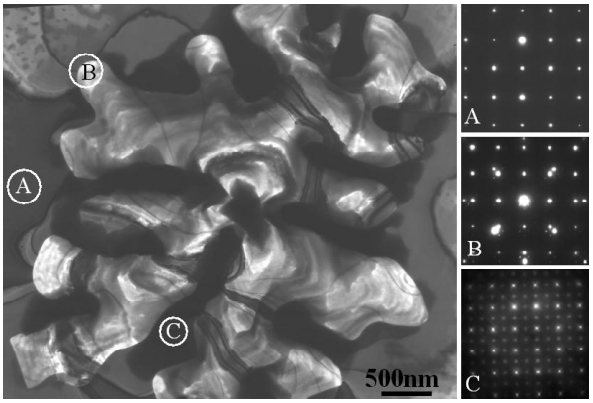

Figure 2: Typical morphology of dendritic oxide islands obtained during oxidation of Cu-15at.%Au(100) films at 600°C in pO_2= 5×10^{-4} Torr. The diffraction patterns indicate A) regions of Cu-Au solubility, B) epitaxial Cu_2O islands on single-phase Cu-Au alloy regions, C) regions where the alloy concentration has evolved as oxidation progresses, such that the $CuAu_3$ ordered phase has formed.

A gradual transition occurs from initially compact island shapes to a dendritic morphology as the islands grow (Figure 3). Oxide islands nucleate with a square shape and retain this shape during the initial growth. The islands then exhibit a gradual transition to a dendritic shape as growth slows along the direction normal to the island edges, i.e., <110> Cu_2O, while maintaining a faster growth rate along the directions of the island corners. In contrast, the oxide islands formed during oxidation of pure Cu(001) under the same conditions have an initially square shape that transforms to a rectangular morphology as growth proceeds as shown in our previous work [3]. The contrast featured in Figure 3 reveal that the alloy film regions adjacent to the island edges become Au-rich, while there is almost no excess Au accumulation in the alloy film adjacent to the island corners.

A useful quantity for characterizing complex growth patterns and establishing a relationship to the growth mechanism is the fractal dimension, D_f. Using the box-counting

method [8], we have estimated D_f of the islands at different growth stages. Our results show that the islands evolve from D_f = 2.0 to a stable value of 1.87, indicating a transition in the rate-limiting mechanism of oxidation from oxygen surface diffusion to diffusion of copper through the increasingly gold-rich regions adjacent to the islands [9].

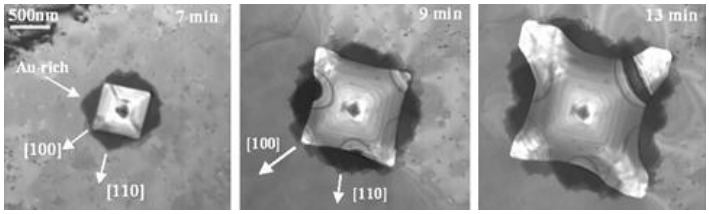

Figure 3: *In situ* TEM observation of the growth of a Cu_2O island on a Cu-5%Au(100) surface at 600°C, a crossover from the initially compact structure to dendritic growth is observed as time progresses.

Future plans

Anisotropic oxide growth behaviors have been observed during the oxidation of crystalline metals of different crystallographic orientations [10-14]. It has been speculated that these behaviors originate from the dependency of initial oxide formation on the crystallographic orientation of oxidizing metal surfaces [12, 15]. However, experimental evidence supporting this speculation has been lacking due to the inability of traditional techniques to elucidate the correlation between surface structures and initial oxide formation. Due to the insensitivity of the *in situ* TEM technique in detecting surface atomic structures, some of the information such as the structure of the oxygen chemisorbed layer on oxidizing surfaces is unavailable. We will therefore employ a recently purchased environmental UHV STM/AFM in Zhou's lab to study the oxidation of Cu surfaces. We will particularly focus on the effect of oxygen surface chemisorption on the nucleation and growth of oxide islands by determining and comparing the activation energies for oxide nucleation and growth on oxygen-chemisorbed Cu(100), (110) and Cu(111) surfaces.

We will continue the *in situ* TEM experiments and examine the effect of alloy composition and crystallographic orientation on dendritic oxide growth. Because the formation of dendritic oxide films is due to the ramification of initially compact islands, we speculate that the dendritic oxide morphology also depends on the crystallographic orientation of oxidizing Cu-Au surfaces since the shape of initially compact oxide islands is different for different substrate orientations. The correlation between the crystallographic orientation of the oxidizing surfaces and the critical island size for oxide shape transition as well as the resulting dendritic morphology of the oxide film will be established experimentally by *in situ* TEM visualization of the oxidation behavior of Cu-Au(100), (110) and (111) surfaces. Besides the alloy composition and the crystallographic orientation, we will also examine the effect of oxygen partial pressure and oxidation temperature on the morphological evolution of dendritic oxide films. We speculate that the growth of complex oxide morphology observed from Cu-Au oxidation may represent a general behavior in the oxidation of other alloy systems containing one reactive component such as Cu, Fe, etc., and one noble component, such as Au, Pd, Pt, Ag etc., which does not form stable oxides under normal conditions. Dendritic oxide growth may also occur in those alloy systems containing two reactive components, in which the oxide growth out of one alloying component can be facilitated or suppressed by the oxide formation of the other component under some oxidation conditions. To verify the above speculation, we will extend the study to other alloy systems such as Fe-Pd containing one reactive component and one noble component, and then to binary alloys containing two reactive components at a later stage of this project.

We plan to develop a kinetic model to simulate the dendritic oxide growth observed during the oxidation of Cu-Au alloys. We will test a model in which O atoms generated by a random function are added to a growing oxide island through surface diffusion. Due to their high surface mobility, oxygen atoms can wander to energetically favorable sites where they are trapped. The

probability of oxygen atoms sticking to a vacant site at the periphery of the growing island depends on the number of its occupied nearest neighbors. The more occupied nearest neighbors, the larger the probability that the vacant site will be occupied by oxygen. Our simulations will also incorporate the effect of Au segregation on the oxide growth. This can be achieved by coupling oxygen site occupation with simultaneous Au rejection from a growing oxide island to its unoccupied nearest neighbors. The probability of Au rejection from a lattice site depends on the alloy composition, which can be realized in the simulation by using a two-dimensional lattice containing two sub-lattices with their ratio corresponding to the alloy composition. The sticking probability of oxygen to a vacant site adjacent to the growing oxide island depends not only on the number of nearest neighbors occupied by oxygen atoms, but also on the number of nearest neighbors occupied by Au atoms. The larger the number of nearest neighbors occupied by Au atoms, the smaller the probability of the vacant site being occupied will be. The critical island size of the dendritic shape transition as well as the fractal dimension of the oxide film will be used as prominent structure features to make connections between experimental observations and simulations.

References

1 B. B. Mandelbrot, *The Fractal Geometry of Nature* (Freeman, San Francisco, 1982).
2 P. Meakin, *Fractals, Scaling, and Growth Far from Equilibrium* (Cambridge University Press, Cambridge, England, 1998).
3 G. W. Zhou and J. C. Yang, Phys. Rev. Lett. **89**, 106101 (2002).
4 G. W. Zhou and J. C. Yang, Applied Surface Science **210**, 165 (2003).
5 G. W. Zhou and J. C. Yang, Applied Surface Science **222**, 357 (2004).
6 G. W. Zhou, X. D. Chen, D. Gallagher, and J. C. Yang, Appl. Phys. Lett. **93**, 123104 (2008).
7 G. W. Zhou, J. A. Eastman, R. C. Birtcher, P. M. Baldo, J. E. Pearson, L. J. Thompson, L. Wang, and J. C. Yang, Journal of Applied Physics **101**, 033521 (2007).
8 T. Vicsek, *Fractal Growth Phenomena* (World Scientific, New Jersey, 1992).
9 G. W. Zhou, L. Wang, R. C. Birtcher, P. E. Baldo, J. E. Pearson, J. C. Yang, and J. A. Eastman, Physical Review Letters **96**, 226108 (2006).
10 F. W. Young, J. V. Cathcart, and A. T. Gwathmey, Acta Metall. **4**, 145 (1956).
11 Y. Zhou, X. S. Jin, Y. M. Mukovskii, and I. V. Shvets, Journal of Physics: Condensed Matter **16**, 1 (2004).
12 F. H. Yuan, E. H. Han, C. Y. Jo, T. F. Li, and Z. Q. Hu, Oxidation of Metals **60**, 211 (2003).
13 K. R. Lawless and A. T. Gwathmey, Acta Metall. **4**, 153 (1956).
14 T. N. Rhodin, Journal of the American Chemical Society **73**, 3143 (1951).
15 G. W. Zhou and J. C. Yang, Surface Science **531**, 359 (2003).

DOE Sponsored Publications from Current Grant

None

Atomic Layer Deposition (ALD) of Metal and Metal Oxide Films: A Surface Science Study

Francisco Zaera
zaera@ucr.edu
Department of Chemistry, University of California, Riverside, CA 92521

i) Program Scope

ALD is poised to become one of the dominant technologies for the growth of nanometer-sized conformal films in many industrial applications. In microelectronics in particular, the growth of diffusion, adhesion, and protection barriers and of metal interconnects is central to the buildup of diodes, transistors, and other elements within integrated circuits. All these processes require the deposition of isotropic films on complex topographies under mild conditions and with monolayer control. ALD is particularly suited to satisfy all those conditions, but many questions concerning the underlying surface chemistry need to be answer before it can find widespread use.

In this project, surface-sensitive techniques such as X-ray photoelectron (XPS), Auger electron (AES), low-energy ion scattering (LEIS), temperature programmed desorption (TPD), and infrared (IR) spectroscopies will be used for surface characterization and kinetic studies of ALD processes under realistic conditions. Our initial focus will be on the study of processes for the deposition of metal (Cu) interconnects and metal oxide (HfO_2) high k dielectric films, both central components in the microelectronics industry. Specific questions will be addressed in terms of the kinetics and mechanisms of the reactions involved, and also in connection with the composition and morphology of the resulting films. This knowledge will be directed to the design of ALD processes that operate under the mildest conditions possible and deposit stoichiometric and pure films with good density, low resistance, and smooth surfaces.

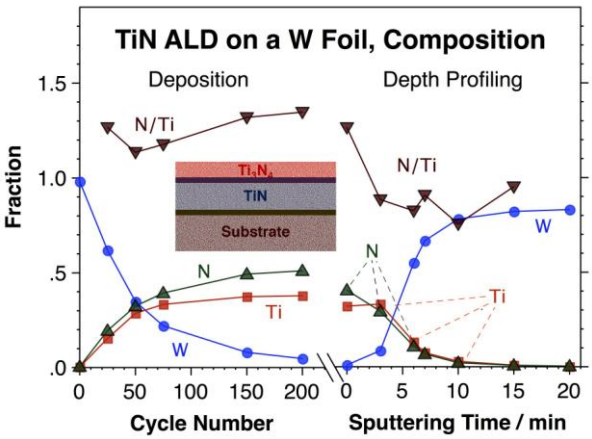

Fig. 1. Summary of XPS data for the ALD of titanium nitride films using $TiCl_4$ and NH_3. Shown are W (the substrate), N, and Ti average atomic surface concentrations and N/Ti atomic ratios measured as a function of the number of ALD cycles during film growth (left) and the sputtering time once a thick film had been grown (right). N/Ti ratios higher than unity were always observed during growth but not after light sputtering, indicating the formation of a thin Ti_3N_4 layer on top of the growing TiN film. The results suggest that the reduction of the titanium ions occurs via disproportionation of the $TiCl_4$ precursor, not by reaction with ammonia as commonly thought.

ii) Recent Progress

In the past few years we in our laboratory have embarked in a project to adapt modern surface science techniques for the study of the surface chemistry of chemical precursors relevant to ALD processes. Our initial studies, funded by a grant from the US National Science Foundation, have focused on the ALD of metal nitride films. [1-5]. Although not directly connected to the

project described in this proposal, that work helps illustrate the power of our surface-science approach to answer some of the key questions associated with the optimization of ALD processes. For instance, XPS data from studies on the deposition of TiN films using $TiCl_4$ and ammonia according highlighted some surprising findings, in particular the formation of a thin Ti_3N_4 layer on top of the growing TiN film all throughout the deposition process. Evidence for this comes both from the soichiometry of the films (Fig. 1) and the position of the Ti XPS peaks, which provide information about oxidation states [1-3]. These results suggest that reduction may occur during the $TiCl_4$, not ammonia, half-cycle.

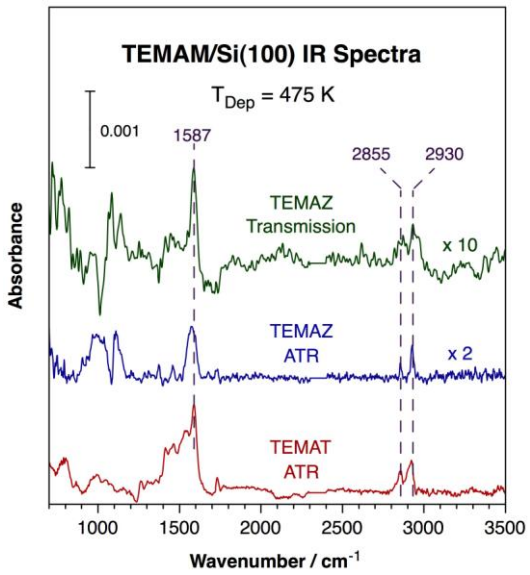

Fig. 2. Infrared absorption spectra from Si(100) surfaces after saturation with TEMAM at 475 K. Three traces are shown, for spectra of TEMAT and TEMAZ recorded using the ATR IR setup (bottom two traces), and for data of TEMAZ taken with the transmission IR apparatus (top trace). All these spectra share similar prominent peaks at 1587, 2855 and 2930 cm^{-1}, all associated with a surface imine.

To test the feasibility of using infrared spectroscopy for the proposed work, we have also carried out a few preliminary experiments on the adsorption of tetrakis(ethylmethyl amido)metal compounds, with zirconium (TEMAZ) and titania (TEMAT). Early work was done on a silica high-surface-area support [2; 3], but more recently both ATR and transmission setups have been tested using Si(100) wafers [5]. The data obtained so far, exemplified in Fig. 2, have proven quite rich in information, pointing to partial decomposition upon adsorption. Note in particular the evidence for the formation of an imine intermediate. The chemistry of dialkylamido-based precursors has in fact been shown to be quite rich [6-9], and to include protonolysis of the dialkylamido ligands to afford amido, imido, and even nitrido ligands in either terminal or bridging bonding configurations (consistent with our observations), and also direct metal-carbon bond-formation steps. All these possibilities will be probed in the future by combining IR experiments with characterization using the other techniques at our disposal, XPS and TPD in particular.

Finally, some years ago we carried out extensive studies on the thermal chemistry of metal carbonyls on nickel and platinum substrates in connection with metal CVD processes [10-15]. That research helped us develop some useful methodologies for the mechanistic investigation of ALD processes proposed here. For instance, RAIRS was used to identify $Fe(CO)_4$ and $Fe(CO)_3$ adsorbed intermediates during the deposition of iron films with an iron pentacarbonyl precursor [12]. ^{13}CO isotope labeling was then employed to prove the reversibility of that decarbonylation [15]. Another particularly interesting demonstration of that work was the use of a combination of LEIS and AES experiments to determine the nature of the films in their initial stages of growth [11]. Specifically, using the fact that LEIS and AES provide compositional information for different surface depths, it was possible to determine that, in the case of iron films grown using $Fe(CO)_5$, the deposition occurs via a three-dimensional island growth, not via the more desirable layer-by-layer mode (Fig. 3)

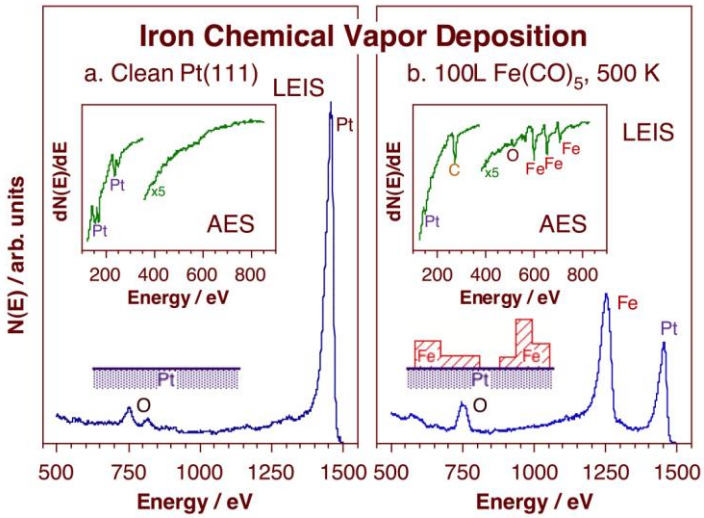

Fig. 3. LEIS and AES spectra before (left) and after (right) CVD growth of an iron film using $Fe(CO)_5$. Because of the different sampling depths of each technique, their combined results provide a fairly good indication of the morphology of the resulting films. In this case, ~30% of the substrate still remains uncovered (according to the LEIS data) even after deposition of seven Fe monolayer-equivalents (according to the AES traces), indicating three-dimensional film growth.

iii**) Future Plans**

We propose to start this project by addressing ALD processes for both metal and high k films while also continue developing new instrumentation for these surface-science studies. The work on Cu ALD will include the following:

- A systematic XPS and TPD study of the surface chemistry of the sec-butyl amidinate, a key Cu ALD precursor, as a function of exposure and deposition temperature.
- A characterization of the surface chemistry of amidine ligands alone, focusing on the parameters that control selectivity between hydrogenation (desirable) and dehydrogenation (undesirable, leading to the deposition of surface impurities) reactions.
- A set of measurements to determine the conditions required for the activation of the copper complex in the absence versus in the presence of coadsorbed hydrogen., the second reactant used in ALD.
- A characterization of the thermal stability and compositional profile of the copper films deposited on different substrates to test the possibility of nucleation, diffusion, mixing, and/or alloy formation.

In terms of high k oxide films, our initial research will focus on the growth of hafnium oxides using alkylamide complexes, starting with tetrakis(ethylmethylamido)hafnium (TEMAHf). The following experiments are suggested:

- A detailed TPD and IR study of the surface chemistry of each half process to identify the surface species formed at each step of the ALD cycle and to detect any byproducts and side reactions leading the deposition of impurities.
- A complementary XPS characterization of the surfaces resulting from each half cycle as a function of exposure time and pressure and substrate temperature, as illustrated for TiN deposition in Fig. 1.

- A test of different oxidants, with particular focus on a comparison between water and N_2O. The latter has, to the best of our knowledge, not been tried before, and promises to provide a viable alternative to avoid the problems in process design associated with the "stickiness" of water.
- An investigation of the role of the substrate in the initial stages of the deposition.

iv) References

[1] H. Tiznado, F. Zaera, "Surface Chemistry in the Atomic Layer Deposition of TiN Films from $TiCl_4$ and Ammonia", J. Phys. Chem. B. 110 (2006) 13491.
[2] H. Tiznado, M. Bouman, B.-C. Kang, I. Lee, F. Zaera, "Mechanistic Details of Atomic Layer Deposition (ALD) Processes for Metal Nitride Film Growth", J. Mol. Catal. A 281 (2007) 35.
[3] M. Xu, H. Tiznado, B.-C. Kang, M. Bouman, I. Lee, F. Zaera, "Mechanistic Details of Atomic Layer Deposition (ALD) Processes", J. Kor. Phys. Soc. 51 (2007) 1063.
[4] F. Zaera, "The Surface Chemistry of Thin Film Atomic Layer Deposition (ALD) Processes for Electronic Device Manufacturing", J. Mater. Chem. 18 (2008) 3521.
[5] S. Bocharov, Z. Zhang, T. P. Beebe Jr, A. V. Teplyakov, "Structure of a thin barrier film deposited from tetrakis-(dimemylamino)-titanium onto a Si(100)-2X1 substrate", Thin Solid Films 471 (2005) 159.
[6] A. Togni, L. M. Venanzi, "Nitrogen donors in organometallic chemistry and homogeneous catalysis", Angew. Chem., Int. Ed. 33 (1994) 497.
[7] K. Koo, G. L. Hillhouse, "Carbon-nitrogen bond formation by reductive elimination from nickel(II) amido alkyl complexes", Organometallics 14 (1995) 4421.
[8] J. F. Hartwig, "Directly-observed beta-hydrogen elimination of a late transition metal amido complex and unusual fate of imine byproducts", J. Am. Chem. Soc. 118 (1996) 7010.
[9] P. L. Holland, R. A. Andersen, R. G. Bergman, "Synthesis, characterization, isomerization, and reactivity of dimeric cyclopentadienylnickel amido complexes", J. Am. Chem. Soc. 118 (1996) 1092.
[10] F. Zaera, "A thermal desorption and X-ray photoelectron spectroscopy study of the surface chemistry of iron pentacarbonyl", J. Vac. Sci. Technol. A 7 (1989) 640.
[11] F. Zaera, "Kinetic study of the chemical vapor deposition of iron films using iron pentacarbonyl", Langmuir 7 (1991) 1188.
[12] F. Zaera, "Mechanism for the decomposition of iron pentacarbonyl on Pt(111): Evidence for iron tetracarbonyl and iron tricarbonyl intermediates", Surf. Sci. 255 (1991) 280.
[13] F. Zaera, "Tungsten hexacarbonyl thermal decomposition on nickel(100) surfaces", J. Phys. Chem. 96 (1992) 4609.
[14] M. Xu, F. Zaera, "Mechanistic studies of the thermal decomposition of metal carbonyls on Ni(100) surfaces in connection with chemical vapor deposition processes", J. Vac. Sci. Technol. A14 (1996) 415.
[15] M. Xu, F. Zaera, "Evidence for ligand exchange in iron pentacarbonyl adsorbed on Ni(100) surfaces", Surf. Sci. 315 (1994) 40.

v) Publications resulting from work supported by the DOE project over the last two years

Funding from DOE for this project is expected to start October 1st, 2009.
There are yet no publications resulting from work supported by this DOE Project.

SCIENCE OF HETEROEPITAXY FOR ENERGY-EFFICIENT LIGHTING

Jung Han
jung.han@yale.edu
Department of Electrical Engineering
Yale University, New Haven, CT 06520

Program Scope

The past two decades have witnessed a phenomenal development of III-nitride (III-N) semiconductor from laboratory explorations to ubiquitous applications in information storage and display. As the field is expanding to energy-efficient solid state lighting and high power electronics, further breakthroughs in III-N epitaxy are needed to enable and propel technological advances. We note that the advances in III-N epitaxy have been made in largely empirical and knob-turning way. The constant need to map out immense growth parametric space fosters a culture emphasizing the development of viable growth recipes. The recent excitement in pursuing epitaxy along unconventional directions (non-polar [1], semi-polar [2], and nitrogen-polar [3], for examples) and the apparent challenges in crystal growth on these low-symmetry surfaces call for a deeper and more comprehensive understanding of the heteroepitaxial process. This program aims to firstly establish a scientific and coherent model over a diverse range of heteroepitaxial phenomena occurred in III-N growth, from nucleation to coalescence, on a variety of crystallographic planes. Secondly, selective area growth is employed as an accurate and flexible method to monitor and record growth kinetics that determine the microstructural and morphological properties. Lastly, this program seeks an active and effective control of the dynamic process of heteroepitaxy through the use of intrinsic and extrinsic morphactants, designed to alter the anisotropy of growth kinetics, to create new dimensions and new paradigm in heteroepitaxial control that is at the heart of contemporary production of solid-state lighting devices.

Recent Progress

Mesoscopic crystal growth phenomena are governed by minimization of energy (surface tension and strain), which was first analyzed mathematically by Wulff [4]. The so-called "kinetic Wulff diagram" or *v*-plot (growth velocity versus surface orientation) has shown to accurately predict the shape evolution under non-equilibrium conditions [5]. Recently, we constructed GaN *v*-plots based on observed stable facets (minima in growth rate) across a broad crystallographic space [6]. Three-dimensional mapping of the *v*-plots as a function of growth condition was accomplished. While the concept of Wulff plot has been largely confined to textbooks, we provide examples of varying complexity to illustrate its value in interpreting growth dynamics and, ultimately, in facilitating a rational control of heteroepitaxial process.

Growth rates were measured from SAG islands [6] grown similarly to conventional epitaxial lateral overgrowth experiments. Samples employed in this study include *c*-plane, *m*-plane, *a*-plane, N-polar, and semi-polar (11$\underline{2}$2) GaN. The use of mask patterns with annular window openings facilitates the measurement of all facets relevant to heteroepitaxial dynamics (Fig 1) including *slow-growth, convex facets* (labeled in red) on the outer ring and *fast-growth, concave facets* (labeled in blue, yellow, green, and magenta) delineating the inner voids. Measuring the rate of advance along all these orientations enable the construction of 3-D *v*-plots shown in Fig 2 for two different growth conditions.

The *v*-plot mappings open numerous pathways to understanding and controlling GaN heteroepitaxy. To demonstrate its usefulness and broad applicability, we considered the morphology of islands on semipolar {11$\underline{2}$2} planes, an example with high anisotropy and complexity. The 3D *v*-plot in Fig 2 can be sliced through the origin by a {11$\underline{2}$2} plane. The truncated *v*-plot (not shown) including all the cusps and valleys can be used to interpret the shape of an island (or SAG mesas, Fig 3) on the semipolar {11$\underline{2}$2} plane.

In addition, island shape-evolution during coalescence can be determined by comparing the curvature of the coalescence front to that of the appropriate *v*-plot. We have developed a model to explain the existence and persistence of morphological imperfection in the form of pits and striations on *a*-plane GaN grown on *r*-plane sapphire (Figs 4) [7]. Asymmetric *a*-GaN islands influence the initial coalescence by forming networks of voids and ridges roughly along [0001]. From geometric analysis, we have determined that pyramidal (11$\underline{2}$2) and {10$\underline{1}$2} planes emerge at the points of contact between ridges. These planes "zip up" the elongated grooves along Ga-polar and N-polar directions, respectively, leaving behind much shallower, straight grooves and interwoven pits (Fig 4c) that account for the typical morphology of a-plane GaN frown by MOCVD. The correlation of GaN heteroepitaxy with Wulff plot is still at its infancy. We expect this approach to effectively guide the design and optimization of nonpolar and semipolar growth.

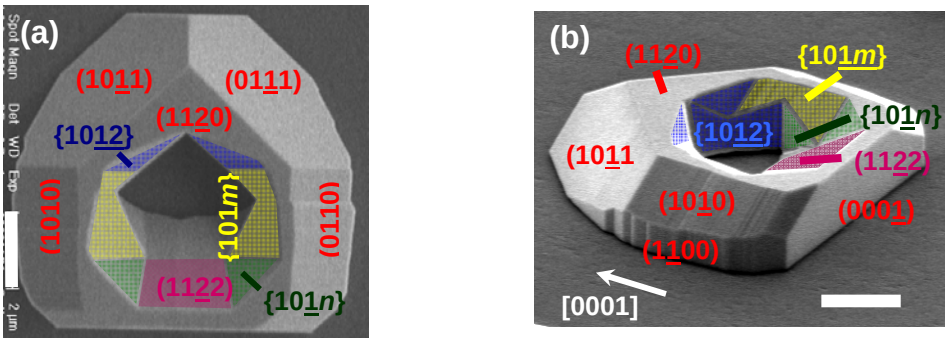

Fig. 1 (left) SEM (a) plan and (b) perspective views of *a*-plane SAG GaN grown using an annular mask opening. Slow, stable facets compose the island perimeter. Fast concave facets, represented by saddle points in Fig. 1, are present within the enclosed void (highlighted). These facets include {10$\underline{1}$2} (blue), {11$\underline{2}$2} (magenta), facets vicinal to {10$\underline{1}$1} (green), and facets vicinal to {10$\underline{1}$0} (yellow). The scale bars are 2μm.

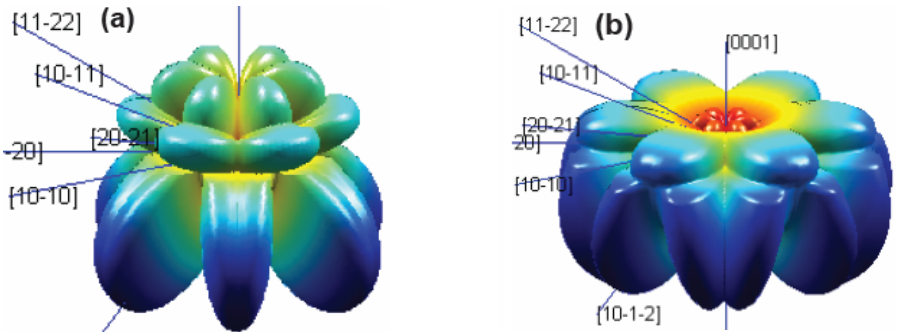

Fig. 2 Kinetic Wulff plots (growth rate versus surface orientation) for MOCVD GaN growth at (a) 1070 ºC, 100 mbar, V/III: 250 and (b) 1000 ºC, 300 mbar, V/III: 500.

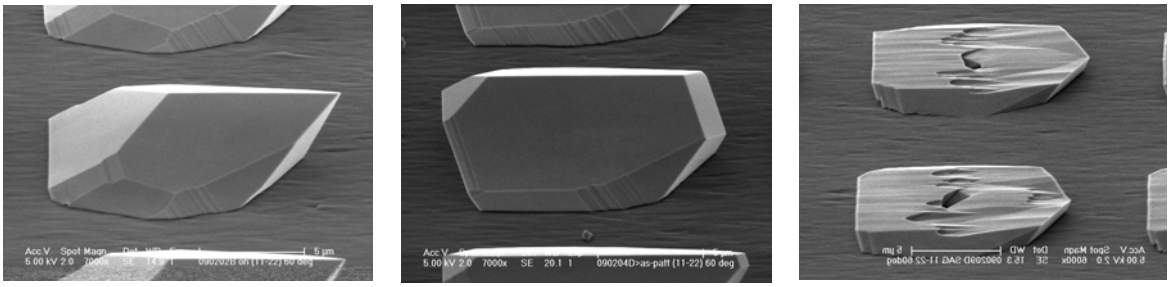

Fig 3 SEM images of GaN islands through selective area growth on semipolar (11$\underline{2}$2) planes.

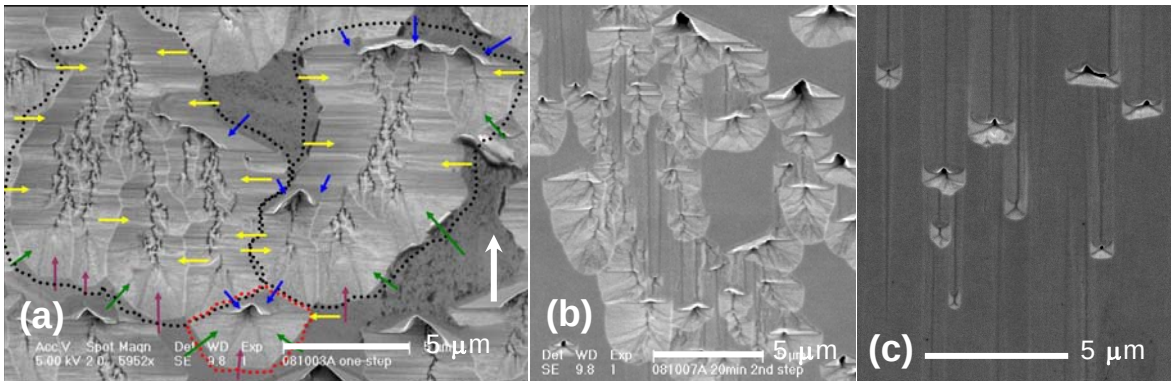

Fig. 4 (middle) SEM images of *a*-plane GaN morphological evolution (a) after a high V/III growth step, (b) after 20 minutes of a subsequent low V/III growth step, and (c) continuing to 40 minutes at low V/III. The initial step forms both large and small ridges that define the location and size of both striations and pits. The concave growth geometry requires each facet emerging during coalescence to be a Wulff saddle point. Colored arrows correspond to the same facets as in Fig 1.

Future Plans

Based on the foundational works carried out recently in the heteroepitaxy of a-plane, m-plane, and semipolar GaN, we have a high anticipation for the scientific outcomes and impact of this program. This program will proceed along four different yet intertwined directions, the first and second ones center on heteroepitaxial sciences while the third and four ones bear great technological relevance to solid state lighting.

1. During the first 18 months of this project, we will continue the mapping and construction of kinetic Wulff plot (*v*-plot) using both intrinsic (growth condition-based) and extrinsic (dopants or additives) morphactants to fully explore the "elasticity" of *v*-plot for GaN. This study will provide a scientific framework for interpretation and rational design of GaN heteroepitaxial processes.
2. We will develop a qualitative model (and possibly a semi-quantitative one through collaboration with Sandia National Labs) of morphological evolution that is coupled with the information of *v*-plots.
3. The correlation of morphological evolution with the final microstructural quality, including the control and elimination of defects such as stacking faults and dislocations through morphology engineering.
4. The application of shape and morphology control to non-planar, mesoscale patterned growth for next generation GaN optoelectronic and electronic devices.

References

[1]M. C. Schmidt, K.-C. Kim, H. Sato, N. Fellows, H. Masui, S. Nakamura, S. P. DenBaars, and J. S. Speck, Jpn. J. Appl. Phys., Part 2 **46**, L126 (2007); M. D. Craven, S. H. Lim, F. Wu, J. S. Speck, and S. P. DenBaars, Appl. Phys. Lett. **81**, 469 (2002).

[2] X. Ni, Ü. Özgür, A. A. Baski, H. Morkoç, L. Zhou, D. J. Smith, and C. A. Tran, , Appl. Phys. Lett. **90**, 182109 (2007).

[3] S. Keller, N. A. Fichtenbaum, F. Wu, D. Brown, A. Rosales, S. P. Den-Baars, J. S. Speck, and U. K. Mishra, J. Appl. Phys. **102**, 083546 (2007).

[4] G. Wulff, Z. Kristallogr. **34**, 449 (1901).

[5] D. Du, D. J. Srolovitz, M. E. Coltrin, and C. C. Mitchell, Phys. Rev. Lett. **95**, 155503 (2005).

[6] Q. Sun, C. D. Yerino, T.-S. Ko, Y. S. Cho, I.-H. Lee, J. Han, and M. E. Coltrin, J. Appl. Phys. **104**, 093523 (2008).

[7] C. D. Yerino, Q. Sun, B. Leung, and J. Han, submitted to Appl. Phys. Lett. (2009).

Growth and *in situ* Characterization of Novel Thin Films using Angle-Resolved Photoemission Spectroscopy

R. G. Moore[1] and Z. –X. Shen[2]
zxshen@stanford.edu
[1]Stanford Synchrotron Radiation Lightsource
[2]Stanford Institute for Materials and Energy Sciences
SLAC National Accelerator Laboratory, Menlo Park, CA 94025

Program Scope

This project will enable SLAC and the Stanford Institute for Materials and Energy Sciences (SIMES) to take an important step in creating a world class program on novel materials grown under non-equilibrium conditions using molecular beam epitaxy (MBE). While such materials provide exciting opportunities for grand challenge science and energy applications, they are typically made in isolation and rarely available for investigation by some of the most sophisticated modern experimental tools such as angle-resolved photoemission spectroscopy (ARPES). This mismatch between opportunity and reality is largely driven by the difficulties of both MBE and ARPES techniques –only institutions with sufficient resources and capabilities of scale can initiate this science. Leveraging its world leading ARPES capability at the Stanford Synchrotron Radiation Lightsource (SSRL), and the growing materials strength of SIMES, we propose to develop such a program at SLAC.

Recent Progress

This project will develop a sophisticated materials synthesis system to be adjoined to the newly funded SSRL ARPES beamline. Several of the DOE grand challenges address the necessity for precise control of atomic structure and full understanding of the emerging properties. The past decade has seen revolutionary advances in the growth of novel materials: precise atomic control of thin films, growth of nanostructures and manipulation of surfaces now happen on a routine basis [1-5]. Layer by layer growth of exotic crystals and heterostructures allows the possibility to fabricate materials with tailored properties. The tools and techniques are already in place to not only synthesize such materials, but to examine their crystallographic and transport properties. Such control enables researchers to better understand how structure, and the precise control of structure, affects physical properties. Despite the advances, there are still unresolved questions as to the underlying mechanisms responsible for the unusual and exotic states that emerge. While atomic control of structure is imperative for the study of fundamental properties, atomic positions alone

do not present the complete picture. Many body interactions arise and manipulate the behavior of electrons within the material and thus change the underlying electronic structure. While thin films and heterostructures have advanced our understanding of the superconducting state, for example, manipulation and reconstruction of the underlying electronic structure in these materials is still a mystery [6,7]. Atomic and electronic structure play complementary roles in physics and one must fully understand both to develop a coherent picture of such exotic physics.

On a parallel front, advances in ARPES have enabled unprecedented access to the electronic structure of materials [8-10]. Energy resolution on the order of a few meV and direct multi-dimensional mapping capability pushes ARPES to the forefront for understanding the most challenging material problems of our times. Modern ARPES, as exemplified by SSRL ARPES beamline 5-4, has become an indispensible tool in the study of quantum physics in solids. The newly funded SSRL ARPES beamline will extend the existing ARPES capabilities ensuring SSRL remains at the forefront of condensed matter research for years to come. However, one of the major limitations of the ARPES technique is its inherent surface sensitivity. High energy and momentum resolution require low photon energies which, in turn, limit the probing depth. Thus far, the majority of ARPES studies have been limited to single crystals with layered structure, capable of *in situ* cleaving. As such, ARPES has been able to observe electronic reconstructions on the cleaved surface, but has been limited in learning how to manipulate the electronic structure due to the necessity of studying bulk crystals.

Future Plans

In order to push beyond current frontiers of modern physics and address the DOE grand challenges, a full understanding of both atomic *and* electronic structure is required. Manipulating atomic structure is not enough as we must learn to manipulate electronic structures as well. The marriage of epitaxial and photoemission techniques would allow unprecedented access and new directions in materials research. Building materials atom by atom, layer by layer, and understanding the resulting electronic structure will open new frontiers in band engineering with potential applications to energy and material science including: superconducting, photovoltaic, magnetoelastic, thermoelectric, ferroelectric and nano-structured materials to name a few. Only by fully understanding novel films can they be tailored to advance technologies such as solar and thermoelectric energy generation. In addition, the coupling of complementary techniques will attract a new breed of users: materials synthesis experts who likely have never had access to the tools offered by the synchrotron community. A cutting-edge synchrotron based-materials synthesis system would become a cornerstone in the SLAC materials program.

Both MBE and ARPES are challenging techniques and require great efforts for success. The existing SSRL ARPES beamline has demonstrated its world leading capabilities numerous times and the growing strength of the SIMES materials synthesis programs present new opportunities for advancement. Planning is already underway for the new SSRL ARPES beamline to include a new insertion device capable of full polarization control over a wide energy range (7-30eV for linear polarization 20-150eV for circular polarization) and a new endstation for high resolution conventional and spin resolved ARPES measurements. The new beamline coupled with the planned 500mA and top-off mode operations at SSRL will enable new areas of condensed matter research with 15-20 times the existing flux of the current ARPES beamline.

The initial goal of this project will be to gain the necessary knowledge and experience for development of a state-of-the-art synchrotron based materials synthesis system. The ongoing development of SIMES materials labs will allow access to various epitaxial techniques. Each technique has advantages and disadvantages and the techniques best suited for synchrotron based research must be identified. Initial proof-of-principle experiments with existing materials synthesis systems are currently being developed within the SIMES labs. A small scale MBE system adjoined to an existing laser ARPES system will be utilized to perform initial experiments and gain essential experience in thin film synthesis and *in situ* characterization by ARPES. These activities will enable the team to develop a detailed DOE proposal creating a leading program taking full advantage of the combined power of MBE materials capability and synchrotron ARPES capability for frontier materials and energy science research.

References

1. I. Bozovic, IEEE T. Appl. Supercon. **11**, 2686 (2001).
2. W. L. Yang, J. D. Fabbri, T. M. Willey, J. R. I. Lee, J. E. Dahl, R. M. K. Carlson, P. R. Schreiner, A. A. Fokin, B. A. Tkachenko, N. A. Fokina, W. Meevasana, N. Mannella, K. Tanaka, X. J. Zhou, T. van Buuren, M. A. Kelly, Z. Hussain, N. A. Melosh and Z. –X. Shen, Science **316**, 1460 (2007).
3. N. Manyala, J. F. DiTusa, G. Appli and A. P. Ramirez, Nature **454**, 976 (2008).
4. Y. Z. Wu, A. K. Schmid, M. S. Altman, X. F. Jin and Z. Q. Qiu, Phys. Rev. Lett. **94** 027201 (2005).
5. O. Matsumoto, A. Utsuki, A. Tsukada, H. Yamamoto, T. Manabe and M. Naito, Phys. Rev. B **79**, 100508 (2009).
6. A. Gozar, G. Logvenov, L. F. Kourkoutis, A. T. Bollinger, L. A. Giannuzzi, D. A. Muller and I. Bozovic, Nature **455**, 782 (2008).

7. P. Abbamonte, L. Venema, A. Rusydi, G. A. Sawatzky, G. Logvenov and I. Bozovic, Science **297**, 581 (2002).
8. W. S. Lee, I. M. Vishik, K. Tanaka, D. H. Lu, T. Sasagawa, N. Nagaosa, T. P. Devereaux, Z. Hussain and Z. –X. Shen, Nature **450**, 81 (2007).
9. D. H. Lu, M. Yi, S. –K. Mo, A. S. Erickson, J. Analytis, J. –H. Chu, D. J. Singh, Z. Hussain, T. H. Geballe, I. R. Fisher and Z. –X. Shen, Nature **455**, 81 (2008).
10. D. Hsieh, D. Qian, L. Wray, Y. Xia, Y. S. Hor. R. J. Cava and M. Z. Hasan Nature **452**, 970 (2008).

DOE Sponsored Publications from Existing Grant

This project is currently not funded. A DOE proposal will be submitted in the near future outlining the details of the project scope and pathways to achieving the desired goals. This project will take advantage of the synergy between the existing programs within the SLAC community, coupling the experience of SSRL with the new insights from the newly founded SIMES.

Creating a New Class of Materials: Multidimensional Multilayer Films.

Paul B. Mirkarimi
Mirkarimi1@llnl.gov
Lawrence Livermore National Laboratory
Livermore, CA. 94550

Program Scope

Multilayer films are a clear demonstration of the saying "the whole is greater than the sum of the parts", with a myriad of unique properties, many unforeseen, made possible by modulating the composition in the film growth direction. However, multilayer films generally utilize a modulation of the composition in only one of the three space dimensions in which physical matter resides. What if one were able to develop techniques and tools to *generally* synthesize films with composition modulations in two and three dimensions? What new properties might arise from these *multidimensional multilayers*?

We propose to create a new class of multicomponent, multifunctional materials: multidimensional multilayer films. Figures 1 (a), (b), and (c), show multilayer films with one-, two-, and three-dimensional composition modulations respectively.

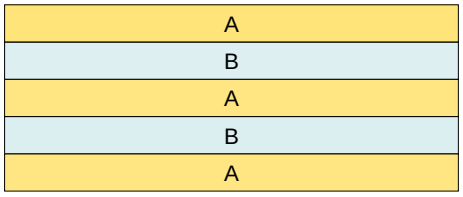

(a) One-dimensional (standard)

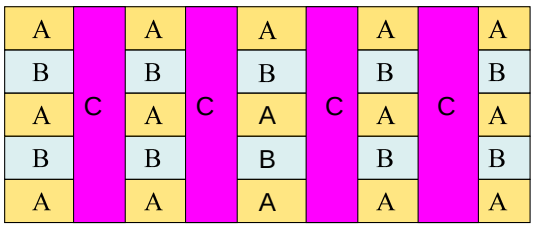

(b) Two-dimensional

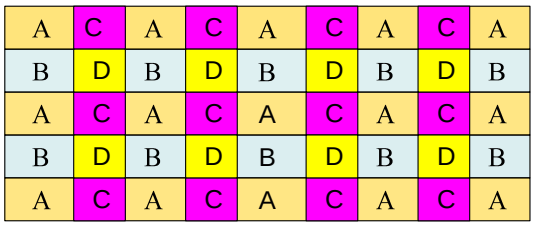

(c) Three-dimensional

Figure 1. Multilayer film with a (a) one-dimensional, (b) two-dimensional and (c) three-dimensional composition modulation.

Progress

Strength enhancement in multilayer films (an example)

Mirkarimi et al.[1] and others have shown that dramatic strength enhancements are possible by introducing a one-dimensional composition modulation into thin films. It is believed

that a Koehler-type[2] of hardening mechanism dominates the observed strengthening enhancements. In this mechanism, the difference in shear elastic moduli between the layers results in a dislocation energy gradient between layers; the dislocations want to remain in the low energy layers and a greater force is needed to move the dislocations (i.e., the material is stronger). However, note that this dramatic strength enhancement is obtained by limiting the dislocation motion in only one of three possible dimensions, as illustrated in Figure 2 below. If one were able to fabricate a three dimensional multilayer, as illustrated in Figure 3 below, one would expect much greater dislocation confinement and hence greater strengthening.

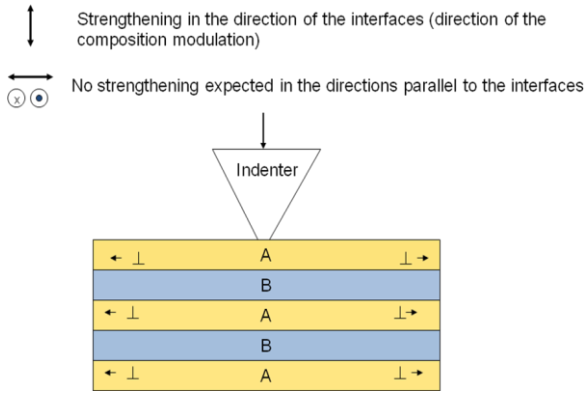

Figure 2. Strengthening in a Koehler-type strengthening mechanism.

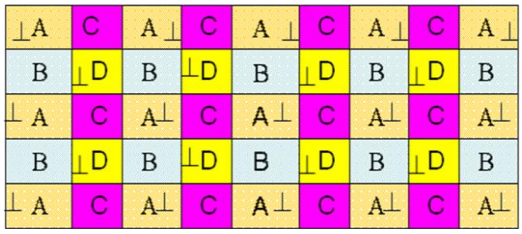

Figure 3. Dislocation confinement in a three composition modulation.

Fabricating multidimensional multilayer thin films

A key challenge in fabricating these materials will be to directionally deposit in holes (for 3D multilayer) and vias (for 2D multilayer); Figure 4 illustrates this for holes and 3D multilayers.

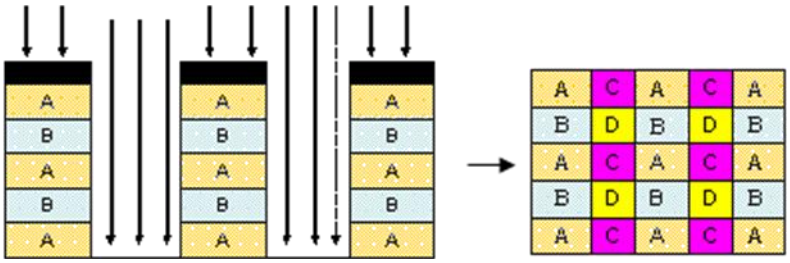

Figure 4. Directional deposition in holes to form a three dimensional multilayer.

As part of the CRADA to develop extreme ultraviolet (EUV) lithography, a candidate technique for fabricating powerful microprocessor and memory chips[3], and subsequent research sponsored by Intel Corporation, we developed techniques to use films to control the topology of substrate surfaces[4,5,6]. Early advances in this work were recognized with an R&D 100 award[7]. Figure 4 below shows an XTEM image of a sample fabricated using

a special coat-and-etch film deposition process (utilizing silicon films) to fill in a ~70 nm wide via, enabling a highly EUV reflective multilayer film to be deposited afterwards. We have also used this process with materials other than Si, we have used it on holes and vias with aspect ratios different than 1, and we have filled in holes much smaller than 70 nm.

In Figure 6 below we show the process where we used a Mo/Si multilayer instead of Si, and where we intentionally turned down the via filling effect to leave a depression at the surface.

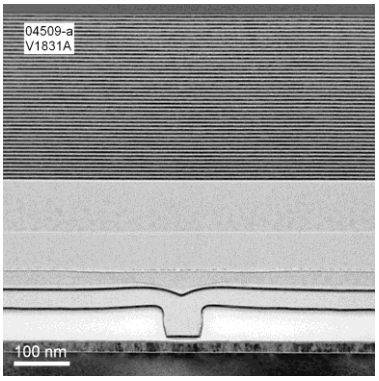

Figure 5. Depositing within a via using our coat-and-etch film process.

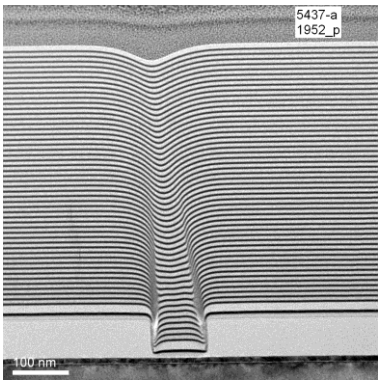

Figure 6. Filling a via with Mo/Si, where the via filling process was turned down to produce a depression at the surface.

Future Work

We plan to couple the national labs' materials expertise, a unique ion beam sputter tool with a directional coating capability, state-of-the-art FIB tool, nanofabrication expertise, nanowriter, and other unique facilities, to synthesize/fabricate this new class of materials.

We have envisioned and created process flows to fabricate these new thin film materials, using either focused ion beam technology or electron beam lithography to open up the holes and vias (process flows are too lengthy to discuss in detail in this abstract).

For materials of interest for strengthening, transition metal nitrides would be good materials to choose from due to the demonstrating strengthening in one dimensional composition modulations in these material systems[1] as well as the fact that the materials are strong/hard to begin with and the technological implications would be greater. Superhard nitride films such as c-BN[8] may also be considered down the road, particularly since the added dimensionality may provide a method for stress compensation[9] to enable thicker films to be deposited. Also note that if these multidimensional multilayer films could be successfully fabricated, they would provide a crisp, clean platform (more straightforward than nanocrystalline materials for example) for studying important scientific topics such as dislocation dynamics at interfaces.

It has been observed that by fabricating a one dimensional composition modulation utilizing the Cu/Nb multilayer system, materials with significantly enhanced radiation resistant properties could be obtained[10]. This suggests that by introducing additional dimensionality to these multilayer materials one might obtain even greater radiation resistant properties as well as to learn more about the mechanisms behind the observed properties.

In general, there are a myriad of instances where introducing a one dimensional composition modulation enhances the properties of materials and increasing the dimensionality of the composition modulation is likely to lead to new science and enhanced properties, with the concomitant technological implications.

References

1. P.B. Mirkarimi, S.A. Barnett, K.M. Hubbard, T.R. Jervis, and L. Hultman, J. Mater. Res. 9, 1456 (1994).
2. J. C. Koehler, Phys. Rev. B 2, 547 (1970).
3. P.B. Mirkarimi, in *Encyclopedia of Nanoscience and Nanotechnology*, H.S. Nalwa, ed, American Scientific (2004), Vol. 3, p. 297.
4. P.B. Mirkarimi and D.G. Stearns, Appl. Phys. Lett. 77, 2242 (2000).
5. P.B. Mirkarimi, E. Spiller, S.L. Baker, V. Sperry, D.G. Stearns, and E.M. Gullikson, J. Microlith., Microfab., Microsyst. 3, 140 (2004).
6. P.B. Mirkarimi, E. Spiller, S.L. Baker, D.G. Stearns, J.C. Robinson, D.L. Olynick, F. Salmassi, J.A. Liddle, T. Liang, and A.R. Stivers, J. Nanosci. Nanotechnol. 6, 28 (2006).
7. R&D Magazine, 45, 66 (2003).
8. P.B. Mirkarimi, K.F. McCarty, and D.L. Medlin, Mater. Sci. Eng. Rep. R21 (1997).
9. P.B. Mirkarimi, Opt. Eng. 38, 1246 (1999).
10. A. Misra, M.J. Demkowicz, X. Zhang, and R.G. Hoagland, JOM 59, 62 (2007).

Intrinsic and laser-irradiation-induced properties of doped ZnO films

S.A. Chambers (PI)[a], T.C. Droubay[a], T.C. Kaspar[a], J. McCloy[a], J. Ryan[a], C.M. Wang[a], V. Shutthanandan[a], L. Wang [b], G.E. Exarhos[a], D.R. Gamelin[c], C.R. Johnson[c], K.M. Whittaker[c], S.M. Heald[d], D.E. Keavney[d], A. Ney[e], T. Kammermeier[e], K. Ollefs[e], S. Ye[e], V. Ney[e], F. Wilhelm[f], A. Rogalev[f]

[a]Pacific Northwest National Laboratory, Richland, WA

[b]Carleton College, Northfield, MN, [c]University of Washington, Seattle, WA

[d]Argonne National Laboratory, Argonne, Ill

[e]Universität Duisburg-Essen, Duisberg, Germany

[f]European Synchrotron Radiation Facility, Grenoble, France

I. Program scope

This program focuses on the growth and properties of doped transition metal and complex oxide thin films. This subtask focuses on the properties of ZnO, a useful oxide semiconductor, doped with Co, Mn and/or electronic dopants. Co- and Mn-doped ZnO have been very heavily investigated because of claims that they readily exhibit room-temperature ferromagnetism, making them desirable in semiconductor spintronics. In most of the literature on Co- and Mn-doped ZnO, the experiments needed to establish the true characteristics of these materials have not been done. Most notably, atom-specific spectroscopies required to positively identify the properties of the dopant are omitted. Our approach is to utilize such spectroscopies, principally x-ray absorption spectroscopy (XAS) in its many variants, to adequately characterize our epitaxial films, and use the resulting insight to understand the magnetic and electronic transport behavior. Electrical conductivity in ZnO is often thought to arise from oxygen vacancies most often created by a slightly reducing atmosphere during deposition or post-deposition annealing. In such materials, low-pulse-energy femtosecond laser excitation above the bandgap produces transient changes in conductivity with recovery on the order of picoseconds. However, the effect of longer pulse width, higher fluence irradiation on film conductivity has only recently been considered, and is a current focus in our program.

II. Recent Progress

Our approach to optimizing the pulsed laser deposition (PLD) growth of Co:ZnO and Mn:ZnO in order to achieve the highest degree of structural perfection, as well as compositional homogeneity, involves judicious choice of target material, and the use of an off-axis geometry to avoid the inclusion of "molten droplets". To this end, we have used target materials that are homogeneous on the nanometer scale. In this approach, pressed agglomerations of Co:ZnO and Mn:ZnO nanoparticles have been utilized. Film thickness and composition were determined using a combination of x-ray reflectivity (XRR), Rutherford backscattering (RBS), and proton induced x-ray fluorescence (PIXE). The film composition was found to be nominally the same as that of the target, but films became somewhat enriched in Co when grown in lower oxygen pressure due to the preferential re-evaporation of ZnO at the growth temperature.

The degree of structural quality and homogeneity that can be achieved in Co- and Mn-doped ZnO epitaxial films is best assessed by a combination of high-resolution XRD and XAS. X-ray absorption near-edge spectroscopy (XANES) yields information on the

Co charge state whereas extended x-ray absorption fine structure (EXAFS) and x-ray linear dichroism (XLD) are highly sensitive to the details of atomic positions of near-neighbor atoms in the vicinity of the x-ray-absorbing atom.

The structural perfection that can be achieved and monitored by this approach is illustrated in Fig. 1 where we show high-resolution XRD and Co K-edge XANES and XLD. The out-of-plane (Fig. 1a) and in-plane (Fig. 1b) scans yield widths of 0.061^{o} and 0.073^{o}, respectively, revealing excellent crystallinity for both. Figs. 1 c - f show Zn and Co K-edge XANES (c & d) for the electric field vector oriented parallel and perpendicular to the *c* axis, and XLD (e & f) obtained by taking the difference of the XANES measured with the two polarizations.

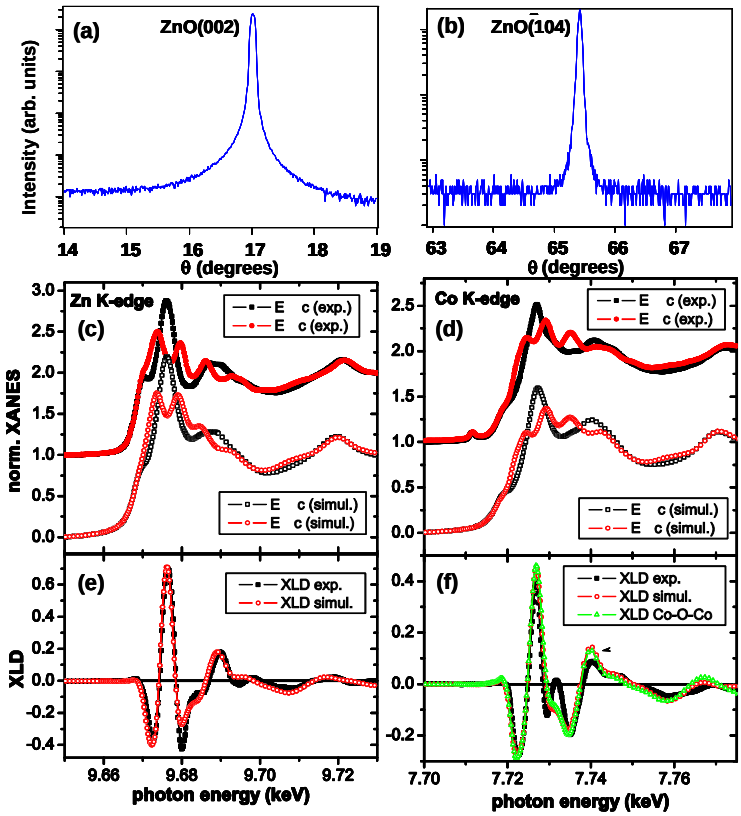

Fig. 1 High-resolution XRD out-of-plane (a) and in-plane (b) scans, along with Zn (c & e) and Co (d & f) XANES (c & d) and XLD (e & f) for 500 nm $Co_{0.1}Zn_{0.9}O$/ α-Al_2O_3 (0001) by off-axis PLD in 10 mTorr O_2.

These absorption thresholds reveal that Zn and Co are both in the +2 formal charge state. There is thus no Co(0) present within the detection limit, which for the present films thicknesses, is equivalent to saying that at least 95% of the Co is Co(II). Changing the x-ray polarization modifies the oscillator strength for excitation of K-shell electrons into unoccupied *p* states. For epitaxial films, the linear dichroism thus probes the extent of crystallographic perfection near the absorbing atom. The XANES & XLD can be simulated using a muffin-tin potential, multiple-scattering based formalism coded as FDMNES, and these simulations are also shown in Figs. 1c-f. One of the inputs is the percentage of absorbing atoms located in lattice sites. Comparison to experiment allows this percentage to be determined. Doing so reveals that at least 95% of the Co is at Zn sites, ruling out metallic Co, as well as antisite and interstitial site occupation.

The as-grown Co:ZnO films are highly resistive, and paramagnetic as judged by vibrating sample magnetometry and Co L-edge x-ray magnetic circular dichroism. Several LDA calculations in the literature predict that doping Co:ZnO *n*-type will activate ferromagnetism via carrier-mediated exchange interaction, and a number of experimental papers claim to have verified this prediction. We have co-doped our films with Al as well as interstitial Zn to make them *n*-type, but have found that the films remain paramagnetic from 300K to 5K, *unless some of the structural Co(II) is reduced to Co(0)*. This reduction can occur when the film is made *n*-type by Zn indiffusion. We have detected Co(0) by Co 2*p* XPS depth profiling, and identified the phase as CoZn using EXAFS, at levels of a few % of the total Co present. Such trace quantities are sufficient to result in hysteresis loops that are easily mistaken for intrinsic ferromagnetism.

Measuring accurate electronic transport properties of highly resistive films is a challenge which few other groups have met successfully. We have demonstrated the ability to reliably measure sheet resistances up to 10^{12} Ω /square (film resistivities of ≥ ~10^{9} Ω-cm) using a unique low-current, buffered-voltage measurement method. D.C. measurements of resistivities of this magnitude present unique challenges as very low applied currents and extremely long wait times are required to ensure that equilibrium voltages are reached in the presence of potentially large surface capacitances. We have carried out measurements on samples requiring seven orders of magnitude in the applied current, representing a resistivity range of thirteen orders of magnitude. Such high resistivities are characteristic of highly pure, crystallographically excellent ZnO films, such as those described above. The ability to measure the associated transport properties enables intrinsic and defect/impurity induced conductivity to be distinguished. Recent investigations include magnetoresistance and Hall effect measurements at low temperature for Co- and Mn-doped ZnO. With isothermal, low-temperature measurements, there is a narrow window of available currents, bounded on the high end by currents which induce deleterious resistive heating, and on the low end by the response voltage above the noise floor of the measuring meter.

Finally, the optical and electrical properties of solution-deposited and *rf* sputter-deposited doped ZnO films on silica were investigated following post-growth pulsed laser irradiation at room temperature. Transparent, *n*-type ZnO films were subjected to unfocused, 4-nsec Nd:YAG laser pulses at 355 nm or 266 nm at fluences below the damage threshold (~ 5 - 150 mJ/cm^2). Film densification, index change and marked increase in conductivity were observed following irradiation at room temperature in air, in flowing CO, and under vacuum. Despite irradiation conditions near the film damage threshold, all films continued to show high optical transparency (~90%). Laser fluences required to activate conductivity varied depending upon the dopant and exposure time. Resistivities of films treated in air were of the order of 16 Ω-cm. The resistivity dropped by an order of magnitude for irradiation in a CO environment and a comparable decrease was seen following irradiation in vacuum. The conductivity increase is attributed to oxygen vacancy formation and subsequent free-carrier excitation. All irradiated films became insulating again after days of air exposure, in addition to recovering their original film thickness and index. The conducting state could be recovered upon successive irradiation-equilibration cycles within the initial laser footprint. Raman spectra of treated films revealed an increase in the LO/TO mode intensity ratio following irradiation that recovered to initial values upon equilibration. These results are consistent with laser-

stimulated reduction of ZnO. Following treatment, ambient air diffuses into the film, promoting oxidation and reversion to the initial non-conducting state.

III. Future Plans

It is still not known if *p*-type Mn:ZnO exhibits intrinsic ferromagnetism via *pd* exchange interaction because ZnO has not yet been effectively doped *p*-type. We plan to test new *p*-type doping schemes and explore the resulting magnetic and magnetotransport properties. We also plan to carry out magnetoresistance and anomalous Hall effect mesurements on Co- and Mn-doped ZnO, as well as explore laser irradiation of *n*-ZnO at elevated temperatures followed by quenching. Rapid quenching is expected to contract the lattice sufficiently to frustrate oxygen diffusion and retain the conducting state. Such studies are important for the continued development of transparent conducting oxide films for use in photovoltaic cells and solid state lighting modules.

IV. Selected Sponsored Publications in 2008-2009

1. S.A. Chambers, "Surface Science Opportunities in the Electronic Structure of ZnO". Invited perspective on the article "Quantitative analysis of surface donors in ZnO" by D.C. Look. Surf. Sci. **601**, 5313 (2008).
2. A. Ney, S. Ye, K. Ollefs, T. Kammermeier, V. Ney, T.C. Kaspar, S.A. Chambers, F. Wilhelm RA. Rogalev, "Absence of Intrinsic Ferromagnetic Interactions of Isolated and Paired Co Dopant Atoms in $Zn_{1-x}Co_xO$ with High Structural Perfection", Phys. Rev. Lett. **100**, 157201 (2008).
3. Y.J. Li, T.C. Kaspar, T.C. Droubay, Z. Zhu, V. Shutthanandan, P. Nachimuthu, S.A. Chambers, "Electronic Properties of H and D doped ZnO Epitaxial Films", Appl. Phys. Lett. **92**, 152105 (2008).
4. T.C. Kaspar, T. Droubay, S.M. Heald, M.H. Engelhard, P. Nachimuthu, S.A. Chambers, "Hidden Ferromagnetic Secondary Phases in Cobalt-doped ZnO Epitaxy Films", Phys. Rev. **B 77**, 201303(R) (2008).
5. T.C. Kaspar, T.C. Droubay, Y. Li, S.M. Heald, P. Nachimuthu, C.M. Wang, V. Shutthanandan, C.A. Johnson, D.R. Gamelin, and S.A. Chambers, "Lack of Ferromagnetism in *n*-type Co-doped ZnO Epitaxial Thin Films, New J. Phys. **10**, 055010 (2008).
6. Y.J. Li, T.C. Kaspar, T.C. Droubay, A.G. Joly, P. Nachimuthu, Z. Zhu, S. Shutthanandan, S.A. Chambers, "A Study of H- and D-Doped ZnO Epitaxial Films Grown by Pulsed Laser Deposition", J. Appl. Phys. **104**, 053711 (2008).
7. T. C. Droubay, T. C. Kaspar, B. P. Kaspar, S. A. Chambers, "Cation dopant distributions in nanostructures of transition-metal doped ZnO", Phys. Rev. **B 79**, 075324 (2009).
8. T.C. Droubay, D.J. Keavney, T.C. Kaspar, S.M. Heald, C.M. Wang, C.A. Johnson, K.M. Whitaker, D.R. Gamelin, and S.A. Chambers, "Correlated Substitution in Paramagnetic Mn-doped ZnO Epitaxial Films", Phys. Rev. **B 79**, 155203 (2009).
9. Steve M Heald, Tiffany Kaspar, Tim Droubay, V. Shutthanandan, Scott Chambers, Abbas Mokhtari, Anthony H. Behan, Harry J. Blythe, James R. Neal, A. Mark Fox, Gillian A. Gehring, "XAFS and Magnetization Characterization of the Metallic Co Component in Co-doped ZnO Thin Films", Phys Rev. B 79, 075202 (2009).
10. S.A. Chambers, "Epitaxial Growth and Properties of Doped Transition Metal and Complex Oxide Films", invited review article for Advanced Materials, in press (2009).
11. A. Ney, K. Ollefs, T. Kammermeier, S. Ye, V. Ney, M. Opel, S. T. B. Goennenwein, R. Gross, T. C. Kaspar, M. H. Engelhard, S. A. Chambers, J. Simon, W. Mader, S. Zhou, K. Potzger, S. M. Heald, J. C. Cezar, A. Rogalev, F. Wilhelm, "Advanced Spectroscopic Synchrotron Techniques to Unravel the Intrinsic Properties of Dilute Magnetic Oxides -- the Case of Co:ZnO", Nat. Mat., submitted (2009).
12. A. Ney, T. Kammermeier, K. Ollefs, S. Ye, V. Ney , T. C. Kaspar, S. A. Chambers, F. Wilhelm and A. Rogalev "Anisotropic paramagnetism of Co-doped ZnO epitaxial films", Phys. Rev. B, submitted (2009).

The Atomic and Electronic Structure of Oxide Superlattices

Amish Shah[1], A. Bhattacharya[2] and Jian-Min Zuo[1]*
*Email, jianzuo@illinois.edu
1 Dept. of Materials Science and Engineering and Materials Research Laboratory, University of Illinois, Urbana-Champaign, IL 61801;
2 Materials Science Division, Argonne National Laboratory, Argonne, Illinois 60439

Program Scope

An epitaxial interface between two strongly correlated transition metal oxides can lead to emergent electronic states at the interface, because the explicit breaking of translational symmetry can nucleate new electronic phases.[1] This phenomenon is very different from semiconductor-semiconductor or metal-semiconductor interface physics, which is determined purely by carrier depletion and bending of the sp bonded valence bands. Recent studies have shown that new interfacial states in oxides can be designed and constructed using physical vapor deposition techniques (for a review, see ref [2]), and when the interface is repeated in close spacing (~a few unit cells), it can lead to bulk-like properties.[3,4] Perovskites have a corner-linked octahedral network structure that can accommodate different ions and a large amount of lattice strain during epitaxial growth. Some strongly correlated perovskites also exhibit competing orders involving charge and spin, resulting in a heightened sensitivity to temperature, external fields, and strain[5]. By combining different perovskites in an epitaxial superlattice, the interruption of translational lattice symmetry and strain can be used to favor one competing order over others.

The challenge in oxide interface research is to control interfacial atomic structure and discover its electronic structure. Ultimately, for transition metal oxide interfaces, we must know the type of atoms and their 3-D position at the interface in order to gain a quantitative understanding of interfacial electronic structures. To achieve this goal, we have developed a research program to address a number of issues related to oxide interfaces and their characterization based electron imaging, diffraction, and energy loss spectroscopy.

Recent Progress:

Atomic structure of oxide superlattices: We use a combination of aberration-corrected (AC), high angle annular dark field (HAADF), scanning transmission electron microscopy (STEM) and electron nanodiffraction to characterize the atomic structure of oxide superlattices. AC-HAADF-STEM provides atomic resolution and sensitivity to detect metal cations. Electron nanodiffraction is sensitive to both metal cations and oxygen. The contrast from annular dark field (ADF) STEM also can be used to distinguish between rough and sharp interfaces[4]. The new generation of AC-STEM also can be used to acquire images with large field of views without suffering large sample drifts. For example, it is possible to acquire atomic-level images at field of views greater than 100 nm x 100 nm. This is a useful aid to diffraction since if we are able to acquire a large amount of pixels in the STEM image, we can directly determine from the image where weak spots spot in the Fourier spectrum originate. Using this technique, we have

investigated several $LaMnO_3$-$SrMnO_3$ (LMO-SMO) superlattices grown on (001) $SrTiO_3$ by molecular beam epitaxy. In some LMO-SMO superlattices, the fast Fourier transform (FFT) of the image shows weak reflections from two orthorhombic domains of LMO, which are confirmed by nanoarea electron diffraction. Using a mask of weak reflections in the FFT, we observe weak reflections and their distribution in the superlattice. Surprisingly, both domains are observed but some layers are dominated by one of the two domains (see Figure 1 for an example). We have performed such studies for several similar samples of different layer thicknesses. When the $LaMnO_3$ film was 6 unit cells in thickness or greater, the weak reflections were present in diffraction patterns, but when the $LaMnO_3$ film was 4 unit cells or thinner, the domain structures were absent. The above results demonstrate film-thickness dependent atomic structure, which will be important for understanding the electronic properties of ultrathin oxide superlattices[3].

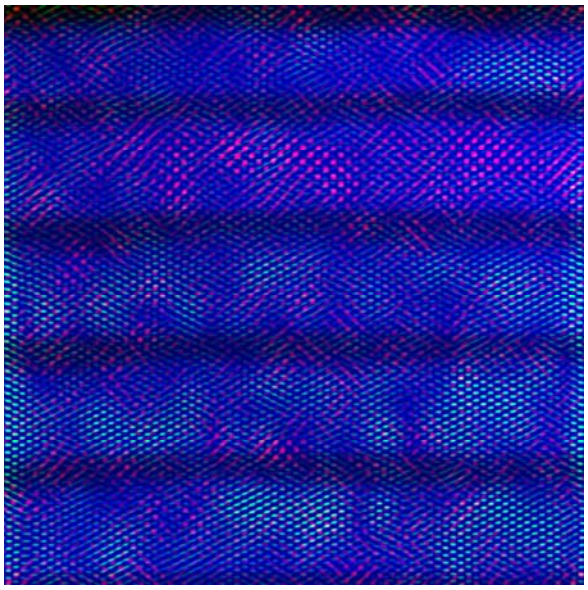

Figure 1. RGB image formed by overlay of STEM image and images from inverse FFTs of masked weak reflections for a $LaMnO_3$-$SrMnO_3$ superlattice grown on $SrTiO_3$. The image show two types of domain structures in the $LaMnO_3$ layer (bright).

Interfacial electronic structure of oxide superlattices: Understanding interfacial electronic reconstruction at oxide interfaces requires fabrication of chemically abrupt and defect-free interfaces and experimental probes to characterize the interfacial atomic structure and charge distribution. Electron microscopy can detect atoms directly at interfaces and probe their electronic structure by electron energy loss spectroscopy (EELS). We carried out an atomic resolution study of the electronic structure of MBE-grown 12 x 4 $LaMnO_3$-$SrMnO_3$ and 2 x 2 $LaMnO_3$-$SrTiO_3$ superlattices (in collaboration with Eckstein, University of Illinois) and their interfaces by EELS. We correlated the interfacial electronic structure with the interfacial atomic structure using atomic resolution Z-contrast scanning transmission electron microscopy (STEM). In STEM-EELS, we measure the site-specific unoccupied states of oxygen atoms and transition metals. The interface electronic structure is mapped using a step size of one spectrum per 1 Å or per 0.5 Å. The high spatial resolution allows a direct mapping of the holes distribution. In the LMO-SMO system we found experimental evidence for extra states (holes) near the Fermi level in the EELS data and their dependence on abruptness of interface. In the LMO-SMO system, an asymmetric hole occupation directly related to the asymmetric atomic structure observed in STEM. In $LaMnO_3$-$SrTiO_3$, we mapped the fine electronic structure of the unoccupied states at atomic resolution (See Figure 2 for an example). We found site-dependent electronic structure of oxygen and a film thickness dependent conduction band edge level for $SrTiO_3$.

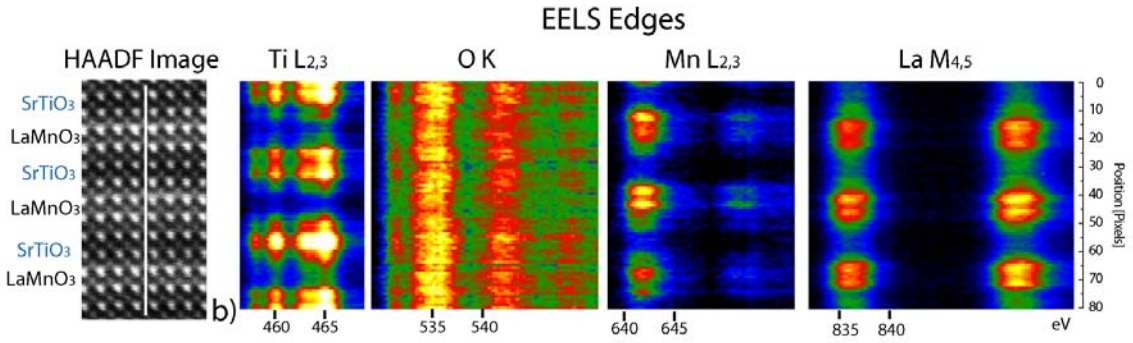

Figure 2. STEM HAADF image of a $LaMnO_3$-$SrTiO_3$ superlattice. EELS chemical maps of Ti, O, Mn, and La shows both spatial mapping of the elements and electronic structural information. For example, the presence of 4 peaks in the Ti $L_{2,3}$ edge indicates a 4+ valence on the Ti site.

Future Plans:

In the immediate future, we plan to complete the atomic and electronic structure characterization of the $LaMnO_3$-$SrMnO_3$ series. We would like to understand the asymmetry observed at the two interfaces. We would like to extract information about local dielectric constant from the low loss EELS spectra. We would also like to understand the source of these asymmetries in combination with synchrotron and neutron studies carried out at ANL. For electron diffraction, we aim to quantify the diffraction intensity to extract information about the atomic structure of $LaMnO_3$ and $SrMnO_3$ and their interfaces. The experiment will be carried out at different temperatures to study their temperature dependence. We also want to use diffraction to observe if the larger unit cell is present. Other systems we would like to study include $SrTiO_3$-$LaMnO_3$, $SrTiO_3$-$SrVO_3$, $LaAlO_3$-$SrTiO_3$, and $LaNiO_3$-$LaMnO_3$. These systems show charge ordering behavior at the Ti, V, Ni, and Mn sites. Furthermore, we plan on using an aberration corrected STEM primarily, where we can use a 1 Å for far better EELS spatial resolution, which has not be demonstrated previously for perovskite superlattices.

Reference:

[1] S. Okamoto and A. J. Millis, "Electronic reconstruction at an interface between a Mott insulator and a band insulator," Nature **428**, 630-633 (2004); N. Reyren, S. Thiel, A. D. Caviglia, L. F. Kourkoutis, G. Hammerl, C. Richter, C. W. Schneider, T. Kopp, A. S. Ruetschi, D. Jaccard, M. Gabay, D. A. Muller, J. M. Triscone, and J. Mannhart, "Superconducting interfaces between insulating oxides," Science **317**, 1196-1199 (2007); R. Pentcheva and W. E. Pickett, "Correlation-driven charge order at the interface between a Mott and a band insulator," Physical Review Letters **99** , 016802 (2007); B. R. K. Nanda and S. Satpathy, "Electronic and magnetic structure of the (LaMnO3)(2n)/(SrMnO3)(n) superlattices," Physical Review B **79** (5), 054428 (2009).

[2] D. G. Schlom, L. Q. Chen, X. Q. Pan, A. Schmehl, and M. A. Zurbuchen, "A thin film approach to engineering functionality into oxides," J. Am. Ceram. Soc. **91**, 2429-2454 (2008).

[3] A. Bhattacharya, S. J. May, Sget Velthuis, M. Warusawithana, X. Zhai, B. Jiang, J. M. Zuo, M. R. Fitzsimmons, S. D. Bader, and J. N. Eckstein, "Metal-insulator transition and its relation to magnetic structure in $(LaMnO_3)_{(2n)}/(SrMnO_3)_{(n)}$ superlattices," Physical Review Letters **100**, 257203 (2008).

[4] S. J. May, A. B. Shah, S. G. E. te Velthuis, M. R. Fitzsimmons, J. M. Zuo, X. Zhai, J. N. Eckstein, S. D. Bader, and A. Bhattacharya, "Magnetically asymmetric interfaces in a $LaMnO_3/SrMnO_3$ superlattice due to structural asymmetries," Physical Review B (Condensed Matter and Materials Physics) **77** (17), 174409-174405 (2008).

[5] M. B. Salamon and M. Jaime, "The physics of manganites: Structure and transport," Reviews of Modern Physics **73** (3), 583-628 (2001).

DOE Sponsored Publications in 2007-2009

1) S. Smadici, P. Abbamonte, A. Bhattacharya, X. F. Zhai, B. Jiang, A. Rusydi, J. N. Eckstein, S. D. Bader, and J. M. Zuo, "Electronic reconstruction at SrMnO3-LaMnO3 superlattice interfaces," Physical Review Letters **99** (19), 196404 (2007).
2) A. Bhattacharya, S. J. May, S. Velthuis, M. Warusawithana, X. Zhai, B. Jiang, J. M. Zuo, M. R. Fitzsimmons, S. D. Bader, and J. N. Eckstein, "Metal-insulator transition and its relation to magnetic structure in $(LaMnO_3)(2n)/(SrMnO_3)(n)$ superlattices", *Physical Review Letters* 100, 257203 (2008).
3) S. J. May, A. B. Shah, S. Velthuis, M. R. Fitzsimmons, J. M. Zuo, X. Zhai, J. N. Eckstein, S. D. Bader, and A. Bhattacharya, "Magnetically asymmetiric interfaces in a $LaMnO_3/SrMnO_3$ superlattice due to structural asymmetries", *Physical Review B* 77, 174409 (2008)
4) A. B. Shah, X. F. Zhai, B. Jiang, J. G. Wen, J. N. Eckstein, and J. M. Zuo, "Electron energy-loss study of the electronic structure of atomic scale $SrTiO_3$-$SrMnO_3$-$LaMnO_3$ superlattices", *Physical Review B* 77, 115103 (2008)
5) A. B. Shah, Q. M. Ramasse,[3] X. Zhai, J. G. Wen, S. J. May, I. Petrov, A. Bhattacharya, P. Abbamonte, J. N. Eckstein and J. M. Zuo. "Probing Interfacial Electronic Structures of Oxide Superlattices at Atomic Resolution", Advanced Materials, Progress report, submitted and under review, 2009

Invited talks

1) "Characterization of Oxide Superlattices", DoD workshop on strongly correlated oxides, Washington, DC, Feb., 2008
2) "Modeling Electron Diffraction and Imaging in Microscopes with Aberration Correctors for Quantitative Materials Structural Analysis", Microscopy Society of America, 2008 annual meeting, Albuquerque, New Mexico, Aug. 5, 2008
3) "Aberration Corrected Electron Probes and their applications for structure determination", Tsinghua-FEI Workshop on Cs-Corrected TEM, Tsinghua University, Oct. 15, 2008
4) "Theory and Practice of Electron Diffraction", ASU Workshop on HREM, Arizona State University, Jan. 9, 2009
5) "The Atomic Structure of Supported Nanoparticles and electronic structure of oxide superlattices", National Center for Electron Microscopy, Lawrence Berkeley National Laboratory, March, 11, 2009.
6) "Quantitative electron diffraction and applications to materials science", Spring MRS Meeting, San Francisco, April 18, 2009
7) "Quantitative Convergent Beam Electron Diffraction and Nanodiffraction", European Workshop on Advanced TEM measurement techniques for Materials Science, La Gaillarde, France, May 29, 2009

The Oxide MBE program at the Center for Nanoscale Materials at Argonne.

Anand Bhattacharya
anand@anl.gov
Materials Science Division and Center for Nanoscale Materials,
Argonne National Laboratory, Argonne IL 60439.

In this talk, I will present an overview of the oxide-MBE program at the Center for Nanoscale Materials (CNM) at Argonne. The Oxide MBE system was installed in Fall of 2007 as a user facility within the Electronic and Magnetic Materials and Devices Group at the CNM. At this time, this system serves a number of user proposals, the CNM core science program on complex oxides and the Digital Synthesis FWP based in the Materials Science Division. In the first part of this talk, I will describe some of the essential features of oxide-MBE, particularly aspects of the design of our system that enables the synthesis of high quality thin films, heterostructures and superlattices of a broad range of complex oxide materials, with relatively rapid turnaround between different materials. I will briefly describe the materials that we have synthesized in the course of these research programs till date. In the second part of this talk I will outline the motivations for the CNM core science program in complex oxides, which seeks to explore these materials at the nanoscale. As we now know, the complex oxides display a very rich array of physical phenomena, often involving competing ground states that are very close in energy to one another. This may lead to coexisting nanoscale regions of very disparate electronic and magnetic properties (*eg.* 'stripes' in the nickelates and cuprates or mixed-phase regions within the manganites), and this has been studied extensively, particularly with scanning probes. An aspect that has received relatively lesser attention is the sensitivity of the properties of complex oxides to being patterned or otherwise confined at the nanoscale. I will describe our approaches to creating patterned structures, and the progress that we have made in realizing such structures. We probe these structures using a number of different techniques, including scanning probes (in collaboration with the scanning probe effort at the CNM). I will describe a few initial results that have been realized in these studies.

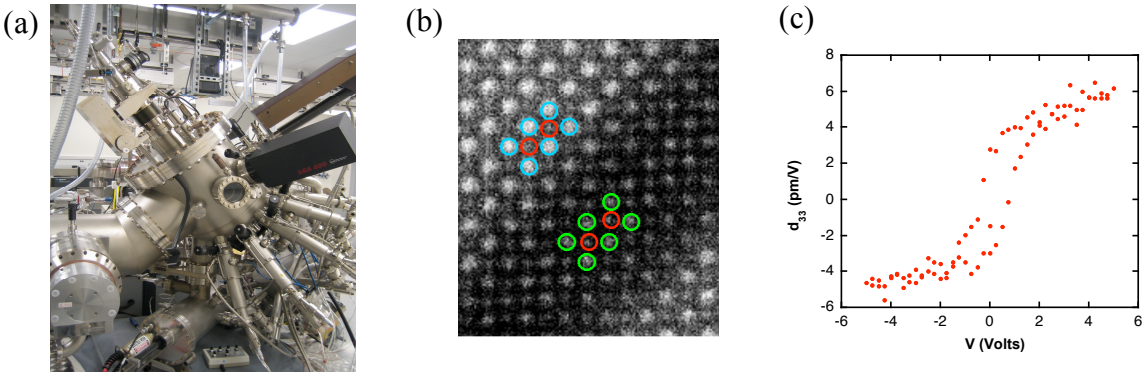

Fig. 1. (a) The oxide MBE system at Argonne's Center for Nanoscale Materials. (b) Scanning transmission electron microscopy image of a $LaMnO_3/SrMnO_3$ superlattice grown in the CNM MBE system. The La atoms are relatively brighter because of their higher atomic number (courtesy A. Shah, J.-M. Zuo, UIUC). (c) A hysteresis loop measured with a piezo-force microscope on a 23 nm $BaTiO_3$ film grown in the CNM MBE system (courtesy T. Santos, CNM, Seungbom Hong, MSD, Argonne).

Project Title: "Multifunctional Nanostructure for Magnetoelectric and Spintronics Applications" ***Grant #DE-FG02-08ER46526***

Investigators (12)**:** *R.S. Katiyar, M. Gomez, G. Morell, L. Fonseca, W. Otano^, O. Perales[+], M.S. Tomar[+], Y. Ishikawa, R.Palai, R. Thomas, A. Kumar, V. Makrov* (University of Puerto Rico, Rio Piedras, Mayaguez[+], Cayey^)

Email: rkatiyar@hpcf.upr.edu

Abstract:

CMOS compatible *Multifunctional Materials* to meet the near future demand of miniaturization of Si based technology and for the next generation technology beyond Si, were the goals of this project. During the past year, the researchers have been actively involved in the synthesis and characterization of various *functional oxides and silicides* to accomplish this goal. We designed and optimized multiferroic nanostructures for numerous electronics applications, because of their potential advantages over conventional electronics devices, such as NVRAM, sensors and actuators, spin valves, data storage systems, due to high speed, low power consumption, radiation hard, and low costs. Many of these devices need a stack of thin film nanostructures (superlattices and heterostructures) and therefore, major part of our efforts in this period focused on demonstrating the feasibility of fabricating multiferroic thin film heterostructures apart from the single phase materials. Some of the materials screened so far showed multifunctional properties especially for spintronics and magnetoelectric applications.

Dilute Magnetic semiconductors

ZnCuO films showed nearly single crystalline phase (≤ 3% Cu doping) with ferromagnetic behavior (Ms ~ 0.76 μ_B/Cu) that reduced on further increase in Cu doping. Moreover, the 1%Cu doped ZnO thin film is epitaxial and free from any interfacial reaction with the substrate (Al_2O_3). Pure and Ni-doped $In_{2-x}Ni_xO_3$ (x=0.0, 0.01, 0.05, 0.1) nanocystalline powders were synthesized and studies indicated that Ni ions are indeed occupying interstitial sites in the host In_2O_3. The room and low-temperature magnetic characterizations showed no evidence of ferromagnetism.

The electrospinning technique has been used to fabricate ZnO and ZnO [Fe, Mn] fibers and ribbons. $ZnFe_2O_4$ spinel was prepared by the electrospinning technique using sol-gel precursors with different polymers. The XRD confirmed the zinc ferrite formation in the cubic spinel structure and the SEM images show the formation of fibers and ribbons in a diameter range of 100 to 500 nm as seen in Figure 1c. The magnetic hysteresis loops of $ZnFe_2O_4$ were measured at room temperature showing typical hysteresis loops as a function of heat-treatment. Magnetization, remnance and coercivity increased with increasing the heat-treatment temperature. Figure 1 b &c shows the AFM topographic and MFM magnetic signal in 3-dimensions of a sample heated at 600 °C. The topographic contrast observed in the magnetic image is believed to correspond to magnetic domains in the sample.

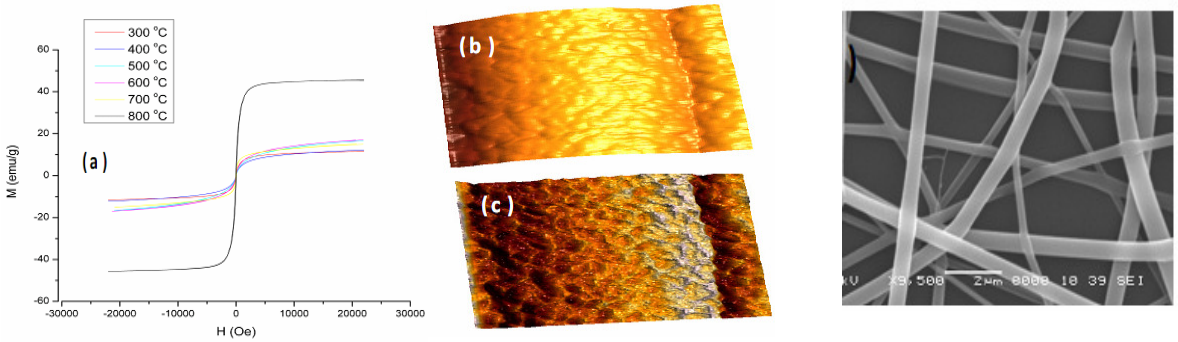

Figure 1 *(a) Magnetic measurements for $ZnFe_2O_4$ spinel phase heat-treated at different temperatures. (b)&(c) Atomic force microscopy topography (top) and corresponding MFM image (bottom) in 3-dimensions of a sample heated at 600 °C. (c) SEM micrographs of fibers and ribbons.*

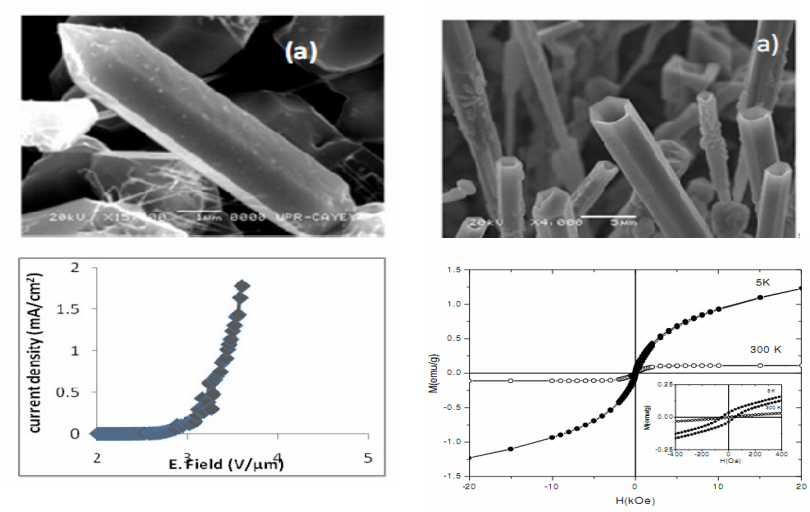

Fig.2 (a) SEM image of a $CrSi_2$ microwire (b) SEM image of $Cr_{0.50}$ $Fe_{0.48}$ $Mn_{0.02}$ Si microwires (c) field emission effects (d) M-H hysteresis

Two new transition metals silicide nanowires were synthesized by Chemical Vapor Transport method: one is Cobalt silicide (CoSi) and the other is the Chromium, Iron, Manganese alloy silicide. The EDS line scans and mappings revealed that the wire grows in a core shell structure in which CoSi is forming the core and the shell is made of silica. The electron diffraction studies showed that the core nanostructure is a single crystal with the c-axis oriented along the growing direction. For the of Cr_x $Fe_yMn_{(1-x-y)}Si$ we were able to grow nano- and micro-wires as shown in Figure 2a &b. The EDS analyses gave atomic ratios consistent with $Cr_{0.50}$ $Fe_{0.48}$ $Mn_{0.02}$ Si and the electron diffraction patterns also confirmed a single crystal structure. The SQUID measurements done on the alloy silicide structures gave a Curie temperature of 10K (Figure 2d). Figures 2c shows the current density versus electric field intensity and the Fowler-Nordheim plot respectively. A turn-on electric field of 1.62 V/μm for an emission current density of 0.1 μA/cm^2 was measured. The maximum current density was 1.86 mA/cm^2 at an electric field of 3.6 V/μm. The data fits well the linear relationship given by the Fowler-Norheim relation. The results demonstrate an excellent electrical contact between the silicon substrate and the nanowires.

Multiferroic Heterostructures

We have fabricated heterostructures and superlattices of ferroelectric, $Ba_{1-x}Sr_xTiO_3$ (BSTO), T_C~ 310K and CMR manganites (ferromagnetic), $La_{2/3}Sr_{1/3}MnO_3$ (LSMO), T_C~ 310K using pulsed laser deposition. Our fabricated heterostructures using 20nm thick LSMO/BSTO/LSMO show multiferroic properties. Highly oriented $Pb(Zr_{0.53}Ti_{0.47})O_3$ (PZT)/$CoFe_2O_4$ multilayered nanostructures (MLNs) were grown on MgO substrate by PLD using LSCO as conducting bottom electrode. Low fatigue and strong temperature and frequency dependent magneto-electric coupling suggest MLNs utility for Dynamic Magneto-Electric Random Access Memory (DMERAM) as described in Reference 2. Layered nanostructures (LNs) of the commercial ferroelectric $Pb(Zr_{0.53}Ti_{0.47})O_3$ (PZT) and the natural ferroic relaxor $Pb(Fe_{0.66}W_{0.33})O_3$ (PFW) were also fabricated with periodicity of PZT/PFW/PZT (~ 5/1/5 nm, thickness ~ 250 nm) on MgO substrate with high remanent polarization (P_r) of about 33 μC/cm^2 and magnetization of 5.32 emu/cc. Very low leakage current densities were obtained ~ 10^{-7} – 10^{-5} A/cm^2 over 500 kV/cm.

Dielectric films have attracted much attention for active and passive devices in silicon-based integrated circuits. Traditionally, dynamic random access memory (DRAM) capacitor and transistor gate uses highly scalable silicon based dielectrics such as SiO_2, SiO_2/Si_3N_4 and Si_3N_4 in the planar geometries and lately in 3D structures. $DyScO_3$ films were grown on platinized silicon and Si substrates by pulsed liquid injection MOCVD. Dielectric constant was around 22 and the capacitance was stable with the voltage, frequency and the temperature variation. These results suggest that $DyScO_3$ films can be considered as high-k material for and DRAM applications and buffer layer for MFIS devices.

The polarization bistability of ferroelectric material offers the possibility to develop high-density, low power, faster write speed, maximum write-erase cycles and radiation resistance NVRAM; alternate to both DRAM and Flash. Multiferroic BFO thin film and high-*k* DSO insulating buffer were fabricated on

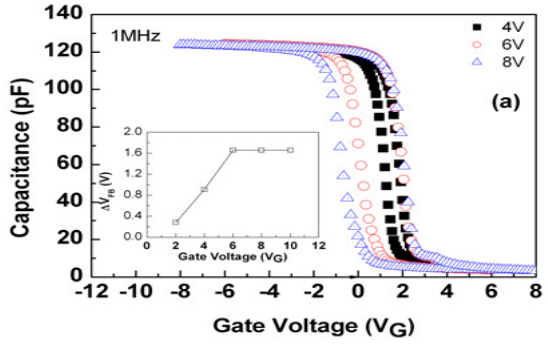

Si and the MFIS diodes were tested for the memory applications. The ferroelectric polarization of BFO gives rise to a memory window of 1.7 V. The magnitude of the memory window demonstrates that BFO has potential in FET FeRAM applications. Lead free ferroelectric, $Bi_{3.25}Nd_{0.75}Ti_3O_{12}$ with Pr ~20.0 $\mu C/cm^2$, E_c ~ 62kV/cm, ε_r ~ 400 and tanδ ~ 0.04 were successfully synthesized. MFIS diodes were fabricated by depositing $Bi_{3.25}Nd_{0.75}Ti_3O_{12}$ ferroelectric film on p-type silicon substrate with an amorphous high-k $DyScO_3$ film. The clockwise CV hysteresis and a memory window of about 0.7V were obtained.

Figure 3*(a)Capacitance-voltage (C-V) characteristics of the Pt/BFO/DSO / p-Si structure with sweep voltages of 4, 6 and 8 V; inset shows the variation of memory window with sweep voltage range.*

Magnetoelectric multiferroics

Basic studies in terms of the structural properties of epitaxial BFO, grown on (111) $SrTiO_3$ substrates, revealed magnetic behavior of $BiFeO_3$ that cannot be described by the Ising Model (*cited as one of the best papers of the Year 2008 by the editors of J. Physics – Condensed Matter*). By investigating low temperature Raman scattering from magnons in the only room temperature single phase magnetoelectric multiferroic $BiFeO_3$, we discovered two new spin reorientation transitions at lower temperatures, namely at 140K and 200K (*also cited as one of the best papers of the Year 2008 by the editors of J. Physics – Condensed Matter*). Polycrystalline $BiFe_{1-x}Ti_xO_3$, $BiFe_{0.9}Ti_{0.05}Co_{0.05}O_3$, $BiFe_{1-x}Ti_xO_3$ thin films on Pt/Ti/SiO_2/ Si (100) substrates were also tested. Up to 5% Ti in the BFO lattice reduces the leakage current substantially and a further increase deteriorates the insulting properties. The magnetic properties were completely lost by Ti substitution and which supports the fact that ferromagnetic properties of pure BFO are intrinsic and not from the Fe_2O_3 trace amount. Considerable enhancement in the ferroelectric properties was observed at room temperature in $Bi(Fe_{0.95}Cr_{0.05})O_3$ compared to BFO.

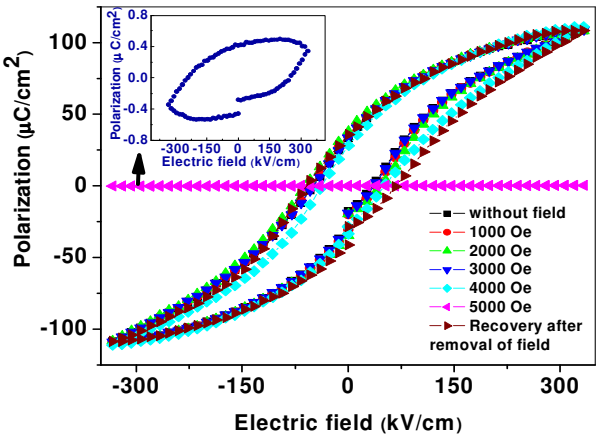

Fig. 4 *Strong M-E coupling in PZT-PFW thin films at room temperature. Inset showed the enlarged*

New room-temperature, single-phase, multiferroic magnetoelectric, $PbZr_{0.46}Ti_{0.34}Fe_{0.13}W_{0.07}O_3$, with polarization loss (<4%), and resistivity (typically 10^8 -10^9 ohm-cm) equal to or superior to $BiFeO_3$ was developed. Figure 4 showed that $PbZr_{0.42}Ti_{0.38}Fe_{0.13}W_{0.07}O_3$ compounds having enormously greater ME effect: switching not from +Pr to –Pr with applied magnetic field, H, but from Pr to zero with applied H of merely 0.5 Tesla. Dielectric properties and magnetic hysteresis revealed the coexistence of relaxor ferroelectricity and weak ferromagnetism at room temperature in PFN films.

Work Plan for the Year 2:

1. $Bi_4Ti_3O_{12}$ based materials have shown large ferroelectric polarization and some evidence of magnetic coupling at low temperature (5K) when Bi is replaced by Gd. If the lattice is distorted by partial replacement of Bi and Ti, it is expected that such material may show strong magnetic coupling also.
2. TiO_2 is a wide gap semiconductor with possibility of p and n doping. It also offers the possibility for magnetic coupling when Ti ion is substituted by cobalt ion.
3. To find the electronic band structure and excitonic transitions at UV region wide band gap in ZnO, In_2O_3, and $CuAlO_2$ by doping Be, Mg, Al. To investigate the room temperature ferromagnetism in Fe and Ni doped In_2O_3 and $CuAlO_2$ thin films.
4. Novel class of magnetoelectric multiferroic with alternate ferroelectric and ferromagnetic/antiferromagnetic/multiferroic layers and its vice versa (i.e. $Pb(Zr,Ti)O_3$ (PZT) - $CoFe_2O_4$(CFO), PZT-$La_{0.67}Ca_{0.33}MnO_3$(LCMO), PZT-$PbFe_{0.66}W_{0.33}O_3$ (PFW), PZT-$PbFe_{0.5}Nb_{0.5}O_3$ (PFN), and PZT-$PbFe_{0.5}Ta_{0.5}O_3$ (PFT).
5. Find the magneto electric coupling effect in $BiFeO_3/CoFe_2O_4$, $BiFeO_3/BaTiO_3$ multilayer at room temperature. Characterization of the ZnO and ZnO[Fe, Mn] nano ribbons prepared using the electrospinning technique and the nanofibers prepared by dc sputtering.
6. Investigate heterostructures and superlattices for giant mangetoresistance (GMR) devices using CMR manganites (LSMO or LCMO) as a free layer and ferroelectrics (BSTO) as a spacer layer and tunnel magnetoresistance (TMR) devices using CMR manganites as an active layer and multiferroic ($BiFeO_3$) as a space layer.
7. Novel high-k material by Atomic layer deposition for the gate-oxide and buffer layer realization.

List of Publications Year 1:

1. Positive temperature coefficient of resistivity (PTCR) and negative differential resistivity in lead iron tunstate-lead zirconate titate**;** Ashok Kumar, R.S. Katiyar, and J. F. Scott, *Applied physics Letters* (2009) (In press).
2. Dynamic magneto-electric multiferroics PZT/CFO multilayered nanostructure, Ashok Kumar, N. Ortega, and R. S. Katiyar, *Recent Developments in Ferroelectric Nanostructures and Multilayers JMS*, (2009) (In press)
3. Strain induced artificial multiferroicity in $Pb(Zr_{0.53}Ti_{0.47})O_3$ / $Pb(Fe_{0.66}W_{0.33})O_3$ layered nanostructure at ambient temperature Ashok Kumar, C. Rinaldi, R.S. Katiyar, J. F. Scott, Recent Developments in Ferroelectric Nanostructures and Multilayers; *JMS*,(in press 2009).
4. Low temperature synthesis and Raman scattering of Mn-doped ZnO nanopowders, Boqian Yang, Ashok Kumar, Noel Upia, Peter Feng, and R.S. Katiyar, Journal of Raman Spectroscopy (2009) (In press)
5. Temperature-Dependent Structural Disintegration of Delafossite $CuFeO_2$, Shojan P. Pavunny, Ashok Kumar, N.M. Murari, R. Thomas, and R.S. Katiyar *MRS Spring 2009 Proceedings*, (in press 2009)
6. Preferential grain growth and improved fatigue endurance in Sr substituted PZT thin films on Pt(111)/TiOx/SiO_2/Si substrates, N. K. Karan, R. Thomas, S. P. Pavunny, J. J. Saavedra-Arias, N. M. Murari, and R. S. Katiyar, *J. Alloys and Compounds.*, (Accepted) (In Press)
7. Structural, electrical and magnetic properties of chemical solution deposited Bi $(Fe_{0.95}Cr_{0.05})O_3$ thin films on platinized silicon substrates N.M.Murari, R. Thomas, A.Winterman, R.E. Melgarejo, S.P. Pavunny and R. S. Katiyar, J. Appl. Phys. **105** (2009).
8. Structural, electrical and magnetic properties of chemical solution deposited $BiFe_{1-x}Ti_xO_3$ and $BiFe_{0.9}Ti_{0.05}Co_{0.05}O_3$ thin films, N. M. Murari, R. Thomas, R. E. Melgarejo, S. P. Pavunny, and R. S. Katiyar, *J. Appl. Phys.* (2009) (accepted)
9. Multiferroics $Pb(Fe_{0.66}W_{0.33})_{0.80}Ti_{0.20}O_3$ thin films: A room temperature relaxor ferroelectric and weak ferromagnetic, Ashok Kumar, I. Rivera, and R.S. Katiyar, *MS&T08 (Material Science and Technology 2008 Conference and Exhibition Proceeding* (2009) (accepted)

Conduction Mechanisms and Structure of Ionomeric Single-Ion Conductors
Part 1: Structure

Ralph H. Colby, Janna K. Maranas, Karl T. Mueller, James Runt
Materials Research Institute, Penn State University, University Park, PA 16803
and Karen I. Winey
Materials Science and Engineering, University of Pennsylvania, Philadelphia, PA 19104

Program Scope

Our group combines expertise in a variety of aspects of static and dynamic properties of ionomers to study the same set of materials: Low glass transition temperature ionomers that primarily comprise polyethers with sulfonated anions and either Li^+, Na^+ or Cs^+ counterions. The ether oxygens in these polymers play a vital role, solvating the ions and preventing the microphase separation of ions that occurs in conventional ionomers. We aim to thoroughly understand ion conduction mechanisms in this class of materials, with the ultimate goal of being able to design ionomer membranes for facile ion transport.

Recent Progress Part 1: Structure

Polyethylene glycol (PEG)-based polyester ionomers with variable ion content have been synthesized, with the structure given below. A mixture of neutral dimethyl isophthalate and dimethyl 5-sulfo isophthalate sodium salt were used with M = 600 PEG to produce a range of ion contents with nomenclature PEG600-x%C (x% is the mole% of sulfonated phthalates 0%, 2.5%, 6%, 11%, 17%, 49%, 70%, 85%, 100%; C is the cation Li, Na, Cs).

Room temperature X-ray scattering on PEG600-100%Li, PEG600-100%Na and PEG600-100%Cs, shown in the figure at left, exhibit the amorphous halo of PEO at high q = 17 nm^{-1}, with cation-dependent scattering at lower q. The broadened amorphous halo of the Cs ionomer may also be showing the spacing of cations in quadrupoles, at ~18 nm^{-1}. PEG600-100%Cs also shows a peak at ~7.5 nm^{-1}, indicating some sort of local structural ordering of ions. PEG600-100%Na shows no sign of any ionomer peak, while at ~2.7 nm^{-1}, PEG600-100%Li does.

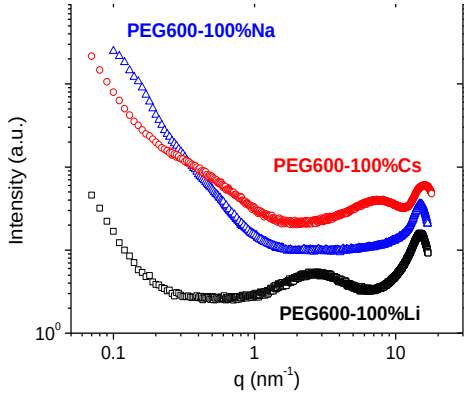

It should be noted that all the materials of this study have very low glass transition temperatures (far below room temperature) and relatively low molecular weight (<10K),

allowing them to reach thermodynamic equilibrium rapidly. The terminal relaxation time of these ionomers is only a few seconds at 25 °C. During the variable-temperature X-ray scattering experiments discussed next, the samples were annealed at each temperature for 10 min before data collection. As a result, we believe the morphology we observed should be close to the equilibrium state of the materials. All data are reproducible in both heating and cooling.

Increasing the temperature of the PEG600-100%Li causes the peak at ~2.7 nm^{-1} to increase in intensity, and the peak position shifts very slightly to lower angle (~2.5 nm^{-1} at 150 °C). Increasing temperature in all the PEG-100%Na and 100%Cs ionomers causes an "ionomer peak" to form at 2-3 nm^{-1} (with PEG segment length = 400, 600, 900; only the PEG600 data are shown below).

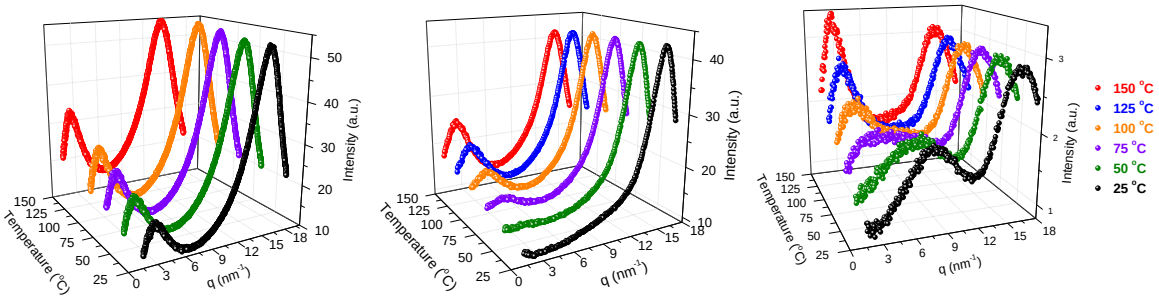

PEG 600 -100%Li PEG 600 -100%Na PEG 600 -100%Cs

We are developing scattering models, based on the Kinning-Thomas model for roughly spherical ionic aggregates and the Debye function for ionic chains to help us interpret such SAXS data in terms of quantitative populations of various ion states. All of the ionomers show the usual "ionomer upturn" at low q in SAXS, and we have studied this in more detail using ultra-small angle x-ray scattering (USAXS) at Argonne. The USAXS data show that the low q upturn continues to as low q as we can measure. The PEG600-Na (100% sulfonated) data shown here demonstrate that the low q upturn and the shoulder near 10^{-2} Å^{-1} are reasonably insensitive to temperature, while again showing the growth of an ionomer peak at 2-3 nm^{-1} at elevated temperature.

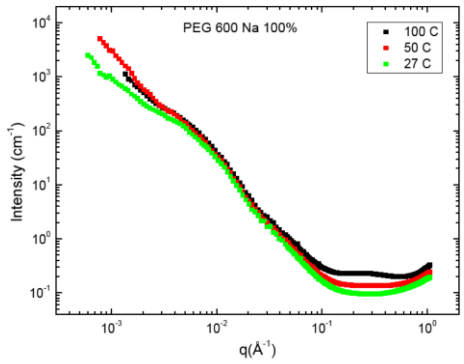

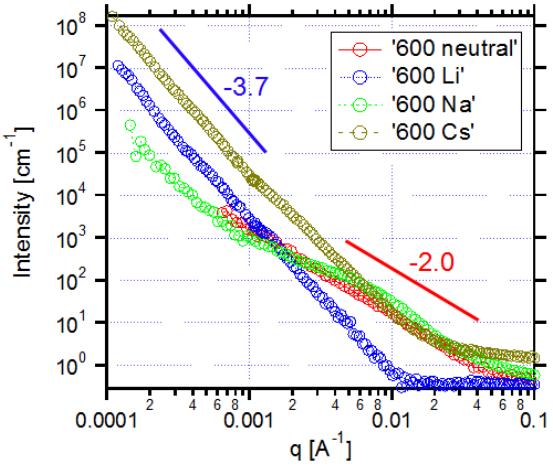

USAXS scattering on the PEG600-100%Li and PEG600-100%Cs shown at right suggest that the low q upturn with slope -3.7 is quite similar for the ionomers with various counterions but the shoulder

near 10^{-2} $Å^{-1}$ is only seen for PEG600-100%Na. The fact that the low q upturn is also evident in the neutral counterpart PEG600-0% (shown in red and labeled '600 neutral' in the figure to the left above) leads us to the tentative conclusion that the low q upturn in ionomers is primarily caused by critical fluctuations of ionic impurities.

Density functional theory (DFT) calculations have been performed on the benzene sulfonate anion with Li^+, Na^+ and K^+ counterions, using Gaussian98 for input of force fields in the MD simulations described below. These quantum chemistry calculations are done at 0 K in vacuum, meaning that they provide a lower bound on the separation distances of ions in various states. Shown at left is the equilibrated quadrupole for two Li^+ ions (purple) with two benzene sulfonate anions (dark grey is C, light grey is H, yellow is S, red is O). The cation – anion spacings in quadrupoles are consistently larger than those observed in contact ion pairs, as detailed in the Table below, taking the S – cation distance as the measure of the spacing.

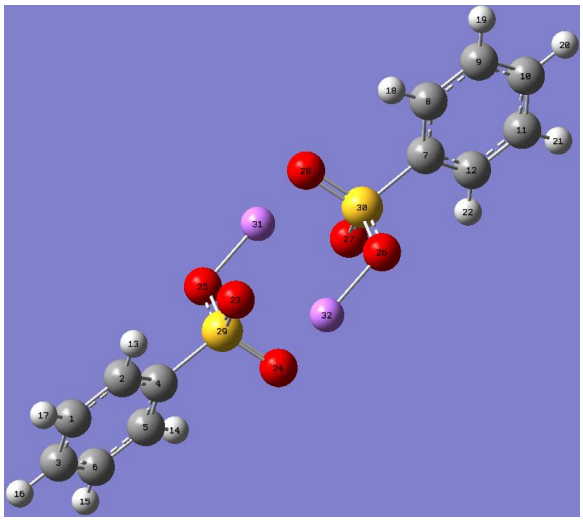

Cation	S – cation (Å) ion pair	S – cation (Å) quadrupole	S – S (Å) quadrupole	cation – cation (Å) quadrupole
Li^+	2.37	2.46	4.09	3.51
Na^+	2.74	2.88	4.59	3.40
K^+	3.13	3.30	5.09	4.12

.

Solvation of cations and anions by the ether-oxygen of PEO is well known to play an important role in PEO-based ion conducting membranes. Solvation by multiple ether-oxygens has been studied by adding 1-6 DME (dimethyl ethers) to the ions of interest and also to the studies of contact ion pairs and quadrupoles discussed above. The figure at the left shows the cumulative effect of solvation of ions by multiple DME saturates at 5 or 6 DME because no additional DME can fit around a given ion. Li^+ is solvated by DME more than Na^+ and the cations are solvated much more than the anions that have been studied. The cumulative effect of 5 ether-oxygens coordinating around Li^+ (480 kJ/mol) is comparable to the

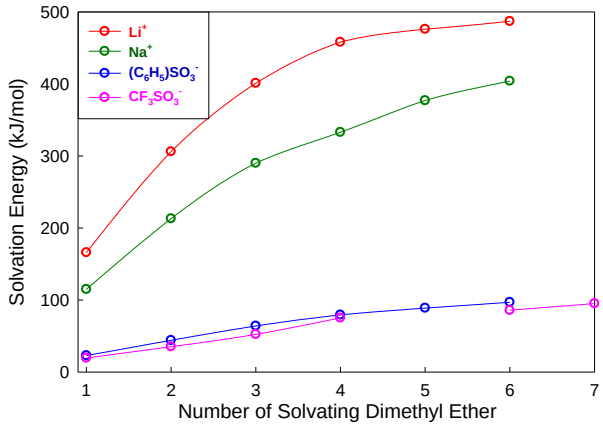

association energy of the benzene sulfonate Li^+ contact pair (640 kJ/mol), confirming that solvation by ether oxygens plays a vital role in our ionomers.

Force fields for the PEG-based polyester ionomers have been developed using those known and well-tested for poly(ethylene oxide) and poly(ethylene terephthalate). The force fields for the sulfonate group have been estimated by the DFT calculations described above. MD simulation of the 100% sulfonated polyester ionomers based on M = 600 PEG with Na^+ counterions has been equilibrated at 343K. This simulation is being compared with quasi-elastic neutron scattering data to assess the force fields utilized.

One powerful aspect of MD simulations is that potentials can be easily adjusted to explore their consequences. In the figure on the left, the orange curve is the radial pair distribution function for Na – S with our best force-fields (labeled accurate). This g(r) is compared with two others that have adjusted force fields; the teal curve has enhanced Na – S interactions and the pink curve has enhanced Na – O interactions. All three show evidence for three ion states with significant populations: contact pairs (2.7 – 3.6 Å), quadrupoles (3.2 – 4.5 Å) and separated pairs that have an ether oxygen between the cation and the anion (7.0 – 8.5 Å for the accurate g(r)). The same three ion states are being utilized to interpret data from NMR and dielectric spectroscopies discussed in Part 2.

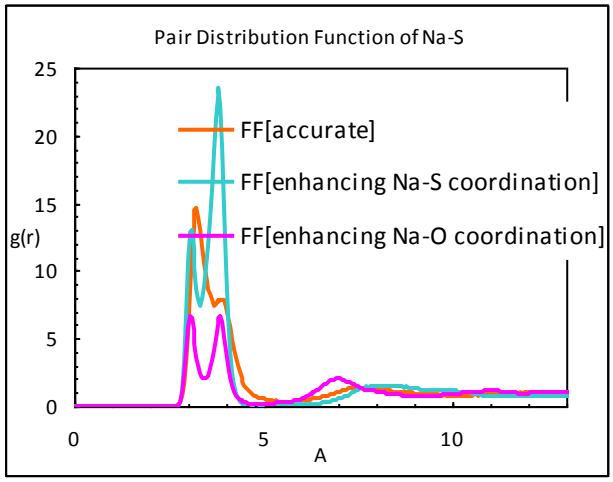

Future Plans: Part 1: Structure

We are combing these characterization methods and calculations to fully determine the populations of various ion states (isolated ion pairs, conducting triple ions and quadrupoles) in these polyether ionomers. We are also synthesizing the next generation of low-T_g ionomers with polysiloxane backbones and both polar and weak-binding ionic side groups. Our *ab initio* calculations suggest that the oxygen in the siloxane backbone is nearly as good at solvating cations as the oxygen in PEO, and has identified weak-binding anions and polar groups that can be added as side groups to these polysiloxanes.

DOE Sponsored Publications in 2008-2009 from Current Grant

1. D. Fragiadakis, S. Dou, R.H. Colby, and J. Runt, Molecular Mobility, Ion Mobility, and Mobile Ion Concentration in Poly(ethylene oxide)-based Polyurethane Ionomers, *Macromolecules* **41**, 5723 (2008).
2. D. Fragiadakis, S. Dou, R. H. Colby and J. Runt, Molecular Mobility and Li^+ Conduction in Polyester Copolymer Ionomers based on Poly(ethylene oxide), *J. Chem. Phys.* **130**, 064907 (2009).
3. M. Lu, J. Runt and P. C. Painter, An Infrared Spectroscopic Study of a Polyester Copolymer Ionomer based on Poly(ethylene oxide), *Macromolecule*s, submitted.

Conduction Mechanisms and Structure of Ionomeric Single-Ion Conductors
Part 2: Dynamics

Ralph H. Colby, Janna K. Maranas, Karl T. Mueller, James Runt
Materials Research Institute, Penn State University, University Park, PA 16803
and Karen I. Winey
Materials Science and Engineering, University of Pennsylvania, Philadelphia, PA 19104

Program Scope

Our group combines expertise in a variety of aspects of static and dynamic properties of ionomers to study the same set of materials: Low glass transition temperature ionomers that primarily comprise polyethers with sulfonated anions and either Li^+, Na^+ or Cs^+ counterions. The ether oxygens in these polymers play a vital role, solvating the ions and preventing the microphase separation of ions that occurs in conventional ionomers. We aim to thoroughly understand ion conduction mechanisms in this class of materials, with the ultimate goal of being able to design ionomer membranes for facile ion transport.

Recent Progress Part 2: Dynamics

^{7}Li pulsed-gradient spin-echo (PGSE) experiments were carried out to determine the self-diffusion coefficients of lithium cations in PEG600-6%Li, PEG600-11%Li and PEG600-17%Li at 290K and 298K, summarized in the table below.

Sample	Self Diffusion Coefficients Measured at 298 K	Self Diffusion Coefficients Measured at 290 K
PEG600 Li 6%	2.22×10^{-13} m^2/s	1.16×10^{-13} m^2/s
PEG600 Li 11%	1.76×10^{-13} m^2/s	9.04×10^{-14} m^2/s
PEG600 Li 17%	1.52×10^{-13} m^2/s	7.04×10^{-14} m^2/s

Using the Nernst-Einstein equation, self-diffusion coefficient of Li^+ was calculated from the measured temperature dependence of conductivity from dielectric spectroscopy on the same ionomers (described below) and compared with the self-diffusion coefficients measured by ^{7}Li NMR in the figure to the left. The NMR data logically have larger D than expected from the Nernst-Einstein equation, because ion pairs contribute to diffusion but not to conduction. The NMR data also change the order, with lowest ion content showing the largest D and the strongest deviation from Nernst-Einstein expectations, indicating large populations of ion pairs in the lightly sulfonated polymers.

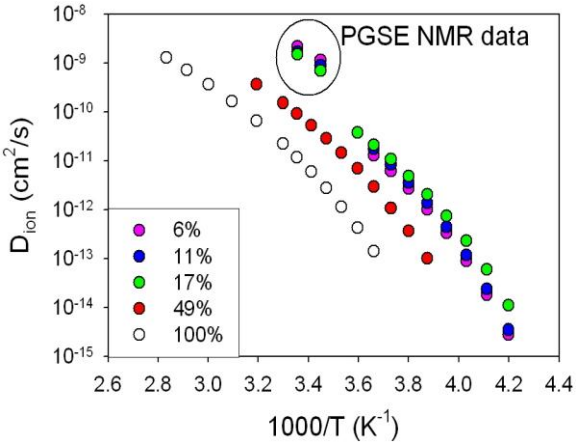

Also consistent with dielectric results discussed below, the larger ion content polymers

have significant populations of quadrupoles that act as crosslinks to raise Tg, and do not contribute to either conduction or diffusion of ions.

We have continued investigations of PEG600-Na ionomers with 6%, 11%, 17% and 100% sulfonation utilizing an array of solid-state nuclear magnetic resonance (NMR) studies. These include single pulse ^{23}Na magic angle spinning (MAS) NMR, single pulse ^{13}C MAS NMR (with ^{1}H decoupling), and new variable temperature ^{1}H/^{13}C cross polarization MAS (CPMAS) NMR (with ^{1}H decoupling). Similar experiments were performed on a lithium-exchanged series of PEG600 ionomers with sulfonation levels of 6%, 11%, 17% and 100%. These include single pulse ^{7}Li MAS NMR, single pulse ^{13}C (with ^{1}H decoupling) MAS NMR, and ^{1}H/^{13}C CPMAS NMR.
For the PEG600-100%Na sample we also detect a downfield shift and broadening in the ^{23}Na resonance as the temperature is raised from 294 to 373 K, which is consistent with a greater variety of ionomeric states as temperature is increased, as in the SAXS experiments reported in Part 1.

We use the Novocontrol GmbH Concept 40 broadband dielectric spectrometer to study polymer segmental relaxations and ion dynamics, from temperatures far below T_g up to 120^{o}C. This experiment directly measures the conductivity and the static dielectric constant of ionomers.[1,2]
Electrode polarization was analyzed with the 1953 Macdonald model to determine that the conducting ion content displayed an Arrhenius temperature dependence with activation energy 22 kJ/mol for Li^+ and Na^+ in our fully sulfonated PEG600-based polyurethanes[1] and our study of the random copolyester ionomers[2] find activation energy systematically increasing with ion content (from 8.4 kJ/mol for PEG600-6%Li to 18 kJ/mol for PEG600-100%Li). Mobility and conductivity displayed strongly non-Arrhenius temperature dependences with Vogel temperatures similar to that of the α-relaxation of the polymer, confirming that polymer segmental motion of PEO is required for ion conduction in this class of materials.
The static dielectric constant of all the ionomers we have studied is proportional to 1/T, as shown in the figure below and also as expected by the 1936 Onsager model. Thermal randomization causes the dielectric constant of liquids to decrease in this way as temperature is raised. Ionomers with Na^+ counterions have 2X larger dielectric constant[1] than the same ionomers with Li^+ counterions at 120^{o}C, and this dielectric constant ratio increases as temperature is lowered (to about 3X at the lowest temperatures that we can measure static dielectric constant). This suggests that Na^+ ionomers form more separated pairs than Li^+ ionomers. We applied the 1936 Onsager model to the temperature dependence of the static dielectric constant shown in the figure on the left.[2] After subtracting the contribution from the

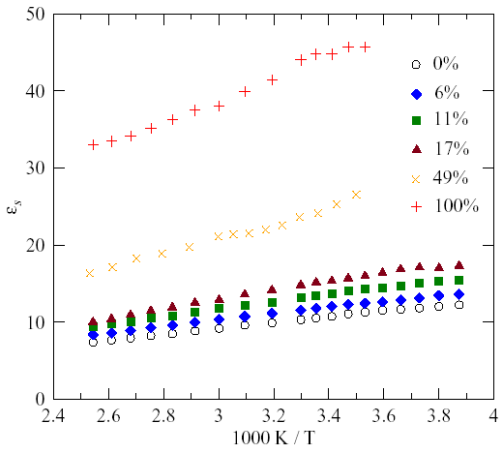

neutral polymer (PEG600-0, shown as the open circles) the remaining contributions to dielectric constant are attributed exclusively to ions, and were used to evaluate an effective dipole moment of ions (assuming all ions are in the same state) that is significantly larger than the contact pair, independent of temperature and ion content! One simple explanation for that is the formation of a significant population of separated pairs, consistent with MD simulation results discussed in Part 1. However, the *ab initio* calculations discussed in Part 1 suggest that the separated pair is higher energy than the contact pair and the FTIR results discussed below find no evidence for separated pairs. Another possible explanation is linear string-like chains of ions and their consequences on other measurements are now being considered.

In collaboration with Professor Paul Painter at Penn State, Fourier transform infrared (FTIR) spectroscopy was used to investigate the copolyester ionomers[3] based on PEG-600. The difference spectra to the left indicate no detectable free SO_3^- anions (or solvent separated pairs!) expected at 1033 cm^{-1}, significant populations of Na^+—SO_3^- contact ion pairs expected at 1042 cm^{-1}, and measurable quantities of SO_3^- anions that are coordinated with two Na^+ (quadrupoles and higher aggregates) expected at 1048 cm^{-1}. The band at 1048 cm^{-1} due to aggregates increased in intensity relative to that due to ion pairs at 1042 cm^{-1} as temperature was raised, consistent with the SAXS experiments on these materials reported in Part 1.

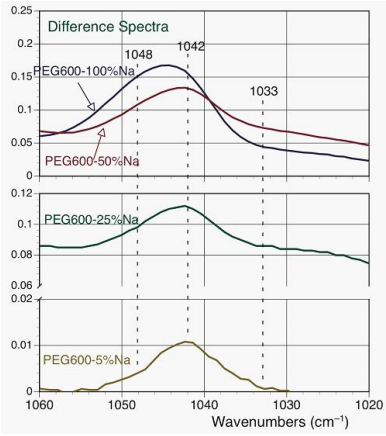

The PEG600-based polyester ionomer copolymers with variable ion content (mole% of sulfonated phthalates 0%, 2.5%, 6%, 11%, 17%, 49%, 100%) with Na^+ counterions have been studied with the Disc Chopper Spectrometer (1.3 ps – 50 ps; 4 Å – 11 Å) and the High Flux Backscattering Spectrometer (240 ps – 2 ns; 3.5 Å – 10 Å) methods at NIST, at 298K, 323K and 348K. For all of these ionomers and the neutral PEG600-0, two decays in S(q,t) are observed, with contributions that are independent of ion content. As the figure to the left shows, the faster process has a much weaker dependence on ion content than the slower process. These relaxations are apparently parts of the β-relaxation seen in dielectric spectroscopy, believed to be associated with local chain twisting of the PEO portions of the polymers. Extrapolating the time extracted from the β-relaxation peak observed at lower temperatures in dielectric spectroscopy, using the observed Arrhenius temperature dependence, leads to an expected β-relaxation time of 5 ns (or 5000 ps) at 298K. The β-relaxation in dielectric spectroscopy is very broad (roughly four decades in frequency at half-height) and apparently includes both of the relaxations observed in quasi-elastic neutron scattering.

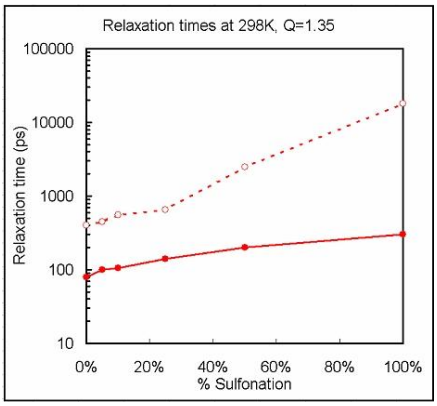

The data presented here are the first proof that the β-relaxation of our ionomers is comprised of multiple relaxations.

PEG600-100%Li has $l_B/\sigma \approx 13$ and our best estimates of ion pair populations suggest that PEG600-100%Li has nearly all ions in pairs with little or no free ions. PEG600-6%Li has $l_B/\sigma \approx 40$; our best estimates of ion populations suggest that PEG600-6%Li has 65% of the ions in ion pairs and 35% of the ions in quadrupoles. Hence, our PEG-based polyester ionomers seem to have most of the ions in pairs and quadrupoles. This is due to the solvating power of the PEO ether oxygens, preventing the ion pairs and quadrupoles from microphase separating to form the conventional ion domains seen in many ionomers. To attain higher dielectric constant ($l_B/\sigma < 10$) in PEG-based polyester ionomers, we would need to increase the ion content significantly. That would push the PEG-based polyester ionomers into the regime of free ions in equilibrium with ion pairs and likely boost conductivity greatly. Unfortunately, we know that PEG400-100%Li has T_g = 285K, 27K above the T_g of PEG600-100%Li. Apparently the close proximity of ion pairs favors the formation of quadrupoles which raise T_g.
Our PEG-based polyester ionomers have vanishingly small populations (fraction of order 10^{-9}) of truly free ions. The dominant conducting ion species is a triple ion of $Li^+—SO_3^-—Li^+$, with fraction of order 10^{-3}. The $Li^+—SO_3^-—Li^+$ triple ion exchanges its extra Li^+ cation with other isolated $Li^+—SO_3^-$ ion pairs. Segmental motion of the polymer allows the two species to approach each other and then move apart after the random exchange. Such a 'hopping' mechanism involving exchange between positive triple ions and ion pairs, facilitated by segmental motion of the polymer, seems at least qualitatively consistent with all of our observations thus far.

Future Plans
It is clear that PEG-based ionomers have limitations; raising the dielectric constant by simply adding more ions to the system also raises T_g. For this reason we are now synthesizing the next generation of low-T_g ionomers with polysiloxane backbones (with inherent T_g = -123 ^oC) and both polar and weak-binding ionic side groups. Our *ab initio* calculations suggest that the oxygen in the siloxane backbone is nearly as good at solvating cations as the oxygen in PEO, and has identified weak-binding anions and polar groups that can be added as side groups to these flexible polysiloxane backbones.

References and DOE Sponsored Publications in 2008-2009 from Current Grant
1. D. Fragiadakis, S. Dou, R.H. Colby, and J. Runt, Molecular Mobility, Ion Mobility, and Mobile Ion Concentration in Poly(ethylene oxide)-based Polyurethane Ionomers, *Macromolecules* **41**, 5723 (2008).
2. D. Fragiadakis, S. Dou, R. H. Colby and J. Runt, Molecular Mobility and Li^+ Conduction in Polyester Copolymer Ionomers based on Poly(ethylene oxide), *J. Chem. Phys.* **130**, 064907 (2009).
3. M. Lu, J. Runt and P. C. Painter, An Infrared Spectroscopic Study of a Polyester Copolymer Ionomer based on Poly(ethylene oxide), *Macromolecule*s, submitted.

Nanoparticles Stabilize Thin Polymer Films: A Fundamental Study to Understand the Phenomenon

Michael E. Mackay,[1] Tzu-Chia Tseng,[1] Venkat Padmanabhan[1] and Amalie Frischknecht[2]
mem@udel.edu

[1]Department of Materials Science and Engineering
University of Delaware, Newark, DE 19716

[2]Center for Integrated Nanotechnologies
Sandia National Laboratories, Albuquerque, NM 87185

Program Scope

A new understanding of thermodynamics at the nanoscale resulted in a recently discovered first order phase transition that nanoparticles in a polymer film will all segregate to the supporting substrate. This is an unusual phase transition that was predicted using a modeling technique developed at Sandia National Laboratories and required the equivalent of many computational years on one computer. The original observation was made in this project through careful experimentation, however, it was the computational effort that demonstrated it was a phase transition which occurs only in a polymer film.

The utility of this phenomenon is the thermodynamic force is so large that a liquid film approximately 50 - 100 nm thick will rise above a ~150 nm sized object, defying gravity and surface tension, rather than disassemble the nanoparticle layer. Basically, the polymer molecules in the thin film push the nanoparticles to the substrate and hold them there by an entropic force. The film will rise above objects rather than disassembling the nanoparticle layer and so we have found it is possible to make both liquid and solid films that are rough. Applications include optical coatings, solar cells and films which will wet any substrate even under very adverse conditions.

Recent Progress

Simulations. In a fluid mixture of particles with different sizes, the distribution of the particles near a substrate is determined by the complex interplay among the steric effects and the particular particle-wall and particle-particle interactions [1]. If all the fundamental forces acting on a collection of particles at any given surface were known, it would be possible to design systems so that particles assembled in desired locations. An example of a step in this direction is self-assembly of a polymer-nanoparticle system [2], in which the nanoparticles segregated to the solid substrate when the entropic forces were dominant or to the air interface if the dielectric properties were properly tuned.

It has been shown that when there is a size anisotropy, a binary hard-sphere mixture, exhibits a phenomenon resulting in “depletion” potential [3, 4]. The larger spheres will tend to locate next to the substrate because the overall system entropy loss per unit area is less. In the present study we determine if it is possible to displace the larger particles by introducing an attraction between the small particles and the wall. Both fluids density functional theory and discontinuous molecular dynamics simulations demonstrate that at a certain attractive potential, which is on the order of the thermal energy, the large particles can indeed be dislodged from the surface layer so the small particles are now the major surface component. We use a combination of the “White-Bear” functional [5] and mean-field attractions to study the system of binary fluid mixture close to an attractive surface. We show that as we increase the strength of attraction (ε_{wf}) between the small spheres and the wall, their density near the wall increases. There is a transitional value, ε_{wf}^{*}, beyond which the concentration of the small spheres at the wall is higher.

In Figure 1, we show the density profiles of the small and big spheres with two different wall-fluid attraction strengths, for a volume fraction, Φ_{small} = 0.22. The open symbols represent the simulation data and the dotted line is obtained from the density functional theory. For a weak wall-fluid attraction, the density of the big spheres near the wall is high as a result of the depletion effect caused by the size anisotropy. As the wall-fluid attraction strength is

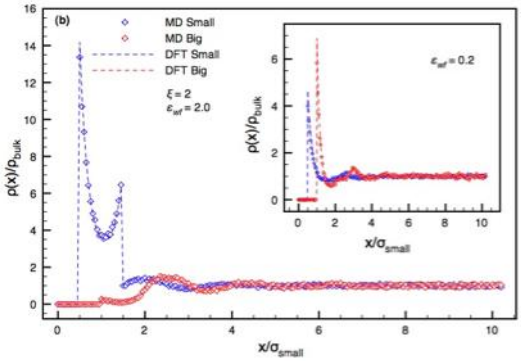

Fig.1 Density profiles for ε_{wf} = 2.0. *Inset*: ε_{wf} = 0.2.

increased, the peak corresponding to the density of the big spheres, slowly diminishes while a second peak in the density distribution of the small spheres begin to appear. The attraction between the wall and the small particles acts against the entropic force that arises due to the size anisotropy. This attraction pulls more small particles closer to the wall dislodging the bigger particles.

Figure 2 shows the concentration profiles of the small and big spheres, for Φ_{small} = 0.22. These concentration profiles demonstrate that, for the weak wall-fluid attraction, apart from the purely geometrical constraints near the wall, the big particles are enriched and the small particles depleted. But, for a stronger wall-fluid attraction, the enthalpic force due to the attraction between the small spheres and the wall dominates over the entropic force, resulting in the small spheres replacing the big spheres at the wall.

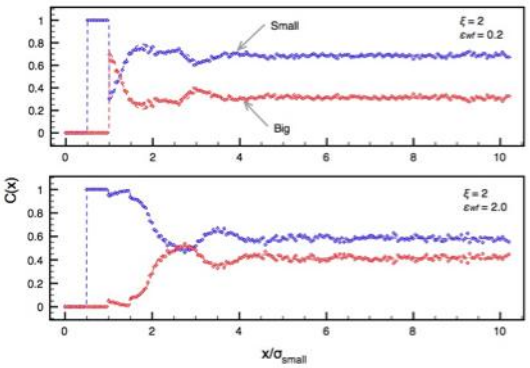

Fig.2 Concentration profiles for - Top: ε_{wf} = 0.2. Bottom: ε_{wf} = 2.0.

To study the effect of mutual attraction of particles in addition to the wall-fluid attractions, we added fluid-fluid square-well attractions to the small spheres. Figure 3 shows the concentrations of the small and big spheres as a function of ε_{wf} for various values of ε_{ff} for ξ = 2 and Φ_{small} = 0.22. ε_{wf}^{*} dropped to lower values as the fluid-fluid attractions got stronger. This effect of mutual attraction of particles can be understood by the fact that the wall-fluid attraction leads to an enhancement of the particles near the wall, and the fluid-fluid attraction pulls even more of them into those peaks since they want to be near each other. This leads to a decrease in the wall-fluid attraction required to obtain a 50-50 concentration of the particles near the wall, with an increase in the fluid-fluid attractions. Figure 4 shows the transitional wall-fluid attraction strength ε_{wf}* as a function of fluid-fluid attraction strength ε_{ff} for three different size ratios.

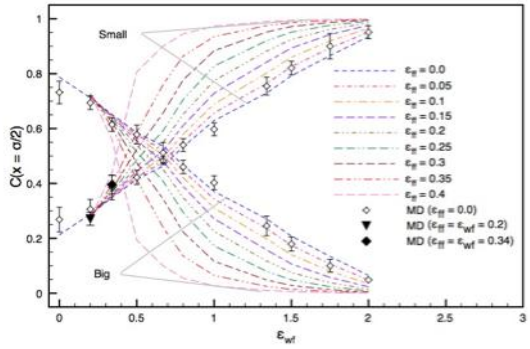

Fig.3 Concentration near wall as a function of ε_{wf}.

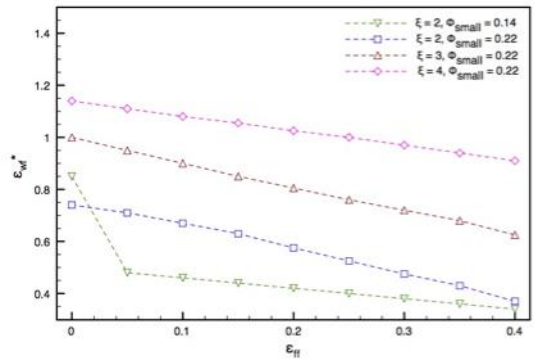

Fig.4 ε_{wf}* as a function of ε_{ff}.

Experiments. In the experiments, we used cadmium selenide (CdSe) quantum dots (QD's) with core radii of 2 nm and polystyrene (PS) to demonstrate the assembly phenomenon in thin polymer films. Solution blends of CdSe QD's and linear polystyrene (PS) were spin coated to silicon substrates and thermally annealed well above the glass transition temperature of PS. QDs were found to assemble to interfaces in PS films by a combination of entropy and enthalpy [6].

In the cross-sectional transmission electron microscopy (TEM) image (Figure 5a), the pyridine stabilized QD's (p-QD's), assembled to the substrate in the PS film after annealing due to their larger surface energy than PS (enthalpy) and also the entropy gain by the polymer. The p-QD's packed densely on the substrate as shown in a top view image (Figure 5b) though a Fourier transform shows no long range order (inset). Furthermore, we are able to manipulate the direction of nanoparticle assembly by simply changing the steric layer of the CdSe QDs. If QD's with much thicker steric layer, oleic acid (o-QD's), were spin coated together with p-QD's and then annealed, o-QD's were found to assemble to the air interface (Figure 5c) due to their lower surface energy while the p-QD's still assembled to the substrate. In addition, if the silicon substrate was decorated sparsely with large SiO_2 particles and a layer of p-QD's and PS was spin coated on top and annealed, p-QD's assembled along the substrate and around the silica particle (Figure 5d).

The assembly energy of nanoparticles to the solid substrate is so large that a liquid film can follow surface protrusions that are larger than the film thickness and not dewet. As shown in Figure 6, large SiO_2 particles were firstly deposited onto a silicon substrate and PS films of various thicknesses containing p-QD's were spin coated onto this rough substrate and thermally annealed. A 180 thick film results in a fairly flat surface that becomes rougher as the nominal film thickness is decreased to 120 nm and then 40 nm, shown by the atomic force microscope (AFM) images (Figure 6a). A similar film was prepared (Figure 6b) with PS that was crosslinked [2] then another layer of p-QD and PS was deposited on top and thermally annealed; the p-QD outlined the original air interface while segregating onto the top of the first layer. Even though the film was curved above the SiO_2 particle but still stayed three-dimensionally stable. This result is striking since the SiO_2 particles would be nucleation sites for dewetting in such thin films without the QD's. The reason is that disassembling the nanoparticle layer requires more energy than that gained by dewetting from this rough surface.

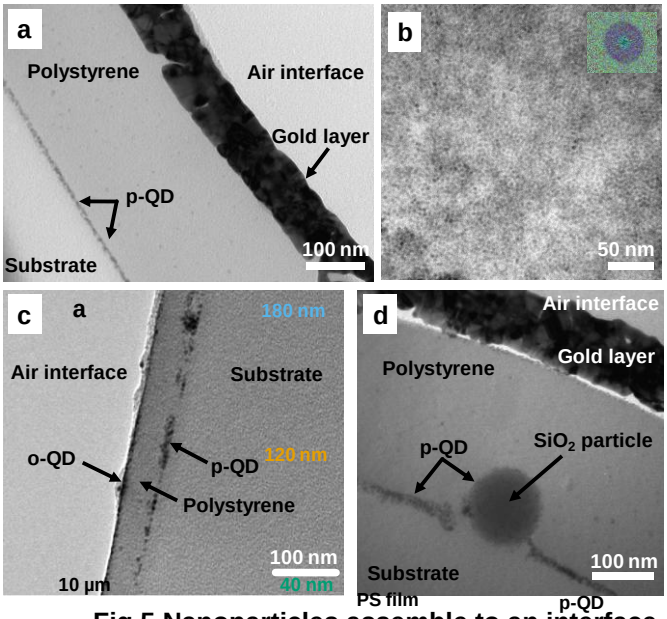

Fig.5 Nanoparticles assemble to an interface dictated by a combination of entropy and enthalpy.

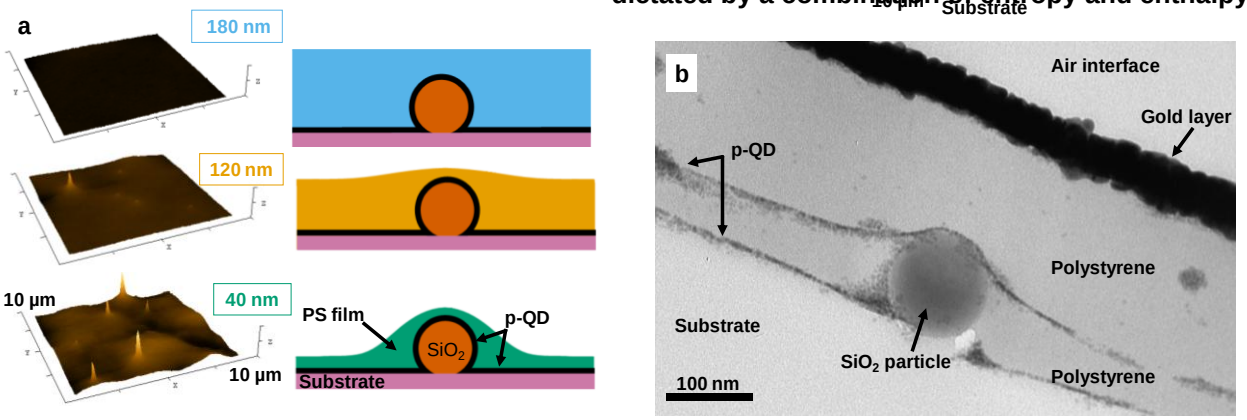

Fig.6 Three-dimensional liquid surfaces.

To model the film profile, a continuum theory for film morphology [7] was used in which we minimize an interfacial free energy as a function of the film thickness. The cartoon in Figure 7a illustrates the parameters we used for the calculation. In a nominal 92 nm thick film (Figure 7b), the height profile (h(x)) as a function of distance from the center of the particle agrees well with the experimental values. The film height above the particle apex (h_0) is similar to the film thickness far from the sphere (h_∞) for large film thicknesses (Figure 7c), while it approaches a value of *ca.* 25 nm for thinner films. The size dispersity of the SiO_2 particles (121 ± 14 nm) explains the larger error bars of thinner films.

Future Plans

The proposed activities will be conducted by the researchers to build on the above discoveries to develop a more fundamental understanding of the assembly process through development of new theoretical, as well as experimental, tools and to generalize the self assembly process from two-dimensions to one- and three-dimensions. Specifically we propose to:

1. Achieve directed assembly of nanoparticles between given objects

- Preliminary results show that we can assemble nanoparticles in one dimension along an object and we will work on assembling them between objects.

2. Develop theoretical capabilities describing nanoparticle filled polymer films between a solid substrate and vapor to more accurately model the thin polymer films
3. Use PRISM theory to calculate bulk nanoparticle – polymer interactions.

We have recently written a new PRISM code that allows the polymer to adopt any configuration rather than that when no nanoparticles are present. The polymer molecules swell as seen in our experiments, we will continue this study in tandem with the thin film work since it allows us to more fully understand polymer – nanoparticle interactions.

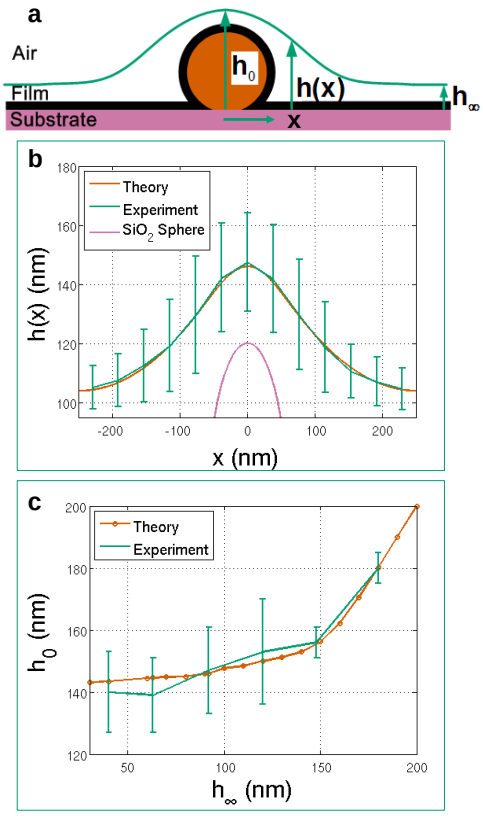

Fig.7 Calculated film profiles agree well with the experimental results.

References

1. Lajovic, M. Tomsic, and A. Jamnik, Acta Chim. Slov., **56**, 145 (2009).
2. M. E. Mackay et al., Nano Letter, **7**, 484 (2007).
3. R. Roth, and S. Dietrich, Phys. Rev. E, **62**, 6926 (2000).
4. D. Dinsmore, P. B. Warren, W. C. K. Poon, and A. G. Yodh, Europhys. Lett., **40**, 337 (1997).
5. R. Roth, R. Evans, A. Lang, and G. Kahl, J. Phys.: Cond. Matter **14**, 12063 (2002).
6. T.-C. Tseng et al., Submitted.
7. R. Seemann, S. Herminghaus and K. Jacobs, J. Phys.: Cond. Mat., 2001, **13**, 4925-4938.

DOE Sponsored Publications in 2007 – 2009 from the Current Grant

1. Yaklin, M.A., Duxbury, P.M., and Mackay, M.E., Control of nanoparticle dispersion in thin polymer films. *Soft Matter* **4**, 2441 (2008).
2. Tuteja, Anish, Duxbury, Phillip M., and Mackay, Michael E., Polymer chain swelling induced by dispersed nanoparticles. *Phys. Rev. Letters* **100**, 077801 1 (2008).
3. McGarrity, E. S., Frischknecht, A. L., and Mackay, M. E., Phase behavior of polymer/nanoparticle blends near a substrate. *J. Chem. Phys.* **128**, 154904 (2008).
4. McGarrity, E. S., Duxbury, P. M., Mackay, M. E., and Frischknecht, A. L., Calculation of entropic terms governing nanoparticle self-assembly in polymer films. *Macromolecules* **41**, 5952 (2008).
5. McGarrity, E. S., Frischknecht, A. L., Frink, L. J. D., and Mackay, M. E., Surface-induced first-order transition in athermal polymer-nanoparticle blends. *Phys Rev Lett* **99** (2007).
6. Krishnan, R. S. et al., Self-assembled multilayers of nanocomponents. *Nano Letters* **7**, 484 (2007).
7. Krishnan, R. S. et al., Improved polymer thin-film wetting behavior through nanoparticle segregation to interfaces. *J. Phys.: Cond Matter* **19**, 356003 (2007).
8. Holmes, Melissa A., Mackay, Michael E., and Giunta, Rachel K., Nanoparticles for Dewetting Suppression of Thin Polymer Films used in Chemical Sensors. *J. Nanopart. Res.* **9**, 753 (2007).

Diblock Copolymers under Nano-Confinement

Qiang (David) Wang and David S. Dandy
q.wang@colostate.edu
Department of Chemical and Biological Engineering
Colorado State University, Fort Collins, CO 80523-1370

Program Scope

Our DOE project (DE-FG02-07ER46448) is a computational study on the simultaneous application of two orthogonal external fields to achieve long-range (over microns) three-dimensional (3D) order in self-assembled nanostructures of block copolymers. In particular, for the self-assembled lamellar or cylindrical morphology in diblock copolymer (DBC) films under nano-confinement, we use a topographically or chemically patterned substrate to control its in-plane ordering, and an electric field applied perpendicular to the film to achieve the perpendicular orientation desirable in applications such as nanolithography.

As the first step, we need to understand in detail the effects of nano-confinement, which is of both fundamental and practical interest. Nano-confinement strongly affects and can thus be used to control the self-assembled morphology of block copolymers. The confinement dimensions, geometries and patterns of the confining surfaces, and surface preferences all have significant effects on the self-assembled morphology under nano-confinement.[1] Here, we use real-space parallel self-consistent field (SCF) calculations with high accuracy[2] to study the self-assembled morphology of diblock copolymers (DBC) in several systems, including lamellae- or cylinder-forming DBC confined between two homogeneous surfaces, on topologically patterned substrates, and on chemically patterned substrates. The stable phases are identified through free-energy comparisons, and our SCF results are compared with corresponding experiments. Much richer phase behaviors are found in these nano-confined systems, with complex morphologies that are very different from those found in the bulk.

Recent Progress

We have developed a new FORTRAN 90 code for the 3D SCF calculations needed in our project. The code can be used for DBC in either bulk or confined geometries, and is parallelized using the message-passing interface (MPI) for large-scale and high-accuracy SCF calculations. To demonstrate the capability and versatility of this code, we have mapped out the phase diagrams of lamellae-forming symmetric DBC A-B confined between two parallel, flat and homogeneous surfaces. By finely tuning the surface separation and interactions with the two blocks, we found the various complex morphologies shown in Fig. 1 that cannot be obtained in the bulk. The free-energy data provided by our high-accuracy SCF calculations also reveal in detail the formation mechanism of these morphologies, which is due to the subtle balance among chain conformational entropy, surface preferences, and A-B repulsion. This work demonstrates that understanding and predicting the self-assembled morphology of DBC under nano-confinement will help us obtain the optimal morphologies for targeted applications, and real-space SCF calculation is a powerful tool for this purpose.

In collaboration with the Almaden Research Center at IBM, we have also studied the bending of lamellae controlled by topographic guiding patterns. As shown in Fig. 2(a), lamellae-

forming symmetric DBC polystyrene-*block*-poly(methylmethacrylate) are confined between a pair of neutral, elbow-like sidewalls on a neutral substrate. By varying the elbow-pattern angle θ, the titling angle φ of lamellae with respect to the sidewalls is measured and plotted in Fig. 2(b). Based on the experimental findings, we performed 2D SCF calculations, with all the input parameters taken directly from the experiments. The SCF predictions are in good agreement with experiments as shown in Fig. 2(b), and the free-energy information provided by our SCF calculations clearly explains the interesting φ-θ relationship observed in the experiments. This work clearly shows that high-accuracy SCF calculations can be used to understand and predict the self-assembled structures of block copolymers on topographically patterned substrates, directly related to our DOE project.

Finally, we have also studied cylinder-forming asymmetric DBC thin films on chemically stripe-patterned substrates, in collaboration with an experimental group in Korea. In this work, we demonstrated that, by carefully controlling the substrate pattern (size, period, and interactions with the two blocks) and film thickness, directed assembly using a substrate pattern *incommensurate* with the bulk morphology of block copolymers may induce well ordered, complex nanostructures in the copolymer thin film. This is different from the idea of epitaxy[3] or density multiplication[4] where *commensurate* substrate patterns were used. Moreover, as shown in Fig. 3, our SCF calculations are in good agreement with experimental observations, and further provide detailed 3D structures inside thin films and their formation mechanisms that are difficult to resolve in experiments.

Future Plans

With our high-performance parallel SCF code, we will proceed to investigate the different mechanisms (dielectric contrast *vs*. ion effects) proposed for the electric-field alignment of lamellae and cylinders confined between two homogeneous and flat surfaces. We will also study in detail the effects of topographically patterned substrates on the confined morphology of lamellae-forming and cylinder-forming diblock copolymers. Finally, we will identify the optimal conditions under which perpendicular nanostructures (lamellae and cylinders) with long-range 3D order can be obtained by combined external fields, which will allow knowledge-based rational design (instead of trial-and-error experiments in a large parameter space) to achieve such nanostructures.

References

1. *Q. Wang,* "Monte Carlo Simulations of Nano-Confined Block Copolymers", Chap. 16 in **Nanostructured Soft Matter: Experiment, Theory, Simulation and Perspectives**, 495-527, ed. A. V. Zvelindovsky, Springer, 2007.
2. *D. Meng and Q. Wang*, "Hard-Surface Effects in Polymer Self-Consistent Field Calculations", **J. Chem. Phys., 126**, 234902 (2007).
3. *S. O. Kim, H. H. Solak, M. P. Stoykovich, N. J. Ferrier, J. J. de Pablo, and P. F. Nealey*, "Epitaxial Self-Assembly of Block Copolymers on Lithographically Defined Nanopatterned Substrates", **Nature 424**, 411 (2003).
4. *R. Ruiz, H. Kang, F. A. Detcheverry, E. Dobisz, D. S. Kercher, T. R. Albrecht, J. J. de Pablo, P. F. Nealey*, "Density Multiplication and Improved Lithography by Directed Block Copolymer Assembly", **Science, 321**, 936 (2008).

DOE Sponsored Publications in 2007-2009 from Current Grant

A. *S. O. Kim, B. H. Kim, D. Meng, D. O. Shin, C. M. Koo, H. H. Solak, and Q. Wang*, "Novel Complex Nanostructure from Directed Assembly of Block Copolymers on Incommensurate Surface Pattern", **Adv. Mater., 19** (20), 3271-3275 (2007) [***Frontispiece***]; **20** (5), 866 (2008).
B. *Q. Wang*, "Effects of Interaction Range and Compressibility on Microphase Separation of Diblock Copolymers: Mean-Field Analysis", **J. Chem. Phys., 129**, 054904 (2008).
C. *Q. Wang and Y. Yin*, "Fast Off-Lattice Monte Carlo Simulations with 'Soft' Repulsive Potentials", **J. Chem. Phys., 130**, 104903 (2009).
D. *S.-M. Park, M. Dong, C. T. Rettner, D. S. Dandy, Q. Wang, and H.-C. Kim*, "Bending of Lamellar Microdomains of Block Copolymers on Non-Selective Surfaces", **Macromolecules**, submitted (2009).
E. *D. Meng and Q. Wang*, "Mixed Lamellae in Symmetric Diblock Copolymer Thin Films as Stable Phases", **Phys. Rev. Lett.**, to be submitted (2009).
F. *D. Meng and Q. Wang*, "Complex Morphologies in Symmetric Diblock Copolymer Thin Films", **Soft Matter**, to be submitted (2009).
G. *D. Meng and Q. Wang*, "Stimuli-Response of Charged Diblock Copolymer Brushes", **Macromolecules**, to be submitted (2009).

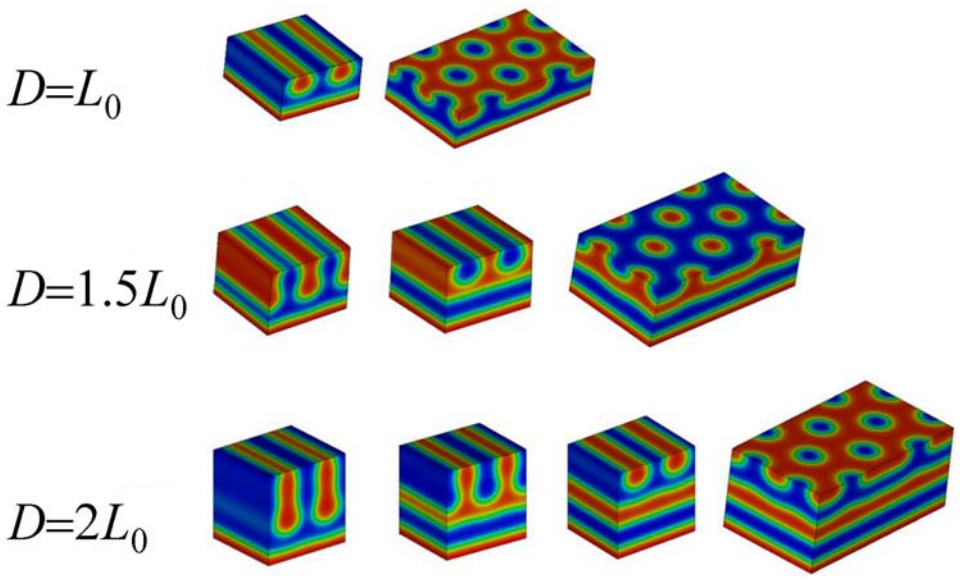

Fig. 1. Novel complex nanostructures formed by symmetric DBC A-B confined between two parallel, flat and homogeneous surfaces (placed at the top and bottom of each morphology, not shown for clarity), obtained from our SCF calculations. The red corresponds to A-rich regions and the blue for B-rich regions, and periodic boundary conditions are applied in the lateral directions. D denotes the film thickness and L_0 the bulk lamellar period. From Refs. [E,F].

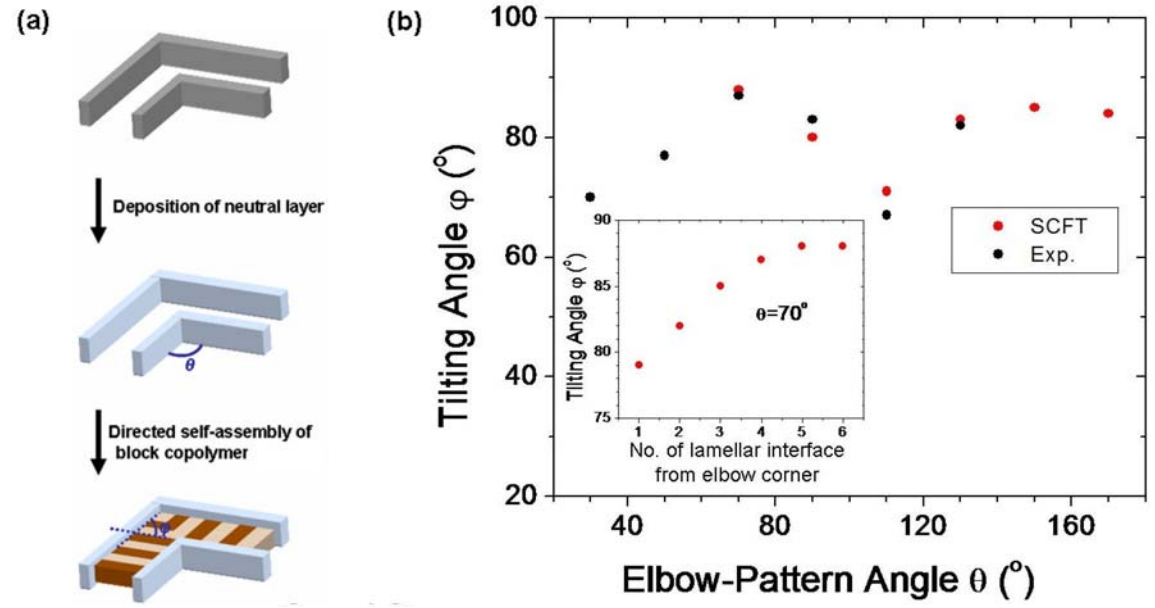

Fig. 2. Bending of lamellae of symmetric DBC A-B by topographic guiding patterns. The SCF results in the inset of part (b) can be used to explain the experimentally observed decrease of lamellae titling angle φ (with respect to the elbow-like sidewalls) as the elbow-pattern angle θ decreases from 70º. From Ref. [D].

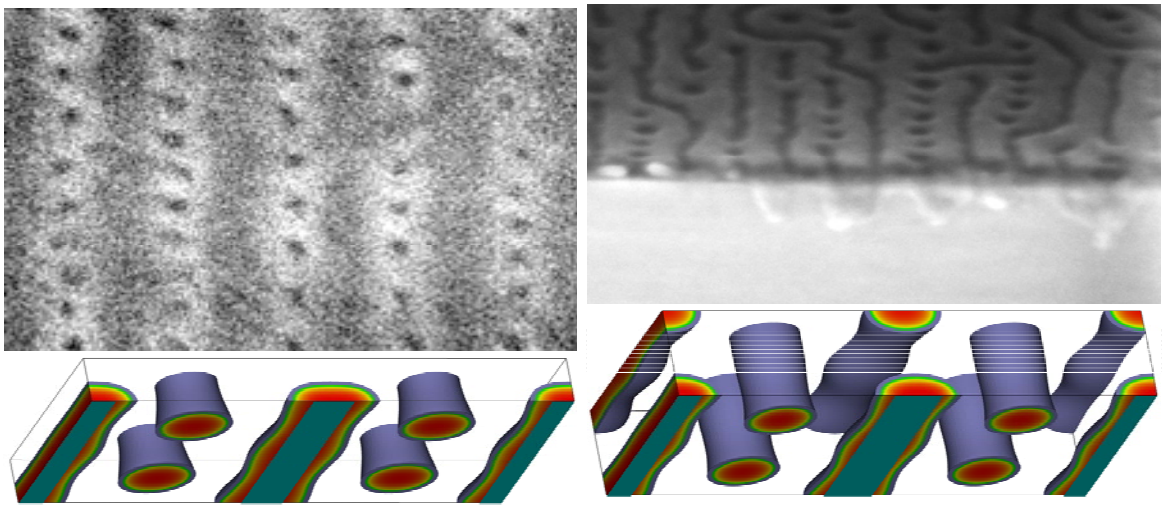

Fig. 3. Novel complex nanostructures of cylinder-forming diblock copolymers on incommensurate substrate pattern. The pre-patterned substrate consists of alternating neutral and preferential stripes and its pattern period is 100 nm, which is more than twice of the bulk inter-cylinder distance of 45 nm of the copolymer; the preferential stripes attract the minority (dark/red) block. **Left:** Plane-view SEM image (top) and SCF results (bottom) indicating well ordered arrays of parallel half-cylinders on preferential stripes (shown in teal) and perpendicular cylinders on neutral stripes (not shown for clarity) in a 20-nm-thick film. **Right:** Cross-sectional SEM image (top) and SCF results (bottom) indicating two layers of parallel half-cylinders on preferential stripes and perpendicular cylinders on neutral stripes in a 40-nm-thick film. From Ref. [A].

AC Electrohydrodynamic Instabilities in Thin Liquid Films: A Route to Hydrodynamic Self-Assembly of Topographical Patterns on Soft Materials

Scott A. Roberts and Satish Kumar
kumar@cems.umn.edu
Department of Chemical Engineering and Materials Science
University of Minnesota, Minneapolis, MN 55455

Program Scope

Surface topography has a significant impact on the optical, adhesive, and wetting properties of materials [1]. For thin films of soft materials such as polymers, controlling surface topography in order to tailor associated properties to desired specifications is a crucial processing challenge. In this program, we are using theoretical tools to explore fundamentally new ways of creating and controlling the surface topography of thin films of soft materials that make use of principles from hydrodynamics and self-assembly. These methods are worthy of exploration because they have the potential to considerably advance state-of-the-art technologies as well as fundamental scientific understanding. Our focus to date has been on analyzing how AC electric fields lead to the formation of topographical patterns on the surfaces of thin liquid films through hydrodynamic instabilities.

Recent Progress

When DC electric fields are applied to a thin liquid film, the interface may become unstable and form a series of pillars [2], as shown in Figure 1.

Figure 1: The top panel shows a schematic of the problem setup. Layer 2 is a thin liquid film, typically a polymer, whereas Layer 1 could be another polymer, a low-molecular-weight fluid, or air. The bottom panel shows a series of pillars that form after the interface becomes unstable due to an applied electric field. The film thicknesses, pillar widths, and pillar spacings are ~100-1000 nm.

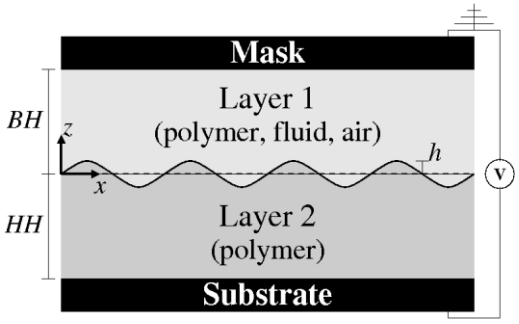

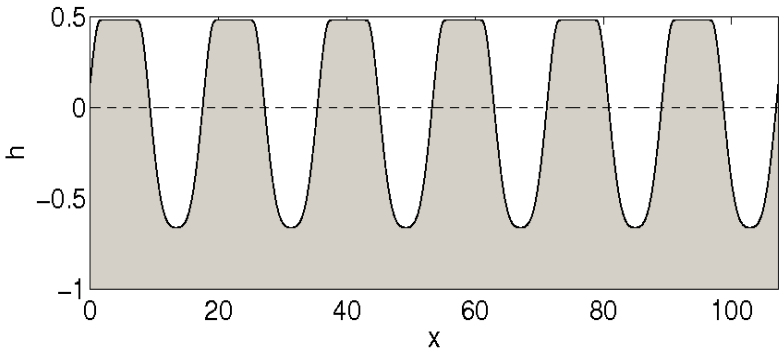

The formation of these pillars provides a route through which surface topography can be created on thin polymer films. Being able to precisely control surface topography is crucial to the advancement of technologies such as coatings, plastic electronics, and biomaterials. Our work examines the possibility of using AC electric fields to exert further control over the size and shape of the pillars. The basic idea is that an AC field introduces two new parameters, the amplitude and the frequency of the voltage oscillation, which could potentially be manipulated to create new phenomena not seen when only DC fields are applied.

The mathematical model used in our study is based on well-established equations of electrohydrodynamics [3]. The model assumes that the fluids involved have (i) Newtonian rheological behavior, (ii) thicknesses much smaller than their characteristic lateral dimensions (thereby allowing the use of the well-known lubrication approximation, which yields great simplification of the governing equations), and (iii) the ability to accumulate charge at fluid-fluid interfaces (so-called leaky dielectric fluids). At its core, the model consists of two coupled nonlinear partial differential equations for the height of the liquid-fluid interface (see Figure 1) and the charge at that interface. Both linear stability analysis and nonlinear simulations (via finite-difference methods) were performed over a wide range of parameters.

In the limit that the fluids behave as perfect dielectric materials, linear stability analysis shows that the influence of an AC field can be understood by considering an effective DC field. For leaky dielectric films, Floquet theory is applied to carry out the linear stability analysis, and it reveals that high frequencies may be used to inhibit the accumulation of interfacial free charge, leading to a lowering of growth rates and wavenumbers. Moreover, the stability analysis shows that by tuning the relative contribution of the DC and AC components of the applied electric field as well as the oscillation frequency, much greater control over the pillar wavelength and growth rate can be achieved compared to the case where only DC fields are present.

Nonlinear simulations confirm the results of the linear stability analysis while also uncovering two additional mechanisms for tuning overall pillar height and width through adjustment of the amplitude and frequency of the AC field. One mechanism involves pillar thinning, as illustrated in Figure 2. A DC field can be used initially to create a given pillar structure. Then, after a given time, an AC component to the field can be switched on. Because of the transient nature of the AC field, the pillars will start to thin, and these smaller structures could be locked in by lowering the temperature.

Figure 2: Evolution of a single pillar (light grey) for a DC field and after an AC field is applied (dark grey). The panels are for increasing time, with the one on the left being for the earliest time.

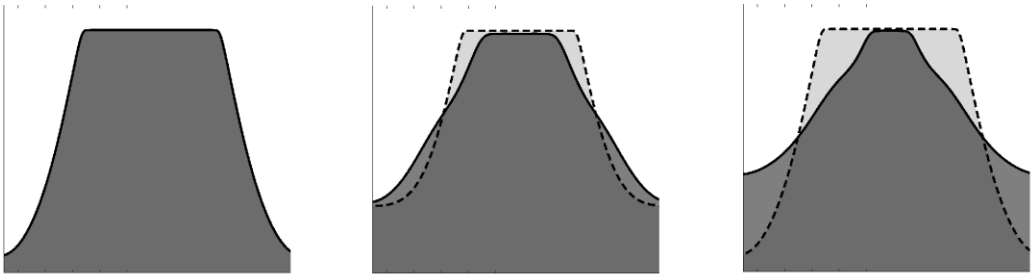

Another mechanism involves peak splitting. Here, rather than obtaining pillars which have flat tops, we observe pillars with small crowns, as depicted in Figure 3.

Figure 3: Evolution of peak splitting. The original peak in the left panel is shown as a dashed line in subsequent panels.

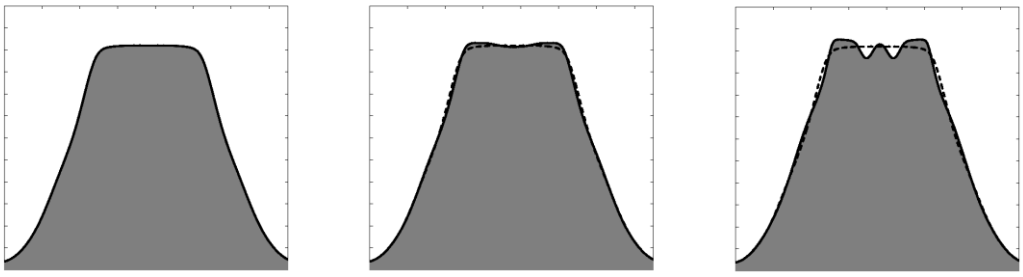

When only a DC field is present, a flat top is obtained because of a balance between the electrostatic potential and repulsive van der Waals forces from the top electrode. The presence of an AC field breaks this balance by causing the pillar heights to oscillate. The oscillation then leads to a local instability at the pillar tops which turns a flat surface into one with small crowns. Again, this smaller-scale structure could be locked in by lowering the temperature. It is important to emphasize that neither the pillar thinning nor the peak splitting are observed when only DC fields are applied. Both are new phenomena that arise due to the use of an AC field [4].

Future Plans

Currently we are analyzing AC electrohydrodynamic instabilities in systems with three thin liquid films. The geometry is similar to that shown in Figure 1, except that there are two polymer layers underneath Layer 1. This geometry is also extremely relevant to the applications mentioned above, but is much more difficult to investigate due to the presence of two deformable interfaces. Preliminary results show that the oscillation frequency can be tuned to precisely regulate the amount of free charge residing at each interface, which could allow for unprecedented control over the topographical pattern resulting from the electrohydrodynamic instability.

We are also planning to investigate how tangential electric fields can be used to further manipulate topographical patterns, and the effects of using a rheological model that accounts for the viscoelasticity of the polymer films. In addition, some effort is being devoted to learning new theoretical methods that have been used to analyze the stability of bulk flows of polymeric liquids [5] because of the potential of these methods to provide significant new insights into the stability of topographical patterns on thin polymer films (e.g., how stable the patterns are in the presence of external noise or thermal fluctuations). A long-term is goal is to develop a multiscale simulation tool that uses molecular-level (e.g., Brownian dynamics) and macroscopic (e.g., finite element) simulations to connect molecular-level information (e.g., polymer chain stiffness, excluded volume interactions, etc.) to macroscopic features (e.g., surface roughness, width of topographical features, etc.). We expect that each of these efforts will advance the fundamental understanding needed to create materials of desired nanoscale structure, which can ultimately be exploited in modern technologies.

References

[1] H. Assender, V. Bliznyuk, and K. Porfyrakis, How surface topography relates to materials' properties, Science 297 (2002) 973.

[2] S. Y. Chou, L. Zhuang, and L. Guo, Lithographically induced self-construction of polymer microstructures for resistless patterning, Appl. Phys. Lett. 75 (1999) 1004; E. Schäffer, T. Thurn-Albrecht, T. P. Russell, and U. Steiner, Electrically induced structure formation and pattern transfer, Nature 403 (2000) 874.

[3] D. A. Saville, Electrohydrodynamics: The Taylor-Melcher leaky dielectric model, Annu. Rev. Fluid Mech. 29 (1997) 27.

[4] S. A. Roberts and S. Kumar, AC Electrohydrodynamic Instabilities in Thin Liquid Films, J. Fluid Mech. 631 (2009) 255.

[5] N. Hoda, M. R. Jovanović, and S. Kumar, Energy amplification in channel flows of viscoelastic fluids, J. Fluid Mech. 601 **(**2008) 407.

DOE Sponsored Publications from Current Grant

S. A. Roberts and S. Kumar, AC Electrohydrodynamic Instabilities in Thin Liquid Films, J. Fluid Mech. 631 (2009) 255-279.

Large Electrocaloric Effect near Room Temperature in P(VDF-TrFE) Based Ferroelectric Polymers

Qiming Zhang
qxz1@psu.edu
Materials Research Institute and Department of Electrical Engineering,
The Pennsylvania State University, University Park, PA 16802

Program Scope

The electroactive effect (ECE) may provide an efficient means to realize solid state high efficiency cooling devices for a broad range of applications such as on-chip cooling, air-conditioning, and refrigeration. However, the small ECE in the materials developed in the past makes it not practical for these applications. Basic molecular and nanostructural considerations, experimental results, and phenomenological theory all suggest the existence of giant ECE, i.e., $\Delta T>10\ ^{o}C$ and isothermal entropy change $\Delta S>60J/(kgK)$, in the ferroelectric poly(vinylidene fluoride-trifluoroethylene) (P(VDF-TrFE)) based polymers [1,2], which are much larger than that from the ferroelectric ceramic ($\Delta T < 2.5$ °C [3]), crystal ($\Delta T < 1$ °C [4]), and antiferroelectric thin film ($\Delta T \sim 12$ °C, $\Delta S < 8$ J/(kgK) [5]). In the current grant we investigate the ECE in normal ferroelectric P(VDF-TrFE), in the relaxor ferroelectric polymer, and in several related ferroelectric polymers. Combining these studies with the molecular, nano- and micro-structures studies, an understanding of how various parameters in a ferroelectric polymer influence the electrocaloric effect and how to achieve very high ECE in polymeric materials will be developed.

Recent Progress

P(VDF-TrFE) 55/45 copolymers and P(VDF-TrFE-CFE) 59.2/33.6/7.2 terpolymers were chosen for the investigation. By characterizing the pyroelectric coefficient of these polymers under different electric fields, the ECE was deduced from the Maxwell relation. For this study, polymer films of 0.4 to 2 μm thick were prepared by spin cast method, using dimethylformamide (DMF) as the solvent at a concentration of 12 wt% for copolymer and 10 wt% for terpolymer. The solutions were spin-coated onto an aluminum coated glass substrate at 2000 rpm for 2 min, and annealed in a vacuum oven at 140 °C for copolymer and 100 °C for terpolymer for 2 hrs to remove the solvent and to crystallize the films. An aluminum coating was then evaporated on the polymer surface to serve as top electrode. The dielectric properties as a function of temperature were characterized using a multi-frequency LCR meter (HP4284A) equipped with a temperature chamber. The electric displacement - electric field (D-E) loops at different temperatures were measured using a Sawyer-Tower circuit with a temperature controller. The use of very thin films allowed the characterization of ECE in these polymers to high electric field (>300 MV/m). More recently, in collaboration with Dr. Z. Kutnjak at Josef Stefan Institute in Slovenia, direct measurement on the isothermal entropy change and the adiabatic temperature change were

conducted, up to a field of 120 MV/m for the copolymer films and 75 MV/m for the terpolymer films. For the direct measurement, polymer films of 5 to 8 μm were prepared.

The D-E loops were measured at 1 kHz for different temperatures above the F-P transition and different electric fields for P(VDF-TrFE) 55/45. The Maxwell equations were used to calculate the isothermal entropy change and adiabatic temperature change. The results are presented in Fig. 1 (a). Inset is the electric displacement D as a function of temperature (pyroelectric coefficient) at different fields. It was found that $\Delta S>55$ J/(kgK) and $\Delta T>12$ °C can be produced for E=209 MV/m. The phenomenological theory was used to calculate the ΔS and ΔT based on the dielectric constant and electric displacement as a function of temperature at low electric fields. Results are presented in Fig. 1 (b). The results are consistent with the experimental measurements. The slightly higher values from the phenomenological theory are due to the amorphous phase in the experimental samples while the theory is for crystalline phase and clamped boundary conditions in the experiment.

The entropy change as a function of square of electric displacement is presented in Fig. 1 (c). As can be seen the slope is nearly independent of temperature, which confirms the phenomenological results that $\Delta S=-1/2\beta\Delta D^2$ for copolymer at temperature above the F-P transition [6].

Direct measurements on the ΔS and ΔT were carried out using a specially designed calorimeter at Josef Stefan Institute in Slovenia, in which the temperature change was recorded when an E field was applied or removed. The direct measurement results are consistent with the Maxwell equation derived results. All the results are consistent with the phenomenological theory for normal ferroelectric copolymers.

Relaxor ferroelectric terpolymer P(VDF-TrFE-CFE) 59.2/33.6/7.2 mol% has an average phase transition temperature near room temperature [1,2], which is lower than the P(VDF-TrFE) 55/45 copolymers (~ 70 °C) [1,2]. Figure 2(a) presents the dielectric properties measured at different frequencies as function of temperature. Figure 2(b) is D~E loop measured at 30 ^{o}C. The slim D~E loop indicates very low ferroelectric loss during the polarization switch, suggesting an ideal cooling cycle with very low loss. Figure 3 shows the direct measurement of ΔS and ΔT for terpolymers at E=8, 45.6 and 74.4 MV/m, respectively. An isothermal entropy change > 14 J/(kgK), and an adiabatic temperature change > 3.5 °C have been gained at a field of 74 MV/m. Since ΔS and ΔT are proportional to ΔD^2, it can be deduced that $\Delta T > 12$ °C and $\Delta S > 50$ J/(kgK) at E=150 MV/m can be achieved at room temperature. It should be noted that at 30 °C, the D-E loop shows that the polarization is not saturated, indicating a higher D could be obtained at higher fields (>200 MV/m). In fact, in the random oriented dipole system, a polarization could be induced in terms of the alignment of dipoles in a large electric field. Furthermore, the polarization can be further enhanced in polymer due to the nonlinear behavior caused by the deformation of dipoles in a high electric field [7].

Future Plans

We will develop calorimeter for direct measurement of ECE in ferroelectric polymers to fields above 200 MV/m. In the current set-up at Josef Stefan Institute in Slovenia, the highest field that can be applied to the polymer films is limited to below 75 MV/m for the terpolymer and 120 MV/m for the copolymer. At fields > 200 MV/m, the ΔS and ΔT will be larger than 60 J/(kgK) and 12 °C, respectively, for terpolymer at room temperature. We will expand this investigation to nanocomposites and blends where the polymer nanostructures can be modified [8,9]. Furthermore, the large ECE and magnetocaloric effect (MCE) observed in ferroelectric materials and ferromagnetic materials also suggest an investigation of the approach of using elastic stress to induce entropy change and temperature change (elastocaloric effect), which could be significant in polar-polymers as well. These studies will be carried out in the future. Modeling works will be carried out to establish quantitatively structure-property-functional performance relationship.

References

1. Bret Neese, Baojin Chu, Sheng-Guo Lu, Yong Wang, E. Furman, and Q. M. Zhang, Science **321** (2008) 821.
2. Sheng-Guo Lu and Qiming Zhang, Adv. Mater. **21** (2009) 1983.
3. B. A. Tuttle and D. A. Payne, Ferroelectrics **37** (1981) 603.
4. H. Baumgartner, Helv. Phys. Acta **23** (1950) 651.
5. A. S. Mischenko, Q. Zhang, J. F. Scott, R. W. Whatmore, and N. D. Mathur, Science **311** (2006) 1270.
6. B. Neese, S. G. Lu, B. J. Chu, and Q. M. Zhang, Appl. Phys. Lett. **94** (2009) 042910.
7. S. G. Lu, B. Neese, B. J. Chu, Y. Wang, and Q. M. Zhang, Appl. Phys. Lett. **93** (2008) 042905.
8. Baojin Chu, B. Neese, Minren Lin, Sheng-Guo Lu, and Q. M. Zhang, Appl. Phys. Lett. **93** (2008) 152903.
9. Baojin Chu, Minren Lin, Breet Neese, Xin Zhou, Qin Chen, and Q. M. Zhang. Appl. Phys. Lett. **91** (2007) 122909.

DOE Sponsored Publications in 2007 – 2009 from Current Grant

∗ "Large Electrocaloric Effect in Ferroelectric Polymers near Room temperature", Bret Neese, Baojin Chu, Sheng-Guo Lu, Yong Wang, E. Furman, and Q. M. Zhang, Science **321** (2008) 821.

∗ "Electrocaloric Materials for Solid-State Refrigeration", Sheng-Guo Lu and Qiming Zhang, Adv. Mater. **21** (2009) 1983.

∗ "Electrocaloric Effect of the relaxor Ferroelectric P(Vinylidene Fluoride – Trifluoroethylene – Chlorofloroethylene) terpolymer", B. Neese, S. G. Lu, B. J. Chu, and Q. M. Zhang, Appl. Phys. Lett. **94** (2009) 042910.

∗ "Large Electric Tunability in P(Vinylidene Fluoride – Trifluoroethylene) Based Polymers", S. G. Lu, B. Neese, B. J. Chu, Y. Wang, and Q. M. Zhang, Appl. Phys. Lett. **93** (2008) 042905.

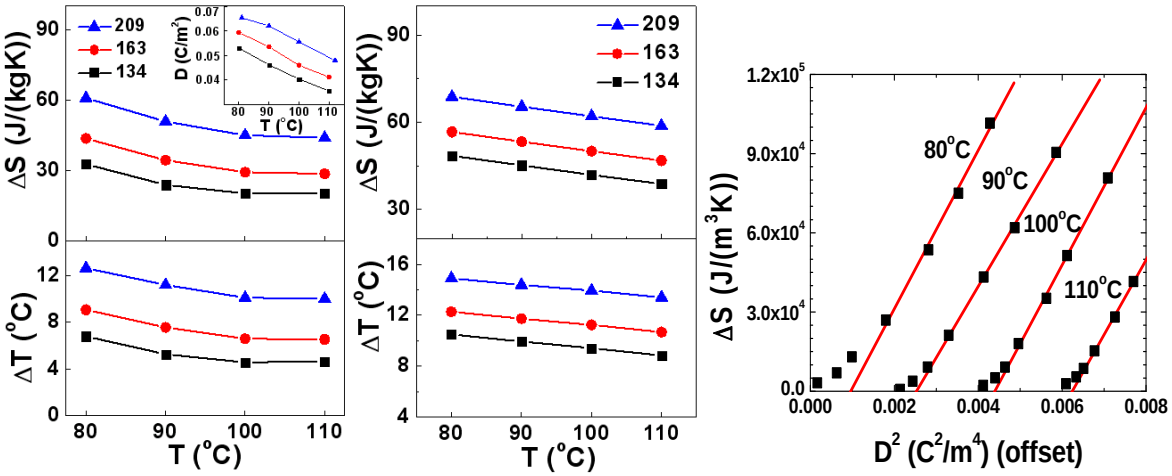

(a) (b) (c)

Fig. 1. (a) ΔS and ΔT as a function of temperature derived from Maxwell equation at E=134, 163, and 209 MV/m. Inset shows the electric displacement versus temperature obtained from D-E loops. (b) ΔS and ΔT as a function of temperature derived from phenomenological theory. (c) ΔS as a function of square of electric displacement for P(VDF-TrFE) 55/45 copolymers.

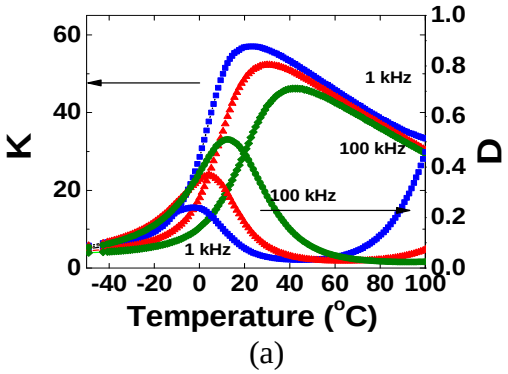

(a)

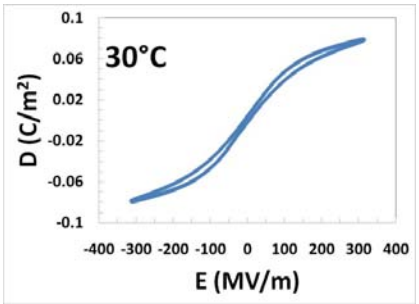

(b)

Fig. 2. (a) Dielectric properties as a function of temperature and (b) D~D loop at 30 C for the 59.2/33.6/7.2 terpolymer

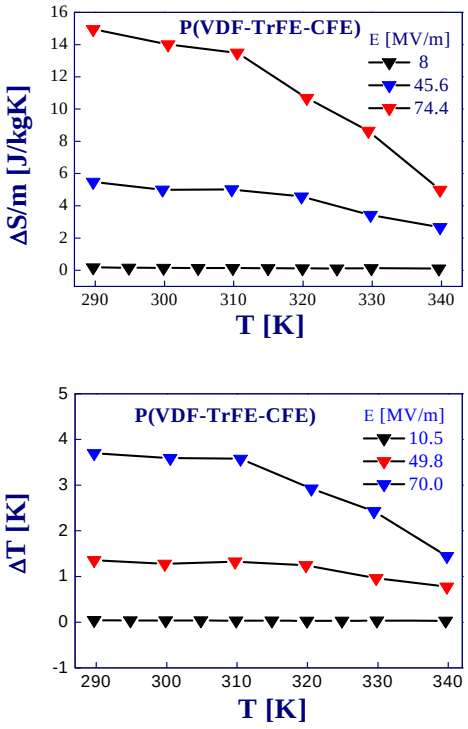

Fig. 3. Directly measured ΔS and ΔT at different E fields vs T for 59.2/33.6/7.2 terpolymer

.

Thin Film Polymer Nanoparticle Composites: Morphology and Dynamics

Peter F. Green,
pfgreen@umich.edu
Department of Materials Science and Engineering, University of Michigan, Ann Arbor, MI 48109

Program Scope

The properties of polymers are known to undergo significant changes with the incorporation of nanoparticles of varying chemistries, even at very small nanoparticle concentrations [1]. Changes of a diverse range of properties, from mechanical and thermal to optical and electronic, occur, depending on the functionalities of the polymer and the nanoparticles. A major challenge in PNC systems is the fact that they possess non-equilibrium morphologies (aggregation, particle bridging interactions and phase separation at various length scales) due to the complex interplay between enthalpic and entropic interactions [2].

One effective strategy to control the morphology, specifically nanoparticle dispersion, of PNCs is to graft polymer chains onto the nanoparticles [3,4]. Polymer chains of varying chemistries, and degrees of polymerization, N, are grafted onto nanoparticles of diameter D with different grafting densities, σ. The grafted nanoparticles are placed into polymer hosts of varying different chemistries and chain degrees of polymerization, P. These parameters, N, P, σ and polymer chemistry enable control of the entropic and enthalpic interactions and hence the morphologies of the systems [4]. We performed research in the following areas: (1) dynamics of bulk and thin film nonoparticle/polymer mixtures; (2) Phase behavior of thin film polymer/nanoparticle mixture

I. Dynamics of bulk and thin film nonoparticle/polymer mixtures

We examined the role of nanoparticle size, host degree of polymerization and grafting chain degree of polymerization on the glass transition and translational dynamics of a series of PNCs. Specifically, dielectric spectroscopy and differential scanning calorimetry studies were performed on bulk mixtures of unentangled, low molecular weight polystyrene (PS), of degree of polymerization P=50, with polystyrene-grafted gold nanoparticles, Au(D)-PS_N. Hereafter these mixtures will be identified as PS(P)Au(D)/PS_N.

The degree of polymerization of the PS host chains was P=48 and that of the chains grafted onto the gold nanoparticles was N=10; the size of the gold nanoparticles was D=5 nm. Scanning transmission electron microscopy (STEM) of microtomed sections of the samples revealed that the nanoparticles were dispersed uniformly throughout the samples, at least for samples of ϕ<3.wt.% of gold [7]. These mixtures containing Au(5)PS_{10} nanoparticles exhibited $T_g(\phi)$'s substantially below those of pure PS, $T_g(\phi=0)$. The decrease was an unprecedented 10 degrees centigrade. The relaxation dynamics in this composition range were approximately two orders of magnitude faster than pure PS, as shown in Figure 2. Notably, the decrease in the dynamics is qualitatively consistent with the drop in T_g.

We performed additional experiments involving much longer grafted PS chains, N=480, onto nanoparticles of the same size, D=5 nm; this sample is identified: PS(50)/Au(5)-PS_{480}. The glass transition temperatures of these mixtures exhibited the opposite dependence on composition; they increased with increasing concentration. In addition, the dielectric

spectroscopy measurements revealed that the relaxation times increased in a manner qualitatively consistent with the increases in T_g (Fig. 2). We will propose physical mechanisms to explain the changes in T_g (related to dynamic Percolation) and the chain dynamics.

1b Future research:

We plan to examine the role of particle size on the properties. Experiments on the dynamics involving different naoparticle sizes (up to D~20 nm) will be considered. The large effects are expected to diminish with increasing nanoparticle size. In addition we will perform complimentary experiments on grfted layers onto flat surfaces to get better insight into the role of the melt/brush interactions.

Positron Annihilation spectroscopy will be used to examine the free volume distribution in these systems, to get further insight inn to the fundamental origins of the T_g and dynamics changes. This will be done in collaboration with David Gidley, Professor of Physics, here at the University of Michigan. Preliminary studies have begun.

Finally, we are also studying the dynamics of mixtures of polyisoprene (PI) and the PS-grafted nanoparticles. Our preliminary results reveal the existence of additional relaxation peaks that reflect the influence of side chain/nanoparticle interactions. This phenomenon is not observed in the PS/Ps-grafted Au systems.

2. Phase behavior of thin film polymer/nanoparticle mixture

In the foregoing we discussed the properties of <u>bulk properties</u> of polymer nanocomposites and showed how the Au(5)-PS_{10} nanoparticles, particles were distributed uniformly throughout the host (P=5), particularly at low nanoparticle concentrations. *In thin films, however, surprising phenomena, associated with the confinement and the role of interfaces, were observed*. The behavior is not predictable based on the bulk phase behavior. Two following control dispersion of the grafted nanoparticles. At sufficiently high grafting densities, wherein the melt chains are expelled from the brush, aggregation of the nanoparticles is favored. The driving force is due to the finite interfacial tension that exists between the grafted layers and the free melt chains when the brush is “dry.” Consequently, the system minimizes its free energy by nanoparticle aggregation, in order to minimize the unfavorable contact between the brush and the host. Note that for particles with the same grafting density, the particle-particle attraction decreases with decreasing particle size because the wet brush/dry brush transition only occurs for larger grafting density with increasing particle curvature. There are two additional considerations that influence particle-particle dispersion. If the particles reside in proximity, with free melt chains confined between them, the melt chains experience a loss of conformational entropy. This cost is relieved only with the exclusion of the chains from between the particles. This entropic cost of confinement increases with the length of the free melt chains. Secondly, the entropy of mixing favors dispersion of the nanoparticles.

We are studyng three types of systems. In the first we are studying the phase behavior of PS(P)/Au-PS_N mixtures where D varies from 2 to 6 nm, N varies from 10 to 480 and P varies from 1000 to 10^4. One of the Key findings is that when the size of the 2nm particle is smaller than the size of the host chains, the nanoparticles are completely dispersed. However, when it

increases, the particles phase separate and segregate to the interfaces. In principle we have shown how we can control the spatial location of the nanoparticles in the thin film. We have published the initial proof on concept in the Journal Soft Matter 2009 (impact factor ~5) and have a manuscript in preparation.

2b Future research:

We are continuing to map put the phase space in the PS(P)/Au-PS(N) system. In addition, we are now examining a case of a miscible blend where the host is poly phenylene oxide (PPO) and on another case poly tetra methyl bisphenol polycarboate (TMPC). These polymers are miscible with polystyrene. Our preliminary findings reveal that the in some cases the entropic interactions can be sufficiently strong that they dominate the phase behavior of the system. They can force phase separation even when the enthalpic interactions would favor miscibility and vice versa.

References

1. see for example: K. I. Winey, R. A. Vaia, Mrs Bulletin 32 (2007) 314-319.
2. A. Jayaraman, K. S. Schweizer, Macromolecules 41 (2008) 9430-9438.
3. R. Krishnamoorti, MRS Bulletin 32 (2007) 341-347.
4. "Control of the entropic interactions and phase behavior of athermal nanoparticle/homopolymer thin film mixtures," Luciana Meli, Abraham Arceo and Peter F. Green, Soft Matter (communication), **Soft Matter**, 2009, 5, 533.

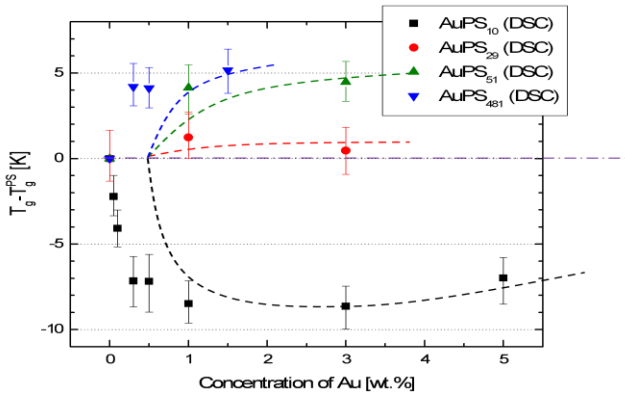

Figure 1: The changes in the glass transition temperature are shown here with composition. For the PS(50)/Au(5)-PS_{10} samples, the T_g decreased whereas for the T_g increased, PS(50)/Au(5)-PS_{480} samples.

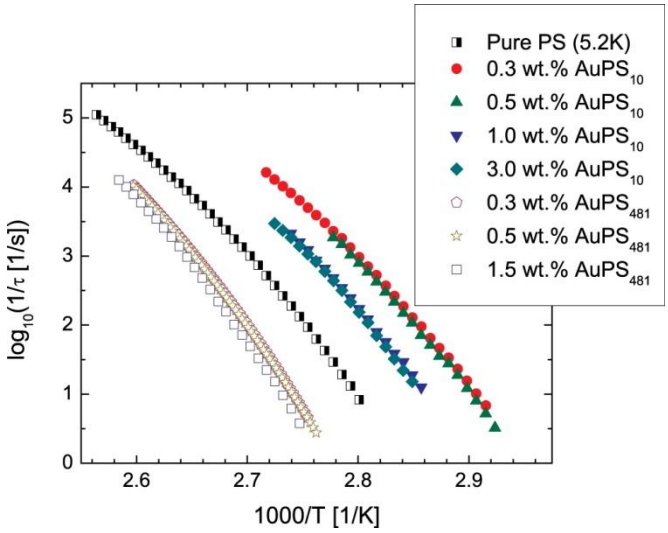

Figure 2: The temperature dependencies of the relaxation times (longest relaxation times), t, are shown here for nanocomposites containing various Au weight fractions for different nanocomposite mixtures. Pure PS is represented by the black symbols.

Publications from grant (August 2007-Present)

1. "Polymer chain dynamics and glass transition in athermal polymer/nanoparticle mixtures," Hyun Joon Oh, Peter F. Green, **Nature Materials**, 2009, 8, 139.
2. "Aggregation and Coarsening of Ligand-Stabilized Gold Nanoparticles in Poly(methyl methacrylate) Thin Films," Luciana Meli and Peter F. Green, **ACS Nano**, 2008, 2 (6), pp 1305–1312.
3. "Glass Transition of polymer/nanoparticle thin film mixtures: Role of entropically directed forces on nanocrystal Distribution," A. Acero, L. Meli, P.F. Green, **Nano letters** 2008, 8, 2271-2276.
4. "Role of diblock copolymers toward controlling the glass transition in thin polymer films," Hyunjoon Oh, Peter F. Green; **Macromolecules**, 2008, 41, 2561.
5. "Local polymer dynamics in polymer-C_{60} mixtures," Kropka, J., Garcia-Sakai, V. and Green P.F.; **Nano Letters** (Letter), 2008, 1061.
6. "Control of the entropic interactions and phase behavior of athermal nanoparticle/homopolymer thin film mixtures," Luciana Meli, Abraham Arceo and Peter F. Green, Soft Matter (communication), **Soft Matter**, 2009, 5, 533.

Manuscripts Submitted

"Phase Behavior of Thin Film Brush-Coated Nanoparticles/Homopolymer Mixtures." Jenny Kim and Peter F. Green (submitted)

"Control of Morphology and its effect on the Optical Properties of Polymer Nanocomposites," *Chelsea Chen and Peter F. Green (submitted)*

(This page intentionally left blank.)

Session VI

Energy Frontier Centers and Nanocenters

Session Chair: Karen Winey, University of Pennsylvania

(This page intentionally left blank.)

DOE Energy Frontier Research Center on Nanostructuring for Efficient Energy Conversion (CNEEC)

Stacey F. Bent and Fritz Prinz
sbent@stanford.edu
Departments of Chemical Engineering and Mechanical Engineering
Stanford University, Stanford, CA 94305

A new DOE Energy Frontier Research Center (EFRC) on Nanostructuring for Efficient Energy Conversion (CNEEC) has been established at Stanford University, partnering with the Danish Technical University, Carnegie Institution, and HRL Laboratories. CNEEC seeks to understand and solve cross-cutting fundamental problems at the nanoscale for improved energy conversion efficiency in devices such as photovoltaics, fuel cells, and batteries.

The overarching goal of the Center is to increase the efficiency of energy conversion devices by manipulating materials at the nanometer scale. We will develop the fabrication and characterization methodologies to understand how nanostructuring can optimize transport, light absorption, and reaction kinetics and thermodynamics in materials, each of which will be used to improve performance and efficiency in energy conversion and storage devices. Our research will provide a scientific foundation of underlying physical and chemical phenomena shared by a diverse range of energy conversion processes, and exploit them in devices for break-out high-efficiency, cost-effective energy technologies.

CNEEC will support three research thrusts:

- Tuning Thermodynamics/Kinetics by Nanostructuring
- Photon Management
- Optimizing Charge Transport at Reduced Sizes and Dimensions

We view these three themes as universal cross-cutting topics which underlie virtually all attempts to improve energy conversion efficiency. CNEEC will employ nanostructuring to generate high gradients, high surface-to-volume ratios, and low dimensionality, and identify ways in which such engineered structures can enhance materials properties such as light absorption, charge transport, and catalytic activity that are critically important for many energy conversion systems. We will exploit these properties to tune thermodynamic equilibria and kinetic properties, to vary photonic behavior through quantum confinement for efficient photon capture, and to reduce distances for charge transport. We will manipulate sub-nanometer particles – namely electrons, photons, ions, atoms, and molecules – by tuning material properties through nanostructuring.

Based on such fundamental work, we will build and test device structures that demonstrate how our fundamental advances can improve the efficiency of photovoltaics, batteries, photoelectrochemical fuel synthesis, fuel cells, supercapacitors, and hydrogen storage. The nanoscale design principles we will pursue will provide the foundation for a sustainable energy

future that will require a collection of energy technologies working in concert to produce, store, and consume the 20 TW of energy that humans will soon demand. Although there are many existing technologies for energy conversion, they cannot provide renewable or sustainable solutions at scale because they are either too inefficient or too expensive. It is thus critical to improve the efficiency of these conversion devices and systems.

The Stanford team brings expertise in *ab initio* design, synthesis, characterization, simulation, and device fabrication. Our partners will complement the program in both experimental and theoretical efforts. The Technical University of Denmark brings world-class expertise in theory to elucidate underlying phenomena and to guide the design of new materials and structures. Carnegie Institution offers expertise in biological sciences and bioengineering. HRL Laboratories provides first-rate scientific research and a link to industrial partners.

This talk will describe the fundamental themes encompassed by the Center and will outline the overall research strategies planned for CNEEC. Some examples of the experimental approaches taken by the Center will be presented.

CENTER FOR SOLAR AND THERMAL ENERGY CONVERSION IN COMPLEX MATERIALS

Peter F. Green
University of Michigan, Ann Arbor, MI

Program Scope/Mission

A large multidisciplinary research team will perform to develop the science necessary to understand and to mitigate energy loss processes that occur in low dimensional, and/or complex nanostructured, organic, inorganic, and hybrid materials for *high efficiency* photovoltaic (PV) and thermoelectric (TE) energy conversion.

Future Plans

In PV and TE materials, energy conversion processes are controlled, in part, by the dynamics and interactions between charge carriers and phonons. In PVs, the transfer of energy from photons to electrons occurs through a series of identifiable stages: charge separation, diffusion, charge transfer, charge separation and finally harvesting. Each stage is characterized by different length scales (0.1 nm-10^2 nm) and time scales (10^{-9}-10^{-15} s) and involves intrinsic energy losses. The interconversion between heat and electricity in TEs is characterized by the figure of merit, ZT. $ZT=S^2\sigma T/\kappa$, where S is the Seebeck coefficient, σ is the electronic conductivity and κ is the thermal conductivity, which is controlled by the dynamics of phonons and charge carriers. Enhancing ZT requires decoupling $S^2\sigma$ and κ through nano-structural design. The research will involve cross-cutting efforts in theory, computation, materials growth/synthesis/fabrication, and physical property measurements, including the use ultrafast optical spectroscopy techniques. This effort will lead to a fundamental understanding of the dynamics and interactions of charge carriers and phonons, which is essential to control and to "tailor" the conversion efficiencies of low dimensional, and/or complex nanostructured, organic, inorganic, and hybrid materials for TE and PV applications.

Research on inorganic PVs will focus primarily on low dimensional materials, including arrays of quantum dots and rods. Low dimensional and nanostructured materials show exceptional promise for high efficiency energy conversion. These materials will be fabricated using various self-assembly and patterning strategies, including focused ion beam nanopatterning and selective-array epitaxy. By varying the sizes and the spatial locations of dots and rods in 2D and 3D, the interactions between them may be controlled. The densities of electronic states increase with reduced dimensionality. Moreover, the carrier/phonon interactions, photon absorption/emission, electron/hole recombination and transport are necessarily controllable under conditions of reduced dimensionality and spatial organization. Intermediate band semiconductors, specifically dilute semiconductor alloys, will be considered in this study. Intermediate band- semiconductors are advantageous for overcoming intrinsic losses, associated with thermalization and absorption, experienced by *p-n* junction solar cells. Through a combination of density functional theory (DFT) and molecular simulations, a fundamental understanding of the energy conversion processes will be developed, leading to a series of materials design rules.

Materials for organic PVs present unique challenges and opportunities for improved efficiency and lower cost. Research will focus on thin-film systems comprising: (1) novel small molecules;

(2) conjugated linear chain polymers; (3) dendritic and (4), caged molecules in which the chemical functionalities can be controlled. Self-assembly and patterning strategies will be used to control film morphology (e.g. length scales of phase separation, molecular ordering), which in turn can enhance exciton and charge carrier transport and separation. Molecular dynamics simulations and DFT will accompany chemical synthesis and thin-film processing, and help interpret measurements of ultra-fast energy conversion processes at organic-organic and organic-inorganic interfaces.

The overall aim of our thermoelectrics effort will be to study the fundamental mechanisms that can increase the ZT of a material by maximizing the Seebeck coefficient and electronic conductivity, while minimizing thermal conductivity. Nanostructuring and changes in dimensionality will be used to control carrier and phonon transport, as well as carrier/phonon interactions. Reducing the dimensionality leads to singular features, and enhanced response in the densities of electronic states. Nanostructuring, as well as reduced dimensionality, leads to enhanced scattering of mid-range frequency phonons, which are responsible for heat transport. Conjugated single molecules, specifically metal-molecule-metal junctions, will be investigated for TE applications. Because charge transport is controlled by discrete energy levels, the Seebeck coefficient in conjugated molecules is expected to be large; the thermal conductance is expected to be low due to the significant mismatch between the vibrational spectrum of the molecule and the metal. Simulation and modeling will provide critical insights into the relationship between nano-structure and transport mechanisms, and thereby provide guidance for the structural design of the next-generation TE materials.

The issues associated with nanostructuring TE and PV devices to achieve high energy conversion efficiency are very similar. By manipulating dimensionality of materials structures, their chemical composition, and building block functionality, the dynamics and interactions of phonons and charge carriers can be controlled and studied in both spatial and temporal regimes. In particular, we will utilize advanced ultrafast optical spectroscopy techniques to investigate these processes over a wide range of time scales in different classes of materials. In addition, the molecular and electronic structure of these materials will be determined using a combination of state-of-the art microscopies, x-ray diffraction, and neutron scattering techniques, complemented by detailed computer simulations.

In summary, through combined experimental, theoretical, and computational efforts, we will discover and develop the science associated with energy conversion mechanisms in photovoltaic and thermoelectric devices, fabricated using materials (inorganic, organic, and hybrid organic/inorganic) that possess low-dimensional and/or complex nanostructures. As outcome of our research we will have critically addressed the grand scientific challenges associated with: (1) control of materials processes at the level of electrons; (2) understanding and controlling properties of matter that emerge from the complex correlations of atomic or electronic constituents and (3) characterizing and controlling matter away from equilibrium. The team is composed of 28 Principal and Senior investigators, in addition to many post docs and students.

Session IVd

Thin Films: Fabricating Nanostructure from Films: Synthesis and Processing

Session Chair: Francisco Zaera, University of California-Riverside

(This page intentionally left blank.)

Synthesis of Submonolayer Type-II Quantum Dots to Enhance Materials Properties of Wide Bandgap Semiconductors

M. C. Tamargo,[1] I. L. Kuskovsky,[2] and G. F. Neumark[3]
[1)] *Department of Chemistry, The City College of New York, New York, NY 10031*
[2)] *Department of Physics, Queens College, Flushing, New York 11367*
[3)] *Department of Applied Physics & Applied Mathematics, Columbia University, New York, NY 10027*

Project Scope

Type-II semiconductor nanostructures, in which the bands are staggered: that is, the material with the lower potential energy for electrons has the higher potential energy for holes, or alternatively, the material with lower potential for holes has the higher potential for electrons have unique physical properties. The spatial separation of electrons and holes gives rise to relatively long carrier lifetimes and to a dependence of photoemission and photocurrents on the intensity of excitation, as well as on the external electric and magnetic fields. Moreover, it tends to suppress Auger recombination. These properties, as well as others that result from the type-II band alignment, provide unique opportunities for new and enhanced materials.

We are presently studying the ways to manipulate the shutter sequence of the various sources during MBE growth, incorporating delay times between them, and modifying the source fluxes to fabricate composite nanostructures with sub-monolayer nano-islands of ZnTe embedded in ZnSe (type-II QDs). In addition, we consider ways to incorporate other impurities (N or Mg) at will within the nano-islands, and thus modify the resulting material properties, such as band alignment and conductivity type.

Recent Progress

We have grown undoped ZnTe nanoislands as well as those doped with N embedded in a ZnSe matrix. For these, the predicted band alignment is such that holes are confined in the ZnTe regions. The dot confinement energy and band alignment in the heterostructure was controlled by altering the dot size (smaller dots will have a lower carrier "ionization" energy). The size and density of QDs have been controlled by adjusting growth parameters including delay times and deposition times or by changing the fluxes and/or flux ratios of the elements forming the QDs.

For example, Fig. 1 (left) shows the low temperature PL spectra of a set of ZnTe/ZnSe samples grown with different Te deposition temperature (or Te fluxes). For the sample with Te deposition temperature of 215˚C, sharp emission lines - typically present in samples with extremely low Te concentration [1, 2] - are observed. Upon increasing the Te source temperature, the PL peak positions exhibit drastic red shifts, suggesting the formation of larger nano-islands and/or nano-islands with higher Te fraction. [3]

Furthermore, other time parameters in our growth protocol (Ref. [4] and references therein) provide additional opportunities to control the size of the dots. An example is shown in Fig. 1 (right) where it is observed that samples grown with longer wait time $t_{all\text{-}off}$ exhibit PL spectra with the peak at higher energies. We propose that the effect of $t_{all\text{-}off}$ on QD size derives from Te desorption [5], a clue that we plan to explore—and, if possible, exploit—in future work.

Another important observation is that the size and density of QDs can be controlled not only by adjusting the growth parameters but also by the number of repeats (or "delta-layers"). For instance, three repeats (or "δ^3-layers") give larger and denser dots as evidenced from magneto-optical experiments, [6] where we observed higher orbital momentum transitions at larger fields for samples grown with single delta-layer. Moreover, the magneto-optical experiments [4, 7] on samples with single-delta layer demonstrated the presence of QDs by exhibiting oscillations in the PL intensity as a function of the magnetic field (Fig. 2). These unexpected phenomena have been attributed to the optical Aharonov-Bohm (AB) effect in type-II QDs [6, 8]. The value of the magnetic field B_0 allows one to estimate the lateral size of the dots - the higher the field the smaller the dots. The highest value for B_0 reported in Ref. [6] was 1.79 T, which suggests that the QDs formed in the δ-ZnSe:Te sample are indeed smaller. Assuming the model developed in Ref. [6] is valid here we estimate the radius of the quantum dots to be less than 9 nm.

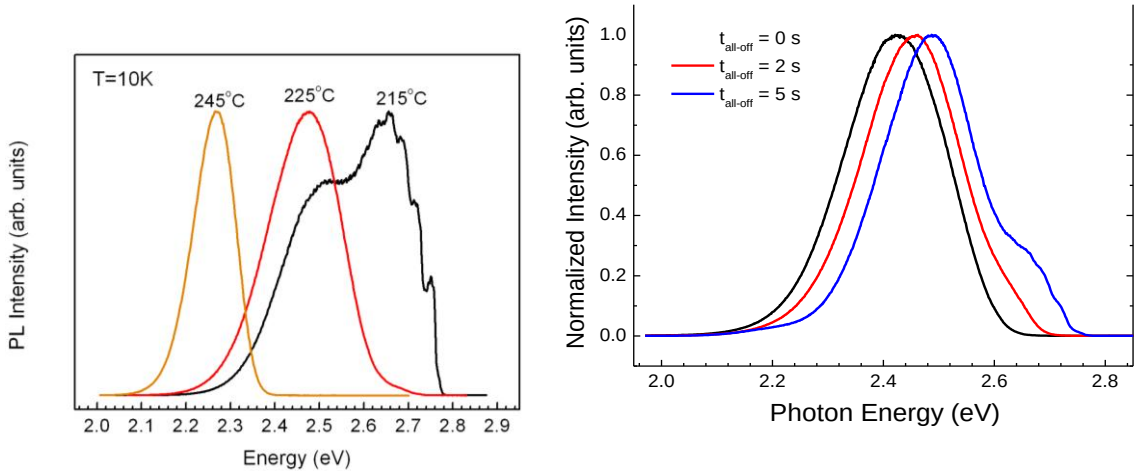

Figure 1 Nitrogen doped ZnTe/ZnSe QDs PL: (left) is a function of temperature of the Te effusion cell (i.e. Te flux); (right) is a function of tall-off.

The presence of type-II QDs was confirmed by PL studies at temperatures above 40 K, where a "green" band that is usually associated with the type-II ZnTe/ZnSe QDs appears. This band indeed showed strong dependence of the energy on the excitation intensity (Fig. 3). Therefore, it is apparent that we can fabricate type-II QDs even with minimal amounts of deposited Tellurium.

Most of our previous experience has been with the growth of ZnTe nanoislands embedded in a ZnSe matrix. As described above, we adjusted the dot confinement energy and band alignment by altering the

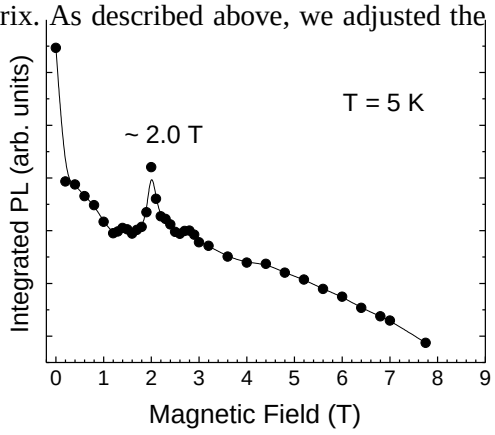

Figure 2 The integrated PL intensity of a δ-ZnSe:Te sample as a function of magnetic field. The peak at ~2.0 T corresponds to the electronic transition to non-zero orbital momentum.

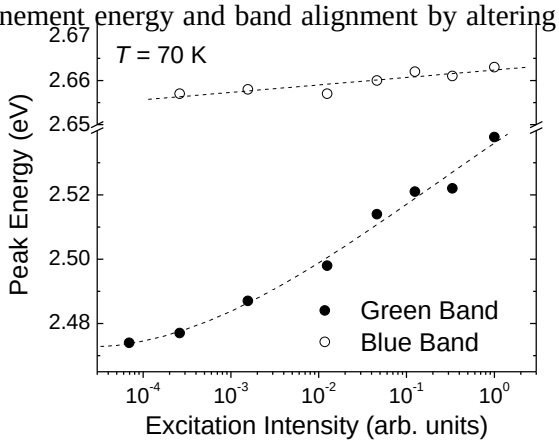

Figure 3 Peak position of the blue and green bands as functions of excitation intensity as obtained via the two Gaussians fitting. The dashed lines are for eye guidance only.

dot size via variation of growth parameters. Alternatively, one can change the chemical composition of the dots and/or the barrier. For example, the incorporation of Mg within the nanoisland increases the QD band gap, raising the conduction band and lowering the valence band relative to that of bulk ZnTe. The anticipated result is the simultaneous reduction of the valence band offset (relative to the surrounding ZnSe barrier) and hole confinement energy. The incorporation of Mg in the dot can be accomplished if one introduces a Mg flux simultaneously with the Te "on" step of the shuttering sequence. Preliminary results using such alternate growth protocol described above suggest that Mg is indeed incorporated in the dots, and not in the barrier material. While x-ray diffraction demonstrates that Mg has been incorporated in the structure, room temperature reflectance measurements (Fig. 4) shows that the absorption edge (and thus the bandgap) of the ZnTe(Mg) QDs in ZnSe structure is the same as that of ZnSe (2.7 eV). Hall

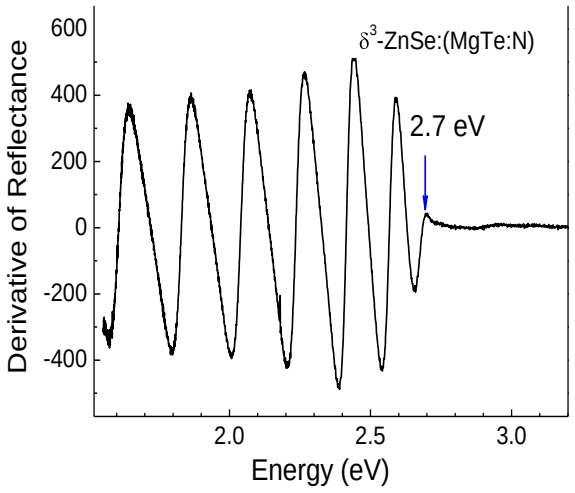

Figure 4 Room temperature reflectance of ZnTe(Mg) QDs in ZnSe matrix

Effect measurements of these samples gave the first instance in which a p-type conductivity of free holes could be measured (although the concentration of free carriers is still rather small). These experiments suggest that addition of Mg in the dots indeed has the effect of lowering the confinement energy of holes in the p-type doped ZnTe nanoislands, making the carriers more easily ionized.

Future Plans

We will emphasize the growth of type-II QDs of the ZnMgTe/ZnSe and ZnCdTe/ZnSe materials as modifications of the ZnTe/ZnSe materials previously studied. We will also explore changing of size of the dots by modification of the growth shutter sequence. The purpose will be to alter the confinement energy of the holes confined in the dots. We will continue to thoroughly investigate the optical and structural properties of these nanostructures to confirm our ability to adjust the bandstructure of the materials. We will explore the growth of type II ZnSe QDs embedded in ZnTe layers to obtain electron confinement, which has never been previously demonstrated.

We will optimize the growth of type II systems for electrons, and also grow coupled and uncloupled stacked QD systems, by varying the barrier spacer thickness. We will also explore strain engineering of the QDs. Enhanced p-type doping of ZnSe by the ZnMgTe(N) QDs will be further investigated. We will investigate the enhanced n-type doping of ZnTe via ZnSe(Cl) nanoislands.

References

[1] A. Muller, P. Bianucci, C. Piermarocchi, M. Fornari, I. C. Robin, R. Andre, and C. K. Shih, Phys. Rev. B **73**, 081306 (2006).
[2] I. L. Kuskovsky, C. Tian, G. F. Neumark, J. E. Spanier, I. P. Herman, W. C. Lin, S. P. Guo, and M. C. Tamargo, Phys. Rev. B **63**, 155205 (2001).
[3] Y. Gu, I. L. Kuskovsky, M. van der Voort, G. F. Neumark, X. Zhou, M. Munoz, and M. C. Tamargo, Phys. Stat. Sol. (b) **241**, 515 (2004).
[4] Y. Gong, W. MacDonald, G. F. Neumark, M. C. Tamargo, and I. L. Kuskovsky, Phys. Rev. B **77**, 155314 (2008).
[5] S. Tatarenko, B. Daudin, and D. B.-L. Cunff, Appl. Phys. Lett. **66**, 1773 (1995).
[6] I. L. Kuskovsky, W. MacDonald, A. O. Govorov, L. Muroukh, X. Wei, M. C. Tamargo, M. Tadic, and F. M. Peeters, Phys. Rev. B **76** 035342 (2007).
[7] I. L. Kuskovsky, Y. Gong, G. F. Neumark, and M. C. Tamargo, Supperlattice Microst **Article in Press** (2009).
[8] I. R. Sellers, V. R. Whitesides, I. L. Kuskovsky, A. O. Govorov, and B. D. McCombe, Phys. Rev. Lett. **100**, 136405 (2008).

DOE Sponsored Publications in 2007-2009 from Current Grant:

1. M. C. Tamargo, Q. Zhang, I. Kuskovsky, A. Shen and G. F. Neumark, Molecular Beam Epitaxy Growth and Properties of Type II Quantum Dots of Wide Bandgap II-VI Semiconductors, J. Vac. Sci. Technol. B (submitted for publication)
2. I. L. Kuskovsky, Y. Gong, G. F. Neumark, and M. C. Tamargo, *Photoluminescence and magneto-optical properties of multilayered type-II ZnTe/ZnSe quantum dots*, Supperlattice Microst **Article in Press** (2009).
3. V. A. Shuvayev, **I. L. Kuskovsky**, L. I. Deych, Y. Gu, Y. Gong, G. F. Neumark, M. C. Tamargo, and A. A. Lisyansky, *Dynamics of the radiative recombination in cylindrical nanostructures with type-II band alignment*, Phys. Rev. B **79**, 115307 (2009).
4. I. R. Sellers, V. R. Whiteside, **I. L. Kuskovsky**, A. O. Govorov, B. D. McCombe, *Aharanov-Bohm excitons at elevated temperatures in type-II ZnTe/ZnSe quantum dots*, Phys. Rev. Lett. **100**, 136405 (2008)
5. Y. Gong, W. MacDonald, G. F. Neumark, M. C. Tamargo, and **I. L. Kuskovsky**, *Optical Properties and Growth Mechanism of Multiple Type-II ZnTe/ZnSe Quantum Dots Grown by Migration Enhanced Epitaxy*, Phys. Rev. B. **77**, 155314 (2008)
6. M. C-K. Cheung, A. N. Cartwright, I. R. Sellers, B. D. McCombe, and **I. L. Kuskovsky**, *Time-resolved photoluminescence of type-II quantum dots and isoelectronic centers in Zn-Se-Te superlattice structures*, Appl. Phys. Lett. **92**, 032106 (2008)
7. I. R. Sellers , V. R. Whiteside, **I. L. Kuskovsky**, A. O. Govorov and B. D. McCombe, *Modulation of the Aharanov-Bohm Effect in Type-II II-VI ZnTe/ZnSe quantum dots by a Far-Infrared lase*r, Physica E, **40**, 1819-1823 (2008)
8. I. L. Kuskovsky, W. MacDonald, A. O. Govorov, L. Mouroukh, X. Wei, M. C. Tamargo, M. Tadic, F. M. Peeters, Optical Aharonov Bohm Effect in Stacked Type-II Quantum Dots, Phys. Rev. B. 76, 035342 (2007)

Group IV Semiconductor Nanomembranes
New Properties through Novel Synthesis and Strain Engineering

Max G. Lagally and Mark A. Eriksson
Lagally@engr.wisc.edu
University of Wisconsin-Madison, Madison WI 53706

Program scope

Semiconductor nanomembranes, very thin crystalline sheets with thicknesses ranging from less than 5 nm to ~500nm, represent a vehicle for both significant scientific discoveries and for energy related nanotechnologies. They are flexible, can be freestanding or transferred to other hosts, or can be layered to put crystalline materials next to each other that nature would not allow. They can be strain engineered so that they contain localized periodic strain or roll into tubes or other shapes. They can be lithographically patterned into nanowires and hybrid structures.

With appropriate synthesis and processing, dramatically new or changed mechanical, electronic, and thermoelectric properties can be induced. Functionally new materials can be made. Surfaces become more important, creating the opportunity for new sensing capabilities. Even photonic and electro-optic properties can be affected by appropriate strain engineering.

Our program addresses a broad spectrum of synthesis, processing, and characterization themes in Group IV semiconductors (specifically Si and Ge, although what is stated above should be generally true for other semiconductor nanomembranes). Specifically our interests have focused on 1) strain engineering and the use of strain to modify properties in very thin sheets or ribbons; 2) integration of membranes via transfer, bonding, and growth to create new properties; 3) novel characterization and development of tools and methods therefore; 4) theoretical interpretation and prediction via collaboration with Feng Liu (Utah) and theorists locally; and exploring the use of nanomembranes to address grand challenges as envisioned by DOE-BES.

Recent Progress

We have made significant progress on several fronts during the past two years, in novel-materials development focused on Si and Ge nanomembranes, in characterization of unique properties of nanomembranes, and in providing a theoretical understanding of processes and properties. The successes include

a) New method to increase strain in a strained trilayer membrane, beyond limitations of kinetic critical thicknesses.
b) Dislocation engineering with nanomembranes – making biaxially strained defect-free Si(110) via growth and release; a material that cannot be made any other way. A study in dislocation and twin suppression that can serve as a model for other systems.
c) Si nanoribbons and ordered quantum dots – a nanostrain lattice causing an electronic superlattice and miniband formation.
d) Hybrid-orientation and hybrid-composition nanomembrane synthesis, for possible thermoelectric materials studies.
e) Nanoribbon fabrication for thermoelectric studies.
f) Characterization of the modifications in conduction band structure of Si with biaxial strain, via membrane formation.
g) Measurement of conduction band changes due to quantum size effect for 1D confinement, including influence of surface roughness.
h) Measurement of localized strain-modified band structure using photoelectron spectroscopy.
i) Surface modified electronic transport in nanomembranes.
j) Thermopower measurements in low-doped Si nanoribbons.
k) Vertical transport through stacked membranes, possible use in novel solar cells.

We summarize briefly a few highlights from the above list with images.

1. **Defect-free SiGe growth substrate**. By a clever application, we are able to avoid critical-thickness considerations in introducing strain in trilayer membranes and also to provide a defect free SiGe substrate with high Ge composition. The basic idea is to grow the stressor SiGe layer so thick and at high enough Ge composition so that 3D islands form. But the beginning wetting layer is still flat. By releasing the membrane, removing the bounding Si layers and flipping the Si Ge layer we have a very flat high concentration SiGe substrate free of any dislocations. This substrate can serve as the basis for high-strain defect-free tensile Si, useful not only for fundamental studies of electron transport and band structure but also eventually for solar energy conversion and photodetectors.

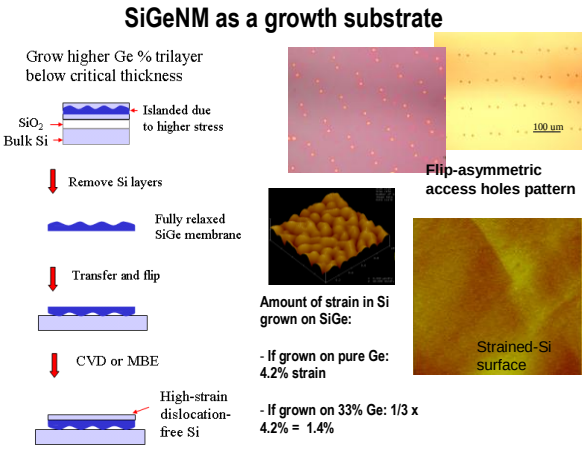

Figure 1. Process flow for SiGeNM and AFM results

2. Dislocation-free isotropically strained Si(110) NMs. Strained Si(110) cannot be grown by conventional techniques, but is useful for its high hole conductivity. We have devised a way using NM growth to do so. By careful analysis of the anisotropy of stress and strain, we discovered a generally useful way create isotropic strain even if the elastic constants are anisotropic. Figure 2 illustrates how this works. Because the elastic constants of Si and Ge are anisotropic in equivalent ways, the stress will be anisotropic but the strain will be isotropic.

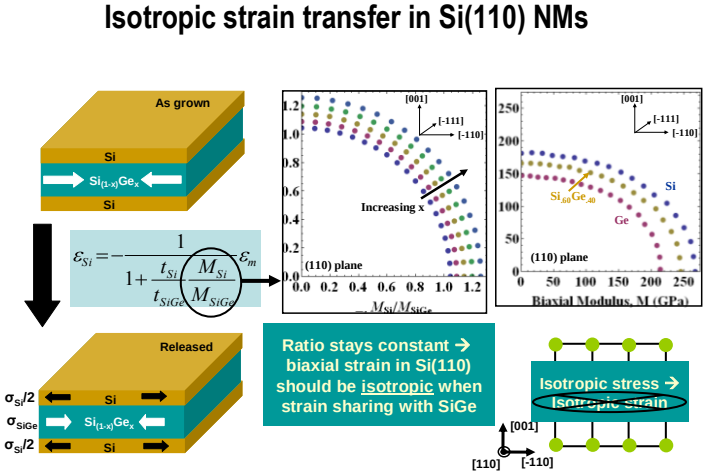

Figure 2 Illustration of strain transfer in NM growth and release when moduli are anisotropic

3. Photoelectron microscopy (PEEM) combined with x-ray absorption spectroscopy (XAS) to determine local-strain induced band structure changes. As part of our efforts on this grant we found we could grow a regular array of nanostressors (the "hut" quantum dots) on very thin Si nanoribbons to create a strain lattice. Collaborator Feng Liu calculated (see his abstract) that the strain lattice will create a band gap modulation, as the band structure of Si is sensitive to strain (measurements see below). How to measure this band gap modulation at the 50-100nm spatial resolution required, however, was a critical question. XAS can measure conduction band offsets. We found we could combine it with PEEM at the synchrotron to make such measurements. Figure 3 shows some early results. We certainly expect to continue to exploit and expand this technique in future work.

4. XAS measurements of conduction band structure changes with strain. Because with membranes we are able to make uniformly strained samples with various levels of strain, we were able to provide a quantitative determination of how the conduction band changes and splits with strain. Feng Liu provided

theoretical support. Some surprising results, inconsistent with prior theoretical work, were found, especially in how the energy positions of bands changed with strain.

5. Surface modified electronic transport in SiNMs. With very thin membranes, the surface begins to dominate the bulk. As we showed earlier, for typically low doped Si, the effects on electronic transport begin already at 200nm. [Thus all Si nanowire studies are affected by surfaces unless they are highly or degeneratively doped]. We have begun to modify the surface chemical condition to explore quantitatively how surface states, surface species, and surface roughness affect conductivity. The changes can be many orders of magnitude, and thus good control of these processes will open new possibilities for sensors. In the process, because we have very well defined systems, we appear to be addressing a large amount of confusion in the literature, and perhaps bringing order to the subject. We have also begun such studies on individual nanoribbons made from membranes

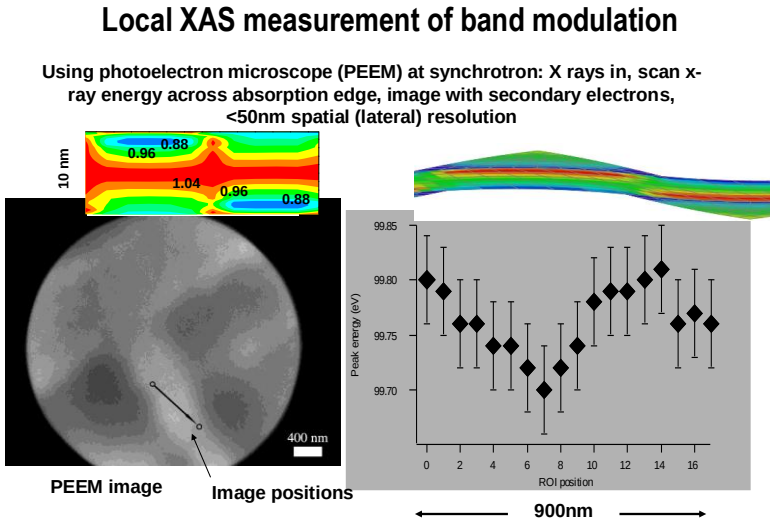

Figure 3. PEEM measurement of onset of absorption spectrum along a bent NR

6. Thermoelectric nanomaterials. This topic is of great interest to us, from both a processing point of view and from our capability to make relevant measurements. We already described in 3. above that we can make a strain lattice that in turn is a band gap lattice, in essence a single-element heterostructure. We calculated for this lattice miniband formation that could be valuable for thermoelectric nanowires. A recent result is shown in Fig. 4. We can also fabricate nanoribbons and create hybrid-composition membranes to make compositionally varying nanoribbons. Most recently we have made initial thermopower measurements on a low-doped individual ribbons, with interesting results. In parallel we are studying the effect of roughness on the electrical-transport portion of the thermoelectric figure of merit.

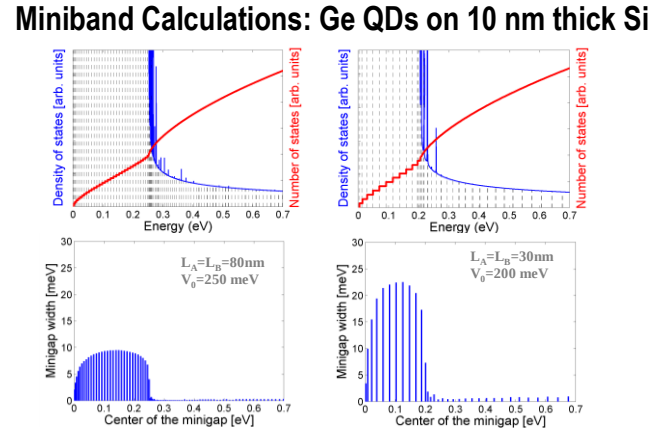

Figure 4. Miniband calculations for a strain lattice corresponding to experiment

Future work

It should be evident that the opportunities for novel energy-related science are legion with nanomembranes. In particular, we will be addressing membrane layering and vertical transport, with an eye toward novel photovoltaic approaches. More complexity in general will be introduced in materials and combinations. We expect to use Ge much more, for various reasons, and C for a different set of reasons. We expect to develop methods for uniaxial strain introduction and measurement. We certainly will expand our efforts in understanding the role of the surface. Our thermoelectric efforts are just beginning and we expect to be able to make a significant contribution there in the future.

Selected publications supported by this grant in the last two years

1. "Silicon Nanomembranes", **M.G. Lagally**, MRS Bulletin 32, 57 (2007). (invited)
2. "Elastically Strain Sharing Nanomembranes: Flexible and Transferable Strained Silicon and Silicon-Germanium Alloys", S. A. Scott and **M. G. Lagally**, J. Phys. D40, R1 (2007) (invited).
3. "Structure of Elastically Strain-Shared Silicon (110) Nanomembranes", A. C. Opotowsky, S. A. Scott, D. E. Savage, and **M. G. Lagally**, New J. of Physics 9, 270 (2007).
4. "Routes Toward Lateral Self-Organization of Quantum Dots: The Model System SiGe on Si(001)", Chr. Teichert and **M.G. Lagally**, Ch.2 in Lateral Alignment of Epitaxial Quantum Dots, ed. Oliver G. Schmidt, Springer Series on Nanoscience and Technology (2007)
5. "Directed Self-Assembly of Quantum Dots by Local Chemical Potential Control via Strain Engineering on Patterned Substrates", M-H Huang, **Feng Liu**, and **M. G. Lagally**, in Lateral Alignment of Epitaxial Quantum Dots, ed. Oliver G. Schmidt, Springer Series on Nanoscience and Technology 2007.
6. "Single-electron quantum dot in Si/SiGe with integrated charge measurement", C. B. Simmons, M. Thalakulam, N. Shaji, L. J. Klein, Hua Qin, R. H. Blick, D. E. Savage, **M. G. Lagally**, S. N. Coppersmith, **M. A. Eriksson**, Appl. Phys. Letters 91, 213103 (2007).
7. "Thermally Processed High-Mobility MOS Thin-Film Transistors on Transferable Single-Crystal Elastically Strain-Sharing Si/SiGe/Si Nanomembranes", H.-C. Yuan, M. M. Roberts, D. E. Savage, **M. G. Lagally**, G. K. Celler, and Z.Q. Ma, IEEE Transactions on Electron Devices 55, 810 (2008).
8. "Electronically Driven Structure Changes of Silicon Captured by Femtosecond Electron Diffraction", M. Harb, R. Ernstorfer, Ch. T. Hebeisen, G. Sciaini, Weina Peng, Th. Dartigalongue, **M. A. Eriksson, M. G. Lagally**, S. G. Kruglik, and R. J. D. Miller, Phys. Rev. Letters 100, 155504 (2008).
9. "Spin Blockade and Coherence Enhanced Transport in a Few-Electron Si/SiGe Double Quantum Dot", N. Shaji, C. B. Simmons, M. Thalakulam, L. J. Klein, H. Qin, H. Luo, D. E. Savage, **M. G. Lagally**, A. J. Rimberg, R. Joynt, M. Friesen, R. H. Blick, S. N. Coppersmith, and **M. A. Eriksson**, Nature Physics 4, 540 (2008).
10. "Influence of Strain on Band Structure in Strained Silicon Nanomembranes", C. Euaruksakul, Z. W. Li, F. Zheng, F. J. Himpsel, C. S. Ritz, B. Tanto, D. E. Savage, X. S. Liu, and **M. G. Lagally**, Phys. Rev. Letters 101, 147403 (2008).
11. "Excitation of Longitudinal and Transverse Coherent Acoustic Phonons in Nanometer Free-Standing Films of (001)-Si", M. Harb, W. Peng, G. Sciaini, Ch.T. Hebeisen, R. Ernstorfer, **M.A. Eriksson, M.G. Lagally**, S. G. Kruglik, and R. J. D. Miller, Phys. Rev. B79 0194301 (2009).
12. "Nanomechanical Architectures – Mechanics-Driven Fabrication Based on Crystalline Membranes", **F. Liu, M. G. Lagally**, and Ji Zang, MRS Bulletin 34, 190 (2009). (invited)
13. "Mechano-electronic Superlattices in Silicon Nanomembranes", Minghuang Huang, C. S. Ritz, B. Novakovic, D.C.Yu, Yu Zhang, F. Flack, D. E. Savage, I. Knezevic, P. G. Evans, **F. Liu,** and **M. G. Lagally**, ACS Nano 3, 721 (2009).
14. "Control of Island Growth with Mechanically Responsive Single-Crystal Nanomembrane Substrates", H.-J. Kim-Lee, D.E. Savage, C.S. Ritz, **M.G. Lagally,** and K.T. Turner, Phys. Rev. Letters 102, 226103 (2009)
15. "Influence of Surface Chemical Modification on Charge Transport Properties in Ultra-thin Silicon Membranes", S. A. Scott, W. Peng, A. M. Kiefer, H.-Q. Jiang, I. Knezevic, D. E. Savage, **M. A. Eriksson, and M. G. Lagally**, ACS Nano 3, 1683 (2009).
16. "Effects of Ge Adsorption on Dewetting and Thermal Agglomeration of Thin Silicon-on-Insulator", P.P. Zhang, B. Yang, P. Rugheimer, M. Roberts, D.E. Savage, **F. Liu**, and **M. G. Lagally**, J. Phys. D 42, 175309 (2009).
17. "Charge sensing and controllable tunnel coupling in a Si/SiGe double quantum dot"
C. Simmons, M. Thalakulam, B. Rosemeyer, B. Van Bael, E. Sackmann, D.E. Savage, **M.G. Lagally**, R. Joynt, M. Friesen, S. Coppersmith, and **M.A. Eriksson**, Nanoletters 9 3234 (2009).
18. "Strain – band structure relationships in Si(001) and Si(110) nanomembranes", C. Euaruksakul, F. Chen, B. Tanto, C. S. Ritz, D. M. Paskiewicz, F. J. Himpsel, D. E. Savage, Zheng Liu, Yugui Yao, **Feng Liu**, and **M. G. Lagally**, Phys. Rev. B, in press
19. "Globally and Locally Strained Si Nanomembranes Fabricated by Elastic Strain Sharing", F. Cavallo, D. M. Paskiewicz, and **M. G. Lagally**, Springer Series in Materials in press (review)
20. "Semiconductors turn soft: inorganic nanomembranes", Francesca Cavallo and **M. G. Lagally,** Soft Matter, submitted (invited)
21. "Step- and stress-driven nanostructure formation in the initial roughening of silicon-on-insulator", S. Seo, C. Euaruksakul, D. E. Savage, **M. G. Lagally**, and P. G. Evans, Phys. Rev. Letters, final review

Strain Superlattice: A combination of strain-induced self-assembly and strain-engineered band structure

Feng Liu (fliu@eng.utah.edu)
Department of Materials Science & Engineering
University of Utah, Salt Lake City, UT 84112

Program Scope

The nanotechnology of the future demands controlled and consistent fabrication of different classes of nanostructures that posses unique properties distinct from their conventional bulk counterparts. In the last decade, strain induced self-assembly process in epitaxial growth has become an attractive route to fabricate thin-film-based semiconductor nanostructures [1]. Recently, our experimental collaborators has demonstrated the ability to create a novel form of self-assembled nanostructures by growing SiGe quantum dots (nanostressors) on both sides of a Si nanomembrane and/or nanoribbon [2], as shown in Fig. 1. When a Si nanomembrane is thinned down to nanometer thickness, its mechanical compliance makes it fundamentally different from bulk materials or supported thin films. In particular, the growth of nanostressors on ultrathin Si membranes takes advantage of this mechanical compliance to create a "strain lattice" consisting of very small regions of high local strain, and which in turn provides a strong and precise feedback for self-assembly of the nanostressors with a high degree of ordering [2]. Consequently, the strain lattice in the Si membrane produces a modulation in the electronic band structure that extends through the thickness of the membrane, creating an electronic superlattice (SL).

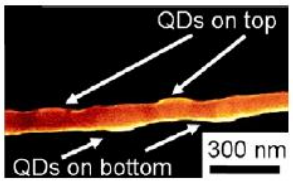

Fig. 1. SEM image of a Si nanoribbon strain modulated by self-assembled SiGe QDs (nanostressors) on its top and bottom surfaces.

Conventionally, a SL is always consisted of alternating epitaxial layers with different compositions in order to create an artificial one-dimensional (1D) periodic potential to modulate band gaps [3]. The strain SL, however, is made of pure Si with energy bands modulated by periodic strain. This new type of SL, on the one hand, revives the conventional concept of SL to not only new materials of one composition but also to new structures of 2D nanomembranes and 1D nanowires; on the other hand, expands the application of strain engineering to new territories combining the strain induced self-assembly of nanostructures with strain engineered band structures. It may potentially find new applications, such as in thermoelectric devices.

Recent Progress

In correlation with experimental studies, we have performed theoretical calculations to map out the electronic phase diagram of a Si strain SL. One key feature to identify a semiconductor SL is the formation of narrow subbands as described in Kronig-Penny model. According to the band offset scheme, the SL can be in addition classified into different types for different carrier confinement behaviors. It's long known that for compositional SL, these properties depend on the layer composition and layer thickness. For example, in the so-called "short-period" SLs, electronic states from different layers are strongly hybridized, so that the Kronig-Penny model breaks down and the SL behaves like an alloy [4]. Also, a transition from type I to type II is observed in GaAs/AlAs SLs when the layer thickness is varied, resulting in a change of the SL's optic property [4].

In the newly found strain SLs, it is clear that the strain magnitude and period play the same roles as layer composition and thickness in the conventional compositional SL. However, the relationship between the electronic properties and strain magnitude/period must be established for strain SLs, in order to characterize their electronic phase (SL phase vs. alloy phase) and SL type (type-I vs. type-II). Using first-principles calculations, we have recently constructed the electronic phase of a Si strain SL where uniaxial strain along (100) direction is periodically applied, as shown in Fig. 2. Band structures and charge distributions are calculated as a function of strain magnitude/period, to evaluate the degree of carrier confinement in terms of band edge local density of states (LDOS) and single valley wavefunctions.

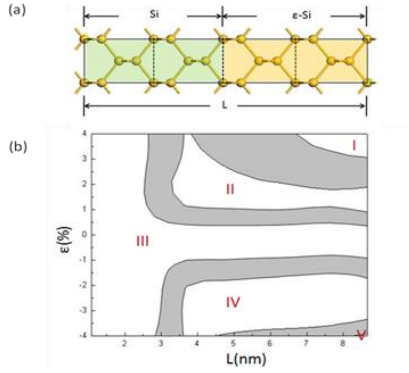

Fig. 2. (a) Schematics of atomic structures to model the strain SL. (b) Electronic phase diagram: I. partial type-II SL, II. electron confinement, III. Alloy, IV. electron confinement, V. type-I SL.

We found that there are five phases in this system under different combinations of strain magnitude (ε) and period (L). When either ε or L is small (Region III), the carriers "see" the average strain rather than the periodic strain, and the system behaves like the alloy phase. Compressive strain ($\varepsilon < -4\%$, $L > 8$nm) can give rise to type-I SL (Region I) in which the electrons and holes are both strongly confined in the strained layers. In contrast, tensile strain (e.g. $\varepsilon > 3\%$, $L > 6$nm) leads to a situation where only electrons in one single valley are confined in the unstrained layers, while the holes are confined in the strained layers. We refer to it as the partial type-II phase (Region V). In the intermediate regions (II and IV), holes are extended, but electrons are confined, which is defined as the electron-confined phase. The five phases are separated by broad boundaries (the grey bands in Fig. 2b), which indicates a crossover behavior rather than the real phase transition. The phase diagram as shown in Fig. 2 provides a useful knowledge base for designing Si strain SLs to engineer band structures for potential applications.

Recent progress on other projects:

1. Effect of Surface Bonding on Nanoribbon Wiggling:

The Si nanomembranes and nanoribbons provide one important class of stretchable electronic materials. Thus, it is important to study the elastic properties (such as stretchability) of Si nanomembranes and nanoribbons, especially after they are transferred on to a surface for certain applications. Recently, a very interesting wiggling phenomenon was observed in SiGe nanoribbon bonded to SOI substrate, as shown in Fig. 3. To understand the wiggling process and its characteristic properties, we have performed linear stability analysis based on a continuum model, to establish a scaling rule between the wiggling period and surface bonding area, in relation to the ratio of strain energy over interfacial bonding energy.

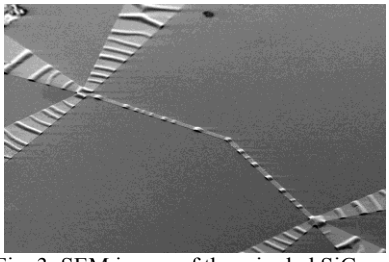
Fig. 3. SEM image of the wiggled SiGe nanoribbon on SOI substrate fabricated as a Hall-bar structure. (Courtesy of Prof. Blick of UW-Madison)

2. Quantum Manifestations of Graphene Edge Stress and Edge Instability:

Quantum effects have been widely shown for electronic structure and energetic quantities of low-dimensional nanostructures. Recently, we demonstrated for the first time the quantum manifestations of mechanical quantities in edge stress of graphene [5], the thinnest solid-state nanomembrane of only one-atomic-layer thick. We discover that quantum confinement can lead to stress oscillations, which in turn "quantum mechanically" modify the edge twisting and warping instability, as shown in Fig. 4. We further show that H edge saturation and Stone-Wale edge reconstruction can improve the chemical stability of graphene edges by lowering the edge energy, and also enhance their mechanical stability by converting compressive edge stress towards tensile so as to stabilize the planar edge structure. These first-principles findings, which cannot be captured by classical methods, give new insights to the understanding of mechanical stability of graphene-based nanostructures. We expect the quantum manifestation of mechanical properties such as stress to exist generally in many low-dimensional nanostructures.

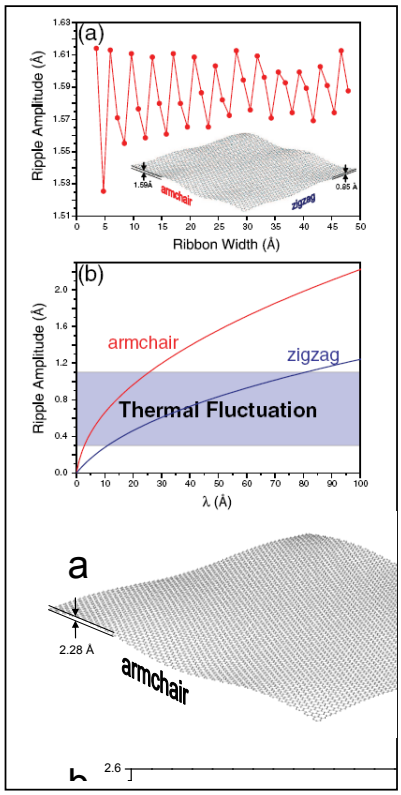

Future Plans

We will continue to expand our current studies as described above in the following areas:

(1) Continue with more extensive theoretical analyses and computer simulations on the "designing principle and process optimization" of nanomechanical architectures of nanofilms, focusing on nanomembranes and nanoribbons.
(2) Extend the study of SiGe nanomembranes/nanowires to other materials.
(3) Continue with study of electronic properties of nanomembranes and nanoribbons.
(4) Initiate new study on transport properties of nanomembranes and nanoribbons.
(5) Initiate new study on optoelectronic properties of nanomembranes and nanoribbons.

References

1. "Modeling and Simulation of Strain-Mediated Nanostructure Formation on Surface", Feng Liu, in "*Handbook of Theoretical and Computational Nanotechnology*", eds. M. Rieth and W. Schommers, Chapter 10, 577-625 (2006). (**invited book chapter**).
2. "Mechano-electronic Superlattices in Silicon Nanomembranes", M. Huang, C. S. Ritz, B. Novakovic, D. Yu, Y. Zhang, F. Flack, D. E. Savage1, P. G. Evans1, I. Knezevic, Feng Liu, and M. G. Lagally, *ACS Nano*, **3**, 721 (2009).
3. L. Esaki, and R. Tsu, IBM J. Res. Devel. **14** (1970).
4. J. Ihm, Applied Physics Letters **50**, 1068 (1987).
5. "Quantum Manifestations of Graphene Edge Stress and Edge Instability: A First-Principles Study", B. Huang, M. Liu, N. Su, J. Wu, W. Duan, B. Gu and Feng Liu, *Phys. Rev. Lett*. **102,** 166404 (2009).

The DOE funded publications in the last two years

1. "Influence of germanium on thermal dewetting and agglomeration of the silicon template layer in thin silicon-on-insulator", *J. Phys. D: Appl. Phys*. **42**, 175309 (2009).
2. "Quantum Manifestations of Graphene Edge Stress and Edge Instability: A First-Principles Study", B. Huang, M. Liu, N. Su, J. Wu, W. Duan, B. Gu and Feng Liu, *Phys. Rev. Lett*. **102, 166404** (2009).
3. "Nanomechanical Architecture --- A Mechanics-Driven Nanofabrication Approach", Feng Liu, M. G. Lagally and J. Zang, *MRS Bulletin* **34**, 190 (2009). (**Invited review**).
4. "Mechano-electronic Superlattices in Silicon Nanomembranes", M. Huang, C. S. Ritz, B. Novakovic, D. Yu, Y. Zhang, F. Flack, D. E. Savage1, P. G. Evans1, I. Knezevic, Feng Liu, and M. G. Lagally, *ACS Nano*, **3**, 721 (2009).
5. "Mechanical Wave Propagation in Carbon Nanotubes Driven by an Oscillating Tip Actuator", M. Chen, J. Zang, D. Xiao and Feng Liu, *J. Appl. Phys.* **105**, 026102 (2009).
6. "First-principles study of electronic properties of biaxially strained silicon: Effects on charge carrier mobility", D. Yu and Feng Liu, *Phys. Rev. B* **78**, 245204 (2008).
7. "Theory of Directed Nucleation of Strained Islands on Patterned Substrates" H. Hu, H.J. Gao and Feng Liu, *Phys. Rev. Lett*. **101, 216102** (2008).
8. "Dual-surfactant effect on enhancing p-type doping in III-V semiconductor thin films" Junyi Zhu, Feng Liu, G.B. Stringfellow, *Phys. Rev. Lett*. **101, 196103** (2008).
9. "Magnetism in Nanopatterned Graphite Film", L. Chen, D. Yu, Feng Liu, *Appl. Phys. Lett*. **93**, 223106 (2008).
10. "Unified Design Rule for Nanomagnetism in Graphene", D. Yu, E. M. Lupton, H.J. Gao, C. Zhang and Feng Liu, *Nano Res.* **1**, 497 (2008).
11. "Enhanced growth instability of a strained film on a wavy substrate", Hangyao Wang, Yu Zhang, and Feng Liu, *J. Appl. Phys.* **104**, 054301 (2008).
12. "Collective Magnetic Behavior of Graphene Nanohole Superlattices", D. Yu, E. M. Lupton, M. Liu, W. Liu and Feng Liu, *Nano Res*. **1**, 56 (2008).
13. "Suppression of spin-polarization in graphene nanoribbon by edge defect and impurity", Bing Huang, Feng Liu, Jian Wu, Bing-Lin Gu, and Wenhui Duan, *Phys. Rev. B* **77**, 153411 (2008).
14. "Modified Timoshenko formula for bending of ultrathin strained bi-layer films", Ji Zang and Feng Liu, *Appl. Phys. Lett*. **92**, 021905 (2008).
15. "Making a field effect transistor on a single graphene nanoribbon by selective doping", Bing Huang, Qimin Yan, Gang Zhou, Jian Wu, Bing-Lin Gu, Wenhui Duan, and Feng Liu, *Appl. Phys. Lett*. **91**, 253122 (2007).
16. "Synthesis of Carbon Nanotubes by Rolling Up Patterned Graphene Nanoribbons Using Selective Atomic Adsorption", Decai Yu and Feng Liu, *Nano Lett*. **7**, 3046 (2007).
17. "Bending of Si Nano-Cantilever Induced by Molecular Adsorption: A Modified Stoney Formula for the Calibration of Nanomechanochemical Sensors", Ji Zang and Feng Liu, *Nanotechnology*, **18**, 405501 (2007).
18. "Confining P diffusion in Si by an As-doped barrier layer", Lugang Bai, Decai Yu, Guang-Hong Lu, Feng Liu, Q. Wang, and Hamza Yilmaz, *Appl. Phys. Lett.* **91**, 061926 (2007).
19. "Intrinsic current-voltage characteristics of graphene nanoribbon transistors and effect of edge doping", Q. Yan, B. Huang, J. Yu, F. Zheng, J. Zang, J. Wu, B. Gu, Feng Liu, and W. Duan, *Nano Lett*. **7**, 1469 (2007).
20. "Mechanism for Nanotube Formation from Self-Bending Nanofilms Driven by Atomic-Scale Surface-Stress Imbalance", Ji Zang, Minghuang Huang, and Feng Liu, *Phys. Rev. Lett.* **98, 146102** (2007).
21. "MD simulation of structural and mechanical transformation of single-walled carbon nanotubes under pressure", J. Zang, O. Aldás-Palacios and Feng Liu, *Commun. Comput. Phys.* **2**, 451 (2007). (**invited review**).
22. "Impurity mediated absorption continuum in single-walled carbon nanotubes", C. Zhang, J.C. Chao, X.G. Guo and Feng Liu, *Appl. Phys. Lett.* **90**, 023106 (2007).
23. "Directed Self-assembly of Quantum Dots by Local-Chemical-Potential control via Strain Engineering on Patterned Substrates", Hangyao Wang, Feng Liu, and M. Lagally, in "Lateral Alignment of Epitaxial Quantum Dots", Ed., O. Schmidt, Springer, Chapter 20, page 524 **(2007). (invited book chapter).**

Session IVe

Thin Films: Fabricating Nanostructure from Films: Synthesis and Processing (cont.)

Session Chair: David Geohegan, Oak Ridge National Laboratory

(This page intentionally left blank.)

Design and Synthesis of Nanomaterials

Michael L. Simpson, Jason D. Fowlkes, Miguel Fuentes-Cabrera, Joseph A. Horton, Anatoli V. Melechko, Philip D. Rack, G. Malcolm Stocks

Program Scope: The objective of this program is to perform basic research that provides a new level of understanding of the mechanisms that control the organization of nanostructured materials. Specifically, the primary focus is the assembly and controlled synthesis of elemental and multi-component nanoparticles on surfaces by the destabilization of thin solid films. Specifically we are studying how intrinsic thermodynamic alloy properties; micro- and nanostructure; and thin film size, geometry and dimensionality affect surface wave instabilities and hole nucleation. Furthermore, we are studying the subsequent dynamics in both the solid and liquid state through substrate or pulsed laser heating with the goal of elucidating the behavior of thin film materials during the dewetting process. The fundamental understanding of synthesis processes based on thin-film destabilization makes possible the directed assembly of metal alloy nanoparticles with designed composition, structure, orientation and spatial arrangement.

Recent Progress: As described in the scope of work we are investigating thin film instabilities in both the liquid state (via nanosecond pulsed laser heating) and the solid state via standard annealing. Furthermore we are correlating experimental observations to multiple time and length scale computational approaches.

Liquid State Instability and Transport

Pulsed laser treated thin films and patterned nanostructures have been investigated and the relative time and length scales associated with the thermocapillary transport and instability mechanisms which results in correlated nanoparticle assemblies. Lithographically patterned nickel circles, squares, and triangles have been pulsed laser treated and the nanosecond liquid lifetimes and resultant front velocities have been correlated to the in-plane and out-of-plane nanoscale radius of curvature. Pseudo 1-dimensional nanoscale lines of nickel have also been studied and the time and length (particle size and spacing) scale for the nanoparticles assembly were determined by non-linear 3-dimensional hydrodynamic simulations to be due to substrate-mediated Rayleigh instabilities. Figure 1 shows the scanning electron micrographs of pulsed laser dewetted nickel patterns and lines resulting from sequential pulsed laser irradiation and liquid induced transport. Also shown are the simulated 3-dimensional hydrodynamic simulation results which show good time and length scale agreement with the experimental results. In addition to these fundamental studies assembled silicon and nickel particles have been used as templates for organized growth of vertically aligned carbon nanofibers.

Solid State Instability and Transport

The early focus for the solid state dewetting studies has been on the behavior of Cu-Ni alloy thin films during solid state dewetting. We have observed segregation in the Cu-Ni alloy thin films during solid state destabilization on Si which is in contrast to behavior expected for the isomorphous system. Thin films of Cu-Ni and Ti-Cu-Ni were formed on Si and subjected to annealing temperatures from 300^{o}C - 700^{o}C. Scanning Electron Microscopy (SEM) micrographs and Energy-Dispersive X-ray spectroscopy(EDX) mapping of these films reveal the formation of Cu-rich clusters on the surface prior to complete dewetting of the film in the range of temperatures much lower than dewetting of Ni film (figure 2). The size and density of the Cu-rich regions increased with the increase in annealing temperatures. The partial segregation has been correlated with hole nucleation during initial stages of thin film dewetting and the Ni-rich regions lag behind copper rich regions in particle formation in the temperature range from 400-600^{o}C. Films heated to 700^{o}C do not display segregation of Cu-Ni alloy.

Computational Studies

The goal of our program is to apply various ab-initio, molecular dynamics and continuum models to intersect the various time and length scale phenomena of the experimental program. We have initially studied the thin film dewetting of the nickel in the solid and liquid state using a LAMMPS simulation package (AIREBO potential was used to mimic the C-C interaction; the Ni-C interaction was described with a Lennard-Jones potential; and finally EAM was used to describe the Ni-Ni interaction]. Preliminary results compare favorably with experimental studies in that the simulated dewetting velocities of the liquid state (~150m/s) are on the same order of magnitude as the experimental values (90m/s). Figure 3 shows simulated cross sections of the liquid nickel dewetting profiles as a function of the liquid lifetime. Using this approach, we will try to extract surface energies (and wetting angles) as this could facilitate continuum models which describe instability and transport behavior.

Future Plans: We will continue to investigate liquid and solid state dewetting phenomena in the thin film elements and alloys. For the liquid state dewetting we plan on investigating copper ring dewetting patterns to compare the competing retraction velocities, Rayleigh-type, and thin film instabilities. Additionally by varying the radius of curvature of the ring, we can investigate how the azimuthal LaPlace pressure has on the instability and transport. For the solid state dewetting, we plan on investigating patterned nanoscale featured with confined dimensionality similar to our initial liquid phase studies to compare relevant time and length scales associated with the surface diffusion driven process. Initially we will study individual elemental Cu and Ni and then progress to alloy thin films. For our computational efforts, we will use a Reactive Force-field (ReaxFF) to study the de-wetting of Cu on Si (111). Early results contradict experimental results in that the simulations show that Cu wets the silicon surface. Thus we are investigating the source of the discrepancy which could be due to: 1) the force-field is not representing the physics correctly; 2) the Si surface used in the experiment is not the Si(111) surface; 3) is the reconstruction of the Si(111) surface playing a role in de- wetting? 4) The surface is damaged (contains defects) or is not clean. To address the initial issue, we have begun studying the deposition of Cu in Si(111) and the diffusion of Cu in bulk Si (from the T to the H site) using first-principles and techniques and the ReaxFF. To address the last issue we have also started to carry out simulations of an H-terminated Si (111) surface. Preliminary results show that for the H-terminated surface copper prefers to form islands instead of wetting.

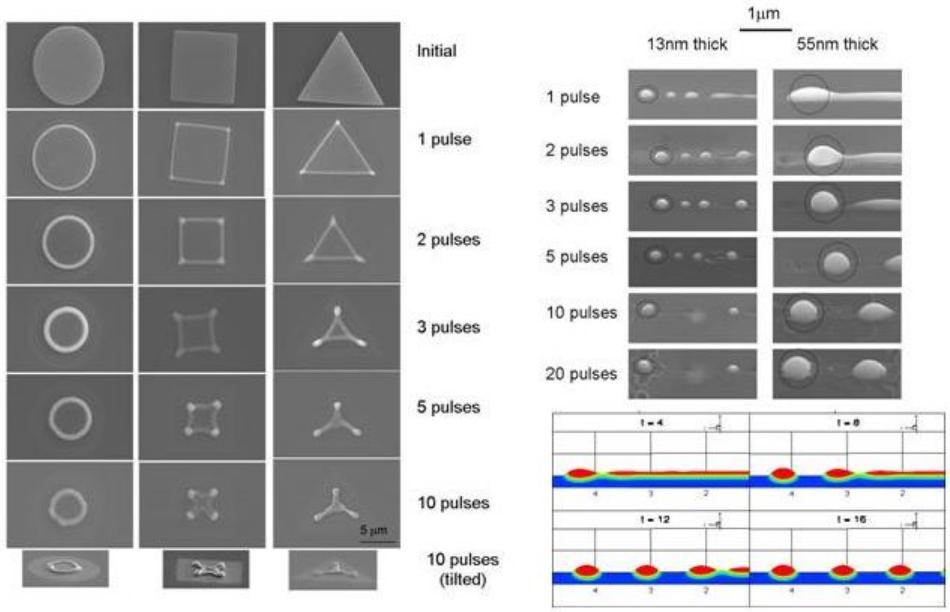

Figure 1. Left: Pulsed laser dewetting of patterned nickel shapes which contract due to in-plane and out-of-plane radii of curvature. Right: SEM images (top) and 3-d hydrodynamic simulations of the nanoparticle assembly from laser treated patterned nickel lines.

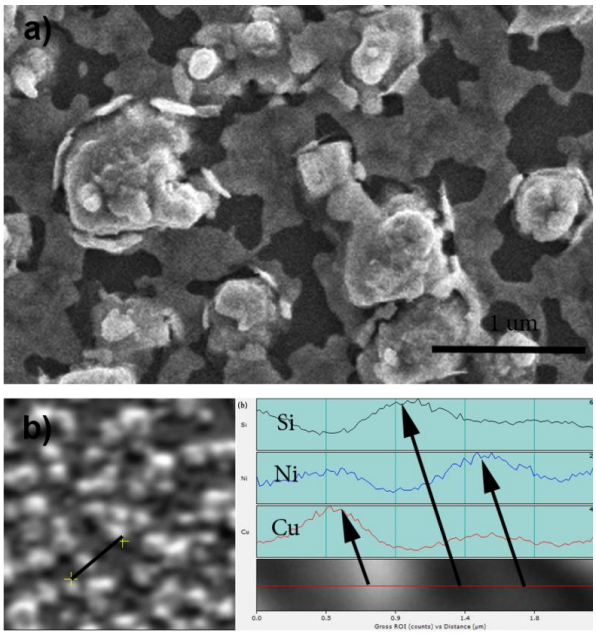

Figure 2. Solid state segregation in a CuNi alloy thin film on Si: a) Scanning electron micrograph of a 50 nm film with 75 at% of Cu annealed in vacuum for 1 hour at 500C; b) An EDX line scan (indicated in the left panel), arrows indicate Cu-rich, Si-rich, and Ni-reach areas.

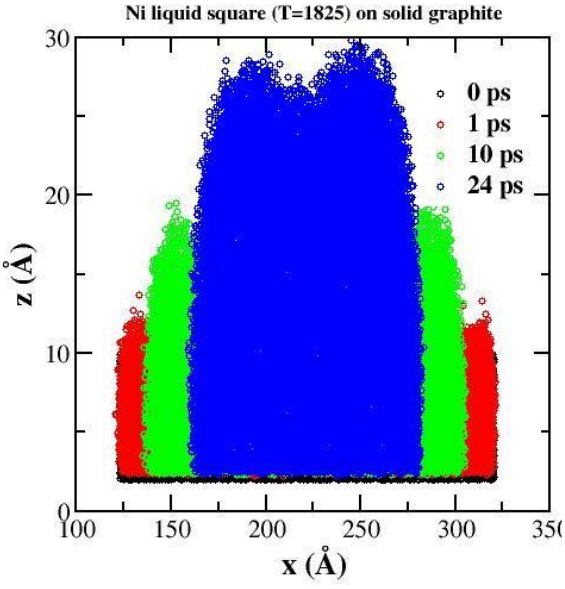

Figure 3. Simulated liquid dewetting profiles of a nanoscale nickel square.

Publications (previous 2 years)

1. Melechko AV, Desikan R, McKnight TE, Klein KL, Rack PD. *Synthesis of vertically aligned carbon nanofibers for interface with live systems*. Journal of Physics D, (2009) (in press)
2. Peckys, DB, Melechko AV, Simpson, ML, McKnight, TE, *Immobilization and release strategies for DNA delivery using carbon nanofiber arrays and self-assembled monolayers*. NANOTECHNOLOGY, SN 0957-4484, PD APR 8, PY 2009, VL 20, IS 14, AR 145304
3. Fletcher, BL, Retterer, ST, McKnight, TE, Melechko AV, Fowlkes, JD, Simpson, ML, Doktycz, MJ *Actuatable membranes based on polypyrrole-coated vertically aligned carbon nanofibers*. ACS NANO SN 1936-0851, PD FEB, PY 2008, VL 2, IS 2, P 247-254
4. Fowlkes, J. D., B. L. Fletcher, S. T. Retterer, Melechko AV, M. L. Simpson and M. J. Doktycz. *Size-selectivity and anomalous subdiffusion of nanoparticles through carbon nanofiber-based membranes*. Nanotechnology 19(41): 415301. (2008)
5. Fuentes-Cabrera, M., M. I. Baskes, Melechko AV and M. L. Simpson. *Bridge structure for the graphene/Ni(111) system: A first principles study*. Physical Review B (Condensed Matter and Materials Physics) 77(3): 035405-5. (2008)
6. Guan, Y. F., R. C. Pearce, A. V. Melechko, D. K. Hensley, M. L. Simpson and P. D. Rack. *Pulsed laser dewetting of nickel catalyst for carbon nanofiber growth*. Nanotechnology 19(23): Artn 235604. (2008)
7. Klein, KL, Melechko AV, McKnight TE, Retterer, ST, Rack, PD, Fowlkes, JD, Joy, DC, Simpson, ML. *Surface characterization and functionalization of carbon nanofibers*. Journal of Applied Physics, SN 0021-8979, PD MAR 15, PY 2008, VL 103, IS 6, AR 061301
8. Mann, DGJ, McKnight TE, McPherson, JT, Hoyt, PR, Melechko AV, Simpson, ML, Sayler, GS. *Inducible RNA interference-mediated gene silencing using nanostructured gene delivery arrays*. ACS NANO, SN 1936-0851, PD JAN, PY 2008, VL 2, IS 1, BP 69-76
9. Rack, P. D., Y. Guan, J. D. Fowlkes, A. V. Melechko and M. L. Simpson (2008). *Pulsed laser dewetting of patterned thin metal films: A means of directed assembly*. Applied Physics Letters 92(22): Artn 223108.
10. Retterer, S. T., A. Melechko, D. K. Hensley, M. L. Simpson and M. J. Doktycz (2008). *Positional control of catalyst nanoparticles for the synthesis of high density carbon nanofiber arrays*. Carbon 46(11): 1378-1383.
11. Sorge, K. D., K. L. Klein, A. V. Melechko, C. L. Finkel, O. Malkina, T. Leventouri, J. D. Fowlkes, P. D. Rack and M. L. Simpson (2008). *Magnetic properties of Fe-Co catalysts used for carbon nanofiber synthesis*. Journal of Applied Physics 104(3): 033909.
12. Melechko, A. V., K. L. Klein, J. D. Fowlkes, D. K. Hensley, I. A. Merkulov, T. E. McKnight, P. D. Rack, J. A. Horton and M. L. Simpson (2007). *Control of carbon nanostructure: From nanofiber toward nanotube and back*. Journal of Applied Physics 102(7): 074314-7.
13. Randolph, SJ, Fowlkes, JD, Melechko AV, Klein, KL, Meyer, HM, Simpson, ML, Rack, PD. *Controlling thin film structure for the dewetting of catalyst nanoparticle arrays for subsequent carbon nanofiber growth.* NANOTECHNOLOGY, SN 0957-4484, PD NOV 21, PY 2007, VL 18, IS 46, AR 465304

Nanoscale Morphology Evolution Under Ion Irradiation

Michael J. Aziz
maziz@harvard.edu
Harvard School of Engineering and Applied Sciences
Cambridge MA 02138

Program Scope

The ability to understand and control the properties of matter on nanometer length scales is a major thrust in materials chemistry and physics today. Mastery of fundamental science at this length scale will have profound implications for a wide variety of future discoveries and applications in the chemical and biological sciences as well as in materials science and condensed matter physics.

This program is a combined experimental and theoretical study of the fundamental physical principles governing nanoscale surface morphology evolution during sputter erosion using ions with energies roughly in the range 0.1 to 30 keV. The ability of ion beams to control solid state material morphologies on molecular dimensions has permitted the fabrication of solid-state single-biomolecule detectors [1] and may become the basis for nanoscale morphology control in the mass production of a wide variety of nanoscale devices.

In this presentation I will report on our studies of the spontaneous formation of topographic patterns such as those shown in Fig. 1 during spatially uniform ion beam irradiation of initially flat surfaces. This method has created features as small as 15 nm in semiconductors [2] and 7 nm in polymers [3]. For a rigorous comparison of theory and experiment, we are focusing on the simplest possible systems: elemental, amorphous, isotropic materials under inert ion irradiation.

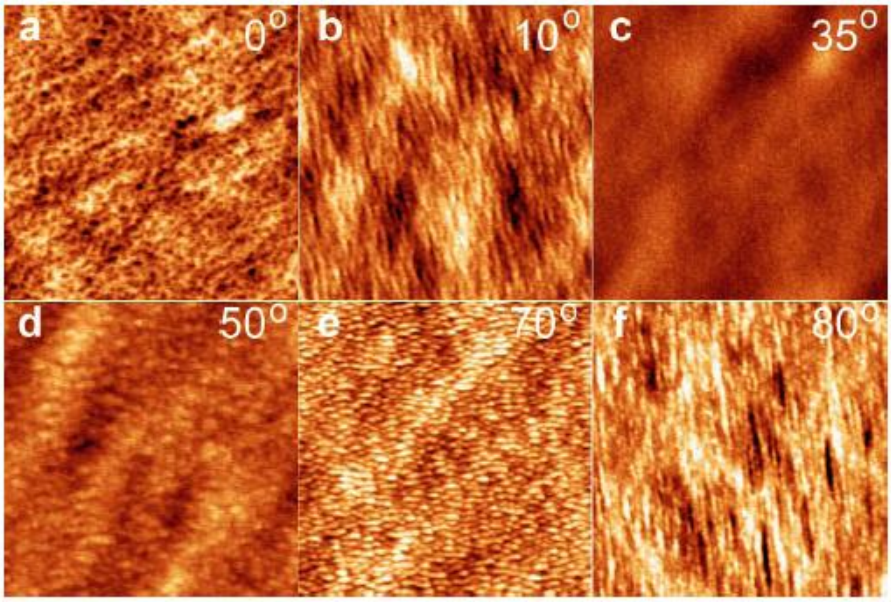

Fig. 1. Patterns formed by 250 eV argon ion irradiation of room-temperature Si(001), which immediately becomes amorphous and isotropic. Angle from normal incidence is indicated in corner of image. Projected direction of ion beam is from bottom to top on page.

The Bradley-Harper linear stability theory for a flat surface under uniform ion irradiation [4] is the widely accepted "classical" starting point for understanding self-organized nanoscale pattern formation. The theory predicts that the evolving surface topography function $h(x,t)$ (here, for simplicity, we are describing evolution in only one independent spatial dimension, although the actual theory includes two independent spatial dimensions) is governed by the following partial differential equation (PDE)

$$\frac{\partial\left(h-\bar{h}\right)}{\partial t}=S\left(b\right)\frac{\partial^2 h}{\partial x^2}-B\frac{\partial^4 h}{\partial x^4}, \tag{1}$$

where $\bar{h}$ is the mean height, b is the local surface slope, and B is a materials parameter involving the surface diffusivity and describing gradual relaxation. If the "curvature coefficient" S is negative then a flat surface is unstable. Bradley-Harper theory predicts the linear instability of a flat surface topography to a sinusoidal modulation of *some* wave vector for *any* incidence angle: S is always negative in *some* direction (including the direction in the surface perpendicular to the ion beam).

Recent Progress

We have been studying the topographic patterns formed on silicon surfaces as the "control parameters" of ion energy and incidence angle are varied. We found regions of parameter space where a flat surface is stable, as shown in Fig. 1(c) and indicated by the "phase diagram" in Fig. 2.

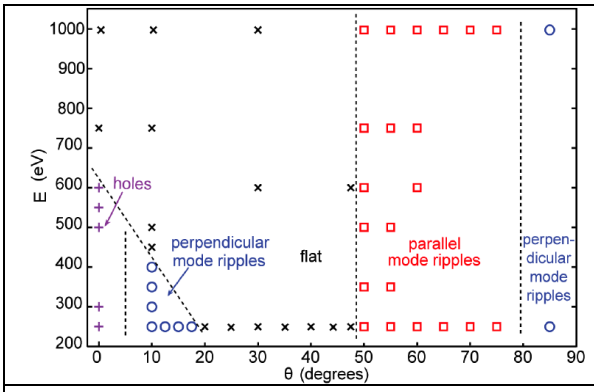

Fig. 2. Phase diagram for pattern formation on room-temperature silicon upon argon ion irradiation. θ is deviation from normal incidence, E is ion beam kinetic energy.

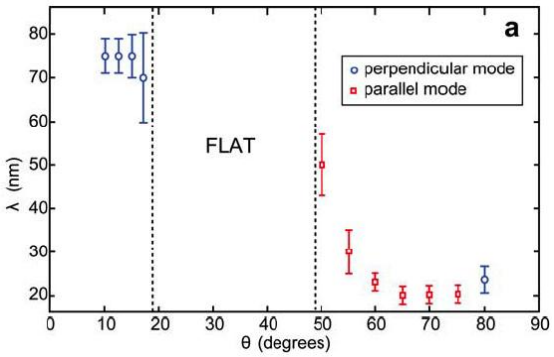

Fig. 3. Diverging pattern wavelength exhibited by parallel mode ripples (Type II bifurcation) near 50 degrees as flatness is approached from higher angle; constant pattern wavelength (Type I bifurcation) for perpendicular mode ripples near 20 degrees as flatness is approached from lower angle.

The observation of a regime of stability contradicts the classical theory, but is readily resolved as discussed below. Other contradictions present more difficult puzzles.

Sharp boundaries between stable and unstable regimes in control parameter space are known as *bifurcations*. Nonequilibrium pattern formation theory [5] predicts that near bifurcations pattern formation features are universal, depending only on general characteristics of the dynamics, such as its symmetries, degree of criticality (i.e. whether the amplitude vanishes continuously or discontinuously), and whether the characteristic length scale vanishes, diverges or remains finite at bifurcation.

As shown in Fig. 3, when we follow the wavelength of the emerging corrugation vs. control parameter as we pass from a regime of ripples to a regime of flatness, the wavelength diverges in the high-angle regime (this is called a Type II bifurcation) for parallel mode ripples (wave vector parallel to projected ion beam) and stays constant in the low-angle regime (called a Type I bifurcation) for perpendicular mode ripples (wave vector perpendicular to projected ion beam).

We have theoretically examined physically-motivated phenomena that may be influencing the linear stability of a flat surface but may not be encompassed by the classical theory, e.g. the formation of craters with rims at ion impact points. For all such phenomena whereby a pattern develops from the cumulative response to localized changes brought about with each ion impact, we have proven that Eq. (1) still describes the surface evolution but the magnitude and sign and b-dependence of S can change. Importantly, other spatial derivatives of the height do not enter the stability equation, as long as we are discussing *linear stability*, i.e. the initial stability/instability criterion for infinitesimal perturbations. S can readily change signs, which explains the appearance of regions of stability of a flat surface in the phase diagram, but *the characteristic wavelength of the instability should diverge* – i.e. the bifurcation should be Type II. Experimentally, near 10° from normal incidence we observe the constant wavelength indicating Type I bifurcations. We have thereby proven that these features do not come from the accumulation of a local response to an ion impact. Candidate *non-local* mechanisms include the evolution of stress (which is a very

long-range effect) and re-deposition of sputtered atoms after very long distance displacements (long compared to the pattern wavelength) through the vacuum.

From Crater Functions to Phase Diagrams

We have developed a new theoretical methodology for deriving the governing partial differential equation for surface evolution from the accumulation of topographic responses to individual ion impacts. The local response (the "crater function" $\Delta h(x-x')$, with x' the impact point) can be obtained by experiment (e.g. STM images) or simulation (e.g., Molecular Dynamics). Although no two craters are completely identical, only the average over many craters matters. The theory exploits a separation in length scale between the topographic changes due to a single ion impact and the emerging pattern. It also exploits a separation in time scale between the "prompt regime", in which kinetic energy-induced sputter erosion and bombardment-induced surface mass transport go to completion, and the "gradual regime" in which thermally-activated morphological relaxation processes occur (leading to the last term in Eq. (1)). The theory derives for the prompt regime, *without any free parameters*, the *S* coefficients (there is one for each independent spatial dimension, *x* and *y*) in Eq. (1), from the crater functions. Prior to this work, the best models for the *S* coefficients contained adjustable parameters, and in many cases there was no way to tell the magnitude. A flat surface is stable if both S_x and S_y are positive.

The theoretical formalism starts with an expression for the net result of accumulated responses to single ion impacts:

$$\frac{\partial h(x,t)}{\partial t} = \int_{-\infty}^{\infty} I(x')\Delta h(x-x')dx', \tag{3}$$

in terms of the single-impact crater function $\Delta h(x-x')$ and the ion flux over the surface *I*. The complete description evolution of an initially-flat interface in the "prompt regime" (including the values of the *S* coefficients) then follows from some complicated but rigorous math:

$$\frac{\partial h(x,y,t)}{\partial t} = I\tilde{M}^{(0)} + \varepsilon\nabla\bullet I\tilde{M}^{(1)} + \frac{1}{2}\varepsilon^2\nabla\bullet\nabla\bullet I\tilde{M}^{(2)} \tag{4}$$

where ε is the amplitude of the modulation and the $\tilde{M}$'s are simply combinations of moments of the average crater function. For linear stability the terms of order ε^2 are insignificant and the $\tilde{M}^{(1)}$ term determines whether a flat surface is stable.

To obtain converged crater functions from Molecular Dynamics simulations, we have been collaborating with Kai Nordlund and Juha Samela of the University of Helsinki. They have obtained preliminary results from a large number of impact simulations at a variety of incidence angles, and more thorough calculations are under way at present. When we compute the moments from their preliminary results we obtain the predictions for stability vs. instability in Fig. 4. This result is highly significant for several reasons:

1. For the first time, a theory predicts the existence of a transition to flatness with zero free parameters;
2. The predicted divergence of the wavelength with decreasing angle is qualitatively consistent with the experiments for parallel-mode ripples;
3. The crossover to perpendicular mode ripples at 75° is consistent with experiment;
4. The predicted absence of the instability below 20°, where the experiments clearly show the presence of an instability, indicates that non-local mechanisms (such as elastic stress) must be responsible for them.
5. The actual value of the instability wavelength is set by not just *S* but also by the material relaxation parameter *B*. This parameter might vary with incidence angle depending on the actual relaxation mechanism, but only *S* should be responsible for wavelength divergence, just as *S* is solely responsible for flatness. For a more quantitative treatment of the wavelength of the instability, we may need to understand the gradual-regime relaxation mechanism better.

Future Plans

We plan to complete the molecular dynamics study, obtain well-converged results, and analyze the results to compare with experiment qualitatively and quantitatively.

We plan to investigate stress development as a potential origin of the low-angle instability.

At an incidence angle of about 50°, where we see the diverging length scale that is predicted by local theory, we plan to investigate the amplification kinetics as the transition to flatness is approached. This investigation will be carried out using real-time synchrotron X-ray diffraction in collaboration with Karl Ludwig (Boston University). Very near the bifurcation points, the number of possible terms in a governing PDE is reduced and so we are able to perform much more reliable tests of theory with experiments in this regime. The amplification rate becomes so slow near the bifurcation point that it becomes difficult to make sufficiently accurate measurements with cook-and-look experiments; hence the synchrotron experiments are called for.

We will study the saturation amplitude, where amplification comes to a halt and the amplitude approaches steady state. This is the best regime for a rigorous test of non-linear terms (once we have well established linear behavior).

Finally, we plan to complete a series of experiments and the development of a model for the closing of nanopores by ion irradiation induced stresses.

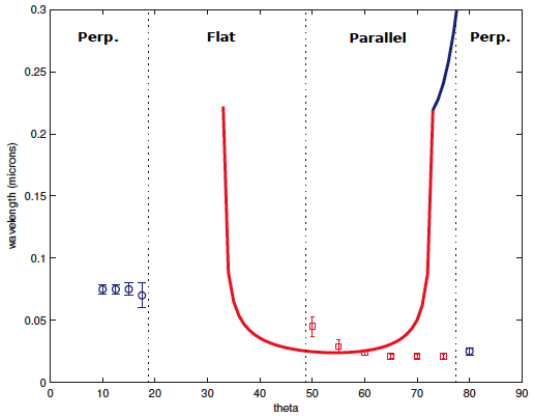

Fig. 4. Predicted vs experimental pattern wavelength vs. incidence angle at 250 eV. Data points and vertical dotted lines indicate experimental results: Perpendicular mode ripples at low angle (blue points); flat stability at intermediate angle (no points); parallel mode ripples at high angle (red points); perpendicular mode at very high angle (blue point). Theory predicts flat stable surfaces for low angles extending to about 30°, parallel mode ripples from 30° to about 75° (red line), and perpendicular mode ripples above 75° (blue line).

References

[1]J. Li, D. Stein, C. McMullan, D. Branton, M.J. Aziz, and J. Golovchenko, *Nature* **412**, 166 (2001); J. Li, M. Gershow, D. Stein, E. Brandin, and J.A. Golovchenko, *Nature Materials* **2**, 611 (2003).

[2]S. Facsko, T. Dekorsy, C. Koerdt, C. Trappe, H. Kurz, A. Vogt, and H.L. Hartnagel, *Science* **285**, 1551 (1999).

[3]Q. Wei, J. Lian, S. Zhu, W. Li, K. Sun, and L. Wang, *Chem. Phys. Lett.* **452**, 124 (2008).

[4]R.M. Bradley and J.M. Harper, *J. Vac. Sci. Technol. A* **6**, 2390 (1988).

[5]M.C. Cross and P.C. Hohenberg, *Reviews of Modern Physics* **65**, 851 (1993).

Publications Acknowledging DOE support - Past 2 Years

D.P. Adams, M.J. Aziz, G. Hobler, W.J. MoberlyChan, T. Schenkel, "Fundamentals of FIB Nanostructural Processing: Below, At and Above the Surface", *MRS Bulletin* **32** (5), 424-32 (2007).

B. Davidovitch, M.J. Aziz, and M.P. Brenner, "On the Stabilization of Ion Sputtered Surfaces", *Phys. Rev. B* **76**, 205420 (2007).

C.S. Madi, B. Davidovitch, H.B. George, S.A. Norris, M.P. Brenner, and M.J. Aziz, "Multiple Bifurcation Types and the Linear Dynamics of Ion Sputtered Surfaces", *Phys. Rev. Lett.* **101**, 246102 (2008).

B. Davidovitch, M.J. Aziz, and M.P. Brenner, "Linear Dynamics of Ion Sputtered Surfaces: Instability, Stability and Bifurcations", *J. Phys. Cond. Mat*. **21**, 224019 (2009).

S.A. Norris, M.P. Brenner, and M.J. Aziz, "From Crater Functions to PDEs: A New Approach to Ion Bombardment Induced Nonequilibrium Pattern Formation", *J. Phys. Cond. Mat.* **21**, 224017 (2009).

C.S. Madi, H.B. George, and M.J. Aziz, "Linear Stability and Instability Patterns in Ion- Sputtered Silicon", *J. Phys. Cond. Mat.* **21**, 224010 (2009).

Mechanisms of sputter ripple formation: coupling among energetic ions, surface kinetics, stress and composition

Eric Chason and Vivek Shenoy
Brown University, Division of Engineering, Providence, RI 02806
DOE Award number: DE-FG02-01ER45913

Program Scope

Sputtering solid surfaces with low energy ions induces a surprising array of nanoscale pattern forming behavior [1]. Depending on the ion beam and material parameters, the surface can spontaneously develop highly uniform waves (sputter ripples) or even arrays of nanoscale quantum dots. We want to understand the processes that control ripple formation because they provide a window into the non-equilibrium kinetic processes that occur under the combined effects of energetic particle bombardment and defect-mediated transport. These processes control the formation and stability of nanoscale structures and the behavior of materials subjected to high flux environments. Because the pattern is self-organizing, we can also potentially utilize sputter rippling as an inexpensive method for creating nanoscale structures over large areas, e.g., for magnetic storage [2] alignment of liquid crystals [3], optoelectronic materials [4] or enhanced catalysis [5].

A great deal of our understanding has come from a linear instability approach (known as the BH theory [6]) that considers the surface evolution as a competitive balance between various roughening and smoothing processes occurring during ion bombardment. The roughening is attributed to a sputter yield that depends on the surface curvature while the smoothing is based primarily on the diffusion of defects. In our earlier work under this DOE program, we quantified how this balance depends on the processing conditions and developed a "kinetic phase diagram" that illustrates the different types of pattern forming behavior in different kinetic regimes. As shown in figure 1, depending on the temperature and flux, the patterning may be controlled by the direction of the ion beam (labeled B-H instability), the crystallographic orientation of the surface (Schwoebel) or lead to no patterning at all (layer-by-layer erosion). The linear instability approach has provided a useful and intuitive framework for considering different forms of pattern formation. Many aspects of ripple formation, such as the transitions between different types of behavior under different conditions, can be understood within this picture.

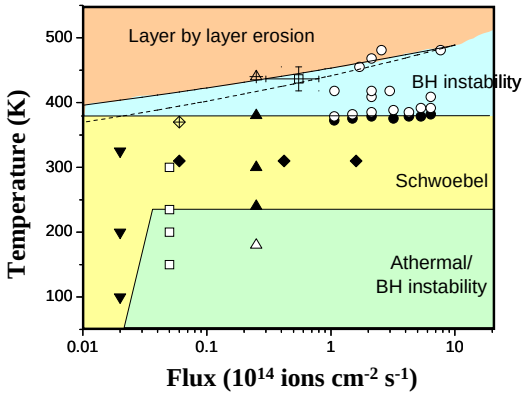

Figure 1. Kinetic phase diagram shows regimes of pattern formation observed on Cu(001) surfaces at different fluxes and temperatures.

However, systematic studies of ripple formation kinetics over recent years have

exposed significant shortcomings of this approach. For instance, the growth rate of ripples in experiments has been found to be significantly faster than predicted by the theory (200 times faster in our measurements on Cu(100) [1]). Other observed features of pattern formation (e.g., the formation of quantum-dot-like patterns at normal ion incidence) fall outside the scope of the linear theory. These observations suggest that there must be additional roughening mechanisms in the real systems that are not included in the previous models. In addition, our models predict other pattern forming behavior (the development of composition modulation on alloy surfaces) that has not been observed yet. We are therefore using an integrated combination of multiscale modeling and real-time experiments to probe the mechanisms at work during ripple formation in order to develop a fuller quantitative understanding of how surfaces evolve under ion bombardment

Recent Progress

Ion-induced stress as ripple driving force - One potential mechanism that we have identified as a source of surface roughening is stress which can lead to a morphological instability similar to the BH mechanism (referred to as the Asaro-Tiller-Grinfeld or ATG instability). Using an optical wafer curvature technique [7], we directly measured the stress induced in the near surface region by low energy ions and determined that the magnitude (in the range of 0.5 – 2 GPA) was sufficient to affect the surface evolution. We extended the linear instability model by combining the effects of stress induced roughening with the BH mechanism to predict the evolution of different Fourier components on the surface [8]. The model predicts that the ripple will grow faster in the presence of stress than in the simple BH theory, with a rate that rises as the wavevector approaches the value predicted by the ATG theory. Figure 2 shows how the growth rate increases significantly over the BH prediction as the stress increases.

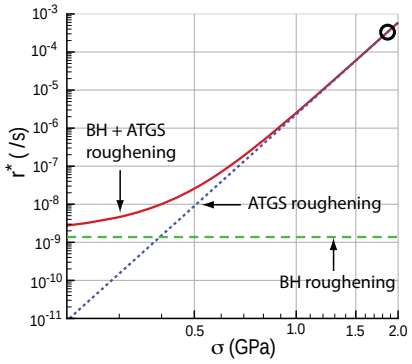

Figure 2. Results of model for effect of stress on ripple growth rate.

Kinetic Monte Carlo simulations of ripple formation mechanisms – We have developed kinetic Monte Carlo (KMC) models of ripple formation to test different atomistic mechanisms and understand their effect on ripple formation. Recently, we have studied the effect on ripple evolution of including 1) multiple ion-induced defects per ion and 2) barriers to transport between different levels on the surface (known as Ehrlich-Schwoebel or ES barriers). Preliminary results of the roughening rate as a function of wavevector for different transport and defect scenarios (single defect, multiple defect and ES barrier) suggest that the ripple amplitude grows faster when multiple defects and ES barriers are included relative to the BH sputter effects alone, but not enough to explain the discrepancy between experiments and theory.

Ion-induced prediction of composition modulations on alloy surfaces - We have recently extended the instability model to consider the sputtering of alloy surfaces [9] and found that sputtering can be used to produce composition modulations on the surface, in addition to height modulations. Composition modulations arise when each component of the alloy (A, B) has a different sputter yield (Y_A, Y_B) and/or surface diffusivity (D_A, D_B). The results of the model indicate that the surface will develop modulations in the height and also in the composition on the surface (figure 3). Depending on the relative values of the diffusivities and sputter yields, the phase between the surface height and the composition modulation can be changed, i.e., if $D_A/D_B > Y_A/Y_B$, then the composition of A will be enriched at the bottom of the ripple. For the opposite case, the composition of A will be enriched at the top of the ripple. The theory predicts that the composition

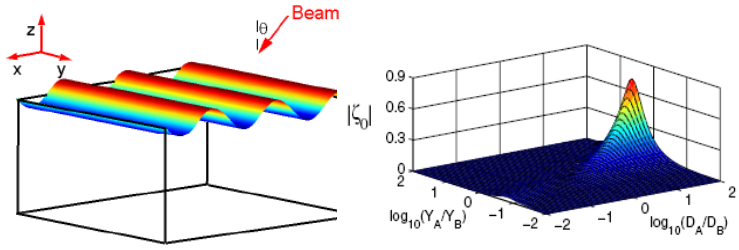

Figure 3. (a) Schematic of composition modulations (shown by color variations) that accompany shape modulations on an alloy surface predicted by our theory. (b) The amplitude of composition as a function of the ratio of the yields and diffusivities.

modulations can be significant. The amplitude of the composition modulation (ζ) depends on the relative values of the diffusivity and yield as shown in figure 3; the maximum modulation can be as large as 0.7.

Future Plans

In the future, we will measure the stress induced by the incoming ion for comparison with the MD simulations. A model of surface evolution will be developed that incorporates effects of stress, sputtering and surface transport into a single model. The results from the MD simulations will also be used to obtain the distribution of defects around the ion trajectory to be put into the KMC simulation. This will allow us to determine with an atomistic model how the ion-induced redistribution of surface atoms couples into the patterning. We will also study sputtering of alloy surfaces to look for composition modulations predicted by the theory developed by Shenoy. We will prepare samples by electrodeposition of amorphous alloys to eliminate the need for single crystal samples. A KMC model for alloy surfaces will also be developed to support the experiments. In other work, we are continuing to develop an SEM with an ion source for studying ripple formation in real time. When the resolution is sufficiently improved, we plan to use the SEM to study the direction of ripple travel on single-crystal surfaces.

References

1. Wai Lun Chan and Eric Chason, "*Making waves: kinetic processes controlling surface evolution during low energy ion sputtering*", Applied Physics Reviews, in press.
2. C. Teichert, *Self-organized semiconductor surfaces as templates for nanostructured magnetic thin films*, Appl. Phys. A 76, 653 (2003).

3. S.-C. A. Lien, P. Chaudhari, J. A. Lacey, R. A. John, J. L. Speidell, "*Active-matrix display using ion-beam-processed polyimide film for liquid crystal alignment*," IBM J. of Res. And Dev. 42, 537 (1998).
4. S. Facsko, T. Dekorsy, C. Koerdt, C. Trappe, H. Kurz, A. Vogt and H. L. Hartnagel, "*Formation of ordered nanoscale semiconductor dots by ion sputtering*", Science 285, 1551 (1999).
5. F. Zaera, "*The surface chemistry of catalysis: new challenges ahead*", Surf. Sci. 500, 947 (2002).
6. R. M. Bradley, J. M. E. Harper, *"Theory of ripple topography induced by ion bombardment",* J. Vac. Sci. Technol. A 6, 2390 (1988).
7. Wai Lun Chan , Eric Chason, "*Irradiation stress in Cu induced by low energy ions: experiment and modeling*", J. Vac. Sci. Tech. A26, 44 (2008).
8. N.V. Medhekar, W. L. Chan, V.B. Shenoy, E. Chason, "*Stress-enhanced Pattern Formation on Surfaces during Low-Energy Ion-Bombardment"*, J. Physics Cond Mat. 21, 224021 (2009).
9. V. B. Shenoy, W. L. Chan, and E. Chason, "*Compositionally modulated ripples induced by sputtering of alloy surfaces"*, Phys. Rev. Lett., submitted

Publications in the last two years

1. *"Spontaneous patterning of surfaces by low energy ion beams*", in Materials Science with Ion Beams, E. Chason and W.L. Chan, ed. H. Bernas (Springer Verlag, Berlin, 2008) (in press).
2. Wai Lun Chan , Eric Chason, "*Irradiation stress in Cu induced by low energy ions: experiment and modeling"*, J. Vac. Sci. Tech. A26, 44 (2008)
3. Basic Research Needs for Materials under Extreme Environments, E. Chason (one of multiple authors), Report of DOE workshop on Materials Under Extreme Environments (http://www.er.doe.gov/bes/reports/files/MUEE_rpt.pdf).
4. A. Ramasubramanian and V. Shenoy, "*Dynamics of nanoscale ripple relaxation on alloy surfaces*", Phys,. Rev. E 77, 1 (2008)
5. E. Chason, W. L. Chan, "*Kinetic Monte Carlo simulations compared with continuum models and experimental properties of pattern formation during ion beam sputtering,*", J. Physics Cond Mat. 21, 224016 (2009).
6. N.V. Medhekar, W. L. Chan, V.B. Shenoy, E. Chason, "*Stress-enhanced Pattern Formation on Surfaces during Low-Energy Ion-Bombardment"*, J. Physics Cond Mat. 21, 224021 (2009).
7. V.B. Shenoy, A. Ramasubramanian, "*Kinetic composition locking on faceted alloy surfaces*", Acta Mat 57, 196 (2009)

Author Index

(This page intentionally left blank.)

Author Index

Participants

(This page intentionally left blank.)

Thad Adams
Savannah River National Laboratory
803-725-5510
thad.adams@srnl.doe.gov

Pulickel Ajayan
Rice University
713-348-5904
ajayan@rice.edu

Mark Asta
University of California, Davis
530-754-8656
mdasta@ucdavis.edu

Michael Aziz
Harvard School of Engineering and Applied Sciences
617-495-9884
maziz@harvard.edu

Stacey Bent
Stanford University
650-723-0385
sbent@stanford.edu

Anand Bhattacharya
Argonne National Laboratory
630-252-6518
anand@anl.gov

Ivan Bozovic
Brookhaven National Laboratory
631-344-4973
bozovic@bnl.gov

Nigel Browning
Lawrence Livermore National Laboratory
925-424-5563
browning20@llnl.gov

Scott Chambers
Pacific Northwest National Laboratory
509-371-6517
sa.chambers@pnl.gov

Eric Chason
Brown University
401-863-2317
eric_chason@brown.edu

Xidong Chen
Cedarville University
937-766-3236
chenx@cedarville.edu

Hans Christen
Oak Ridge National Laboratory
865-574-5965
christenhm@ornl.gov

George Chumanov
Clemson University
864-656-2339
gchumak@clemson.edu

Ralph Colby
Pennsylvania State University
814-863-3457
rhc@plmsc.psu.edu

Mildred Dresselhaus
Massachusetts Institute of Technology
617-253-6864
millie@mgm.mit.edu

Timothy Droubay
Pacific Northwest National Laboratory
509-371-6488
tim.droubay@pnl.gov

James Eckstein
University of Illinois
217-244-7709
eckstein@illinois.edu

Gyula Eres
Oak Ridge National Laboratory
865-574-5494
eresg@onrl.gov

Gregory Exarhos
Pacific Northwest National Laboratory
509-371-6243
greg.exarhos@pnl.gov

Kristen Fichthorn
Pennsylvania State University
814-863-4807
fichthorn@psu.edu

Ian Fisher
Stanford Institute for Materials and Energy Science
SLAC National Accelerator Laboratory
650-723-5821
irfisher@stanford.edu

Jason Fowlkes
Oak Ridge National Laboratory
865-223-2902
fo2@ornl.gov

Miguel Fuentes-Cabrera
Oak Ridge National Laboratory
865-574-2206
fuentescabma@ornl.gov

Mary Galvin
US DOE Office of Basic Energy Sciences
301-903-8334
Mary.Galvin@science.doe.gov

David Geohegan
Oak Ridge National Laboratory
865-576-5097
geohegandb@ornl.gov

Bonnie Gersten
US DOE Office of Basic Energy Sciences
301-903-0002
Bonnie.Gersten@science.doe.gov

Peter Green
University of Michigan
734-763-2445
pfgreen@umich.edu

Jung Han
Yale University
203-432-7567
jung.han@yale.edu

Kai Ming Ho
Ames Laboratory/Iowa State University
515-294-1960
kmh@ameslab.gov

Joe Horton
Oak Ridge National Laboratory
301-903-7369
joe.horton@science.doe.gov

Linda Horton
US DOE Office of Basic Energy Sciences
301-903-7506
linda.horton@science.doe.gov

Hanchen Huang
University of Connecticut
860-486-9037
hanchen@uconn.edu

Peter D. Johnson
Brookhaven National Laboratory
631-344-3705
pdj@bnl.gov

Lawrence Jones
Ames Laboratory
515-294-5236
jonesll@ameslab.gov

Richard Kelley
US DOE Office of Basic Energy Sciences
301-903-6051
richard.kelley@science.doe.gov

Wayne King
Lawrence Livermore National Laboratory
925-423-6547
king17@llnl.gov

Aravinda Kini
US DOE Office of Basic Energy Sciences
301-903-3565
a.kini@science.doe.gov

Carolyn Koh
Colorado School of Mines
303-273-3237
ckoh@mines.edu

Refik Kortan
US DOE Office of Basic Energy Sciences
301-903-3308
refik.kortan@science.doe.gov

Matthew Kramer
Ames Laboratory
515-294-0276
mjkramer@ameslab.gov

Satish Kumar
University of Minnesota
612-625-2558
kumar@cems.umn.edu

Igor L. Kuskovsky
Queens College, The City University of New York
718-997-3367
Igor.Kuskovsky@qc.cuny.edu

Max Lagally
University of Wisconsin-Madison
608-263-2078
lagally@engr.wisc.edu

Chengdu Liang
Oak Ridge National Laboratory
865-574-8408
liangcn@ornl.gov

Chekesha Liddell
Cornell University
607-342-3775
cliddell@ccmr.cornell.edu

Feng Liu
University of Utah
801-587-7719
fliu@eng.utah.edu

Jun Liu
Pacific Northwest National Laboratory
509-375-4443
jun.liu@pnl.gov

Glenn Lockwood
Rutgers University
732-445-3083
glock@rci.rutgers.edu

Thomas Lograsso
Ames Laboratory
515-294-8425
lograsso@ameslab.gov

Michael Mackay
University of Delaware
302-831-6194
mem@udel.edu

Janna Maranas
Pennsylvania State University
814-863-6228
jmaranas@psu.edu

Michael Markowitz
US DOE Office of Basic Energy Sciences
301-903-6779
mike.markowitz@science.doe.gov

R. William McCallum
Ames Laboratory
515-294-4736
mccallum@ameslab.gov

Anatoli Melechko
North Carolina State University
865-566-2713
anatoli_melechko@ncsu.edu

Mikhail Mendelev
Ames Laboratory
515-294-2795
mendelev@ameslab.gov

Paul Mirkarimi
Lawrence Livermore National Laboratory
925-423-4848
Mirkarimi1@llnl.gov

Robert Moore
Stanford Synchrotron Radiation Lightsource
650-926-4539
rgmoore@slac.stanford.edu

Karl Mueller
Pennsylvania State University
814-863-8674
ktm2@psu.edu

Ralph Napolitano
Iowa State University
515-294-9101
ralphn@iastate.edu

Alexandra Navrotsky
Peter A. Rock Thermochemistry Laboratory
NEAT ORU, University of California, Davis
530-752-3292
anavrotsky@ucdavis.edu

George S. Nolas
University of South Florida
813-974-2233
gnolas@cas.usf.edu

David Norris
University of Minnesota
612-625-2043
dnorris@umn.edu

Roberto Paiella
Boston University
617-353-8883
rpaiella@bu.edu

Cedomir Petrovic
Brookhaven National Laboratory
631-344-5065
petrovic@bnl.gov

Alex Puretzky
Oak Ridge National Laboratory
865-241-9482
puretzkya@ornl.gov

Philip Rack
University of Tennessee, Oak Ridge National Lab
865-974-5344
prack@utk.edu

Ramamoorthy Ramesh
Univ. of California, Lawrence Berkeley National Lab
510-642-2347
rramesh@berkeley.edu

James Runt
Pennsylvania State University
814-863-2749
runt@matse.psu.edu

Raymond Schaak
Pennsylvania State University
814-865-8600
res20@psu.edu

Andrew Schwartz
US DOE Office of Basic Energy Sciences
301-903-3535
andrew.schwartz@science.doe.gov

Shelley Scott
University of Wisconsin-Madison
608-265-4119
sscott@cae.wisc.edu

Vivek Shenoy
Brown University
401-863-1475
Vivek_Shenoy@brown.edu

Michael Simpson
Oak Ridge National Laboratory
865-574-8588
simpsonML1@ornl.gov

Jay Switzer
Missouri University of Science and Technology
573-341-2071
jswitzer@mst.edu

Lee-Ann Talley
Oak Ridge Institute for Science and Education
865-576-2077
Lee-Ann.Talley@orise.orau.gov

Maria Tamargo
The City College of New York
212-650-7941
mtamargo@ccny.cuny.edu

Meng Tao
University of Texas at Arlington
817-272-1353
mtao@uta.edu

Patricia Thiel
Ames Laboratory
515-294-8985
thiel@ameslab.gov

Thiyaga P. Thiyagarajan
US DOE Office of Basic Energy Sciences
301-903-9706
P.Thiyagarajan@science.doe.gov

Reji Thomas
University of Puerto Rico
787-751-4210
etreji@yahoo.com

Katsuyo Thornton
University of Michigan
734-615-1498
kthorn@umich.edu

Salvatore Torquato
Princeton University
609-258-3341
torquato@princeton.edu

Darrell Velegol
Pennsylvania State University
814 865-8739
velegol@psu.edu

Peter Voorhees
Northwestern University
847-491-7815
p-voorhees@northwestern.edu

Qiang Wang
Colorado State University
970-491-2763
q.wang@colostate.edu

Karen Winey
University of Pennsylvania
215-898-0593
winey@seas.upenn.edu

Stanislaus S. Wong
Brookhaven National Laboratory
631-344-3178
sswong@bnl.gov

Zhili Xiao
Northern Illinois University
815-753-3506
zxiao@niu.edu

Boris Yakobson
Rice University
713-348-3572
biy@rice.edu

Mina Yoon
Oak Ridge National Laboratory
865-574-6153
myoon@ornl.gov

Francisco Zaera
University of California, Los Angeles
951-827-5498
zaera@ucr.edu

Qiming Zhang
Pennsylvania State University
814-863-8994
qxz1@psu.edu

Zhuomin Zhang
Georgia Institute of Technology
404-385-4225
zhuomin.zhang@me.gatech.edu

Guangwen Zhou
Binghamton University
607-777-5084
gzhou@binghamton.edu

Pavel Zinin
HIGP, University of Hawaii
808-956-9960
zinin@soest.hawaii.edu

Steven Zinkle
Oak Ridge National Laboratory
865-574-4065
zinklesj@ornl.gov

Jian-Min Zuo
University of Illinois
217-244-6504
jianzuo@illinois.edu